Signals and Communication Technology

Ming Ding
Hanwen Luo

Multi-point Cooperative Communication Systems: Theory and Applications

上海交通大學出版社
SHANGHAI JIAO TONG UNIVERSITY PRESS

Springer

Signals and Communication Technology

For further volumes:
http://www.springer.com/series/4748

Ming Ding • Hanwen Luo

Multi-point Cooperative Communication Systems: Theory and Applications

Springer
上海交通大學出版社
SHANGHAI JIAO TONG UNIVERSITY PRESS

Ming Ding
Sharp Laboratories of China Co., Ltd.
Department of Electrical Engineering
Shanghai Jiao Tong University
Shanghai
China, People's Republic

Hanwen Luo
Department of Electrical Engineering
Shanghai Jiao Tong University
Shanghai
China, People's Republic

ISSN 1860-4862
ISBN 978-3-642-34948-5 ISBN 978-3-642-34949-2 (eBook)
SJTUP's ISBN 978-7-313-09112-3
DOI 10.1007/978-3-642-34949-2
Springer Heidelberg New York Dordrecht London

Library of Congress Control Number: 2013932878

Printed on acid-free paper

Springer is part of Springer Science+Business Media (www.springer.com)

Preface

This book is about multipoint cooperative communication, a key technology to overcome the long-standing problem of limited transmission rate caused by inter-point interference. However, the multipoint cooperative communication is not an isolated technology. Instead, it covers a vast range of research areas such as the multiple-input multiple-output system, the relay network, channel state information issues, inter-point radio resource management operations, coordinated or joint transmissions, etc. We suppose that any attempt trying to thoroughly analyze the multipoint cooperative communication technology might end up working on a cyclopedia for modern communication systems and easily get lost in discussing all kinds of cooperative communication schemes as well as the associated models and their variations. Therefore, in this book we take a systematic approach to study the multipoint cooperative communication systems in a novel and general framework, which helps our readers to get a clear picture about the technology map and where the addressed topics fit in.

Goals of This Book

Recently, there is a huge surge of research activities in the theories and applications of multipoint cooperative communication technologies. Besides, the multipoint cooperative communication has also found its way in the state-of-the-art international communication networks, for example, the fourth generation (4G) cellular systems. Hence, the first goal of this book is to conduct a well-organized survey and introduce our readers to the exciting progress of researches on cooperative communications both in academic communities and in industrial standardizations. The second and third goals of this book are presenting some of our theoretical studies on the multipoint cooperative communication and discussing the related applications in the advanced cellular systems. In the theory part of this book, our readers might be interested to know that instead of combating the interference, technologies have evolved to adopt the philosophy of exploiting the interference to improve the transmission rate by joint processing among multiple points. In the application part of this book, our readers might be quite excited to watch the campaigns of promoting the coordinated multipoint (CoMP) system in the standardization of the 4G cellular network. Also, our readers can learn how to design suboptimal cooperative communication schemes with considerations of practical systems.

Structure of This Book

In order to attain our goals, we have properly arranged this book. Chapter 2 is the key part of this book, which discusses the fundamentals of wireless digital communication, several selected topics that have laid the foundation for the multipoint cooperative communication, and a thorough survey on the state of the researches on cooperative communication technologies by classifying all the existing schemes into eight categories. This chapter is presented with the purpose to help our readers to get a large technical picture about the history and new development in each area of multipoint cooperative communications so that the positions and connections of the topics to be treated in the following chapters can be better understood. Among the dozens of technical topics raised in Chap. 2, we select four topics respectively addressed in Chaps. 3, 4, 5 and 6, as the examples of theoretical studies in the multipoint cooperative communication. Please note that a thorough analysis of all the topics listed in Chap. 2 would be a mammoth undertaking, which cannot be accomplished by this book with limited space. Finally, Chaps. 7 and 8 discuss the application of the CoMP system in the 4G network, including the downlink transmission and uplink reception schemes of CoMP, as well as the related specification works and the simulation results from the perspective of a practical cellular network.

Audience of This Book

This book is meant for the scientist, researcher, engineer or student who works in the field related to wireless communication and wants to know the essence of multipoint cooperative communication as well as its aspects of theoretical studies and practical applications. In particular, for readers who are interested in obtaining a high-level understanding of multipoint cooperation, reading Chap. 2 is probably enough. Besides, Chap. 2 is self-contained and almost requires no background of digital communication at all. For readers who are doing research in the multipoint cooperative communication, it might be more efficient to go straightly into Chaps. 3, 4, 5 and 6 to check whether our results are relevant and helpful. If not, a careful study on Chap. 2 and some of the references therein might turn out to be beneficial. Moreover, details of practical considerations when designing a cooperative communication network can be found in the second part of this book, that is, Chaps. 7, 8 and 9. These chapters are very useful for readers who intend to get a quick idea about what's going on regarding the CoMP system in the 4G network, and those who want to check whether the system assumptions in their studies are reasonable or whether their proposals can be applied in the future multipoint cooperative communication systems.

Acknowledgement

First, we would like to thank the students in our research laboratory for their selfless supports in preparing this book. Particular thanks are due to: Jian Huang who helped us painstakingly arrange most parts of our manuscript according to the format required by Springer; Jing Deng who proofread many chapters and provided quite a few constructive suggestions for revision; Jun Zou, Meng Zhang, Yi Qin, Shi Liu, Youlong Wu and Jiamei Qin who helped us with some editing work in Chaps. 2, 3, 5 and 6; Cheng Qian who worked with us on the simulation of all the schemes in Chap. 8. Second, we would like to express our gratitude to Wen Chen from Shanghai Jiao Tong University for his critical comments and helpful advice for improvement on Chaps. 2, 3 and 6. Third, Sayantan Choudhury from Sharp Laboratories of America, Inc., Nogami Toshizoh and Shimezawa Kazuyuki from Sharp Telecommunication & Image Technology Laboratories helped us to improve the presentation of Chap. 5. Ahmad Khoshnevis from Sharp Laboratories of America, Inc. gave us many constructive inputs on Chaps. 7 and 8. Oh Wahoh and Tsuboi Hidekazu from Sharp Telecommunication & Image Technology Laboratories provided valuable help to us regarding the system-level simulations in Chap. 4. Fourth, many chapters of this book have benefitted from our discussions with Zeng Yang, Renmao Liu, Lei Huang, Chen Chen, Yongming Liang and Yingyu Zhang from Sharp Laboratories of China Co., Ltd.

We would also like to thank the publishing team of Springer and Shanghai Jiao Tong University Press. In particular, many thanks to: Guangliang Li and Dan Li for their encouragement and support throughout the preparation of this book; Virgin Gomez who nicely coordinated and supervised the publishing process of this book; and the editorial staff for their professionalism in producing the proof with high quality, especially helping us double-check each and every sentence, equation and reference link in this book.

Regarding the key part of this book (i.e., Chap. 2), I want to mention several individuals for special acknowledgement. An interesting fact is that Chap. 2 of this book is a direct result of my promise to explain “wireless communication” to my fiancée, Minwen Zhou, who is now pursuing her career as a naturalist and philosopher. She is the most brilliant person I have ever met. From time to time, I'm amazed by her non-linear thinking and using vivid analogy between two conceptually different objects during our talks. Her intellectual capability is something I do not yet possess. Still, I hope I'm doing a good job trying to think like her in the preparation of Chap. 2. I suppose that our readers largely benefit from her because without Chap. 2 this book will just lose its soul and degenerate to a magazine with fragmented topics. Besides, Chap. 2 owes an intellectual debt to two of my close friends, Dawei Wang and Wuyang Jiang. Some contents in this chapter are related to the discussions with them. Their useful feedback and constructive comments have made this chapter much colorful. Even today, I can still recall the joyful time when Dawei Wang and I were discussing about the possibility of estimating the audience ratings by analyzing signal variations in the radio frequency chain of the broadcasting transmitter. Wuyang Jiang, on the other hand, sometimes is a quiet listener. But when he reiterates my statement in another way with his own thoughts, usually we can get deeper understanding of the discussed topic or find new problems for further study.

Finally, it should be noted that any views presented in this book do not reflect the views of our university and company. We highly welcome any feedback to further improve this book.

Contents

Abbreviations

2G	The Second Generation
3G	The Third Generation
3GPP	The Third Generation Partner Project
3GPP2	The Third Generation Partner Project 2
4G	The Fourth Generation
ADSL	Asymmetric Digital Subscriber Line
AF	Amplify-and-Forward
AGP	Autonomous Global Precoding
AMC	Adaptive Modulation and Coding
AMPS	Advanced Mobile Phone Service
ANC	Analogue Network Coding
AoA	Angle-of-Arrival
AoD	Angle-of-Departure
ARQ	Automatic Repeat reQuest
AS	Antenna Selection
ASI	Antenna Selection Indicator
ASK	Amplitude Shift Keying
AS-SFNP	Antenna Selection - Single Frequency Network Precoding
AWGN	Additive White Gaussian Noise
BC	Broadcast Channel
BD	Block Diagonalization
BER	Bit Error Rate
BF	BeamForming
BLAST	Bell Labs Layered Space-Time
BLER	BLock Error Rate
BP	Band Part
bps	bits per second
BPSK	Binary Phase Shift Keying
BS	Base Station
CAZAC	Constant Amplitude Zero Autocorrelation Codes
CB	Coordinated Beamforming

CC	Coded Cooperation
CDF	Cumulative Distribution Function
CDI	Channel Direction Indicator
CDM	Code Division Multiplexing
CDMA	Code Division Multiple Access
C/I	Carrier-to-Interference ratio
CFF	Common Feedback Framework
CoMP	Coordinated Multi-Point
CP	Cyclic Prefix
CQI	Channel Quality Indicator
CRC	Cyclic Redundancy Check
CRS	Common Reference Signal
CS	Coordinated Scheduling
CS/CB	Coordinated Scheduling / Coordinated Beamforming
CSG	Closed Subscriber Group
CSI	Channel State Information
CSIR	Channel State Information at the Receiver
CSI RS	CSI Reference Signal
CSIT	Channel State Information at the Transmitter
CVQ	Channel Vector Quantization
DAS	Distributed Antenna System
dB	deci-Bel
DCS	Dynamic Cell Selection
DF	Decode-and-Forward
DFT	Discrete Fourier Transform
DFT-S-OFDM	DFT-Spread OFDM
DL	DownLink
DM RS	DeModulation RS
DMF	Doubly Matched Filter
DORS	Distributed Orthogonal Relay Selection
DPC	Dirty Paper Coding
DS-CDMA	Direct-Sequence Code Division Multiple Access
DSP	Digital Signal Processor
DVB	Digital Video Broadcasting
DVB-H	Digital Video Broadcasting–Handheld
DVB-T	Digital Video Broadcasting–Terrestrial
DZF-GCM	Doubly ZF-Greedy Capacity Maximization
EDGE	Enhanced Data rates for GSM Evolution
EESM	Exponential Effective SINR Mapping
ETSI	European Telecommunications Standards Institute
EUR	Edge UE Resource
E-UTRA	Evolved-UTRA
E-UTRAN	Evolved-UTRAN
EVD	Eigen-Value Decomposition
EvDO	Evolution Data Optimized

FB	Full Buffer
FDD	Frequency Division Duplex
FDM	Frequency Division Multiplexing
FDMA	Frequency Division Multiple Access
FEC	Forward Error Correction
FFR	Fractional Frequency Reuse
FFT	Fast Fourier Transform
FPGA	Field Programmable Gate Array
FRU	Frequency Resource Unit
FSK	Frequency Shift Keying
FTP	File Transfer Protocol
GCM	Greedy Capacity Maximization
GERAN	GSM EDGE Radio Access Network
GMSK	Gaussian Minimum-Shift Keying
GMM	Greedy MSE Minimization
GI	Guard Interval
GP	Global Precoding
GPRS	General Packet Radio Service
GPS	Global Positioning System
GSM	Global System for Mobile communication
HARQ	Hybrid Automatic Repeat reQuest
HD-FDD	Half-Duplex FDD
HII	High Interference Indicator
HSDPA	High Speed Downlink Packet Access
HSPA	High Speed Packet Access
HSUPA	High Speed Uplink Packet Access
HTTP	Hyper Text Transfer Protocol
IA	Interference Alignment
IC	Interference Channel
ICI	Inter-Carrier Interference
ICIC	Inter-Cell Interference Coordination
IDFT	Inverse Discrete Fourier Transform
IEEE	Institute of Electrical and Electronics Engineers
IFFT	Inverse Fast Fourier Transform
i.i.d.	independently and identically distributed
IMT	International Mobile Telecommunications
INR	Interference-to-Noise Ratio
IoT	Internet of Things
IP	Internet Protocol
IRC	Interference Rejection Combining
ISD	Inter-Site Distance
ISI	Inter-Symbol Interference
ITU	International Telecommunication Union
JR	Joint Reception
JT	Joint Transmission

LAN	Local Area Network
LMMSE	Linear MMSE
LoS	Line-of-Sight
LP	Local Precoding
LS	Least Squares
LTE	Long Term Evolution
LTE-A	Long Term Evolution - Advanced
MAC	Medium Access Channel
MAP	Maximum A posteriori Probability
MBMS	Multimedia Broadcast and Multicast Service
MBSFN	Multimedia Broadcast Single Frequency Network
MCS	Modulation and Coding Scheme
MF	Matched Filter
MIMO	Multiple-Input Multiple-Output
MISO	Multiple-Input Single-Output
ML	Maximum Likelihood
MMSE	Minimum Mean Squared Error
MRC	Maximum Ratio Combining
MRT	Maximum Ratio Transmission
MSC	Mobile Switch Controller
MSE	Mean Square Error
MSH	More Softer Hand-Off
MU	Multi-User
MUI	Multi-User Interference
MU-MIMO	Multi-User MIMO
NF	Noise Figure
NGMN	Next Generation Mobile Networks
NLoS	Non-Line-of-Sight
N-MIMO	Network MIMO
OB	Opportunistic Beamforming
OFDM	Orthogonal Frequency Division Multiplexing
OFDMA	Orthogonal Frequency Division Multiple Access
OI	Overload Indicator
PA	Power Amplifier
PAPR	Peak-to-Average Power Ratio
PC	Personal Computer
PDCCH	Physical Downlink Control CHannel
PDF	Probability Density Function
PDSCH	Physical Downlink Shared CHannel
PER	Packet Error Rate
PF	Proportional Fairness
PMI	Precoding Matrix Indicator
PSD	Power Spectral Density
PTI	Precoding Type Indicator
PRB	Physical Resource Block

PSK	Phase Shift Keying
PUCCH	Physical Uplink Control CHannel
PUSCH	Physical Uplink Shared CHannel
QAM	Quadrature Amplitude Modulation
QoE	Quality of Experience
QoS	Quality-of-Service
QPSK	Quadrature Phase Shift Keying
RAC	Resource Access Control
RAN	Radio Access Network
RAT	Radio Access Technology
RB	Resource Block
RE	Resource Element
RF	Radio Frequency
RI	Rank Indicator
RN	Relay Node
RNC	Radio Network Controller
RNTP	Relative Narrowband Transmit Power
RRC	Radio Resource Control
RRH	Remote Radio Head
RRM	Radio Resource Management
RS	Reference Signal
SC-FDMA	Single Carrier Frequency Division Multiple Access
SCM	Spatial Channel Model
SCME	Spatial Channel Model Extension
SCP	Single Cell Processing
SDM	Space Division Multiplexing
SDMA	Spatial Division Multiple Access
SDP	Semi-Definite Programming
SFBC	Space-Frequency Block Code
SFN	Single Frequency Network
SFNP	Single Frequency Network Precoding
SH	Soft Hand-off
SIC	Successive Interference Cancellation
SIMO	Single-Input Multiple-Output
SINR	Signal-to-Interference-plus-Noise Ratio
SIP	Sequential and Incremental Precoding
SIR	Signal-to-Interference Ratio
SISO	Single-Input Single-Output
SNR	Signal-to-Noise Ratio
SON	Self-Optimizing Networks
S-O	Semi-Orthogonal
SRS	Sounding Reference Signal
STBC	Space-Time Block Code
SU	Single-User
SU-MIMO	Single-User MIMO

SVD	Singular Value Decomposition
TB	Transport Block
TCP	Transmission Control Protocol
TDD	Time Division Duplex
TDM	Time Division Multiplex
TDMA	Time Division Multiple Access
TD-SCDMA	Time Division Synchronous Code Division Multiple Access
TF	Transport Format
THP	Tomlinson-Harashima precoding
TM	Transmission Mode
TSG	Technical Specification Group
TTI	Transmit Time Interval
TU	Typical Urban
UE	User Equipment
UL	UpLink
ULA	Uniform Linear Array
UMTS	Universal Mobile Telecommunications System
UTRA	Universal Terrestrial Radio Access
UTRAN	Universal Terrestrial Radio Access Network
WAN	Wide Area Network
WCDMA	Wideband Code Division Multiple Access
WG	Working Group
WiMAX	Worldwide interoperability for Microwave Access
WINNER	Wireless world INitiative NEw Radio
WLAN	Wireless Local Area Network
WRC	World Radiocommunication Conference
WLP	Weighted Local Precoding
ZF	Zero-Forcing
ZF-BF	Zero-Forcing Beamforming
ZMCSCG	Zero-Mean Circularly Symmetric Complex Gaussian

Chapter 1
Introduction

Abstract This chapter gives an introduction of this book. First, we begin with a large picture by reviewing the fast development of wireless communication in the past half century with the emphasis on the cellular network. Second, we discuss the future and key technologies of the enhanced fourth generation (4G) international telecommunication network based on analysis of challenges and requirements in the next decade. Third, among the discussed key technologies, we focus on the multipoint cooperative communication and present its background to readers. Finally, we indicate the scope and outline of this book to complete this introduction.

Keywords Cellular network • 3G • 4G • Enhanced 4G • Small cell • Three-dimensional MIMO • CoMP • Multipoint cooperative communication

1.1 A Brief History of the International Mobile Telecommunication Systems

With the continuously growing demands for high data rate and reliable connection in wireless communication, the mobile telecommunication system, also widely known as the cellular network, has undergone several revolutionary developments in the past half century.

The first generation (1G) cellular network is a frequency division multiple access (FDMA) analog system. The story began in 1960, when a two-way analog mobile phone system operated by a high-power base station (BS) was put to use in New York, USA. However, at that time only 12 user equipments (UEs) were able to access the system simultaneously in the city. In order to increase the system capacity, in 1979, Bell labs proposed a ground-breaking concept of cell (MacDonald 1979), which consists of three novel ideas, that is, frequency reuse, sectorization, and intercell handover. The purpose of constructing a cellular system is to allow more UEs to access the system simultaneously. To fulfill that purpose, the power of a BS

M. Ding and H. Luo, *Multi-point Cooperative Communication Systems: Theory and Applications*, Signals and Communication Technology, DOI 10.1007/978-3-642-34949-2_1,

should be decreased, rather than increased, thus creating a small quasi-hexagonal coverage area called cell. Moreover, a wide area can be covered by plenty of the non-overlaid cells with the associated BSs providing wireless communication service to UEs randomly distributed in the area. To further increase the system capacity, a cell can be splitted into several sectors using directional antennas. It was in year 1983 that the famous advanced mobile phone service (AMPS) system was officially deployed in USA, which marked the birth of the 1G cellular network. It should be noted that Japan also launched a similar 1G system, which is known as the MCS-L1 system. In the following decade, small improvement was made on the 1G system, such as narrowing the frequency channels to accommodate more UEs in each cell.

The second generation (2G) cellular network is a digital system based on time division multiple access (TDMA) combined with FDMA. In 1990, the American AMPS system was upgraded to the digital AMPS (DAMPS) system, which adopts QPSK modulation, frequency division duplex (FDD), and narrow-band TDMA technologies. DAMPS was specified in the USA standardization IS-54, which later became IS-136. A similar system to DAMPS, which is called pacific digital cellular (PDC) system, was deployed in Japan in 1993. However, the true winner of the 2G cellular network came from Europe, that is, the Global System for Mobile communication (GSM), which claimed to have achieved one billion subscribers before 2005. The GSM system featured on Gaussian filtered continuous-phase frequency shift keying (FSK) modulation, FDD, and wide-band TDMA/FDMA technologies. To keep the competitiveness of the GSM system, the enhancement of general packet radio service (GPRS), mainly designed for data transmission with packet switch, was introduced as an upgrade to the GSM network in 2001. Later on, the GPRS system evolved into the enhanced data rate for GSM evolution (EDGE) system, in which adaptive modulation and coding (AMC) schemes were employed. The GSM system with GPRS or EDGE enhancement can be viewed as a super 2G or 2.5G network, and it paved the way for the development of the third generation (3G) cellular networks. Another 2G network worthy of mentioning is the narrow-band code division multiple access (CDMA) system proposed by Qualcomm company. The technical details were captured in the IS-95A specification, which was upgraded to IS-95B as a standard of another 2.5G cellular network in 1995.

The development of the 3G system commenced in 1997, when International Telecommunication Union (ITU) posted the invitation for technical proposals on the design of 3G networks. Fifteen proposals were received, including wide-band CDMA (WCDMA) from Europe and Japan, CDMA2000 (narrow-band CDMA, upgraded from IS-95B) from USA, and TD-SCDMA from China. The mentioned three proposals were carefully evaluated and finally adopted by ITU in 2000. The standardization of WCDMA was taken care of by the Third Generation Partner Project (3GPP) organization. Another organization 3GPP2 was responsible for the standardization activities of CDMA2000 and TD-SCDMA. In 2000, 3GPP2 released an upgrade for CDMA 2000, that is, CDMA 2000 1xEV-DO (Evolution-Date Only), where dedicated carriers for data transmission were designed. In 2003, another upgrade for CDMA2000 was presented, that is, CDMA 2000 1xEV-DV

(Evolution-Date and Voice), where voice service was further enhanced. 3GPP also made some prominent progress in 2005, when a downlink upgrade for WCDMA, that is, high-speed downlink packet access (HSDPA), was officially announced and deployed. In the following year, the uplink upgrade for WCDMA was launched also by 3GPP, which was high-speed uplink packet access (HSUPA). In October of year 2007, ITU approved the worldwide interoperability for microwave access (WiMAX) system to be the fourth member of the 3G standards. The unexpected move of WiMAX in such a late stage of 3G era intensified the competition of the upcoming fourth generation (4G) standardization.

In fact, 3GPP has long ago realized that the wireless IP technology, represented by the Wireless Local Area Network (WLAN) and WiMAX systems, may pose serious threats to the traditional cellular network. In order to respond to the upcoming challenge, since 2004, 3GPP has been devoting most of its efforts to the design of a new and competitive cellular network (Sesia et al. 2009), that is, the long-term evolution (LTE) system based on the orthogonal frequency division multiplexing (OFDM) technology. The first release of the LTE system (LTE Release 8), also known as the super 3G or 3.9G system, was launched in 2009 and has been deployed around the world since 2010. The reason why LTE Release 8 system was not recognized as a 4G candidate system is that 3GPP wanted to present an even more powerful solution than the LTE Release 8 system for the 4G arena. To that end, in April of 2008 3GPP called a workshop meeting in Shenzhen, China, to discuss the LTE Release 10 network as an official 4G candidate system (3GPP 2010a), which is also referred to as the LTE-Advanced (LTE-A) system.

The LTE-A network boasts of many desirable features, such as backward compatibility with the LTE system, wide system bandwidth (e.g., 100 MHz), high-peak rate (e.g., 1Gbps for downlink, 500Mbps for uplink), smooth support for various services, and good user experience. The key technologies of the LTE-A system include OFDM transmission, multiple-input multiple-output (MIMO) technology, limited-bit channel state information (CSI) feedback technique, multipoint cooperative communication, carrier aggregation, low peak-to-average power ratio (PAPR) uplink multiple access scheme, and multimedia broadcast and multicast service (MBMS) (Parkvall et al. 2008). Among them, multipoint cooperative communication is one of the core technologies which can improve both the cell-edge and overall throughputs of the system.

Like the worldwide invitation event for the 3G cellular network in 1997, in September of 2009 ITU invited for the technical proposals on the 4G system. One month later, six proposals were received, which came from China (one TDD LTE-A proposal), Japan (two proposals respectively based on LTE-A and WiMAX), Korea (one WiMAX proposal), 3GPP (one LTE-A proposal), and USA (one WiMAX proposal). The evaluation period was estimated to be one year. In October 2010, Chongqing, China, ITU officially announced that the air interface technologies for the 4G network should be LTE-A and WiMAX. As a result, many existing cellular operators have declared their intentions to quickly deploy the LTE-A network from year 2012 due to the booming development of mobile Internet.

1.2 The Future of Wireless Communication: The Enhanced 4G Network

1.2.1 Challenges in the Next Decade

The fourth generation of wireless communication networks, represented by the LTE-A and WiMAX systems, are able to provide communication service of high transmission rate and good experience for UEs. But they still cannot fully meet the users' demands in the next few years. At present, the number of mobile connections is about 5.5 billion and is estimated to rise to 7.3 billion by 2015 (Gartner 2012). In particular, the growth rate of smartphone UEs will be quite significant. In year 2011, there were about 4.28 million smart mobile terminals purchased by customers, and that sales number will quickly double to more than one billion in 2015 (Pyramid 2012).

Deep market penetration of powerful mobile communication devices such as laptops, smartphones, and tablets largely boosts the growth of wireless data traffic. Some examples of new data services are application software download, real-time navigation, and personal cloud data management and sharing. In recent years, the worldwide wireless data traffic has been steadily increasing by more than 100% per year (Cisco 2012). So it is expected that after 10 years, the wireless communication system should be upgraded to generate 1,000 times of data traffic provided by the current system so as to satisfy the basic requirement of communication service. On the other hand, the voice traffic that is subjected to the relatively slow growth rate of population will not see fast development in the near future.

In addition to the challenge of data traffic explosion, another challenge stems from the rise of the mobile Internet communication. Currently, about 70% of Internet access is initiated by mobile terminals (Softbank 2012), and the ratio continues going up, which shows a paradigm-shifting change in user habit from the traditional PC Internet to the mobile Internet. The next decade will be another golden time for the IT industry since the mobile Internet has spawned a number of new businesses, such as software development targeting for handheld communication devices with touch-controlled screen, location-based social network applications, and real-time cloud application/content service. The impacts on the wireless communication system are twofolds. First, it has been forecasted that mobile video will boom at a compound annual growth rate (CAGR) of 90% through 2016 (Cisco 2012), which is the highest growth rate of any mobile application category. And by 2016, mobile video will account for over 70% of total mobile data traffic (Cisco 2012). Consequently, significant growth of the mobile video traffic calls for real-time transmission with relatively high quality of service (QoS) and high reliability of the cellular network. Second, at present and in the future, 70∼80% of the mobile data traffic takes place in indoor and hot-spot areas (Fujitsu 2012), which raises the issue of enhanced coverage of the wireless communication service.

Furthermore, machine-to-machine (M2M) communication has been gradually transformed from a lab toy to a viable business as operators are now creating their M2M portfolios. According to Machina (2011), over 12 billion M2M devices are expected in 2015, excluding PCs, TVs, and handheld mobile devices. And M2M devices will be actively interworking with each other in fields such as smart cities, smart grids, healthcare, and public safety. By 2020, the world will be populated with 20 billion M2M units, and their data traffic will have a 500% increase compared with today (Bell et al. 2011). Therefore, how to design the future wireless communication system in order to accommodate such colossal number of M2M devices is also a subject that needs further study.

1.2.2 Development Requirements

Considering the challenges over the next decade, some general requirements of the enhanced 4G wireless communication system can be foreseen as follows:

- To achieve high wireless broadband capacity and focus on the optimization for the local area cell.
- To further improve the customer experience, especially for the cell-edge UEs.
- Considering that the available spectrum will not expand by 1,000 folds, studies on new technologies to further improve the spectral efficiency should be continued.
- Higher frequency spectrums (e.g., 5GHz or even higher) should be put into use to obtain larger communication bandwidths.
- Inter-network cooperation should be operated among 2G/3G/4G, WLAN, WiMAX, and LTE/LTE-A systems for data traffic offloading.
- To optimize the network for diverse devices, applications, and services.
- To enhance the system to support large amount of M2M communications.
- To strive for flexible, smart, and cost-efficiency network planning and deployment.

1.2.3 Key Technologies

In order to fulfill the development requirements discussed in Sect. 1.2.2, in June 2012, 3GPP organization called a special workshop meeting to discuss the key technologies of the enhanced 4G wireless communication system. At the meeting, 42 proposals were presented and discussed, and three key technologies were identified as follows:

- Enhanced small-cell technology (NSN 2012; Ericsson and ST-Ericsson 2012; Nokia 2012; Huawei and HiSilicon 2012; Qualcomm 2012; Telecom 2012; NTT 2012; Deutsche 2012; Alcatel-Lucent 2012; Fujitsu 2012; AT&T 2012; Panasonic 2012; SK 2012; Samsung 2012; Renesas 2012; Intel 2012; China Unicom 2012; CATT 2012; CMCC 2012; Vodafone 2012; ZTE 2012; China Telecom 2012; KDDI 2012; SHARP 2012; Hitachi 2012; MediaTek 2012; ITRI 2012)

- Three-dimensional (3D) MIMO technology (NSN 2012; Ericsson and ST-Ericsson 2012; Orange 2012; Huawei and HiSilicon 2012; NTT 2012; NEC 2012; Deutsche 2012; Alcatel-Lucent 2012; Fujitsu 2012; AT&T 2012; SK 2012; Samsung 2012; CATT 2012; ETRI 2012; CMCC 2012; ZTE 2012; Motorola 2012; China Telecom 2012; KDDI 2012; MediaTek 2012)
- Enhanced coordinated multipoint (CoMP) technology (Ericsson and ST-Ericsson 2012; Orange 2012; Telefonica 2012; Telecom 2012; NTT 2012; Deutsche 2012; Dish 2012; Alcatel-Lucent 2012; Fujitsu 2012; AT&T 2012; Panasonic 2012; SK 2012; Samsung 2012; Renesas 2012; Intel 2012; CATT 2012; ETRI 2012; Softbank 2012; CMCC 2012; ZTE 2012; Motorola 2012; China Telecom 2012; KDDI 2012; SHARP 2012; Hitachi 2012; MediaTek 2012; ITRI 2012; Broadcom 2012)

To discuss it as an interesting fact, various companies seemed to show their preferences on the candidate technologies based on their business interests, rather than technical considerations. BS equipment vendors (Ericsson and ST-Ericsson 2012; Huawei and HiSilicon 2012), for example, tended to adopt the first key technology because infrastructure reconstruction due to the introduction of small cells would bring them a large number of new orders. Operators (Orange 2012; Telefonica 2012; Telecom 2012), on the other hand, strongly promoted the third technology because of its low-cost investment on software upgrade only. Other innovative manufactures showed their support for the second technology (NSN 2012; Alcatel-Lucent 2012; Samsung 2012), trying to make the 4G wireless communication system more competitive in the future. Brief introductions of the three key technologies are provided in the following.

1.2.3.1 Enhanced Small-Cell Technology

Data transmission sum-rate in a unit area (1 m^2) can be roughly expressed as the product of three factors, that is, spectrum bandwidth (Hz), spectral efficiency (bps/Hz), and cell density (cells/m^2) (NTT 2012). On one hand, frequency spectrum is a very scarce resource, especially the low-frequency band with small propagation loss. In the next decade, the bandwidth of the available spectrum is at most $2 \sim 3$ times as that of the current spectrum (SK 2012). On the other hand, the campaign of improving the spectral efficiency advances at a very slow pace. In the SINR regime for most working mobile devices, for example, $5 \sim 15$ dB, the spectral efficiency of the 4G system is already very close to the Shannon's capacity limit so that future improvement becomes quite hard at a painful cost of high complexity. Thus, in order to increase the transmission rate of a wireless communication system by hundreds or one thousand of times, the most direct and efficient way is to perform cell-splitting so as to create a huge number of small cells in the network, which can rapidly increase the cell density and in turn boost the network capacity dramatically.

In the enhancement for small-cell systems, many new topics are worthy of studying. First, the protocol of the hybrid TDD/FDD network should be considered.

It is well known that the FDD system has been commonly used for the case of wide coverage and/or symmetrical downlink/uplink traffic, while the TDD system is mostly applicable to hot spots of local coverage with flexible traffic patterns (Sesia et al. 2009). Thus, in future networks, small cells will prioritize a TDD scheme over an FDD one. Moreover, the ratio between the downlink and uplink subframes in a TDD scheme should be semi-statically configured in small cells so that the data service is able to adapt to the fast change of traffic patterns (3GPP 2012). In the extreme case, a TDD small cell with zero traffic may even intelligently shut itself down to save electrical power. The conventional macro cell, however, should still use the FDD technology to cover a wide area. Therefore, it needs further investigation on how to enable mobile UEs to seamlessly switch between TDD and FDD systems. Second, the interference issue in the hybrid TDD/FDD network should be dealt with. In general, there are two new types of interference in the hybrid TDD/FDD network, that is, (1) intercell interference between the TDD small cell and FDD macro cell; (2) interlink interference between the uplink and downlink transmissions resulted from nonuniform configurations of TDD subframes in difference small cells. Third, due to the very limited coverage of small cells, the distance-dependent attenuation of radio waves is relatively small. Thus, high-frequency band can be employed for the transmission in small cells, which opens a whole new research area of optimization on OFDM systems considering the propagation characteristics of the high-frequency radio waves. Fourth, as for the connections from abundant small cells to the core network, if we build up an all-fiber underground network with high-capacity and low-latency connections, then the corresponding capital investment will be too vast to be afforded by the operators. A more feasible way is to use wireless backhaul transmissions to link the small cells with the existing macro BSs, which already have access to the core network by means of wired connections. However, the data traffic rate on the mentioned wireless backhaul will be ultrahigh since one typical macro BS may be required to assist the service in tens of small cells, all with high traffic volumes. Thus, the design of ultrahigh wireless backhaul transmissions becomes a critical challenge in various small cell scenarios. Good news is that we can safely assume that both the small-cell BS and macro cell BS are immobile with relatively stable inter-BS channel conditions, and the BSs will carry sophisticated hardware platforms with powerful signal processing capabilities. Therefore, various advanced transmitter and receiver algorithms can be considered for the wireless backhaul design.

1.2.3.2 Three-Dimensional (3D) MIMO Technology

The 3D MIMO technology represents a new approach to improve the efficiency of spectrum utilization. At present, transmit and receive antennas are usually placed in the form of one-dimensional (1D) linear arrays, which can only resolve the azimuth angles, thus forming beams in two-dimensional (2D) horizontal directions for the multiuser (MU) MIMO operation. Considering that the future wireless communication system will be widely used in urban areas, where high buildings and large mansions will reform the 2D communication environment into a 3D one, transmit and receive antennas should be arranged on a plane grid, that is, a 2D antenna array, to generate 3D beams with both horizontal and vertical directions so that UEs on different floors of a building can simultaneously communicate with the BS (Alcatel-Lucent 2012).

The 3D MIMO technology mainly includes two research topics. The first one is the modeling of 3D channels (Shafi et al. 2006), which needs to verify the mathematical model and perform parameter fitting with the field test results. The 3D channel modeling is a key step for the study of 3D MIMO technology since any MIMO transceiver design largely depends on the propagation characteristics of the specific multi-antenna channels. Current researches on MIMO channel modeling are mostly devoted to the 2D channel which cannot resolve the elevation angles (3GPP 2011). This simplification is reasonable under the assumptions of the conventional large-radius cell with small elevation angle difference and 1D linear antenna arrays. The second topic is the 3D beamforming, which calls for investigations on the design of reference signals, 3D beamforming codebook, enhanced 3D MIMO channel state information (CSI) feedback, 3D MU MIMO operation, advanced spatial domain interference coordination, etc. In the 3D MIMO channel modeling, it is generally not necessary to consider the 2D antenna array since the 3D communication environment always exists irrespective of the antenna setup. However, in the study of the 3D beamforming, the 2D antenna array should be fully taken into account when designing the MIMO schemes.

1.2.3.3 Enhanced CoMP Technology

The CoMP technology, more generally known as the multipoint cooperative communication technology, indicates that multiple UEs can simultaneously receive their signals from one or multiple transmission points in a coordinated or joint-processing manner. This technology requires the network to collect CSI from the distributed transmission points to the UE and perform smart radio resource management (RRM) and multipoint cooperation, so that UEs' experience can be greatly improved by pooling together the radio resource throughout the network and making effective use of it.

In 3GPP, it has been agreed that the CoMP function will be adopted by the LTE release 11 system (MCC Support 2012), an improved version of the LTE-A network. Note that the CoMP schemes are mainly employed in the downlink (3GPP 2010b), while the uplink CoMP is mostly a multi-BS implementational issue, which is transparent to UEs (Clerckx et al. 2009). However, the LTE release 11 system only considers simple noncoherent CoMP schemes such as dynamic point selection and basic joint transmission. In the enhanced 4G system, it is necessary to study the coherent joint transmission scheme with enhanced CSI feedback, smart selection of transmission points/antennas, joint precoding and power allocation algorithms, etc.

1.3 Background of Multipoint Cooperative Communication

Among the previously introduced key technologies, the multipoint cooperative communication technology will be the focus of this book. In this section, we present its background and briefly discuss a systematical framework to address this topic.

In the last decade, the multipoint cooperative communication technology attracted tremendous attention thanks to the rapid development in the theory of MIMO transmission. In MIMO systems, the generalized models of the uplink and downlink channels are known as the multiple access channel (MAC) and the broadcast channel (BC), respectively. An important theoretical finding is that for single-antenna UEs, duality exists between the capacity region of an MAC system and that of a BC network (Caire and Shamai 2003; Caire 2006; Yu and Cioffi 2004). Moreover, the capacity duality also holds for multi-antenna UEs (Weingarten et al. 2004; Vishwanath et al. 2003; Viswanath and Tse 2003). Further studies even show that the capacity duality is still valid when each transmit antenna is subjected to an individual power constraint in BC or MAC (Yu and Lan 2007). The answers to these fundamental questions have profound implications for the multipoint cooperative communication technology because each point in the network is nothing but a set of colocated antennas so that the multipoint system can be viewed as a combination of BC and MAC. The deeper the MIMO theory goes, the clearer the picture of the multipoint cooperative communication technology will emerge.

From a general viewpoint of cooperative communications, a lot of academic research work in wireless communication belongs to this populous family. Some related topics include relay technologies, network MIMO technologies, opportunistic beamforming (OB), radio resource reuse schemes, multicell joint scheduling/power control schemes, soft/more softer hand-off technique (SH/MSH), interference alignment (IA) schemes, femtocell-related technologies, and spatial domain coordinated beamforming (CB). Although these topics may seem lack of commonality at first glance, they are essentially various embodiments of different strategies to treat the interpoint interference issue. Some notable strategies, for example, are interference cancellation, coordination, avoidance, suppression, randomization, and recently proposed interference utilization.

A general framework of cooperative communication was addressed in Gesbert et al. (2010) to provide us a large technical picture, in which existing cooperative communication schemes are classified into four categories based on whether data sharing is conducted and whether CSI sharing is available. Furthermore, in this book we consider a third factor, that is, whether time-frequency synchronized transmission or reception (TFSTR) is operated, to refine the classification of cooperative communication technologies. In our new framework, resource reuse schemes, as well as selection and muting of BS/relay/antenna, are treated separately due to their non-TFSTR features. Besides, since recent development both in academic communities and in industrial standardization activities shows a paradigm-shifting philosophy of exploiting the interference based on TFSTR, we can distinguish the conventional cooperative communication schemes from the modern ones from the TFSTR aspect. In Sect. 2.7, we will discuss the existing multipoint cooperative communication technologies using the proposed framework.

1.4 Scope of This Book

This book studies on the theory and applications of multipoint cooperative communication systems. Recent research activities in this area are comprehensively addressed and systematically analyzed. If ideal assumptions are considered, that is, full CSI at the transmitter (CSIT), unlimited signal processing capabilities, and interpoint backhaul connections with infinite capacity and zero latency, then the theoretical performance of cooperative communication can be derived from the generalized MIMO MAC or BC system (see Sect. 1.3). Current researches on the theory of multipoint cooperative communication are based on practical constraints such as limited-bit CSI feedback, linear precoding, and nonideal backhaul links.

In this book, we mainly consider four elements of constraints. The first element is the imperfectness of CSIT. It is well known that if CSI is available at the transmitter side, then a large performance gain can be achieved by adaptive transmission through the perceived channel (Love et al. 2008). However, even in a time division duplex (TDD) system, perfect CSI is difficult to acquire because response of transmit/receive antennas and interference strength at the receiver side cannot be inferred from channel reciprocity (Sesia et al. 2009). Besides, the issue of imperfect CSIT becomes more serious in the multipoint communication scenario since more CSIT for distributed transmission points should be collected (Gesbert et al. 2010). Therefore, imperfect CSIT should be taken into account when designing the cooperative communication schemes. The second element is the discrepancy of the CSI definition in the academic and industrial fields. In most academic researches, CSI refers to the direct information of channel vectors or matrices (Love et al. 2008; Santipach and Honig 2004), while in practical systems, in order to save the feedback overhead, CSI generally indicates the transmission recommendation (Santipach and Honig 2004), including the layer number of MIMO transmissions (RI, rank indicator), index of the preferred precoder in a codebook (PMI, precoding matrix indicator), and index of the appropriate transport format with a certain payload size (CQI, channel quality indicator). Hence, CSI based on transmission recommendation should be considered in the theoretical studies on cooperative communication. The third and fourth elements are about the low-complexity signal processing and the practical backhaul connections, respectively.

Considering one or several elements of practical constraints, we carefully select four research topics as examples of theoretical studies on multipoint cooperative communication technology. Taking the first and second elements into account, we address relay/antenna selection for the amplify-and-forward (AF) MIMO relay network and interference coordination for the uplink FDMA cellular network.

Besides, adding the third element into our consideration, we investigate the linear precoding for multipoint joint transmission (JT) with ideal backhaul conditions. Furthermore, considering all four elements, we propose a sequential and incremental precoding scheme with nonideal backhaul conditions for the downlink JT network.

As for the applications of the multipoint cooperative communication technology, we address the CoMP system in the LTE Release 10/11 networks. The CoMP transmission/reception in the 4G cellular network is the most advanced cooperative communication scheme that has ever been put to commercial use. Its development in the industrial standardization activities is reviewed and its key design of a common CSI feedback framework is treated based on the ongoing discussions in 3GPP and the requirements of the enhanced 4G network in the future.

To sum up, the scope of this book covers the theoretical studies on multipoint cooperative communication with practical constraints and its exciting applications in the state-of-the-art 4G wireless communication networks.

1.5 Book Outline

This book is divided into two parts. The first part addresses the theory of multipoint cooperative communication, which consists of six chapters, that is, Chaps. 1, 2, 3, 4, 5 and 6.

In Chap. 1, an introduction of this book is presented, including discussions on the past and future of wireless communication from a high-level point of view, some background of multipoint cooperative communication, and the structure of this book.

In Chap. 2, existing works related to multipoint cooperative communication technologies are discussed in great details, with emphases on the fundamentals of wireless digital communication, several selected topics that have laid the foundation for multipoint cooperative communication, and a thorough survey on the state of the researches on multipoint cooperative communication technologies by classifying all the existing schemes into eight categories. This chapter is presented with the purpose to help readers to get a large technical picture and thus better understand the positions of the topics to be treated in the following chapters.

In Chap. 3, relay/antenna selection for the amplify-and-forward (AF) multiple-input multiple-output (MIMO) relay network is addressed as an example of the sixth category of multipoint cooperative communication technology. Three greedy relay/antenna selection algorithms are proposed, and the effectiveness of the proposed schemes is corroborated by simulation results, followed by comprehensive discussions on the performance comparison of various algorithms to provide more insights on this topic.

In Chap. 4, interference coordination for the uplink frequency division multiple access (FDMA) cellular network is treated as an example of the seventh category of multipoint cooperative communication technology. An advanced interference coordination scheme is proposed, which consists of six steps with the key design lying in the enhanced UE categorization and resource-access control policies. This chapter is highlighted by the discussions on the methodology and implementation of the system-level simulation, which will be used in the following chapters.

In Chap. 5, linear precoding for multipoint joint transmission (JT) with ideal backhaul conditions is discussed as an example of the eighth category of multipoint cooperative communication technology. Various precoding schemes, for example, the global precoding (GP), local precoding (LP), weighted local precoding (WLP), single frequency network precoding (SFNP) schemes, together with a proposed antenna selection (AS) single frequency network precoding (AS-SFNP) scheme, are presented, analyzed, and compared in aspects of performance, complexity as well as feedback overhead.

In Chap. 6, a sequential and incremental precoding scheme with nonideal backhaul conditions for the downlink JT network is proposed as an example of the eighth category of multipoint cooperative communication technology. The objective is to minimize the maximum of the sub-stream mean square errors (MSE), which dominates the average bit error rate (BER) performance of the system. The key problem is first illustrated and solved with a two-BS JT system, and the results are then generalized to multi-BS JT systems.

The second part of this book addresses the applications of multipoint cooperative communication in practical cellular networks, which is composed of three chapters, that is, Chaps. 7, 8 and 9.

In Chap. 7, the CoMP system in LTE networks is discussed in details. Main topics of this chapter include the implicit CSI feedback in LTE Release 8/9/10 and its implications on the standardization progress of CoMP in LTE Release 10/11. Besides, overall scheme descriptions and specification works, as well as some simulation analysis for the CoMP system in LTE Release 11, are presented.

In Chap. 8, a key design of the CoMP system in LTE Release 11, that is, the common feedback framework (CFF), is investigated. Four candidates of CFF options are presented with the emphases on feedbacks of co-phase information and aggregated channel quality indicator (CQI). System-level simulation is conducted to compare the cell-edge throughput performance of CoMP schemes with various CFF options and the non-CoMP scheme. Some discussions on the adopted CFF option in LTE Release 11 and the further development of the CoMP CFF are also provided.

In Chap. 9, some concluding remarks are provided to complete our discussions on multipoint cooperative communication.

1.6 Conclusion

The international telecommunication system has marched beyond the LTE-A network, which is a 4G mobile communications standard developed by 3GPP with the goal of significantly enhancing the system performance of throughput, coverage, QoE, etc. One of the key technologies of the LTE-A and future LTE networks is the multipoint cooperative communication technology that has attracted much attention in both academic and industrial fields. In this book, we will discuss the theoretical studies on multipoint cooperative communication with practical constraints and its design in the enhanced 4G wireless communication networks.

References

3GPP (2008) TR 36.913: requirements for further advancements for E-UTRA (LTE-Advanced) (V8.0.0). Accessed 2008

3GPP (2010) TS 36.213: physical layer procedures (V10.0.1). http://www.3gpp.org/ftp/Specs/archive/36_series/36.213/36213-a01.zip. Accessed 2010

3GPP (2010) TR 36.814: further advancements for E-UTRA physical layer aspects (V9.0.0). http://www.3gpp.org/ftp/Specs/archive/36_series/36.814/36814-900.zip. Accessed 2010

3GPP (2011) TR 25.996 V10.0.0: spatial channel model for Multiple Input Multiple Output (MIMO) simulations (Release 10). http://www.3gpp.org/ftp/Specs/archive/25_series/25.996/25996-a00.zip. Accessed Mar 2011

3GPP (2012) 3GPP TR 36.828 V2.0.0: further enhancements to LTE TDD for DL-UL interference management and traffic adaptation (Release 11). http://www.3gpp.org/ftp/Specs/archive/36_series/36.828/36828-200.zip. Accessed June 2012

Alcatel-Lucent (2012) RWS-120014: towards LTE RAN evolution. In: 3GPP workshop on Release 12 Onward, Ljubljana, Slovenia, 11–12 June 2012. http://www.3gpp.org/ftp/workshop/2012-06-11_12_RAN_REL12/Docs/RWS-120014.zip

AT&T (2012) RWS-120018: AT&T view of release 12 in the North America marketplace. In: 3GPP workshop on Release 12 Onward, Ljubljana, Slovenia, 11–12 June 2012. http://www.3gpp.org/ftp/workshop/2012-06-11_12_RAN_REL12/Docs/RWS-120018.zip

Bell Labs Modeling, Machina Research, Pyramid Research, Beecham (2011) M2M Market. Accessed 2011

Broadcom (2012) RWS-120051: new concept to maximize the benefit of interference rejection at the UE receiver: interference suppression subframes (ISS). In: 3GPP workshop on Release 12 Onward, Ljubljana, Slovenia, 11–12 June 2012. http://www.3gpp.org/ftp/workshop/2012-06-11_12_RAN_REL12/Docs/RWS-120051.zip

Caire G (2006) MIMO downlink joint processing and scheduling: a survey of classical and recent results. In: Workshop on information theory and its applications, Los Angeles, USA

Caire G, Shamai S (2003) On the achievable throughput of a multiantenna Gaussian broadcast channel. IEEE Trans Inform Theory 49(7):1691–1706

CATT (2012) RWS-120025: views on LTE R12 and beyond. In: 3GPP workshop on Release 12 Onward, Ljubljana, Slovenia, 11–12 June 2012. http://www.3gpp.org/ftp/workshop/2012-06-11_12_RAN_REL12/Docs/RWS-120025.zip

China Telecom (2012) RWS-120037: views on REL-12 and onwards. In: 3GPP workshop on Release 12 Onward, Ljubljana, Slovenia, 11–12 June 2012. http://www.3gpp.org/ftp/workshop/2012-06-11_12_RAN_REL12/Docs/RWS-120037.zip

China Unicom (2012) RWS-120024: considerations on further enhancement and evolution of UMTS/LTE network in R12 and onwards. In: 3GPP workshop on Release 12 Onward, Ljubljana, Slovenia, 11–12 June 2012. http://www.3gpp.org/ftp/workshop/2012-06-11_12_RAN_REL12/Docs/RWS-120024.zip

Cisco (2012) Cisco visual networking index: global mobile data traffic forecast update, 2011–2016. http://www.cisco.com/en/US/solutions/collateral/ns341/ns525/ns537/ns705/ns827/white_paper_c11-520862.pdf. Accessed 14 Feb 2012

Clerckx B, Lozano A, Sesia S, Rensburg CV, Papadias CB (2009) 3GPP LTE and LTE advanced. EURASIP J Wireless Commun Network 2009, Article ID: 472124

CMCC (2012) RWS-120029: views on LTE Rel-12 & beyond. In: 3GPP workshop on Release 12 Onward, Ljubljana, Slovenia, 11–12 June 2012. http://www.3gpp.org/ftp/workshop/2012-06-11_12_RAN_REL12/Docs/RWS-120029.zip

Deutsche Telekom (2012) RWS-120012: Deutsche Telekom requirements and candidate technologies. In: 3GPP workshop on Release 12 Onward, Ljubljana, Slovenia, 11–12 June 2012. http://www.3gpp.org/ftp/workshop/2012-06-11_12_RAN_REL12/Docs/RWS-120012.zip

Dish Network (2012) RWS-120013: release 12 prioritization concepts. In: 3GPP workshop on Release 12 Onward, Ljubljana, Slovenia, 11–12 June 2012. http://www.3gpp.org/ftp/workshop/2012-06-11_12_RAN_REL12/Docs/RWS-120013.zip

Ericsson, ST-Ericsson (2012) RWS-120003: Views on Rel-12. In: 3GPP workshop on Release 12 Onward, Ljubljana, Slovenia, 11–12 June 2012. http://www.3gpp.org/ftp/workshop/2012-06-11_12_RAN_REL12/Docs/RWS-120003.zip

ETRI (2012) RWS-120026: a proposal for potential technologies for Release 12 and onwards. In: 3GPP workshop on Release 12 Onward, Ljubljana, Slovenia, 11–12 June 2012. http://www.3gpp.org/ftp/workshop/2012-06-11_12_RAN_REL12/Docs/RWS-120026.zip

Fujitsu Limited (2012) RWS-120016: requirements and technical considerations for RAN Rel.12 & onwards. In: 3GPP workshop on Release 12 Onward, Ljubljana, Slovenia, 11–12 June 2012. http://www.3gpp.org/ftp/workshop/2012-06-11_12_RAN_REL12/Docs/RWS-120016.zip

Gartner (2012) Mobile Services, Worldwide, 2008–2016, 2Q12 Update. www.gartner.com/id=2050315. Accessed 15 June 2012

Gesbert D, Hanly S, Huang H, Shamai S, Simeone O, Wei Y (2010) Multi-cell MIMO cooperative networks: a new look at interference. IEEE J Sel Areas Commun 28(9):1380–1408

Hitachi (2012) RWS-120040: views on enhancement of system capacity and energy efficiency toward Release12 and onward. In: 3GPP workshop on Release 12 Onward, Ljubljana, Slovenia, 11–12 June 2012. http://www.3gpp.org/ftp/workshop/2012-06-11_12_RAN_REL12/Docs/RWS-120040.zip

Huawei Technologies, HiSilicon (2012) RWS-120006: views on Rel-12 and onwards for LTE and UMTS. In: 3GPP workshop on Release 12 Onward, Ljubljana, Slovenia, 11–12 June 2012. http://www.3gpp.org/ftp/workshop/2012-06-11_12_RAN_REL12/Docs/RWS-120006.zip

Intel (2012) RWS-120023: LTE Rel-12 and beyond: requirements and technology components. In: 3GPP workshop on Release 12 Onward, Ljubljana, Slovenia, 11–12 June 2012. http://www.3gpp.org/ftp/workshop/2012-06-11_12_RAN_REL12/Docs/RWS-120023.zip

ITRI, HTC (2012) RWS-120042: potential technologies and road map for LTE release 12 and beyond. In: 3GPP workshop on Release 12 Onward, Ljubljana, Slovenia, 11–12 June 2012. http://www.3gpp.org/ftp/workshop/2012-06-11_12_RAN_REL12/Docs/RWS-120042.zip

KDDI (2012) RWS-120047: KDDI's views on LTE Release 12 onwards. In: 3GPP workshop on Release 12 Onward, Ljubljana, Slovenia, 11–12 June 2012. http://www.3gpp.org/ftp/workshop/2012-06-11_12_RAN_REL12/Docs/RWS-120047.zip

Love D, Heath R, Lau V, Gesbert D, Rao B, Andrews M (2008) An overview of limited feedback in wireless communication systems. IEEE J Sel Areas Commun 26(8):1341–1365

MacDonald V H (1979) The cellular concept. Bell Syst Technical J 58(1), Jan 1979. http://www.alcatel-lucent.com/bstj/vol58-1979/articles/bstj58-1-15.pdf

Machina Research (2011) M2M global forecast & analysis 2010–20. www.machinaresearch.com/m2mglobal2020.html. Accessed Oct 2011

MCC Support (2012) Draft report of 3GPP TSG RAN WG1 #70 v0.1.0. In: 3GPP TSG RAN WG1 #70, Qingdao, China, 13–17 Aug 2012. http://www.3gpp.org/ftp/tsg_ran/WG1_RL1/TSGR1_70/Report/Draft_ReportWG1#70_v010.zip

MediaTek (2012) RWS-120041: beyond LTE-A: MediaTek's view on R12. In: 3GPP workshop on Release 12 Onward, Ljubljana, Slovenia, 11–12 June 2012. http://www.3gpp.org/ftp/workshop/2012-06-11_12_RAN_REL12/Docs/RWS-120041.zip

Motorola Mobility (2012) RWS-120035: considerations for LTE Rel-12 and beyond. In: 3GPP workshop on Release 12 Onward, Ljubljana, Slovenia, 11–12 June 2012. http://www.3gpp.org/ftp/workshop/2012-06-11_12_RAN_REL12/Docs/RWS-120035.zip

NEC (2012) RWS-120011: where to improve Rel-12 and beyond: promising technologies. In: 3GPP workshop on Release 12 Onward, Ljubljana, Slovenia, 11–12 June 2012. http://www.3gpp.org/ftp/workshop/2012-06-11_12_RAN_REL12/Docs/RWS-120011.zip

Nokia Corporation (2012) RWS-120004: LTE evolving towards local area in release 12 and beyond. In: 3GPP workshop on Release 12 Onward, Ljubljana, Slovenia, 11–12 June 2012. http://www.3gpp.org/ftp/workshop/2012-06-11_12_RAN_REL12/Docs/RWS-120004.zip

NSN (2012) RWS-120002: release 12 and beyond for C^4 (cost, coverage, coordination with small cells and capacity). In: 3GPP workshop on Release 12 Onward, Ljubljana, Slovenia, 11–12 June 2012. http://www.3gpp.org/ftp/workshop/2012-06-11_12_RAN_REL12/Docs/RWS-120002.zip

NTT DOCOMO, INC (2012) RWS-120010: requirements, candidate solutions & technology roadmap for LTE Rel-12 Onward. In: 3GPP workshop on Release 12 Onward, Ljubljana, Slovenia, 11–12 June 2012. http://www.3gpp.org/ftp/workshop/2012-06-11_12_RAN_REL12/Docs/RWS-120010.zip

Orange (2012) RWS-120005: views on release 12. In: 3GPP workshop on Release 12 Onward, Ljubljana, Slovenia, 11–12 June 2012. http://www.3gpp.org/ftp/workshop/2012-06-11_12_RAN_REL12/Docs/RWS-120005.zip

Panasonic (2012) RWS-120019: major drivers, requirements and technology proposals for LTE Rel-12 Onward. In: 3GPP workshop on Release 12 Onward, Ljubljana, Slovenia, 11–12 June 2012. http://www.3gpp.org/ftp/workshop/2012-06-11_12_RAN_REL12/Docs/RWS-120019.zip

Parkvall S, Dahlman E, Furuskär A, Jading Y, Olsson M, Wänstedt S, Zangi K (2008) LTE-advanced – evolving LTE towards IMT advanced. IEEE Veh Technol Conf 2008:1–5

Pyramid Research (2012) Smartphone forecast. www.pyramidresearch.com/SmartphoneForecasts.htm. Accessed April 2012

Qualcomm (2012) RWS-120007: 3GPP RAN Rel-12 & beyond. In: 3GPP workshop on Release 12 Onward, Ljubljana, Slovenia, 11–12 June 2012. http://www.3gpp.org/ftp/workshop/2012-06-11_12_RAN_REL12/Docs/RWS-120007.zip

Renesas Mobile Europe (2012) RWS-120022: LTE Rel-12 and beyond. In: 3GPP workshop on Release 12 Onward, Ljubljana, Slovenia, 11–12 June 2012. http://www.3gpp.org/ftp/workshop/2012-06-11_12_RAN_REL12/Docs/RWS-120022.zip

Samsung Electronics (2012) RWS-120046: technologies for Rel-12 and onwards. In: 3GPP workshop on Release 12 Onward, Ljubljana, Slovenia, 11–12 June 2012. http://www.3gpp.org/ftp/workshop/2012-06-11_12_RAN_REL12/Docs/RWS-120046.zip

Santipach W, Honig ML (2004) Asymptotic capacity of beamforming with limited feedback. In: IEEE International Symposium on Information Theory (ISIT), Chicago, IL, USA, June 2004, p 289

Sesia S, Toufik I, Baker M (2009) LTE: the UMTS long term evolution. Wiley, Chichester

Shafi M, Zhang M, Moustakas AL et al (2006) Polarized MIMO channels in 3-D: models, measurements and mutual information. IEEE J Sel Area Commun 24(3):514–527

SHARP (2012) RWS-120039: evolving RAN towards Rel-12 and beyond. In: 3GPP workshop on Release 12 Onward, Ljubljana, Slovenia, 11–12 June 2012. http://www.3gpp.org/ftp/workshop/2012-06-11_12_RAN_REL12/Docs/RWS-120039.zip

Softbank Mobile (2012) RWS-120048: a view on requirements on Rel-12 and onwards from an operator's viewpoint. In: 3GPP workshop on Release 12 Onward, Ljubljana, Slovenia, 11–12 June 2012. http://www.3gpp.org/ftp/workshop/2012-06-11_12_RAN_REL12/Docs/RWS-120048.zip

SK Telecom (2012) RWS-120020: efficient spectrum resource usage for next-generation N/W. In: 3GPP workshop on Release 12 Onward, Ljubljana, Slovenia, 11–12 June2012. http://www.3gpp.org/ftp/workshop/2012-06-11_12_RAN_REL12/Docs/RWS-120020.zip

Telecom Italia (2012) RWS-120009: Telecom Italia requirements on 3GPP evolution. In: 3GPP workshop on Release 12 Onward, Ljubljana, Slovenia, 11–12 June 2012. http://www.3gpp.org/ftp/workshop/2012-06-11_12_RAN_REL12/Docs/RWS-120009.zip

Telefonica (2012) RWS-120008: new solutions for new mobile broadband scenarios. In: 3GPP workshop on Release 12 Onward, Ljubljana, Slovenia, 11–12 June 2012. http://www.3gpp.org/ftp/workshop/2012-06-11_12_RAN_REL12/Docs/RWS-120008.zip

Viswanath P, Tse DN (2003) Sum capacity of the vector Gaussian broadcast channel and uplink-downlink duality. IEEE Trans Inform Theory 49(8):1912–1921

Vishwanath S, Jindal N, Goldsmith A (2003) Duality, achievable rates, and sum-rate capacity of MIMO broadcast channels. IEEE Trans Inform Theory 49(10):2658–2668

Vodafone (2012) RWS-120031: Vodafone view on 3GPP RAN release 12 and beyond. In: 3GPP workshop on Release 12 Onward, Ljubljana, Slovenia, 11–12 June 2012. http://www.3gpp.org/ftp/workshop/2012-06-11_12_RAN_REL12/Docs/RWS-120031.zip

Weingarten H, Steinberg Y, Shamai S (2004) The capacity region of the Gaussian MIMO broadcast channel. Conf Info Sci Syst 174

Yu W, Cioffi JM (2004) Sum capacity of Gaussian vector broadcast channels. IEEE Trans Inform Theory 50(9):1875–1892

Yu W, Lan T (2007) Transmitter optimization for the multi-antenna downlink with per-antenna power constraints. IEEE Trans Signal Process 55(6):2646–2660

ZTE (2012) RWS-120034: views on 3GPP Rel-12 and beyond. In: 3GPP workshop on Release 12 Onward, Ljubljana, Slovenia, 11–12 June 2012. http://www.3gpp.org/ftp/workshop/2012-06-11_12_RAN_REL12/Docs/RWS-120034.zip

Chapter 2
Related Work

Abstract In this chapter, we address the existing work related to multipoint cooperative communication technologies. First, we discuss the fundamentals of wireless digital communication as a preparation for the following in-depth investigations on plenty of new concepts and technologies. Second, we review several selected topics that have laid the foundation for cooperative communication, for example, the orthogonal frequency-division multiplexing (OFDM) transmission, the multiple-input multiple-output (MIMO) system, the MIMO relay network, the multiuser (MU) MIMO theory, and channel state information (CSI) feedback methods. Third, we perform a thorough survey on the state of the researches of multipoint cooperative communication technology by classifying all the existing schemes into eight categories according to three factors, that is, whether data sharing is conducted, whether CSI sharing is allowed, and whether time-frequency synchronized transmission or reception (TFSTR) is operated. In this chapter, we present a large technical picture about the history and new development in each area of multipoint cooperative communication, which helps to show the positions of the topics to be treated in the following chapters.

Keywords Wireless digital communication • OFDM • MIMO • Relay • MU MIMO • CSI feedback • Multipoint cooperative communication • Classification

2.1 Fundamentals of Wireless Digital Communication

Before presenting our studies on the multipoint cooperative communication, it is beneficial to perform a survey on the existing cooperative communication technologies in a systematic way so that we can understand the relations among different research topics in this field and identify the areas that need to be further investigated. However, the multipoint cooperative communication is not an isolated technology. Instead, it covers a wide range of research areas such as multiple-input multiple-output (MIMO) systems, relay networks, channel state information

M. Ding and H. Luo, *Multi-point Cooperative Communication Systems: Theory and Applications*, Signals and Communication Technology, DOI 10.1007/978-3-642-34949-2_2,

(CSI) feedback, and radio resource management (RRM) operations. And before introducing these topics, let us first look at some fundamentals of wireless digital communication as a preparation for the following discussions on plenty of new concepts and schemes.

This book is not intended to be a textbook for graduate students majored in information and communication systems, and hence we will try to avoid overusing mathematical expressions in order to present more insights on the relations among various basic concepts and how the communication system works on a general basis. To keep it simple, there are only three basic questions we should ask about a wireless digital communication system, that is:

1. What form of communication?
2. How to communicate?
3. When/where to communicate?

2.1.1 What Form of Communication

In a word, communication is to carry some form of information by use of some medium from one end to another. Some conventional information forms are as follows:

- Verbal message: It is the most primitive form of information, quite effective for human beings.
- Text: The text information generated by human handwriting is usually not reliable due to misspelling, expression misusage, misreading, etc. The first error-free form of text was created by the stereotype printing invented by the Chinese people around the eleventh century.
- Hard copy material: Some examples are photo, facsimile, printed image, reproduction by a copying machine, etc.
- Electronic document: This kind of information file is usually encoded with binary bits and appended by cyclic redundancy check (CRC) codes to ensure its integrity.

As for the carriers of information, human beings play an important role for a very long time, even in today's express delivery service. When a worker from FedEx knocks your door and presents you some real estate papers in hard copy, he or she becomes a perfect embodiment of communication, that is, he or she carries some information in the form of the hard copy material from your agent to you. To increase the speed of human delivery, various kinds of mechanical moving platforms have been invented and put to use in the past centuries, such as land-based vehicle, locomotive, intercontinental ocean liner, and aircraft. With the invention of telephone in 1876, electronic signals traveling along metal, for example, twisted pair lines, were introduced as the carrier of the verbal message. Later on, telephone was upgraded to facsimile machine, which was able to exchange information in the form of hard copy materials between two terminals. In 1907, electromagnetic wave debuted as the text information carrier in the new service of telegraph. The invention of telegraph was extremely remarkable because it could finish the long-distance information transportation through thin air in a lightning speed. This kind of instantaneous wireless connection with other people living far away had never been experienced by the entire human race. In recent decades, electromagnetic wave becomes more and more important as a versatile information carrier in wireless communication. For example, the world has seen its wide applications in radio, TV broadcasting, satellite relaying, and cellular service. Now it is even marching forward and reshaping the infrastructure of the Internet. Earlier the personal computer (PC) Internet was a communication means based on electronic signals conveyed by twisted pair lines, copper, or fibers to transport electronic documents from one PC to another. In the new era of the mobile Internet, our personal devices are beginning to rely on electromagnetic wave to send/receive electronic files to/from the core network without any metal or silicon based wire. Therefore, in wireless digital communication, electromagnetic wave is the main information carrier and the conveyed information can be voice (e.g., cell-phone calls), text (e.g., short message service), electronic documents (e.g., Google Map navigation on tablets), etc. If someday quantum mechanisms were fully understood, then perhaps we would invent a "quantum Internet" in the future, which employs intertwined quantum particles to carry quantum-state coded information from the earth to another planet in our solar system or maybe in another galaxy.

2.1.2 How to Communicate

For wireless digital communication, the transmitter generates electromagnetic waves with some key parameters configured according to a finite set of one-to-one mapping rules from combinations of information bits to wave-shape parameters. The mapping process is called modulation. To explain it in more details, suppose that we have a set of M combinations of source bits represented by $\Pi = \{\pi_1, \pi_2, \ldots, \pi_M\}$, and we also have a same-sized set of wave-shape parameter configurations shown as $\Omega = \{\omega_1, \omega_2, \ldots, \omega_M\}$, then the one-to-one mapping from π_i to ω_i ($i \in \{1, 2, \ldots, M\}$) is defined as modulation. Upon receiving the modulated signal, the receiver can extract the information bits by detecting the interested parameters of the electromagnetic wave and looking up a demodulation table, which reverses the entries and outputs of the modulation mappings. The configurable wave-shape parameters can be amplitude, frequency, phase, or some combination of two or more parameters.

The digital modulation based on amplitude configuration generates a signal expressed as

$$s_m(t) = A_m g(t) \cos(2\pi f_c t), \tag{2.1}$$

where A_m belongs to an amplitude modulation set $\Omega_{\mathrm{A}} = \{A_1, A_2, \ldots, A_M\}$ consisting of M discrete values. Obviously, A_m bears $\log_2 M$ information bits. $g(t)$ is the spectrum-shaping function and f_{c} is the carrier frequency. The digital modulation scheme represented by (2.1) is generally known as the amplitude shifting keying (ASK), where "keying" means striking a key to play a certain note in music. A vivid example of the ASK is the signal lamp employed on naval vessels, which is a visual signaling device typically sending Morse code by opening and closing shutters mounted in front of the lamp. The Ω_{A} of the mentioned signal lamp can be simply written as $\Omega_{\mathrm{A}} = \{0, A\}$, where 0 and A indicates closing and opening of the shutters, respectively.

The digital modulation based on frequency configuration gives a signal shown as

$$s_m(t) = Ag(t)\cos(2\pi f_m t), \tag{2.2}$$

where f_m is selected from a frequency modulation set $\Omega_{\mathrm{F}} = \{f_1, f_2, \ldots, f_M\}$. Similar to A_m in (2.1), f_m can also carry $\log_2 M$ information bits. This digital modulation scheme is referred to as frequency-shifting keying (FSK). Perhaps the most interesting application of the FSK is the traffic light system with $\Omega_{\mathrm{F}} = \left\{f_{\mathrm{g}}, f_{\mathrm{r}}, f_{\mathrm{y}}\right\}$, where f_{g}, f_{r}, and f_{y} denote the frequency of green light, red light, and yellow light, respectively.

Furthermore, the signal of the digital modulation based on phase configuration can be written as

$$s_m(t) = Ag(t)\cos(2\pi f_{\mathrm{c}} t + \varphi_m), \tag{2.3}$$

where $\varphi_m \in \Omega_{\mathrm{P}} = \{\varphi_1, \varphi_2, \ldots, \varphi_M\}$. The modulation scheme given by (2.3) is called phase-shifting keying (PSK). Because the parameter of phase can barely be perceived by human organs, it's hard to present a daily-life example to let readers have some concrete sense about how the PSK modulation works. Here we want to make an analogy between the phase of an electromagnetic wave and the face of a dice to shed some light on the PSK. A dice usually has six faces, with each face displaying an integer result. If we consider an electromagnetic wave as a dice, then its initial state at $t = 0$ in (2.3), that is, $Ag(0)\cos(\varphi_m)$, is just like a perceivable face of the dice. And different φ_ms represent different faces. Hence, the phase shifting in (2.3) can be well illustrated by a picture of spinning a dice, only that no randomness is involved in the PSK modulation process. Instead, the transmitter carefully turns the PSK dice as an interpretation of the source bits for the receiver to read.

Finally, a typical example of the combination of more than one wave parameter configuration is the quadrature amplitude modulation (QAM), which combines ASK and PSK to form a two-dimensional modulation set described by $\Omega_{\mathrm{QAM}} = \{(A_1, \varphi_1), \ldots, (A_m, \varphi_n), \ldots, (A_M, \varphi_N)\}$. According to (2.1) and (2.3), the corresponding signal can be expressed as

$$s_{m,n}(t) = A_m g(t)\cos(2\pi f_{\mathrm{c}} t + \varphi_n). \tag{2.4}$$

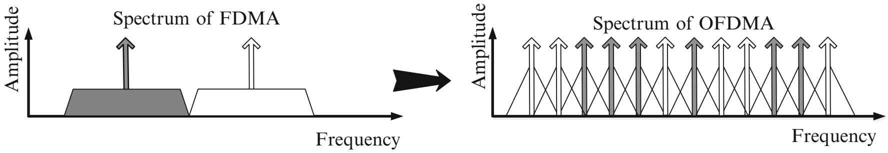

Fig. 2.1 Comparison of the spectrums of FDMA and OFDMA

2.1.3 When/Where to Communicate

In wireless digital communication, no device shall occupy all the time and frequency resources in the universe for the purpose of its own wireless communication. In practice, a lot of user equipments (UEs) share the time-frequency medium, which is usually divided into multiple channels for UEs to access. Here, channel is the answer to the question of when/where to communicate.

The simplest channel division method is perhaps the time division multiple access (TDMA), which divides the transmission period into time slots allocated to different UEs. TDMA scheme still works today in the Global System for Mobile communication (GSM) system (see Sect. 1.1). Another way to construct the channels is the frequency-division multiple access (FDMA) scheme, where frequency sub-bands are defined as channels. In our daily life, most broadcasting systems such as radio and television, adopt an FDMA approach because broadcasting is usually non-interrupting throughout the day time. Code division multiple access (CDMA) is another well-known scheme, which employs coded sequences to create low-interference channels for multiple UEs to transmit simultaneously on the same time-frequency resource. The CDMA technology is not as complicated as it appears. Let us imagine that we are now attending a symphony concert. When the orchestral tuning note is played, various musical instruments will produce sounds with the same pitch at a similar loudness. Nevertheless, you may still have no trouble in recognizing that a clarinet and a violin have just joined the tuning operation, because those two instruments do sound differently compared with other ones. The reason behind this human capability is nothing else than the CDMA technique. To be more specific, the timbre of a musical instrument, plays the role of the code sequence in CDMA, which is characterized by the spectrum and envelope of its sound. Our brain, much like a CDMA receiver, first picks up the unique timbre of a musical instrument, then performs signal matching to filter out the sound track of that particular instrument.

Recently, another two channel division schemes have attracted extensive attention. The first scheme is the space division multiple access (SDMA) method, which originates from the MU MIMO technology. The basic idea of SDMA is to serve multiple users simultaneously using multiple transmission beams generated by the multi-antenna array. The other one is the orthogonal frequency-division multiple access (OFDMA) scheme. The difference between FDMA and OFDMA from the perspective of frequency spectrum is illustrated in Fig. 2.1, where the

FDMA breaks the whole system bandwidth into two channels of frequency spectrum chunks centered on carriers with grey or white color, while the OFDMA defines a great number of narrowbands each with a subcarrier and groups contiguous or noncontiguous narrowbands into channels. The details of OFDMA will be discussed in Sect. 2.2, but the basic principle of OFDMA can be easily explained here by drawing an analogy between OFDMA and a piano. We know that a piano has many keys on its board, which perform the same function as the subcarriers in OFDMA. For example, the piano key associated with the note of middle C will give a sound with its frequency around 261.626 Hz, which can be considered as a subcarrier frequency. When we press several piano keys together, not necessarily contiguous keys, a multi-key sound will thus be created, though it may not be pleasant to listen to. Nevertheless, the purpose of the OFDMA communication is not about good sounding, so any combination of subcarriers can be grouped as a channel like the multi-key sound and allocated to a certain UE for transmitting modulated signals, the process of which is usually called scheduling in RRM. Just to mention it as an interesting fact, in music, acoustically good combinations of multiple notes are called chords, which can deliver pleasant sounds to human ears.

If we further consider a two-way communication, then there will be forward and backward channels. The forward channel is for the UE to transmit, while the backward channel to receive. The construction of the two-way channels falls into the design of duplex mode, that is, when/where to transmit and receive. Currently, the state-of-the-art communication equipment still has a serious problem in simultaneously transmitting and receiving signals on the same time-frequency resource because the power of the transmitted signal is typically orders of magnitude larger than that of the received signal, rendering a sure failure of the reception. Therefore, time division duplex (TDD) or frequency-division duplex (FDD), that is, separating the two-way channels in time domain or frequency domain, is widely used in practical systems.

A clear understanding of what, how, and when/where of a communication scheme can help readers to capture the essence of the system design. For example, readers may have some interests to review previous knowledges in Sect. 1.1 that GSM is an FDD, TDMA/FDMA, FSK modulated, voice transmission system, and in the next few years we may be served by a TDD, OFDMA, QAM modulated, packet data transmission system. Also it might be interesting to consider the possibility of a much more advanced system, which is characterized by space division duplex (SDD), CDMA/OFDMA, high-order QAM modulated, and packet data transmission.

2.2 OFDM Technology

The basic idea of the OFDM technology has been explained in Sect. 2.1 using an analogy between OFDM subcarriers and piano keys. In this section, we discuss it in more details. The OFDM transmission was first addressed in Chang (1966) as a

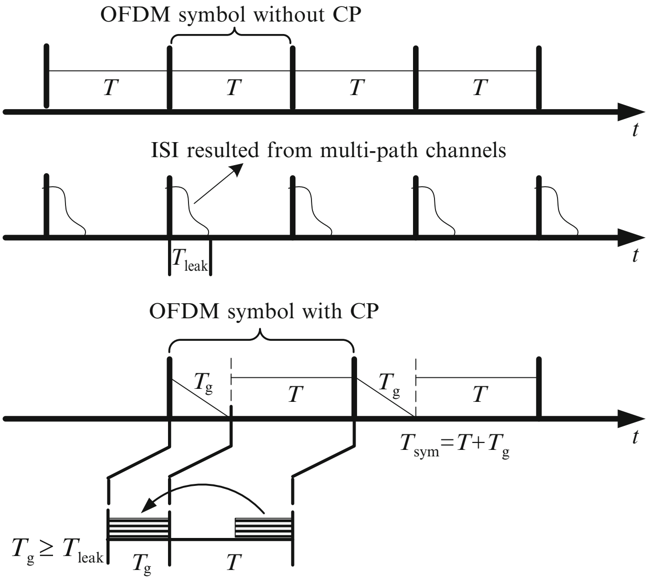

Fig. 2.2 Illustration of CP in OFDM symbols

multi-carrier modulation scheme with high spectral efficiency, which was originally designed for military communication purposes. However, due to lack of powerful processing chips, it was difficult to put the OFDM technology into practical usage. In year 1971, the authors Weinstein and Ebert (1971) proposed that inverse discrete Fourier transform (IDFT) and discrete Fourier transform (DFT) could be employed as the means of OFDM modulation and demodulation, respectively. In recent years, with the fast development in electronic devices, such as digital signal processor (DSP) and field-programmable gate array (FPGA), the IDFT and DFT operations for OFDM have become very easy with low complexity and low cost. In addition, the authors Peled and Ruiz (1980) proposed an interesting solution to mitigate the inter-symbol interference (ISI) by inserting a cyclic prefix (CP) between two contiguous OFDM symbols so that the leakage from the previous symbol in multipath fading channels would be buried in CP to protect the integrity of the current symbol. An illustration of inserting CP between OFDM symbols is provided in Fig. 2.2, in which the length of the useful part of an OFDM symbol is denoted as T, and those of ISI and CP are denoted as T_{leak} and T_{g}, respectively. With $T_{\text{g}} \geq T_{\text{leak}}$, ISI can be completely removed and the total length of an OFDM symbol becomes $T_{\text{sym}} = T + T_{\text{g}}$. Note that a conventional way to construct CP is to duplicate the rear part of an OFDM symbol with length T_{g} and dock it to the front of the OFDM symbol as illustrated in Fig. 2.2. It should also be noted that the introduction of CP will incur a time efficiency loss of $\eta_{\text{loss}} = T_{\text{g}}/T_{\text{sym}}$, which takes a value between 0.2 and 0.25 in practical systems (3GPP 2011a).

Owing to its easy implementation and inherent ability to combat the multipath fading channels, the OFDM technology has been widely used in many high-rate data transmissions such as digital video broadcasting (DVB) standards (ETSI 2001), wireless local area network (WLAN) (IEEE 1999), and asymmetric digital subscriber line (ADSL) (Bingham 2000). Moreover, it has also been accepted as the air interface technology for the 4G cellular networks, that is, worldwide interoperability for microwave access (WiMAX) and Long-Term Evolution-Advanced (LTE-A) (see Sect. 1.1).

In the OFDM transmission, each usable subcarrier is loaded with a QAM or PSK symbol $a(k)$, where k denotes the subcarrier index. The time-domain complex baseband samples $b(l)$ of an OFDM symbol with N subcarriers are generated by performing the N-point IDFT as

$$b(l) = \frac{1}{\sqrt{N}} \sum_{k=-N_{\mathrm{u2}}}^{N_{\mathrm{u1}}} a(k) \exp\left(\mathrm{j}\frac{2\pi kl}{N}\right), -N_g \le l \le N-1, \tag{2.5}$$

where the number of used subcarriers is $N_{u1} + N_{u2} + 1 = N_u \le N$. And the useful part of each OFDM symbol occupies a time duration of T, which corresponds to N samples. Besides, N_g is the number of CP samples. The resulting symbol is then transmitted through the multipath fading channel, the finite impulse response of which is $h(l)$. Assuming that perfect timing/frequency synchronization has been achieved, the received complex baseband signal is sampled with a periodicity $T_{\mathrm{s}} = T/N$ and can be expressed as

$$r(m) = \exp(\mathrm{j}\psi) \sum_{l} b(m-l)\ h(l) + n(m), \tag{2.6}$$

where ψ is an arbitrary phase factor and $n(m)$ is the sample of complex noise in time domain.

Conducting the N-point DFT after discarding the CP of N_g samples from $r(m)$, the received frequency domain signal can be written as

$$\begin{aligned} z(k) &= \frac{1}{\sqrt{N}} \sum_{m=0}^{N-1} r(m) \exp\left(-\mathrm{j}\frac{2\pi mk}{N}\right) \\ &= a(k)H(k) + \bar{n}(k), \quad -N_{\mathrm{u1}} \le k \le N_{\mathrm{u2}}, \end{aligned} \tag{2.7}$$

where $H(k)$ is the frequency response of the channel associated with the k-th subcarrier and $\bar{n}(k)$ denotes the noise in frequency domain. Then, $a(k)$ can be recovered by performing various filtering functions on $z(k)$ at the receiver.

In LTE/LTE-A networks, OFDMA has been adopted for the downlink transmission, that is, multiple UEs are served by a BS on different groups of subcarriers. For the uplink, however, single-carrier frequency division multiple access (SC-FDMA) is applied due to considerations on reducing the peak-to-average power ratio (PAPR) of uplink signals sent from UE. In SC-FDMA, the frequency resource allocated for a UE must consist of contiguous subcarriers and the UE's data symbols should be spread over its frequency resource by the DFT operation. Hence, in LTE/LTE-A networks, SC-FDMA is also called DFT-Spread OFDM.

2.3 MIMO Technology

2.3.1 Capacity of a MIMO System

MIMO transmission schemes require that both the transmitter and the receiver should be equipped with multiple antennas. The channel responses of the transmit-receive antenna pairs constitute a matrix of channel coefficients. An illustration of a MIMO system is provided in Fig. 2.3.

The MIMO technology can be dated back to year 1908, when Marconi proposed that the problem of channel fading could be alleviated by utilizing multiple independent antennas for transmission. Nearly 90 years later, Foschini from the Bell labs invented the space-time coding technology, that is, Bell labs layered space-time (BLAST) coding, to improve the reliability of multi-antenna transmissions (Foschini 1996). In 1999, for the first time from the information theory perspective, Telatar showed that when the received SNR is high the capacity of a MIMO system scales linearly with the SNR in dB. Besides, the order of the capacity increasing slope, also known as the multiplexing gain, equals to the minimum number of transmit and receive antennas (Telatar 1999).

One of the most basic problems of a point-to-point MIMO system is its capacity as well as the capacity-achieving transceiver design. Suppose that in a MIMO

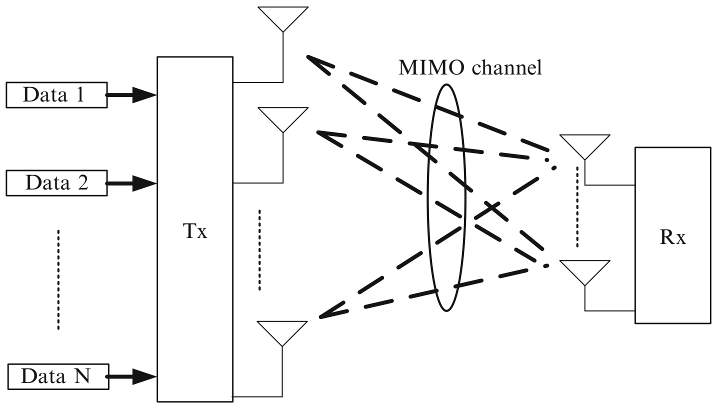

Fig. 2.3 Illustration of a MIMO system

system, the transmit and receive nodes, respectively, have N_{T} and N_{R} antennas. Then the received signal $\mathbf{y} \in \mathbb{C}^{N_{\mathrm{R}} \times 1}$ can be expressed as

$$\mathbf{y} = \mathbf{H}\mathbf{x} + \mathbf{n}, \tag{2.8}$$

where $\mathbf{H} \in \mathbb{C}^{N_{\mathrm{R}} \times N_{\mathrm{T}}}$ is the channel matrix, $\mathbf{x}$ is the transmitted signal vector, and $\mathbf{n}$ is the zero-mean circularly symmetric complex Gaussian (ZMCSCG) noise vector with $\mathrm{E}\left\{\mathbf{n}\mathbf{n}^{\mathrm{H}}\right\} = N_0 \mathbf{I}_{N_{\mathrm{R}}}$, where $(\cdot)^{\mathrm{H}}$, $\mathrm{E}\{\cdot\}$, and $\mathbf{I}_{N_{\mathrm{R}}}$ denote conjugate transpose, expectation operator, and an $N \times N$ identity matrix, respectively. Without loss of generality, we assume that the covariance matrix of $\mathbf{x}$ is $\mathbf{Q}_{\mathbf{x}} = \mathrm{E}\left\{\mathbf{x}\mathbf{x}^{\mathrm{H}}\right\}$ and the power constraint at the transmitter can be written as

$$\mathrm{tr}\left\{\mathbf{Q}_x\right\} \leq P, \tag{2.9}$$

where $\mathrm{tr}\{\cdot\}$ denotes the trace of a matrix and P is the maximum transmit power. Considering time-variant MIMO channels, we can obtain the ergodic capacity of a MIMO system shown as (Tse and Viswanath 2005)

$$C = \max_{\mathbf{Q}_{\mathbf{x}}:\mathrm{tr}\{\mathbf{Q}_{\mathbf{x}}\} \leq P} \mathrm{E}\left\{\log_2 \det\left(\mathbf{I}_{N_{\mathrm{R}}} + \frac{1}{N_0}\mathbf{H}\mathbf{Q}_{\mathbf{x}}\mathbf{H}^{\mathrm{H}}\right)\right\}, \tag{2.10}$$

where, $\det(\cdot)$ denotes the determinant operation. If we recall the interpretation of a determinant operation as the volume calculation, then Eq. (2.10) can be interpreted as noise ball packing in the signal-noise sphere (Tse and Viswanath 2005) and (2.10) can be reformulated as

$$C = \max_{\mathbf{Q}_{\mathbf{x}}:\mathrm{tr}\{\mathbf{Q}_{\mathbf{x}}\} \leq P} \mathrm{E}\left\{\log_2 \left(\frac{\det\left(N_0 \mathbf{I}_{N_{\mathrm{R}}} + \mathbf{H}\mathbf{Q}_{\mathbf{x}}\mathbf{H}^{\mathrm{H}}\right)}{\det\left(N_0 \mathbf{I}_{N_{\mathrm{R}}}\right)}\right)\right\}, \tag{2.11}$$

where the numerator and denominator in the logarithm term represent the volumes of a signal-noise ball and a noise ball, respectively. When $\mathbf{H}$ experiences fast fading, and there is no channel state information (CSI) at the transmit side, the capacity-maximization strategy is known as the equal power allocation on all transmit antennas (Tse and Viswanath 2005), that is,

$$\mathbf{Q}_{\mathbf{x}} = \frac{P}{N_{\mathrm{T}}}\mathbf{I}_{N_{\mathrm{T}}}. \tag{2.12}$$

Substituting (2.12) into (2.10), yields

$$C_{\mathrm{no\_CSI}} = \mathrm{E}\left\{\log_2 \det\left(\mathbf{I}_{N_{\mathrm{R}}} + \frac{P/N_0}{N_{\mathrm{T}}}\mathbf{H}\mathbf{H}^{\mathrm{H}}\right)\right\}. \tag{2.13}$$

When $\mathbf{H}$ experiences block fading, that is, $\mathbf{H}$ is a deterministic matrix during a given time interval, and $\mathbf{H}$ varies independently across different time intervals, the transmit side may be able to acquire the full CSI, for example, from receiver's feedback in an FDD system or channel reciprocity in a TDD system. The optimal transmit strategy (Tse and Viswanath 2005) to maximize the system capacity is addressed in the following.

We perform the singular value decomposition (SVD) on $\mathbf{H}$ and get

$$\mathbf{H} = \mathbf{U}\boldsymbol{\Lambda}\mathbf{V}^{\mathrm{H}}, \tag{2.14}$$

where $\mathbf{U} \in \mathbb{C}^{N_{\mathrm{R}}\times N_{\mathrm{R}}}$ and $\mathbf{V} \in \mathbb{C}^{N_{\mathrm{T}}\times N_{\mathrm{T}}}$ are unitary matrices and $\boldsymbol{\Lambda} \in \mathbb{C}^{N_{\mathrm{R}}\times N_{\mathrm{T}}}$ is a semi-definite diagonal matrix with diagonals λ_i s, that is, singular values, being the square root of the eigenvalues of $\mathbf{H}\mathbf{H}^{\mathrm{H}}$. Substituting (2.14) into (2.8), we have

$$\mathbf{y} = \mathbf{U}\boldsymbol{\Lambda}\mathbf{V}^{\mathrm{H}}\mathbf{x} + \mathbf{n}. \tag{2.15}$$

Let $\tilde{\mathbf{y}} = \mathbf{U}^{\mathrm{H}}\mathbf{y}$, $\tilde{\mathbf{x}} = \mathbf{V}^{\mathrm{H}}\mathbf{x}$, and $\tilde{\mathbf{n}} = \mathbf{U}^{\mathrm{H}}\mathbf{n}$. Then we can rewrite (2.15) as

$$\tilde{\mathbf{y}} = \boldsymbol{\Lambda}\tilde{\mathbf{x}} + \tilde{\mathbf{n}}, \tag{2.16}$$

where

$$\tilde{y}_i = \begin{cases} \lambda_i \tilde{x}_i + \tilde{n}_i & 1 \le i \le \min\left(N_{\mathrm{R}}, N_{\mathrm{T}}\right) \\ \tilde{n}_i & \min\left(N_{\mathrm{R}}, N_{\mathrm{T}}\right) < i \le N_R \end{cases}. \tag{2.17}$$

In (2.17), $\min(\cdot)$ outputs the minimum value. From (2.16) and (2.17), we can conclude that the deterministic MIMO channel can be decomposed to $\min\left(N_{\mathrm{R}}, N_{\mathrm{T}}\right)$ independent single-input single-output (SISO) sub-channels and the accumulation of the sub-channel capacities gives the MIMO system capacity (Tse and Viswanath 2005), which is shown as

$$C_{\mathrm{full\_CSI}} = \sum_{i=1}^{\min(N_{\mathrm{R}},N_{\mathrm{T}})} \log_2\left(1 + \lambda_i^2 P_i\right), \tag{2.18}$$

where P_i is the transmit power loaded onto the i-th sub-channel. With some standard convex optimization procedure, the capacity-maximization power allocation can be obtained as

$$P_i = \left(\mu - \frac{1}{\lambda_i^2}\right)^+ P, \tag{2.19}$$

where $(x)^+ = \max(x, 0)$ and μ is chosen to satisfy (2.9) with equality met therein, that is,

$$\sum_{i=1, P_i>=0}^{L} P_i = P. \tag{2.20}$$

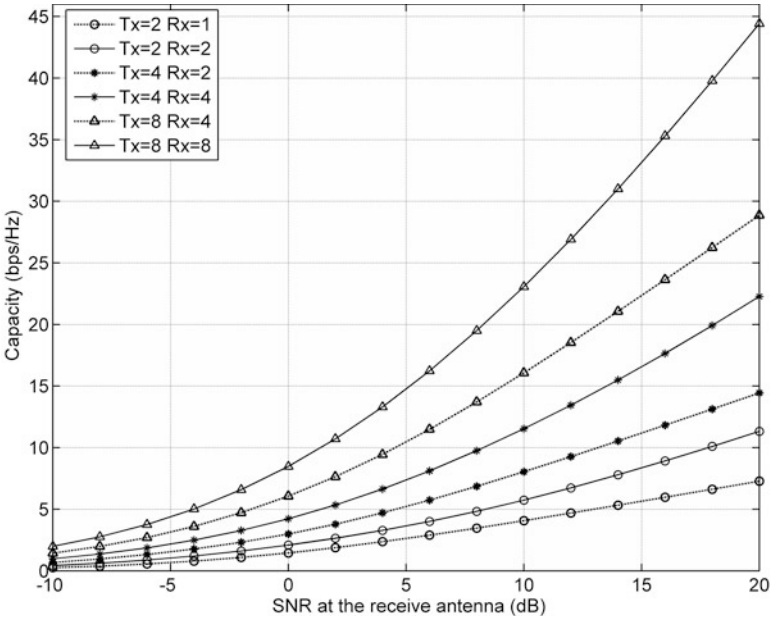

Fig. 2.4 Ergodic capacity of a deterministic MIMO system

Hence, we have

$$\mathbf{Q}_{\mathbf{x}} = \begin{bmatrix} P_1 & & & \\ & P_2 & & \\ & & \ddots & \\ & & & P_L \end{bmatrix}. \tag{2.21}$$

From (2.18), we can see that the capacity of a deterministic MIMO system depends on the sub-channel gains, that is, the eigenvalues of $\mathbf{HH}^{\mathrm{H}}$ and the power-loading result. An interesting finding from (2.19) is that more power goes to the sub-channel with a larger gain, leading to an even higher sub-channel capacity. Figure 2.4 shows the simulation results of the ergodic capacity of the deterministic MIMO system for various antenna setups in Rayleigh fading channels (Proakis 2001). From Fig. 2.4, we can clearly observe the slopes of the capacity curves in high SNR regime, which indicate the multiplexing gains as addressed in Telatar (1999).

From (2.16) to (2.19), it can be seen that the capacity-achieving transmission strategy should be sending $\tilde{\mathbf{x}} = \mathbf{V}^{\mathrm{H}}\mathbf{x}$ with power loading shown in (2.19), which is usually referred to as the water-filling power allocation. Note that the transmit optimization process is generally called precoding (Mai and Paulraj 2007). It should also be noted that with a Wiener filter (Proakis 2001) employed at the receiver, the optimal transmission strategy to minimize the sum MSE of the deterministic MIMO system is also $\tilde{\mathbf{x}} = \mathbf{V}^{\mathrm{H}}\mathbf{x}$, but with a different power-loading function given by Palomar et al. (2003)

$$P_i = \left(\mu \frac{1}{\lambda_i} - \frac{1}{\lambda_i^2}\right)^+ P. \tag{2.22}$$

As for the signal detection and decoding at the receiver, some conventional algorithms include matched filtering (MF), zero-forcing (ZF) filtering, minimum mean square error (MMSE) filtering, least square (LS) algorithm, maximum likelihood (ML) algorithm, and maximum a posteriori (MAP) algorithm. Among them, the MF, ZF, and MMSE filters are linear detectors. The MF filter focuses on capturing the signal part, which is effective in low SNR regime. On the other hand, the ZF filter tries to completely mitigate the interference part, which gives good performance in high SNR regime. The MMSE filter strikes a balance between maximizing the signal part and minimizing the interference part by projecting the received signal onto a subspace, which generates the minimum MSE (Tse and Viswanath 2005). The LS, ML, and MAP algorithms generally belong to the nonlinear decoders, which need to jointly process multiple detected signal symbols by exhaustively searching over all possible symbol transmissions and making comparison between the hypotheses and the observed vector. The symbol sequence can be decoded according to various criteria, such as minimizing the Euclidean distance (LS), maximizing the likelihood metric (ML), and maximizing the posterior probability (MAP). A MAP algorithm without consideration of the prior probability of the transmitted symbols degenerates to an ML algorithm. Furthermore, an ML algorithm under the condition of additive white Gaussian noise (AWGN) channels becomes an LS algorithm. On top of the aforementioned detection filters or decoding algorithms, we can employ the successive interference cancellation (SIC) technique (Wolniansky et al. 1998; Foschini et al. 1999) to enhance the system performance. The basic idea of the SIC technique is to sort the superimposed signals in a descending order of their received power then iteratively detect or decode, reconstruct, and subtract the signals from the received signal until all signals are separated. When the capacity-achieving transmit strategy described by (2.16) and (2.19) is employed, the optimal receiver is unexpectedly simple, which only requires $\mathbf{U}^{\mathrm{H}}$ as a linear filter, that is, $\tilde{\mathbf{y}} = \mathbf{U}^{\mathrm{H}}\mathbf{y}$. In fact, this receiver is nothing but the aforementioned MF filter.

When the capacity-achieving transmit strategy is not operated, no matter how to improve the receiving function linearly or nonlinearly, the system capacity will not achieve its maximum because the water-filling power allocation shown in (2.19) cannot be relegated to the receiver. However, some receiving functions can be performed by the transmitter. For instance, the SIC technique can be replaced by the dirty paper coding (DPC) scheme (Costa 1983) conducted before the transmission if full CSI is available at the transmitter. The basic principle of DPC is that if the transmitter has perfect knowledge of the upcoming interference, then it can pre-compensate the undesirable signal symbol by symbol so as to create an interference-free communication link. Although superb performance can be offered by the DPC scheme, its complexity is prohibitively high, which is difficult to be implemented in practical systems. Alternatively, two low-complexity-oriented nonlinear transmission schemes can achieve comparable performance with the DPC scheme, which are the Tomlinson-Harashima precoding (Erez et al. 2005) and trellis-convolutional precoding (Yu et al. 2005) schemes.

2.3.2 Space-Time Block Codes

Another fundamental aspect of the MIMO system is its diversity gain, which can increase the reliability of the wireless communication. In general, the diversity gain is strongly related to the number of independent versions of the received signal. The degree of the diversity gain can be roughly represented by the order of bit error rate (BER) decreasing slope with respect to SNR increase in dB when the SNR is high. At the end of last century, space-time block codes (STBC) were proposed to harvest the diversity gain of the MIMO system (Alamouti 1998; Tarokh et al. 1999). Perhaps the most renowned STBC scheme is the Alamouti coding (Alamouti 1998), which just requires a linear filter to decompose the joint decoding of the block codes into two independent decoding processes. Considering a MISO system with two transmit antennas and one receive antenna, we briefly elaborate on how the Alamouti STBC works. We denote h_1 and h_2 as the channel coefficients for the links from the first and second transmit antennas to the receive antenna, respectively. Furthermore, let x_1 and x_2 be two consecutive symbols for transmission, which are stacked into a vector $\mathbf{x} = [x_1, x_2]^{\mathrm{T}}$. Suppose that the channel coefficients remain unchanged during two time slots, then the Alamouti STBC dictates that the two transmitting antennas should send $[x_1, x_2]^{\mathrm{T}}$ and $\left[-x_2^*, x_1^*\right]^{\mathrm{T}}$, respectively, in the first and second time slots. The received signals y_1 and y_2 in the two time slots can be written as

$$y_1 = h_1 x_1 + h_2 x_2 + n_1 \tag{2.23}$$

and

$$y_2 = -h_1 x_2^* + h_2 x_1^* + n_2, \tag{2.24}$$

where n_1 and n_2 represent the ZMCSCG noise variables at the receiver in the first and second time slots, respectively. With some mathematical manipulations, (2.23) and (2.24) can be combined into

$$\mathbf{y} = \mathbf{H}\mathbf{x} + \mathbf{n}, \tag{2.25}$$

where $\mathbf{y} = \left[y_1, y_2^*\right]^{\mathrm{T}}$, $\mathbf{n} = \left[n_1, n_2^*\right]^{\mathrm{T}}$, and the effective channel is denoted as

$$\mathbf{H} = \begin{bmatrix} h_1 & h_2 \\ h_2^* & -h_1^* \end{bmatrix}. \tag{2.26}$$

Obviously, $\mathbf{H}$ is an orthogonal matrix with its two columns being orthogonal to each other. Therefore, we have

$$\mathbf{H}^{\mathrm{H}}\mathbf{H} = \alpha \mathbf{I}_2, \tag{2.27}$$

where $\alpha = |h_1|^2 + |h_2|^2$. Apply the MF filter on $\mathbf{y}$ and we can obtain

$$\begin{aligned}\tilde{\mathbf{y}} &= \mathbf{H}^{\mathrm{H}}\mathbf{y} \\ &= \mathbf{H}^{\mathrm{H}}\left(\mathbf{H}\mathbf{x} + \mathbf{n}\right) \\ &= \alpha\mathbf{x} + \tilde{\mathbf{n}},\end{aligned} \tag{2.28}$$

where $\tilde{\mathbf{n}} = \mathbf{H}^{\mathrm{H}}\mathbf{n}$ is still a ZMCSCG noise vector. From (2.28), we can see that the decoding of x_1 has been separated from that of x_2, which helps to reduce the complexity at the receiver.

However, in STBC the multiplexing gain is usually sacrificed in exchange for the diversity gain. An interesting discussion on the trade-off between the multiplexing and diversity gains can be found in Zheng and Tse (2003). The main conclusion is that if a MIMO system is assumed to transmit L independent data streams, that is, the multiplexing gain equals to L, then the diversity gain of each data stream is at most $(N_{\mathrm{T}} - L)(N_{\mathrm{R}} - L)$. The intuition behind this statement is that in order to support L-independent data streams, at least L transmit-receive antenna pairs should be reserved for multilayer MIMO transmissions, while the remaining $(N_{\mathrm{T}} - L)$ transmit antennas and $(N_{\mathrm{R}} - L)$ receive antennas can be designed to provide full diversity for each data stream.

2.3.3 Antenna Array Gain

In Fig. 2.4, it can be observed that a certain performance gap exists between the capacity curves of $(\mathrm{Tx} = 2, \mathrm{Rx} = 2)$ and $(\mathrm{Tx} = 4, \mathrm{Rx} = 2)$ and between those of $(\mathrm{Tx} = 4, \mathrm{Rx} = 4)$ and $(\mathrm{Tx} = 8, \mathrm{Rx} = 4)$. This phenomenon can only be attributed to the size of the antenna array, which is usually called antenna array gain. Note that the antenna array gain does not come from the straightforward power boosting of more antenna elements. In fact, the total transmit power should always satisfy (2.9) no matter how many antennas are involved.

The basic principle of the antenna array gain is closely related to a commonly asked question, which seems very simple but turns out to be quite difficult to answer. The question is whether the following equation of signal combining holds:

$$\sin t + \sin t = 2 \sin t. \tag{2.29}$$

At first glance, we may want to readily accept (2.29), partly because the very basic mathematics tells us that one plus one yields two and partly because the overthrow of (2.29) will be unthinkable since most of the publications in wireless communication are somehow based on this premise. However, if we recall the more general law of conservation of energy, then we may find ourselves get into a troublesome dilemma as follows. It is easy to show that the power of a signal $\sin t$ is 0.5, and hence the total power of the left-hand side of (2.29) should be 1. But the power of the right-hand side of (2.29) apparently equals to 2!

If we adhere to the law of conservation of energy, then (2.29) should be rewritten as

$$\sin t + \sin t = \sqrt{2} \sin t. \tag{2.30}$$

Some students majored in circuitry system may even enthusiastically conduct a circuitry experiment to show us the undisputable correctness of (2.30). We also suppose that (2.30) is indeed correct in most cases, for example, in circuitry systems. But it doesn't necessary imply that (2.29) is wrong in all cases. In wireless communication, radio wave signals travel in omnidirections, so multiple transmitted radio waves on the same frequency will intervene with each other and create both constructive and destructive signal combinings in the space. There will be some place wherein constructive signal combining shown by (2.29) occurs. But there will also be other place wherein multiple signals are cancelled out with each other, that is,

$$\sin t - \sin t = 0. \tag{2.31}$$

If we consider (2.29) together with (2.31), and those signal combining cases in-between them, then we can state that the energy conservation law is valid for the whole space. However, in the study of wireless communication, we are usually concerned with a particular position of an interested UE so that (2.29) is often presented and (2.31) is omitted by default. In other words, the power gain in (2.29) is just a result of power redistribution in the whole electromagnetic field, not a violation of the energy conservation law by doubling the power using mathematics. In MISO systems with unit-norm channel coefficients, the power gain exhibited in (2.29) is the fundamental reason behind the antenna array gain, and it is easy to show that more antenna elements can deliver higher power gains. Suppose that signals are transmitted from N_{T} antenna elements with equal power allocation for each antenna and total power constrained to one, then the constructively combined signal can be formulated as

$$\sum_{1}^{N_{\mathrm{T}}} \sqrt{\frac{2}{N_{\mathrm{T}}}} \sin t = \sqrt{2N_{\mathrm{T}}} \sin t. \tag{2.32}$$

The power of the left-hand side in (2.32) is one and that of the right-hand side jumps to N_{T}. Therefore, the considered electromagnetic field generated by N_{T} transmit antennas can offer an SNR gain as large as N_{T} in some place with coherent signal combining. In Fig. 2.5, we plot the ergodic capacity of the deterministic MISO system with unit-norm channel coefficients and we can easily observe an

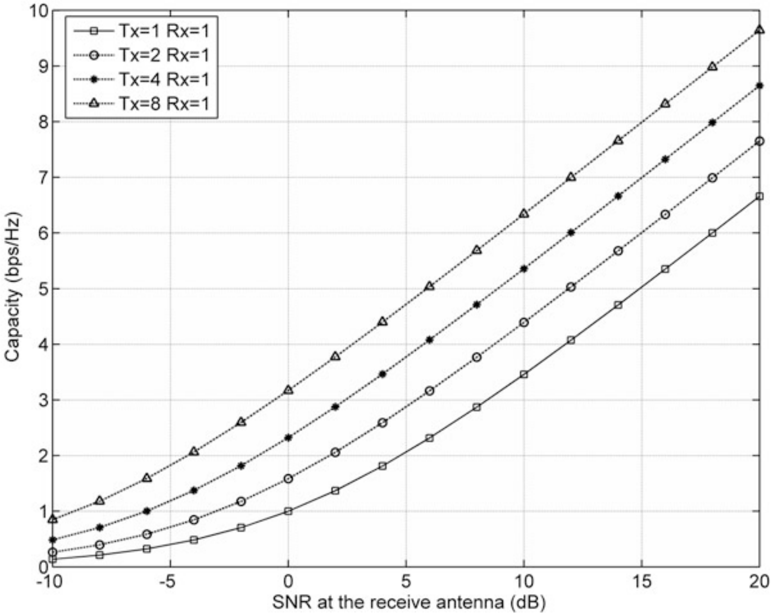

Fig. 2.5 Ergodic capacity of a deterministic MISO system with unit-norm channel coefficients

SNR gain of approximately $\log_{10} N_{\mathrm{T}}$ dB in high SNR regime. Note that the antenna array gain is actually more significant in low SNR regime since the system capacity can be nearly doubled or tripled when several more transmit antennas are activated.

In MIMO systems with fading channel models, the power gain shown by (2.32) is incorporated into the eigenvalue derivation in (2.14). Moreover, the antenna array gain in MIMO systems is generally larger than $\log_{10} N_{\mathrm{T}}$ dB (Antonia 2004) as can be observed in Fig. 2.4. Note that an interesting discussion about the trade-off between the diversity and array gains for correlated MIMO channels can be found in Yildirim et al. (2010), wherein the authors pointed out that the array gain increases while the diversity gain degrades with increased correlation of the MIMO channels, and hence the practical communication system should be designed to adaptively achieve a beneficial balance between the array and diversity gains.

2.3.4 MIMO-OFDM Technology

In essence, the OFDM technology converts a frequency-selective channel resulted from the multipath environment into per-subcarrier flat-fading sub-channels. Hence, OFDM transmission can overcome the undesirable multipath fading and support high-rate broadband wireless communication in practical scenarios. Considering that subcarrier is the basic element in OFDM, we can conclude that OFDM is a narrowband technology, which is able to exploit the channel-selective gains for more effective communication by means of radio resource scheduling and link adaptation (LA). On the other hand, the MIMO technology is also a narrowband technology, which takes advantage of the channel selectivity in space domain as well as in frequency domain to boost the spectral efficiency.

Therefore, the OFDM and MIMO technologies can be naturally combined to form a MIMO-OFDM technology, which performs opportunistic communication on frequency-space channels with high SINR gain for the scheduled UE. Together with the UE selection and OFDMA process, the MIMO-OFDM technology can make the best of every single frequency subcarrier resource to achieve a large overall throughput. Due to its superior performance, the MIMO-OFDM technology has become one of the core parts of the fourth generation of wireless communication networks (Sesia et al. 2009; 3GPP 2010a).

2.4 Relay Technology

2.4.1 Relaying Protocols

Currently, the bottleneck of the wireless communication development is still the scarcity of frequency spectrums. In particular, the low-frequency spectrums with wide coverage are hard to come by. In October of 2007, the World Radio-communication Conference (WRC07) was held in Geneva, Swiss. During the conference, International Telecommunication Union (ITU) specified four new frequency spectrums for 3G and 4G systems, which were 3.4G∼3.6 GHz (200 MHz bandwidth), 2.3G∼2.4 GHz (100 MHz bandwidth), 698 M∼806 MHz (108 MHz bandwidth), and 450 M∼470 MHz (20 MHz bandwidth), which are illustrated in Fig. 2.6.

As can be seen from Fig. 2.6, most working spectrums are beyond 2 GHz, which are able to accommodate high data rate transmissions in the 4G system, for example, the LTE-A network. However, it is well known that the signal attenuation of an electromagnetic wave with higher frequency tends to be more severe. Therefore, the coverage radius of a future BS operating on high-frequency spectrums will be significantly smaller than that of the BS at present. Moreover, the coverage of high data rate transmissions will be even smaller since more bits require more received

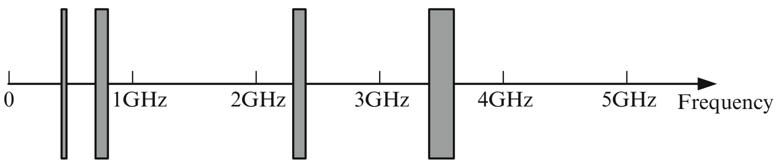

Fig. 2.6 New working spectrums of 3G/4G systems recommended by ITU in 2007

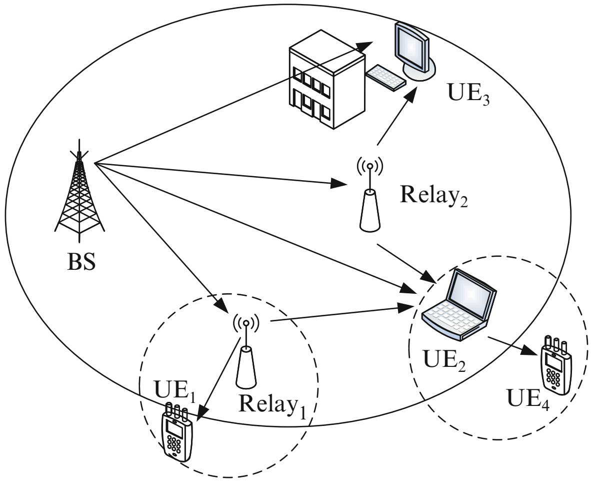

Fig. 2.7 Illustration of a cellular system deployed with relay nodes

power for successful decoding if we assume that the target per-bit received power is kept the same.

In order to increase the received power at the UE side, two straightforward approaches can be considered. The first approach calls for a great many of micro-BSs to run the service, with each micro-BS controlling the radio resources of one micro-cell. The UE's received power can be largely boosted due to the shortened distance between the UE and the BS. The second approach appeals to the MIMO technology, which can form a strong signal beam toward the UE. The first approach will significantly increase the operator's capital investment in the network infrastructure and may cause some regulatory issues. On the other hand, the second approach is able to beam up the received power of the single-stream transmission, while the multi-stream transmission still faces many difficulties such as limited antenna slots installed in the handset UE, high SNR required to fuel the capacity of the multi-stream MIMO transmission to increase linearly (Telatar 1999), and complicated signal processing to mitigate interstream/inter-UE interference in SU/MU MIMO (Tse and Viswanath 2005).

In order to cope with the problem, relay technologies attract continuous attention these years, both in academic and industrial fields. The basic idea of relay is to deploy low-cost and low-power nodes in the network, which receive and forward the signal sent from the BS, thus extending the system coverage and achieving the diversity gain to combat the fading channels (Pabst et al. 2004). A cellular network deployed with relay nodes is illustrated in Fig. 2.7. As can be seen from Fig. 2.7, a UE can also serve as a relay node, for example, UE$_2$ helps to relay the signal from the BS to UE$_4$. Since there are plenty of UEs in the network, the signal can be forwarded from multiple UEs with independent channels and the BER at the destination will decrease significantly due to multi-UE diversity gains (Hong et al. 2007). In the following, we will briefly discuss the existing relay protocols.

We consider a basic three-node relay communication system, which is illustrated in Fig. 2.8. For simplicity, TDD mode is assumed for the relay node, that is, the

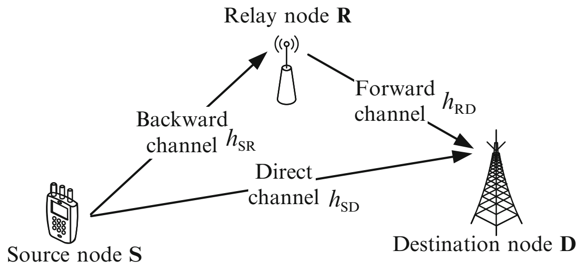

Fig. 2.8 Illustration of a relay communication system with three nodes

relay node receives the signal from the source node and forwards the signal to the destination node in two separate time slots. And all of the three nodes in Fig. 2.8 are assumed to have only one antenna. The MIMO relay system will be addressed later.

In the first time slot, the source node **S** transmits the signal to the relay node **R** and destination node **D**, and the received signal at **R** and **D** can be, respectively, expressed as

$$y_{\text{SR}} = h_{\text{SR}} x + n_{\text{SR}} \tag{2.33}$$

and

$$y_{\text{SD}} = h_{\text{SD}} x + n_{\text{SD}}. \tag{2.34}$$

In (2.33) and (2.34), x is the source data symbol constrained by

$$\mathrm{E}\left\{|x|^2\right\} \leq P_{\text{s}}, \tag{2.35}$$

where $|\cdot|$ gives the absolute value and P_{s} is the maximum transmission power of **S**. Besides, h_{SR} and h_{SD} are the coefficients of the backward channel (**S** to **R**) and the direct channel (**S** to **D**), respectively. n_{SR} and n_{SD}, respectively, represent the AWGN at **R** and **D** when receiving the signal from **S**.

When the relay node **R** receives y_{SR}, it will perform some sort of signal processing on it denoted as $\mathrm{G}\left(y_{\text{SR}}\right)$, where $\mathrm{G}\left(\cdot\right)$ is a general function that depends on the corresponding relay protocol. Two widely studied relay protocols are amplify-and-forward (AF) relaying (Laneman et al. 2004) and decode-and-forward (DF) relaying (Laneman and Wornell 2003).

For the AF relay, the received analogue signal is simply amplified and forwarded to the destination node **D**. Thus, the associated $\mathrm{G}\left(\cdot\right)$ can be described as

$$\mathrm{G}\left(y_{\text{SR}}\right) = \alpha y_{\text{SR}}, \tag{2.36}$$

where α is the amplifying factor, limited by the relay transmission power constraint expressed as

$$\mathrm{E}\left\{\left|\mathrm{G}\left(y_{\text{SR}}\right)\right|^2\right\} \leq P_{\text{r}}, \tag{2.37}$$

where P_{r} is the maximum transmission power at the relay node **R**. The primary problem of the AF relaying is that the noise at **R** will also be amplified, which may overwhelm the weak received signal.

When the source node **S** is not far from the relay node **R**, the DF relaying protocol is usually employed, in which the relay detects and decodes x from y_{SR}, and then re-encodes the signal before the forwarding operation. If the DF relay successfully unpacks the source data symbols, then the useful signal can be fully regenerated without the undesirable noise amplification in the AF relaying protocol. Hence, the $\mathrm{G}(\cdot)$ in a DF relay is given by

$$\mathrm{G}(y_{\mathrm{SR}}) = \sqrt{P}x, \tag{2.38}$$

where P is chosen to satisfy (2.37).

In the second time slot, the relay node **R** forwards $\mathrm{G}(y_{\mathrm{SR}})$ to the destination node **D**. The received signal at **D** can be written as

$$y_{\mathrm{RD}} = h_{\mathrm{RD}} \times g(y_{\mathrm{SR}}) + n_{\mathrm{RD}}, \tag{2.39}$$

where h_{RD} is the coefficient of the forward channel (**R** to **D**) and n_{RD} is the noise at **D**.

Suppose that the two time slots of the TDD relay transmission are of the same period and the noise power $\sigma_{\mathrm{n}}^2 = 1$. Then, for the AF relaying, α can be obtained according to (2.40) if the maximum powers in (2.35) and (2.37) are granted.

$$\alpha = \sqrt{\frac{P_{\mathrm{r}}}{|h_{\mathrm{SR}}|^2 P_{\mathrm{s}} + 1}}. \tag{2.40}$$

The capacity of an AF relay system can be presented by Laneman et al. (2004)

$$C_{\mathrm{AF}} = \frac{1}{2}\log_2\left(1 + P_{\mathrm{s}}|h_{\mathrm{SD}}|^2 + \frac{P_{\mathrm{s}}P_{\mathrm{r}}|h_{\mathrm{SR}}|^2|h_{\mathrm{RD}}|^2}{P_{\mathrm{s}}|h_{\mathrm{SR}}|^2 + P_{\mathrm{r}}|h_{\mathrm{RD}}|^2 + 1}\right), \tag{2.41}$$

where the factor 1/2 is a penalty on the TDD relay protocol occupying two time slots to complete one end-to-end transmission.

Besides, the capacity of a DF relay system can be expressed as (Laneman et al. 2004; Laneman and Wornell 2003)

$$C_{\mathrm{DF}} = \frac{1}{2}\min\left\{\log_2\left(1 + P_{\mathrm{s}}|h_{\mathrm{SR}}|^2\right), \log_2\left(1 + P_{\mathrm{s}}|h_{\mathrm{SD}}|^2 + P_{\mathrm{r}}|h_{\mathrm{RD}}|^2\right)\right\}, \tag{2.42}$$

which shows that the end-to-end capacity is dominated by the minimum value of the capacities associated with two distinct paths, that is, the direct path from **S** to **D** and the relaying path from **S** to **R** then to **D**.

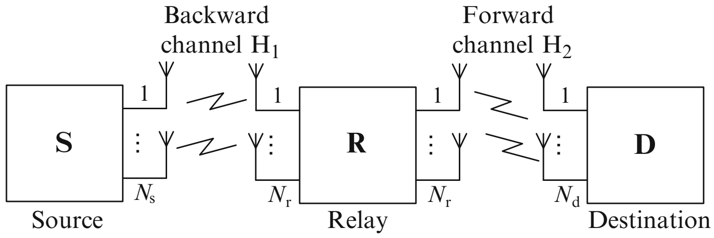

Fig. 2.9 Illustration of a MIMO relay system with one source, one relay, and one destination

In addition to the AF and DF protocols, the relay node can also perform various coding schemes on y_{SR} before forwarding the packet to the destination node. Some practical coding schemes include convolutional channel coding (Stefanov and Erkip 2004) and distributed space-time coding (Jing and Hassibi 2006).

It should be noted that although the introduction of relay nodes can improve the system coverage, it doesn't promise to decrease the interference in the network. On the contrary, the more relay nodes in the network, the more interference may be observed by UEs. Therefore, stringent transmission power constraints on relay nodes are essential to make the system work properly.

2.4.2 *One-Way MIMO Relay Technology*

The combination of MIMO and relay technologies is often referred to as the MIMO relay technology, where multiple antennas are mounted on the source, relay, and destination nodes in order to achieve both multiplexing and diversity gains. A MIMO relay system with one source, one relay, and one destination is illustrated in Fig. 2.9, where the source node **S**, relay node **R,** and destination node **D** are equipped with N_s, N_r, and N_d antennas, respectively. Compared with the single-antenna three-node model plotted in Fig. 2.8, the MIMO relay model shown in Fig. 2.9 consists of two hops of MIMO transmission, in which the two-hop interstream interference problem should be carefully studied. Besides, the relaying protocols discussed in Sect. 2.4.1 can be naturally applied for this upgraded relay model. It should be noted that in an AF MIMO relay network, the processing function $G(\cdot)$ at the relay node is more than just a power amplification shown in (2.40). Instead, a compound processing matrix containing receive filter, power-loading factors, and transmit precoder should be designed for the MIMO relay node **R**.

Let us also consider a TDD AF relaying, that is, transmissions take place in two separate time slots. During the first time slot, the source node **S** transmits to the relay node **R** and the received signal can be expressed as

$$\mathbf{y}_r = \mathbf{H}_1\mathbf{x} + \mathbf{n}_1, \tag{2.43}$$

where $\mathbf{H}_1 \in \mathbb{C}^{N_r \times N_s}$ denotes the backward channel matrix. $\mathbf{x}$ is the source-data signal vector, the elements of which are chosen independently from the same constellation and satisfy $\mathrm{E}\{\mathbf{x}\mathbf{x}^{\mathrm{H}}\} = \sigma_x^2 \mathbf{I}_{N_s}$. $\mathbf{n}_1$ is a zero-mean circularly symmetric complex Gaussian (ZMCSCG) noise vector with $\mathrm{E}\{\mathbf{n}_1\mathbf{n}_1^{\mathrm{H}}\} = \sigma_1^2 \mathbf{I}_{N_r}$, and it is statistically independent of $\mathbf{x}$. During the second time slot, the relay node forwards the received signal to the destination node $\mathbf{D}$ after multiplying a matrix $\mathbf{Q}$ to $\mathbf{y}_r$, and the signal arriving at $\mathbf{D}$ is written as

$$\begin{aligned}\mathbf{y}_d &= \mathbf{H}_2\mathbf{Q}\mathbf{y}_r + \mathbf{n}_2 \\ &= \mathbf{H}_2\mathbf{Q}\mathbf{H}_1\mathbf{x} + \mathbf{H}_2\mathbf{Q}\mathbf{n}_1 + \mathbf{n}_2 \\ &= \mathbf{H}\mathbf{x} + \mathbf{n},\end{aligned} \tag{2.44}$$

where $\mathbf{Q}$ is the linear compound processing matrix at the MIMO relay node $\mathbf{R}$. $\mathbf{H}_2 \in \mathbb{C}^{N_d \times N_r}$ stands for the forward channel matrix, and $\mathbf{n}_2$ is a ZMCSCG noise vector at the destination node $\mathbf{D}$ with $\mathrm{E}\{\mathbf{n}_2\mathbf{n}_2^{\mathrm{H}}\} = \sigma_2^2 \mathbf{I}_{N_d}$. Besides, we denote $\mathbf{H} = \mathbf{H}_2\mathbf{Q}\mathbf{H}_1 \in C^{N_d \times N_s}$ as the effective MIMO relay channel, and $\mathbf{n} = \mathbf{H}_2\mathbf{Q}\mathbf{n}_1 + \mathbf{n}_2$ represents the equivalent noise vector. Considering the power constraint at the relay node $\mathbf{R}$, $\mathbf{Q}$ should satisfy

$$\mathrm{tr}\left\{\mathbf{Q}\left(\sigma_x^2\mathbf{H}_1\mathbf{H}_1^{\mathrm{H}} + \sigma_1^2\mathbf{I}_{N_r}\right)\mathbf{Q}^{\mathrm{H}}\right\} \le P_r, \tag{2.45}$$

where P_r is the maximum transmit power at $\mathbf{R}$.

First, we discuss the capacity-maximization strategy for the considered AF MIMO relay system. According to (2.10), the capacity of (2.44) can be expressed as

$$\mathrm{C}(\mathbf{Q}) = \frac{1}{2}\log_2 \det\left(\mathbf{I}_{N_s} + \sigma_x^2\mathbf{H}^{\mathrm{H}}\mathbf{R}_n^{-1}\mathbf{H}\right), \tag{2.46}$$

where $\mathbf{R}_n = \sigma_1^2\mathbf{H}_2\mathbf{Q}\mathbf{Q}^{\mathrm{H}}\mathbf{H}_2^{\mathrm{H}} + \sigma_2^2\mathbf{I}_{N_d}$ and similar to (2.41) the scalar 1/2 is a penalty on the capacity of the TDD relaying transmission. Through Eigen-Value Decomposition (EVD) operations, we can get

$$\mathbf{H}_1\mathbf{H}_1^{\mathrm{H}} = \mathbf{U}_1\mathbf{\Lambda}_1^2\mathbf{U}_1^{\mathrm{H}} \tag{2.47}$$

and

$$\mathbf{H}_2^{\mathrm{H}}\mathbf{H}_2 = \mathbf{V}_2\mathbf{\Lambda}_2^2\mathbf{V}_2^{\mathrm{H}}, \tag{2.48}$$

where $\mathbf{\Lambda}_1 = \mathrm{diag}\{\lambda_{1,1}, \lambda_{1,2}, \ldots, \lambda_{1,N_s}\}$ and $\mathbf{\Lambda}_2 = \mathrm{diag}\{\lambda_{2,1}, \lambda_{2,2}, \ldots, \lambda_{2,N_d}\}$ are diagonal matrices whose diagonal elements are the square roots of eigenvalues of $\mathbf{H}_1\mathbf{H}_1^{\mathrm{H}}$ and $\mathbf{H}_2^{\mathrm{H}}\mathbf{H}_2$ arranged in a descending order. The optimal $\mathbf{Q}$ that maximizes $\mathrm{C}(\mathbf{Q})$ can be derived as (Medina et al. 2007; Tang and Hua 2007)

$$\mathbf{Q}^{\mathrm{opt}} = \mathbf{V}_2\mathbf{\Phi}\mathbf{U}_1^{\mathrm{H}}, \tag{2.49}$$

where $\mathbf{\Phi} = \operatorname{diag}\{\varphi_1, \varphi_2, \ldots, \varphi_{N_\mathrm{s}}\}$ is a $N_\mathrm{s} \times N_\mathrm{s}$ diagonal matrix and φ_i s, where $i \in \{1, 2, \ldots, N_s\}$ are given by

$$|\varphi_i|^2 = \frac{\sigma_2^2}{\sigma_1^2\left(\sigma_x^2\lambda_{1,i}^2 + \sigma_1^2\right)}\left[\sqrt{\omega\frac{\sigma_x^2\lambda_{1,i}^2}{\lambda_{2,i}^2} + \left(\frac{\sigma_x^2\lambda_{1,i}^2}{2\lambda_{2,i}^2}\right)^2} - \frac{\sigma_x^2\lambda_{1,i}^2}{2\lambda_{2,i}^2} - \frac{\sigma_1^2}{\lambda_{2,i}^2}\right]^+, \tag{2.50}$$

where the parameter ω should be chosen that the following power constraint formulated from (2.45) is met with equality:

$$\sum_{i=1}^{N_s}\left(\sigma_x^2\lambda_{1,i}^2 + \sigma_1^2\right)|\varphi_i|^2 \leq P_\mathrm{r}. \tag{2.51}$$

Next, we discuss the sum MSE minimization strategy. To reduce the implementation complexity, we suppose that a linear decoder $\mathbf{W}$ is applied at $\mathbf{D}$ for signal detection, that is, the estimated data vector becomes

$$\tilde{\mathbf{x}} = \mathbf{WHx} + \mathbf{Wn}. \tag{2.52}$$

For a given $\mathbf{Q}$, the optimal receiver filter to minimize the sum MSE is the Wiener filter (Tse and Viswanath 2005) expressed as

$$\hat{\mathbf{W}} = \sigma_x^2\mathbf{H}^\mathrm{H}\left(\sigma_x^2\mathbf{H}\mathbf{H}^\mathrm{H} + \mathbf{R}_\mathrm{n}\right)^{-1}. \tag{2.53}$$

Then the sum MSE on condition of $\mathbf{Q}$ can be written as

$$\mathrm{J}(\mathbf{Q}) = \sigma_x^2 tr\left\{\left(\sigma_x^2\mathbf{H}^\mathrm{H}\mathbf{R}_\mathrm{n}^{-1}\mathbf{H} + \mathbf{I}_{N_\mathrm{s}}\right)^{-1}\right\}. \tag{2.54}$$

The optimal $\mathbf{Q}$ that minimizes $\mathrm{J}(\mathbf{Q})$ takes the same form as in (2.49) and φ_i s are obtained from (Guan and Luo 2008)

$$|\varphi_i|^2 = \frac{1}{\left(\sigma_x^2\lambda_{1,i}^2 + \sigma_1^2\right)\lambda_{2,i}^2}\left(\sqrt{\frac{\sigma_2^2\sigma_x^2\lambda_{1,i}^2\lambda_{2,i}^2}{\xi\left(\sigma_x^2\lambda_{1,i}^2 + \sigma_1^2\right)}} - \sigma_2^2\right)^+, \tag{2.55}$$

where the parameter ξ should be chosen that the power constraint in (2.45) is met with equality.

It should be noted that if there exists direct link between $\mathbf{S}$ and $\mathbf{D}$, the optimal transceiver strategies in the AF MIMO relay system are more complicated. The optimal precoding schemes targeted for capacity-maximization and MSE minimization can be found in Munoz et al. (2007) and Rong and Gao (2009), respectively.

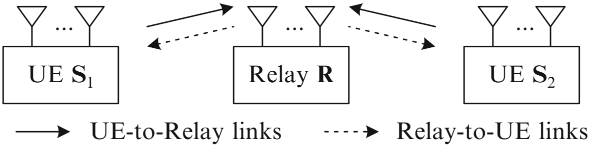

Fig. 2.10 Illustration of a two-way MIMO relay system

2.4.3 Two-Way MIMO Relay Technology

In a two-way relay system, two UEs communicate with each other via the help of a relay node. An illustration of a two-way MIMO relay system is presented in Fig. 2.10, wherein two UEs and one relay node are denoted as $\mathbf{S}_1$, $\mathbf{S}_2$, and $\mathbf{R}$, respectively. Each UE is equipped with N_s antennas and the relay has N_r antennas.

For the two-way MIMO relay system, we can apply the DF relaying protocol (Laneman and Wornell 2003), which breaks the two-way relaying process into an uplink UE-to-relay MU MIMO transmission phase and a downlink relay-to-UE MU MIMO broadcast phase. The AF relaying protocol (Laneman et al. 2004) can also be employed in the two-way MIMO relay node $\mathbf{R}$, which is usually referred to as the analogue network coding (ANC) (Katti et al. 2007). With the ANC and TDD relaying protocol, two UEs concurrently transmit information to the relay in a first phase, and then the relay amplifies and forwards the superimposed signal to both UEs in a second phase.

During the first phase, $\mathbf{S}_1$ and $\mathbf{S}_2$, respectively, transmit data vector $\mathbf{x}_1 \in \mathbb{C}^{N_\mathrm{s}\times 1}$ and $\mathbf{x}_2 \in \mathbb{C}^{N_\mathrm{s}\times 1}$ to $\mathbf{R}$ with $\mathrm{E}\left\{\mathbf{x}_i\mathbf{x}_i^\mathrm{H}\right\} = \sigma_x^2\mathbf{I}_{N_\mathrm{s}}$, $\forall i = 1, 2$. The received signal at the relay node $\mathbf{R}$ can be expressed as

$$\mathbf{y}_\mathrm{r} = \mathbf{H}_1\mathbf{x}_1 + \mathbf{H}_2\mathbf{x}_2 + \mathbf{n}_\mathrm{r}, \tag{2.56}$$

where $\mathbf{H}_i \in \mathbb{C}^{N_\mathrm{r}\times N_\mathrm{s}}$, $\forall i = 1, 2$, denotes the backward channel from $\mathbf{S}_i$ to $\mathbf{R}$. Besides, $\mathbf{n}_\mathrm{r}$ represents a ZMCSCG noise vector at $\mathbf{R}$ with $\mathrm{E}\left\{\mathbf{n}_\mathrm{r}\mathbf{n}_\mathrm{r}^\mathrm{H}\right\} = \sigma_\mathrm{r}^2\mathbf{I}_{N_\mathrm{r}}$. During the second phase, the relay node $\mathbf{R}$ multiplies $\mathbf{y}_\mathrm{r}$ with a processing matrix $\mathbf{Q}$ and then broadcasts $\mathbf{Q}\mathbf{y}_\mathrm{r}$ to both UEs. We assume that the relay node $\mathbf{R}$ is subject to a power constraint given by

$$\mathrm{tr}\left\{\mathbf{Q}\left(\sigma_x^2\mathbf{H}_1\mathbf{H}_1^\mathrm{H} + \sigma_x^2\mathbf{H}_2\mathbf{H}_2^\mathrm{H} + \sigma_\mathrm{r}^2\mathbf{I}_{N_\mathrm{r}}\right)\mathbf{Q}^\mathrm{H}\right\} \leq P_\mathrm{r}, \tag{2.57}$$

where P_r is the maximum transmit power at $\mathbf{R}$.

Considering the channel reciprocity in TDD systems, the observed signal at $\mathbf{S}_i$ can be written as

$$\mathbf{y}_i = \mathbf{H}_i^\mathrm{H}\mathbf{Q}\mathbf{H}_{\bar{i}}\mathbf{x}_{\bar{i}} + \mathbf{H}_i^\mathrm{H}\mathbf{Q}\mathbf{H}_i\mathbf{x}_i + \mathbf{H}_i^\mathrm{H}\mathbf{Q}\mathbf{n}_\mathrm{r} + \mathbf{n}_i, \tag{2.58}$$

where $\bar{i} = 1$ if $i = 2$ and $\bar{i} = 2$ if $i = 1$, and $\mathbf{H}_i^{\mathrm{H}}$ denotes the forward channel matrix from $\mathbf{R}$ to $\mathbf{S}_i$ in the considered TDD system. $\mathbf{n}_i \in \mathbb{C}^{N_{\mathrm{s}} \times 1}$ is a ZMCSCG noise vector at $\mathbf{S}_i$ with $\mathrm{E}\left\{\mathbf{n}_i \mathbf{n}_i^{\mathrm{H}}\right\} = \sigma_i^2 \mathbf{I}_{N_{\mathrm{s}}}$. Assuming $\mathbf{H}_i^{\mathrm{H}} \mathbf{Q} \mathbf{H}_i$ is perfectly known to $\mathbf{S}_i$ through training by reference signals, then $\mathbf{S}_i$ can completely remove the self-interference term $\mathbf{H}_i^{\mathrm{H}} \mathbf{Q} \mathbf{H}_i \mathbf{x}_i$ and get

$$\begin{aligned} \hat{\mathbf{y}}_i &= \mathbf{H}_i^{\mathrm{H}} \mathbf{Q} \mathbf{H}_{\bar{i}} \mathbf{x}_{\bar{i}} + \mathbf{H}_i^{\mathrm{H}} \mathbf{Q} \mathbf{n}_{\mathrm{r}} + \mathbf{n}_i \\ &= \mathbf{H}_{i,\mathrm{eq}} \mathbf{x}_{\bar{i}} + \mathbf{n}_{i,\mathrm{eq}}, \end{aligned} \tag{2.59}$$

where $\mathbf{H}_{i,\mathrm{eq}} = \mathbf{H}_i^{\mathrm{H}} \mathbf{Q} \mathbf{H}_{\bar{i}}$ and $\mathbf{n}_{i,\mathrm{eq}} = \mathbf{H}_i^{\mathrm{H}} \mathbf{Q} \mathbf{n}_{\mathrm{r}} + \mathbf{n}_i$. According to Tse and Viswanath (2005), the maximum rate for $\mathbf{S}_i$ is given by

$$R_i = \frac{1}{2} \log_2 \det \left(\mathbf{I}_{N_{\mathrm{s}}} + P_{\mathrm{s}} \mathbf{H}_{i,\mathrm{eq}} \mathbf{H}_{i,\mathrm{eq}}^{\mathrm{H}} \boldsymbol{\Phi}_i^{-1} \right), \tag{2.60}$$

where $\boldsymbol{\Phi}_i = \mathrm{E}\left\{\mathbf{n}_{i,\mathrm{eq}} \mathbf{n}_{i,\mathrm{eq}}^{\mathrm{H}}\right\} = \sigma_{\mathrm{r}}^2 \mathbf{H}_i^{\mathrm{H}} \mathbf{Q} \left(\mathbf{H}_i^{\mathrm{H}} \mathbf{Q}\right)^{\mathrm{H}} + \sigma_i^2 \mathbf{I}_{N_{\mathrm{s}}}$ and the pre-log factor is resulted from half duplex relaying. From (2.60), the sum rate for the two-way MIMO relay system can be simply written as $R_1 + R_2$. Note that the optimal transceiver strategy to maximize the sum rate of a two-way MIMO relay system is generally more difficult to derive than that of the one-way one.

Similar to that in the one-way MIMO relay system, the relay node $\mathbf{R}$ in Fig. 2.10 can also perform some kind of coding on $\mathbf{y}_{\mathrm{r}}$ before the broadcasting phase. In general, the coding scheme at $\mathbf{R}$ acts as a mapping function from the received signal $\mathbf{y}_{\mathrm{r}}$ to the broadcasting message $\mathbf{y}_{\mathrm{b}}$, which belongs to a new technology called physical network coding (Koike et al. 2009).

2.5 Multiuser MIMO Technology

2.5.1 System Model

The studies on downlink and uplink multiuser (MU) MIMO technologies are, respectively, based on the broadcast channel (BC) and multiple access channel (MAC) models (Cover and Thomas 1991; Dighe et al. 2003) as illustrated in Figs. 2.11 and 2.12, respectively. Here, we suppose that one BS provides communication service to K UEs. The BS-to-UE transmission is defined as the downlink communication shown by the BC model, while the UE-to-BS transmission as the uplink communication given by the MAC model. In addition, let the numbers of antennas at BS and UE be M and N, respectively. Moreover, we denote $\mathbf{H}_i \in \mathbb{C}^{N \times M}$ and $\mathbf{H}_i^{\mathrm{H}} \in \mathbb{C}^{M \times N}$, respectively, as the BS-to-UE and UE-to-BS channel matrices for UE i considering the channel reciprocity between the BS and UE.

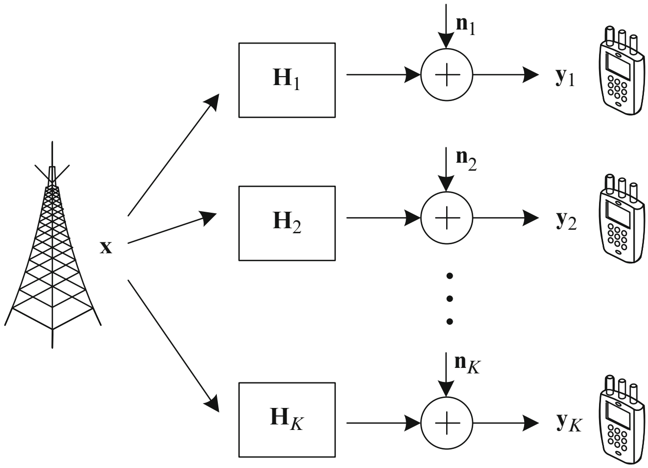

Fig. 2.11 Illustration of a BC model

Fig. 2.12 Illustration of a MAC model

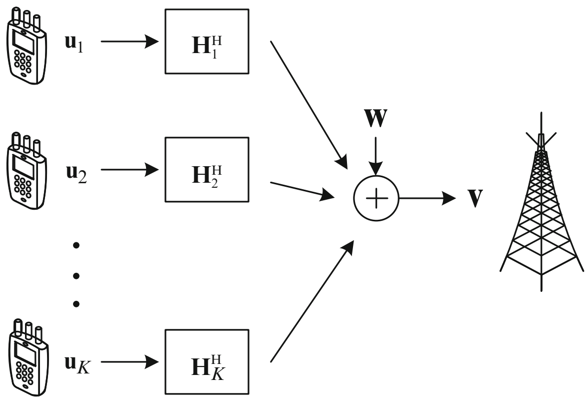

2.5.2 MU MAC Model

First, we consider the MU MAC model illustrated by Fig. 2.12. The received signal vector $\mathbf{v}$ at the BS can be described as

$$\mathbf{v} = \mathbf{H}_1^{\mathrm{H}}\mathbf{u}_1 + \cdots + \mathbf{H}_K^{\mathrm{H}}\mathbf{u}_K + \mathbf{w} = \mathbf{H}^{\mathrm{H}} \begin{bmatrix} \mathbf{u}_1 \\ \vdots \\ \mathbf{u}_K \end{bmatrix} + \mathbf{w}, \tag{2.61}$$

where $\mathbf{u}_i$ is the transmitted signal of UE i, $\mathbf{w}$ is a ZMCSCG noise vector with $\mathrm{E}\left\{\mathbf{w}\mathbf{w}^{\mathrm{H}}\right\} = \mathbf{I}_M$, and $\mathbf{H}$ is denoted as $\mathbf{H} = \left[\mathbf{H}_1^{\mathrm{H}}, \ldots, \mathbf{H}_K^{\mathrm{H}}\right]^{\mathrm{H}}$. In addition, each UE is power constrained by

$$\mathrm{tr}\left\{\mathbf{Q}_i\right\} \leq P_i, \tag{2.62}$$

where $\mathbf{Q}_i = \mathrm{E}\left\{\mathbf{u}_i\mathbf{u}_i^{\mathrm{H}}\right\}$ and P_i is the maximum transmit power of UE i. For a fixed group of covariance matrices $(\mathbf{Q}_1, \ldots, \mathbf{Q}_K)$, the capacity region of the MU MAC can be expressed as (Cover and Thomas 1991)

$$\sum_{i \in S} R_i \leq \log_2\left(\det\left(\mathbf{I}_M + \sum_{i \in S} \mathbf{H}_i^{\mathrm{H}}\mathbf{Q}_i\mathbf{H}_i\right)\right), \forall S \subseteq \{1, \ldots, K\}. \tag{2.63}$$

As an example, we set $K = 2$ and examine (2.63) in more details. For a certain pair of covariance matrices $(\mathbf{Q}_1, \mathbf{Q}_2)$, (2.63) can be rewritten as

$$R_1 \leq \log_2\left(\det\left(\mathbf{I}_M + \mathbf{H}_1^{\mathrm{H}}\mathbf{Q}_1\mathbf{H}_1\right)\right), \tag{2.64}$$

$$R_2 \leq \log_2\left(\det\left(\mathbf{I}_M + \mathbf{H}_2^{\mathrm{H}}\mathbf{Q}_2\mathbf{H}_2\right)\right), \tag{2.65}$$

$$\begin{aligned} R_1 + R_2 &\leq \log_2\left(\det\left(\mathbf{I}_M + \mathbf{H}_1^{\mathrm{H}}\mathbf{Q}_1\mathbf{H}_1 + \mathbf{H}_2^{\mathrm{H}}\mathbf{Q}_2\mathbf{H}_2\right)\right) \\ &= \log_2\left(\det\left(\mathbf{I}_M + \mathbf{H}^{\mathrm{H}}\begin{pmatrix}\mathbf{Q}_1 & \\ & \mathbf{Q}_2\end{pmatrix}\mathbf{H}\right)\right). \end{aligned} \tag{2.66}$$

Among them, (2.64) corresponds to the capacity-achieving scheme for UE_1, that is, decoding the signal of UE_1 after the interference from UE_2 has been completely removed by a SIC receiver. In a similar way, (2.65) describes the capacity upper limit for UE_2. The capacity of UE_1 and UE_2 in full cooperation but with block diagonal transmit covariance matrices is bounded by (2.66). Combining (2.64), (2.65), and (2.66), we can obtain a pentagon-shaped MAC capacity region for fixed $(\mathbf{Q}_1, \mathbf{Q}_2)$ as illustrated in Fig. 2.13.

Take different $(\mathbf{Q}_1, \mathbf{Q}_2)$ and we can get a cluster of pentagon-shaped regions from (2.64), (2.65), and (2.66), the union of which gives the capacity region of MAC if we consider a sum power constraint for the two UEs, that is,

$$\mathrm{tr}\left\{\mathbf{Q}_1\right\} + \mathrm{tr}\left\{\mathbf{Q}_2\right\} \leq P, \tag{2.67}$$

where P is the maximum sum power of UE_1 and UE_2. It should be noted that the strategy to achieve the capacity of full UE cooperation is the TDM-based MMSE-SIC nonlinear receiver (Tse and Viswanath 2005), that is, the time slot is divided into two parts, in the first and second parts of which the BS employs the SIC receiver in favor of UE_1 and UE_2, respectively.

From (2.63) and the extension of the sum power constraint (2.67) to the case of more than two UEs, that is,

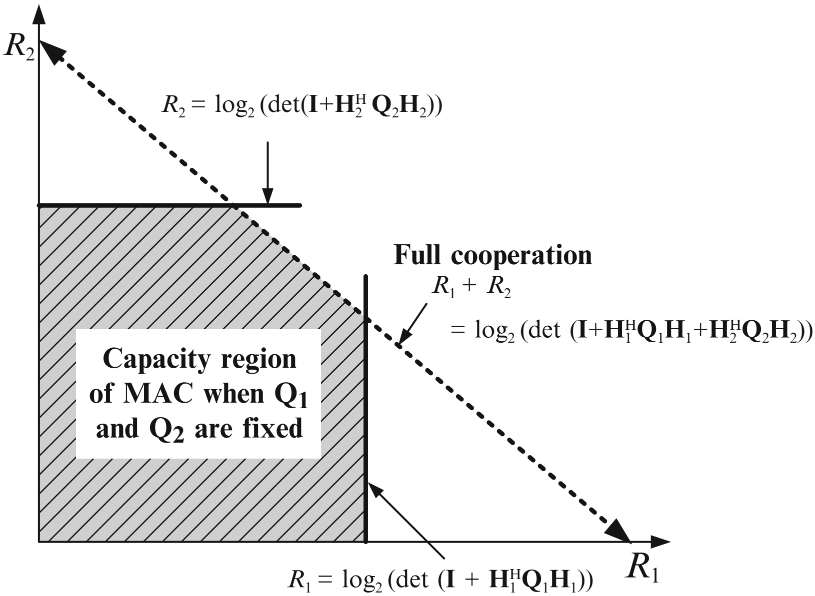

Fig. 2.13 Capacity region for a two-UE MAC model when $\mathbf{Q}_1$ and $\mathbf{Q}_2$ are fixed

$$\sum_{i=1}^{K} \operatorname{tr}\{\mathbf{Q}_i\} \le P, \tag{2.68}$$

we can get the rate tuple union as the MAC capacity region formulated as

$$R_{\mathrm{MAC}}^{\text{sum-power}}(\mathbf{H}, P) = \bigcup_{\mathbf{Q}_i} \left\{ (R_1, \ldots, R_K) \left| \sum_{i \in S, \forall S \subseteq \{1,\ldots,K\}} R_i \le \log_2 \left(\det \left(\mathbf{I}_M + \sum_{i \in S} \mathbf{H}_i^{\mathrm{H}} \mathbf{Q}_i \mathbf{H}_i \right) \right) \right. \right\}. \tag{2.69}$$

2.5.3 MU BC Model

Next, we investigate the MU BC model illustrated by Fig. 2.11. The received signal $\mathbf{y}_i$ at UE i can be expressed as

$$\mathbf{y}_i = \mathbf{H}_i \mathbf{x}_i + \mathbf{n}_i, \tag{2.70}$$

where $\mathbf{x}_i$ is the signal sent from the BS to UE i and $\mathbf{n}_i$ is the ZMCSCG noise vector at UE i with $\mathrm{E}\left\{\mathbf{n}_i \mathbf{n}_i^{\mathrm{H}}\right\} = \mathbf{I}_N$.

When the UEs are equipped a single antenna, the capacity region of the MISO BC was presented in Caire and Shamai (2003) and Caire (2006). However, when multi-antenna UEs are involved, the BC capacity region is much more difficult to identify. In Yu and Cioffi (2004), the authors proposed that the capacity region of the MIMO BC can be obtained by the DPC technique. Suppose that UEs are encoded in an order represented by $\pi(\cdot)$, that is, UE $\pi(i)$ will be the i-th UE to be encoded. Then the achievable rate of UE $\pi(i)$ can be written as (Yu and Cioffi 2004)

$$R\left(\pi(i), \mathbf{Q}_{\pi(j)}\right) = \log_2 \left(\frac{\det\left(\mathbf{I}_N + \mathbf{H}_{\pi(i)} \left(\sum\limits_{j \geq i} \mathbf{Q}_{\pi(j)}\right) \mathbf{H}^{\mathrm{H}}_{\pi(i)}\right)}{\det\left(\mathbf{I}_N + \mathbf{H}_{\pi(i)} \left(\sum\limits_{j > i} \mathbf{Q}_{\pi(j)}\right) \mathbf{H}^{\mathrm{H}}_{\pi(i)}\right)} \right), \ (i = 1, \ldots, K), \tag{2.71}$$

where $\mathbf{Q}_{\pi(j)} = \mathrm{E}\left\{\mathbf{x}_{\pi(j)}\mathbf{x}^{\mathrm{H}}_{\pi(j)}\right\}$ is the transmit covariance matrix of UE $\pi(j)$. And $\mathbf{Q}_{\pi(j)}$ should satisfy the sum power constraint at BS shown as

$$\begin{aligned} \mathrm{tr}\left\{\sum_{j=1}^{K} \mathbf{Q}_{\pi(j)}\right\} &= \mathrm{tr}\left\{\mathbf{Q}_{\mathbf{x}}\right\} \\ &\leq P, \end{aligned} \tag{2.72}$$

where $\mathbf{Q}_{\mathbf{x}} = \mathrm{diag}\left\{\mathbf{Q}_{\pi(1)}, \mathbf{Q}_{\pi(2)}, \ldots, \mathbf{Q}_{\pi(K)}\right\}$ and P is the maximum transmit power at BS. Then the capacity region of MIMO BC by DPC should be the union of achievable rate tuples on condition of all possible $\pi(\cdot)$ and $\mathbf{Q}_{\mathbf{x}}$ (Weingarten et al. 2004), which can be formulated as

$$R^{\text{sum-power}}_{\text{BC, DPC}}(\mathbf{H}, P) = \bigcup_{\pi(\cdot), \mathbf{Q}_{\mathbf{x}}} \left\{\left(R\left(\pi(1), \mathbf{Q}_{\pi(j)}\right), \ldots, R\left(\pi(K), \mathbf{Q}_{\pi(j)}\right)\right)\right\}, \tag{2.73}$$

where $R\left(\pi(i), \mathbf{Q}_{\pi(j)}\right)$ is computed using (2.71).

2.5.4 Duality of the MAC and BC Capacity Regions

An interesting question is about the relation between $R^{\text{sum-power}}_{\text{MAC}}(\mathbf{H}, P)$ and $R^{\text{sum-power}}_{\text{BC, DPC}}(\mathbf{H}, P)$. In Vishwanath et al. (2003) and Viswanath and Tse (2003), the authors proved the equivalence of these two capacity regions. Thus, the duality between the MAC and BC capacity regions was established as illustrated by Fig. 2.14 for a two-UE model.

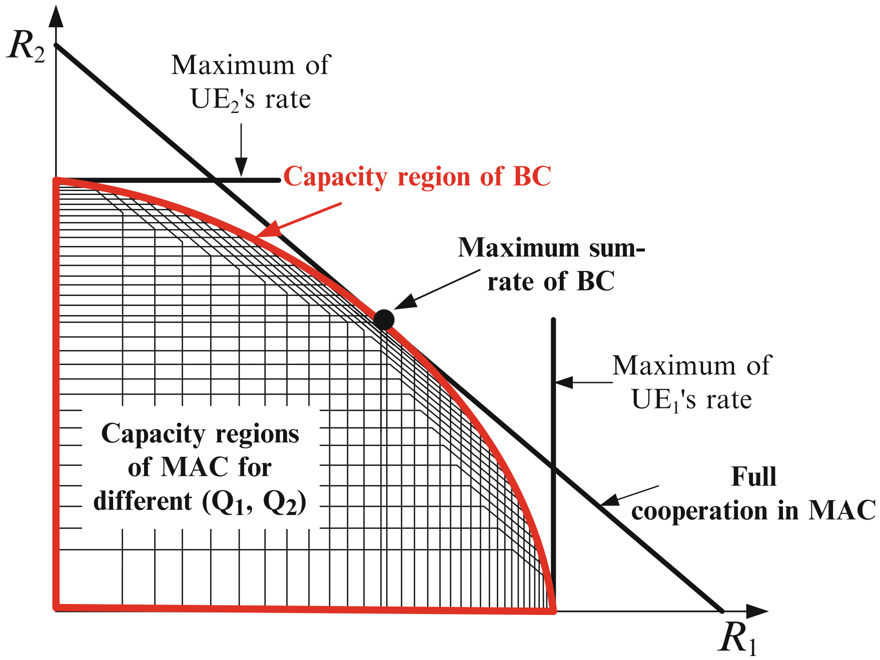

Fig. 2.14 Duality of the MAC and BC capacity regions for a two-UE model

As an example, we conduct a numerical simulation for the case when $M = 4$, $N = 2$, $K = 2$, and $P = 10$. In the simulation, the coefficients of $\mathbf{H}_1^{\mathrm{H}}$ and $\mathbf{H}_2^{\mathrm{H}}$ are randomly generated according to the Rayleigh fading model (Proakis 2001) shown as

$$\mathbf{H}_1^{\mathrm{H}} = \begin{bmatrix} 0.1048 - 0.4416\mathrm{i} & 1.1699 + 0.0070\mathrm{i} \\ 0.1036 + 0.9046\mathrm{i} & 0.4720 - 0.8422\mathrm{i} \\ 0.6977 - 0.1094\mathrm{i} & 0.1132 + 0.4511\mathrm{i} \\ -0.4358 - 0.3217\mathrm{i} & 0.3305 - 1.2169\mathrm{i} \end{bmatrix} \tag{2.74}$$

and

$$\mathbf{H}_2^{\mathrm{H}} = \begin{bmatrix} 0.7817 - 0.0276\mathrm{i} & -0.3694 + 0.3533\mathrm{i} \\ 0.7931 - 0.4793\mathrm{i} & -1.3169 + 0.0316\mathrm{i} \\ 0.3617 + 0.4353\mathrm{i} & 0.5655 - 0.0469\mathrm{i} \\ 0.1579 + 0.9729\mathrm{i} & -0.4112 - 0.7454\mathrm{i} \end{bmatrix}. \tag{2.75}$$

The simulated capacity regions of MAC and BC are plotted in Fig. 2.15, which serves as a concrete embodiment of the duality relation between $R_{\mathrm{MAC}}^{\mathrm{sum\text{-}power}}(\mathbf{H}, P)$ and $R_{\mathrm{BC,DPC}}^{\mathrm{sum\text{-}power}}(\mathbf{H}, P)$.

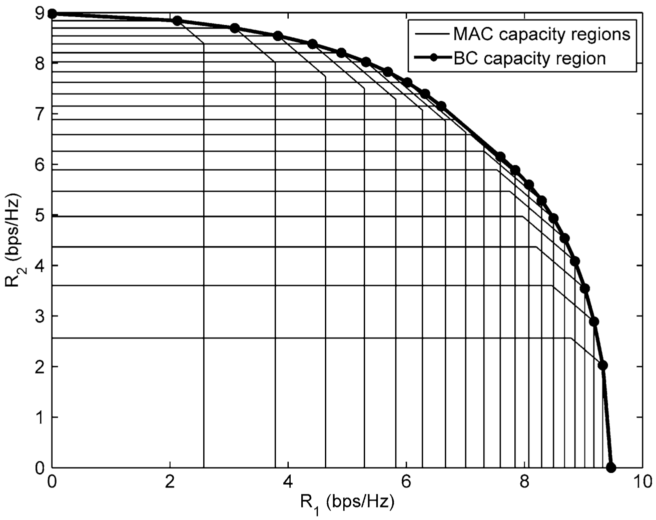

Fig. 2.15 Example of the duality of the MAC and BC capacity regions for a two-UE model

2.5.5 MU MIMO Schemes in Practical Systems

From the analysis in Sects. 2.5.2 and 2.5.3, it can be concluded that the capacity-achieving strategies in MU MIMO systems generally demand nonlinear signal processing such as the SIC receiver or DPC operation at the transmitter. The implementation of SIC receiver is relatively easy since the BS is usually equipped with devices of high signal processing capabilities. However, the employment of DPC in practical systems is quite another story, partly due to the very high complexity of UE-wise and symbol-wise encoding process, partly because of the requirement of perfect or nearly perfect CSI in DPC. Although some suboptimal DPC schemes were proposed in Caire and Shamai (2003), the DPC technique is still far from practical uses. This has motivated the research in low-complexity-oriented linear precoding schemes (Mai and Paulraj 2007), for example, zero-forcing beamforming (ZF-BF) for single-antenna UEs (Yoo and Goldsmith 2006) and block diagonalization (BD) precoding for multi-antenna UEs (Spencer et al. 2004). The basic idea of ZF-BF and BD precoding is to transmit each UE's signal in the null space spanned by other UE channel vectors/matrices so that inter-UE interference can be completely mitigated. It was proved in Yoo and Goldsmith (2006) that the ZF-BF can achieve asymptotically optimal performance compared with the DPC scheme at high SNR when full CSI is available at the BS. Besides, a joint optimization of linear precoding matrix and linear receive filter was proposed in Pan et al. (2004), wherein the transceiver functions of each multi-antenna UE are iteratively computed based on the BD principle. Moreover, when the UE number is large, the capacity of the MU BC system also grows with the UE number according to a double logarithm scaling law due to the multi-UE diversity gain provided by UE scheduling (Sharif and Hassibi 2007). Furthermore, the BD precoding scheme was proposed to be used in a multicell scenario in Shim et al. (2008) to simultaneously suppress inter-UE and intercell interference. Although the interference power is minimized in the ZF-BF or BD precoding scheme, it doesn't necessarily maximize the signal power at the same time. On the contrary, the useful signal usually suffers from considerable power loss due to forced signal steering away from the subspace spanned by other UE channel vectors/matrices. Therefore, an alternative signal-to-leakage-plus-noise ratio (SLNR) approach was proposed in Sadek et al. (2007), which suggested maximizing the ratio of the signal power over the interference leakage power plus the noise power. In the SLNR precoding scheme, each UE precoder can be derived without the knowledge of other UE transmission processing information so that iterative algorithms are generally not necessary.

2.6 CSI Feedback Technology

The term "CSI feedback" refers to a process, in which a UE reports its CSI to a BS so that the BS can perform adaptive transmission and appropriate radio resource management (RRM) operations. There are primarily three CSI feedback approaches in the literature (3GPP 2010a, b; Love et al. 2008; Ericsson 2009; Texas 2009).

1. Direct CSI feedback: The UE quantizes all elements in a channel matrix and feeds back the quantized real part and imaginary part of the elements to the BS (Ericsson 2009). Alternatively, the UE can analogously modulate all elements in the channel matrix and sends them back to the BS. Also, the UE can apply the vector quantization technique (Santipach and Honig 2004) on the channel matrix column by column and feeds back the indices of the vector indices to the BS. Thus, the BS can reconstruct a relatively accurate channel matrix from the quantized CSI fed back from the UE.
2. Statistical CSI feedback: The UE extracts some form of statistical information, for example, covariance matrix, from a MIMO channel, quantizes the statistical CSI and then feeds it back to the BS. Thus, the BS can obtain the statistical CSI and optimize the transmission strategy based on this coarse CSI.
3. Feedback of transmission recommendations based on codebook searching (3GPP 2010b, 2011a): A finite set of transmission recommendations is predefined by a codebook which is stored in both the UE and the BS. Commonly used codebook includes contents such as channel rank indicator (RI) and/or precoding matrix indicator (PMI) and/or channel quality indicator (CQI). As have been explained in Sect. 1.4, RI indicates the number of parallel sub-channels for single-stream or multi-stream transmissions, PMI carries the spatial domain transmission information, and CQI measures the channel quality in terms of achievable paylaod size. Upon detection of a channel matrix, the UE searches in the codebook for an optimal transmission strategy and feeds back the corresponding

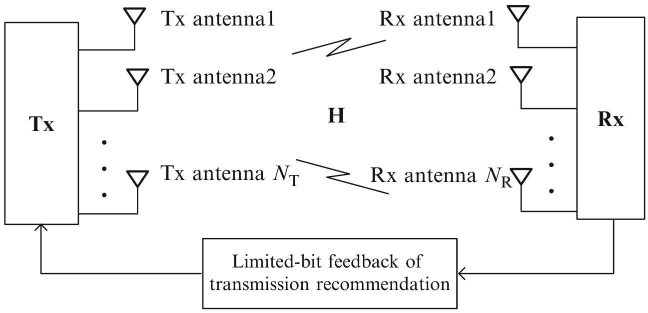

Fig. 2.16 Illustration of limited-bit feedback of transmission recommendation for MIMO systems

content indices to the BS. Then, the BS can simply follow the transmission recommendation given by the UE or translate the reported information into new forms of CSI for alternative implementations.

Among the above three approaches, the direct CSI feedback scheme can deliver the best performance, but it is difficult to be applied for practical systems due to its very high feedback overhead (Ericsson 2009). Moreover, in the multi-antenna multi-BS cooperative communication system, the overhead associated with the direct CSI feedback grows in proportion to the increased number of BSs and thus it will become even more impractical to employ. The feedback of transmission recommendations based on codebook search, also known as implicit CSI feedback, has the lowest feedback overhead, but with an unsatisfactory performance since it cannot accurately describe the channel matrix so that the transmitter is unable to make full use of the MIMO channel by finely tuning the transmission strategy. However, this scheme is extremely easy to implement and can typically quantize the CSI within a few bits. Hence, it has been widely applied in practical FDD systems (3GPP 2010b, 2011a). The statistical CSI feedback scheme, on the other hand, can achieve a good trade-off between the performance and overhead in some specific antenna configurations. For example, when the uniform linear array (ULA) is employed at BS and UE, the corresponding channel matrix can be decomposed in angular domain (Tse and Viswanath 2005) and exhibits evident statistical CSI.

Currently, in LTE and LTE-A systems, the feedback of transmission recommendations based on codebook search as illustrated in Fig. 2.16 has been employed for downlink transmissions. To be more specific, in LTE/LTE-A networks, there are two CSI feedback channels, that is, physical uplink control channel (PUCCH) and physical uplink shared channel (PUSCH). In general, the PUCCH is configured for the transmission of periodic and basic transmission recommendations with low payload, while the PUSCH is used for the report of burst, extended CSI with high payload. For CSI feedback on PUCCH, the CSI contents, for example, RI, PMI, and CQI, are transmitted in different subframes. For that on PUSCH, on the other hand, self-contained transmission recommendations are fed back within one subframe to keep the completeness of a CSI report.

In recent years, some active topics of the single-cell limited-bit CSI feedback in academic researches (Love et al. 2008) include contents of limited-bit CSI (Thoen et al. 2001; Love and Heath 2003; Zheng et al. 2007), codebook design for the precoding operation (Lau et al. 2004; Kim et al. 2007; Clerckx et al. 2008; Abe and Bauch 2007), allocation of feedback bits among multiple UEs (Taesang et al. 2007; Jindal 2006), and RRM operations based on reported CSI (Sun and Honig 2003a, b; Yao and Giannakis 2005; Sampei and Harada 2007), etc. Most of these results are derived for the case of single-antenna UEs due to its analytical tractability. In Taesang et al. (2007) and Jindal (2006), the authors investigated the impact of vector-channel quantization error on system throughput. It was found that when ZF precoding is operated for multiple single-antenna UEs, the number of CSI feedback bits should grow proportionally with the product of UE's SNR in dB and the number of BS antennas so as to achieve the full multiplexing gain of the MU MISO system. The above conclusion was extended to a multi-antenna multi-UE scenario with a modified definition of quantization error for channel matrices in Ravindran and Jindal (2008). Moreover, the authors Moon et al. (2010) analyzed the impact of channel matrix quantization errors on system throughput in multi-antenna multi-UE cases. Recently, in Zhang et al. (2009a, 2011), the authors further considered the CSI delay issue and investigated how the CSI feedback delay and quantization error jointly affect the performance of system throughput.

When multiple cooperative BSs are involved, the limited CSI feedback bits should be smartly divided among the BSs so that multicell CSI is collected effectively in the sense that the performance of the cooperative communication is optimized (Bhagavatula and Heath 2011a, b). Generally speaking, there are two main factors that determine the allocation of CSI feedback bits among multiple BSs, that is, channel quality and feedback delay. In Bhagavatula and Heath (2011a), the authors proposed that if the total number of CSI feedback bits is fixed, then in general more bits should be used to quantize the channels with higher gains when coordinated beamforming (CB) is operated. Further discussions on joint assessment of channel gain and feedback delay for this bit-allocation problem can be found in Bhagavatula and Heath (2011b). For multi-BS joint transmission (JT) systems, similar conclusion can be found in Kim et al. (2012) and Xu et al. (2008) that a channel with higher SNR deserves more quantization bits for its CSI feedback. In addition, the authors Wu et al. (2011) investigated the quantization and feedback of inter-BS relative phase information, which can facilitate coherent combining of signals sent from multiple BSs in JT operations.

2.7 Survey of Multipoint Cooperative Communication Technologies

In a multipoint cooperative communication network, each transmit/receive point no longer separately conducts its signal processing operations. Instead, multiple nodes will jointly or cooperatively perform the signal transmission and/or reception. Here, the term “point” may refer to a BS, relay, UE, or just an antenna. It should be noted that the importance of the multipoint cooperative communication technology is more pronounced in MIMO systems since the interference problem is much more severe in MIMO networks than in single-input single-output (SISO) networks (Catreux et al. 2000; Blum 2003). In a multipoint SISO system, the interference can be considered as isotropic signals, while in a MIMO multipoint scenario, the interference becomes unpredictable in spatial domain because of multi-antenna beamforming or precoding performed by neighbor points.

From a general perspective of cooperative communication, a variety of researches in wireless communication contributes to its prosperity in the last decade. Some related topics include MIMO relay system, network MIMO technologies, opportunistic beamforming, radio resource reuse schemes, multicell joint scheduling/power control schemes, soft/more softer hand-off technique, interference alignment schemes, femtocell-related technologies, and spatial domain coordinated beamforming, etc. Although these topics may seem lack of commonality, they actually belong to the same family of multipoint cooperative communication technology.

A general framework of cooperative communication has been addressed in Gesbert et al. (2010) to provide us a large technical picture, in which existing cooperative communication schemes are classified into four categories based on whether data sharing is conducted and whether CSI sharing is available. In this book, we propose that a third factor should be considered in the classification of cooperative communication schemes, which is whether time-frequency synchronized transmission or reception (TFSTR) is operated. Our motivations to introduce the third factor are twofold:

1. Resource reuse schemes, as well as selection and muting of transmission point (TP), for example, BS, relay, or antenna(s), are widely used in practical systems. They are clearly characterized by non-TFSTR features and hence should be treated separately.
2. In the non-TFSTR-based cooperative communication schemes, a traditional philosophy of interference avoidance or coordination is often adopted. However, recent development both in academic communities and in industrial standardization activities has evolved out a paradigm-shifting philosophy based on TFSTR, which is to exploit the interference, instead of staying away from it. Therefore, it is helpful to distinguish the conventional cooperative communication schemes from the modern ones from the TFSTR aspect.

Our views on the classification of multipoint cooperative communication technologies are summarized in Table 2.1. The schemes in the 3rd, 4th, 5th and, 6th categories are generally based on traditional approaches to deal with the interference issue, while those in the 7th and 8th categories are developed in the most recent years, which are more sophisticated than the conventional schemes.

Table 2.1 Classification of multipoint cooperative communication technologies

	Without data sharing	With data sharing
With TFSTR and without CSI sharing	The 1st category	The 2nd category
Without TFSTR and without CSI sharing	The 3rd category	The 4th category
Without TFSTR and with CSI sharing	The 5th category	The 6th category
With TFSTR and with CSI sharing	The 7th category	The 8th category

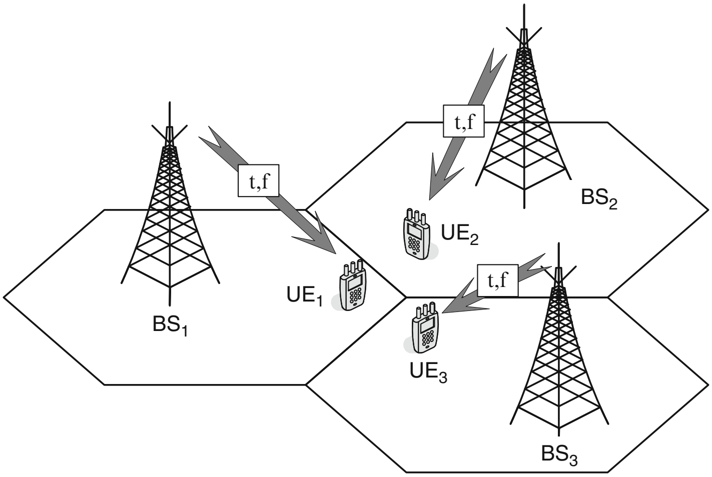

Fig. 2.17 Illustration of a single-cell processing scheme

2.7.1 The First Category of Multipoint Cooperative Communication

The first category of multipoint cooperative communication is characterized by TFSTR with no data sharing and no exchange of interpoint CSI, which implies distributed signal processing carried out in standalone transmission points. This scenario exhibits the lowest cooperation level with very limited prior information to facilitate the cooperative communication. Actually, scheme in this category usually serves as a benchmark, such that other advanced multipoint cooperative communication schemes are compared against it.

2.7.1.1 Single-Cell Processing

Single-cell processing (SCP) is a typical example of the first category of multipoint cooperative communication technologies. An illustrative diagram of the SCP scheme is presented in Fig. 2.17, where three UEs and their respectively associated

BSs, each takes charge of RRM operations in one hexagonal cell, are depicted. Signal transmission and reception in one BS are independent from those in another BS, that is, BS_1, BS_2, and BS_3 independently provide communication service to UE_1, UE_2, and UE_3, respectively. It should be noted that in Fig. 2.17 we stamp the same framed text "t,f" onto the illustrative arrows of transmissions from BS_1, BS_2, and BS_3 to indicate the TFSTR feature of SCP.

In SCP, very limited cooperation can be conducted among BSs. Perhaps the most basic form of cooperative communication is the network planning (3GPP 2008). The primary function of the network planning is to properly deploy a large number of BSs with certain maximum transmission powers to meet the cell coverage requirements while keeping the overall interference as low as possible. Obviously, an SCP system is in general interference-limited since it is lack of effective methods to tackle the inevitable interference from adjacent cells.

2.7.1.2 Opportunistic Beamforming

In the first category of multipoint cooperative communication technologies, one may think that no cooperation scheme is worthy of noting since we don't have much to do without the knowledge of data and CSI, plus TFSTR implying 100% of signal collision from multiple transmission points. Here, we'd like to show an interesting exception in this basic category of cooperative communications.

In 1995, it was shown from information theory that at a certain time if a BS communicates with the UE with the best channel link condition, then the mutual information between the BS and the UE can be maximized (Knopp and Humblet 1995). Later on, in So and Cioffi (2009), Viswanath et al. (2002), Ozdemir and Torlak (2006), and Sanayei et al. (2007), the authors proposed a novel scheme of opportunistic beamforming (OB) in MU-MIMO systems to save the CSI feedback overhead. The basic procedure of the OB scheme can be explained as follows (So and Cioffi 2009). First, a BS generates several pseudorandom beamforming vectors. Second, the BS broadcasts some reference signals (RSs) known by all served UEs using the said beamforming vectors. Third, UE feeds back a CQI as well as an index of a selected beam vector only if the SINR associated with the selected beamforming exceeds a predefined threshold. Finally, for each beam vector, the UE with the highest CQI obtains the communication opportunity. It should be noted that UE's CSI feedback overhead is kept very low since each UE only needs to report a CQI together with a corresponding beam index; while the PMI feedback is not necessary in the OB scheme. In a scenario where there are many active UEs, it is relatively safe to assume that every randomly generated beam will be opportunistically adopted by some UE with a good performance. It has been proved in Ozdemir and Torlak (2006) that the capacity of the OB scheme is comparable with that of the optimal beamforming scheme when the number of UEs in the network is large.

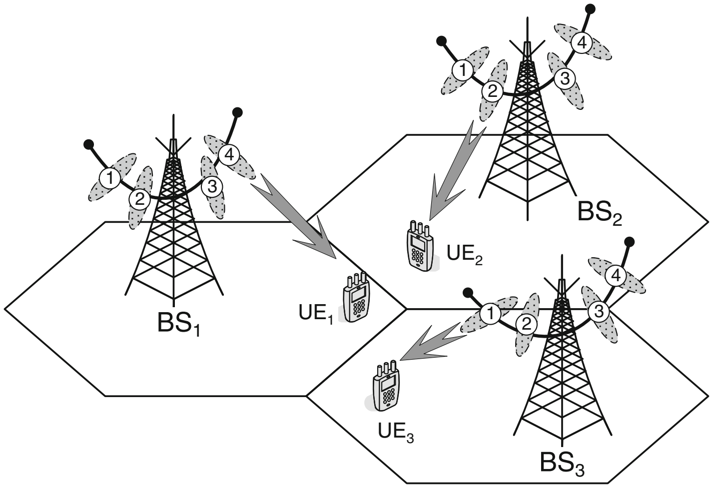

Fig. 2.18 Illustration of opportunistic beamforming in a multicell scenario

In fact, the OB scheme, originally designed for the MU-MIMO system, can be directly applied in the multipoint cooperative communication scenarios. An example of a multi-BS OB scheme as illustrated by Fig. 2.18, operates in a TFSTR manner and requires no data and CSI sharing. In Fig. 2.18, three BSs broadcast beams with indices ①, ②, ③, and ④ in four sequential times slots, respectively. From the illustrative beam directions, when the three BSs simultaneously transmit RSs using beam ①, UE_3 served by BS_3 should experience a desirable channel condition, which allows a good signal reception with low interference. Similarly, UE_1 in BS_1 and UE_2 in BS_2 should show their preferences on beam ④ and ②, respectively. Then, the indices of the UE-selected beams should be reported to the BSs for RRM operations. A scheme like the one illustrated by Fig. 2.18 was proposed by Huawei company (2008a) at the LTE-A standardization conference. Similar discussions can also be found in some academic papers (Vemula et al. 2006).

2.7.2 *The Second Category of Multipoint Cooperative Communication*

The second category of multipoint cooperative communication takes a further step than the first category by admitting data sharing in the network, leading to broadcast operations based on the multipoint infrastructure. The shared data can be transmitted on the same time-frequency resource throughout the network, which achieves a power gain by noncoherent signal combining at the receiver and diversity gain from distributed SCP transmissions.

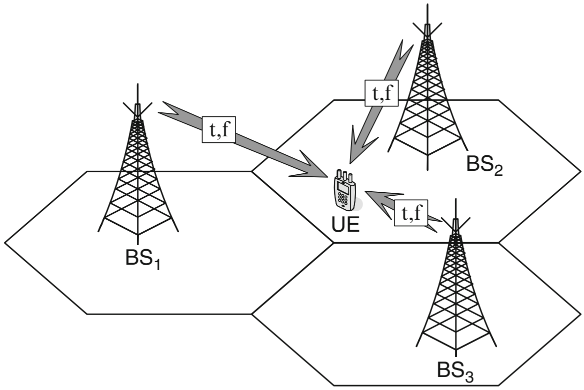

Fig. 2.19 Illustration of an SFN system

2.7.2.1 Single-Frequency Network Broadcasting

Single-frequency network (SFN) consists of synchronized radio transmission points located in distributed geological positions. These transmitters send the same signal on certain time-frequency resources to provide reliable broadcasting service to UEs. Such technology has already been adopted by the LTE/LTE-A system as a means to deliver the multimedia broadcast and multicast service (MBMS) to UEs (3GPP 2010b). The SFN transmission is illustrated by Fig. 2.19, where three BSs transmit the same signal to a UE.

Compared with the conventional way of signal broadcasting from a super radio tower, usually situated at the center of a city, the SFN transmission holds many advantages. First, dead zones with poor SINR can be well covered by short-range multipoint transmissions from various directions. Second, a UE's quality of experience (QoE) is consistent across the whole network since the UE is able to enjoy the macro-diversity and power gain when it approaches the cell-edge region. Third, the distributed transmissions of the cellular SFN produce less electromagnetic radiation than the centralized transmission from one broadcasting tower, which is usually energized by a very high power so that the broadcasting signals can march to a far-reaching distance.

2.7.3 The Third Category of Multipoint Cooperative Communication

Similar to the first category of communication cooperation, in the third category, neither data sharing nor CSI exchange is granted. However, non-TFSTR operations are considered here, leading to hard/fractional resource reuse schemes in frequency and/or time domain. Suppose that we divide the whole time-frequency resources into several parts and one cell is only authorized to use one part, then we may

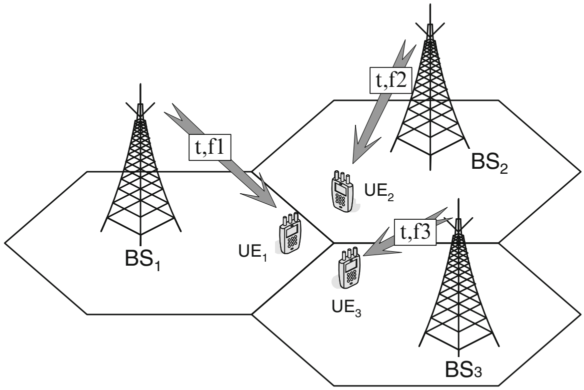

Fig. 2.20 Illustration of a hard frequency reuse scheme

design that one cell's resource part can only be reused by cells located some distance away so that the intercell interference will significantly diminish with the radio propagation across multiple cells.

2.7.3.1 Hard/Fractional Frequency Reuse

First proposed by the Bell labs (MacDonald 1979), the hard frequency reuse scheme has so profound meaning for the cellular network that its impact is still lingering today. In the early time of the cellular communication, transmit antennas were mounted on a tall and high-power BS tower, which looked down at a very large area and provided service to the UEs in it. However, with the continuous increase of UEs, the capacity of the giant BS will soon appear inadequate since the BS power cannot be unlimitedly increased and the power boosting provides no multiplexing gain at all. Therefore, the Bell labs proposed to employ multiple low-power BSs and exploit the signal attenuation of radio waves due to propagation loss such that one segment of frequency spectrum used by a BS can be reused by another BS some distance away where the signal power diminishes below the noise power level. A coverage area managed by a lower-power BS with one segment of frequency spectrum is named as cell. In order to achieve high multiplexing gains, the coverage of each cell is designed to be relatively small and plenty of cells are laid on a wide area to provide the system coverage. To sum up, the hard frequency reuse scheme represents a paradigm-shifting methodology of deploying multiple small BSs instead of building up a super BS, which turns out to be the core part of the pioneering cellular networks.

A hard frequency reuse scheme is illustrated in Fig. 2.20, where three BSs adopt different segments of the frequency spectrum, that is, f1, f2, and f3, to serve their UEs. An improvement on the hard frequency reuse scheme is to split the whole frequency resource into two sets, one set is applied with the hard frequency reuse scheme and the other set is universally used by all cells, usually only assigned to the cell-interior UEs with low transmit powers to decrease the intercell interference. Such scheme is called the fractional frequency reuse scheme (Huawei 2005a), which will be discussed in more details in Chap. 4.

It should be noted that in the early practice of cellular networks, the reuse factor F, that is, the number of the resource partition sets segments of the frequency spectrum, is relatively large. For example, F ranges from 9 to 11 in the AMPS network (1G system, see Sect. 1.1) and its value becomes 4∼7 for the GSM system (ETSI 1996). The larger the F is, the farther the resource reuse distance and the lower the interference level will be, but the system capacity will suffer from a higher loss. In Hanly and Whiting (1993), the authors proved that for a network with a reuse factor F, its capacity decreases by a factor of F compared with an interference-free SCP system. In the modern 3G cellular network enabled by the CDMA technology, the reuse factor aggressively takes the value of 1, that is, universal reuse, due to the unique capability of CDMA to suppress the intercell interference. From an operator's point of view, universal reuse means saving considerable investment on the acquisition of new frequency spectrums. Therefore, universal reuse is an explicit design goal of the 4G cellular network, for example, the LTE/LTE-A system (3GPP 2008).

2.7.3.2 Hard Time Reuse

The hard time reuse scheme works in a similar way as the hard frequency reuse scheme except it is applied in time domain (Hanly and Whiting 1993). In Sharif and Hassibi (2007), the performance and complexity of the hard time reuse, DPC, and ZF receiver schemes are carefully compared. A prominent example of the hard time reuse scheme is its recent application in the heterogeneous network involving femtocells. A femtocell refers to a very small cell, usually only covers an apartment, office, or meeting room (Claussen et al. 2008; Chandrasekhar et al. 2008). The BS associated with a femtocell can provide service to a specific group of UEs, that is, closed subscriber group (CSG) UEs, or to any UEs in its coverage.

Currently, a large portion of mobile phone traffics takes place in the indoor environment (Fujitsu 2012), and hence the market of indoor wireless communication is of great importance to operators. In order to maintain the competitiveness of the cellular network in the future and properly respond to the challenges posed by alternative wireless IP technologies such as wireless local area network (WLAN), the femtocell scheme was proposed as a means to provide better indoor coverage with low cost and prevent macro-BSs being overwhelmed by huge indoor traffic loads.

An illustration of a femtocell within a macro-cell is depicted in Fig. 2.21. In Fig. 2.21, the indoor UE gains access to the cellular network from the femto-BS without connecting to the macro-BS. Obviously, the indoor communication link quality is much better than that of the long-distance, building-penetrating channel between the macro-BS and the UE, leading to high QoE for the UE. However, the interference issue is aggravated in this scenario because an outdoor UE walking into

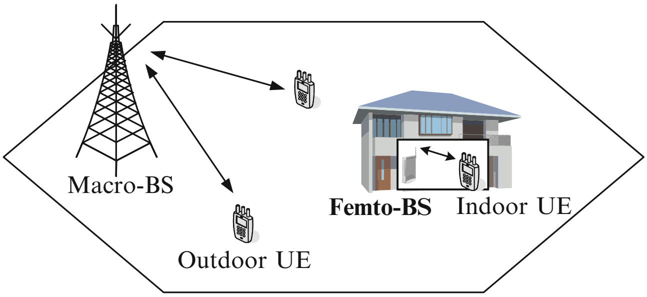

Fig. 2.21 Illustration of a femtocell within a macro-cell coverage

the femtocell coverage may jam the femto-BS due to its high uplink transmission power, and a femto-BS may also interfere with an outdoor UE from a close range.

In the LTE/LTE-A system, for simplicity, no backhaul interface exists between the femto-BS and macro-BS (3GPP 2010b). Therefore, no data sharing and CSI exchange is possible in the heterogeneous network illustrated by Fig. 2.21. The primary cooperative communication scheme to deal with the interference problem is based on a hard time reuse scheme, that is, the macro-BS periodically gives up some uplink and downlink subframes in time domain for the femto-BSs in its coverage to use (3GPP 2011a). It should be noted that other than femtocells, there exists another kind of small cells, that is, picocells, which have backhaul communication links with macro-cells (3GPP 2010b). A pico-BS can be used like a relay to provide service in dead zones of a cell. More importantly, pico-BSs can be deployed in hot spots such as shopping malls, train stations, and entertainment centers, where the wireless communication traffic loads are tremendously large and cannot be accommodated by macro-BSs with wide coverage. Actually, a pico-BS can be treated in the same way as a macro-BS except with a relatively small transmission power. Thus, all the eight categories of multipoint cooperative communication technologies discussed in this section can be applied for pico-BSs.

2.7.4 The Fourth Category of Multipoint Cooperative Communication

In this category, the cooperative communication operates in a non-TFSTR manner with data sharing, but without any form of interpoint CSI exchange. Thus, one or more versions of the data may arrive at the receiver to enhance the SINR of the data. The AF relaying scheme discussed in Sect. 2.4.1 is a typical example of this category of cooperative communication technologies. In practice, a simple AF relay node is also called radio repeater, which usually operates in an FDD manner, that is, the backward and forward links are separated in frequency domain.

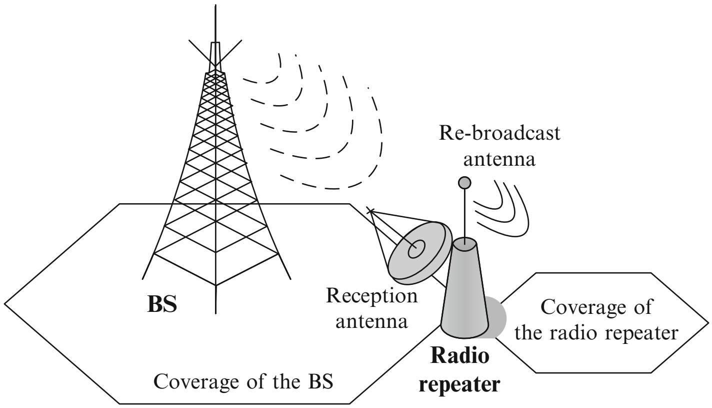

Fig. 2.22 Illustration of a radio repeater system

2.7.4.1 Radio Repeater

A radio repeater receives a weak, band-pass signal and rebroadcasts it with power amplification, so that it allows communication between two or more nodes that are unable to communicate directly with each other due to long distance or obstructions (Lee et al. 2008). For an FDD radio repeater system, the backward transmission is operated on an input frequency spectrum, where the radio repeater employs a band-passing filter to collect the signal sent by the source node. Then the forward transmission is shifted onto an output frequency spectrum, where the radio repeater amplifies and retransmits the received signal to the destination node. An illustration of a radio repeater system is presented in Fig. 2.22, wherein the downlink coverage of the BS is effectively extended by the employment of the radio repeater. Note that multiple radio repeaters can be deployed in the system to further boost the power of the amplified signals and achieve some diversity gains.

In the radio repeater system, the backward transmission from the source node has two purposes. One is to conduct data sharing with the radio repeater(s) through air interface and the other is to perform non-TFSTR operation to provide isolation on the transmitter and receiver of the radio repeater. In practice, isolating the radio repeater receiver from its transmitter is achieved by setting sufficient space bewteen the input and output frequencies. Modern radio repeater is also able to retransmit cellular signals inside a building. It is usually equipped with an external, directional antenna to receive the cellular signal, which is then amplified and rebroadcasted locally, providing massively improved signal strength. Compared with a BS, the radio repeater is a much more cost-efficient means to cover a wide region, especially in rural areas. Besides, the deployment of radio repeaters is simple, fast, and flexible, which can quickly remove blind spots or dead zones in the network. However, the interference and noise levels of the network may be greatly increased with the introduction of radio repeaters because they cannot distinguish the intercell interference and thermal noise from the useful signal before the amplification.

2.7.5 The Fifth Category of Multipoint Cooperative Communication

From this category on, we will discuss about more advanced multipoint cooperative communication technologies with the availability of interpoint CSI. In the fifth category, the cooperative nodes cannot share data, but they have the capabilities of CSI exchange and non-TFSTR operation. The corresponding cooperation schemes are directly enhanced from those in the third category, which are agnostic of any CSI. In general, with interpoint CSI and non-TFSTR, one can manage the communication resources in a smart way that interpoint interference will be adaptively coordinated or sometimes completely avoided.

2.7.5.1 Adaptive Frequency Reuse

The adaptive frequency reuse scheme, which is an upgraded version of the hard frequency reuse scheme, belongs to the fifth category of cooperative communication. The basic idea is to adaptively change the share or portion of the frequency resource used by a cell according to the intercell CSI about the incoming interference. A typical application of this technology is the multicell scheduling scheme (Gjendemsjoe et al. 2008; Kiani and Gesbert 2008), which carefully assesses the network interference based on multicell joint scheduling results and comes up with an optimized RRM decision.

In the LTE/LTE-A network, there is an adaptive frequency reuse scheme based on an intercell high-interference indicator (HII) (Sesia et al. 2009; 3GPP 2010c). The HII scheme, similar to the one proposed in Kiani and Gesbert (2008), is a proactive interference coordination scheme in the uplink, which is illustrated by Fig. 2.23. In Fig. 2.23, each BS estimates how strong its UEs may interfere with neighbor BSs in the uplink based on UEs' geometry information, for example, a cell-edge UE tends to emit strong interference toward its most adjacent non-serving cell. After a BS scheduler performs the uplink resource allocation, the BS can predict on which frequency sub-band(s) and to which cell(s) its UEs may inject strong interference. Such forecast information of the upcoming interference will be conveyed by the HII signaling and sent to neighbor BSs through backhaul links. The BSs receiving the HII signaling will apply interference countermeasures on the indicated frequency sub-band(s), such as transmission muting (i.e., adjustment of the hard frequency reuse pattern), urgent rescheduling an cell-interior UE to take the interference (i.e., performing fractional frequency reuse by means of RRM scheduling), or heavier channel code protection, etc. It should be noted that the HII signaling can be designed as broadcast information and sent to all neighbor BSs. However, such kind of cell-wide crying out may alarm too many BSs to take defensive stances and employ conservative transmission schemes, which might offset the performance gain provided by the HII signaling. Therefore, in the LTE/LTE-A system, the HII is designed to be a cell-specific signaling (3GPP 2010c).

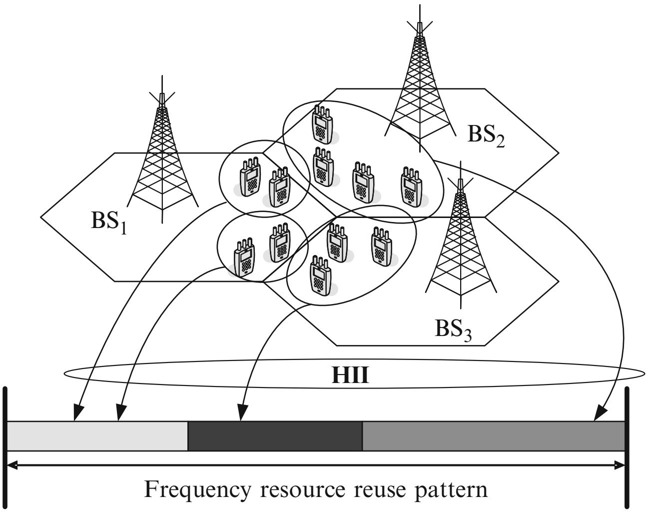

Fig. 2.23 Illustration of an adaptive frequency reuse scheme based on HII

To sum up, the adaptive frequency reuse scheme is operated before the occurrence of uncoordinated interference thanks to the inter-point CSI exchange, which can effectively prevent interference jamming. Thus, the cell-edge UEs can greatly benefit from this technology. However, full adaptive frequency reuse scheme may require complete information exchange of scheduling results, leading to a large inter-point signaling overhead. In addition, the adaptive frequency reuse scheme is typically effective in a multicell scenario with low or medium traffic load (Ericsson 2007) so that there are some spare frequency resources to support dynamic change of frequency reuse patterns.

2.7.6 *The Sixth Category of Multipoint Cooperative Communication*

In the sixth category, the cooperative communication is supported by data and CSI sharing as well as non-TFSTR operations. Since the data is available at multiple points and we also have some form of CSI indicating which point(s) may provide good signal strength, we can smartly activate some point(s) to perform the cooperative transmission with better performance and less power consumption compared with the full transmission from all available points.

2.7.6.1 MIMO Relay Transmission

The MIMO relay transmissions discussed in Sects. 2.4.2 and 2.4.3 generally belongs to this technology category. The non-TFSTR feature is justified by their two-phase

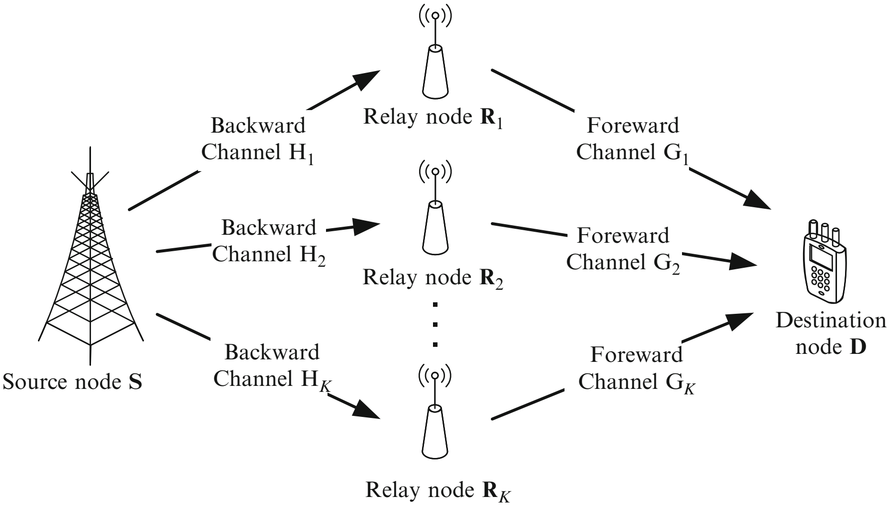

Fig. 2.24 Illustration of a MIMO multi-relay network

relaying protocol. Besides, both data sharing and CSI exchange are conducted between the source and relay nodes.

2.7.6.2 Relay/Antenna Selection

When multiple MIMO relays exist in the network, they can retransmit the source signal to the UE in a coordinated manner so that the multi-antenna array gain and diversity gain can be achieved. If all the relay antennas participate in the relay transmission on the same time-frequency resource, advanced precoding and power control schemes should be devised, which belong to the eighth category of cooperative communication to be addressed later. Here, we discuss about a non-TFSTR scheme, that is, relay/antenna selection, where only a part of relays or relay antennas are activated during the transmission.

The system model of a MIMO multi-relay network is illustrated by Fig. 2.24, where the source node **S**, the destination node **D**, and each relay node $\mathbf{R}_k (k \in \{1, 2, \ldots, K\})$ are equipped with N_s, N_d, and N_r antennas, respectively.

Suppose that the transmit time interval is divided into two time slots, the first and second time slots of which are assigned to the backward and forward transmissions, respectively. The CSI of the backward and forward channels is measured at the relay nodes and destination node, respectively. Then the source node obtains the CSI from relays and performs relay/antenna selection to activate some relay antennas from a total of KN_r^2 receive-transmit antenna pairs. For the unselected antenna pairs, they can be muted to decrease the interference level in the network or they can be used to serve other UEs.

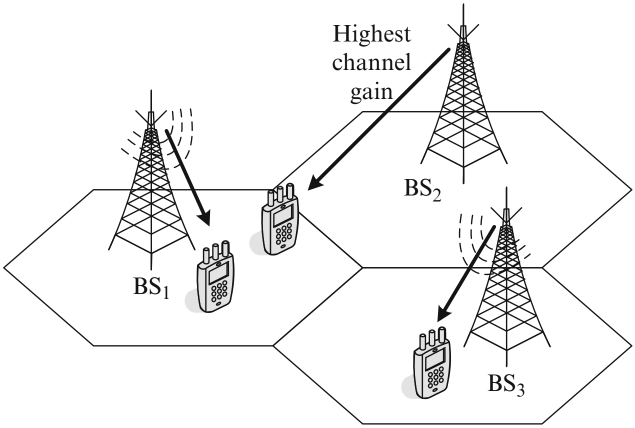

Fig. 2.25 Illustration of a dynamic cell selection scheme

2.7.6.3 Cell Selection and Blanking

Similar to relay/antenna selection, BS can also be smartly turned on and off according to the multicell CSI. In the LTE-A system, a scheme called dynamic cell selection (DCS) has been adopted (3GPP 2011b). In the DCS scheme, the UE data will be delivered to multiple BSs from the core network, and the UE will periodically monitor the multicell channels and report the corresponding CSI to its serving BS. Note that the serving BS does not necessarily mean the BS with the largest signal strength at the UE, especially during the inter-BS handover process. According to 3GPP (2010b), the serving BS is generally defined as the BS sending downlink control signalings, for example, downlink scheduling grant, to the UE. For actual data transmission on a certain time-frequency resource, the serving BS can order a BS with the highest channel gain, probably not the serving BS itself, to undertake the transmission task. The DCS scheme is illustrated in Fig. 2.25, where BS_2 takes over the transmission for a UE associated with BS_1.

In addition to the basic DCS scheme addressed above, in Zhang et al. (2004) the authors proposed a more advanced scheme of dynamically selecting multiple BSs for cooperative transmission. Later in Hoydis et al. (2010), the authors discussed the optimal number of cooperative BSs in the multicell DCS scheme.

Besides the DCS scheme, which activates some BS(s), there is also a dynamic cell blanking (DCB) scheme (3GPP 2011b) with a functionality of deactivating some BS(s) emitting strong interference. The DCB scheme is illustrated in Fig. 2.26, where BS_2 is activated for transmission and BS_1 is deactivated to reduce its strong interference to the UE.

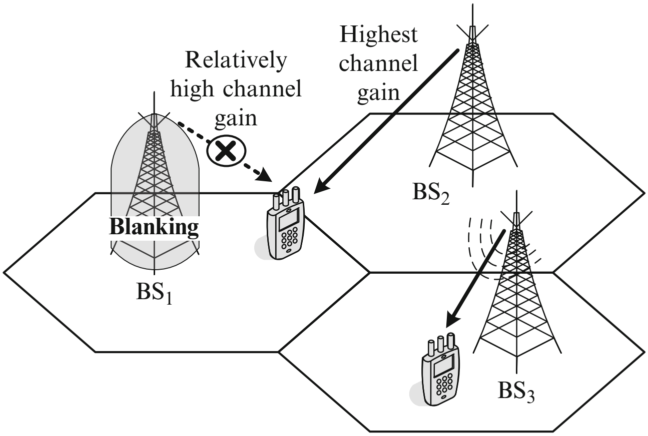

Fig. 2.26 Illustration of a dynamic cell blanking scheme

2.7.7 The Seventh Category of Multipoint Cooperative Communication

In this technology category, TFSTR is operated without data sharing, implying that the network is flooded with interpoint interference from all directions. The only resource we have here to combat the interference is the interpoint CSI. Based on the CSI knowledge, we can perform smart interference coordination so that most communication links can dodge serious hits from dominant interferers. Some practical schemes include soft resource reuse methods based on interpoint load balancing, joint scheduling together with advanced power control policies, spatial domain interference coordination using MIMO technologies to steer signal away from interference or vice versa, and interference alignment to reserve certain signal subspace for burying multipoint interference so that the interference can be perfectly contained and become harmless.

2.7.7.1 Soft Frequency Reuse

A soft frequency reuse scheme is in essence an improved version of the adaptive frequency use scheme addressed in Sect. 2.7.5.1. The enhancement of the soft frequency reuse lies in that each frequency resource will no longer be designated as usable or unusable in a cell. Instead, every frequency resource can be used by all cells, but with different power levels. In a general soft frequency reuse scheme (Caire et al. 2008), all frequency resources are divided into F parts. For one cell, some frequency resource segments are defined as the primary resource and the other

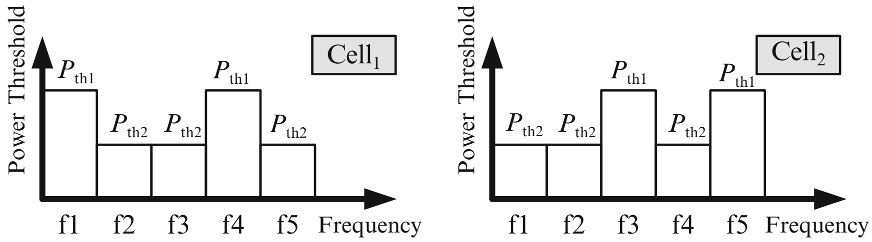

Fig. 2.27 Illustration of downlink power masks for different cells

segments the secondary resource. On the primary resource, the transmission power is set to be higher than a threshold P_{th1} to achieve a large throughput performance. However, for the secondary resource, its priority is to keep the intercell interference low. Therefore, the corresponding transmission power must not exceed another threshold P_{th2}. Each cell can adjust its primary/secondary resource together with P_{th1} and P_{th2} based on multicell coordinations. Hence, the equivalent reuse factor of a soft frequency reuse scheme is always 1, while that of a fractional frequency reuse scheme (see Sect. 2.7.3.1) or an adaptive frequency reuse scheme (see Sect. 2.7.5.1) takes a value between 1 and F.

It should be noted that P_{th1} is usually larger than P_{th2}, and the resulted shape of the power thresholds across the frequency spectrum is called power mask (Caire et al. 2008), which is illustrated in Fig. 2.27. In Fig. 2.27, we assume Cell$_1$ and Cell$_2$ are adjacent cells, and Cell$_1$ transmits with high power on frequency resources f1 and f4, that is, the primary resource. In order to coordinate the intercell interference, Cell$_2$ smartly lower the transmission power on f1 and f4 and establish its primary resource on f3 and f5. With the employ of power mask, both the cell-edge and cell-interior UEs are able to access larger system bandwidth, and thus the BS can make more efficient scheduling decisions to achieve a higher spectral efficiency. Considering the extreme case when $P_{\mathrm{th2}} = 0$ (Choi and Andrews 2008), we can see that the soft frequency reuse scheme will degenerate to the adaptive frequency reuse scheme.

In the soft frequency reuse scheme, the main problem is how to determine the multicell power masks in a dynamic way to achieve high performance. Some existing works studied multicell coordinated scheduling and traffic load-balancing schemes (Das et al. 2003; Sang et al. 2008; Jing et al. 2008). In Jing et al. (2008), the authors proposed an interesting scheduling algorithm, where two adjacent BSs alternately schedule cell-edge UEs and cell-interior UEs. Other works investigated distributed BS power control (Kiani and Gesbert 2008; Kiani et al. 2007) or multicell joint scheduling and power allocation (Tralli et al. 2004; Gesbert et al. 2007a) to improve the overall system throughput. Among them, in Gesbert et al. (2007a) the authors discussed the suboptimal numerical results of joint scheduling and power allocation. It should be noted that the global optimal solution is computationally very complex to find because the problem of multicell scheduling and power allocation is generally non-convex and shown to be NP-hard (Luo and Zhang 2008).

In Stolyar and Viswanathan (2008, 2009), Venturino et al. (2009), and Yu et al. (2010), the authors devised iterative algorithms to update the scheduling table and power control results in all BSs to achieve relatively satisfactory performances. A relatively new approach to treat the problem is based on the noncooperative game theory (Basar and Olsder 1999; Saad et al. 2009), which allows distributed power optimization in each BS (Gesbert et al. 2007a; Han et al. 2007; Alpcan et al. 2006). Another new method is the price-based spectrum management proposed in Shi et al. (2008) and Wang et al. (2008), where each BS is encouraged to try its best to lower the transmission power because the BS has to virtually pay for the interference it causes. It should be noted that the so-called interference price is actually a quantized measure on the effects of the interference, the relevant factors of which include bandwidth of the occupied spectrum, interference strength, and fairness among UEs. Last but not least, the inter-BS synchronization issue should be carefully looked into (Zhang et al. 2008), otherwise the soft frequency reuse scheme will suffer from considerable performance degradation due to misalignment of the dynamically changed power masks of multiple cells.

In the 4G system, the soft frequency reuse method plays an active role (Huawei 2005b; Wimax 2006). For example, in the LTE/LTE-A downlink system, there exists a simple soft frequency reuse scheme based on the CSI exchange among BSs by means of backhaul communications on a long-periodicity basis. The related CSI is carried by the relative narrowband transmission power (RNTP) control signaling (3GPP 2008), which is essentially a promise made by a BS to all neighbor BSs about its sub-band P_{th2} across the downlink frequency spectrum shown in Fig. 2.27. After receiving the RNTP information, a BS can smartly manage its radio resource to prepare itself for the upcoming interference.

Also, in the uplink of the LTE/LTE-A system, a soft frequency reuse scheme similar to the one based on the RNTP signaling is adopted. First, a BS measures the intensity of uplink interference on each frequency sub-band caused by UEs from adjacent BSs. In a case when the interference exceeds a predetermined threshold, the BS will note that an event of interference overload has occurred. Then, the BS broadcasts an overload indicator (OI) control signaling to all BSs through backhaul communication links (Sesia et al. 2009; 3GPP 2010c). The OI signaling explicitly indicates whether or not overloaded interference has emerged per frequency sub-band. A BS having received the OI will check its scheduling history and determine whether the interference overload is caused by its UEs according to some geometry information reported by UEs, for example, path loss to the victim cell. If an interferer UE is identified, then its serving BS will take certain measures in order to suppress the interference, for example, reducing the UE's transmission power on the frequency sub-band indicated by the OI and rescheduling another UE to use the frequency sub-band. The soft frequency reuse scheme based on OI the OI signaling is illustrated in Fig. 2.28.

The method of indicating an interference overload event per frequency sub-band is simple and flexible and allows for quick response to strong interference. However, unlike the proactive scheme based on the RNTP signaling, it is a reactive scheme, which cannot mitigate the interference beforehand and may regulate the cell-edge UEs too often due to their tendency to produce relatively large intercell interference.

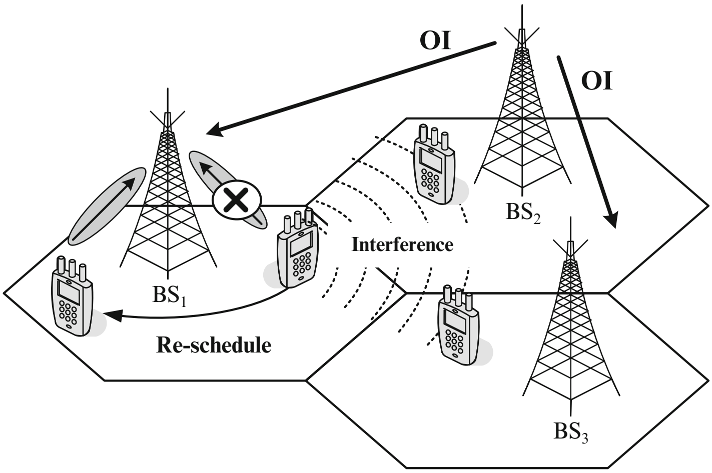

Fig. 2.28 Illustration of a soft frequency reuse scheme based on OI

2.7.7.2 Spatial Domain Interference Coordination

In a spatial domain interference coordination scheme, each BS adjusts the transmission beam directions and power-loading factors for its scheduled UEs to reduce their interference in the network based on the intercell spatial domain CSI exchanged among BSs. This system can be generalized to a model in information theory called interference channel (IC), that is, independent transceiver pairs with inter-pair interference. Currently, the capacity region of the IC model is still unknown (Gesbert et al. 2007a), even for the simplest two-user Gaussian interference channel. Nevertheless, some good progress has been made recently. In Shang et al. (2006), the authors deduced a lower bound of the sum capacity for the vector Gaussian interference channel by use of the superposition code technique. Moreover, in Etkin et al. (2008), the authors showed that a scheme splitting the transmitted information of two UEs into a private information part to be decoded only at own receiver and a common information part to be decoded at both receivers can achieve to within one bps/Hz of the capacity region of the Gaussian interference channel.

Although the spatial domain interference coordination scheme cannot achieve a performance close to the theoretical limit, it is easy to implement and useful in practical systems. The treatment of spatial domain interference can be dated back to the researches of optimal receiver in condition of colored interference (Winters et al. 1994). Most recent works are devoted to the problem of finding the optimal downlink beamforming vectors with minimum power consumption under a set of UE SINR constraints (Dahrouj and Yu 2008). In Jorswieck et al. (2008) and Lindblom et al. (2009), the authors proposed practical solutions based on MF and ZF precoding schemes for the cases of instantaneous CSI and statistical CSI. In Zakhour et al. (2009), the authors investigated a distributed downlink beamforming scheme based on a virtual SINR, which was similar to the SLNR

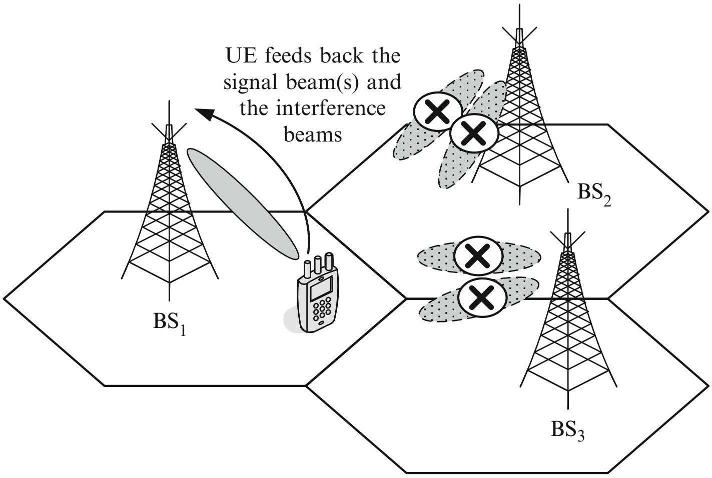

Fig. 2.29 Illustration of a dynamic spatial domain interference coordination scheme

discussed in Sect. 2.5.5. Additionally, in Dahrouj and Yu (2010), the authors studied a coordinated beamforming scheme for the multicell multi-antenna wireless system based on the Lagrangian duality theory.

During the standardization of the LTE-A system, a dynamic spatial domain interference coordination scheme was proposed in Alcatel-Lucent (2009) as illustrated by Fig. 2.29. In Fig. 2.29, the UE feeds back the signal beam(s) to its serving BS denoted as BS_1. Besides, the UE also reports the undesirable interference beams of neighbor BSs, for example, BS_2 and BS_3. After inter-BS CSI exchanging by the backhaul communication, BS_2 and BS_3 will avoid steering the signal toward the directions indicated by the said interference beams.

In a simpler spatial domain interference coordination scheme, it doesn't require the instantaneous CSI from the UE. Instead, each BS semi-statically determines and declares its beam pattern in a distributed way so that low-interference and high-interference regions are created by chance (Huawei 2008b). This scheme is illustrated in Fig. 2.30, wherein interference leakages from adjacent cells are coordinated by tuning the beam directions or avoided using beam deactivation in some cells, thus cell-edge UEs with the low-interference beams can take the opportunity and enjoy communication service with high SINR. In order not to let any UE always be overshadowed by high interference, all BSs in the network should periodically alter the beam patterns and broadcast the changes through backhaul links.

2.7.7.3 Interference Alignment

The basic idea of the interference alignment (IA) technology is to sacrifice a certain signal subspace to contain the multipoint interference so that the other signal

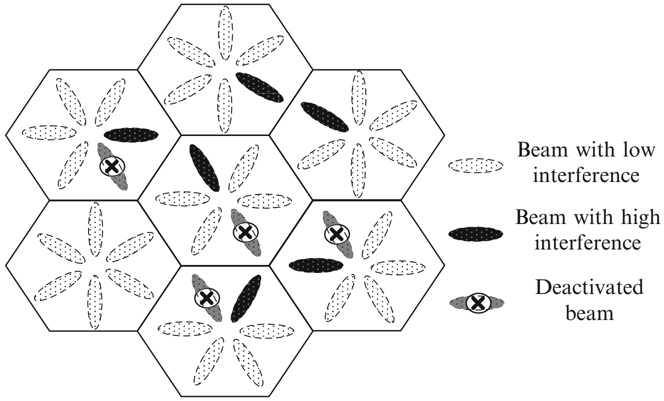

Fig. 2.30 Illustration of a semi-static spatial domain interference coordination scheme

subspaces are free from interference, thus achieving high spectral efficiency. The said signal subspace for burying the interference can be constructed in time and/or frequency and/or spatial domains. In Cadambe and Jafar (2008), the authors proved that for a network consisting of K UEs, when the IA technique is applied at the transmitter and ZF detection is used at each UE, the multiplexing gain of each UE can be as high as $K/2$. In other words, no matter how large the network size is, the IA technology promises that half the degrees of freedom in the system can be used for transmission without interference. Besides, in Gomadam et al. (2008), Peters and Health (2009), and Yu et al. (2009), the authors studied the feasibility of the IA technology in arbitrary setups of multi-UE and multi-antenna communications. At the LTE-A standardization meeting, a spatial domain IA scheme was proposed in Alcatel-Lucent (2009), as illustrated by Fig. 2.31. In Fig. 2.31, the UE not only feeds back the CSI of its signal space but also recommends the beamforming directions of BS2 and BS3 so that the interference from these two BSs can be aligned and buried in the UE's null space.

2.7.8 *The Eighth Category of Multipoint Cooperative Communication*

The highest level of multipoint cooperation will be discussed in this subsection, that is, cooperative communication based on TFSTR with data and CSI sharing. Schemes in this category generally require joint control of multiple points to form a virtual super node so that the optimization of transmission or reception can be performed on a high level. Perhaps the earliest application of this category of technologies can be dated back to about 20 years ago, when the soft/more softer handover procedure (Viterbi et al. 1994) was proposed for the CDMA system to

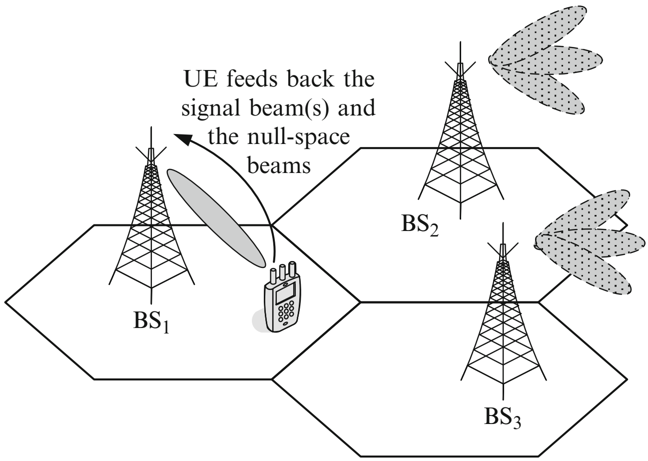

Fig. 2.31 Illustration of a spatial domain interference alignment scheme

allow cell-edge UEs to remain connected with multiple BSs during the handover process. Recent development in this area includes studies on multi-BS multi-relay networks and joint transmission (JT)/joint reception (JR) schemes, also known as the network MIMO technology.

2.7.8.1 Soft/More Softer Handover

The soft handover (SH) technique (Viterbi et al. 1994) is designed for the intra-frequency cell switching for mobile UEs. In the SH process, a mobile UE is temporarily connected to both the original and target BSs, which transmit the same downlink data to the UE and perform joint processing for the UE's uplink transmission. The link associated with the original BS will be terminated only when QoS-guaranteed communication is established between the target BS and the UE. The SH method is one of the key technologies in CDMA systems, which can significantly improve the robustness of the mobility management (Jing et al. 2007) performed by the mobile switch controller (MSC) entity. In Fig. 2.32, we provide an illustration of the SH technology. As seen from Fig. 2.32, when a UE moves from BS$_3$ toward BS$_1$, the MSC will track the UE's geometry information according to the UE's measurement report based on the received RSs. If the qualities of links from BS$_3$ and BS$_1$ to UE are comparable, BS$_1$ will be activated to co-work with BS$_3$ and they will jointly provide service to the UE. Afterward, as the UE continues its movement, BS$_3$ will relinquish the control of the UE to BS$_1$ if the link quality between BS$_3$ and the UE is below a certain threshold. For SH process in the CDMA system, joint decoding of UE data involving multiple BSs was first discussed in Hanly (1996), where it was proposed that multiple BSs should perform maximum ratio combining (MRC) followed by MF detection to increase the received SNR.

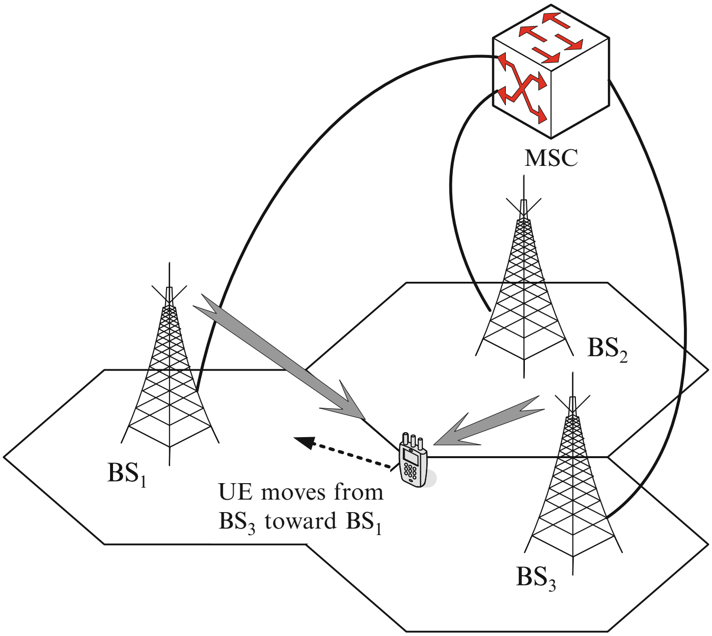

Fig. 2.32 Illustration of the soft handover technology

In addition, there is an enhanced version of the SH technique, that is, the more softer handover (MSH) scheme, referring to the SH between different sectors managed by the same BS. Both the SH and the MSH schemes are designed to improve the continuity of the mobile communication service, which has a large impact on UE's experience. Other than the SH and MSH schemes, there is another kind of handover strategy called hard handover. In the hard handover scheme, the link between the original BS and the UE should be cut off before that between the target BS and the UE being established. In our framework of technology survey, the hard handover scheme belongs to the sixth category of multipoint cooperative communication technologies. In practice, the combination of different handover strategies may be applied. For instance, a UE located between two sectors of a BS and at the same time near the boundary of a cell controlled by another BS will trigger both intra-BS MSH and inter-BS SH. As another example, a UE at the central point of an area triangulated by three BSs may invoke a rare case of 3-BS SH.

2.7.8.2 Joint Transmission/Reception

The model of joint transmission (JT) from multiple points to multiple UEs can be viewed as a MIMO BC with distributed transmit antennas. Similarly, the model of

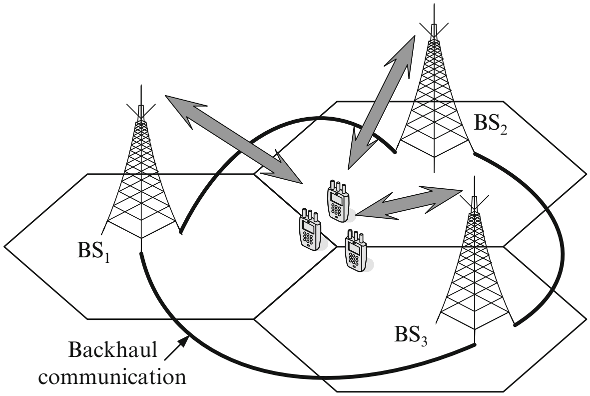

Fig. 2.33 Illustration of the JT/JR technology

joint reception (JR) can be generalized as a MIMO MAC with distributed receive antennas. The JT/JR technology is illustrated in Fig. 2.33, where the two-way arrows indicate downlink and uplink communications.

As have been discussed in Sect. 2.7.8.1, the studies on JR begun with the signal combining technique designed for the CDMA system (Hanly 1996). Regarding the MU detection in JR, it can be performed by a centralized processing unit or conducted in a distributed manner (Gesbert et al. 2007b; Ng et al. 2004; Aktas et al. 2008). Besides, if inter-UE cooperation is considered, larger system capacity can be expected (Simeone et al. 2008a).

The research on JT can also be dated back to the mid-1990s of the last century. In Wyner (1994), the author proposed BSs placed on a linear array and a hexagonal grid as two cellular models for the theoretical analysis of JT. These two models are generally known as the Wyner models and some variations can also be found in the literature, for example, in Somekh et al. (2009). The Wyner model with BSs placed on a linear array is illustrated by Fig. 2.34, in which the inter-BS interference is assumed to be only caused by several adjacent BSs. For instance, in Fig. 2.34, UE_m receives the useful signal from BS_m and the interference is generated from $2k$ adjacent BSs, that is, BS_{m-k} to BS_{m-1} and BS_{m+1} to BS_{m+k}. The Wyner model shown in Fig. 2.34 presents a simplified and tractable mathematical model for investigating practical cases, such as the highway and corridor scenarios (Venkatesan et al. 2007). It should be noted that in the Wyner model, different path losses for UEs are usually not considered for simplicity (Caire et al. 2008).

With the development of information theory on MIMO systems, multi-antenna multipoint JT, also known as the network MIMO technology, draws increasing attention in the literature (Karakayali et al. 2006). This is due to the fact that JT can exploit the interference channels, not only offering significant MIMO array gain but also macro-diversity gain but also improving the rank condition of the communication channel (Zhang and Dai 2004). In Shamai and Zaidel (2001), the authors pointed out that in the case of perfect backhaul connection among BSs, the downlink multipoint JT model is essentially the same as that of a MIMO BC model, except that each BS should be subjected to an individual power constraint in JT.

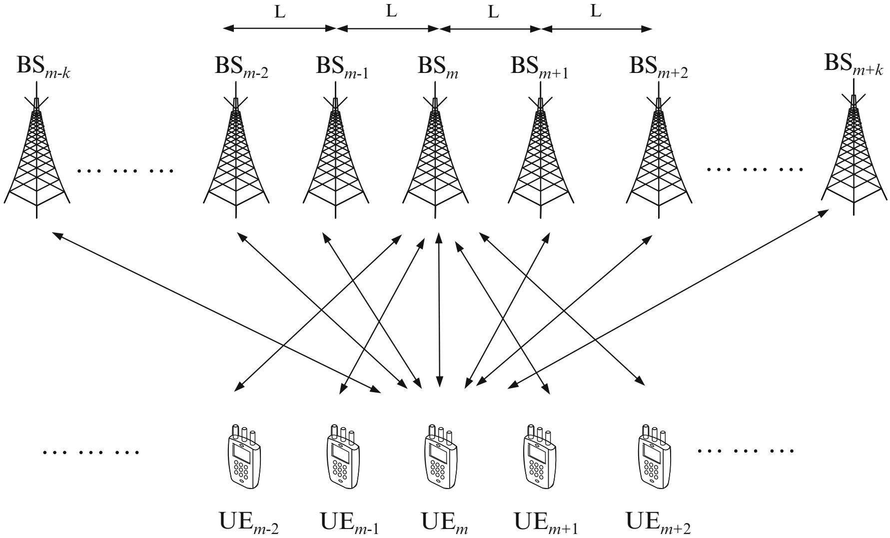

Fig. 2.34 Illustration of the Wyner model with BSs placed on a linear array

As for the MIMO BC model, it is well known that the optimal transmission strategy based on the capacity-maximization criterion (Zhang and Dai 2004) is the DPC technique (Costa 1983). Some simplified multipoint DPC schemes can be found in Jafar et al. (2004) and Simeone et al. (2009). However, for practical systems, each cooperating BS should have an independent power source, thus the studies on MIMO BC with per-BS power constraint are more meaningful. It should be noted that the DPC capacity region of MIMO BC with a more general per-antenna power constraint has been obtained by the duality theory in Yu and Lan (2007). This work was later extended to solve some MIMO BC problems with linear power constraints (Zhang et al. 2009b; Huh et al. 2009). Due to the high complexity of the DPC operation, linear precoding schemes for the conventional MIMO BC (Schubert and Boche 2004; Peel et al. 2005; Stojnic et al. 2006) based on ZF or BD precoding (Spencer et al. 2004; Choi and Murch 2004; Pan et al. 2004) (see Sect. 2.5.5) were extended to the multipoint JT network with per-BS power constraints. Multi-BS ZF precoding was investigated in Boccardi and Huang (2006) and Karakayali et al. (2007), while its BD version was treated in Liu et al. (2009) and Zhang et al. (2009c). Most existing schemes adopt the approach of first admitting a sum power constraint for the multipoint JT problem and then scaling down the solution to satisfy the local power constraint at each BS (Zhang and Dai 2004). Obviously, the two-step precoding design is strictly suboptimal. In contrast, direct incorporation of the per-BS power constraint into the optimization problem will usually generate a better solution (Zhang 2010). Regarding the performance loss between the multipoint DPC precoding and linear precoding, in Somekh et al. (2009) the authors studied the system capacity performance of a multi-BS JT scheme based on joint ZF precoding and distributed UE selection. It has been shown that even with the simple implementations of linear precoding and conventional UE scheduling, the system capacity is still asymptotically optimal.

At present, there are still many open questions for JT. First, the information capacity of a JT network needs further study considering nonideal factors such as channel fading, large-scale path loss, as well as imperfect CSI. Second, the multipoint JT network is composed of a large number of antenna elements, which makes the transmission and reception schemes very complex, especially when iterative algorithms are involved. Therefore, how to reduce the complexity of precoding and decoding schemes is a topic worthy of studying (Weingarten et al. 2006). Third, limitations of the interpoint backhaul connection, for example, unreliable connectivity, finite capacity, and unpredictable latency, should be taken into account when designing the JT system (Zakhour and Gesbert 2010). Partial ZF or partial DPC processing has been considered in Bagheri et al. (2010) and Hari and Yu (2010) to cope with the issue of data sharing through backhaul links of limited capacity. Fourth, in Zhang et al. (2007, 2009c), and Boccardi and Huang (2007), the authors proposed the framework of applying JT inside each cluster of multiple BSs and employing other low-level cooperative communication strategies to mitigate the intercluster interference. And hence, the BS clustering algorithm for JT operation should be further investigated for a well-balanced scheme with reasonable network complexity and CSI feedback overhead. Some popular BS clustering schemes are, for example, the nearest BS clustering, interference minimization clustering, and dynamic clustering algorithms (Marsch and Fettweis 2007; Papadogiannis et al. 2008). In Somekh et al. (2007a), the authors indicated that BS clustering will reduce the multiplexing gain of the JT system and discussed the performance loss factor when the number of BSs in each cluster takes an even integer or an odd one. As for the intercluster interference mitigation, we can apply the third or fifth category of multipoint cooperative communication technologies, for example, resource reuse and power control policies (Caire et al. 2008; Katranaras et al. 2009) or the seventh category of multipoint cooperative communication technologies such as the spatial domain beam coordination schemes (Zhang et al. 2009c).

2.7.8.3 Multi-BS Multi-relay Networks

If JT or JR technology is applied on multiple relays and they are connected to a BS by means of wireless interface, then the one-BS multi-relay network can be viewed as a concatenated model of a one-hop BC (BS $\rightarrow$ relay) with a one-hop JT (relay $\rightarrow$ UE) or a one-hop JR (UE $\rightarrow$ relay) with a one-hop MAC (relay $\rightarrow$ BS). An illustration of a multi-BS multi-relay network is provided in Fig. 2.35. In Simeone et al. (2007), the authors studied an upgraded Wyner model with multiple BS-relay pairs and no BS-UE direct links, where each pair consisting of one BS and one AF relay. The work in Simeone et al. (2007) was generalized for the application in multi-BS joint processing (Somekh et al. 2007b) and further extended to DF relaying protocol (Simeone et al. 2008b).

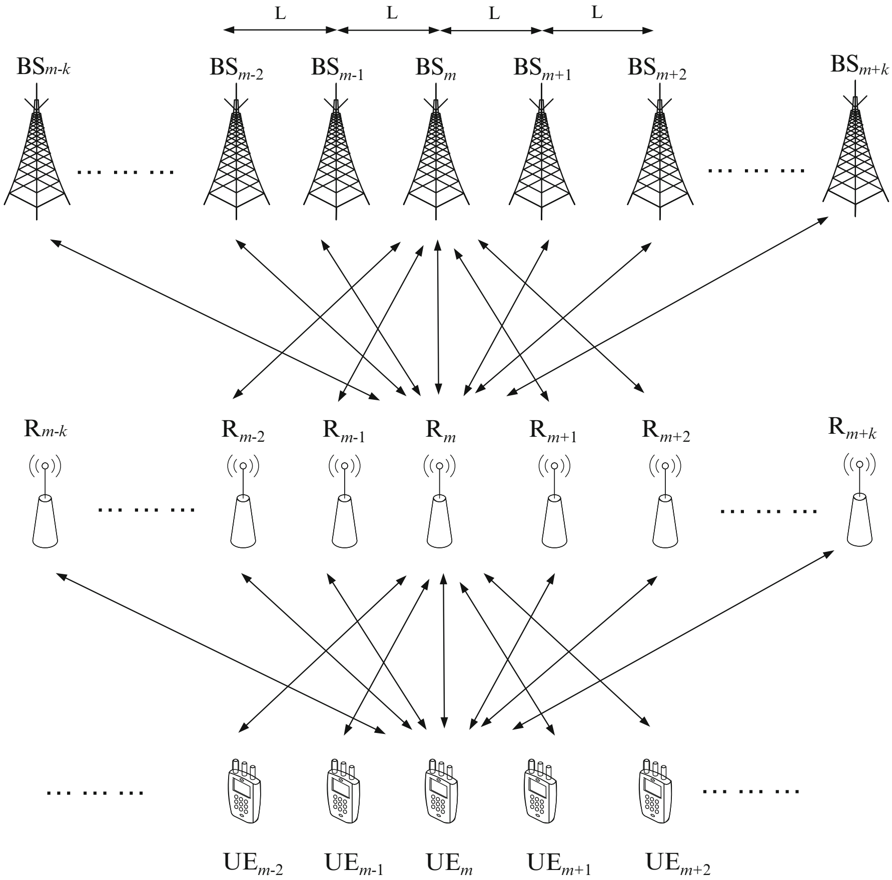

Fig. 2.35 Illustration of a multi-BS multi-relay network

2.8 Conclusion

The multipoint cooperative communication is not an isolated technology. Instead, it covers a very wide range of research topics. In order not to make our book become a magazine composed of fragmented chapters, we address the related work in a systematic way so that our selected topics in the following chapters are interconnected on a high level. After some warm-up discussions on the fundamentals and basic technologies of the modern wireless digital communication, recent research activities in multipoint cooperative communication are comprehensively addressed and analyzed in this chapter. Based on whether data sharing is conducted, whether CSI sharing is allowed, and whether TFSTR is operated, all the existing multipoint cooperative communication schemes are classified into eight categories. In the proposed framework of eight technology categories, the first four categories don't require sharing of CSI so that they treat the intercell interference as unpredictable and useless signals, leading to passive and simple multipoint cooperative communication schemes. On the other hand, the latter four categories take advantage of the multipoint CSI and perform more active signal processing functionalities in an interference-cognitive way. Among them, the last two categories of multipoint cooperations are particularly sophisticated because of the TFSTR feature, resulting in a high spectral efficiency. The following chapters will focus on the latter four technology categories.

References

3GPP (2008) TR 36.913: requirements for further advancements for E-UTRA (LTE-Advanced) (V8.0.0). Accessed 2008

3GPP (2010a) TS 36.213: physical layer procedures (V10.0.1). http://www.3gpp.org/ftp/Specs/archive/36_series/36.213/36213-a01.zip. Accessed 2010

3GPP (2010b) TR 36.814: further advancements for E-UTRA physical layer aspects (V9.0.0). http://www.3gpp.org/ftp/Specs/archive/36_series/36.814/36814-900.zip. Accessed 2010

3GPP (2010c) TS 36.423: X2 application protocol (X2AP) (V9.4.0). http://www.3gpp.org/ftp/Specs/archive/36_series/36.423/36423-940.zip. Accessed 2010

3GPP (2011a) TS 36.211 V10.1.0: physical channels and modulation (Release 10). http://www.3gpp.org/ftp/Specs/archive/36_series/36.211/36211-a10.zip. Accessed Mar 2011

3GPP (2011b) TR 36.819: coordinated multi-point operation for LTE (V2.0.0). http://www.3gpp.org/ftp/Specs/archive/36_series/36.819/36819-200.zip. Accessed Sept 2011

Abe T, Bauch G (2007) Differential codebook MIMO precoding technique. In: Global telecommunications conference, 2007. GLOBECOM 07. IEEE:3963–3968

Aktas E, Evans J, Hanly S (2008) Distributed decoding in a cellular multiple access channel. IEEE Trans Wireless Commun 7(1):241–250

Alamouti SM (1998) A simple transmit diversity technique for wireless communications. IEEE J Sel Area Commun 16(8):1451–1458

Alcatel-Lucent (2009) R1-091782: Estimation of extended PMI feedback signalling required for user intra-cell and inter-cell coordination. In: 3GPP TSG RAN WG1 #57 Meeting, San Francisco, USA, 4–8 May, 2009

Alpcan T, Basar T, Dey S (2006) A power control game based on outage probabilities for multicell wireless data networks. IEEE Trans Wireless Commun 5(4):890–899

Antonia MT (2004) Random matrix theory and wireless communications. Found Trends Commun Inform Theor 1(1):1–182

Bagheri H, Motahari AS, Khandani AK (2010) Zero-forcing for the symmetric interference channel with conferencing encoders. In: IEEE International Symposium Information Theory (ISIT), Austin, TX, USA, pp 370–374

Basar T, Olsder GJ (1999) Dynamic noncooperative game theory, 2nd edn, Classics in applied mathematics. SIAM, Philadelphia

Bhagavatula R, Heath RW (2011a) Adaptive bit partitioning for multicell intercell interference nulling with delayed limited feedback. IEEE Trans Signal Process 59(8):3824–3836

Bhagavatula R, Heath RW (2011b) Adaptive limited feedback for sum-rate maximizing beamforming in cooperative multicell systems. IEEE Trans Signal Process 59(2):800–811

Bingham JAC (2000) ADSL, VDSL, and multicarrier modulation. Wiley, New York. Accessed 2000

Blum RS (2003) MIMO capacity with interference. IEEE J Sel Area Commun 21(5):793–801

Boccardi F, Huang H (2006) Zero-forcing precoding for the MIMO broadcast channel under per-antenna power constraints. In: IEEE SPAWC, Cannes, France, 2006, pp 1–5
Boccardi F, Huang H (2007) Limited downlink network coordination in cellular networks. In: IEEE international symposium on personal indoor and mobile radio communication, Athens, Greece, pp 1–5
Cadambe VR, Jafar SA (2008) Interference alignment and degrees of freedom of the K-user interference channel. IEEE Trans Inform Theor 54(8):3425–3441
Caire G (2006) MIMO downlink joint processing and scheduling: a survey of classical and recent results. In: Workshop on information theory and its applications, Los Angeles, USA
Caire G, Shamai S (2003) On the achievable throughput of a multiantenna Gaussian broadcast channel. IEEE Trans Inform Theor 49(7):1691–1706
Caire G, Ramprashad S, Papadopoulos H, Pepin C, Sundberg C-E (2008) Multiuser mimo downlink with limited inter-cell cooperation: approximate interference alignment in time, frequency and space. In: IEEE annual Allerton conference on communication, control, and computing, Illinois, USA, 2008, pp 730–737
Catreux S, Driessen PF, Greenstein LJ (2000) Simulation results for an interference-limited multiple-input multiple-output cellular system. IEEE Commun Lett 4(11):334–336
Chandrasekhar V, Andrews JG, Gatherer A (2008) Femtocell networks: a survey. IEEE Commun Mag 46(9):59–67
Chang RW (1966) Synthesis of band-limited orthogonal signals for multichannel data transmission. Bell Syst Tech J 46:1775–1796
Choi W, Andrews JG (2008) The capacity gain from intercell scheduling in multi-antenna systems. IEEE Trans Wireless Commun 7(2):714–725
Choi LU, Murch RD (2004) A transmit preprocessing technique for multiuser MIMO systems using a decomposition approach. IEEE Trans Wireless Commun 3(1):20–24
Claussen H, Ho LTW, Samuel LG (2008) An overview of the femtocell concept. Bell Labs Tech J 13(1):221–245
Clerckx B, Zhou YX, Kim S (2008) Practical codebook design for limited feedback spatial multiplexing, communications. In: IEEE international conference on communications, Beijing, China, pp 3982–3987
Costa M (1983) Writing on dirty paper. IEEE Trans Inform Theor 29(3):439–441
Cover TM, Thomas JA (1991) Elements of information theory. Wiley-Interscience, New York
Dahrouj H, Yu W (2008) Coordinated beamforming for the multi-cell multi-antenna wireless system. In: IEEE Conference on Information Sciences and Systems (CISS), Princeton, NJ, USA, pp 429–434
Dahrouj H, Yu W (2010) Coordinated beamforming for the multicell multi-antenna wireless system. IEEE Trans Wireless Commun 9(5):1748–1759
Das D, Viswanathan H, Rittenhouse G (2003) Dynamic load balancing through coordinated scheduling in packet data systems. INFOCOM 2003, Twenty-Second annual joint conference of the IEEE computer and communications, San Francisco, USA, 2003, pp 786–796
Dighe PA, Mallik K, Jamuar SS (2003) Analysis of transmit-receive diversity in Rayleigh fading. IEEE Trans Commun 51(4):694–703
Erez U, Shamai S, Zamir R (2005) Capacity and lattice strategies for canceling known interference. IEEE Trans Inform Theor 51(1):3820–3833
Ericsson (2007) R1-074444: on inter-cell interference coordination schemes without/with traffic load indication. In: 3GPP TSG-RAN WG1 meeting #50-bis, Shanghai, China, 8–12 Oct 2007
Ericsson (2009) On CSI feedback for ITU requirement fulfilling CoMP schemes. In: 3GPP, R1-092024. Accessed 2009
Etkin R, Tse D, Wang H (2008) Gaussian interference channel capacity to within one bit. IEEE Trans Inform Theor 54(12):5534–5562
ETSI (2001) ETSI EN 300 744. Digital Video Broadcasting (DVB): Framing structure, channel coding and modulation for digital terrestrial television. http://www.etsi.org/deliver/etsi_en/300700_300799/300744/01.05.01_40/en_300744v010501o.pdf. Accessed 2001

Foschini GJ (1996) Layered space-time architecture for wireless communication in fading environments when using multi-element antennas. Bell Lab Tech J 1(2):41–59

Foschini GJ, Golden GD, Valenzuela RA, Wolniansky PW (1999) Simplified processing for high spectral efficiency wireless communication employing multi-element arrays. IEEE J Sel Area Commun 17(11):1841–1852

Fujitsu Limited (2012) RWS-120016: requirements and technical considerations for RAN Rel.12 & onwards. In: 3GPP workshop on Release 12 Onward, Ljubljana, Slovenia, 11–12 June 2012. http://www.3gpp.org/ftp/workshop/2012-06-11_12_RAN_REL12/Docs/RWS-120016.zip

Gesbert D, Kiani SG, Gjendemsjø A, Øien GE (2007a) Adaptation, coordination, and distributed resource allocation in interference-limited wireless networks. Proc IEEE 95(12):2393–2409

Gesbert D, Kountouris M, Heath R, Chae C-B, Salzer T (2007b) Shifting the MIMO paradigm. IEEE Signal Process Mag 24(5):36–46

Gesbert D, Hanly S, Huang H, Shamai S, Simeone O, Wei Y (2010) Multi-cell MIMO cooperative networks: a new look at interference. IEEE J Sel Area Commun 28(9):1380–1408

Gjendemsjoe A, Gesbert D, Oien G, Kiani S (2008) Binary power control for sum rate maximization over multiple interfering links. IEEE Trans Wireless Commun 7(8):3164–3173

Gomadam K, Cadambe VR, Jafar SA (2008) Approaching the capacity of wireless networks through distributed interference alignment. IEEE global communications conference, New Orleans, USA, 2008, pp 1–6

GSM ETSI TC-SMG (1996) Digital cellular telecommunication system (Phase 2) Principles of telecommunication services supported by a GSM Public Land Mobile Network (PLMN). Accessed March 1996. http://www.etsi.org/deliver/etsi_gts/02/0201/05.01.00_60/gsmts_0201v050100p.pdf

Guan W, Luo HW (2008) Joint MMSE transceiver design in non-regenerative MIMO relay systems. IEEE Commun Lett 12(7):517–519

Han Z, Ji Z, Liu KJR (2007) Non-cooperative resource competition game by virtual referee in multi-cell OFDMA networks. IEEE J Sel Area Commun 25(6):1079–1090

Hanly SV (1996) Capacity and power control in spread spectrum macrodiversity radio networks. IEEE Trans Commun 44(2):247–256

Hanly SV, Whiting PA (1993) Information-theoretic capacity of multi-receiver networks. Telecommun Syst 1(1):1–42

Hari S, Yu W (2010) Partial zero-forcing precoding for the interference channel with partially cooperating transmitters. In: IEEE International Symposium Information Theory (ISIT), Austin, Texas, 2010, pp 2283–2287

Hong YW, Huang WJ, Chiu FH, Kuo CCJ (2007) Cooperative communications in resource-constrained wireless networks. IEEE Signal Process Mag 24(3):47–57

Hoydis J, Kobayashi M, Debbah M (2010) On the optimal number of cooperative base stations in network MIMO systems. http://adsabs.harvard.edu/abs/2010arXiv1003.0332H

Huawei (2005a) Inter-cell interference mitigation. In: 3GPP, R1-050629. Accessed 2005

Huawei (2005b) Soft frequency reuse scheme for UTRAN LTE. In: 3GPP, R1-050507. Accessed 2005

Huawei (2008a) Some results on DL coordinated beam switching for interference management in LTE- Advanced. In: 3GPP, R1-084352. Accessed 2008

Huawei (2008b) DL coordinated beam switching for interference management in LTE-advanced. In: 3GPP, R1-083236. Accessed 2008

Huh H, Papadopoulos H, Caire G (2009) MIMO broadcast channel optimization under general linear constraints. In: IEEE International Symposium Information Theory (ISIT), Seoul, Korea, 2009: 2664–2668

IEEE (1999) Standard 802.11a. Part 11: Wireless LAN Medium Access Control (MAC) and Physical Layer (PHY) specifications: high-speed physical layer in 5 GHz Band. Accessed 1999

Jafar SA, Foschini G, Goldsmith AJ (2004) Phantomnet: exploring optimal multicellular multiple antenna systems. EURASIP J Appl Signal Process, 2004(1):591–604

Jindal N (2006) MIMO broadcast channels with finite-rate feedback. IEEE Trans Inform Theor 52(11):5045–5060

Jing Y, Hassibi B (2006) Distributed space-time coding in wireless relay networks. IEEE Trans Wireless Commun 5:2006

Jing S, Tse DNC, Soriaga JB, Hou J, Smee JE, Padovani R (2007) Downlink macro-diversity in cellular networks. In: IEEE international symposium on information theory, Glasgow, Scotland, 2007, pp 1–5

Jing S, Tse DNC, Hou J, Soriaga JB, Smee JE, Padovani R (2008) Multi-cell downlink capacity with coordinated processing. In: EURASIP J Wireless Commun Network, Vienna, Austria, 2008: Article ID: 586878

Jorswieck E, Larsson EG, Danev D (2008) Complete characterization of the Pareto boundary for the MISO interference channel. IEEE Trans Signal Process 56(10):5292–5296

Karakayali M, Foschini G, Valenzuela R (2006) Network coordination for spectrally efficient communications in cellular systems. IEEE Wireless Commun 13(4):56–61

Karakayali K, Yates R, Foschini G, Valenzuela R (2007) Optimum zero-forcing beamforming with per-antenna power constraints. In: IEEE international symposium information theory, Nice, France, 2007, pp 101–105

Katranaras E, Imran M, Hoshyar R (2009) Sum-rate of linear cellular systems with clustered joint processing. IEEE Veh Technol Conf 8(4):1910–1921

Katti S, Gollakota S, Katabi D (2007) Embracing wireless interference: analog network coding. ACM SIGCOMM, September 2007, pp 397–408

Kiani SG, Gesbert D (2008) Optimal and distributed scheduling for multicell capacity maximization. IEEE Trans Wireless Commun 7(1):288–297

Kiani SG, Gesbert D, Øien GE (2007) Maximizing multi-cell capacity using distributed power allocation and scheduling. IEEE wireless communications and networking conference, 2007, pp 1690–1694

Kim JH, Park SY, Love DJ (2007) Partial channel state information unitary precoding and codebook design for MIMO broadcast systems. In: Global telecommunications conference, 2007. GLOBECOM 07. IEEE, pp 1607–1611

Kim D, Shin OS, Sohn I, Lee KB (2012) Channel feedback optimization for network MIMO systems. IEEE Trans. Vehicular Technology 2012

Knopp R, Humblet P (1995) Information capacity and power control in single cell multiuser communications. IEEE Int Conf Commun 1:331–335

Koike AT, Popovski P, Tarokh V (2009) Optimized constellations for two–way wireless relaying with physical network coding. IEEE J Sel Area Commun 27(5):773–787

Laneman JN, Wornell GW (2003) Distributed space-time-coded protocols for exploiting cooperative diversity in wireless networks. IEEE Trans Inform Theor 49(10):2415–2425

Laneman JN, Tse DNC, Wornell GW (2004) Cooperative diversity in wireless networks: efficient protocols and outage behavior. IEEE Trans Inform Theor 50(12):3062–3080

Lau V, Liu Y, Chen TA (2004) On the design of MIMO block-fading channels with feedback-link capacity constraint. IEEE Trans Commun 52(1):62–70

Lee M, Keum B, Lee HS, Kim JW (2008) A radio repeater interference cancellation model for mobile communication systems. In: Wireless and mobile communications, 27 July –1 Aug 2008, pp 376–381

Lindblom J, Karipidis E, Larsson EG (2009) Elfishness and altruism on the MISO interference channel: the case of partial transmitter CSI. IEEE Commun Lett 13(9):667–669

Liu W, Ng SX, Hanzo L (2009) Multicell cooperation based SVD assisted multi-user MIMO transmission. In: IEEE vehicular technology conference, Barcelona, Spain, 2009, pp 1–5

Love DJ, Heath RW (2003) Equal gain transmission in multiple-input multiple-output wireless systems. IEEE Trans Commun 51(7):1102–1110

Love D, Heath R, Lau V, Gesbert D, Rao B, Andrews M (2008) An overview of limited feedback in wireless communication systems. IEEE J Sel Areas Commun 26(8):1341–1365

Luo ZQ, Zhang S (2008) Dynamic spectrum management: complexity and duality. IEEE J Sel Topics Signal Process 2(10):57–73

MacDonald VH (1979) The cellular concept. Bell Syst Tech J 58(1), January 1979. http://www.alcatel-lucent.com/bstj/vol58-1979/articles/bstj58-1-15.pdf

Mai V, Paulraj A (2007) MIMO wireless linear precoding. IEEE Signal Process Mag 24(5):86–105
Marsch P, Fettweis G (2007) A framework for optimizing the uplink performance of distributed antenna systems under a constrained backhaul. In: IEEE international conference on communications, Glasgow, Scotland, 2007, pp 975–979
Medina OM, Vidal J, Agustin A (2007) Linear transceiver design in nonregenerative relays with channel state information. IEEE Trans Signal Process 55(6):2593–2604
Moon SH, Kim JS, Lee I (2010) Limited feedback design for block diagonalization MIMO broadcast channels with user scheduling. In: IEEE global communications conference, 2010, pp 1–5
Munoz O, Vidal J, Agustin A (2007) Linear transceiver design in no regenerative relays with channel state information. IEEE Trans Signal Proces 55:2593–2604
Ng B, Evans J, Hanly S (2004) Distributed linear multiuser detection in cellular networks based on Kalman smoothing. In: IEEE Globecom, Dallas, Texas, USA, 2004, 134–138
Ozdemir O, Torlak M (2006) Performance of opportunistic beamforming with quantized feedback. In: Global telecommunications conference, 2006, pp 1–5
Pabst R, Walke BH, Schultz DC, Yanikomeroglu H, Mukherjee S, Viswanathan H, Lett M, Zirwas W, Dohler M, Aghvami H, Falconer DD, Fettweis GP (2004) Relay-based deployment concepts for wireless and mobile broadband radio. IEEE Commun Mag 42(9):80–89
Palomar DP, Cioffi JM, Lagunas MA (2003) Joint Tx-Rx beamforming design for multicarrier MIMO channels: a unified framework for convex optimization. IEEE Trans Signal Process 51(9):2381–2401
Pan ZG, Wong KK, Ng TS (2004) Generalized multiuser orthogonal space division multiplexing. IEEE Trans Wireless Commun 3(6):1969–1973
Papadogiannis A, Gesbert D, Hardouin E (2008) A dynamic clustering approach in wireless networks with multi-cell cooperative processing. In: IEEE international conference on communication (ICC), Beijing, China, 2008, pp 4033–4037
Peel CB, Hochwald B, Swindlehurst AL (2005) A vector perturbation technique for near capacity multi-antenna multi-user communication–Part I: channel inversion and regularization. IEEE Trans Commun 53(1):195–202
Peled A, Ruiz A (1980) Frequency domain data transmission using reduced computational complexity algorithms. IEEE Int Conf Acoust Speech Signal Process 5:964–967
Peters SW, Health RW (2009) Interference alignment via alternating minimization. IEEE international conference on acoustics, speech and signal processing, Taipei, Taiwan, 2009:2445–2448
Proakis JG (2001) Digital communication. McGraw-Hill, New York
Ravindran N, Jindal N (2008) Limited feedback-based block diagonalization for the MIMO broadcast channel. IEEE J Sel Area Commun 26(8):1473–1482
Rong Y, Gao F (2009) Optimal beamforming for non-regenerative MIMO relays with direct link. IEEE Commun Lett 13:926–928
Saad W, Han Z, Debbah M, Hjorungnes A, Basar T (2009) Coalitional game theory for communication networks [A tutorial]. IEEE Signal Process Mag Special Issue Game Theor 26(5):77–97
Sadek M, Tarighat A, Sayed AH (2007) A leakage-based precoding scheme for downlink multi-user MIMO channels. IEEE Trans Wireless Commun 6(5):1711–1721
Sampei S, Harada H (2007) System design issues and performance evaluations for adaptive modulation in new wireless access systems. Proc IEEE 85(12):2456–2471
Sanayei S, Nosratinia A et al (2007) Opportunistic beamforming with limited feedback. IEEE Trans Wireless Commun 6(8):2765–2771
Sang A, Wang X, Madihian M, Gitlin RD (2008) Coordinated load balancing, handoff/cell-site selection, and scheduling in multi-cell packet data systems. Wireless Netw 14(1):103–120
Santipach W, Honig ML (2004) Asymptotic capacity of beamforming with limited feedback. In: IEEE international symposium on information theory (ISIT), June 2004, pp 289
Schubert M, Boche H (2004) Solution of the multiuser downlink beamforming problem with individual SINR constraints. IEEE Trans Veh Technol 53(1):18–28
Sesia S, Toufik I, Baker M (2009) LTE: the UMTS long term evolution. Wiley, Somerset

Shamai S, Zaidel B (2001) Enhancing the cellular downlink capacity via co-processing at the transmitting end. IEEE Veh Technol Conf 3:1745–1749

Shang X, Chen B, Gans MJ (2006) On the achievable sum rate for MIMO interference channels. IEEE Trans Inform Theor 52(9):4313–4320

Sharif M, Hassibi B (2007) A comparison of time-sharing, DPC, and beamforming for MIMO broadcast channels with many users. IEEE Trans Commun 55(1):11–15

Shi C, Berry RA, Honig ML (2008) Distributed interference pricing for OFDM wireless networks with non-separable utilities. In: IEEE Conference on Information Sciences and Systems (CISS), 2008, pp 755–760

Shim S, Kwak JS, Heath RW, Andrews JG (2008) Block diagonalization for multi-user MIMO with other-cell interference. IEEE Trans Wireless Commun 7(7):267–2681

Simeone O, Somekh O, Bar-Ness Y, Spagnolini U (2007) Uplink throughput of TDMA cellular systems with multicell processing and amplify-and-forward cooperation between mobiles. IEEE Trans Wireless Commun 6(8):2942–2951

Simeone O, Somekh O, Kramer G, Shamai S, Poor HV (2008a) Cellular systems with multicell processing and conferencing links between mobile stations. Information theory and applications workshop, 2008, pp 361–365

Simeone O, Somekh O, Kramer G, Poor HV, Shamai S (2008b) Uplink sum-rate analysis of a multi-cell system with feedback. In: IEEE annual Allerton conference on communication, control, and computing, Monticello, USA, 2008, pp 1030–1036

Simeone O, Somekh O, Poor HV, Shamai S (2009) Downlink multicell processing with limited backhaul capacity. EURASIP J Adv Signal Proc: article ID: 840814

So J, Cioffi JM (2009) Feedback reduction scheme for downlink multiuser diversity. IEEE Trans Wireless Commun 8(2):668–672

Somekh O, Zaidel B, Shamai S (2007a) Sum rate characterization of joint multiple cell-site processing. IEEE Trans Inform Theor 53(12):4473–4497

Somekh O, Simeone O, Poor HV, Shamai S (2007b) Cellular systems with full-duplex amplify-and-forward relaying and cooperative basestations. In: IEEE international symposium on information theory, 2007, pp 16–20

Somekh O, Simeone O, Bar-Ness Y, Haimovich A, Shamai S (2009) Cooperative multi-cell zero-forcing beamforming in cellular downlink channels. IEEE Trans Inform Theor 55(7):3206–3219

Spencer QH, Swindlehurst AL, Haardt M (2004) Zero-forcing methods for downlink spatial multiplexing in multiuser MIMO channels. IEEE Trans Signal Process 52(2):461–471

Stefanov A, Erkip E (2004) Cooperative coding for wireless networks. IEEE Trans Wireless Commun 52(9):1470–1476

Stojnic M, Vikalo H, Hassibi B (2006) Maximizing the sum-rate of multiantenna broadcast channels using linear preprocessing. IEEE Trans Wireless Commun 5(9):2338–2342

Stolyar AL, Viswanathan H (2008) Self-organizing dynamic fractional frequency reuse in OFDMA systems. In: IEEE conference on computer and communications (INFOCOM), 2008: 691–699

Stolyar AL, Viswanathan H (2009) Self-organizing dynamic fractional frequency reuse for besteffort traffic through distributed inter-cell coordination. IEEE Conference on Computer Communications (INFOCOM), 2009, pp 1287–1295

Sun Y, Honig ML (2003a) Asymptotic capacity of multicarrier transmission over a fading channel with feedback. In: Proceedings of the IEEE international symposium on information Theory, June–July 2003, 40

Sun Y, Honig ML (2003b) Minimum feedback rates for multicarrier transmission with correlated frequency-selective fading. Proc IEEE Glob Telecom Conf 3:1628–1632

Taesang Y, Jindal N, Goldsmith A (2007) Multi-antenna downlink channels with limited feedback and user selection. IEEE J Select Area Commun 25(7):1478–1491

Tang XJ, Hua YB (2007) Optimal design of non-regenerative MIMO wireless relays. IEEE Trans Wireless Commun 6(4):1398–1407

Tarokh V, Jafarkhani H, Calderbank AR (1999) Space–time block codes from orthogonal designs. IEEE Trans Inform Theory 45(5):1456–1467

Telatar EI (1999) Capacity of multi-antenna Gaussian channels. Europ Trans Telecommun 10(6):585–595

Texas Instruments (2009) Implicit feedback in support of downlink MU-MIMO. In: 3GPP, R1-093997. Accessed 2009

Thoen S, Perre LV, Gyselinckx B, Engels M (2001) Performance analysis of combined transmit-SC/receive-MRC. IEEE Trans Commun 49(1):5–8

Tralli V, Veronesi R, Zorzi M (2004) Power-shaped advanced resource assignment (PSARA) for fixed broadband wireless access systems. IEEE Trans Wireless Commun 3(6):2207–2220

Tse D, Viswanath P (2005) Fundamentals of wireless communication. Cambridge University Press, Cambridge

Vemula M, Avidor D, Ling J, Papadias C (2006) Inter-cell coordination, opportunistic beamforming and scheduling. IEEE Int Conf Commun 12:5319–5324

Venkatesan S, Lozano A, Valenzuela R (2007) Network mimo: overcoming intercell interference in indoor wireless systems. In: IEEE Asilomar conference on signals, systems and computers, Monterey, California, USA, 2007, pp 83–87

Venturino L, Prasad N, Wang X (2009) Coordinated scheduling and power allocation in downlink multicell OFDMA networks. IEEE Trans Veh Technol 58(6):2835–2848

Vishwanath S, Jindal N, Goldsmith A (2003) Duality, achievable rates, and sum-rate capacity of MIMO broadcast channels. IEEE Trans Inform Theor 49(10):2658–2668

Viswanath P, Tse DN (2003) Sum capacity of the vector Gaussian broadcast channel and uplink-downlink duality. IEEE Trans Inform Theor 49(8):1912–1921

Viswanath P, Tse D, Laroia R (2002) Opportunistic beamforming using dumb antennas. IEEE Trans Inform Theor 48(6):1277–1294

Viterbi AJ, Viterbi AM, Gilhousen KS, Zehavi E (1994) Soft handoff extends CDMA cell coverage and increases reverse link capacity. IEEE J Sel Area Commun 12(8):1281–1288

Wang F, Krunz M, Cui S (2008) Price-based spectrum management in cognitive radio networks. IEEE J Sel Topics Signal Process 1(2):74–87

Weingarten H, Steinberg Y, Shamai S (2004) The capacity region of the Gaussian MIMO broadcast channel. In: Conference on information sciences and systems, Princeton, New Jersey, USA, 2004, p 174

Weingarten H, Steinberg Y, Shamai S (2006) The capacity region of the Gaussian multiple-input multiple-output broadcast channel. IEEE Trans Inform Theor 52(9):3936–3964

Weinstein SB, Ebert PM (1971) Data transmission by frequency-division multiplexing using the discrete Fourier transform. IEEE Trans Commun Technol 19(5):628–634

Wimax Forum (2006) Mobile WiMAX–Part I: a technical overview and performance evaluation. Accessed 2006

Winters JH, Salz J, Gitlin RD (1994) The impact of antenna diversity on the capacity of wireless communication systems. IEEE Trans Commun 42(2,3,4):1740–1751

Wolniansky PW, Foschini GJ, Golden GD, Valenzuela RA (1998) V-BLAST: an architecture for realizing very high data rates over the rich-scattering wireless channel. In: International symposium on signals, systems, and electronics, 1998, Pisa, Italy, pp 295–300

Wu Y, Luo H, Ding M, Zou J, Li X (2011) Efficient limited feedback for MIMO-relay systems. IEEE Comm Lett 15(2):181–183

Wyner AD (1994) Shannon-theoretic approach to a Gaussian cellular multiple-access channel. IEEE Trans Inform Theor 40(6):1713–1727

Xu W, Zhao C, Ding Z (2008) Optimisation of limited feedback design for heterogeneous users in multi-antenna downlinks. IET Commun 3(11):1724–1735

Yao Y, Giannakis GB (2005) Rate-maximizing power allocation in OFDM based on partial channel knowledge. IEEE Trans Wireless Commun 4(3):1073–1083

Yildirim SA, Safak M, Yanlk ME (2010) Diversity loss-array gain tradeoff in doubly correlated MIMO beamforming systems. In: Signal processing and communications applications conference (SIU), 22–24 April 2010, pp 415–418

Yoo T, Goldsmith A (2006) On the optimality of multianntenna broadcast scheduling using zero-forcing beamforming. IEEE Trans Sel Area Commun 24(3):528–541

Yu W, Cioffi JM (2004) Sum capacity of Gaussian vector broadcast channels. IEEE Trans Inform Theor 50(9):1875–1892
Yu W, Lan T (2007) Transmitter optimization for the multi-antenna downlink with per-antenna power constraints. IEEE Trans Signal Process 55(6):2646–2660
Yu W, Varodayan DP, Cioffi JM (2005) Trellis and convolutional precoding for transmitter-based interference presubtraction. IEEE Trans Commun 53(7):1220–1230
Yu H, Park J, Sung Y, Lee YH (2009) A least squares approach to joint beam design for interference alignment in multiuser interference channels. IEEE international workshop on signal processing advances in wireless communications, 2009, pp 593–597
Yu W, Kwon T, Shin C (2010) Joint scheduling and dynamic power spectrum optimization for wireless multicell networks. In: IEEE Conference on Information Sciences and Systems (CISS), 2010, pp 1–6
Zakhour R, Gesbert D (2010) On the value of data sharing in constrained-backhaul network MIMO. In: International Zurich seminar on communications, Zurich, Switzerland, 2010
Zakhour R, Ho ZKM, Gesbert D (2009) Distributed beamforming coordination in multicell MIMO channels. In: IEEE vehicular technology conference (VTC), 2009: 1–5
Zhang R (2010) Multi-cell block diagonalization with per-base-station power constraints. IEEE J Sel Area Commun 28(9):1435–1445
Zhang H, Dai H (2004) Cochannel interference mitigation and cooperative processing in downlink multicell multiuser MIMO networks. EURASIP J Wireless Commun Netw – Special issue on multiuser MIMO networks, 2004(2):222–235
Zhang H, Dai H, Zhou Q (2004) Base station cooperation for multiuser MIMO: joint transmission and BS selection. In: Conference on Information Sciences and Systems (CISS), 2004, pp 1–6
Zhang J, Chen R, Andrews JG, Heath RW (2007) Coordinated multi-cell MIMO systems with cellular block diagonalization. In: Asilomar Conference on signals, systems and computers, 2007, pp 1669–1673
Zhang H, Mehta NB, Molisch AF, Zhang J, Dai H (2008) Asynchronous interference mitigation in cooperative base station systems. IEEE Trans Wireless Commun 7(1):155–165
Zhang J, Andrews JG, Heath RW (2009a) Block diagonalization in the MIMO broadcast channel with delayed CSIT. In: IEEE global communications conference, 2009, pp 1–6
Zhang L, Zhang R, Liang Y C, Xin Y, Poor HV (2009b) On the Gaussian MIMO BC-MAC duality with multiple transmit covariance constraints. In: IEEE International Symposium on Information Theory (ISIT), 2009, pp 2502–2506
Zhang J, Chen R, Andrews J, Ghosh A, Heath RW (2009c) Networked MIMO with clustered linear precoding. IEEE Trans Wireless Commun 8(4):1910–1921
Zhang J, Kountouris M, Andrews JG, Heath RW (2011) Multi-mode transmission for the MIMO broadcast channel with imperfect channel state information. IEEE Trans Commun 59(3):803–814
Zheng L, Tse DNC (2003) Diversity and multiplexing: a fundamental tradeoff in multiple antenna channels. IEEE Trans Inform Theor 49(5):1073–1096
Zheng X, Xie Y, Li J, Stoica P (2007) MIMO transmit beamforming under uniform elemental power constraint. IEEE Trans Signal Process 55(11):5395–5406

Chapter 3
The Sixth Category: Antenna Selection Technologies

Abstract For the sixth category of multipoint cooperative communication technology, we address the relay/antenna selection schemes for the amplify-and-forward (AF) multiple-input multiple-output (MIMO) relay network in this chapter. First, we discuss the system model of an AF MIMO relay network as well as the value of relay/antenna selection when joint relay precoding cannot be operated. Second, we review the existing relay/antenna selection algorithms and present our motivations of improving the existing schemes. Third, we propose three greedy relay/antenna selection algorithms, that is, doubly zero-forcing (ZF) greedy capacity maximization (DZF-GCM), greedy capacity maximization (GCM), and greedy mean square error (MSE) minimization (GMM) algorithms, to optimize the system based on various performance metrics. The effectiveness of the proposed schemes is corroborated by our simulation results followed by comprehensive discussions on the performance comparison of various algorithms to provide more insights on this topic.

Keywords AF MIMO relay • Antenna selection • Relay selection • Capacity • MSE

3.1 Introduction

The sixth category of multipoint cooperative communication technology has been discussed in Sect. 2.7.6, wherein we have described the key feature of the multiple-input multiple-output (MIMO) relay systems, that is, applying multi-antenna technologies on relay node(s). In a MIMO relay system, both the backward and forward channels are MIMO channels, and hence the system capacity can be largely boosted

M. Ding and H. Luo, *Multi-point Cooperative Communication Systems: Theory and Applications*, Signals and Communication Technology, DOI 10.1007/978-3-642-34949-2_3,

by multiplexing multiple data streams over the two-hop transmissions. However, interstream interference may largely degrade the system performance (Tang and Hua 2007).

Employing precoding technique at the relay node and/or BS can effectively mitigate the interstream interference. A great many of works (Fan and Thompson 2007; Medina et al. 2007; Guan and Luo 2008) have been devoted to solve the optimal precoding problem for the conventional three-point model, that is, one source, one destination, and one relay node (see Sect. 2.4.2). However, in the scenario where multiple MIMO relays are deployed, multi-relay precoding operation requires that relay nodes should be equipped with at least as many antennas as the source and destination nodes to perform interference-suppressing functions. Unfortunately, this may not be a realistic assumption since in practice, especially for cellular networks, relay basically serves as a low-cost and low complexity means to extend the system coverage and improve the spectral efficiency for cell-edge UEs (Pabst et al. 2004). Besides, multi-relay precoding is usually of very high complexity and falls into the eighth category of multipoint cooperative communication technology addressed in Sect. 2.7.8. Therefore, in a system where advanced signal processing cannot be relegated to relay nodes, relay/antenna selection becomes an efficient alternative to extract the performance gains offered by multiple MIMO relays.

Recently, selection techniques have already seen some interesting activities for the amplify-and-forward (AF) MIMO relay networks but mostly limited to single-antenna relay models (Michalopoulos et al. 2008) or limited to single-stream MIMO relay networks (Peters and Heath 2008). Regarding antenna selection for multi-stream AF MIMO relay networks, the authors of Torabi and Frigon (2008) presented an iterative antenna selection scheme based on semi-orthogonality (S-O) among antenna pairs of the relays for a system model where ZF processing is performed at the source and destination nodes. The idea was similar to that in the semi-orthogonal user selection algorithm (Yoo and Goldsmith 2006) for the MIMO broadcast channel (BC) model. Besides, the authors of Torabi and Frigon (2008) proved that the network capacity scales double-logarithmically with the number of relay nodes, which is inferior to the logarithmical capacity scaling law achieved by the “doubly coherent” relaying protocol in Bolcskei et al. (2006) and Nabar et al. (2003). In Zhang and Letaief (2008), another heuristic relay/antenna selection criterion based on harmonic mean of dual-hop sub-channel gains was proposed, which was called distributed orthogonal relay selection (DORS) algorithm. Although the schemes in Torabi and Frigon (2008) and Zhang and Letaief (2008) were effective and of low complexity, the noise terms were ignored in the deductions, which might not be realistic due to the use of noisy power amplifiers (PAs) at the relay nodes. Moreover, instead of using heuristic criteria as in Torabi and Frigon (2008) and Zhang and Letaief (2008), it would be better to develop antenna selection algorithms based on various performance metrics in closed forms and investigate whether the logarithmical capacity scaling law still holds.

3.2 System Model and Existing Technologies

3.2.1 System Model

The system model of an AF MIMO relay network is illustrated in Fig. 3.1, where the source node **S**, destination node **D,** and each relay node $\mathbf{R}_k$ ($k \in \{1, 2, \ldots, K\}$) are equipped with N_s, N_d, and N_r antennas, respectively. $\mathbf{H}_k \in \mathbb{C}^{N_r \times N_s}$ and $\mathbf{G}_k \in \mathbb{C}^{N_d \times N_r}$ denote the backward channels (link from **S** to $\mathbf{R}_k$) and the forward channels (link form $\mathbf{R}_k$ to **D**). All the channels are modeled as block flat fading entries. In this chapter, we only focus on time division duplex (TDD) relaying with the AF protocol, that is, the transmission time interval is divided into two time slots. The first and the second time slot of which are assigned to the backward and the forward transmission, respectively. We also assume that there is no direct link from node **S** to **D** due to long-distance pathloss. It should be noted that if the source node **S** is removed, then the AF MIMO relay model shown in Fig. 3.1 will degenerate to a multi-BS model, and thus the relay/antenna selection schemes discussed in this chapter can be easily adapted to BS/antenna selection schemes for a multi-BS scenario. It should also be noted that if each relay node is equipped with only one antenna, then the antenna selection schemes addressed in the following can be regarded as relay selection schemes.

During the first time slot, L antennas are selected from KN_r relay antennas to receive L data streams sent from **S**. Denote the L antennas are associated with a relay set $\Gamma = \{r(1), r(2), \ldots, r(L)\}$. Note that Γ may contain duplicated elements since more than one antenna can be selected from a single MIMO relay. To illustrate the relationship among L, N_s, N_d, and N_r, we take a practical example that $KN_r \geq N_s, N_d$. Thereby, the multiplexing gain (see Sect. 2.3.1) of the interested system will be limited by $M = \min\{N_s, N_d\}$. If full multiplexing gain is achieved between **S** and **D**, L should be no less than M in order to make the equivalent two-hop relay channel well conditioned.

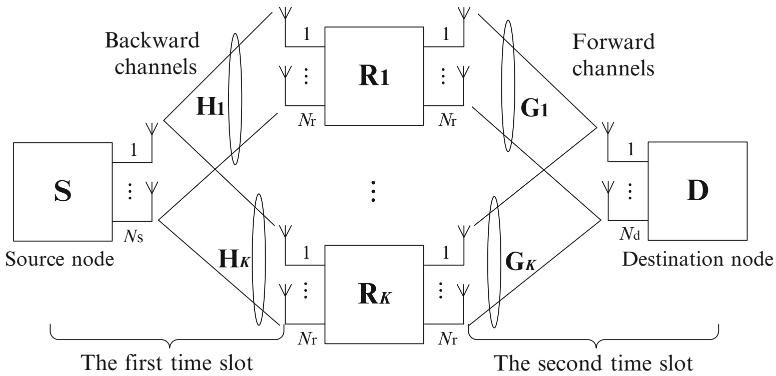

Fig. 3.1 Schematic model of an AF MIMO relay network

Let $\mathbf{H} \in \mathbb{C}^{L\times N_\mathrm{s}}$ represent the compound backward channel. Then we can write $\mathbf{H} = \left[\mathbf{h}^\mathrm{T}_{(b(1),r(1))}, \mathbf{h}^\mathrm{T}_{(b(2),r(2))}, \ldots, \mathbf{h}^\mathrm{T}_{(b(L),r(L))}\right]^\mathrm{T}$, where we use an indices pair $(b(i), r(i))(i \in \{1, 2, \ldots, L\})$ to indicate antenna $b(i)$ mounted on relay $r(i)$ for the i-th selected backward antenna, and $\mathbf{h}_{(b(i),r(i))} \in \mathbb{C}^{1\times N_\mathrm{s}}$ is the channel vector of $\mathbf{S}$ to the i-th selected backward antenna. Let the received signals at L selected antennas be stacked into a vector $\mathbf{r} = [r_1, r_2, \ldots, r_L]^\mathrm{T}$, which is given by

$$\mathbf{r} = \mathbf{HFx} + \mathbf{n}_\mathrm{r}, \tag{3.1}$$

where $\mathbf{x} \in \mathbb{C}^{L\times 1}$ is the transmit signal vector with covariance matrix $\mathrm{E}\left\{\mathbf{x}\mathbf{x}^\mathrm{H}\right\} = \mathbf{I}_L$. $\mathbf{F} \in \mathbb{C}^{N_\mathrm{s}\times L}$ is the precoding matrix employed at $\mathbf{S}$, and $\mathbf{n}_\mathrm{r} \in \mathbb{C}^{L\times 1}$ denotes the zero-mean circularly symmetric complex Gaussian (ZMCSCG) noise vector with covariance matrix $\mathrm{E}\left\{\mathbf{n}_\mathrm{r}\mathbf{n}_\mathrm{r}^\mathrm{H}\right\} = \mathbf{I}_L$. If we incorporate the pathloss and shadowing factor into the total transmit power P_s available at $\mathbf{S}$, the long-term power constraint can be written as

$$\begin{aligned} \mathrm{E}\left\{\mathrm{tr}\left\{\mathbf{Fx}(\mathbf{Fx})^\mathrm{H}\right\}\right\} &= \mathrm{tr}\left\{\mathbf{F}\mathbf{F}^\mathrm{H}\right\} \\ &\le P_\mathrm{s}. \end{aligned} \tag{3.2}$$

In the second time slot, $\mathbf{S}$ keeps silent while relays in Γ amplify and forward the received signal to $\mathbf{D}$. The AF relays' amplifying function can be represented by a diagonal matrix $\mathbf{W} \in \mathbb{C}^{L\times L}$, whose scalar diagonal element $w_i (i \in \{1, 2, \ldots, L\})$ is the gain associated with relay antenna $(f(i), r(i))$. Here, $(f(i), r(i))$ stands for the i-th selected forward antenna, that is, antenna $f(i)$ of relay $r(i)$. It should be pointed out that previously defined $b(i)$ is not necessary to be the same as $f(i)$, but they have to belong to the same relay $r(i)$ because no inter-relay cooperation is assumed. Moreover, the notion of $b(i)$ or $f(i)$ should not be limited to a single physical antenna. For example, the authors of Torabi and Frigon (2008) performed the SVD operation for $\mathbf{H}_k$ and $\mathbf{G}_k$ and gave new definitions for equivalent backward and forward channels. In that case, $b(i)$ and $f(i)$ respectively became the index of the backward and forward eigen modes of relay $r(i)$. Since such kind of signal processing can be applied on any antenna selection scheme for free, we only focus on the straight antenna selection in this chapter.

From (3.1) and the definition of $\mathbf{W}$, the amplified signal transmitted from the selected relay antennas can be expressed by

$$\begin{aligned} \mathbf{t} &= \mathbf{Wr} \\ &= \mathbf{WHFx} + \mathbf{Wn}_\mathrm{r}. \end{aligned} \tag{3.3}$$

Again, let us incorporate the pathloss and shadowing factor into a sum transmit power P_r for relays and formulate the relay power constraint in block fading channels as

$$
\begin{aligned}
\mathrm{E}\left\{\mathrm{tr}\left(\mathbf{t}\mathbf{t}^{\mathrm{H}}\right)\right\} &= \mathrm{tr}\left\{\mathrm{E}\left\{(\mathbf{WHFx}+\mathbf{Wn}_{\mathrm{r}})(\mathbf{WHFx}+\mathbf{Wn}_{\mathrm{r}})^{\mathrm{H}}\right\}\right\} \\
&= \mathrm{tr}\left\{\mathbf{W}^2\left((\mathbf{HF})(\mathbf{HF})^{\mathrm{H}}+\mathbf{I}_L\right)\right\} \\
&\leq P_{\mathrm{r}}.
\end{aligned} \tag{3.4}
$$

Considering equal power allocation across the activated antennas at relays, we have the following expression for w_i according to (3.4) with equality met therein,

$$
w_i = \sqrt{\frac{P_{\mathrm{r}}/L}{\left((\mathbf{HF})(\mathbf{HF})^{\mathrm{H}}+\mathbf{I}_L\right)_{i,i}}}, \tag{3.5}
$$

where $(\mathbf{A})_{i,i}$ is the i-th diagonal element of a matrix $\mathbf{A}$. Under the condition of perfect synchronization in the relay network, signal arriving at $\mathbf{D}$ is given by

$$
\mathbf{y} = \mathbf{Gt} + \mathbf{n}_{\mathrm{d}}, \tag{3.6}
$$

where $\mathbf{n}_{\mathrm{d}} \in \mathbb{C}^{L\times 1}$ stands for the ZMCSCG noise vector at $\mathbf{D}$ with covariance matrix $\mathrm{E}\left\{\mathbf{n}_{\mathrm{d}}\mathbf{n}_{\mathrm{d}}^{\mathrm{H}}\right\} = \mathbf{I}_{N_{\mathrm{d}}}$. $\mathbf{G} \in \mathbb{C}^{N_{\mathrm{d}}\times L}$ denotes the compound forward channel from the activated relay antennas to $\mathbf{D}$, which is a stack of L column vectors $\mathbf{g}_{(f(i),r(i))} \in \mathbb{C}^{N_{\mathrm{s}}\times 1}$, that is, $\mathbf{G} = \left[\mathbf{g}_{(b(1),r(1))}, \mathbf{g}_{(b(2),r(2))}, \ldots, \mathbf{g}_{(b(L),r(L))}\right]$. Substituting (3.3) into (3.6), we get

$$
\begin{aligned}
\mathbf{y} &= \mathbf{Gt} + \mathbf{n}_{\mathrm{d}} \\
&= \mathbf{GWHFx} + \mathbf{GWn}_{\mathrm{r}} + \mathbf{n}_{\mathrm{d}}.
\end{aligned} \tag{3.7}
$$

3.2.1.1 Capacity of the System with Double ZF Processing

Considering suppression of the interstream interference, in a similar way as in Torabi and Frigon (2008), we apply ZF precoding at $\mathbf{S}$ and ZF reception at $\mathbf{D}$ to separate individual data streams. Thereby, the number of selected antenna pairs L shall be limited by the number of antennas mounted at $\mathbf{S}$ or $\mathbf{D}$, that is, $L = M = \min\{N_{\mathrm{s}}, N_{\mathrm{d}}\}$, otherwise the double ZF processing at $\mathbf{S}$ and $\mathbf{D}$ cannot be operated.

In the first time slot, due to the employment of the ZF precoding, $\mathbf{F}$ takes the form written as

$$
\mathbf{F} = \mathbf{H}^{\dagger}\mathbf{\Lambda} = \mathbf{H}^{\dagger}\begin{bmatrix} \lambda_1 & & & \\ & \lambda_2 & & \\ & & \ddots & \\ & & & \lambda_L \end{bmatrix} \tag{3.8}
$$

where $(\cdot)^{\dagger}$ denotes the pseudo-inverse operator. $\mathbf{\Lambda}$ is a diagonal scalar matrix, with diagonal entry $\lambda_i = (\mathbf{\Lambda})_{i,i} (i \in \{1, 2, \ldots, L\})$ being the gain for each parallel backward sub-channel. Substituting (3.8) into (3.2), we obtain the transmission power constraint at **S** shown as

$$\begin{aligned}\operatorname{tr}\left\{\mathbf{H}^{\dagger}(\boldsymbol{\Lambda})^2\left(\mathbf{H}^{\dagger}\right)^{\mathrm{H}}\right\} &= \operatorname{tr}\left\{(\boldsymbol{\Lambda})^2\left(\mathbf{H}^{\dagger}\right)^{\mathrm{H}}\mathbf{H}^{\dagger}\right\} \\ &\le P_{\mathrm{s}}.\end{aligned} \tag{3.9}$$

Suppose that **S** operates at maximum power and equal power allocation among data streams is applied, then we have

$$\lambda_i = \sqrt{\frac{P_{\mathrm{s}}/L}{\left\|\left(\mathbf{H}^{\dagger}\right)_{:,i}\right\|^2}}, \tag{3.10}$$

where $\|\cdot\|$ is the Frobenius-norm operator and $(\mathbf{A})_{:,i}$ extracts the i-th column of a matrix $\mathbf{A}$.

In the second time slot, from (3.3), the transmission signal from selected relay antennas can be rewritten as

$$\begin{aligned}\mathbf{t} &= \mathbf{WHFx} + \mathbf{Wn}_{\mathrm{r}} \\ &= \mathbf{W\Lambda x} + \mathbf{Wn}_{\mathrm{r}}.\end{aligned} \tag{3.11}$$

Then the sum power constraint at relay antennas can be reformulated as

$$\begin{aligned}\mathrm{E}\left\{\operatorname{tr}\left(\mathbf{tt}^{\mathrm{H}}\right)\right\} &= \operatorname{tr}\left\{\mathrm{E}\left\{(\mathbf{W\Lambda x} + \mathbf{Wn}_{\mathrm{r}})\left(\mathbf{W\Lambda x} + \mathbf{Wn}_{\mathrm{r}}\right)^{\mathrm{H}}\right\}\right\} \\ &= \operatorname{tr}\left\{\mathbf{W}^2\left(\boldsymbol{\Lambda}^2 + \mathbf{I}_L\right)\right\} \\ &\le P_{\mathrm{r}}.\end{aligned} \tag{3.12}$$

We also assume that equal power allocation is applied for L selected antennas, thus w_i is given by

$$w_i = \sqrt{\frac{P_{\mathrm{r}}/L}{\lambda_i^2 + 1}}. \tag{3.13}$$

Then, the received signal at **D** becomes

$$\begin{aligned}\mathbf{y} &= \mathbf{Gt} + \mathbf{n}_{\mathrm{d}} \\ &= \mathbf{GW\Lambda x} + \mathbf{GWn}_{\mathrm{r}} + \mathbf{n}_{\mathrm{d}}.\end{aligned} \tag{3.14}$$

Applying ZF filter $\mathbf{G}^{\dagger}$ at **D**, we can separate the data streams and have

$$\begin{aligned}\mathbf{z} &= \mathbf{G}^{\dagger}\mathbf{y} \\ &= \mathbf{W\Lambda x} + \mathbf{Wn}_{\mathrm{r}} + \mathbf{G}^{\dagger}\mathbf{n}_{\mathrm{d}}.\end{aligned} \tag{3.15}$$

Thanks to the doubly ZF processing at **S** and **D** to diagonize the two-hop relay channels, we can write the system capacity in a simple form as

$$\begin{aligned} C &= \frac{1}{2}\sum_{i=1}^{L}\log_2\left(1+\gamma_i\right) \\ &= \frac{1}{2}\sum_{i=1}^{L}\log_2\left(1+\frac{(w_i\lambda_i)^2}{w_i^2+\left\|\left(\mathbf{G}^{\dagger}\right)_{i,:}\right\|^2}\right), \end{aligned} \tag{3.16}$$

where $(\mathbf{A})_{i,:}$ represents the i-th row of a matrix $\mathbf{A}$. γ_i is the SNR for the i-th data steam. Note that the factor 1/2 in (3.16) is a scalar penalty resulted from the TDD relaying protocol.

3.2.1.2 Capacity of the System with General Processing

Besides the double ZF processing, we take a further step to consider a more general transmit and receive processing, which assumes an identity precoding matrix at **S** and the capacity-achieving receiver, that is, MMSE-SIC receiver at **D**. Note that compared with the double ZF processing, the considered general processing relaxes the limitation on L, which merely requires that L should be less than the total number of available relay antennas, that is, KN_{r}. Hence, more relay antennas will be activated in the system, and large capacity gain can be expected.

Employing the identity precoding matrix at **S**, we have

$$\mathbf{F} = \sqrt{\sigma_x^2}\mathbf{I}_{N_{\mathrm{s}}}, \tag{3.17}$$

where σ_x^2 is the transmission power of each antenna at **S**. Substituting (3.17) into (3.2), we can get the power constraint at **S** as

$$\begin{aligned} \mathrm{tr}\left\{\sigma_x^2\mathbf{I}_{N_{\mathrm{s}}}\right\} &= N_{\mathrm{s}}\sigma_x^2 \\ &\leq P_{\mathrm{s}}. \end{aligned} \tag{3.18}$$

Suppose that **S** operates at maximum power and equal power allocation among data streams is applied, then we can calculate σ_x^2 as

$$\sigma_x^2 = P_{\mathrm{s}}/N_{\mathrm{s}}. \tag{3.19}$$

In the second time slot, from (3.3), the amplified signal transmitted from the selected relay antennas can be rewritten as

$$\mathbf{t} = \sigma_x\mathbf{W}\mathbf{H}\mathbf{x} + \mathbf{W}\mathbf{n}_{\mathrm{r}}. \tag{3.20}$$

And the sum power constraint at relay antennas can be reformulated as

$$\begin{aligned}\mathrm{E}\left\{\mathrm{tr}\left(\mathbf{t}\mathbf{t}^{\mathrm{H}}\right)\right\} &= \mathrm{tr}\left\{\mathrm{E}\left\{\left(\sigma_x\mathbf{W}\mathbf{H}\mathbf{x}+\mathbf{W}\mathbf{n}_{\mathrm{r}}\right)\left(\sigma_x\mathbf{W}\mathbf{H}\mathbf{x}+\mathbf{W}\mathbf{n}_{\mathrm{r}}\right)^{\mathrm{H}}\right\}\right\}\\ &= \mathrm{tr}\left\{\mathbf{W}^2\left(\sigma_x^2\mathbf{H}\mathbf{H}^{\mathrm{H}}+\mathbf{I}_L\right)\right\}\\ &\le P_{\mathrm{r}}.\end{aligned} \tag{3.21}$$

Considering equal power allocation across the L-activated relay antennas, we have the following expression for w_i according to (3.21) with equality met therein,

$$\begin{aligned}w_i &= \sqrt{\frac{P_{\mathrm{r}}/L}{\left(\sigma_x^2\mathbf{H}\mathbf{H}^{\mathrm{H}}+\mathbf{I}_L\right)_{i,i}}}\\ &= \sqrt{\frac{P_{\mathrm{r}}/L}{\sigma_x^2\left\|(\mathbf{H})_{i,:}\right\|^2+1}}.\end{aligned} \tag{3.22}$$

Under the condition of perfect synchronization in the relay network, signal arriving at $\mathbf{D}$ is given by

$$\begin{aligned}\mathbf{y} &= \mathbf{G}\mathbf{t}+\mathbf{n}_{\mathrm{d}}\\ &= \sigma_x\mathbf{G}\mathbf{W}\mathbf{H}\mathbf{x}+\mathbf{G}\mathbf{W}\mathbf{n}_{\mathrm{r}}+\mathbf{n}_{\mathrm{d}}\\ &= \mathbf{H}_{\mathrm{eq}}\mathbf{x}+\mathbf{n}_{\mathrm{eq}},\end{aligned} \tag{3.23}$$

where $\mathbf{H}_{\mathrm{eq}} = \sigma_x\mathbf{G}\mathbf{W}\mathbf{H}$ is denoted as the equivalent channel and $\mathbf{n}_{\mathrm{eq}} = \mathbf{G}\mathbf{W}\mathbf{n}_{\mathrm{r}}+\mathbf{n}_{\mathrm{d}}$ as the colored noise term.

Hence, the capacity for the considered system can be expressed as

$$\begin{aligned}C &= \frac{1}{2}\log_2\det\left(\mathbf{I}_{N_{\mathrm{d}}}+\sigma_x^2\mathbf{H}_{\mathrm{eq}}\mathbf{H}_{\mathrm{eq}}^{\mathrm{H}}\mathbf{\Phi}^{-1}\right)\\ &= \frac{1}{2}\log_2\det\left(\mathbf{\Phi}+\sigma_x^2\mathbf{H}_{\mathrm{eq}}\mathbf{H}_{\mathrm{eq}}^{\mathrm{H}}\right)-\frac{1}{2}\log_2\det\left(\mathbf{\Phi}\right),\end{aligned} \tag{3.24}$$

where $\mathbf{\Phi} = \mathrm{E}\left\{\mathbf{n}_{\mathrm{eq}}\mathbf{n}_{\mathrm{eq}}^{\mathrm{H}}\right\} = \mathbf{G}\mathbf{W}(\mathbf{G}\mathbf{W})^{\mathrm{H}}+\mathbf{I}_{N_{\mathrm{d}}}$ is the covariance matrix for $\mathbf{n}_{\mathrm{eq}}$. Note that for the same reason as in (3.16), the factor 1/2 in (3.24) is a scalar penalty resulted from the half duplex relaying.

3.2.1.3 MSE of the System with General Processing

Another commonly used performance metric is the mean square error (MSE), and hence, we continue to analyze the MSE of the system with general processing, which assumes an identity precoding matrix at $\mathbf{S}$ and the minimum MSE (MMSE) receiver (Proakis 2001) at $\mathbf{D}$. In the considered system, more relay antennas will be selected compared with the system with the double ZF processing, thus the performance should be improved in terms of diversity gain, which leads to lower MSE and bit error rate (BER).

The precoding operation at **S** and the corresponding power constraint have been shown in (3.17) and (3.18), respectively. Also the amplified signal sent from the selected relay antennas and its power constraint can be referred to (3.20) and (3.21), respectively. The expression for w_i in (3.22) is still valid if we grant maximum available power to **S** and relay antennas and consider equal power allocation among the data streams at **S** and across the L activated relay antennas.

Here, we'd like to take another step to consider a more practical scenario that each relay node is equipped with only one PA so that only one antenna pair can be activated on each relay for the TDD-based transmission. Besides, each relay node has an independent power supply, the local power of which is bounded by P_{loc}. Thus, the local power constraints at relays can be expressed as

$$\begin{aligned} \mathrm{E}\left\{\left(\mathbf{t}\mathbf{t}^{\mathrm{H}}\right)_{i,i}\right\} &= \left(\mathbf{W}^2\left(\sigma_x^2\mathbf{H}\mathbf{H}^{\mathrm{H}} + \mathbf{I}_L\right)\right)_{i,i} \\ &\leq P_{\text{loc}}. \end{aligned} \tag{3.25}$$

Comparing (3.21) with (3.25), we can see that the selected relay antennas share the fixed maximum power in (3.21) while more power will pour into the system for more selected antennas in (3.25) due to distributed power sources. Assume full-power transmission in (3.25), then we get

$$w_i = \sqrt{\frac{P_{\text{loc}}}{\sigma_x^2\left\|(\mathbf{H})_{i,:}\right\|^2 + 1}}. \tag{3.26}$$

The received signal at **D** can be written as

$$\begin{aligned} \mathbf{y} &= \mathbf{G}\mathbf{t} + \mathbf{n}_{\mathrm{d}} \\ &= \sigma_x\mathbf{G}\mathbf{W}\mathbf{H}\mathbf{x} + \mathbf{G}\mathbf{W}\mathbf{n}_{\mathrm{r}} + \mathbf{n}_{\mathrm{d}} \\ &= \mathbf{H}_{\mathrm{eq}}\mathbf{x} + \mathbf{n}_{\mathrm{eq}}, \end{aligned} \tag{3.27}$$

where $\mathbf{H}_{\mathrm{eq}} = \sigma_x\mathbf{G}\mathbf{W}\mathbf{H}$ is denoted as the equivalent channel and $\mathbf{n}_{\mathrm{eq}} = \mathbf{G}\mathbf{W}\mathbf{n}_{\mathrm{r}} + \mathbf{n}_{\mathrm{d}}$ as the colored noise term. According to Proakis (2001), the MSE of symbol estimation will achieve its minimum value when Wiener filter is employed. The corresponding MSE is presented by

$$\begin{aligned} Q &= \sigma_x^2\mathrm{tr}\left\{\left(\mathbf{I}_{N_{\mathrm{d}}} + \sigma_x^2\mathbf{H}_{\mathrm{eq}}\mathbf{H}_{\mathrm{eq}}^{\mathrm{H}}\boldsymbol{\Phi}^{-1}\right)^{-1}\right\} + \sigma_x^2\left(N_{\mathrm{s}} - N_{\mathrm{d}}\right) \\ &= \sigma_x^2\mathrm{tr}\left\{\boldsymbol{\Phi}\left(\boldsymbol{\Phi} + \sigma_x^2\mathbf{H}_{\mathrm{eq}}\mathbf{H}_{\mathrm{eq}}^{\mathrm{H}}\right)^{-1}\right\} + \beta, \end{aligned} \tag{3.28}$$

where $\mathbf{\Phi} = \mathrm{E}\left\{\mathbf{n}_{\mathrm{eq}}\mathbf{n}_{\mathrm{eq}}^{\mathrm{H}}\right\} = \mathbf{GW}(\mathbf{GW})^{\mathrm{H}} + \mathbf{I}_{N_\mathrm{d}}$ is the covariance matrix for $\mathbf{n}_{\mathrm{eq}}$. And $\beta = \sigma_x^2 (N_\mathrm{s} - N_\mathrm{d})$ is a constant that is free from the minimization of Q, so we will omit β hereafter.

3.2.2 Existing Technologies

3.2.2.1 The S-O Algorithm

In the S-O algorithm (Torabi and Frigon 2008), the orthogonality metric for two vectors $\mathbf{a}$ and $\mathbf{b}$ is defined as

$$\phi(\mathbf{a}, \mathbf{b}) = \frac{\left|\mathbf{a}^{\mathrm{H}}\mathbf{b}\right|}{\|\mathbf{a}\| \, \|\mathbf{b}\|}. \tag{3.29}$$

Obviously, the smaller the value of $\phi(\mathbf{a}, \mathbf{b})$ is, the stronger orthogonality between $\mathbf{a}$ and $\mathbf{b}$ will be. Denote $\mathbf{h}_{k,m}$ and $\mathbf{g}_{k,n}$ as the backward channel vector for $\mathbf{S}$ to the m-th receive antenna on the k-th relay and the forward channel vector from the n-th transmit antenna on the k-th relay to $\mathbf{D}$, respectively. For convenience, we use (k, m, n) to indicate the receive-transmit antenna pair (m, n) on the k-th relay node.

Suppose that the selected l antenna pairs constitute a set $\mathbf{S}_l = \{(r_1, b_1, f_1), (r_2, b_2, f_2), \ldots, (r_l, b_l, f_l)\}$ and the orthogonality metric between the $(l+1)$-th candidate antenna pair (k, m, n) and $\mathbf{S}_l$ is defined as

$$\Gamma_{(k,m,n)}(l+1) = \sum_{i=1}^{l} \max\left\{\gamma_{k,i}(m), \gamma'_{k.i}(n)\right\}, \tag{3.30}$$

where $\gamma_{k,i}(m)$ and $\gamma'_{k.i}(n)$ are respectively given by

$$\gamma_{k,i}(m) = \varphi\left(\mathbf{h}_{r_i,b_i}, \mathbf{h}_{k,m}\right) \tag{3.31}$$

and

$$\gamma'_{k.i}(n) = \varphi\left(\mathbf{g}_{r_i,f_i}, \mathbf{g}_{k,n}\right). \tag{3.32}$$

The basic idea of (3.30) is to check the orthogonality metric sum of the less orthogonal hops between the candidate antenna pair and the already selected relay antennas. The $(l+1)$-th candidate antenna pair is chosen heuristically by minimizing $\Gamma_{(k,m,n)}(l+1)$ (Torabi and Frigon 2008), which can be formulated as

$$(r_{l+1}, b_{l+1}, f_{l+1}) = \arg \min_{(k,m,n,\in T_l)} \left\{\Gamma_{(k,m,n)}(l+1)\right\}. \tag{3.33}$$

The S-O algorithm repeatedly evaluates (3.30) and (3.33) until L antenna pairs are selected. The S-O algorithm is initialized by selecting the antenna pair with the largest harmonic mean of $||\mathbf{h}_{k,m}||^2$ and $||\mathbf{g}_{k,n}||^2$ and it is summarized in Table 3.1.

Table 3.1 The S-O relay/antenna selection algorithm

1.	Initialization: Set the candidate antenna pair set $\Omega = \{(k, m, n)\,\vert 1 \le k \le K,\, 1 \le m \le N_{\mathrm{r}},\, 1 \le n \le N_{\mathrm{r}}\}$, $l = 1, (r_1, b_1, f_1) = \arg \max\limits_{(k,m,n,\in T_1)} \frac{\Vert \mathbf{h}_{k,m} \Vert^2 \Vert \mathbf{g}_{k,n} \Vert^2}{\Vert \mathbf{h}_{k,m} \Vert^2 + \Vert \mathbf{g}_{k,n} \Vert^2}$, $\Omega = \Omega - \{(r_1, b_1, :), (r_1, :, f_1)\}, \mathbf{S}_l = \{(r_1, b_1, f_1)\}$
2.	Iterative loop: For each antenna pair $(k, m, n) \in \Omega$, use (3.30) to compute $\Gamma_{(k,m,n)}(l+1)$ Select the $(l+1)$th antenna pair according to (3.33), $\mathbf{S}_{l+1} = \{\mathbf{S}_l, (r_{l+1}, b_{l+1}, f_{l+1})\}$ Update Ω by $\Omega = \Omega - \{(r_{l+1}, b_{l+1}, :), (r_{l+1}, :, f_{l+1})\}$
3.	Set $l = l+1$, if $l < L$, go to Step 2 Else, terminate with $\mathbf{S}_L$ as the selected relay antenna pairs

3.2.2.2 The DORS Algorithm

In the DORS algorithm, a different orthogonality metric is proposed. Suppose that the selected l receive antennas and l transmit antennas at relay nodes constitute a set $\mathbf{S}_l^{\mathrm{rx}} = \{(r_1, b_1), (r_2, b_2), \ldots, (r_l, b_l)\}$ and a set $\mathbf{S}_l^{\mathrm{tx}} = \{(r_1, f_1), (r_2, f_2), \ldots, (r_l, f_l)\}$, respectively. Let $\mathbf{h}_{m,k}^{\perp(l)}$ be the component of $\mathbf{h}_{m,k}$ orthogonal to the backward channel subspace spanned from $\mathbf{S}_l^{\mathrm{rx}}$ and $\mathbf{g}_{n,k}^{\perp(l)}$ be the component of $\mathbf{g}_{n,k}$ orthogonal to the forward channel subspace given by $\mathbf{S}_l^{\mathrm{tx}}$. Then, the DORS algorithm selects the antenna pair to maximize the harmonic mean of dual-hop sub-channel gains, which is expressed as

$$(r_{l+1}, b_{l+1}, f_{l+1}) = \arg \max_{(k,m,n,\in T_l)} \left\{\Gamma_{(k,m,n)}(l+1)\right\}, \tag{3.34}$$

where $\Gamma_{(k,m,n)}(l+1)$ is

$$\Gamma_{(k,m,n)}(l+1) = \frac{\left\Vert \mathbf{h}_{m,k}^{\perp(l)} \right\Vert \left\Vert \mathbf{g}_{n,k}^{\perp(l)} \right\Vert}{\left\Vert \mathbf{h}_{m,k}^{\perp(l)} \right\Vert + \left\Vert \mathbf{g}_{n,k}^{\perp(l)} \right\Vert}. \tag{3.35}$$

Then the DORS algorithm repeatedly evaluates (3.35) and (3.34) until L antenna pairs are selected. The DORS algorithm is summarized in Table 3.2.

3.2.2.3 Motivations of Improved Algorithms

Both the S-O and DORS algorithms are heuristic relay/antenna selection methods. They adopt semi-orthogonal criteria to guide the selection process and disregard the

Table 3.2 The DORS relay/antenna selection algorithm

1.	Initialization:
	Set the candidate antenna pair set
	$\Omega = \{(k, m, n) \mid 1 \le k \le K,\ 1 \le m \le N_{\mathrm{r}},\ 1 \le n \le N_{\mathrm{r}}\}$,
	$l = 1,\ (r_1, b_1, f_1) = \arg \max\limits_{(k,m,n,\in T_1)} \dfrac{\lVert \mathbf{h}_{m,k} \rVert \lVert \mathbf{g}_{n,k} \rVert}{\lVert \mathbf{h}_{m,k} \rVert + \lVert \mathbf{g}_{n,k} \rVert}$,
	$\Omega = \Omega - \{(r_1, b_1, :), (r_1, :, f_1)\},\ \mathbf{S}_l = \{(r_1, b_1, f_1)\}$
2.	Iterative loop:
	For each antenna pair $(k, m, n) \in \Omega$, use (3.35) to compute
	$\Gamma_{(k,m,n)}(l+1)$
	Select the $(l+1)$th antenna pair according to (3.34)
	$\mathbf{S}_{l+1} = \{\mathbf{S}_l, (r_{l+1}, b_{l+1}, f_{l+1})\}$
	Update Ω by $\Omega = \Omega - \{(r_{l+1}, b_{l+1}, :), (r_{l+1}, :, f_{l+1})\}$
3.	Set $l = l + 1$, if $l < L$, go to Step 2
	Else, terminate with $\mathbf{S}_L$ as the selected relay antenna pairs

noise at the relay nodes, which might not be realistic due to the use of noisy PAs at the relay nodes. Thus, it would be better to develop a relay/antenna selection scheme based on more concrete criteria in closed forms, such as capacity maximization or MSE minimization. Besides, low-complexity-oriented greedy selection schemes like the S-O and DORS algorithms, which select antenna pairs one by one, are still preferred.

Therefore, we propose to derive the closed-form expressions to quantify the capacity increase and/or MSE decrease incurred from adding one more relay antenna pair, followed by designing low-complexity greedy relay/antenna selection algorithms.

3.3 Greedy Antenna Selection Algorithms

3.3.1 Capacity Maximization for the System with Double ZF Processing

Suppose that l antenna pairs $\mathbf{S}_l = \{(r_1, b_1, f_1), (r_2, b_2, f_2), \ldots, (r_l, b_l, f_l)\}$ have been picked out, and let us concentrate on how the $(l+1)$-th antenna pair affects the capacity. Denote the already selected partial backward channel and forward channel respectively as

$$\mathbf{H}^{(l)} = \left[\mathbf{h}_{r_1,b_1}^{\mathrm{T}}, \mathbf{h}_{r_2,b_2}^{\mathrm{T}}, \ldots, \mathbf{h}_{r_l,b_l}^{\mathrm{T}}\right]^{\mathrm{T}} \tag{3.36}$$

and

$$\mathbf{G}^{(l)} = \left[\mathbf{g}_{r_1,f_1}, \mathbf{g}_{r_2,f_2}, \ldots, \mathbf{g}_{r_l,f_l}\right]. \tag{3.37}$$

We consider adding a candidate antenna pair (k, m, n) and write the candidate backward channel and forward channel as

$$\mathbf{H}_{k,m}^{(l+1)} = \left[\left(\mathbf{H}^{(l)} \right)^{\mathrm{T}}, \mathbf{h}_{k,m}^{\mathrm{T}} \right]^{\mathrm{T}} \tag{3.38}$$

and

$$\mathbf{G}_{k,n}^{(l+1)} = \left[\mathbf{G}^{(l)}, \mathbf{g}_{k,n} \right]. \tag{3.39}$$

From (3.10) and (3.13), we have

$$\begin{aligned} (\boldsymbol{\Lambda}_{k,m})_{i,i} &= \sqrt{\frac{P_{\mathrm{s}}/L}{\left(\left(\left(\mathbf{H}_{k,m}^{(l+1)} \right)^{\dagger} \right)^{\mathrm{H}} \left(\mathbf{H}_{k,m}^{(l+1)} \right)^{\dagger} \right)_{i,i}}} \\ &= \frac{\sqrt{P_{\mathrm{s}}/L}}{\left\| \left(\mathbf{H}_{k,m}^{(l+1)} \right)^{\dagger}_{:,i} \right\|}, \end{aligned} \tag{3.40}$$

and

$$(\mathbf{W}_{k,m})_{i,i} = \sqrt{\frac{P_{\mathrm{r}}/L}{(\boldsymbol{\Lambda}_{k,m})_{i,i}^2 + 1}}. \tag{3.41}$$

Hence, from (3.16) we can get the conditional SNR $\gamma_i|_{(k,m,n)}$ expressed as

$$\gamma_i|_{(k,m,n)} = \frac{\left((\mathbf{W}_{k,m})_{i,i} \times (\boldsymbol{\Lambda}_{k,m})_{i,i} \right)^2}{(\mathbf{W}_{k,m})_{i,i}^2 + \left\| \left(\left(\mathbf{G}_{k,n}^{(l+1)} \right)^{\dagger} \right)_{i,:} \right\|^2}, \tag{3.42}$$

and we can obtain the conditional system capacity as

$$C_{k,m,n}^{(l+1)} = \frac{1}{2} \sum_{i=1}^{L} \log_2 \left(1 + \frac{\left((\mathbf{W}_{k,m})_{i,i} \times (\boldsymbol{\Lambda}_{k,m})_{i,i} \right)^2}{(\mathbf{W}_{k,m})_{i,i}^2 + \left\| \left(\left(\mathbf{G}_{k,n}^{(l+1)} \right)^{\dagger} \right)_{i,:} \right\|^2} \right). \tag{3.43}$$

It is critical to find a computationally efficient way to evaluate (3.40), (3.41), and (3.43) iteratively. To this end, we resort to the pseudo-inverse calculation formula in Golub and Loan (1996). For the selected partial backward channel $\mathbf{H}^{(l)}$ and the candidate partial backward channel $\mathbf{H}_{k,m}^{(l+1)}$, we propose Theorem 3.1.

Theorem 3.1. *The pseudo-inverse of* $\mathbf{H}_{k,m}^{(l+1)}$ *can be evaluated as*

$$\left(\mathbf{H}_{k,m}^{(l+1)}\right)^{\dagger} = \left(\left(\left(\mathbf{H}^{(l)}\right)^{\mathrm{T}}, \mathbf{h}_{k,m}^{\mathrm{T}}\right)^{\mathrm{T}}\right)^{\dagger}$$
$$= \begin{pmatrix} \left(\left(\mathbf{H}^{(l)}\right)^{\dagger}\right)^{\mathrm{T}} - \dfrac{\left(\left(\mathbf{H}^{(l)}\right)^{\dagger}\right)^{\mathrm{T}} \mathbf{h}_{k,m}^{\mathrm{T}} \mathbf{p}_{k,m}^{\mathrm{H}}}{\|\mathbf{p}_{k,m}\|^2} \\ \dfrac{\mathbf{h}_{k,m}^{\mathrm{T}} \mathbf{p}_{k,m}^{\mathrm{H}}}{\|\mathbf{p}_{k,m}\|^2} \end{pmatrix}^{\mathrm{T}}, \tag{3.44}$$

where $\mathbf{p}_{k,m} = \left(\mathbf{I}_{N_{\mathrm{s}}} - \left(\mathbf{H}^{(l)}\right)^{\mathrm{T}} \left(\left(\mathbf{H}^{(l)}\right)^{\dagger}\right)^{\mathrm{T}}\right) \mathbf{h}_{k,m}^{\mathrm{T}}$.

Proof. According to Golub and Loan (1996), for any $\mathbf{A} \in \mathbb{C}^{a \times b}, \mathbf{b} \in \mathbb{C}^{a \times 1}$ $(a > b)$, we have

$$[\mathbf{A}\ \mathbf{b}]^{\dagger} = \begin{bmatrix} \mathbf{A}^{\dagger} - \mathbf{A}^{\dagger}\mathbf{b}\mathbf{c} \\ \mathbf{c} \end{bmatrix}, \tag{3.45}$$

where

$$\mathbf{c} = \left(\left(\mathbf{I}_a - \mathbf{A}\mathbf{A}^{\dagger}\right)\mathbf{b}\right)^{\dagger}$$
$$= \frac{\left(\left(\mathbf{I}_a - \mathbf{A}\mathbf{A}^{\dagger}\right)\mathbf{b}\right)^{\mathrm{H}}}{\left\|\left(\mathbf{I}_a - \mathbf{A}\mathbf{A}^{\dagger}\right)\mathbf{b}\right\|^2}. \tag{3.46}$$

The proof is concluded by substituting (3.46) into (3.45) and considering the definition of $\mathbf{p}_{k,m}$ in (3.44).

Similar to Theorem 3.1, for the selected partial backward channel $\mathbf{G}^{(l)}$ and the candidate partial backward channel $\mathbf{G}_{k,n}^{(l+1)}$, we have

$$\left(\mathbf{G}_{k,n}^{(l+1)}\right)^{\dagger} = \left[\mathbf{G}^{(l)}, \mathbf{g}_{k,n}\right]^{\dagger}$$
$$= \begin{bmatrix} \left(\mathbf{G}^{(l)}\right)^{\dagger} - \dfrac{\left(\mathbf{G}^{(l)}\right)^{\dagger} \mathbf{g}_{k,n} \mathbf{q}_{k,n}^{\mathrm{H}}}{\|\mathbf{q}_{k,n}\|^2} \\ \dfrac{\mathbf{g}_{k,n} \mathbf{q}_{k,n}^{\mathrm{H}}}{\|\mathbf{q}_{k,n}\|^2} \end{bmatrix}, \tag{3.47}$$

where $\mathbf{q}_{k,n} = \left(\mathbf{I}_{N_{\mathrm{d}}} - \mathbf{G}^{(l)}\left(\mathbf{G}^{(l)}\right)^{\dagger}\right) \mathbf{g}_{k,n}$.

Table 3.3 The DZF-GCM relay/antenna selection algorithm

1.	Initialization: Set the candidate antenna pair set $\Omega = \{(k, m, n) \,\vert\, 1 \leq k \leq K,\ 1 \leq m \leq N_\mathrm{r},\ 1 \leq n \leq N_\mathrm{r}\}$, $l = 0, \mathbf{S}_l = \emptyset, \mathbf{H}^{(l)} = \mathbf{G}^{(l)} = \emptyset, \left(\mathbf{H}^{(l)}\right)^\dagger = \left(\mathbf{G}^{(l)}\right)^\dagger = \mathbf{0}$
2.	Iterative loop: For each antenna pair $(k, m, n) \in \Omega$, use (3.44), (3.47), and (3.43) to compute $\left(\mathbf{H}_{k,m}^{(l+1)}\right)^\dagger, \left(\mathbf{G}_{k,n}^{(l+1)}\right)^\dagger$, and $C_{k,m,n}^{(l+1)}$, respectively Select the $(l+1)$th antenna pair by maximizing $C_{k,m,n}^{(l+1)}$: $\left(r_{l+1}, b_{l+1}, f_{l+1}\right) = \underset{(k,m,n)\in\Omega}{\arg\max} \left\{C_{k,m,n}^{(l+1)}\right\}$ Update $\mathbf{H}^{(l+1)} = \left[\left(\mathbf{H}^{(l)}\right)^\mathrm{T}, \mathbf{h}_{r_{l+1},b_{l+1}}^\mathrm{T}\right]^\mathrm{T}, \mathbf{G}^{(l+1)} = \left[\mathbf{G}^{(l)}, \mathbf{g}_{r_{l+1},f_{l+1}}\right]$, $\mathbf{S}_{l+1} = \left\{\mathbf{S}_l, \left(r_{l+1}, b_{l+1}, f_{l+1}\right)\right\}$, and $\Omega = \Omega - \left\{\left(r_{l+1}, b_{l+1}, :\right), \left(r_{l+1}, :, f_{l+1}\right)\right\}$
3.	Set $l = l + 1$; if $l < L$, go to Step 2 Else, terminate with $\mathbf{S}_L$ as the selected relay antenna pairs

Note that (3.44) and (3.47) only involve simple calculations such as matrix multiplication and norm operation, which are of low complexity. In addition, it needs to compute $\left(\mathbf{H}^{(l)}\right)^\dagger$ and $\left(\mathbf{G}^{(l)}\right)^\dagger$ for just once at the beginning of each iteration loop. Therefore, combining (3.44), (3.47), and (3.43), we are able to analyze the capacity accurately and efficiently. Furthermore, we propose a doubly ZF greedy capacity maximization (DZF-GCM) antenna selection algorithm (Ding et al. 2010a) summarized in Table 3.3.

3.3.2 *Capacity Maximization for System with General Processing*

In order to analyze the system capacity taking realistic noise into account, we want to evaluate (3.24) without approximation. Obviously, an exhaustive search to maximize (3.24) yields the optimal set of relay antennas. But such a brute-force search will quickly turn out to be prohibitively complex since the size of its search space is at least $\mathrm{C}_{KN_\mathrm{r}^2}^{\min(N_\mathrm{s},N_\mathrm{d})}$ for large KN_r^2, where $\mathrm{C}_{KN_\mathrm{r}^2}^{i}$ counts the events of selecting i antenna pairs from a pool of KN_r^2 candidate antenna pairs. For example, in a case of $N_\mathrm{s} = N_\mathrm{d} = N_\mathrm{r} = 4$ and $K = 6$, the exhaustive search needs to perform approximately 3.3 million trials with each trial demanding a 4-dimensional determinant operation in (3.24), which is computationally time-consuming. Hence, we have to find another way with low complexity to tackle the evaluation of the closed-form capacity given by (3.24). Here, we consider the same approach as in Sect. 3.3.1, which assumes l antenna pairs $\mathbf{S}_l = \{(r_1, b_1, f_1), (r_2, b_2, f_2), \ldots, (r_l, b_l, f_l)\}$ have been selected and then greedily maximizes the capacity when the $(l+1)$-th antenna pair is added to the network.

We recall the definitions of $\mathbf{H}^{(l)}$, $\mathbf{G}^{(l)}$, $\mathbf{H}_{k,m}^{(l+1)}$, and $\mathbf{G}_{k,n}^{(l+1)}$ shown in (3.36), (3.37), (3.38), and (3.39). Regarding the $(l+1)$th antenna pair, for every unselected candidate antenna pair (k, m, n), we calculate the associated relay gain $w_{k,m}^{(l+1)}$ and update the signal amplifying matrix $\mathbf{W}^{(l+1)}$ as

$$\mathbf{W}_{k,m}^{(l+1)} = \begin{bmatrix} \tilde{\mathbf{W}}^{(l)} & \mathbf{0} \\ \mathbf{0} & w_{k,m}^{(l+1)} \end{bmatrix}, \tag{3.48}$$

where $\tilde{\mathbf{W}}^{(l)} = \mathbf{W}^{(l)}\sqrt{l/(l+1)}$ represents the power dilution of the signal amplifying function at the relay nodes due to the additional antenna pair. Besides, according to (3.22), we have

$$w_{k,m}^{(l+1)} = \sqrt{\frac{P_{\mathrm{r}}/(L+1)}{\sigma_x^2 \|\mathbf{h}_{k,m}\|^2 + 1}}. \tag{3.49}$$

In order to efficiently calculate the system capacity shown in (3.24), we present Theorem 3.2.

Theorem 3.2. *The network capacity resulted from the* $(l+1)$*-th additional antenna pair* (k, m, n) *can be evaluated as*

$$\begin{aligned} C_{k,m,n}^{(l+1)} = & \frac{1}{2}\log_2 \det\left(\mathbf{A}^{(l)} + \sum_{i=1}^{4} s_i \mathbf{q}_i \mathbf{q}_i^{\mathrm{H}}\right) \\ & - \frac{1}{2}\log_2 \det\left(\tilde{\boldsymbol{\Phi}}^{(l)}\right) \\ & - \frac{1}{2}\log_2 \det\left(1 + \left(w_{k,m}^{(l+1)}\right)^2 \mathbf{g}_{k,n}^{\mathrm{H}} \left(\tilde{\boldsymbol{\Phi}}^{(l)}\right)^{-1} \mathbf{g}_{k,n}\right), \end{aligned} \tag{3.50}$$

where

$$\begin{aligned} & \tilde{\boldsymbol{\Phi}}^{(l)} = \mathbf{I}_{N_{\mathrm{d}}} + \left(\mathbf{G}^{(l)}\tilde{\mathbf{W}}^{(l)}\right)\left(\mathbf{G}^{(l)}\tilde{\mathbf{W}}^{(l)}\right)^{\mathrm{H}}, \\ & \mathbf{A}^{(l)} = \tilde{\boldsymbol{\Phi}}^{(l)} + \sigma_x^2 \left(\mathbf{G}^{(l)}\tilde{\mathbf{W}}^{(l)}\mathbf{H}^{(l)}\right)\left(\mathbf{G}^{(l)}\tilde{\mathbf{W}}^{(l)}\mathbf{H}^{(l)}\right)^{\mathrm{H}}, \\ & \mathbf{u}_{k,m}^{(l)} = \sigma_x^2 \left(\mathbf{G}^{(l)}\tilde{\mathbf{W}}^{(l)}\mathbf{H}^{(l)}\right) w_{k,m}^{(l+1)} \mathbf{h}_{k,m}^{\mathrm{H}}, \\ & \mathbf{q}_1 = \mathbf{u}_{k,m}^{(l)} + \mathbf{g}_{k,n}, \mathbf{q}_2 = \sqrt{\frac{P_{\mathrm{r}}}{l+1}}\mathbf{g}_{k,n}, \mathbf{q}_3 = \mathbf{g}_{k,n}, \mathbf{q}_4 = \mathbf{u}_{k,m}^{(l)}, \\ & [s_1, s_2, s_3, s_4] = [1, 1, -1, -1]. \end{aligned} \tag{3.51}$$

Proof. From (3.24), the network capacity resulted from the $(l+1)$-th additional antenna pair (k, m, n) is

$$C_{k,m,n}^{(l+1)} = \frac{1}{2}\log_2 \det\left(\mathbf{\Phi}_{k,m,n}^{(l+1)} + \sigma_x^2 \left(\mathbf{H}_{\text{eq}}\right)_{k,m}^{(l+1)} \left(\left(\mathbf{H}_{\text{eq}}\right)_{k,m}^{(l+1)}\right)^{\text{H}}\right)$$
$$- \frac{1}{2}\log_2 \det\left(\mathbf{\Phi}_{k,m,n}^{(l+1)}\right), \tag{3.52}$$

where

$$\begin{aligned}
\mathbf{\Phi}_{k,m,n}^{(l+1)} &= \mathbf{I}_{N_\text{d}} + \left(\mathbf{G}_{k,n}^{(l+1)}\mathbf{W}_{k,m}^{(l+1)}\right)\left(\mathbf{G}_{k,n}^{(l+1)}\mathbf{W}_{k,m}^{(l+1)}\right)^{\text{H}} \\
&= \mathbf{I}_{N_\text{d}} + \left[\mathbf{G}^{(l)}, \mathbf{g}_{k,n}\right]\begin{bmatrix} \tilde{\mathbf{W}}^{(l)} & \mathbf{0} \\ \mathbf{0} & w_{k,m}^{(l+1)} \end{bmatrix}^2 \left[\mathbf{G}^{(l)}, \mathbf{g}_{k,n}\right]^{\text{H}} \\
&= \mathbf{I}_{N_\text{d}} + \mathbf{G}^{(l)}\left(\tilde{\mathbf{W}}^{(l)}\right)^2\left(\mathbf{G}^{(l)}\right)^{\text{H}} + \mathbf{g}_{k,n}\left(w_{k,m}^{(l+1)}\right)^2 \mathbf{g}_{k,n}^{\text{H}},
\end{aligned} \tag{3.53}$$

and

$$\begin{aligned}
\left(\mathbf{H}_{\text{eq}}\right)_{k,m}^{(l+1)} &= \mathbf{G}_{k,n}^{(l+1)}\mathbf{W}_{k,m}^{(l+1)}\mathbf{H}_{k,m}^{(l+1)} \\
&= \left(\mathbf{G}^{(l)}, \mathbf{g}_{k,n}\right)\begin{pmatrix} \tilde{\mathbf{W}}^{(l)} & \mathbf{0} \\ \mathbf{0} & w_{k,m}^{(l+1)} \end{pmatrix}\begin{pmatrix} \mathbf{H}^{(l)} \\ \mathbf{h}_{k,m} \end{pmatrix} \\
&= \mathbf{G}^{(l)}\tilde{\mathbf{W}}^{(l)}\mathbf{H}^{(l)} + \mathbf{g}_{k,n} w_{k,m}^{(l+1)}\mathbf{h}_{k,m}.
\end{aligned} \tag{3.54}$$

Substituting (3.53) and (3.54) into (3.52), and considering the definitions in (3.51), we can simplify $C_{k,m,n}^{(l+1)}$ as follows with some mathematical manipulations,

$$\begin{aligned}
C_{k,m,n}^{(l+1)} &= \frac{1}{2}\log_2 \det\begin{pmatrix} \tilde{\mathbf{\Phi}}^{(l)} + \left(w_{k,m}^{(l+1)}\right)^2 \mathbf{g}_{k,n}\mathbf{g}_{k,n}^{\text{H}} \\ + \sigma_x^2\left(\mathbf{G}^{(l)}\tilde{\mathbf{W}}^{(l)}\mathbf{H}^{(l)} + w_{k,m}^{(l+1)}\mathbf{g}_{k,n}\mathbf{h}_{k,m}\right) \\ \times\left(\mathbf{G}^{(l)}\tilde{\mathbf{W}}^{(l)}\mathbf{H}^{(l)} + w_{k,m}^{(l+1)}\mathbf{g}_{k,n}\mathbf{h}_{k,m}\right)^{\text{H}} \end{pmatrix} \\
&\quad - \frac{1}{2}\log_2 \det\left(\tilde{\mathbf{\Phi}}^{(l)} + \left(w_{k,m}^{(l+1)}\right)^2 \mathbf{g}_{k,n}\mathbf{g}_{k,n}^{\text{H}}\right) \\
&= \frac{1}{2}\log_2 \det\begin{pmatrix} \mathbf{A}^{(l)} + \left(\mathbf{u}_{k,m}^{(l)} + \mathbf{g}_{k,n}\right)\left(\mathbf{u}_{k,m}^{(l)} + \mathbf{g}_{k,n}\right)^{\text{H}} \\ + \left(\dfrac{P_\text{r}}{l+1} - 1\right)\mathbf{g}_{k,n}\mathbf{g}_{k,n}^{\text{H}} - \mathbf{u}_{k,m}^{(l)}\left(\mathbf{u}_{k,m}^{(l)}\right)^{\text{H}} \end{pmatrix} \\
&\quad - \frac{1}{2}\log_2 \det\left(\tilde{\mathbf{\Phi}}^{(l)} + \left(w_{k,m}^{(l+1)}\right)^2 \mathbf{g}_{k,n}\mathbf{g}_{k,n}^{\text{H}}\right).
\end{aligned} \tag{3.55}$$

By invoking the Sherman-Morrison-Woodbury formula (Lutkepohl 1996), we get

$$\left(\mathbf{B} \pm \mathbf{U}\mathbf{T}^{\mathrm{H}}\right)^{-1} = \mathbf{B}^{-1} \mp \mathbf{B}^{-1}\mathbf{U}\left(\mathbf{I} \pm \mathbf{T}^{\mathrm{H}}\mathbf{B}^{-1}\mathbf{U}\right)^{-1}\mathbf{T}^{\mathrm{H}}\mathbf{B}^{-1}, \tag{3.56}$$

where $\mathbf{B} \in \mathbb{C}^{m\times m}$, $\mathbf{U} \in \mathbb{C}^{m\times n}$, $\mathbf{T} \in \mathbb{C}^{m\times n}$. Let $\mathbf{U} = \mathbf{T} = \mathbf{d} \in \mathbb{C}^{m\times 1}$, and we have

$$\begin{aligned}\left(\mathbf{B} \pm \mathbf{d}\mathbf{d}^{\mathrm{H}}\right)^{-1} &= \mathbf{B}^{-1} \mp \mathbf{B}^{-1}\mathbf{d}\left(1 \pm \mathbf{d}^{\mathrm{H}}\mathbf{B}^{-1}\mathbf{d}\right)^{-1}\mathbf{d}^{\mathrm{H}}\mathbf{B}^{-1} \\ &= \mathbf{B}^{-1} \mp \frac{\mathbf{B}^{-1}\mathbf{d}\mathbf{d}^{\mathrm{H}}\mathbf{B}^{-1}}{1 \pm \mathbf{d}^{\mathrm{H}}\mathbf{B}^{-1}\mathbf{d}}.\end{aligned} \tag{3.57}$$

Take the determinant of (3.57) and consider the following equation in Golub and Loan (1996)

$$\det\left(\mathbf{I} \pm \mathbf{U}\mathbf{T}^{\mathrm{H}}\right) = \det\left(\mathbf{I} \pm \mathbf{T}^{\mathrm{H}}\mathbf{U}\right), \tag{3.58}$$

then, we can rewrite (3.57) as

$$\begin{aligned}\det\left(\left(\mathbf{B} \pm \mathbf{d}\mathbf{d}^{\mathrm{H}}\right)^{-1}\right) &= \det\left(\mathbf{B}^{-1}\right)\det\left(\mathbf{I} \mp \frac{\mathbf{d}\mathbf{d}^{\mathrm{H}}\mathbf{B}^{-1}}{1 \pm \mathbf{d}^{\mathrm{H}}\mathbf{B}^{-1}\mathbf{d}}\right) \\ &= \det\left(\mathbf{B}^{-1}\right)\det\left(\mathbf{I} \mp \frac{\mathbf{d}^{\mathrm{H}}\mathbf{B}^{-1}\mathbf{d}}{1 \pm \mathbf{d}^{\mathrm{H}}\mathbf{B}^{-1}\mathbf{d}}\right) \\ &= \det\left(\mathbf{B}^{-1}\right)\det\left(\left(1 \pm \mathbf{d}^{\mathrm{H}}\mathbf{B}^{-1}\mathbf{d}\right)^{-1}\right).\end{aligned} \tag{3.59}$$

From (3.59), we can obtain a log-determinant equation given by (3.60), which is quite useful to evaluate (3.55) iteratively,

$$\log_2\det\left(\mathbf{B} \pm \mathbf{d}\mathbf{d}^{\mathrm{H}}\right) = \log_2\det\left(\mathbf{B}\right) + \log_2\det\left(1 \pm \mathbf{d}^{\mathrm{H}}\mathbf{B}^{-1}\mathbf{d}\right). \tag{3.60}$$

The proof of (3.50) is concluded by substituting (3.60) into (3.55) and applying some mathematical manipulations.

Furthermore, as for the first term in (3.50), we can calculate it by repeatedly making use of (3.57) and (3.60), which is described in Table 3.4.

As shown in the proof of Theorem 3.2, (3.52) has been broken down into several parts shown in (3.50), which can be efficiently computed since $\left(\tilde{\boldsymbol{\Phi}}^{(l)}\right)^{-1}$, $\det\left(\boldsymbol{\Phi}^{(l)}\right)$, and $\left(\mathbf{A}^{(l)}\right)^{-1}$ are irrelevant of (k, m, n) and only computed at the initial stage for each iterative loop. Other computations in (3.50) are no more than several complex vector/matrix multiplications. Hence, based on Theorem 3.2, we propose a greedy capacity maximization (GCM) relay/antenna selection algorithm (Ding et al. 2010b) shown in Table 3.5.

Table 3.4 The iterative calculation method for the first term in (3.50)

1. Initialization:
Set $i = 0, \mathbf{Q}_0 = \mathbf{A}^{(l)}, \mathbf{Q}_0^{-1} = \left(\mathbf{A}^{(l)}\right)^{-1}$
2. Iterative loop:
Set $i = i + 1$
$\mathbf{Q}_i = \mathbf{Q}_{i-1} + s_i \mathbf{q}_i \mathbf{q}_i^{\mathrm{H}}$
$\frac{1}{2}\log_2 \det(\mathbf{Q}_i) = \frac{1}{2}\log_2 \det(\mathbf{Q}_{i-1}) + \frac{1}{2}\log_2 \det\left(1 + s_i \mathbf{q}_i^{\mathrm{H}} \mathbf{Q}_{i-1}^{-1} \mathbf{q}_i\right)$
$\mathbf{Q}_i^{-1} = \mathbf{Q}_{i-1}^{-1} - \frac{s_i \mathbf{Q}_{i-1}^{-1} \mathbf{q}_i \mathbf{q}_i^{\mathrm{H}} \mathbf{Q}_{i-1}^{-1}}{1 + s_i \mathbf{q}_i^{\mathrm{H}} \mathbf{Q}_{i-1}^{-1} \mathbf{q}_i}$
3. If $i < 4$, go to Step 2
Else, terminate with $\frac{1}{2}\log\det(\mathbf{Q}_4)$ as the first term of (3.50)

Table 3.5 GCM relay/antenna selection algorithm

1. Initialization:
Set the candidate antenna pair set
$\Omega = \{(k, m, n) \mid 1 \le k \le K, 1 \le m \le N_{\mathrm{r}}, 1 \le n \le N_{\mathrm{r}}\}$,
$l = 0, \mathbf{S}_l = \emptyset, \mathbf{H}^{(0)} = \mathbf{G}^{(0)} = \mathbf{W}^{(0)} = \emptyset, \mathbf{A}^{(0)} = \mathbf{\Phi}^{(0)} = \mathbf{I}_{N_{\mathrm{d}}}, C_{\mathrm{old}} = 0$
2. Iterative loop:
Compute $\tilde{\mathbf{\Phi}}^{(l)}, \left(\tilde{\mathbf{\Phi}}^{(l)}\right)^{-1}, \det\left(\mathbf{\Phi}^{(l)}\right), \mathbf{A}^{(l)}, \left(\mathbf{A}^{(l)}\right)^{-1}$
For each antenna pair $(k, m, n) \in \Omega$, use (3.50) to compute $C_{k,m,n}^{(l+1)}$
Select the $(l+1)$th antenna pair by maximizing $C_{k,m,n}^{(l+1)}$:
$\left(r_{l+1}, b_{l+1}, f_{l+1}\right) = \arg\max_{(k,m,n)\in\Omega} \left\{C_{k,m,n}^{(l+1)}\right\}$
3. If $\max_{(k,m,n)\in\Omega} \left\{C_{k,m,n}^{(l+1)}\right\} > C_{\mathrm{old}}$, then let $C_{\mathrm{old}} = \max_{(k,m,n)\in\Omega} \left\{C_{k,m,n}^{(l+1)}\right\}$
Set $l = l + 1$; update $\mathbf{H}^{(l+1)} = \left[\left(\mathbf{H}^{(l)}\right)^{\mathrm{T}}, \mathbf{h}_{r_{l+1},b_{l+1}}^{\mathrm{T}}\right]^{\mathrm{T}}, \mathbf{G}^{(l+1)} = \left[\mathbf{G}^{(l)}, \mathbf{g}_{r_{l+1},f_{l+1}}\right]$,
$\mathbf{S}_{l+1} = \left\{\mathbf{S}_l, \left(r_{l+1}, b_{l+1}, f_{l+1}\right)\right\}$, and $\Omega = \Omega - \left\{\left(r_{l+1}, b_{l+1}, :\right), \left(r_{l+1}, :, f_{l+1}\right)\right\}$
Update $\mathbf{W}^{(l+1)} = \mathbf{W}_{r_{l+1},b_{l+1}}^{(l+1)}$ from (3.48); Then go to Step 2
Else, terminate with $\mathbf{S}_L$ as the selected relay antenna pairs

3.3.3 MSE Minimization for the System with General Processing

Since (3.28) is a closed-form expression to evaluate the system MSE, we can perform an exhaustive search to obtain the optimal antenna pair set. However, such method is in fact infeasible considering the required trials could be as large as $\sum_{l=\min(N_{\mathrm{s}},N_{\mathrm{d}})}^{K} \mathrm{C}_K^l \left(N_{\mathrm{r}}^2\right)^l$, where $\left(N_{\mathrm{r}}^2\right)^l$ refers to the number of candidate antenna pairs at each relay node. In a modest example where $N_{\mathrm{s}} = N_{\mathrm{d}} = 4$, $N_{\mathrm{r}} = 2$, and $K = 6$, the exhaustive search would involve approximately 14,000 trials, with each trial requiring the inversion of a matrix of size 4×4 shown in (3.28).

Therefore, instead of dealing with (3.28) directly, we assume l antenna pairs $\mathbf{S}_l = \{(r_1, b_1, f_1), (r_2, b_2, f_2), \ldots, (r_l, b_l, f_l)\}$ have been selected and greedily minimize the MSE by adding the $(l+1)$-th antenna pair to the system.

Again, we recall the definitions of $\mathbf{H}^{(l)}$, $\mathbf{G}^{(l)}$, $\mathbf{H}_{k,m}^{(l+1)}$, and $\mathbf{G}_{k,n}^{(l+1)}$ in (3.36), (3.37), (3.38), and (3.39). For every unselected candidate backward channel $\mathbf{h}_{k,m}$ of $\mathbf{S}$, we calculate the associated relay gain $w_{k,m}$ according to (3.26) as

$$w_{k,m} = \sqrt{\frac{P_{\text{loc}}}{\sigma_x^2 \|\mathbf{h}_{k,m}\|^2 + 1}}, \tag{3.61}$$

where the maximum local power P_{loc} is defined in (3.25) and we have

$$\mathbf{W}_{k,m}^{(l+1)} = \begin{bmatrix} \mathbf{W}^{(l)} & \mathbf{0} \\ \mathbf{0} & w_{k,m} \end{bmatrix}. \tag{3.62}$$

It should be noted that unlike that in (3.48), $\mathbf{W}^{(l)}$ in (3.62) doesn't need to be power diluted when a new antenna pair join $\mathbf{S}_l$ because each relay node has an independent local power constraint in here.

In order to efficiently calculate the system MSE shown in (3.28), we propose Theorem 3.3.

Theorem 3.3. *The network MSE resulted from the* $(l+1)$*-th additional antenna pair* (k, m, n) *can be evaluated as*

$$Q_{k,m,n}^{(l+1)} = \sigma_x^2 tr\left\{\left(\boldsymbol{\Phi}^{(l)} + w_{k,m}^2 \mathbf{g}_{k,n}\mathbf{g}_{k,n}^{\mathrm{H}}\right)\left(\mathbf{C}_{k,m,n}^{(l)}\right)^{-1}\right\}, \tag{3.63}$$

where

$$\begin{aligned}
\boldsymbol{\Phi}^{(l)} &= \mathbf{I}_{N_{\mathrm{d}}} + \left(\mathbf{G}^{(l)}\mathbf{W}^{(l)}\right)\left(\mathbf{G}^{(l)}\mathbf{W}^{(l)}\right)^{\mathrm{H}}, \\
\left(\mathbf{C}_{k,m,n}^{(l)}\right)^{-1} &= \left(\mathbf{B}_{k,m,n}^{(l)}\right)^{-1} - \frac{\left(\mathbf{B}_{k,m,n}^{(l)}\right)^{-1}\mathbf{g}_{k,n}\left(\mathbf{v}_{k,m,n}^{(l)}\right)^{\mathrm{H}}\left(\mathbf{B}_{k,m,n}^{(l)}\right)^{-1}}{1 + \left(\mathbf{v}_{k,m,n}^{(l)}\right)^{\mathrm{H}}\left(\mathbf{B}_{k,m,n}^{(l)}\right)^{-1}\mathbf{g}_{k,n}}, \\
\left(\mathbf{B}_{k,m,n}^{(l)}\right)^{-1} &= \left(\mathbf{A}^{(l)}\right)^{-1} - \frac{\left(\mathbf{A}^{(l)}\right)^{-1}\mathbf{u}_{k,m,n}^{(l)}\mathbf{g}_{k,n}^{\mathrm{H}}\left(\mathbf{A}^{(l)}\right)^{-1}}{1 + \mathbf{g}_{k,n}^{H}\left(\mathbf{A}^{(l)}\right)^{-1}\mathbf{u}_{k,m,n}^{(l)}}, \\
\mathbf{A}^{(l)} &= \boldsymbol{\Phi}^{(l)} + \sigma_x^2\left(\mathbf{G}^{(l)}\mathbf{W}^{(l)}\mathbf{H}^{(l)}\right)\left(\mathbf{G}^{(l)}\mathbf{W}^{(l)}\mathbf{H}^{(l)}\right)^{\mathrm{H}}, \\
\mathbf{u}_{k,m,n}^{(l)} &= \sigma_x^2\left(\mathbf{G}^{(l)}\mathbf{W}^{(l)}\mathbf{H}^{(l)}\right)w_{k,m}\mathbf{h}_{k,m}^{\mathrm{H}} + w_{k,m}^2\mathbf{g}_{k,n}, \\
\mathbf{v}_{k,m,n}^{(l)} &= \sigma_x^2\mathbf{F}_{k,m,n}^{(l)}w_{k,m}\mathbf{h}_{k,m}^{\mathrm{H}}, \\
\mathbf{F}_{k,m,n}^{(l)} &= \mathbf{G}^{(l)}\mathbf{W}^{(l)}\mathbf{H}^{(l)} + w_{k,m}\mathbf{g}_{k,n}\mathbf{h}_{k,m}.
\end{aligned} \tag{3.64}$$

Proof. According to (3.28) and by some mathematical manipulations, the MSE (with β omitted) with $\mathbf{h}_{k,m}$ and $\mathbf{g}_{k,n}$ added to $\mathbf{H}^{(l)}$ and $\mathbf{G}^{(l)}$ can be represented as

$$Q_{k,m,n}^{(l+1)} = \sigma_x^2 tr\left\{\mathbf{\Phi}_{k,m,n}^{(l+1)}\left(\mathbf{\Phi}_{k,m,n}^{(l+1)} + \sigma_x^2\left(\mathbf{G}_{k,n}^{(l+1)}\mathbf{W}_{k,m}^{(l+1)}\mathbf{H}_{k,m}^{(l+1)}\right)\left(\mathbf{G}_{k,n}^{(l+1)}\mathbf{W}_{k,m}^{(l+1)}\mathbf{H}_{k,m}^{(l+1)}\right)^{\mathrm{H}}\right)^{-1}\right\}, \tag{3.65}$$

where

$$\mathbf{\Phi}_{k,m,n}^{(l+1)} = \mathbf{G}_{k,n}^{(l+1)}\mathbf{W}_{k,m}^{(l+1)}\left(\mathbf{G}_{k,n}^{(l+1)}\mathbf{W}_{k,m}^{(l+1)}\right)^{\mathrm{H}} + \mathbf{I}_{N_\mathrm{d}}. \tag{3.66}$$

Substituting (3.66) into (3.65) and applying the matrix/vector definitions in (3.64), we get

$$Q_{k,m,n}^{(l+1)} = \sigma_x^2 tr\left\{\left(\mathbf{\Phi}^{(l)} + w_{k,m}^2\mathbf{g}_{k,n}\mathbf{g}_{k,n}^{\mathrm{H}}\right)\left(\mathbf{A}^{(l)} + \mathbf{u}_{k,m,n}^{(l)}\mathbf{g}_{k,n}^{\mathrm{H}} + \mathbf{g}_{k,n}\mathbf{v}_{k,m,n}^{(l)}\right)^{-1}\right\}. \tag{3.67}$$

Let $\mathbf{B}_{k,m,n}^{(l)} = \mathbf{A}^{(l)} + \mathbf{u}_{k,m,n}^{(l)}\mathbf{g}_{k,n}^{\mathrm{H}}$, from (3.56) we can obtain

$$\left(\mathbf{B}_{k,m,n}^{(l)}\right)^{-1} = \left(\mathbf{A}^{(l)}\right)^{-1} - \frac{\left(\mathbf{A}^{(l)}\right)^{-1}\mathbf{u}_{k,m,n}^{(l)}\mathbf{g}_{k,n}^{\mathrm{H}}\left(\mathbf{A}^{(l)}\right)^{-1}}{1 + \mathbf{g}_{k,n}^{H}\left(\mathbf{A}^{(l)}\right)^{-1}\mathbf{u}_{k,m,n}^{(l)}}. \tag{3.68}$$

Further denote $\mathbf{C}_{k,m,n}^{(l)} = \mathbf{B}_{k,m,n}^{(l)} + \mathbf{g}_{k,n}\left(\mathbf{v}_{k,m,n}^{(l)}\right)^{\mathrm{H}}$. Then, we have

$$\left(\mathbf{C}_{k,m,n}^{(l)}\right)^{-1} = \left(\mathbf{B}_{k,m,n}^{(l)}\right)^{-1} - \frac{\left(\mathbf{B}_{k,m,n}^{(l)}\right)^{-1}\mathbf{g}_{k,n}\left(\mathbf{v}_{k,m,n}^{(l)}\right)^{\mathrm{H}}\left(\mathbf{B}_{k,m,n}^{(l)}\right)^{-1}}{1 + \left(\mathbf{v}_{k,m,n}^{(l)}\right)^{\mathrm{H}}\left(\mathbf{B}_{k,m,n}^{(l)}\right)^{-1}\mathbf{g}_{k,n}}. \tag{3.69}$$

The proof is completed by substituting (3.68) and (3.69) into (3.67).

As shown in (3.63), $Q_{k,m,n}^{(l+1)}$ can be evaluated efficiently since $\left(\mathbf{A}^{(l)}\right)^{-1}$ is free from (k, m, n) and only computed once for each iterative loop. Other computations required by (3.63) are no more than several vector/matrix multiplications. Based on (3.63), we can iteratively activate the antenna pairs one by one as long as the corresponding MSE keeps decreasing. Although this approach cannot guarantee a global optimal solution as the exhaustive search, it has the potential to find a satisfactory local optimal solution because of three facts: (i) Local optimality can be reflected in the nonincreasing MSE based searching, (ii) the noise terms have been correctly incorporated into (3.63), and (iii) l can be as large as K to exploit the diversity gain of the network. Hence, we propose an MMSE-based greedy MSE minimization (GMM) relay/antenna selection algorithm (Ding et al. 2010c) summarized in Table 3.6.

Table 3.6 GMM relay/antenna selection algorithm

1. Initialization:
   Set the candidate antenna pair set
   $\Omega = \{(k, m, n)\,|1 \le k \le K,\ 1 \le m \le N_\mathrm{r},\ 1 \le n \le N_\mathrm{r}\}$,
   $l = 0$, $\mathbf{S}_l = \emptyset$, $\mathbf{H}^{(0)} = \mathbf{G}^{(0)} = \mathbf{W}^{(0)} = \emptyset$, $\mathbf{A}^{(0)} = \mathbf{\Phi}^{(0)} = \mathbf{I}_{N_\mathrm{d}}$, $Q_\mathrm{old} = +\infty$
2. Iterative loop:
   Compute $\mathbf{W}^{(l)}, \mathbf{\Phi}^{(l)}, \mathbf{A}^{(l)}, \left(\mathbf{A}^{(l)}\right)^{-1}$;
   For each antenna pair $(k, m, n) \in \Omega$, use (3.63) to compute $Q_{k,m,n}^{(l+1)}$
   Select the $(l + 1)$th antenna pair by minimizing $Q_{k,m,n}^{(l+1)}$:
   $\left(r_{l+1}, b_{l+1}, f_{l+1}\right) = \arg \min\limits_{(k,m,n)\in\Omega} \left\{Q_{k,m,n}^{(l+1)}\right\}$
3. If $\min\limits_{(k,m,n)\in\Omega} \left\{Q_{k,m,n}^{(l+1)}\right\} < Q_\mathrm{old}$, then let $Q_\mathrm{old} = \min\limits_{(k,m,n)\in\Omega} \left\{Q_{k,m,n}^{(l+1)}\right\}$
   Set $l = l + 1$; update $\mathbf{H}^{(l+1)} = \left[\left(\mathbf{H}^{(l)}\right)^\mathrm{T}, \mathbf{h}_{r_{l+1},b_{l+1}}^\mathrm{T}\right]^\mathrm{T}$, $\mathbf{G}^{(l+1)} = \left[\mathbf{G}^{(l)}, \mathbf{g}_{r_{l+1},f_{l+1}}\right]$,
   $\mathbf{S}_{l+1} = \left\{\mathbf{S}_l, \left(r_{l+1}, b_{l+1}, f_{l+1}\right)\right\}$, $\Omega = \Omega - \left\{\left(r_{l+1}, b_{l+1}, :\right), \left(r_{l+1}, :, f_{l+1}\right)\right\}$
   Update $\mathbf{W}^{(l+1)} = \mathbf{W}_{r_{l+1},b_{l+1}}^{(l+1)}$ from (3.62); Then go to Step 2
   Else, terminate with $\mathbf{S}_L$ as the selected relay antenna pairs

3.4 Simulation and Analysis

We have proposed three greedy relay/antenna selection schemes in Sects. 3.3.1, 3.3.2, and 3.3.3, and hence, we will accordingly divide the simulation discussions into three parts. First, for the system with double ZF processing, we evaluate the capacity performance of the proposed DZF-GCM algorithm. Second, for the system with general processing, we investigate the capacity gain and scaling law of the proposed GCM algorithm. Third, we check the MSE and BER performance of the proposed GMM algorithm for the system with general processing. We will see from the efforts involved in the second and third simulation parts that exhaustive searching is indeed computationally demanding, which only allows us to get very limited data to observe the trend of the performance upper bound.

3.4.1 The Proposed DZF-GCM Algorithm

In the first part of our simulations, we assume $N_\mathrm{s} = N_\mathrm{d} = 4$, $N_\mathrm{r} = 2$, $L = \min\{N_\mathrm{s}, N_\mathrm{d}\} = 4$. All channels are assumed to be uncorrelated Rayleigh fading, the entries of which are modeled as i.i.d. ZMCSCG random variables with unit covariance. And the node **S** can access full CSI to perform the relay/antenna selection algorithm. We denote SNR at node **S** as $SNR_1 = P_\mathrm{s}/N_0$ (with the noise be normalized to 1, i.e., $N_0 = 1$) and SNR at activated relay/antenna points as $SNR_2 = P_\mathrm{r}/N_0$. SNR_1 is set to be 5 or 10 dB, and SNR_2 is equal to 10 dB. 10,000 Monte Carlo runs were conducted for each relay deployment. Note that the simulated case with $SNR_1 < SNR_2$ represents a realistic cellular downlink scenario, in which relays locate closer to the destination terminal **D** than to the source terminal **S**.

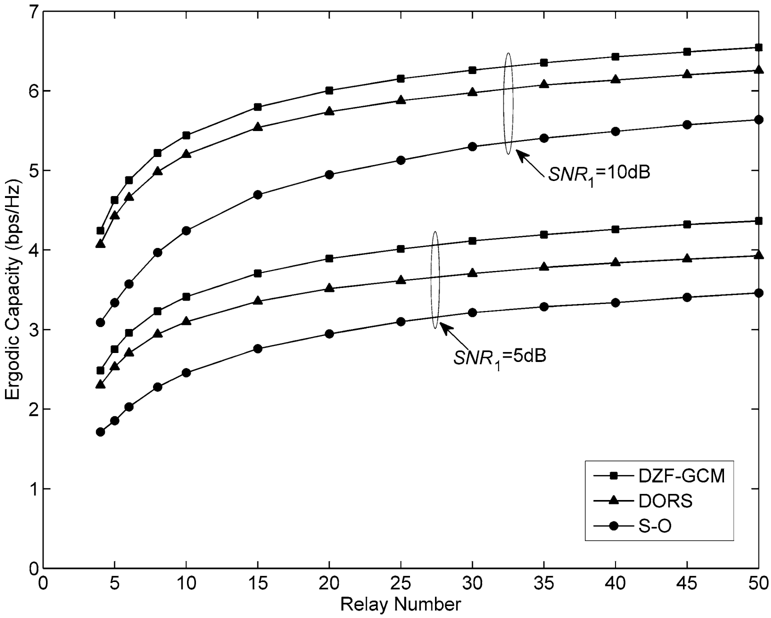

Fig. 3.2 Comparison of system capacities with different relay numbers for the DZF-GCM algorithm

In Fig. 3.2, we plot the ergodic capacity of the proposed DZF-GCM algorithm compared with the S-O and DORS schemes. From the upper set of curves ($SNR_1 = 10$ dB) in Fig. 3.2, we observe that S-O scheme is strictly inferior to the other two by about 15% and the proposed GCM scheme exhibits a moderate improvement compared to the DORS algorithm. Next, let us turn to the lower set of curves where SNR_1 is decreased to 5 dB to stress the noise term at the relay nodes. It is not surprising to find that the GCM scheme largely outperforms the DORS and S-O algorithms by approximately 10% and 30% (20 relays), respectively. The reason behind the results is the fact that the proposed GCM scheme optimally maximizes the capacity with the noise terms accurately reflected in the selection procedure, which becomes essentially important when SNR_1 is low.

3.4.2 The Proposed GCM Algorithm

In the second part of our simulations, we also assume the channels to be uncorrelated Rayleigh fading. The channel coefficients are modeled as i.i.d. ZMCSCG random variables with unit covariance. The antenna configurations are $N_s = N_d = 4$ and $N_r = 2$. Furthermore, we denote the receive SNR at the relay nodes as

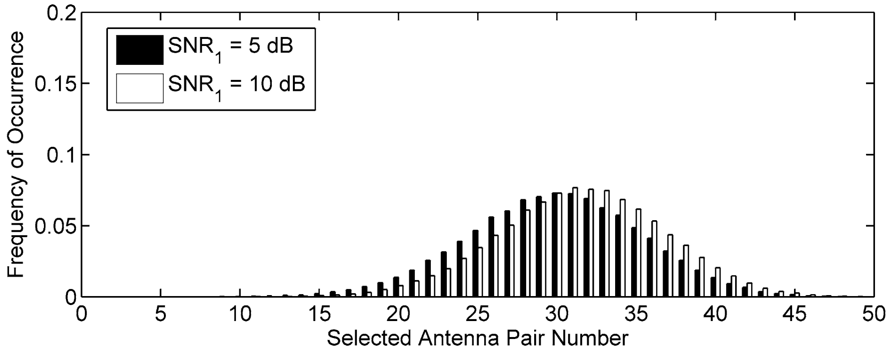

Fig. 3.3 Frequency histogram of the selected antenna pairs for the GCM algorithm

$SNR_1 = P_s/N_0$ and the overall SNR at the destination node as $SNR_2 = P_r/N_0$. Again, SNR_1 is set to be 5 or 10 dB, and SNR_2 is equal to 10 dB. We conduct 10,000 Monte Carlo runs for each relay deployment.

First, we would like to check how many relay antenna pairs tend to be activated in the proposed GCM algorithm, which will be compared with the S-O and DORS algorithm. Figure 3.3 presents the frequency histogram of the selected antenna pairs for the GCM scheme when $K = 40$. We can observe from Fig. 3.3 that the number of selected antenna pairs of the GCM algorithm is much larger than $\min\{N_s, N_d\} = 4$, which is the number of selected antenna pairs in the S-O and DORS algorithm. Besides, when SNR_1 becomes higher, a couple of more antenna pairs will be expected to participate in the AF relaying because the issue of noise amplification at relay nodes becomes less serious. Figure 3.3 also shows that how amazingly the GCM algorithm can handle a large number of MIMO relays, while it is impossible to implement the exhaustive searching for $K = 40$. For example, the combinations of choosing 10 antenna pairs from 40 relays in Fig. 3.3 will exceed one trillion, which is shockingly large. Needless to say, the trials of exhaustively searching for 30 antenna pairs as the GCM algorithm pulls off in Fig. 3.3 will become an astronomically high number.

In Fig. 3.4, we show the ergodic capacity of the proposed GCM algorithm, the DORS and S-O schemes, together with the exhaustive search scheme. Due to the very high complexity of the exhaustive search, we are only able to give the results for cases when $K \leq 8$. From the upper set of curves ($SNR_1 = 10$ dB) in Fig. 3.4, we observe that the proposed GCM scheme largely outperforms the DORS and S-O schemes by more than 25% (20 relays). Furthermore, the capacity gain of the GCM algorithm goes beyond 30% (20 relays) in the lower set of curves where we reduce SNR_1 to 5 dB, representing a more serious noise situation at the relay nodes. Besides, the performance gap between the GCM scheme and the exhaustive search scheme is reasonably small. There are mainly two factors accounting for the improved performance of the proposed GCM scheme. One aspect is that the GCM scheme correctly incorporates the noise terms into the antenna selection process

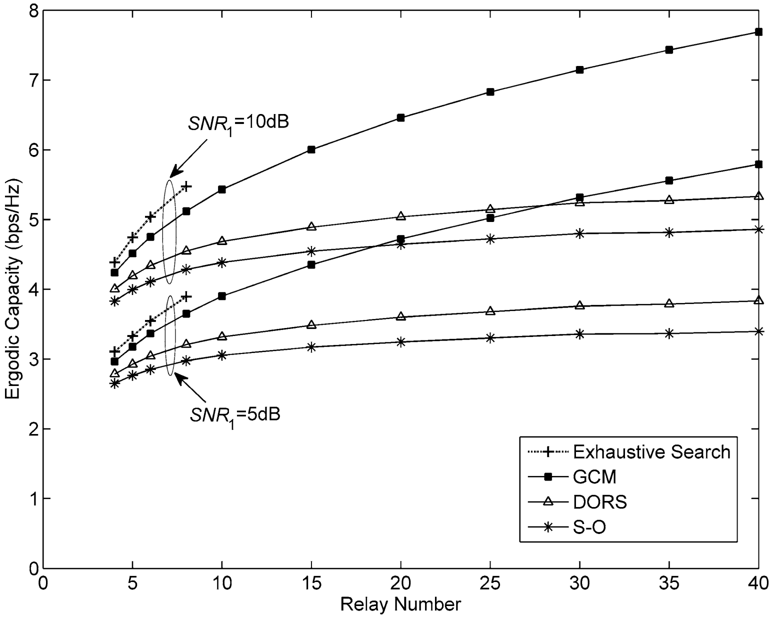

Fig. 3.4 Comparison of system capacities with different relay numbers for the GCM algorithm

unlike the previous schemes. The other aspect, which is more important, is that the DORS and S-O algorithms put restriction on the number of the selected antennas as $L = M = \min\{N_s, N_d\}$, which could waste the diversity and power gain offered by the AF MIMO relay network.

An interesting observation is that the GCM scheme seems to exhibit a higher order of capacity scaling tendency compared to the DORS and S-O algorithms. Since the authors in Torabi and Frigon (2008) established that the network capacity of the S-O algorithm scales asymptotically with $\log\log K$ and it was proved that the achievable upper bound capacity limit of the AF MIMO relay network should be proportional to $\log K$ (Nabar et al. 2003; Bolcskei et al. 2006), we speculate that the network capacity of the GCM scheme should also scale linearly with $\log K$. This speculation is somehow counterintuitive because it seems contradictory to the capacity scaling law for the noncoherent AF relaying protocol in Nabar et al. (2003) and Bolcskei et al. (2006). That law states that if all relays amplify and forward the received signals to the destination node without any kind of coherent signal processing, the network capacity limit will be independent of K, that is, the distributed array gain offered by a large number of relay antennas will be completely lost in the noncoherent AF relaying scheme. On the other hand, the GCM scheme can be viewed as a selective noncoherent AF relaying protocol since the received signal goes right through the backward and forward relay antennas. So it would be surprising to know that the proposed GCM could achieve comparable performance to the "doubly coherent" schemes in Nabar et al. (2003) and Bolcskei et al. (2006).

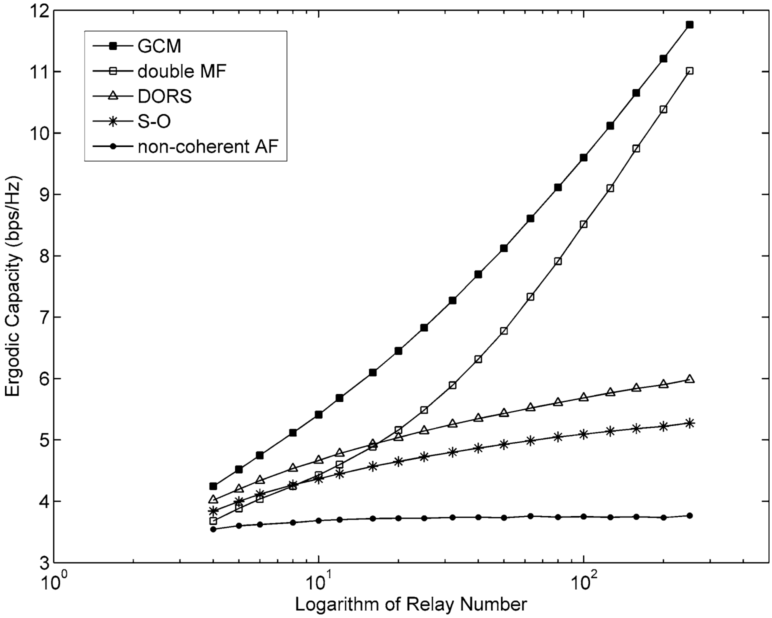

Fig. 3.5 Comparison of asymptotic system capacities for the GCM algorithm

In order to investigate the asymptotic capacity of the aforementioned schemes, we plot the ergodic capacity curves in Fig. 3.5 with emphasis laid on the scaling tendency. The SNRs are set to $SNR_1 = SNR_2 = 10$dB. Furthermore, two curves are added in Fig. 3.5, respectively representing the double MF scheme (Bolcskei et al. 2006) and the noncoherent AF relaying protocol (Nabar et al. 2003; Bolcskei et al. 2006). In the double MF scheme, each relay node performs backward MF reception and forward MF precoding transmission for one data stream, yielding a coherently combined signal at the destination node. As we have explained, in Fig. 3.5 the noncoherent AF relaying scheme leaves a flat trail independent of K, and the DORS and S-O algorithms make the ergodic capacity scale with $\log\log K$. However, both the proposed GCM scheme and the double MF scheme show linearly increasing capacity with respect to $\log K$, which achieves the capacity upper bound in the sense of asymptotic scaling tendency (Nabar et al. 2003; Bolcskei et al. 2006). Therefore, we show by simulation that the capacity of the AF MIMO relay network with relay/antenna selection should be governed by the same logarithmical scaling law.

3.4.3 The Proposed GMM Algorithm

In the third part of our simulations, we adopt a realistic antenna setup as $N_s = N_d = 4$ and $N_r = 2$. The receive SNR at the relay nodes is denoted as $SNR_1 = P_s/N_0$.

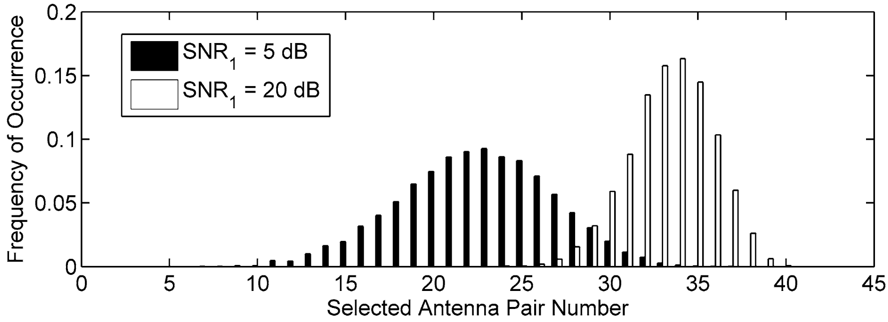

Fig. 3.6 Frequency histogram of the selected antenna pairs for the GMM algorithm

And the receive SNR at the destination node is denoted as $SNR_2 = P_{\mathrm{loc}}/N_0$. SNR_1 is set to be 5 or 20 dB, and SNR_2 is equal to 5 dB. Again, we conduct 10,000 Monte Carlo runs for each relay deployment.

First, we make a brief complexity comparison among the aforementioned schemes. The exhaustive search scheme is nearly impossible to be analyzed when $K > 8$, which is verified by our simulation efforts. The DORS and S-O algorithms stop the antenna selection procedure when $l = M = \min\{N_{\mathrm{s}}, N_{\mathrm{d}}\}$, whereas the proposed GMM scheme tends to select more antennas ($M \leq l \leq K$) until the MSE begins to increase. In each antenna selection loop, although the GMM scheme is more involved than the DORS and S-O algorithms, its implementation is feasible as explained earlier. Figure 3.6 presents the frequency histogram of the selected antenna pairs for the GMM scheme when $K = 40$. It is not surprising to find that less antenna pairs will be expected to participate the relaying when SNR_1 is lower because the received signals at the relay nodes are more likely to vanish under the noise floor. However, we do observe that the GMM scheme will turn on much more relay nodes than the DORS and S-O algorithms, thus making the performance comparison unfair due to the additional power sources. A simple way to separate the power gain from the enhancement offered by the GMM algorithm is to pose a sum power constraint on the selected L forward antennas as in (3.12) and (3.21), that is, instead of allocating P_{loc} for each activated relay node, we dilute the relay power to $P'_{\mathrm{loc}} = M P_{\mathrm{loc}}/L$. Thereby, the sum power at the activated relay nodes will be the same for the DORS, S-O, and GMM schemes.

In Fig. 3.7, we show the average MSE performance versus relay number for the DORS, S-O, GMM, and exhaustive search schemes. From Fig. 3.7, we find that the GMM scheme largely reduces the MSE compared to the DORS and S-O algorithms, with the gain being more conspicuous when the noise issue at the relay nodes is more serious (e.g., the upper set of curves with $SNR_1 = 5$ dB), and K becomes larger. When comparing the curves for the GMM algorithm respectively with sum power constraint and with local power constraint, we can draw the conclusion that the GMM algorithm without the additional power bonus has already reaped most of the

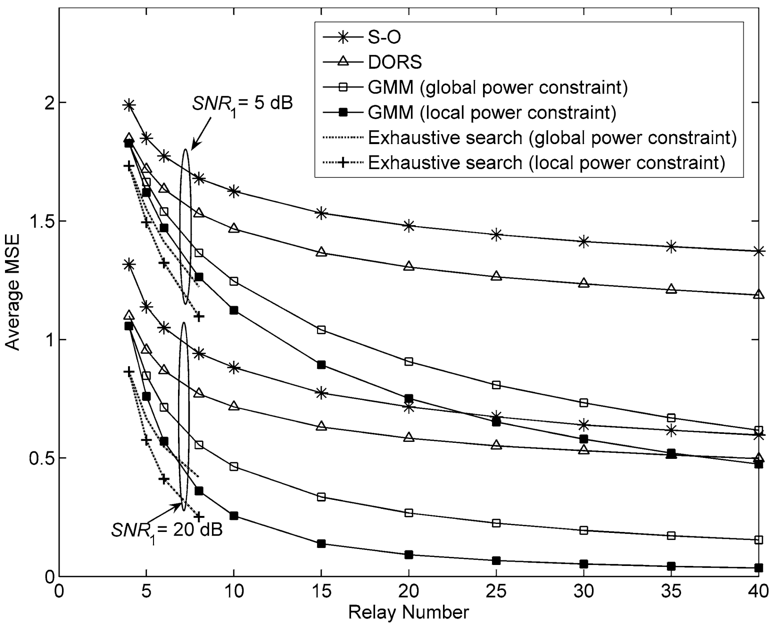

Fig. 3.7 Comparison of system MSE with different relay numbers for the GMM algorithm

performance gain. We also observe that the GMM scheme achieves the performance close to that of exhaustive search, which further confirms the superiority of the proposed scheme.

To illustrate how the MSE performance gains in Fig. 3.7 are interpreted into BER improvement, we plot the average BER curves in Fig. 3.8 with SNR_1 varying from 0 to 30 dB. For all SNR cases, we deploy 15 relays. In addition, we assume that the Wiener filter is employed as the symbol detection filter and the symbols are obtained from the QPSK constellation. As seen from Fig. 3.8, the proposed GMM scheme shows much steeper BER slope than other interested schemes, indicating that more diversity is exploited in our design. With respect to the error floor caused by the limited power in the second hop channels, the proposed GMM scheme also achieves considerable gains. For example, the BER floor of the GMM algorithm with sum power constraint is one order lower than that of the S-O and DORS algorithms. And a much lower BER floor (four orders) compared with the S-O and DORS algorithms is exhibited for the GMM algorithm with local power constraint.

3.5 Conclusion

In this chapter, we propose three greedy antenna selection algorithms, namely, DZF-GCM, GCM, and GMM algorithms. The novelty of the proposed schemes is that the

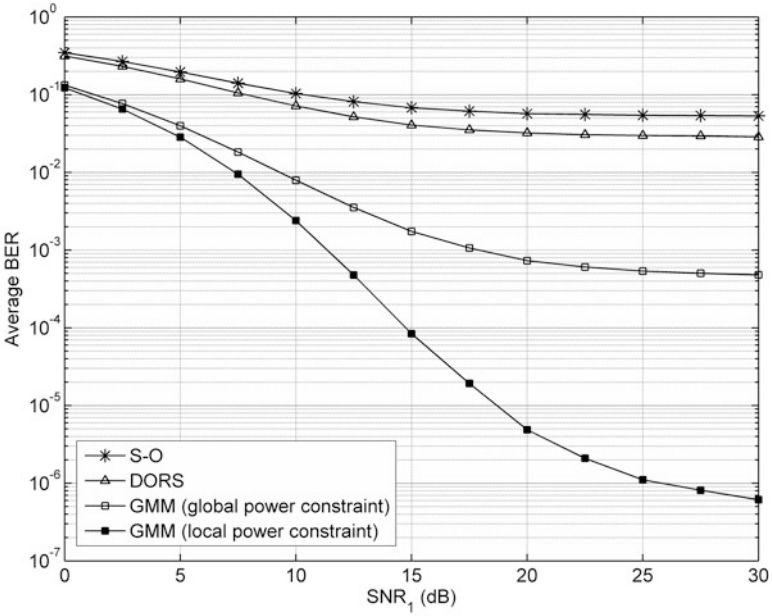

Fig. 3.8 Comparison of average BER with different SNR_1 for the GMM algorithm

closed-form expressions of the capacity increase and MSE decrease resulted from adding one more antenna pair to the AF MIMO relay network are carefully derived, followed by designs of low-complexity greedy relay/antenna selection algorithms. The proposed schemes are either based on the capacity maximization criterion or the MSE minimization criterion. Under the assumption of ZF processing at both transmitter and receiver, simulation results show the proposed DZF-GCM algorithm can achieve higher system capacity than the existing schemes, and the gain is more pronounced in the low SNR regime at the relay nodes. Under the assumption of general processing at both transmitter and receiver, simulation results show that the system capacity obtained from the existing schemes increases with the relay number by the rate of $O(\log\log K)$, while the proposed GCM algorithm can make the system capacity scale like $O(\log K)$ with the relay number, achieving the upper bound of system capacity in the sense of asymptotic capacity. Under the assumption of general processing at both transmitter and receiver, the proposed GMM algorithm can achieve higher diversity gain and lower BER than the existing algorithms, even without the power bonus given by activating more independently powered relay nodes. Moreover, it is well observed that the proposed GCM and GMM algorithms exhibit similar performance compared with the high-complexity exhaustive search method, showing high values of the proposed schemes for both theoretical studies and practical applications.

References

Bolcskei H, Nabar RU, Oyman O, Paulraj AJ (2006) Capacity scaling laws in MIMO relay networks. IEEE Trans Wirel Commun 5(6):1433–1444
Ding M, Liu S, Luo H, Jiang W, Lv J (2010a) Optimum antenna selection with doubly ZF processing for AF MIMO relay systems. IEICE Trans Commun 93(3):762–765
Ding M, Liu S, Luo H, Chen W (2010b) MMSE based greedy antenna selection scheme for AF MIMO relay systems. IEEE Signal Process Lett 17(5):433–436
Ding M, Liu S, Luo H, Wang X (2010c) Antenna selection for AF MIMO relay networks and the capacity scaling tendency. In: IEEE international conference on communications, Cape Town, South Africa, May 2010, pp 1–5
Fan YJ, Thompson J (2007) MIMO configurations for relay channels: theory and practice. IEEE Trans Wirel Commun 6(5):1774–1786
Golub GH, Loan CFV (1996) Matrix computations. The Johns Hopkins University Press, Baltimore
Guan W, Luo HW (2008) Joint MMSE transceiver design in non-regenerative MIMO relay systems. IEEE Commun Lett 12(7):517–519
Lutkepohl H (1996) Handbook of matrices. Wiley, Chichester
Medina OM, Vidal J, Agustin A (2007) Linear transceiver design in non regenerative relays with channel state information. IEEE Trans Signal Process 55(6):2593–2604
Michalopoulos DS, Karagiannidis GK, Tsiftsis TA, Mallik RK (2008) Distributed transmit antenna selection (DTAS) under performance or energy consumption constraints. IEEE Trans Wirel Commun 7(4):1168–1173
Nabar RU, Oyman O, Bolcskei H, Paulraj AJ (2003) Capacity scaling laws in MIMO wireless networks. In: IEEE annual Allerton conference communications, control, and computing, Monticello, pp 378–389
Pabst R, Walke BH, Schultz DC, Yanikomeroglu H, Mukherjee S, Viswanathan H, Lett M, Zirwas W, Dohler M, Aghvami H, Falconer DD, Fettweis GP (2004) Relay-based deployment concepts for wireless and mobile broadband radio. IEEE Commun Mag 42(9):80–89
Peters SW, Heath RW (2008) Nonregenerative MIMO relaying with optimal transmit antenna selection. IEEE Signal Process Lett 15:421–424
Proakis JG (2001) Digital communication. Mc-Graw Hill Press, New York
Tang XJ, Hua YB (2007) Optimal design of non-regenerative MIMO wireless relays. IEEE Trans Wirel Commun 6(4):1398–1407
Torabi MA, Frigon JF (2008) Semi-orthogonal relay selection and beamforming for amplify-and-forward MIMO relay channels. In: IEEE wireless communications and networking conference, Las Vegas, NV, USA, pp 48–53
Yoo T, Goldsmith A (2006) On the optimality of multiantenna broadcast scheduling using zero-forcing beamforming. IEEE J Sel Areas Commun 24(3):528–541
Zhang W, Letaief KB (2008) Opportunistic relaying for dual-hop wireless MIMO channels. In: IEEE global telecommunications conference, New Orleans, LA, USA, pp 3985–3989

Chapter 4
The Seventh Category: Advanced Interference Coordination

Abstract For the seventh category of multipoint cooperative communication technology, we investigate the interference coordination schemes for the uplink frequency division multiple access (FDMA) cellular network in this chapter. First, we elaborate on the topology of a cellular system and show the interference problem in the uplink FDMA network. Second, we discuss the hard, fractional, and soft frequency reuse schemes, and then we address our motivations to improve the static implementation of soft resource reuse scheme with minimum intercell CSI exchanges. Third, we propose an advanced interference coordination scheme that consists of six steps with the key design lying in the enhanced user equipment (UE) categorization and resource-access control policies. In order to verify the effectiveness of the proposed scheme, we resort to the approach of system-level simulation, the methodology and implementation of which are addressed in great details. From the simulation results, it can be observed that compared with the conventional schemes, the proposed scheme can largely increase the efficiency of the trade-off between the cell-edge throughput and the overall throughput, thus showing high values in the study of interference coordination and application for the uplink FDMA cellular network.

Keywords Interference coordination • Uplink cellular network • Frequency reuse • System-level simulation • Cell-edge throughput • Overall throughput

4.1 Introduction

Currently, the long-term evolution (LTE) and LTE-Advanced (LTE-A) systems adopt orthogonal frequency division multiple access (OFDMA) and single carrier frequency division multiple access (SC-FDMA) (see Sect. 2.2) as the multiple access methods respectively for the downlink and uplink transmissions (Sesia et al. 2009). The basic idea is to simultaneously serve many user equipments (UEs) in a cell in a frequency division multiple access (FDMA) manner. Although the

M. Ding and H. Luo, *Multi-point Cooperative Communication Systems: Theory and Applications*, Signals and Communication Technology, DOI 10.1007/978-3-642-34949-2_4,

intra-cell interference can be avoided by the use of FDMA, the intercell co-channel interference, particularly in the uplink FDMA cellular system, is a serious problem which needs to be addressed.

Generally speaking, a cellular system divides a service area into a great number of quasi-hexagonal regions, usually referred to as cell sites (3GPP 2010). Each cell site can be further split into several sectors or cells by the employment of directional antennas. In practice, the number of sectors/cells in each cell site is usually 3 or 6. In an uplink FDMA cellular system, one sector/cell is managed by one base station (BS), which allocates uplink radio resources to UEs and regulates their transmission powers. The uplink radio resources include time slot, frequency sub-band, scramble code, and spatial beam. For a network that frequency resources are universally reused among all the sectors/cells, the co-channel interference will occur when two UEs from adjacent sectors/cells are assigned to use the same frequency sub-band. This uplink co-channel interference is more pronounced when two cell-edge UEs are involved since cell-edge UEs are usually granted with relatively high transmission powers.

There are mainly two approaches to cope with this interference problem. The first one is resource coordination, which can arrange the interference in a desirable way, for example, the hard resource reuse and fractional resource reuse methods addressed in Sect. 2.7.3. The second one is to conduct joint or partially joint scheduling and power allocation operations based on inter-BS communications, for example, the adaptive resource reuse scheme described in Sect. 2.7.5 and the soft resource reuse technology discussed in Sect. 2.7.7.1. The first approach is basically easy to implement and requires small signaling overhead. However, its performance is relatively poorer than that of the second approach. In this chapter, we want to first study some simple scheme in the soft resource reuse technology and then investigate possible improvement for the interested scheme.

4.2 System Model and Existing Technologies

4.2.1 System Model

Figure 4.1 is a schematic diagram showing the topology of a cellular system, together with sector/cell antenna configurations. In Fig. 4.1, UEs are randomly placed in the cellular network. The cell sites are labeled with cell site ID ① $\sim$ ⑦, and each cell site is divided into M sectors/cells, for example, $M = 3$ in Fig. 4.1. For each sector/cell, its radio resource management (RRM) is conducted by a BS, and its cell ID is composed of a cell site ID and a sector ID I_1, I_2, or I_3. Directions of sector/cell antennas are illustrated by arrows in Fig. 4.1. Considering a cell-edge UE x in the sector I_1 of the cell site ① and another cell-edge UE y in the sector I_3 of the cell site ④, which are highlighted by dash-line circles in Fig. 4.1, we can predict that severe uplink co-channel interference will emerge if UE x and y occupy the same uplink radio resource to transmit their signals to the BSs.

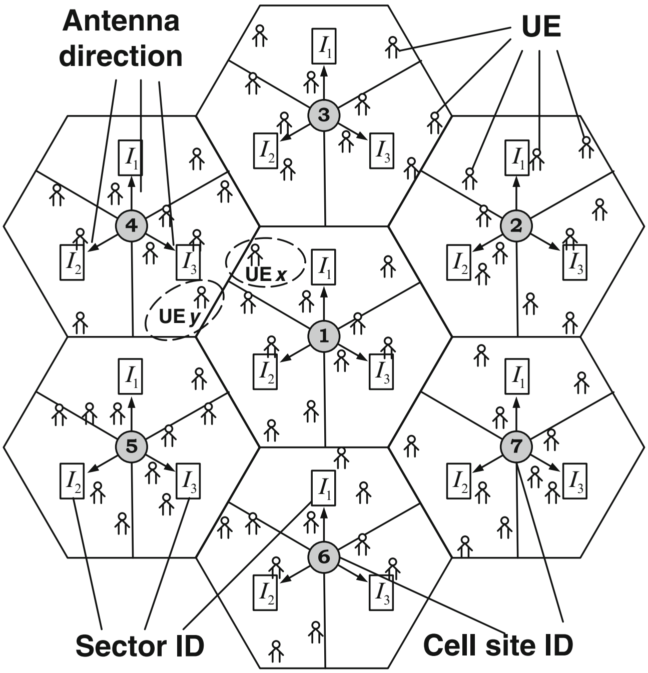

Fig. 4.1 Illustration of a cellular network

4.2.2 Existing Technologies

Two simple schemes are available to cope with the uplink co-channel interference problem. The first scheme is the hard frequency reuse technology and the second is the fractional frequency reuse technology. Although both schemes have been briefly introduced in Sect. 2.7.3.1, we will discuss them in more details in the following.

4.2.2.1 Hard Frequency Reuse Technology

In the hard frequency reuse technology (Hanly and Whiting 1993), each cell can only use part of the system's frequency spectrum, and one cell's frequency resource cannot be reused by adjacent cells; thus intercell co-channel interference between cell-edge UEs can be mostly removed due to the hard frequency spectrum partitioning. However, the frequency reuse factor of this technology is quite low, resulting in a poor performance of overall throughput. An illustration of a hard frequency reuse scheme for a three-cell-site model is depicted in Fig. 4.2, where three hexagonal cell sites are assigned with different frequency resources denoted as f1, f2, and f3.

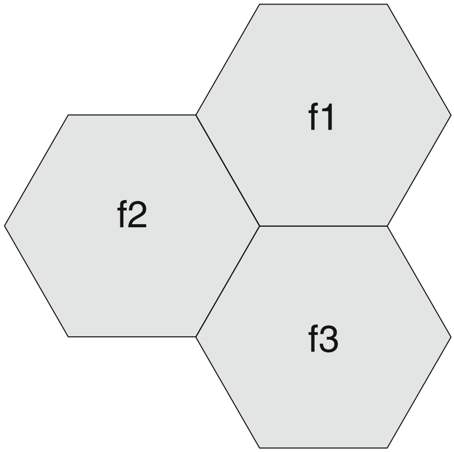

Fig. 4.2 Illustration of a hard frequency reuse scheme for a three-cell-site model

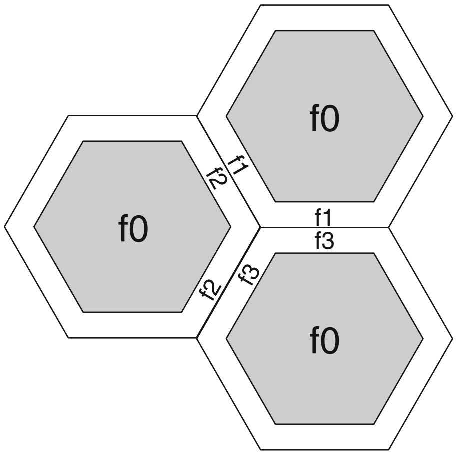

Fig. 4.3 Illustration of a fractional frequency reuse scheme for a three-cell-site model

4.2.2.2 Fractional Frequency Reuse Technology

An improvement to the hard frequency reuse scheme is the fractional frequency reuse method (Alcatel-Lucent 2007), in which each cell reserves some resource referred to as edge UE resource (EUR) for its cell-edge UEs to use and EURs of adjacent cells don't overlap with each other in the network. The core idea of this technology is to protect the cell-edge UEs by allocating to them a dedicated frequency sub-band with intercell interference coordination. Heuristically, we can expect that such method will largely improve the cell-edge throughput as each cell's high-SINR EUR may be more than enough for cell-edge UEs to consume. Besides, all EURs can be further reused by the cell-interior UEs in adjacent cells, leading to a relatively high overall throughput. An illustration of the fractional frequency reuse technology is provided in Fig. 4.3, where the EUR f1, f2, and f3 are respectively set aside for three hexagonal cell sites and f0 is the universal frequency resource for cell-interior UEs. It should be noted that in the conventional fractional

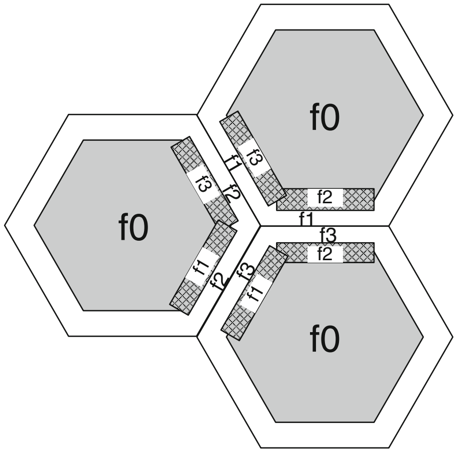

Fig. 4.4 Illustration of the proposed soft frequency reuse scheme for a three-cell-site model

frequency reuse scheme, the union of f1, f2, and f3 has no intersection with f0, which belongs to the third category of multipoint cooperative communication technology. However, if f0 is larger than the union of f1, f2, and f3 or even equals the system bandwidth, then the scheme illustrated by Fig. 4.3 will become a static implementation of soft resource reuse classified into the seventh category of multipoint cooperative communication technology. Obviously, the latter design can achieve higher spectral efficiency.

4.2.2.3 Motivations of Improved Schemes

The hard frequency reuse method holds the merits of easy implementation and low overhead of intercell communication but at the price of a decreased frequency reuse factor. The fractional frequency reuse scheme and the static implementation of soft resource reuse scheme manage to achieve a relatively high-frequency reuse factor without losing the advantages of the hard frequency reuse method. In addition, if some form of channel state information (CSI) is allowed to be exchanged among adjacent cells, though limited amount it may be, the system throughput performance can be further increased. Here we consider improvement for the static implementation of soft resource reuse scheme, which falls into the seventh category of multipoint cooperative communication technology. Our basic idea is to let the BS be able to identify the UEs who have the potential to generate a large amount of interference based on intercell CSI. Then the BS should restrict the usable frequency resource for such UEs in order to reduce the interference emitted to adjacent cells; thus the spectral efficiency of cell-edge UEs can be increased, which in turn will improve the overall throughput of the system since the BS can cut down some frequency resource allocations for cell-edge UEs and accommodate more cell-interior UEs with high transmission rate.

The application of our scheme on a three-cell-site model is illustrated in Fig. 4.4. Compared with Fig. 4.3, Fig. 4.4 shows the new idea that other than the cell-edge and cell-interior UEs, there is another kind of UEs located between the cell-edge and cell-interior regions, which may generate strong interference into the network. So it should be helpful to place additional resource usage restrictions on these UEs to reduce the interference for the sake of cell-edge UEs in adjacent cells. For instance, we can dictate that UEs with potential to generate strong interference are not authorized to access the EURs of adjacent cells, and hence some cell-edge UEs can be saved from being the victims of large interference. The essence of the proposed resource restriction on the strong-interference UEs is to reduce the interference leakage toward other cells from an altruistic viewpoint, which maintains a good communication environment with low interference across the entire network.

4.3 Advanced Interference Coordination Scheme

4.3.1 Overall Description of the Proposed Scheme

Based on the discussions in Sect. 4.2, we propose an advanced interference coordination scheme, which consists of six steps. The key procedure is highlighted in the following.

First, a UE monitors and detects the downlink reference signals (RSs) from multiple neighbor cells, the measurement of which will be reported to its serving BS in a periodic or event-triggering manner. It should be noted that in practical systems, such as the LTE/LTE-A network, the mechanism of RS measurement report already exists (3GPP 2007). Second, the BS performs evaluation on the UE's resistance of interference and tendency of producing interference according to its geometry information reflected in the RS measurement report. The BS will then group UEs into four types based on the evaluation results. Our key design lies in that the BS will assign the four types of UEs to access different parts of the system frequency spectrum. If a UE tends to generate a large amount of interference toward adjacent cells, then the BS will restrict the frequency resource for the UE to use, thus reducing the network interference level from an altruistic perspective so that the cell-edge throughput can be improved. On the other hand, if a UE is not likely to cause much interference to adjacent cells, then the BS will grant the UE to have access to the EUR of the cell if it is available; thus the overall throughput can be increased because the BS scheduler usually works more efficiently on a wider frequency band. Finally, the BS scheduler performs power control, resource allocation, and link adaptation for the served UEs based on the assigned resource-access authorization to the frequency sub-bands.

4.3.2 Implementation Details of the Proposed Scheme

The implementation of the proposed scheme is illustrated in Fig. 4.5, where E1, E2, and E3 are respectively denoted as the EURs for the three cells illustrated by

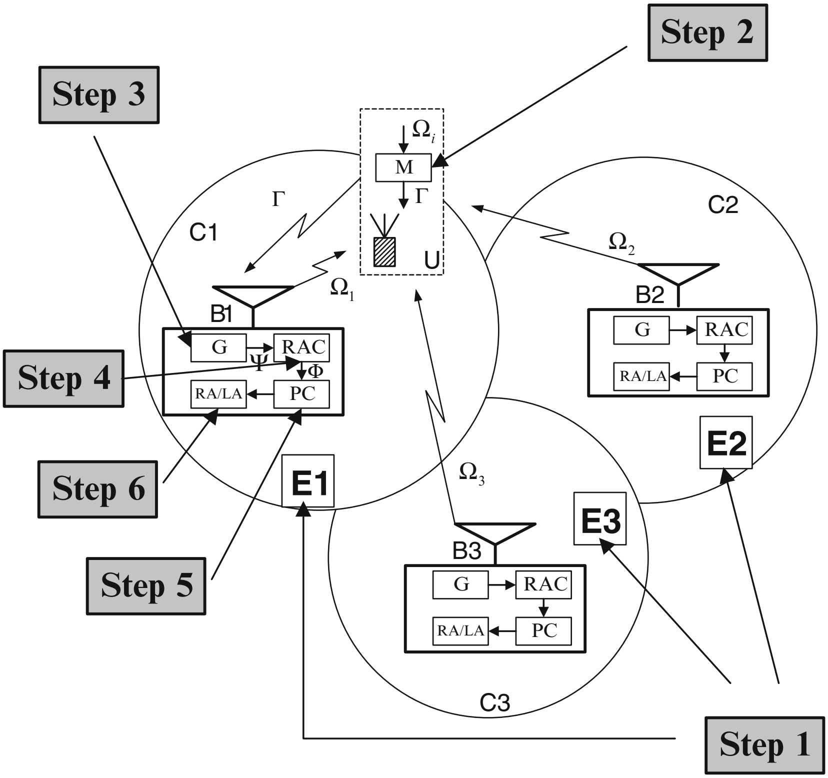

Fig. 4.5 Illustration of the implementation of the proposed scheme for a three-cell model

circles C1, C2, and C3. The three cells are managed by BS entities **B1**, **B2**, and **B3**, respectively. A UE is represented by entity **U** and its serving BS is **B1**. In the entity **U**, module M performs the function of monitoring the downlink RSs Ω_i $(i = 1, 2, 3)$ sent from three BSs, the measurement result of which is contained in a report Γ. After the UE **U** feeds back Γ to **B1**, the BS will then conduct the geometry evaluation and UE categorization in the unit G and obtain the UE categorization result denoted as Ψ. Module RAC is responsible for the resource-access control (RAC), the input and output of which are respectively the UE categorization result Ψ and the RAC result Φ. Finally, the modules PC, RA, and LA are the power control, resource allocation, and link adaptation units, respectively.

The six steps in Fig. 4.5 are elaborated in details as follows.

4.3.2.1 Step 1: Construction of Cell EURs

For a given time t, each cell declares an EUR primarily for the cell-edge UEs, and one cell's EUR doesn't overlap with those of adjacent cells. Suppose that the whole frequency resource set is denoted as $\mathbf{S}$, the elements of which are arranged in an ascending order represented by

$$\mathbf{S} = \{s(i)\,|1 \le i \le C(\mathbf{S}), s(i) < s(i+1), 1 \le s(i) \le C(\mathbf{S})\}, \quad C(\mathbf{S}) = N, \tag{4.1}$$

where $C(\cdot)$ outputs the cardinality of a set. We can divide $\mathbf{S}$ into B candidate EUR sets with no intersection denoted as $\mathbf{S}(j)(j \in \{1, 2, \ldots, B\})$. In each set $\mathbf{S}(j)$, there are $C(\mathbf{S}(j))$ elements written as

$$\mathbf{S}(j) = \left\{s_j(i)\,\middle|1 \le i \le C\left(\mathbf{S}(j)\right), s_j(i) < s_j(i+1), s_j(i) \in \mathbf{S}\right\}, \quad (1 \le j \le B). \tag{4.2}$$

Here, $\mathbf{S}(j)$ satisfies

$$\bigcup_{j=1}^{B} \mathbf{S}(j) \subseteq \mathbf{S}, \tag{4.3}$$

and

$$\mathbf{S}\left(j_k\right) \cap \mathbf{S}\left(j_l\right) = \varnothing, \quad (1 \le j_k,\ j_l \le B, j_k \ne j_l). \tag{4.4}$$

In time t, any two adjacent cells cannot configure the same EUR set. That is to say, for adjacent cells with ID b_k and b_l, we have

$$\mathrm{J}\left(b_k, t\right) \ne \mathrm{J}\left(b_l, t\right), \tag{4.5}$$

where $\mathrm{J}(\cdot)$ maps a cell ID and time t to an EUR set index.

Besides, one cell's EUR can be reused by cell-interior UEs of neighbor cells, which achieves soft frequency reuse. For instance, considering (4.5), the EUR set $\mathbf{S}\left(\mathrm{J}\left(b_k, t\right)\right)$ can be reused by cell-interior UEs in the cell with ID b_l, and the EUR $\mathbf{S}\left(\mathrm{J}\left(b_l, t\right)\right)$ can also be reused by cell-interior UEs in the cell with ID b_k.

In order to further exploit the frequency diversity gain, it's better to construct the EUR sets using frequency hopping. There are generally three ways to construct such kind of EUR sets, that is, localized EURs with contiguous frequency resources, distributed EURs with non-contiguous frequency resources and a regular pattern, and pseudorandomly positioned EURs. They are illustrated respectively in Figs. 4.6, 4.7, and 4.8 for $B = 3$. Note that $\mathbf{S}(1)$, $\mathbf{S}(2)$, and $\mathbf{S}(3)$ are not necessarily of the same size, and the union of $\mathbf{S}(1)$, $\mathbf{S}(2)$, and $\mathbf{S}(3)$ doesn't have to equal set $\mathbf{S}$.

4.3.2.2 Step 2: Report of the Measurement of Downlink RSs

In this step, the UE monitors and detects the downlink RSs Ω_i of the i-th cell. RSs Ω_i can be the synchronization channel signals or common pilot channel signals (Sesia et al. 2009), which contain the cell ID information b_i. The UE's RS

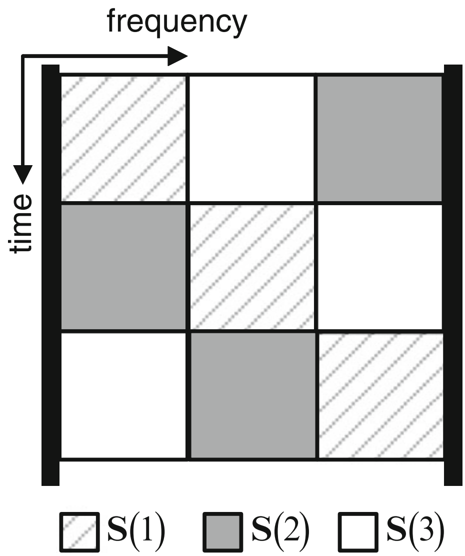

Fig. 4.6 Illustration of localized EURs for $B = 3$

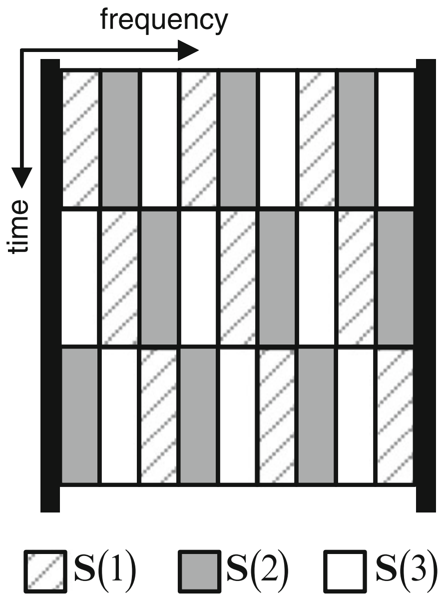

Fig. 4.7 Illustration of distributed EURs for $B = 3$

measurement report Γ should at least include the received power β_i of Ω_i and the corresponding cell ID information b_i. Then at the BS side, the path loss PL_i of the i-th cell can be computed as

$$PL_i = \frac{P_i}{\beta_i}, \tag{4.6}$$

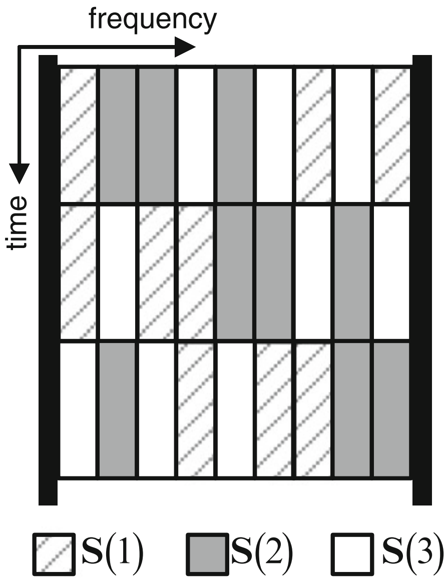

Fig. 4.8 Illustration of pseudorandomly positioned EURs for $B = 3$

where P_i is the transmit power of Ω_i. From (4.6), cell-edge UEs tend to have larger path losses. For simplicity, we denote each UE's serving cell as the first cell, that is, Ω_1, b_1, β_1, P_1, and PL_1 are associated with the serving cell. In addition, it should be noted that the path loss value captures the following channel properties (3GPP 2010):

- Propagation loss of the transmission from the UE to the interested cell
- Shadowing loss caused by radio blocking of large buildings
- Antenna gain related to the angle of departure (AoD) and angle of arrival (AoA) of the UE-to-BS link

Although the proposed scheme demands that the UE should feedback some form of neighbor-cell CSI in Γ to facilitate the advanced interference coordination operations, the overhead does not increase accordingly because such CSI report should be mandatory in practical cellular networks for handover purposes. In 3GPP (2007), it is required that a UE should report 32 values of β_i and the associated cell information b_i to its serving BS in order to assist the network to make possible handover decisions.

4.3.2.3 Step 3: Categorization of UEs Based on Geometry Evaluation

Based on the RS measurement report Γ feedback from the UEs, the BS can evaluate the UEs' resistance of interference and tendency of generating interference to neighbor cells. Here we consider a UE categorization scheme which partitions the set of UEs into four subsets instead of just two subsets, that is, cell-edge UEs and

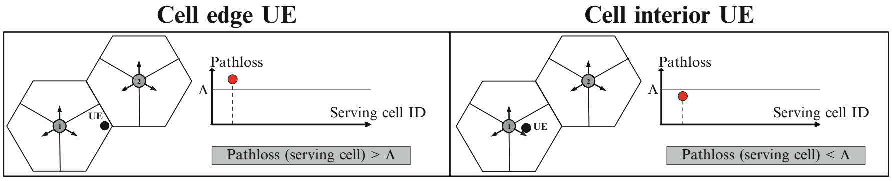

Fig. 4.9 Illustration of dividing UEs into cell-edge UE and cell-interior UE categories

cell-interior UEs. For the two additional groups, we consider another criterion which relates to the expectation of interference leakage generated by the UE, thus dividing the UEs into potential major interfering UEs and potential minor interfering UEs. Combining these two categories with the cell-edge and cell-interior UE categories, we get four types of UEs in total.

To be more specific, the cell-edge UEs or cell-interior UEs are discriminated by the comparison between PL_1 and a pre-configured threshold Λ derived from the λ-percentile point of the serving-cell path loss, that is, a UE is grouped into the cell-edge UE category if its PL_1 is larger than Λ, otherwise it is grouped into the cell-interior UE category. The division of UEs into these two UE categories is illustrated in Fig. 4.9.

In addition, we use $PL_i (i \neq 1)$ to group the UEs into two new categories. For each UE, two largest non-serving-cell path losses are chosen as the metrics for the estimation of potential interference generation. The η-percentile point of the non-serving-cell path loss denoted as a threshold Θ is used to divide the UEs into two groups: potential major interfering UEs and potential minor interfering UEs. The reason why we can perform estimation on the expected intercell uplink interference from downlink path loss information is because downlink and uplink path losses generally share a similar value in FDD systems, which has been exploited in uplink power control process (Sesia et al. 2009). Thereby, smaller downlink path loss indicates larger likelihood of generating undesirable uplink interference.

Combining these two grouping criteria creates a 2-dimensional 2×2 matrix which describes four types of UEs, as illustrated in Fig. 4.10. The categorization of UEs is performed by each BS, the result of which is denoted as Ψ.

The proposed four types of UEs are listed in Table 4.1 for comparison.

4.3.2.4 Step 4: Authorization of Resource Access

Based on the UE categorization result Ψ, the BS authorizes the four types of UE to access the frequency resources of the system. The fundamental principle is to protect the cell-edge UEs in the network and restrict the resource usage of the potential major interfering UEs. The detailed explanations and corresponding examples of the proposed resource coordination scheme are provided as follows.

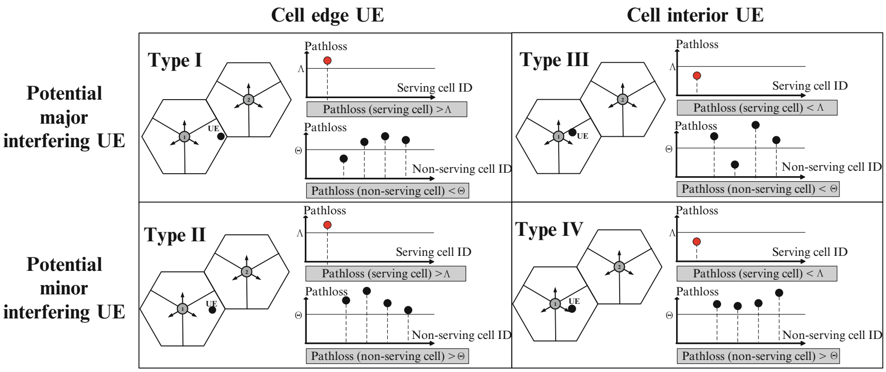

Fig. 4.10 Illustration of four types of UEs in the proposed scheme

Table 4.1 UE categorization table

UE categorization	Description	Criterion
Type I	Cell-edge UE and potential major interfering UE	$PL_1 > \Lambda$ and $\forall i \neq 1$, $PL_i \leq \Theta$
Type II	Cell-edge UE and potential minor interfering UE	$PL_1 > \Lambda$ and $\exists i \neq 1$, $PL_i > \Theta$
Type III	Cell-interior UE and potential major interfering UE	$PL_1 \leq \Lambda$ and $\forall i \neq 1$, $PL_i \leq \Theta$
Type IV	Cell-interior UE and potential minor interfering UE	$PL_1 \leq \Lambda$ and $\exists i \neq 1$, $PL_i > \Theta$

For Type I UEs, that is, UEs at cell-edge area with a potential of generating a high level of interference, they are only authorized to access the EUR of the serving BS described by

$$\mathbf{R}(u,t) = \mathbf{S}\left(\mathrm{J}\left(b_1,t\right)\right), \tag{4.7}$$

where u is the UE's index and $\mathbf{R}(u,t)$ is the set of authorized frequency resources for UE u at time t. Besides $\mathbf{R}(u,t)$, Type I UEs are strictly forbidden to use other frequency resources. This resource-access control policy is illustrated in Fig. 4.11.

The Type II UEs, that is, UEs at cell-edge area with a low level of expected outgoing interference, usually locate at the edge of the serving cell and generate limited intercell interference due to building obstruction, indirect antenna pointing to neighbor cells, etc. Like the Type I UEs, the Type II UEs are also authorized to access the resource shown by (4.7). Optionally, the Type II UEs may be able to have a power boost to improve the uplink data transmission as long as their interference levels are tolerable to adjacent cells. This resource-access control policy is illustrated in Fig. 4.12.

The Type III UEs, that is, UEs locate in the interior area of the serving cell while potentially generating much interference to adjacent cells, can be viewed as hidden

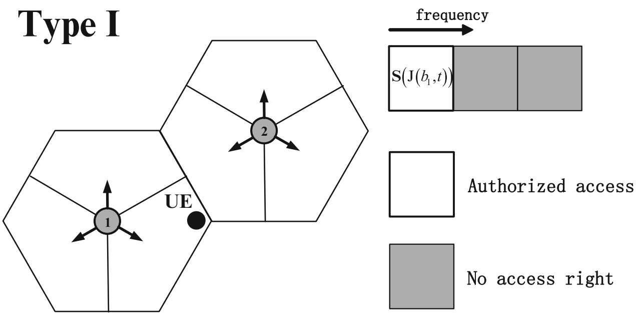

Fig. 4.11 Resource-access authorization for the Type I UEs

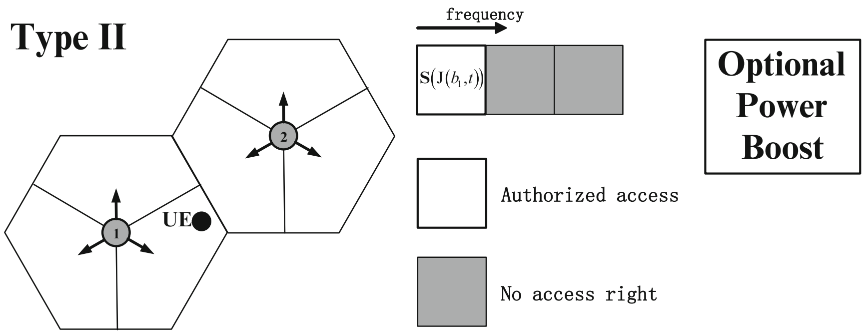

Fig. 4.12 Resource-access authorization for the Type II UEs

interferers in the network. A prominent example emerges at the sector border, where UEs have very good communication links to both sectors/cells. In our proposed scheme, the Type III UEs are forbidden to use the EUR of the serving cell and those EURs of the potentially interfered cells in order to prevent the critical interference hitting the cell-edge UEs in neighbor cells. Hence, $\mathbf{R}(u, t)$ of the Type III UEs can be expressed as

$$\mathbf{R}(u,t) = \mathbf{S} \Big\backslash \left(\mathbf{S}\left(\mathrm{J}\left(b_1, t\right)\right) \cup \left(\bigcup_i \mathbf{S}\left(\mathrm{J}\left(b_i, t\right)\right) \right) \right), \tag{4.8}$$

where b_i is the ID of the potentially interfered cells. However, if $\mathbf{R}(u, t)$ becomes Ø, then we have to create an emergent permission that $\mathbf{R}(u, t) = \mathbf{S}\left(\mathrm{J}\left(b_1, t\right)\right)$. In addition, this type of UEs may have an optional power reduction to further decrease the interference to adjacent cells. The above rule is illustrated in Fig. 4.13.

Finally, the Type IV UEs, that is, UEs at cell-interior area with a low level of expected interference, can access any frequency resource expect the EUR of the serving cell in order not to rob the limited resources intended for the cell-edge UEs. Thus, $\mathbf{R}(u, t)$ of the Type IV UEs can be shown as

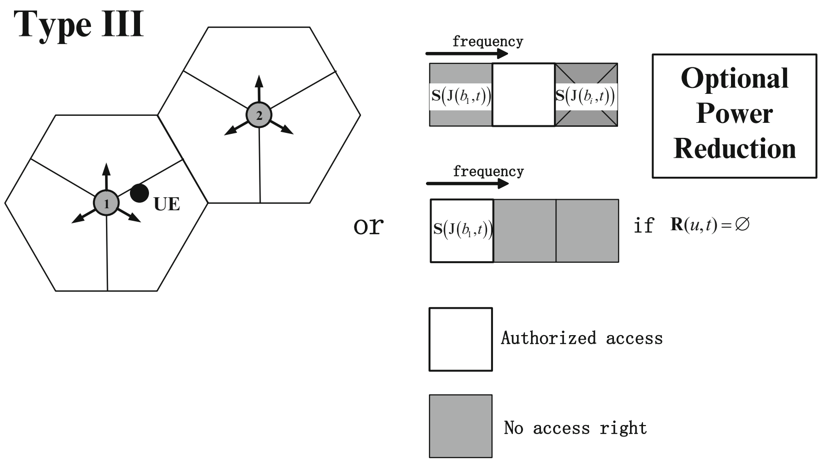

Fig. 4.13 Resource-access authorization for the Type III UEs

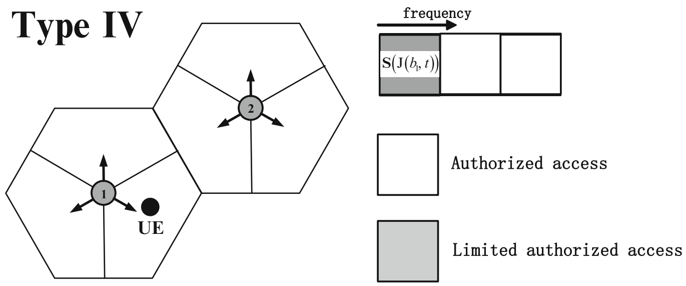

Fig. 4.14 Resource-access authorization for the Type IV UEs

$$\mathbf{R}(u,t) = \mathbf{S} \backslash \left(\mathbf{S}\left(\mathrm{J}\left(b_1, t \right) \right) \right). \tag{4.9}$$

However, when the serving cell's EUR hasn't been used up by the rightful UEs, it can be given to the Type IV UEs. Therefore, the Type IV UEs have limited rights to access the EUR of the serving cell. The discussed resource-access control policy is illustrated in Fig. 4.14.

The proposed resource-access authorization policies is summarized in Table 4.2.

The authorization of resource access made at the BS based on Table 4.2 is denoted as Φ.

Table 4.2 Resource-access authorization policies

UE categorization	Description	Authorized resource
Type I	Cell-edge UE and potential major interfering UE	$\mathbf{R}(u,t)$ shown in (4.7)
Type II	Cell-edge UE and potential minor interfering UE	$\mathbf{R}(u,t)$ shown in (4.7) Optional power boosting
Type III	Cell-interior UE and potential major interfering UE	$\mathbf{R}(u,t)$ shown in (4.8) If $\mathbf{R}(u,t) = \emptyset$, use (4.7) Optional power reduction
Type IV	Cell-interior UE and potential minor interfering UE	$\mathbf{R}(u,t)$ shown in (4.9) Limited right to invoke (4.7)

4.3.2.5 Step 5: Power Control

The uplink transmission power of a UE shall be stringently supervised by the BS so that the UE, especially the cell-edge UE, won't jam the neighbor BSs due to unnecessary high transmission powers. Conventional power control schemes include maximum power control, target SNR power control (Ericsson 2006), and partial path loss compensation power control (Motorola 2006).

The maximum power control scheme allows all UEs to transmit at their highest power level, that is,

$$P(u) = P_{\max}, \tag{4.10}$$

where $P(u)$ is the uplink transmit power of UE u and $P_{\max}$ is the maximum uplink transmit power.

The target SNR power control scheme first sets the power basis to fully compensate the UE's path loss, and then it further raises the transmit power to meet the UE's target SNR. In addition, the granted power shall be bounded by $P_{\max}$. Hence, the target SNR power control scheme can be described as (Ericsson 2006)

$$P(u) = \min\left\{P_{\max}, PL_1(u) \times P_{\text{noise}} \times 10^{\frac{SNR_{\text{tag}}}{10}}\right\}, \tag{4.11}$$

where $PL_1(u)$ is the serving-cell path loss of UE u, P_{noise} is the noise power, and SNR_{tag} is the target SNR in dB scale.

The partial path loss compensation power control scheme grants different power levels for different UEs. For the worst cell-edge UEs defined as UEs with $PL_1(u)$ larger than the x-percentile point of the serving-cell path loss, the BS generously permits them to transmit the signal at the full power $P_{\max}$. For other UEs, the BS only approves a certain power level, which partially compensates $PL_1(u)$ according to a configured factor α. Again, all the UEs' transmit powers shall be limited by $P_{\max}$. Thus, the algorithm can be expressed as (Motorola 2006)

$$P(u) = P_{\max} \times \min\left\{1, \max\left\{r_{\min}, \left(\frac{PL_1(u)}{PL_{x-ile}}\right)^{\alpha}\right\}\right\}, \tag{4.12}$$

where $r_{\min}$ is the ratio of minimum transmit power over $P_{\max}$, PL_{x-ile} is the x-percentile point of the serving-cell path loss, and $\alpha(0 < \alpha \leq 1)$ is the factor of path loss compensation.

4.3.2.6 Step 6: Resource Allocation and Link Adaptation

By means of scheduling algorithms, the BS allocates the frequency resources to the served UEs, taking Φ and power control results into account. Conventional scheduling algorithms include maximum carrier-to-interference ratio (C/I) algorithm, and proportional fairness (PF) algorithm (Ofuji et al. 2002).

The maximum C/I algorithm gives the frequency resource $s(i)$ to the UE who claims to have the largest C/I ratio, that is,

$$\mathrm{A}\left(s(i)\right) = \arg\max_{u}\left\{\frac{\mathrm{Gain}(u, s(i))}{\mathrm{Interf}(s(i))}\right\}, \tag{4.13}$$

where $\mathrm{A}(s(i))$ is the resource allocation function mapping the resource $s(i)$ to its owner u. $\mathrm{Gain}(u,\ s(i))$ is the UE's channel gain on $s(i)$, and $\mathrm{Interf}(s(i))$ is the interference power on $s(i)$.

The PF scheme, on the other hand, doesn't reward the $s(i)$ to the UE with the best channel condition, but to the UE who outperforms its average transmission rate to the largest extent. Suppose that $r(u)$ is the average transmission rate of UE u and $d(u,\ s(i))$ is the instantaneous transmission rate of UE u if it gets $s(i)$. Then the PF algorithm can be expressed as (Ofuji et al. 2002)

$$\mathrm{A}(s(i)) = \arg\max_{u}\left\{\frac{d(u, s(i))}{r(u)}\right\}. \tag{4.14}$$

In the proposed interference coordination scheme, we don't specify which scheduling algorithm(s) should be employed. However, the allocation order of the frequency resources is very important. First, frequency resource units (FRUs) in the set $\mathbf{S}\backslash\left(\mathbf{S}\left(\mathrm{J}\left(b_1, t\right)\right)\right)$ should be allocated to the rightful UEs so that these resource units are fully utilized to prevent unnecessary traffic loading onto the valuable EUR set. Second, FRUs in the EUR set $\mathbf{S}\left(\mathrm{J}\left(b_1, t\right)\right)$ should be scheduled to the authorized UEs. Note that if some FRUs in the EUR set haven't been adopted by any UE after the above two rounds of resource allocation, then the idle FRUs can go to the UEs with limited access right, that is, the Type IV UEs. Such event will happen when there is no cell-edge UE or the EUR set is more than enough for cell-edge UEs or cell-edge UEs abandon the idle FRUs due to deep channel fadings.

Finally, the BS performs link adaptation for the scheduled UEs, that is, the BS adaptively selects the modulation and coding scheme based on the UEs' estimated signal-to-interference plus noise ratio (SINR) so that the expected packet error rate (PER) is controlled to be lower than a predetermined threshold (Qualcomm 2006).

4.4 Simulation and Analysis

4.4.1 Methodology of the System-Level Simulation

The proposed scheme is a system-level resource coordination protocol, which can only be verified by the system-level simulation of the cellular network. To start with, we discuss the methodology of the system-level simulation, which usually consists of four steps as follows.

4.4.1.1 Infrastructure Construction of the Cellular Network

First, we recreate the cellular system topology, together with BS antenna configuration and UE distribution shown in Fig. 4.1 by means of computer programming. Figure 4.15 illustrates the layout of a cellular network in our simulation generated and plotted by the MATLAB software (King 2001).

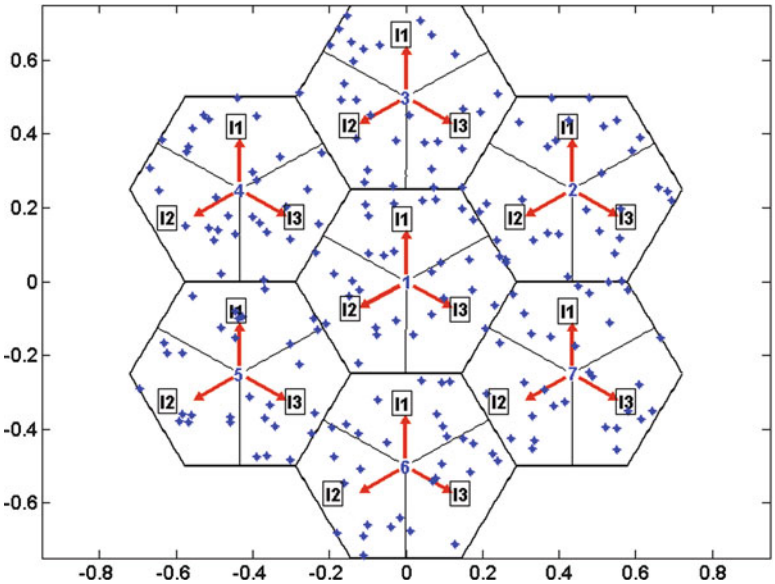

Fig. 4.15 Illustration of the layout of the simulated cellular network ($M = 3$)

In Fig. 4.15, arrows and asterisks represent directional antennas and UEs, respectively. Comparing Fig. 4.1 with Fig. 4.15, we can see that all the primary characteristics of the cellular infrastructure are well captured in our computer simulation. It should be noted that in the system-level simulation, the problem of edge effect around the simulation area, that is, the results collected from the BSs located near the boundary of the simulation area are lack of confidence due to blanked interference from outside, should be carefully considered. A simple solution to tackle the problem is to discard the results of a complete tire of the outmost BSs and only take the results generated from the interior area. Another approach is the advanced wrap-around technique (Sallabi et al. 2005), which extends the simulation area by duplicating the interior cells and placing them outside the simulation area according to some predefined pattern. Thus, the edge effect can be removed because the blank terrains outside the simulation area are filled with duplicated virtual cells that can generate realistic interference. In our simulation, we adopt the first approach for simplicity, that is, only the results collected from cell site ① are used for performance analysis.

4.4.1.2 Model UEs' Uplink/Downlink Channels

Channel modeling with perfect CSI is mainly composed of four parts. The first part is the calculation of path loss values addressed in Sect. 4.3.2.2, which includes a distance-dependent attenuation value derived from the large-scale power attenuation model (Proakis 2001), a shadowing loss based on location-correlated random variable generated from the shadowing model (Gudmundson 1991), and an antenna gain obtained from the antenna pattern and UE's AoA and AoD information with respect to the directional antenna array deployed at the BS (3GPP 2010). The second part is the simulation of fast fading channels, also known as the small-scale channel fadings, which are usually modeled as the Rayleigh fading channels (Zheng and Xiao 2003). The third part is the emulation of interference experienced by the UE. To accurately construct the interference in the network, each interference link should be explicitly generated. In the uplink, the interference comes from the leakage power of neighbor cell UEs to the serving cell. On the other hand, in the downlink, the interference is composed of undesirable signals transmitted from neighbor cells to the UE. The fourth part is the model of ZMCSCG noise, which is related to the environmental temperature (3GPP 2010).

As for the channel impairment resulted from imperfect CSI, the uplink and downlink simulators should consider different factors. For the uplink, imperfect CSI is mostly caused by the inter-UE interference of the uplink RSs, while for the downlink primary concerns are about channel estimation errors and limited-bit CSI feedback addressed in Sect. 2.6.

4.4.1.3 Simulate RRM Functions in BS

According to Sect. 4.3.2, basic RRM functions performed by BS include time-frequency resource allocation (Ofuji et al. 2002), power control (Ericsson 2006; Motorola 2006), and selection of adaptive modulation and coding (AMC) scheme (Qualcomm 2006). All these functions can be simulated by computer programs. For example, the resource scheduling can be represented by an FUR allocation table in the BS, and the AMC selection can be realized by the comparison between the estimated sub-band SINRs with the predefined SINR thresholds inferred from the BER curves of various AMC schemes.

4.4.1.4 Compute the Effective Throughput of the System

For the uplink, the actual SINR of the received signal at the BS on each scheduled time-frequency resource can be obtained from the computer simulation addressed in Sects. 4.4.1.1, 4.4.1.2, and 4.4.1.3. Then according to the mapping technique from SINR to PER (Brueninghaus et al. 2005), the program can obtain a PER and decide whether the simulated packet is successfully decoded by generating a random value in [0, 1) and comparing it with the PER. If the packet has been correctly received at the BS, then the effective bits in the packet will be added to the UE's uplink throughput. Otherwise, retransmission of the packet should be operated. In our simulation, we adopt the same retransmission mechanism as that in the LTE network (3GPP 2010), which is the Hybrid Automatic Repeat reQuest (HARQ) protocol, that is, a combination of forward error-correcting coding and Automatic Repeat reQuest (ARQ) error control. For the downlink, the UE's SINR should also be evaluated, and only the successfully transmitted bits should be counted into the downlink throughput.

It should be noted that an alternative way to determine the correctness of the simulated packet is to perform the real-time link-level decoding process based on the received SINR. However, it is prohibitively complex to conduct such a huge number of real-time link-level simulations for every transmission in a system-level simulator. Therefore, the SINR-to-PER mapping technology addressed in Brueninghaus et al. (2005) is the key to make the system-level simulation possible. The core idea of the SINR-to-PER mapping technology is that multiple subcarrier SINRs in the fading channel can be mapped to an effective SNR in the additive white Gaussian noise (AWGN) channel, in the sense of equivalent PER. A commonly used mapping function is the exponential effective SINR mapping (EESM) (Brueninghaus et al. 2005), the parameters of which are obtained from a substantial number of offline link-level simulations. With the subcarrier SINRs mapped to an effective SNR, we can easily get the PER by looking up an SNR-to-PER table, which is also given by offline simulation results. In short, instead of running real-time simulations, the UE's PER is obtained from checking with the predefined mapping tables in the system-level simulation.

Table 4.3 Parameters of the system-level simulation for LTE uplink (3GPP 2006)

No.	Parameter		Configuration
1	Cellular model and layout		Hexagonal grid, seven cell sites, three sectors/cells per cell site
2	Distance between cell sites		500 m
3	UEs' distribution		Randomly and uniformly distributed in each cell/sector
4	Distance-dependent path loss		$L = 128.1 + 37.6\log_{10}(d)$ dB, d in km
5	Shadowing standard deviation		8 dB
6	Correlation distance of shadowing		50 m
7	Shadowing correlation	Between cell sites	0.5
8		Between cells	1.0
9	Penetration loss		20 dB
10	Antenna pattern		$A_H(\varphi) = -\min\left[12\left(\frac{\varphi}{\varphi_{3dB}}\right)^2, A_m\right]$ $\varphi_{3dB} = 70^\circ$, $A_m = 25dB$
11	BS antenna gain plus cable loss		14 dBi
12	Noise figure at BS		5 dB
13	Thermal noise density		−174 dBm/Hz
14	Minimum distance between UE and BS		35 m
15	UE's speed		3 km/h
16	UE's maximum transmit power $P_{\max}$		24 dBm
17	Number of UE's transmit antennas		1
18	Number of BS's receive antennas		2
19	Carrier frequency		2 GHz
20	System bandwidth		10 MHz
21	Subcarrier interval		15 KHz
22	Number of subcarriers		600
23	Number of subcarriers per FRU $s(i)$		12
24	Number of FRUs in the system N		48 (among the 600 subcarriers, 24 carriers are used for uplink control signaling purposes; the other 576 subcarriers are grouped to 48 FRUs)
25	Transmit time interval (TTI)		1 ms

4.4.2 *Simulation Parameters*

4.4.2.1 System-Level Simulation Parameters

In our simulation, we adopt the system-level simulation parameters of LTE uplink (3GPP 2006) as listed in Table 4.3.

We provide further explanations of the parameters in Table 4.3 as follows:

1. Cellular model and layout: The infrastructure of the cellular network as illustrated in Fig. 4.15.

2. Distance between cell sites: The distance between the center points of adjacent cell sites in Fig. 4.15.
3. UEs' distribution: The description of the probability density function (PDF) of UEs' locations in the cell/sector. In generally, uniform distribution is assumed when no communication hot spot is considered in the simulation scenario.
4. Distance-dependent path loss: The formula to model the large-scale channel attenuation.
5. Shadowing standard deviation: The shadowing value is usually assumed to follow the logarithmic normal distribution (3GPP 2010), that is, the logarithm of the shadowing value conforms to the normal distribution. And the standard deviation of the said normal distribution is denoted as the shadowing standard deviation.
6. Correlation distance of shadowing: Shadowing is usually caused by radio blocking of large buildings, which occupy a certain size of spatial area in the simulated scenario. Thus the shadowing values have relatively strong correlations across some distance (Gudmundson 1991), which is measured by the correlation distance of shadowing.
7. Shadowing correlation—between cell sites: The correlation coefficient of a UE's shadowing values between cell sites. Due to the distributed deployment of cell sites, this correlation coefficient is relatively small.
8. Shadowing correlation—between cells: The correlation coefficient of a UE's shadowing values between cells. Due to the colocated deployment of cells, this correlation coefficient is relatively large.
9. Penetration loss: Any building that contains a significant thickness of concrete or amount of metal will attenuate the radio wave signal. The corresponding power loss due to penetration through walls and floors is represented by this parameter.
10. Antenna pattern: The radiation properties of the antenna as a function of directional angles.
11. BS antenna gain plus cable loss: The power gain at BS receiver before the baseband signal processing.
12. Noise figure at BS: The thermal noise power in the electronic circuits at BS.
13. Thermal noise density: The power spectral density (PSD) of the thermal noise, which relates to the environment temperature.
14. Minimum distance between UE and BS: Due to the antenna down-tilt at BS, UEs at a very close range of BS will experience communication link failure. Thus UEs should be dropped at a distance from BSs to avoid entering the blind spots.
15. UE's speed: This parameter is for modeling time-variant channels.
16. UE's maximum transmit power: The upper limit of UE's transmit power.
17. Number of UE's transmit antennas: The number of transmit antennas equipped at UE.
18. Number of BS's receive antennas: The number of receive antennas equipped at BS.
19. Carrier frequency: The carrier frequency of the spectrum.

Table 4.4 Parameters of the 6-ray TU channel (3GPP 1999)

Path no.	Delay (us)	Relative power (dB)
Path 1	0	−3
Path 2	0.2	0
Path 3	0.5	−2
Path 4	1.6	−6
Path 5	2.3	−8
Path 6	5.0	−10

20. System bandwidth: The bandwidth of the spectrum.
21. Subcarrier interval: The interval between adjacent subcarriers in the OFDM system.
22. Number of subcarriers: The number of available subcarriers in the OFDM system without the guard bands.
23. Number of subcarriers per FRU: The number of subcarriers contained in one $s(i)$.
24. Number of FRUs in the system: The number of available FRUs in the OFDM system without the guard bands and uplink control channels.
25. Transmit time interval (TTI): TTI refers to the minimum time duration of a transmission.

The channel model in our simulation is the 6-ray global system for mobile communication (GSM) typical urban (TU) model (3GPP 1999). Its parameters are presented in Table 4.4.

4.4.2.2 Link-Level Simulation Parameters

Besides the system-level parameters for the LTE uplink simulation specified in 3GPP (2006), other link-level parameters need to be configured, which are shown in Table 4.5.

In the following we further discuss the parameters in Table 4.5:

1. Number of UEs per cell: UEs that can be served by a BS simultaneously are usually limited by the capacity of the control channels.
2. Scheduling algorithm: The scheduling function performed by the BS has been addressed in Sect. 4.3.2.6.
3. Maximum number of FRUs for each UE per TTI: In order not to let UEs with extremely good channel conditions consume all the FRUs, it is beneficial to set a maximum number of FRUs for each UE per TTI to improve the fairness of the system.
4. Retransmission combing: When error occurs in the packet decoding, retransmission will be needed. It is commonly recommended that BS should preserve the soft-bit information of the previously failed transmission and combine it with that of the retransmission to improve the probability of successful decoding (3GPP 2010).

Table 4.5 Configurable link-level parameters of the simulation for LTE uplink

No.	Configurable parameter	Configuration	
1	Number of UEs per cell	40	
2	Scheduling algorithm	PF scheme described in (4.14)	
3	Maximum number of FRUs for each UE per TTI	6	
4	Retransmission combing	Soft chase combing	
5	Maximum number of retransmissions	5	
6	Scheduling of the retransmission	Non-adaptive scheduling	
7	Delay of the retransmission	8 TTIs	
8	Power control algorithm	Fractional path loss compensation algorithm given by (4.12)	
9	Parameter x in (4.12)	95	
10	Parameter α in (4.12)	0.8	
11	Parameter $r_{\min}$ in (4.12)	0.00001	
12	Time granularity of BS scheduling	Per TTI	
13	Delay of BS scheduling	1 TTI	
14	Traffic model	Full buffer (FB)	
15	Receiver type in BS	Minimum mean square error (MMSE) receiver	
16	Expected PER	0.1	
17	Adaptive modulation and coding schemes	QPSK	Coding rate {1/3, 1/2, 2/3, 4/5}
		16QAM	Coding rate {1/2, 2/3, 3/4, 4/5}
18	PER vs. SNR in the AWGN channel	The curves in Qualcomm (2006) shown in Fig. 4.16	
19	Parameter Λ in the proposed scheme	The $\lambda = 10$-percentile point of the path loss to the serving cell	
20	Parameter Θ in the proposed scheme	The $\eta = 95$-percentile point of the path loss to the non-serving cell	

5. Maximum number of retransmissions: When several attempts of retransmission still cannot give a correct decoding of a packet, it is necessary to discard the packet to prevent further wasting of communication resource in case the corrupted packet is beyond repair. In practical systems, the maximum number of retransmissions is usually set to 4 or 5 (3GPP 2010).
6. Scheduling of the retransmission: There are two ways to schedule the retransmission, which are non-adaptive scheduling, that is, retransmitting the packet on the previously scheduled frequency resource, or adaptive scheduling, that is, retransmitting the packet on a new resource with another scheduling. In the LTE/LTE-A network (3GPP 2010), the downlink retransmission operates in the second way, while the uplink one adopts the first approach.

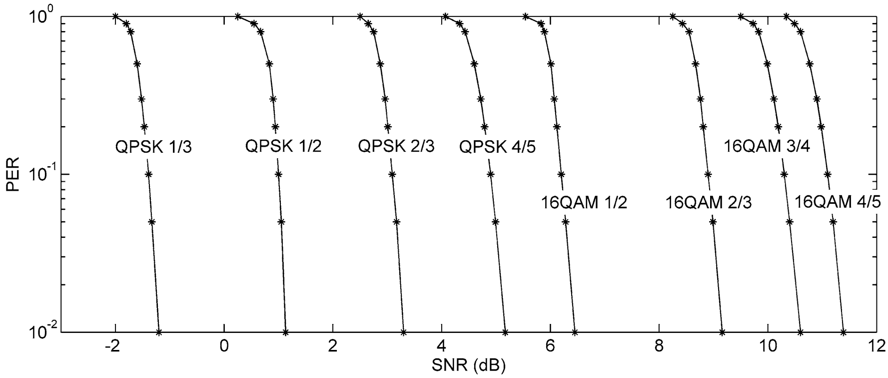

Fig. 4.16 PER versus SNR curves for various AMC schemes in the AWGN channel

7. Delay of the retransmission: The time period between the first transmission and the retransmission.
8. Power control algorithm: The power control function performed by the BS has been addressed in Sect. 4.3.2.5.
9. Parameter x in (4.12): The reference point of the serving-cell path loss in the fractional path loss compensation algorithm (Motorola 2006).
10. Parameter α in (4.12): The factor of path loss compensation in the fractional path loss compensation algorithm (Motorola 2006).
11. Parameter $r_{\min}$ in (4.12): The ratio of minimum transmit power over maximum transmit power in the fractional path loss compensation algorithm (Motorola 2006).
12. Time granularity of BS scheduling: The time granularity based on which the BS scheduling algorithm is operated.
13. Delay of BS scheduling: The time delay between the BS scheduling and the first transmission.
14. Traffic model: The model that describes how the UE's traffic is generated.
15. Receiver type in BS: The receiver structure and capability in BS.
16. Expected PER: The PER target for link adaptation addressed in Sect. 4.3.2.6.
17. Adaptive modulation and coding schemes: The set of candidate modulation and coding schemes, which is a pre-defined lookup table stored in both BSs and UEs (3GPP 2011).
18. PER versus SNR in the AWGN channel: See the details of the SINR-to-PER mapping technique addressed in Sect. 4.4.1.4.
19. Parameter Λ in the proposed scheme: The parameter that generates the threshold to divide the UEs into cell-edge UEs and cell-interior UEs.
20. Parameter Θ in the proposed scheme: The parameter that generates the threshold to divide the UEs into potential major interfering UEs and potential minor interfering UEs.

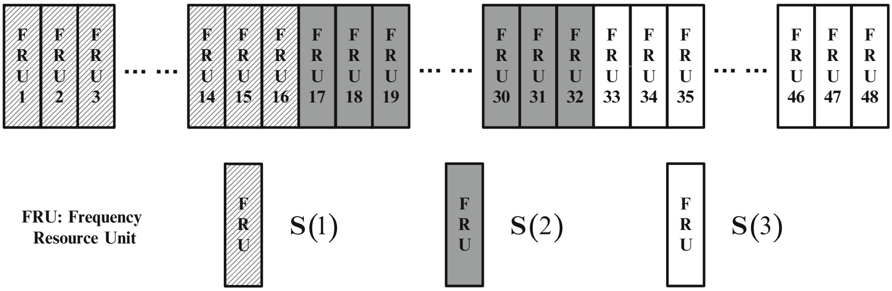

Fig. 4.17 Illustration of construction of **S**(j) by consecutive selection of FRUs

4.4.3 Implementation Details in the Simulation

In order to provide a concrete example of the proposed advanced interference coordination scheme, we address the implementation details of the proposed scheme in our simulation.

4.4.3.1 Step 1: Construction of Cell EURs

According to Table 4.3, we have $N = 48$. Thus $\mathbf{S} = \{s(i)|1 \le i \le C(\mathbf{S}), s(i) < s(i+1), 1 \le s(i) \le 48\}$ and $C(\mathbf{S}) = 48$. Then we divide $\mathbf{S}$ into $B = 3$ disjoint equal-sized EUR sets $\mathbf{S}(j), (1 \le j \le 3)$. A conventional way to construct such EUR sets is to bundle $C(\mathbf{S})/B = 16$ consecutive FRUs as one $\mathbf{S}(j)$. Therefore, $\mathbf{S}(j)$s can be written as

$$\mathbf{S}(1) = \{1, 2, 3, 4, 5, 6, 7, 8, 9, 10, 11, 12, 13, 14, 15, 16\}, \tag{4.15}$$

$$\mathbf{S}(2) = \{17, 18, 19, 20, 21, 22, 23, 24, 25, 26, 27, 28, 29, 30, 31, 32\}, \tag{4.16}$$

$$\mathbf{S}(3) = \{33, 34, 35, 36, 37, 38, 39, 40, 41, 42, 43, 44, 45, 46, 47, 48\}, \tag{4.17}$$

Obviously, $\mathbf{S}(j)$ given by (4.15), (4.16), and (4.17) satisfies (4.3). This EUR construction method is further illustrated in Fig. 4.17.

In order to achieve the frequency diversity gain, $\mathbf{S}(j)$ can also be created by comb-shaped selection of FRUs (Huawei 2005), which can be expressed as

$$\mathbf{S}(1) = \{1, 4, 7, 10, 13, 16, 19, 22, 25, 28, 31, 34, 37, 40, 43, 46\}, \tag{4.18}$$

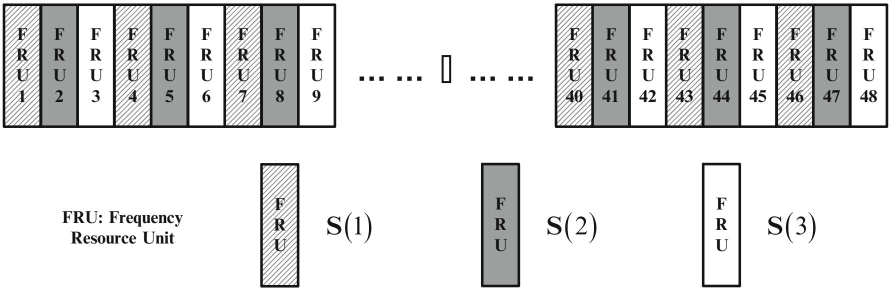

Fig. 4.18 Illustration of construction of **S**(*j*) by comb-shaped selection of FRUs

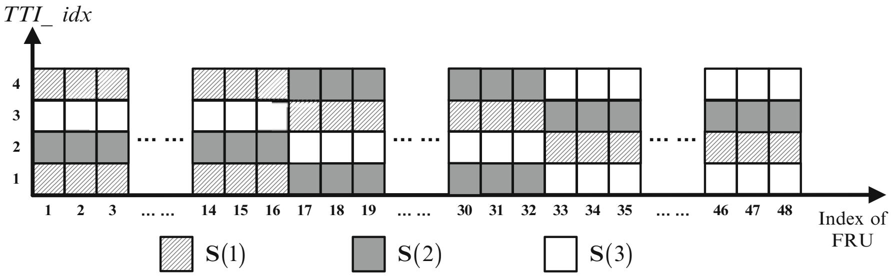

Fig. 4.19 Illustration of the time-frequency structure of **S**(*j*) by consecutive selection of FRUs

$$\mathbf{S}(2) = \{2, 5, 8, 11, 14, 17, 20, 23, 26, 29, 32, 35, 38, 41, 44, 47\}\,, \tag{4.19}$$

$$\mathbf{S}(3) = \{3, 6, 9, 12, 15, 18, 21, 24, 27, 30, 33, 36, 39, 42, 45, 48\}\,, \tag{4.20}$$

Here, (4.18), (4.19), and (4.20) also meet the requirement in (4.3). The illustrative graph of this distributed selection of FRUs is presented in Fig. 4.18.

Moreover, in order to obtain the time diversity gain, we shift the $\mathbf{S}(j)$ for the sectors according to the index of TTI, which can be expressed as

$$\mathrm{J}\,(I_k, TTI\_idx) = \mathrm{mod}\,((I_k + TTI\_idx)\,, 3) + 1, \tag{4.21}$$

where I_k is the sector ID of cell k and TTI_idx is the index of TTI.

Based on (4.21), we can replot Fig. 4.17 as a time-frequency structure of $\mathbf{S}(j)$ by consecutive selection of FRUs shown in Fig. 4.19. Note that previously we have presented the corresponding concept graph in Fig. 4.6.

In a similar way, we can replot Fig. 4.18 as a time-frequency structure of $\mathbf{S}(j)$ by comb-shaped selection of FRUs shown in Fig. 4.20, the concept graph of which can be found in Fig. 4.7.

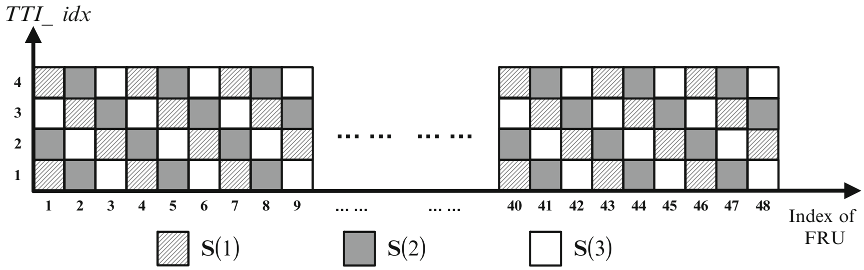

Fig. 4.20 Illustration of the time-frequency structure of **S**(j) by comb-shaped selection of FRUs

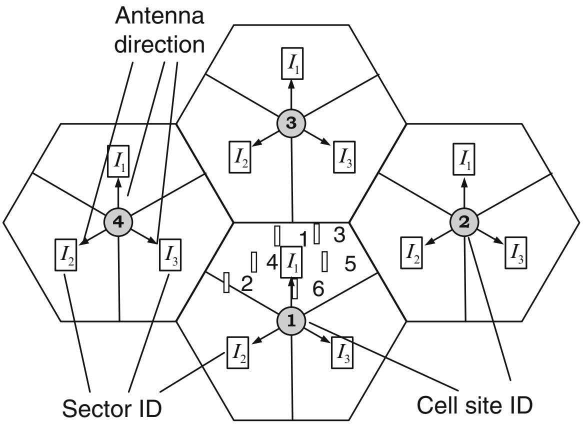

Fig. 4.21 Example of UEs' distribution in the simulation

In our simulation, we choose the time-frequency structure of $\mathbf{S}(j)$ illustrated by Fig. 4.20.

4.4.3.2 Step 2: Report of the Measurement of Downlink RSs

Let us take an example of UEs' distribution in our simulation shown in Fig. 4.21. In Fig. 4.21, we plot six UEs with their locations labeled as #1, #2, #3, #4, #5, and #6, respectively.

The illustrated six UEs should monitor and detect the downlink RSs Ω_i of the i-th neighbor cell with cell ID b_i, which contains the sector ID I_i. For simplicity, we suppose that $I_i = j$ for the j-th sector. After the BS receives the RS measurement report Γ from the UE, the BS can estimate the path losses from neighbor cells to the UE. Among the estimated path losses, the maximum path losses associated with different sector IDs are of particular interest, which can be written as

$$PL\,(I_k) = \max\{\,PL_i\,|\,I_i = I_k\}\,,\,I_k \in \{1,2,3\}. \tag{4.22}$$

4.4.3.3 Step 3: Categorization of UEs Based on Geometry Evaluation

According to the UE categorization table shown in Table 4.1, we can classify the UEs in Fig. 4.21 as follows:

- For the UE at location #1, suppose that we have $PL(1) < \Lambda$, $PL(2) < \Theta$, and $PL(3) < \Theta$. Therefore, the UE is a Type III UE, that is, cell-interior UE and potential major interfering UE.
- For the UE at location #2, suppose that we have $PL(1) < \Lambda$, $PL(2) < \Theta$, and $PL(3) > \Theta$. Therefore, the UE is also a Type III UE, that is, cell-interior UE and potential major interfering UE.
- For the UE at location #3, suppose that we have $PL(1) > \Lambda$, $PL(2) > \Theta$, and $PL(3) < \Theta$. Therefore, the UE is a Type I UE, that is, cell-edge UE and potential major interfering UE.
- For the UE at location #4, suppose that we have $PL(1) < \Lambda$, $PL(2) > \Theta$, and $PL(3) > \Theta$. Therefore, the UE is a Type IV UE, that is, cell-interior UE and potential minor interfering UE.
- For the UE at location #5, suppose that we have $PL(1) > \Lambda$, $PL(2) > \Theta$, and $PL(3) > \Theta$. Therefore, the UE is a Type II UE, that is, cell-edge UE and potential minor interfering UE.
- For the UE at location #6, suppose that we have $PL(1) < \Lambda$, $PL(2) > \Theta$, and $PL(3) > \Theta$. Therefore, the UE is a Type IV UE, that is, cell-interior UE and potential minor interfering UE.

The UE categorization result discussed above is denoted as Ψ.

4.4.3.4 Step 4: Authorization of Resource Access

Following the resource-access authorization policies summarized in Table 4.2, we can order different types of UEs to access different parts of the system frequency spectrum. The details are discussed below:

- For the UE at location #1, which is a Type III UE, according to (4.8), $\mathbf{R}(u,t) = \emptyset$ since $PL(2) < \Theta$ and $PL(3) < \Theta$. Therefore, (4.7) is invoked, that is, $\mathbf{R}(u,t) = \mathbf{S}(\mathrm{J}(b_1,t))$, and power reduction is a further option. For instance, during one TTI, suppose that we have $\mathrm{J}(I_1) = 1$, $\mathrm{J}(I_2) = 2$, and $\mathrm{J}(I_3) = 3$, then considering (4.18), we can get the $\mathbf{R}(u,t)$ for this UE written as

$$\mathbf{R}(u,t) = \{1,\ 4,\ 7,\ 10,\ 13,\ 16,\ 19,\ 22, 25, 28, 31, 34, 37, 40, 43, 46\}. \quad (4.23)$$

- For the UE at location #2, which is also a Type III UE, according to (4.8), we have $\mathbf{R}(u) = \mathbf{S} \backslash (\mathbf{S}(\mathrm{J}(I_1)) \cup \mathbf{S}(\mathrm{J}(I_2))) = \mathbf{S}(\mathrm{J}(I_3))$ since $PL(2) < \Theta$ and $PL(3) > \Theta$. Moreover, this UE's transmit power may be further reduced. For instance, during one TTI, suppose that we have $\mathrm{J}(I_1) = 1$, $\mathrm{J}(I_2) = 2$, and $\mathrm{J}(I_3) = 3$, then considering (4.20), we can get the $\mathbf{R}(u,t)$ for this UE shown as

$$\mathbf{R}(u,t) = \{3, 6, 9, 12, 15, 18, 21, 24, 27, 30, 33, 36, 39, 42, 45, 48\}. \tag{4.24}$$

- For the UE at location #3, which is a Type I UE, according to (4.7), $\mathbf{R}(u,t) = \mathbf{S}(\mathrm{J}(b_1,t))$. For instance, during one TTI, suppose that we have $\mathrm{J}(I_1) = 1$, $\mathrm{J}(I_2) = 2$, and $\mathrm{J}(I_3) = 3$, then considering (4.18), we can get the $\mathbf{R}(u,t)$ for this UE described as

$$\mathbf{R}(u,t) = \{1, 4, 7, 10, 13, 16, 19, 22, 25, 28, 31, 34, 37, 40, 43, 46\}. \tag{4.25}$$

- For the UE at location #4, which is a Type IV UE, according to (4.9), $\mathbf{R}(u,t) = \mathbf{S} \backslash (\mathbf{S}(\mathrm{J}(b_1,t)))$, and this UE also has a limited right to use $\mathbf{S}(\mathrm{J}(b_1,t))$ if it is still available at the end of scheduling. For instance, during one TTI, suppose that we have $\mathrm{J}(I_1) = 1$, $\mathrm{J}(I_2) = 2$, and $\mathrm{J}(I_3) = 3$, then considering (4.19) and (4.20), we can get the $\mathbf{R}(u,t)$ for this UE shown as

$$\mathbf{R}(u,t) = \begin{Bmatrix} 2, 5, 8, 11, 14, 17, 20, 23, 26, 29, 32, 35, 38, 41, 44, 47 \\ 3, 6, 9, 12, 15, 18, 21, 24, 27, 30, 33, 36, 39, 42, 45, 48 \end{Bmatrix}. \tag{4.26}$$

  And the resources with limited access right are

$$\mathbf{R}'(u,t) = \{1, 4, 7, 10, 13, 16, 19, 22, 25, 28, 31, 34, 37, 40, 43, 46\}. \tag{4.27}$$

- For the UE at location #5, which is a Type II UE, according to (4.7), $\mathbf{R}(u,t) = \mathbf{S}(\mathrm{J}(b_1,t))$ and it is optional to further increase the transmit power of this UE. For instance, during one TTI, suppose that we have $\mathrm{J}(I_1) = 1$, $\mathrm{J}(I_2) = 2$, and $\mathrm{J}(I_3) = 3$, then considering (4.18), we can get the $\mathbf{R}(u,t)$ for this UE written as

$$\mathbf{R}(u,t) = \{1, 4, 7, 10, 13, 16, 19, 22, 25, 28, 31, 34, 37, 40, 43, 46\}. \tag{4.28}$$

- For the UE at location #6, which a Type IV UE, according to (4.9), $\mathbf{R}(u,t) = \mathbf{S} \backslash (\mathbf{S}(\mathrm{J}(b_1,t)))$ and this UE also has a limited right to use $\mathbf{S}(\mathrm{J}(b_1,t))$ if it is still available at the end of scheduling. For instance, during one TTI, suppose that we have $\mathrm{J}(I_1) = 1$, $\mathrm{J}(I_2) = 2$, and $\mathrm{J}(I_3) = 3$, then considering (4.19) and (4.20), we can get the $\mathbf{R}(u,t)$ for this UE shown as

$$\mathbf{R}(u,t) = \begin{Bmatrix} 2, 5, 8, 11, 14, 17, 20, 23, 26, 29, 32, 35, 38, 41, 44, 47 \\ 3, 6, 9, 12, 15, 18, 21, 24, 27, 30, 33, 36, 39, 42, 45, 48 \end{Bmatrix}. \tag{4.29}$$

Table 4.6 Example of the FRU allocation order and the target UEs

Order	FRU indices	Target UEs
1	$\left\{\begin{array}{l}2, 5, 8, 11, 14, 17, 20, 23,\\ 26, 29, 32, 35, 38, 41, 44, 47\end{array}\right\}$	UEs at positions #4 and #6
2	$\left\{\begin{array}{l}3, 6, 9, 12, 15, 18, 21, 24,\\ 27, 30, 33, 36, 39, 42, 45, 48\end{array}\right\}$	UEs at positions #2, #4, and #6
3	$\left\{\begin{array}{l}1,\ 4,\ 7,\ 10,\ 13,\ 16,\ 19,\ 22,\\ 25, 28, 31, 34, 37, 40, 43, 46\end{array}\right\}$	UEs at positions #1, #3 and #5
4	The remaining of $\left\{\begin{array}{l}1,\ 4,\ 7,\ 10,\ 13,\ 16,\ 19,\ 22,\\ 25, 28, 31, 34, 37, 40, 43, 46\end{array}\right\}$	UEs at positions #4 and #6

And the resources with limited access right are

$$\mathbf{R}'(u,t) = \{1, 4, 7, 10, 13, 16, 19, 22, 25, 28, 31, 34, 37, 40, 43, 46\}. \tag{4.30}$$

The resource-access authorization result discussed above is denoted as Φ.

4.4.3.5 Step 5: Power Control

In our simulation, we adopt the partial path loss compensation power control scheme described in (4.12). And the optional power boosting or reduction is not operated for simplicity.

4.4.3.6 Step 6: Resource Allocation and Link Adaptation

In our simulation, the PF scheduling algorithm shown in (4.14) is operated at BS based on the resource-access authorization result Φ and UEs' transmit powers. In Fig. 4.21, the BS with cell site ID and sector ID I_1 should first schedule the FRUs in $\mathbf{S}\backslash\mathbf{S}\,(\mathrm{J}\,(I_1))$, then treat those in $\mathbf{S}\,(\mathrm{J}\,(I_1))$.

To be more specific, suppose that we have $\mathrm{J}\,(I_1) = 1$, $\mathrm{J}\,(I_2) = 2$, and $\mathrm{J}\,(I_3) = 3$ during one TTI, the BS should first allocate the FRU set $\mathbf{S}\,(\mathrm{J}\,(I_2))$ in (4.19) to UEs at positions #4 and #6. Then it gives the FRU set $\mathbf{S}\,(\mathrm{J}\,(I_3))$ in (4.20) to UEs at positions #2, #4, and #6. Finally, it allows UEs at positions #1, #3, and #5 to take the FRU set $\mathbf{S}\,(\mathrm{J}\,(I_1))$ in (4.18). After these steps, if $\mathbf{S}\,(\mathrm{J}\,(I_1))$ is not used up, the BS can decide whether the remaining FRUs should be given to the UEs with limited access right, that is, UEs at positions #4 and #6. The above scheduling order is summarized in Table 4.6.

The simulated RRM functions are completed with the link adaptation for the scheduled UEs.

Table 4.7 Throughput performance results: cell-edge and overall

No.	Scheme	Cell-edge 5% point UE throughput (Kbps)	Overall cell throughput (Mbps)	Cell-edge throughput gain at the cost of 1% cell throughput reduction (%)
1	Baseline	82	9.916	–
2	The static implementation of soft frequency reuse	144	9.532	19.5
3	The proposed scheme	148	9.649	29.9

4.4.4 Numerical Results and Discussions

In our simulation, we investigate the 5% point UE throughput as the cell-edge throughput (3GPP 2008), the overall cell throughput (i.e., the sum of UE throughputs in one cell), and the trade-off efficiency between the cell-edge and overall throughputs. A baseline scheme with no interference management is compared with two interested interference coordination schemes, that is, the static implementation of soft frequency reuse scheme (Alcatel-Lucent 2007) and the proposed advanced interference coordination scheme. The numerical results are averaged over ten system-level simulation trials and are presented in Table 4.7.

As can be seen from Table 4.7, the baseline scheme achieves the highest overall throughput among the three schemes but with a very poor cell-edge throughput performance. The static implementation of soft frequency reuse scheme (Alcatel-Lucent 2007) exhibits a much higher cell-edge throughput (144 Kbps, up 75.6% compared with the baseline scheme) but a relatively poor overall throughput (9.532 Mbps, down 3.87% compared with the baseline scheme). From simple calculation, we can find that 1% loss in the overall throughput approximately returns a 19.5% gain in the cell-edge throughput. As for the proposed scheme, a 2.69% decrease in the overall throughput is able to exchange for an 80.5% increase in the cell-edge throughput when it is compared with the baseline scheme. The trade-off efficiency between the cell-edge throughput and the overall throughput is approximately 29.9%, which is shown to be 53.3% more efficient than the static implementation of soft frequency reuse (Alcatel-Lucent 2007).

The reason why the proposed scheme shows excellent performance is that the resource authorization policy in Table 4.2 guarantees an improved communication environment for the cell-edge UEs, and hence they can make use of the frequency resources more efficiently, that is, achieving higher throughput with less FRUs. Moreover, the saved FRUs from the cell-edge UEs are allocated to the cell-interior UEs to increase the overall throughput.

4.5 Conclusion

In this chapter, we propose an advanced interference coordination scheme consisting of UE categorization and resource-access control policies from an altruistic perspective, which aims to reduce the interference to adjacent cells. To verify the effectiveness of the proposed scheme, we resort to the approach of system-level simulation based on a cellular network. Simulation results show that compared with the existing schemes, the proposed scheme can increase the efficiency of the trade-off between the cell-edge throughput and the overall throughput by more than 50%. Therefore, the proposed scheme exhibits high performance in interference coordination and can be implemented with small load of inter-BS signaling, which are very beneficial for the uplink FDMA cellular network. The novelty of the proposed scheme is that the BS assigns different levels of authorization for UEs to access the frequency resource based on the UEs' resistance of interference and tendency of producing interference. If a UE tends to produce a large amount of interference to adjacent cells, the BS will restrict the frequency resource for the UE to use, thus reducing the interference level in the network from an altruistic perspective, and hence the cell-edge throughput can be increased. On the other hand, if a UE is not likely to cause much interference to adjacent cells, the BS will grant the UE to have access to the edge UE resource of the cell if it is available; thus the overall throughput can be improved.

References

3GPP (1999) TS 05.05: Technical Specification Group GSM/EDGE radio access network; radio transmission and reception (Release 1999) (V8.15.0). Accessed 1999

3GPP (2006) TR 25.814: Physical layer aspects for evolved Universal Terrestrial Radio Access (UTRA) (Release 7) (V7.1.0). Accessed 2006

3GPP (2007) TS 25.133: Requirements for support of radio resource management (FDD) (Release 8) (V8.0.0). Accessed 2007

3GPP (2008) TR 36.913: Requirements for further advancements for E-UTRA (LTE-Advanced) (V8.0.0). Accessed 2008

3GPP (2010) TR 36.814: Further advancements for E-UTRA physical layer aspects (V9.0.0). Accessed 2010

3GPP (2011) TS 36.213: Physical layer procedures (V10.0.1). Accessed 2011

Alcatel-Lucent (2007) Interference coordination framework with results. In: 3GPP, R1-073187. Accessed 2007

Brueninghaus K, Astely D, Salzer T et al (2005) Link performance models for system level simulations of broadband radio access systems. In: IEEE international symposium on personal, indoor and mobile radio communications, Berlin, Germany, vol 4, pp 2306–2311

Ericsson (2006) Uplink power control for E-UTRA. In: 3GPP, R1-062861. Accessed 2006

Gudmundson M (1991) Correlation model for shadow fading in mobile radio systems. IET Electron Lett 27(23):2145–2146

Hanly SV, Whiting PA (1993) Information-theoretic capacity of multi-receiver networks. Telecommun Syst 1(1):1–42

Huawei (2005) Inter-cell interference mitigation. In: 3GPP, R1-050629. Accessed 2005
King J (2001) MATLAB 6 for engineers: hands-on tutorial. R.T. Edwards, Inc., Philadelphia, 2001
Motorola (2006) Interference mitigation via power control and FDM resource allocation and UE alignment for E-UTRA uplink and TP. In: 3GPP, R1-060401. Accessed 2006
Ofuji Y, Morimoto A, Abeta S, Sawahashi M (2002) Comparison of packet scheduling algorithms focusing on user throughput in high speed downlink packet access. In: IEEE international symposium on personal, indoor and mobile radio communications, Pavilhão Atlântico, Lisboa, Portugal, vol 3, pp 1462–1466
Proakis JG (2001) Digital communication. Mc-Graw Hill Press, New York
Qualcomm Europe (2006) System analysis for UL SIMO SC-FDMA. In: 3GPP, R1-061525. Accessed 2006
Sallabi F, Lakas A, Shuaib K, Boulmalf M (2005) WCDMA downlink simulator with efficient wrap-around technique. In: IEEE second IFIP international conference on wireless and optical communications networks, Dubai, United Arab Emirates, pp 472–476
Sesia S, Toufik I, Baker M (2009) LTE: the UMTS long term evolution. Wiley, Chichester
Zheng YR, Xiao C (2003) Simulation models with correct statistical properties for Rayleigh fading channels. IEEE Trans Commun 51(6):920–928

Chapter 5
The Eighth Category: Joint Precoding with Ideal Backhaul

Abstract For the eighth category of multipoint cooperative communication technology, we discuss joint precoding schemes with ideal backhaul conditions for the downlink cellular network in this chapter. First, we introduce some of the well-known precoding schemes for joint transmission (JT), that is, the global precoding (GP), local precoding (LP), weighted local precoding (WLP), and single-frequency network precoding (SFNP) schemes. Second, we propose an enhanced SFNP scheme with smart antenna selection (AS) operated at the cooperating base stations (BSs), which is named AS-SFNP scheme. Third, for single-antenna UEs, both analytical lower bounds and simulation results are provided to show that both the proposed AS-SFNP scheme and the WLP scheme achieve performance close to that of the optimal GP scheme in terms of average signal-to-interference-plus-noise ratio (SINR). For multi-antenna UEs, simulation results demonstrate that the proposed AS-SFNP scheme can achieve a larger capacity than the LP, WLP, and SFNP schemes in high-SNR regime. Furthermore, from a system-level simulation of a practical cellular network, the AS-SFNP scheme with a low feedback overhead and low-complexity implementation shows comparable performance of the cell-edge spectral efficiency with the WLP and GP schemes.

Keywords Joint precoding • Ideal backhaul • Single-frequency network precoding • Antenna selection • SINR • Capacity • System-level simulation • Spectral efficiency

5.1 Introduction

The eighth category of multipoint cooperative communication technology addressed in Sect. 2.7.8 has recently attracted considerable interest in the literature, for example, see Gesbert et al. (2010) and references therein. Motivated by these works, downlink multipoint cooperative MIMO technologies have been adopted by the fourth generation (4G) mobile communication standards, such as the 3rd Generation

M. Ding and H. Luo, *Multi-point Cooperative Communication Systems: Theory and Applications*, Signals and Communication Technology, DOI 10.1007/978-3-642-34949-2_5,

Partnership Project (3GPP) Long-Term Evolution-Advanced (LTE-A) network (see Sect. 1.1). In the LTE-A system, the multipoint cooperative communication schemes can be generally divided into two types (3GPP 2010), that is, coordinated scheduling/coordinated beamforming (CS/CB) and joint transmission (JT). When the CS/CB strategy is employed (see the seventh category of multipoint cooperative communication technology introduced in Sect. 2.7.7), the cooperating base stations (BSs) share channel state information (CSI) in various forms, and each BS only transmits data to its served users; while for the JT strategy, both CSI and user data should be shared by all cooperating BSs, and thus each User Equipment (UE) receives data from multiple BSs. Many current research works focus on CS/CB MIMO schemes (Zhang et al. 2009; Dahrouj and Yu 2010; Venturino et al. 2010; Chae et al. 2009). However, the performance of CS/CB strategy is generally interference-limited due to lack of abundant spatial-domain degrees of freedom for perfect inter-BS interference coordination in practical systems (Gesbert et al. 2010). On the other hand, the JT strategy takes a more aggressive approach to cope with the interference problem by transforming the interference from neighbor BSs into useful signals. Usually, the mathematical form of the JT scheme bears a close resemblance to conventional MIMO systems except for its distributed structure (Shamai and Zaidel 2001). From uplink-downlink duality theory (see Sect. 2.5), the capacity region of a downlink JT system can be computed from its dual uplink (Jindal et al. 2004) with the same sum power constraint. These results were later generalized to accommodate the per-antenna power constraint (Yu and Lan 2007) by showing that the per-antenna downlink transmitter optimization problem can be transformed into a dual uplink problem with an uncertain noise. It should be noted that most capacity duality results are based on nonlinear signal processing at the BS side, such as the dirty paper coding (DPC) technique (Costa 1983), which is computationally demanding for precoding across multiple BSs.

Hence, in the JT precoding design for the LTE-A system, linear precoders (Peel et al. 2005) are generally more preferred than the nonlinear precoders (Costa 1983) in order to reduce the system complexity. Some existing linear precoding schemes are global precoding (GP) (Gesbert et al. 2010), local precoding (LP) (TI 2008), weighted local precoding (WLP) (ETRI 2009), single-frequency network precoding (SFNP) (ETRI 2009), etc. The basic idea of the GP scheme is to group multiple BSs together as a virtual BS and apply the extended point-to-point MIMO theory on the multi-BS global channel to obtain a global precoder. The LP scheme, on the other hand, is much simpler. It directly generates each sub-precoder for the sub-channel from each local BS to the UE. The WLP scheme conducts some improvement on the LP scheme by adding a co-phase weight to the per-BS precoder so that quasi-coherent combining of the multi-BS signals can be achieved. Perhaps the simplest JT precoding scheme is the SFNP scheme, in which the same signal with identical precoding is transmitted from multiple BSs to a UE, resulting in an SNR gain at the receiver.

However, the SFNP and LP schemes perform poorly (ETRI 2009) compared with the GP and WLP schemes, but the complexity of the GP scheme and the overhead of the WLP scheme are relatively high. In order to design a precoding scheme that is well-balanced in complexity, feedback overhead, and performance, we propose a novel antenna selection single-frequency network precoding (AS-SFNP) scheme, in which smart antenna selection (AS) is performed at BSs and identical precoders are employed at all cooperating BSs. In contrast with the conventional antenna selection technique where the antenna subset is selected from one transmission point, the AS-SFNP scheme requires distributed antenna selection and different antenna subsets are activated in the cooperating BSs.

5.2 System Model and Existing Technologies

5.2.1 System Model

We consider a single-user (SU) downlink JT scenario, where there are B cooperative BSs and each BS has N_{T} transmit antennas. The data for the target UE equipped with N_{R} antennas is transmitted simultaneously from all cooperative BSs. The channel between BS $b (b \in \{1, 2, \ldots, B\})$ and the UE is denoted as $\mathbf{H}_b \in \mathbb{C}^{N_{\mathrm{R}} \times N_{\mathrm{T}}}$. The UE can report its precoding matrix information either to each individual cooperative BS or to one primary BS. In the latter case, the primary BS should exchange the channel state information (CSI) from the UE among cooperating BSs through the ideal backhaul links. Let $\mathbf{W}_b \in \mathbb{C}^{N_{\mathrm{T}} \times L}$ be the local precoding matrix at BS b, where L is the number of data streams. Without loss of generality, we assume $N_{\mathrm{R}} \leq N_{\mathrm{T}}$ considering that the BS is usually more resourceful than the UE in the aspect of hardware equipment. Thus, we further have $L \leq N_{\mathrm{R}} \leq N_{\mathrm{T}}$ since the number of data streams should be smaller than $M = \min\{N_{\mathrm{R}}, N_{\mathrm{T}}\}$. The received signal at the UE can be described as

$$\mathbf{y} = [\mathbf{H}_1, \mathbf{H}_2, \cdots, \mathbf{H}_B] \begin{bmatrix} \mathbf{W}_1 \\ \mathbf{W}_2 \\ \vdots \\ \mathbf{W}_B \end{bmatrix} \mathbf{x} + \mathbf{n}, \tag{5.1}$$

where $\mathbf{x} \in \mathbb{C}^{L \times 1}$ is the transmission data vector with covariance matrix $\mathrm{E}\left\{\mathbf{x}\mathbf{x}^{\mathrm{H}}\right\} = \mathbf{I}_L$ and $\mathbf{n}$ is an additive interference/noise vector with $\mathrm{E}\left\{\mathbf{n}\mathbf{n}^{\mathrm{H}}\right\} = \mathbf{R}_{\mathrm{n}}$. It should be noted that the interference from outside of the considered B BSs has been incorporated into $\mathbf{n}$. If we treat the interference as white Gaussian signals (Skillermark et al. 2008), then $\mathbf{n}$ can be modeled as an additive zero-mean circularly symmetric complex Gaussian (ZMCSCG) vector with

$$\mathbf{R}_{\mathrm{n}} = N_0 \mathbf{I}_{N_{\mathrm{R}}}. \tag{5.2}$$

Let P be the maximum transmission power at each BS, and we denote per-BS power-to-noise ratio as $\gamma = P/N_0$.

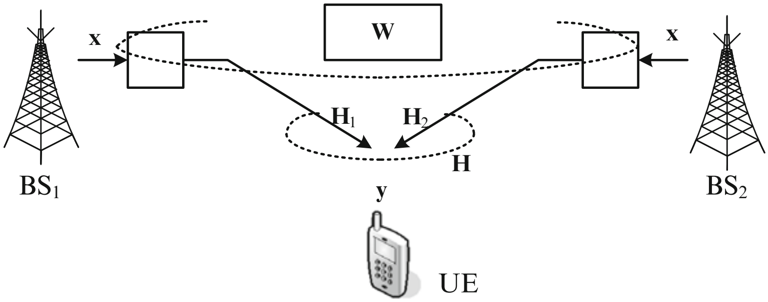

Fig. 5.1 Illustration of the GP scheme for a two-BS model

5.2.2 Existing Technologies

5.2.2.1 The GP Scheme

The GP scheme can be viewed as a generalization of single-BS multi-antenna transmission to cooperative transmission over multiple distributed BSs (Gesbert et al. 2010). For notational convenience, denote the global channel as $\mathbf{H} = [\mathbf{H}_1, \mathbf{H}_2, \ldots, \mathbf{H}_B]$, and the global precoder as $\mathbf{W} = \left[\mathbf{W}_1^{\mathrm{T}}, \mathbf{W}_2^{\mathrm{T}}, \ldots, \mathbf{W}_B^{\mathrm{T}}\right]^{\mathrm{T}}$. Then, we can rewrite (5.1) as

$$\mathbf{y} = \mathbf{HWx} + \mathbf{n}, \tag{5.3}$$

where $\mathbf{W}$ is subjected to a global power constraint given by

$$\mathrm{tr}\left(\mathbf{W}^{\mathrm{H}}\mathbf{W}\right) \leq BP. \tag{5.4}$$

The GP scheme for a two-BS model is illustrated in Fig. 5.1.

The system capacity maximization problem can be formulated as

$$\begin{aligned} \max_{\mathbf{W}} \quad & C(\mathbf{W}) \\ \text{s.t.} \quad & \mathrm{tr}\left\{\mathbf{W}^{\mathrm{H}}\mathbf{W}\right\} \leq BP, \end{aligned} \tag{5.5}$$

where $C(\mathbf{W})$ is the capacity for the global channel $\mathbf{H}$. $C(\mathbf{W})$ with full CSI at the transmit side can be presented as (Tse and Viswanath 2005)

$$C(\mathbf{W}) = \log_2\left(\det\left(\mathbf{I}_{N_{\mathrm{R}}} + \mathbf{HW}(\mathbf{HW})^{\mathrm{H}}\mathbf{R}_{\mathrm{n}}^{-1}\right)\right). \tag{5.6}$$

Conducting the eigenvalue decomposition (EVD) operation on $\mathbf{R_H} = \mathbf{H}^{\mathrm{H}}\mathbf{R}_{\mathrm{n}}^{-1}\mathbf{H}$, we have

$$\mathbf{R_H} = \mathbf{V}\boldsymbol{\Lambda}\mathbf{V}^{\mathrm{H}}, \tag{5.7}$$

where $\mathbf{V} \in \mathbb{C}^{BN_\mathrm{T} \times BN_\mathrm{T}}$ is a unitary matrix. $\mathbf{\Lambda} = \mathrm{diag}\left(\{\lambda_i\}\right)$ is a semi-definite diagonal matrix with the diagonal entries λ_i s being the eigenvalues of $\mathbf{R_H}$ sorted in a descending order.

According to the discussion in Sect. 2.3.1, the optimal solution for problem (5.5) is

$$\bar{\mathbf{W}}^{\mathrm{GP}} = \tilde{\mathbf{V}}\mathbf{\Sigma}, \tag{5.8}$$

where $\tilde{\mathbf{V}} \in \mathbb{C}^{BN_\mathrm{T} \times L}$ contains the L leftmost vectors of $\mathbf{V}$, which correspond to the L largest eigen values $\{\lambda_1, \lambda_2, \ldots, \lambda_L\}$ of $\mathbf{R_H}$. $\mathbf{\Sigma} = \mathrm{diag}\left(\{\sigma_i\}\right)$ is a diagonal water-filling power loading matrix expressed as (Tse and Viswanath 2005)

$$\sigma_i = \sqrt{\left(\mu - \frac{1}{\lambda_i}\right)^+}, \tag{5.9}$$

where $(x)^+ = \max\{x, 0\}$ and μ is the water-filling level chosen to make the power constraint in problem (5.5) tightened to the equality. It should be noted that problem (5.5) is constrained by a global power constraint, that is, the sum power of BSs involved in the JT cannot exceed BP. However, in practical systems, a BS usually has an independent power supply; thus, it makes more sense to adopt a local power constraint per BS. Hence, problem (5.5) should be reformulated to

$$\begin{aligned} \max_{\mathbf{W}} \quad & C\left(\mathbf{W}\right) \\ \text{s.t.} \quad & \mathrm{tr}\left\{\mathbf{W}_b^{\mathrm{H}}\mathbf{W}_b\right\} \le P. \end{aligned} \tag{5.10}$$

Though simple form problem (5.10) may appear to be, its solution can only be found in the form of numerical results by convex optimization software such as the CVX program (Grant et al. 2007). In order to facilitate our analysis in the following, we consider the GP solution shown in (5.8) to give us a tractable capacity upper bound for problem (5.10). We further denote the equivalent channel for the GP scheme as

$$\mathbf{H}_{\mathrm{eq}}^{\mathrm{GP}} = \mathbf{H}\bar{\mathbf{W}}^{\mathrm{GP}}. \tag{5.11}$$

Then, the capacity given by the GP scheme can be rewritten as

$$C_{\mathrm{GP}} = \log_2\left(\det\left(\mathbf{I}_{N_\mathrm{R}} + \mathbf{H}_{\mathrm{eq}}^{\mathrm{GP}}\left(\mathbf{H}_{\mathrm{eq}}^{\mathrm{GP}}\right)^{\mathrm{H}}\mathbf{R}_{\mathrm{n}}^{-1}\right)\right). \tag{5.12}$$

The complexity of the GP scheme is relatively high, which requires an Eigen Value Decomposition (EVD) operation on $\mathbf{R_H}$ with dimension $BN_\mathrm{T} \times BN_\mathrm{T}$ to obtain $\mathbf{V}$. Besides, the quantization of $\bar{\mathbf{W}}^{\mathrm{GP}} \in \mathbb{C}^{BN_\mathrm{T} \times L}$ demands an exhaustive search of precoding codewords in a large-size codebook for BN_T antennas, the feedback overhead of which will also be very high. Moreover, the size of the codebook for the GP scheme varies with B and N_T, which complicates the codebook design.

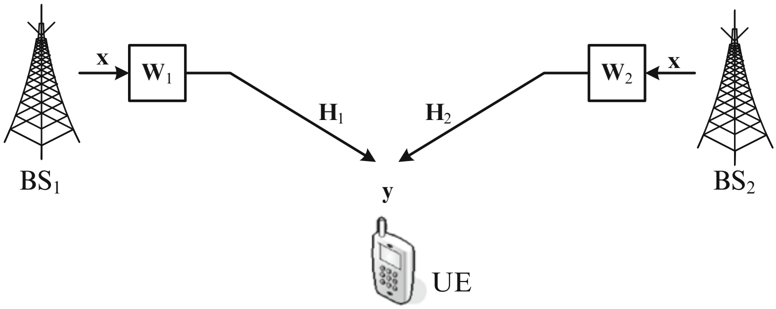

Fig. 5.2 Illustration of the LP scheme for a two-BS model

To sum up, the GP scheme excels in capacity performance, but it requires a large feedback overhead as well as high complexity in computation and codeword search for a global precoder.

5.2.2.2 The LP Scheme

The LP scheme (TI 2008) is based on separate precoding for the individual local channels from the cooperating BSs to the UE. The received signal from the b-th BS can be expressed as

$$\mathbf{y}_b = \mathbf{H}_b \mathbf{W}_b \mathbf{x} + \mathbf{n}, \tag{5.13}$$

where the local precoder $\mathbf{W}_b$ is chosen to match the local channel $\mathbf{H}_b$. The LP scheme for a two-BS model is illustrated in Fig. 5.2.

The capacity maximization problem for the local channel $\mathbf{H}_b$ can be formulated as

$$\begin{aligned} \max_{\mathbf{W}_b} \quad & C(\mathbf{W}_b) \\ \text{s.t.} \quad & \text{tr}\left\{\mathbf{W}_b^{\text{H}} \mathbf{W}_b\right\} \le P, \end{aligned} \tag{5.14}$$

where $C(\mathbf{W}_b)$ is the capacity of the b-th local channel on condition of full CSI available at the b-th BS. It can be written as (Tse and Viswanath 2005)

$$C(\mathbf{W}_b) = \log_2 \left(\det \left(\mathbf{I}_{N_\text{R}} + \mathbf{H}_b \mathbf{W}_b (\mathbf{H}_b \mathbf{W}_b)^{\text{H}} \mathbf{R}_\text{n}^{-1}\right)\right). \tag{5.15}$$

Let $\mathbf{R}_{\mathbf{H}_b} = \mathbf{H}_b^{\text{H}} \mathbf{R}_\text{n}^{-1} \mathbf{H}_b$ and conduct the EVD operation on $\mathbf{R}_\mathbf{H}$, then we have

$$\mathbf{R}_{\mathbf{H}_b} = \mathbf{V}_b \mathbf{\Lambda}_b \mathbf{V}_b^{\text{H}}, \tag{5.16}$$

where $\mathbf{V}_b \in \mathbb{C}^{N_\mathrm{T} \times N_\mathrm{T}}$ is a unitary matrix. $\mathbf{\Lambda}_b = \mathrm{diag}\left(\{\lambda_{b,i}\}\right)$ is a semi-definite diagonal matrix with the diagonal entries $\lambda_{b,i}$ s being the eigenvalues of $\mathbf{R}_{\mathbf{H}_b}$ sorted in a descending order.

Similar to (5.8), the optimal solution for problem (5.14) is

$$\bar{\mathbf{W}}_b^{\mathrm{LP}} = \tilde{\mathbf{V}}_b \mathbf{\Sigma}_b, \tag{5.17}$$

where $\tilde{\mathbf{V}}_b \in \mathbb{C}^{N_\mathrm{T} \times L}$ is comprised of the L leftmost vectors of $\mathbf{V}_b$, which correspond to the L largest eigenvalues of $\mathbf{R}_{\mathbf{H}_b}$. $\mathbf{\Sigma}_b = \mathrm{diag}\left(\{\sigma_{b,i}\}\right)$ is a diagonal water-filling power loading matrix expressed as (Tse and Viswanath 2005)

$$\sigma_{b,i} = \sqrt{\left(\mu_b - \frac{1}{\lambda_{b,i}}\right)^+}, \tag{5.18}$$

where μ_b is the water-filling level, which makes the power constraint in problem (5.14) satisfied with equality.

The combined signal at the UE after the optimal local precoding operations can be written as

$$\mathbf{y} = \left(\sum_{b=1}^{B} \mathbf{H}_b \bar{\mathbf{W}}_b^{\mathrm{LP}}\right) \mathbf{x} + \mathbf{n}. \tag{5.19}$$

We further denote the equivalent channel for the LP scheme as

$$\mathbf{H}_{\mathrm{eq}}^{\mathrm{LP}} = \sum_{b=1}^{B} \mathbf{H}_b \bar{\mathbf{W}}_b^{\mathrm{LP}}. \tag{5.20}$$

And the capacity given by the LP scheme can be reformulated as

$$C_{\mathrm{LP}} = \log_2 \left(\det\left(\mathbf{I}_{N_\mathrm{R}} + \mathbf{H}_{\mathrm{eq}}^{\mathrm{LP}} \left(\mathbf{H}_{\mathrm{eq}}^{\mathrm{LP}}\right)^{\mathrm{H}} \mathbf{R}_{\mathrm{n}}^{-1}\right)\right). \tag{5.21}$$

From (5.17), we can find that although the local precoder $\bar{\mathbf{W}}_b^{\mathrm{LP}}$ matches the local channel $\mathbf{H}_b$ very well, it doesn't guarantee coherent combining of multiple signals sent from different BSs. In the case when destructive combining occurs, the LP scheme will suffer from considerable capacity loss compared with the GP scheme. Nevertheless, the computational burden and codeword search process are of fairly low complexity in the LP scheme since only treatment of small-dimension local channels is involved. As for the feedback overhead, the LP scheme doesn't show any advantage over the GP scheme because multiple quantized $\bar{\mathbf{W}}_b^{\mathrm{LP}}$ s should be fed back to the BSs.

To sum up, the LP scheme can achieve fairly good performance due to precoder optimization for the local channels. Its complexity is also relatively low, but its feedback overhead is comparable to that of the GP scheme, which is quite large.

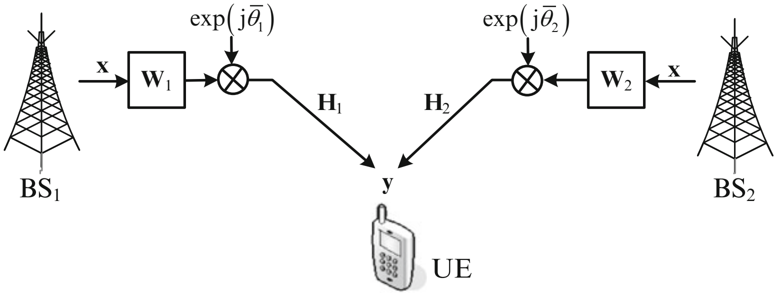

Fig. 5.3 Illustration of the WLP scheme for a two-BS model

5.2.2.3 The WLP Scheme

The WLP scheme extends the idea of the LP scheme by multiplying each precoding matrix with a phase prerotation factor (ETRI 2009) to combine the locally precoded signals in a quasi-coherent way. The received signal resulted from the WLP scheme can be described as

$$\mathbf{y} = \left(\sum_{b=1}^{B} \mathbf{H}_b \bar{\mathbf{W}}_b^{\mathrm{WLP}} \right) \mathbf{x} + \mathbf{n}, \tag{5.22}$$

where $\bar{\mathbf{W}}_b^{\mathrm{WLP}}$ is the weighted local precoder given by

$$\bar{\mathbf{W}}_b^{\mathrm{WLP}} = \exp\left(\mathrm{j}\bar{\theta}_b\right) \bar{\mathbf{W}}_b^{\mathrm{LP}}, \tag{5.23}$$

where $\bar{\theta}_b$ denotes the per-BS phase prerotation factor and $\bar{\mathbf{W}}_b^{\mathrm{LP}}$ is derived from (5.17). The WLP scheme for a two-BS model is illustrated in Fig. 5.3.

The $\{\bar{\theta}_b\}$ should be obtained by joint optimization of $\{\theta_b\}$ shown as

$$\{\bar{\theta}_b\} = \underset{\{\theta_b | b \in \{1,2,\cdots,B\}\}}{\arg\max} \left\{ C_{\mathrm{WLP}}\left(\{\theta_b\}\right) \right\}, \tag{5.24}$$

where $C_{\mathrm{WLP}}\left(\{\theta_b\}\right)$ is the conditional capacity of the WLP scheme expressed as

$$C_{\mathrm{WLP}}\left(\{\theta_b\}\right) = \log_2 \left(\det \left(\mathbf{I}_{N_\mathrm{R}} + \left(\sum_{b=1}^{B} \mathbf{H}_b \exp\left(\mathrm{j}\theta_b\right) \bar{\mathbf{W}}_b^{\mathrm{LP}} \right) \left(\sum_{b=1}^{B} \mathbf{H}_b \exp\left(\mathrm{j}\theta_b\right) \bar{\mathbf{W}}_b^{\mathrm{LP}} \right)^{\mathrm{H}} \mathbf{R}_\mathrm{n}^{-1} \right) \right). \tag{5.25}$$

We further denote the equivalent channel for the WLP scheme as

$$\mathbf{H}_{\mathrm{eq}}^{\mathrm{WLP}} = \sum_{b=1}^{B} \mathbf{H}_b \bar{\mathbf{W}}_b^{\mathrm{WLP}}. \tag{5.26}$$

And the capacity given by the WLP scheme can be written as

$$C_{\mathrm{WLP}} = \log_2 \left(\det \left(\mathbf{I}_{N_{\mathrm{R}}} + \mathbf{H}_{\mathrm{eq}}^{\mathrm{WLP}} \left(\mathbf{H}_{\mathrm{eq}}^{\mathrm{WLP}} \right)^{\mathrm{H}} \mathbf{R}_{\mathrm{n}}^{-1} \right) \right). \tag{5.27}$$

It can be envisaged that with the phase prerotation shown in (5.23), the WLP scheme can restore some capacity loss from the LP scheme. However, drawbacks of the WLP scheme are also very obvious. Additional derivation, quantization, and feedback of $\{\bar{\theta}_b\}$ are required at the UE side on top of the LP operations.

Furthermore, it should be noted that analytical expressions for the optimal $\{\bar{\theta}_b\}$ generally do not exist due to its non-convex form. In other words, it is non-trial to find the solution for the following optimization problem:

$$\begin{aligned} \max_{\{g_b\}} \quad & C'_{\mathrm{WLP}}(\{g_b\}) = \det \left(\mathbf{I}_{N_{\mathrm{R}}} + \left(\sum_{b=1}^{B} \mathbf{H}_b \bar{\mathbf{W}}_b^{\mathrm{LP}} g_b \right) \left(\sum_{b=1}^{B} \mathbf{H}_b \bar{\mathbf{W}}_b^{\mathrm{LP}} g_b \right)^{\mathrm{H}} \mathbf{R}_{\mathrm{n}}^{-1} \right) \\ \text{s.t.} \quad & |g_b| = 1, b \in \{1, 2, \ldots, B\}. \end{aligned} \tag{5.28}$$

However, for some special cases, for example, when $\mathbf{R}_{\mathrm{n}} = N_0 \mathbf{I}_{N_{\mathrm{R}}}$ and $\bar{\mathbf{W}}_b^{\mathrm{LP}}$ is an $N_{\mathrm{T}} \times 1$ vector, we can maximize an upper bound $C'^{\mathrm{UB}}_{\mathrm{WLP}}(\{g_b\})$ of $C'_{\mathrm{WLP}}(\{g_b\})$ shown as

$$\begin{aligned} C'_{\mathrm{WLP}}(\{g_b\}) &= \det \left(N_0 \mathbf{I}_{N_{\mathrm{R}}} + \left(\sum_{b=1}^{B} \mathbf{h}_b g_b \right) \left(\sum_{b=1}^{B} \mathbf{h}_b g_b \right)^{\mathrm{H}} \right) \\ &= \det \left(N_0 \mathbf{I}_{N_{\mathrm{R}}} + \widehat{\mathbf{H}} \mathbf{g} \mathbf{g}^{\mathrm{H}} \widehat{\mathbf{H}}^{\mathrm{H}} \right) \\ &= \det \left(N_0 \mathbf{I}_{N_{\mathrm{R}}} + \widehat{\mathbf{H}} \mathbf{G} \widehat{\mathbf{H}}^{\mathrm{H}} \right) \\ &\le \left(\frac{1}{N_{\mathrm{R}}} \operatorname{tr} \left\{ N_0 \mathbf{I}_{N_{\mathrm{R}}} + \widehat{\mathbf{H}} \mathbf{G} \widehat{\mathbf{H}}^{\mathrm{H}} \right\} \right)^{N_{\mathrm{R}}} \\ &= \left(N_0 + \frac{1}{N_{\mathrm{R}}} \operatorname{tr} \left\{ \widehat{\mathbf{H}}^{\mathrm{H}} \widehat{\mathbf{H}} \mathbf{G} \right\} \right)^{N_{\mathrm{R}}} \\ &= C'^{\mathrm{UB}}_{\mathrm{WLP}}(\{g_b\}), \end{aligned} \tag{5.29}$$

where $\mathbf{h}_b = \mathbf{H}_b \bar{\mathbf{W}}_b^{\mathrm{LP}}$ is an $N_{\mathrm{R}} \times 1$ vector. $\widehat{\mathbf{H}}$, $\mathbf{g}$, and $\mathbf{G}$ denote $[\mathbf{h}_1, \mathbf{h}_2, \ldots, \mathbf{h}_B]$, $[g_1, g_2, \ldots, g_B]^{\mathrm{T}}$ and $\mathbf{g}\mathbf{g}^{\mathrm{H}}$, respectively. Besides, the inequality in (5.29) is obtained from Golub and Loan (1996). Therefore, we can reformulate problem (5.28) into a semi-definite programming (SDP) problem to maximize the term $\mathrm{tr}\left\{\widehat{\mathbf{H}}^{\mathrm{H}}\widehat{\mathbf{H}}\mathbf{G}\right\}$ in $C_{\mathrm{WLP}}^{\prime\mathrm{UB}}(\{g_b\})$, which is shown as

$$
\begin{aligned}
&\max_{\mathbf{g}}\ \mathrm{tr}\left\{\widehat{\mathbf{H}}^{\mathrm{H}}\widehat{\mathbf{H}}\mathbf{G}\right\} \\
&\text{s.t. } \mathbf{G} = \mathbf{g}\mathbf{g}^{\mathrm{H}}, |g_b| = 1, b \in \{1, 2, \ldots, B\}.
\end{aligned} \tag{5.30}
$$

The problem (5.30) is still non-convex because of the constrained form of $\mathbf{G} = \mathbf{g}\mathbf{g}^{\mathrm{H}}$. With some mathematical manipulations, we can reformulate problem (5.30) as

$$
\begin{aligned}
\max_{\mathbf{G}} \quad & \mathrm{tr}\left\{\widehat{\mathbf{H}}^{\mathrm{H}}\widehat{\mathbf{H}}\mathbf{G}\right\} \\
\text{s.t.} \quad & \mathrm{tr}\{\mathbf{G}\mathbf{U}_b\} = 1, b \in \{1, 2, \ldots, B\}, \\
& \mathbf{G} \succeq 0, \mathrm{Rank}\{\mathbf{G}\} = 1,
\end{aligned} \tag{5.31}
$$

where all the entries of $\mathbf{U}_b$ are zero except that its b-th diagonal element equals to one. $\mathbf{G} \succeq 0$ means that $\mathbf{G}$ is positive semi-definite. Problem (5.31) is a non-convex problem due to the rank-one constraint. We then apply the SDP relaxation technique (Huang and Palomar 2010) by omitting the rank-one constraint, which leads to a new optimization problem written as

$$
\begin{aligned}
\max_{\mathbf{G}} \quad & \mathrm{tr}\left\{\widehat{\mathbf{H}}^{\mathrm{H}}\widehat{\mathbf{H}}\mathbf{G}\right\} \\
\text{s.t.} \quad & \mathrm{tr}\{\mathbf{G}\mathbf{U}_b\} = 1, b \in \{1, 2, \ldots, B\} \\
& \mathbf{G} \succeq 0.
\end{aligned} \tag{5.32}
$$

Now problem (5.32) is a standard convex semi-definite programming (SDP) problem and can be solved efficiently using mathematical software packages (Grant et al. 2007). The remaining question is whether problem (5.31) is equivalent to problem (5.32). In (Huang and Palomar 2010), the authors proved that the optimal solution of a SDP problem such as problem (5.32) is always rank one if it has at most three constraints. Therefore, problems (5.31) and (5.32) are equivalent only when the number of cooperative BSs is no more than three. Suppose that $B \leq 3$ and $\bar{\mathbf{G}} = \bar{\mathbf{g}}\bar{\mathbf{g}}^{\mathrm{H}}$ is the optimal solution for problem (5.32), then the optimal solution for the original problem (5.31) or (5.30) is $\mathbf{g} = \bar{\mathbf{g}}$.

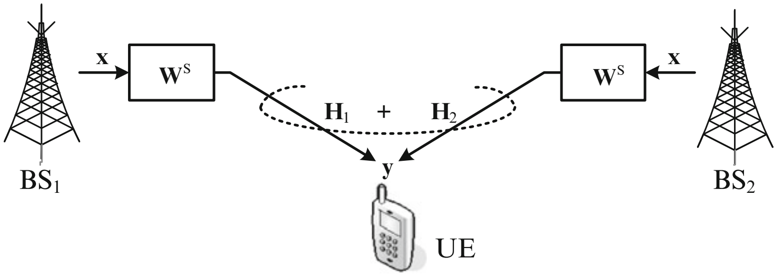

Fig. 5.4 Illustration of the SFNP scheme for a two-BS model

To sum up, the WLP scheme can improve the performance of the LP scheme by quasi-coherent combination of the signals sent from multiple BSs. However, its complexity and feedback overhead associated with the additional phase prerotation weights are relatively high compared with the LP scheme.

5.2.2.4 The SFNP Scheme

Like the LP scheme, the SFNP scheme (ETRI 2009) is another simplification of the GP scheme, in which an identical SFN precoder $\mathbf{W}^{\mathrm{S}} \in \mathbb{C}^{N_{\mathrm{T}}\times L}$ is employed for all cooperating BSs. The UE's received signal of the SFNP scheme can be described as

$$\mathbf{y} = \left(\sum_{b=1}^{B} \mathbf{H}_b\right) \mathbf{W}^{\mathrm{S}}\mathbf{x} + \mathbf{n}, \tag{5.33}$$

where $\mathbf{W}^{\mathrm{S}}$ is subjected to a local power constraint shown as

$$\mathrm{tr}\left\{\left(\mathbf{W}^{\mathrm{S}}\right)^{\mathrm{H}} \mathbf{W}^{\mathrm{S}}\right\} \leq P. \tag{5.34}$$

The SFNP scheme for a two-BS model is illustrated in Fig. 5.4.

Similar to the derivation of the GP precoder, the capacity maximization problem of the SFNP scheme can be formulated as

$$\begin{aligned} &\max_{\mathbf{W}^{\mathrm{S}}} \quad C\left(\mathbf{W}^{\mathrm{S}}\right) \\ &\text{s.t.} \quad \mathrm{tr}\left\{\left(\mathbf{W}^{\mathrm{S}}\right)^{\mathrm{H}} \mathbf{W}^{\mathrm{S}}\right\} \leq P, \end{aligned} \tag{5.35}$$

where $C\left(\mathbf{W}^{\mathrm{S}}\right)$ is the capacity for the composite channel $\sum_{b=1}^{B} \mathbf{H}_b$. $C\left(\mathbf{W}^{\mathrm{S}}\right)$ with full CSI at the transmit side can be presented as (Tse and Viswanath 2005)

$$C\left(\mathbf{W}^{\mathrm{S}}\right)=\log_2\left(\det\left(\mathbf{I}_{N_{\mathrm{R}}}+\left(\sum_{b=1}^{B}\mathbf{H}_b\right)\mathbf{W}^{\mathrm{S}}\left(\left(\sum_{b=1}^{B}\mathbf{H}_b\right)\mathbf{W}^{\mathrm{S}}\right)^{\mathrm{H}}\mathbf{R}_{\mathrm{n}}^{-1}\right)\right). \quad (5.36)$$

Let $\mathbf{R}_{\mathbf{H}^{\mathrm{S}}}=\left(\sum_{b=1}^{B}\mathbf{H}_b\right)^{\mathrm{H}}\mathbf{R}_{\mathrm{n}}^{-1}\left(\sum_{b=1}^{B}\mathbf{H}_b\right)$ and conduct the EVD operation on $\mathbf{R}_{\mathbf{H}^{\mathrm{S}}}$, then we get

$$\mathbf{R}_{\mathbf{H}^{\mathrm{S}}}=\mathbf{V}^{\mathrm{S}}\mathbf{\Lambda}^{\mathrm{S}}\left(\mathbf{V}^{\mathrm{S}}\right)^{\mathrm{H}}, \quad (5.37)$$

where $\mathbf{V}^{\mathrm{S}}\in\mathbb{C}^{N_{\mathrm{T}}\times N_{\mathrm{T}}}$ is a unitary matrix. $\mathbf{\Lambda}^{\mathrm{S}}=\mathrm{diag}\left(\left\{\lambda_i^{\mathrm{S}}\right\}\right)$ is a semi-definite diagonal matrix with the diagonal entries being the eigenvalues of $\mathbf{R}_{\mathbf{H}^{\mathrm{S}}}$ sorted in a descending order. In a similar way as in (5.8), the optimal solution for problem (5.35) is

$$\bar{\mathbf{W}}^{\mathrm{S}}=\tilde{\mathbf{V}}^{\mathrm{S}}\mathbf{\Sigma}^{\mathrm{S}}, \quad (5.38)$$

where $\tilde{\mathbf{V}}^{\mathrm{S}}\in\mathbb{C}^{N_{\mathrm{T}}\times L}$ contains the L leftmost vectors of $\mathbf{V}^{\mathrm{S}}$, which correspond to the L largest eigen values of $\mathbf{R}_{\mathbf{H}^{\mathrm{S}}}$. $\mathbf{\Sigma}^{\mathrm{S}}=\mathrm{diag}\left(\left\{\sigma_i^{\mathrm{S}}\right\}\right)$ is a diagonal water-filling power loading matrix expressed as (Tse and Viswanath 2005)

$$\sigma_i^{\mathrm{S}}=\sqrt{\left(\mu-\frac{1}{\lambda_i^{\mathrm{S}}}\right)^{+}}, \quad (5.39)$$

where μ is the water-filling level allowing the power of $\mathbf{W}^{\mathrm{S}}$ in problem (5.35) take the maximum value.

We further denote the equivalent channel for the SFNP scheme as

$$\mathbf{H}_{\mathrm{eq}}^{\mathrm{S}}=\left(\sum_{b=1}^{B}\mathbf{H}_b\right)\bar{\mathbf{W}}^{\mathrm{S}}. \quad (5.40)$$

Then, the optimal capacity of the SFNP scheme can be expressed as

$$C_{\mathrm{SFNP}}=\log_2\left(\det\left(\mathbf{I}_{N_{\mathrm{R}}}+\mathbf{H}_{\mathrm{eq}}^{\mathrm{S}}\left(\mathbf{H}_{\mathrm{eq}}^{\mathrm{S}}\right)^{\mathrm{H}}\mathbf{R}_{\mathrm{n}}^{-1}\right)\right). \quad (5.41)$$

Compared with the GP, LP, and WLP schemes, the SFNP scheme is much simpler in the precoder derivation. Besides, the SFNP scheme requires a small load of feedback consisting of only one precoder. However, like the LP scheme, the SFNP scheme also has the problem of noncoherent signal combining, which degrades the system performance.

Table 5.1 Comparison of various linear precoding schemes for multi-BS JT

Scheme	Performance	Complexity	Feedback overhead
GP	*Good* (the global channel is considered)	*High* (computationally demanding and time-consuming in codeword search)	*Relatively high* (a large-size global precoder)
LP	*Fairly good* (the local channels are considered)	*Relatively low* (derivation and search of multiple local precoders)	*Relatively high* (multiple local precoders)
WLP	*Better than LP* (quasi-coherent signal combining by phase weights)	*Medium to high* (derivation and search of multiple local precoders and multiple local phase weights)	*High* (multiple local precoders and local phase weights)
SFNP	*Fairly good* (the composite channel is considered)	*Low* (derivation and search of only one SFN precoder)	*Low* (a small-size SFN precoder)

To sum up, the SFNP scheme can achieve fairly good performance because of the optimized precoder for the composite channel. Since only one SFN precoder is of concern in the SFNP scheme, both its complexity and feedback overhead are very low.

5.2.2.5 Motivations of Improved Schemes

We compare the existing linear precoding schemes for JT in terms of performance, complexity, and feedback overhead. The main results are summarized in Table 5.1.

From Table 5.1, we can see that the SFNP scheme exhibits desirable qualities in both complexity and feedback overhead, but it doesn't score well in the aspect of system performance. Therefore, the performance of the SFNP scheme needs to be improved so that we can come up with a more competitive JT precoding scheme. In the following, we propose a precoding scheme which combines the antenna selection (AS) technology and the SFNP scheme, that is, antenna selection single-frequency network precoding (AS-SFNP). The basic idea of the proposed AS-SFNP scheme is to maximize the capacity of the composite channel by smartly activating some of the BS antennas, followed by the SFNP operation.

5.3 Enhanced Single-Frequency Network Precoding Scheme

5.3.1 The Proposed AS-SFNP Scheme

We propose to dynamically select the transmit antennas for the SFNP transmission, which can eliminate the antennas having little or negative contributions on the

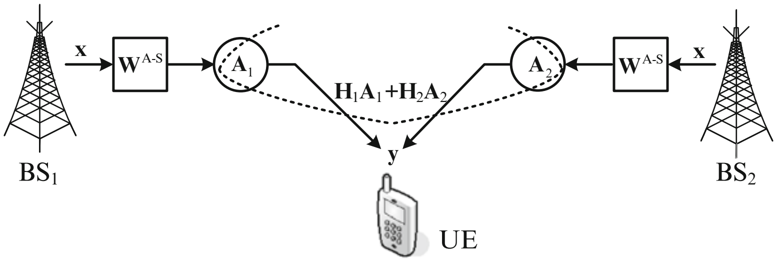

Fig. 5.5 Illustration of the AS-SFNP scheme for a two-BS model

system capacity (Ding et al. 2010). The antenna selection matrix for the b-th BS is represented by a nonnegative diagonal matrix $\mathbf{A}_b$, which is multiplied to the left side of $\mathbf{W}^{\mathrm{S}}$. The i-th diagonal element $a_b(i) \in \{0, 1\}$ of $\mathbf{A}_b$ indicates the AS result for the i-th antenna, with one for activation and zero otherwise. Therefore, the received signal of the proposed AS-SFNP scheme is

$$\mathbf{y} = \left(\sum_{b=1}^{B} \mathbf{H}_b \mathbf{A}_b q_b\right) \mathbf{W}^{\text{A-S}} \mathbf{x} + \mathbf{n}, \tag{5.42}$$

where $\mathbf{W}^{\text{A-S}}$ is the AS-SFN precoder for the cooperating BSs and q_b is an antenna power compensation scalar added to satisfy the local power constraint, which can be represented as

$$q_b = \sqrt{N_{\mathrm{T}}/\operatorname{tr}\{\mathbf{A}_b\}}. \tag{5.43}$$

The proposed AS-SFNP scheme for a two-BS model is illustrated in Fig. 5.5.

The capacity of the AS-SFNP scheme should be optimized over $\{\mathbf{A}_b\}$ and $\mathbf{W}^{\text{A-S}}$, which can be formulated as

$$\begin{aligned} &\max_{\{\mathbf{A}_b\},\mathbf{W}^{\text{A-S}}} C\left(\{\mathbf{A}_b\}, \mathbf{W}^{\text{A-S}}\right) \\ &\text{s.t.} \quad \operatorname{tr}\left\{\left(\mathbf{W}^{\text{A-S}}\right)^{\mathrm{H}} \mathbf{W}^{\text{A-S}}\right\} \le P, \end{aligned} \tag{5.44}$$

where $C\left(\{\mathbf{A}_b\}, \mathbf{W}^{\text{A-S}}\right)$ is expressed as (Tse and Viswanath 2005)

$$\begin{aligned} &C\left(\{\mathbf{A}_b\}, \mathbf{W}^{\text{A-S}}\right) \\ &= \log_2\left(\det\left(\mathbf{I}_{N_{\mathrm{R}}} + \left(\sum_{b=1}^{B} \mathbf{H}_b \mathbf{A}_b q_b\right) \mathbf{W}^{\text{A-S}} \left(\left(\sum_{b=1}^{B} \mathbf{H}_b \mathbf{A}_b q_b\right) \mathbf{W}^{\text{A-S}}\right)^{\mathrm{H}} \mathbf{R}_{\mathrm{n}}^{-1}\right)\right). \end{aligned} \tag{5.45}$$

Due to the fact that $\{\mathbf{A}_b\}$ is independent from the form of optimal $\mathbf{W}^{\text{A-S}}$, we can reformulate (5.44) to a maximization problem of C_{SFNP} conditioned on $\{\mathbf{A}_b\}$, which is written as

$$\begin{aligned} &\max_{\{\mathbf{A}_b\}} \; C_{\text{SFNP}}|_{\{\mathbf{A}_b\}} \\ &\text{s.t. tr}\left\{\left(\mathbf{W}^{\text{A-S}}\right)^{\text{H}}\mathbf{W}^{\text{A-S}}\right\} \leq P, \end{aligned} \tag{5.46}$$

where the conditional capacity $C_{\text{SFNP}}|_{\{\mathbf{A}_b\}}$ of the SFNP scheme is

$$C_{\text{SFNP}}|_{\{\mathbf{A}_b\}} = \log_2\left(\det\left(\mathbf{I}_{N_\text{R}} + \left(\mathbf{H}_{\text{eq}}^{\text{S}}\Big|_{\{\mathbf{A}_b\}}\right)\left(\mathbf{H}_{\text{eq}}^{\text{S}}\Big|_{\{\mathbf{A}_b\}}\right)^{\text{H}}\mathbf{R}_{\text{n}}^{-1}\right)\right). \tag{5.47}$$

In (5.47), $\mathbf{H}_{\text{eq}}^{\text{S}}\Big|_{\{\mathbf{A}_b\}}$ is the conditional equivalent SFN channel given by

$$\mathbf{H}_{\text{eq}}^{\text{S}}\Big|_{\{\mathbf{A}_b\}} = \left(\sum_{b=1}^{B}\mathbf{H}_b\mathbf{A}_b q_b\right)\bar{\mathbf{W}}^{\text{S}}, \tag{5.48}$$

where $\bar{\mathbf{W}}^{\text{S}}$ is the optimal SFN precoder for the composite channel $\sum\limits_{b=1}^{B}\mathbf{H}_b\mathbf{A}_b q_b$.

The optimal AS result is obtained at the UE side by performing an exhaustive search to maximize $C_{\text{SFNP}}|_{\{\mathbf{A}_b\}}$ as

$$\left\{\bar{\mathbf{A}}_b\right\} = \mathop{\arg\max}_{\{\mathbf{A}_b|b\in\{1,2,\cdots,B\}\}}\left\{C_{\text{SFNP}}|_{\{\mathbf{A}_b\}}\right\}. \tag{5.49}$$

We further denote the equivalent channel for the SFNP scheme as

$$\mathbf{H}_{\text{eq}}^{\text{A-S}} = \left(\sum_{b=1}^{B}\mathbf{H}_b\bar{\mathbf{A}}_b q_b\right)\bar{\mathbf{W}}^{\text{A-S}}, \tag{5.50}$$

where $\bar{\mathbf{W}}^{\text{A-S}}$ denotes the optimal SFN precoder for the composite channel with the optimal antenna selection result $\left\{\bar{\mathbf{A}}_b\right\}$. Then, the capacity of the AS-SFNP scheme can be expressed as

$$C_{\text{AS-SFNP}} = \log_2\left(\det\left(\mathbf{I}_{N_\text{R}} + \mathbf{H}_{\text{eq}}^{\text{A-S}}\left(\mathbf{H}_{\text{eq}}^{\text{A-S}}\right)^{\text{H}}\mathbf{R}_{\text{n}}^{-1}\right)\right). \tag{5.51}$$

Compared with the SFNP scheme, the proposed AS-SFNP scheme should be able to greatly improve the capacity performance because of two reasons: (i) It can smartly select the transmit antennas which are mostly beneficial to increase the system capacity; (ii) it redistributes the power of the deactivated antennas onto the selected antennas by q_b, which allows the system to make use of the limited transmission power more efficiently. However, the computational complexity goes up since the SFN operation should be carried out for each antenna selection hypothesis in order to find the optimal $\{\bar{\mathbf{A}}_b\}$, and the feedback overhead also increases due to the additional information of the antenna selection result. For instance, when $B = 3$, $N_{\mathrm{T}} = 4$, the number of possible AS combinations is $(2^4)^3 = 4{,}096$, requiring 12 bits of feedback overhead. Obviously, the exhaustive search shown by (5.49) can be very time-consuming and the overhead becomes quite large. However, it is generally not necessary to search over all combinations of AS from the cooperating BSs, for example, some combinations require shutting down a whole BS, which should be pre-eliminated because of the inefficient usage of the transmit power. Note that the restricted search space method can be exploited not only to reduce the AS complexity and feedback overhead but also to relax the power imbalance problem across the transmit antennas due to antenna muting or antenna power boosting in the AS process.

5.3.2 *Analytical Results for the Single-Antenna UE*

Though simple forms the capacities of the WLP and AS-SFNP schemes may appear to be, the closed-form expressions for the optimal phase prerotation factors and the optimal antenna selection result generally do not exist. So it is difficult to perform a thorough analysis for the system capacity. Hence, we turn our attentions to some mathematically tractable cases such as the vector channels, the analysis of which can provide us some insights on the performance of different precoding schemes for JT.

5.3.2.1 The Average SINR of the GP Scheme

First, we consider the GP scheme. For a single-antenna UE, $\bar{\mathbf{W}}^{\mathrm{GP}}$ in (5.8) degenerates to the matched filter (MF) vector shown as

$$\bar{\mathbf{W}}^{\mathrm{GP}} = \sqrt{BP}\frac{\mathbf{H}^{\mathrm{H}}}{\|\mathbf{H}\|} \times \exp(\mathrm{j}\varphi), \tag{5.52}$$

where φ is an irrelevant random phase misalignment distributed over $[-\pi, \pi)$, which is resulted from the phase difference between the transmitter and receiver. From (5.11), the SINR of the GP scheme is given by

$$
\begin{aligned}
r_{\mathrm{GP}} &= \frac{\mathbf{H}_{\mathrm{eq}}^{\mathrm{GP}}\left(\mathbf{H}_{\mathrm{eq}}^{\mathrm{GP}}\right)^{\mathrm{H}}}{N_0} \\
&= \frac{\mathbf{H}\bar{\mathbf{W}}^{\mathrm{GP}}\left(\mathbf{H}\bar{\mathbf{W}}^{\mathrm{GP}}\right)^{\mathrm{H}}}{N_0} \\
&= \|\mathbf{H}\|^2 B\gamma.
\end{aligned}
\tag{5.53}
$$

The probability density function (PDF) of $\|\mathbf{H}\|^2$ follows a chi-squared distribution $\chi^2\left(2BN_{\mathrm{T}}, 1/2\right)$ (Proakis 2001) expressed as

$$
p(x) = \frac{1}{\sigma^{2BN_{\mathrm{T}}}\, 2^{BN_{\mathrm{T}}}\left(BN_{\mathrm{T}}-1\right)!} x^{BN_{\mathrm{T}}-1} e^{-x/2\sigma^2}, \quad x \geq 0,
\tag{5.54}
$$

and hence, the average SINR of the GP scheme can be easily obtained as

$$
\begin{aligned}
\gamma_{\mathrm{GP}} &= \mathrm{E}\left\{r_{\mathrm{GP}}\right\} \\
&= 2BN_{\mathrm{T}} \times \frac{1}{2} \times B\gamma \\
&= B^2 N_{\mathrm{T}}\gamma.
\end{aligned}
\tag{5.55}
$$

5.3.2.2 The Average SINR of the LP Scheme

Second, we investigate the LP scheme. According to (5.17), when the UE is equipped with one antenna, $\bar{\mathbf{W}}_b^{\mathrm{LP}}$ degenerates to

$$
\bar{\mathbf{W}}_b^{\mathrm{LP}} = \sqrt{P}\frac{\mathbf{H}_b^{\mathrm{H}}}{\|\mathbf{H}_b\|} \times \exp\left(\mathrm{j}\varphi_b\right),
\tag{5.56}
$$

where φ_b is also an irrelevant random phase misalignment distributed over $[-\pi, \pi)$, which is resulted from the phase difference between the transmitter and receiver. From (5.20), the SINR of the LP scheme can be derived as

$$
\begin{aligned}
r_{\mathrm{LP}} &= \frac{\mathbf{H}_{\mathrm{eq}}^{\mathrm{LP}}\left(\mathbf{H}_{\mathrm{eq}}^{\mathrm{LP}}\right)^{\mathrm{H}}}{N_0} \\
&= \frac{\sum_{b=1}^{B}\mathbf{H}_b\bar{\mathbf{W}}_b^{\mathrm{LP}}\left(\sum_{b=1}^{B}\mathbf{H}_b\bar{\mathbf{W}}_b^{\mathrm{LP}}\right)^{\mathrm{H}}}{N_0} \\
&= \sum_{b=1}^{B}\|\mathbf{H}_b\|\exp\left(\mathrm{j}\varphi_b\right)\left(\sum_{b=1}^{B}\|\mathbf{H}_b\|\exp\left(\mathrm{j}\varphi_b\right)\right)^{\mathrm{H}}\gamma.
\end{aligned}
\tag{5.57}
$$

Taking the expectation of r_{LP}, we can get the average SINR for the LP scheme as

$$\begin{aligned}\gamma_{\mathrm{LP}} &= \mathrm{E}\left\{r_{\mathrm{LP}}\right\} \\ &= \mathrm{E}\left\{\left|\sum_{b=1}^{B}\|\mathbf{H}_b\|\exp\left(\mathrm{j}\varphi_b\right)\right|^2\right\}\gamma \\ &= \left(\mathrm{E}\left\{\sum_{b=1}^{B}\|\mathbf{H}_b\|^2\right\}+\mathrm{E}\left\{\sum_{m,n=1,\ m\neq n}^{B}\|\mathbf{H}_m\|\,\|\mathbf{H}_n\|\exp\left(\mathrm{j}\varphi_m\right)\exp\left(\text{-}\mathrm{j}\varphi_n\right)\right\}\right)\gamma \\ &\overset{(a)}{=} B\mathrm{E}\left\{\|\mathbf{H}_b\|^2\right\}\gamma \\ &\overset{(b)}{=} BN_{\mathrm{T}}\gamma. \end{aligned} \tag{5.58}$$

Equation (a) in (5.58) holds because $\|\mathbf{H}_b\|$ and φ_b are independently distributed, and hence, all the multiplication terms with $m \neq n$ are averaged out to zeros. Equation (b) in (5.58) comes from the fact that $\|\mathbf{H}_b\|^2$ conforms to a chi-squared distribution $\chi^2\left(2N_{\mathrm{T}}, 1/2\right)$ (Proakis 2001); thus, we have

$$\mathrm{E}\left\{\|\mathbf{H}_b\|^2\right\} = N_{\mathrm{T}}. \tag{5.59}$$

Comparing (5.58) with the average SINR of the GP scheme shown in (5.55), we can find that the LP scheme suffers from performance loss in terms of average SINR by a factor of B, which is due to the incoherent combining of signals sent from multiple BSs.

5.3.2.3 The Average SINR of the WLP Scheme

Third, we look into the average SINR of the WLP scheme and present Theorem 5.1 in the following.

Theorem 5.1. *The average SINR of the WLP scheme when* $N_{\mathrm{R}} = 1$ *can be expressed as*

$$\gamma_{\mathrm{WLP}} = BN_{\mathrm{T}}\gamma + B\left(B-1\right)\left(\frac{\Gamma\left(N_{\mathrm{T}}+1/2\right)}{\Gamma\left(N_{\mathrm{T}}\right)}\right)^2\gamma, \tag{5.60}$$

where $\Gamma(x)$ *is the gamma function defined as* (Proakis 2001)

$$\Gamma(x) = \int_0^{\infty} t^{x-1}e^{-t}dt, \quad x > 0. \tag{5.61}$$

Proof. In order to achieve the coherent signal combining, it is easy to show that the optimal phase rotations $\{\bar{\theta}_b\}$ in (5.24) should be able to completely cancel out $\{\varphi_b\}$ in (5.56), that is,

$$\bar{\theta}_b = -\varphi_b, \quad b \in \{1, 2, \ldots, B\}. \tag{5.62}$$

From (5.26), the SINR of the WLP scheme is given by

$$\begin{aligned}
r_{\mathrm{WLP}} &= \frac{\mathbf{H}_{\mathrm{eq}}^{\mathrm{WLP}} \left(\mathbf{H}_{\mathrm{eq}}^{\mathrm{WLP}}\right)^{\mathrm{H}}}{N_0} \\
&= \frac{\sum_{b=1}^{B} \mathbf{H}_b \exp\left(\mathrm{j}\bar{\theta}_b\right) \bar{\mathbf{W}}_b \left(\sum_{b=1}^{B} \mathbf{H}_b \exp\left(\mathrm{j}\bar{\theta}_b\right) \bar{\mathbf{W}}_b\right)^{\mathrm{H}}}{N_0} \\
&= \sum_{b=1}^{B} \|\mathbf{H}_b\| \exp\left(\mathrm{j}\bar{\theta}_b + \mathrm{j}\varphi_b\right) \left(\sum_{b=1}^{B} \|\mathbf{H}_b\| \exp\left(\mathrm{j}\bar{\theta}_b + \mathrm{j}\varphi_b\right)\right)^{\mathrm{H}} \gamma \\
&= \left(\sum_{b=1}^{B} \|\mathbf{H}_b\|\right)^2 \gamma.
\end{aligned} \tag{5.63}$$

We can get the average SINR of the WLP scheme by

$$\begin{aligned}
\gamma_{\mathrm{WLP}} &= \mathrm{E}\left\{r_{\mathrm{WLP}}\right\} \\
&= \mathrm{E}\left\{\left(\sum_{b=1}^{B} \|\mathbf{H}_b\|\right)^2\right\} \gamma \\
&= \mathrm{E}\left\{\sum_{b=1}^{B} \|\mathbf{H}_b\|^2 + \sum_{m,n=1,\, m\neq n}^{B} \|\mathbf{H}_m\| \, \|\mathbf{H}_n\|\right\} \gamma \\
&\overset{(a)}{=} \left[B \mathrm{E}\left\{\|\mathbf{H}_b\|^2\right\} + B\left(B-1\right) \mathrm{E}^2\left\{\|\mathbf{H}_b\|\right\}\right] \gamma \\
&\overset{(b)}{=} B N_{\mathrm{T}} \gamma + B\left(B-1\right) \left(\frac{\Gamma\left(N_{\mathrm{T}} + 1/2\right)}{\Gamma\left(N_{\mathrm{T}}\right)}\right)^2 \gamma,
\end{aligned} \tag{5.64}$$

where Equation (a) holds because $\mathbf{H}_b$'s are i.i.d. vectors and Equation (b) is true because according to (Proakis 2001), we have (5.59) and

$$\mathrm{E}\left\{\|\mathbf{H}_b\|\right\} = \left(\frac{\Gamma\left(N_{\mathrm{T}} + 1/2\right)}{\Gamma\left(N_{\mathrm{T}}\right)}\right). \tag{5.65}$$

The proof is concluded by comparing the Equation (b) of (5.64) with (5.60).

If we compare (5.60) with the average SINR of the LP scheme shown in (5.58), we can find that the second term of (5.60) measures the SINR increase resulted from the phase prerotation operation in the WLP scheme. However, (5.60) is an overly optimistic evaluation of the average SINR of the WLP scheme because ideal phase alignment cannot be achieved in practice due to the limited-bit feedback of $\{\bar{\theta}_b\}$. In order to get a more realistic evaluation of the WLP scheme, we consider a quantization codebook for $\{\bar{\theta}_b\}$ and obtain Theorem 5.2 as follows.

Theorem 5.2. *The average SINR of the WLP scheme with limited-bit feedback of $\{\bar{\theta}_b\}$ when $N_{\mathrm{R}} = 1$ can be expressed as*

$$\gamma_{\mathrm{WLP}}^{\mathrm{q}} = BN_{\mathrm{T}}\gamma + B(B-1)\left(\frac{\Gamma(N_{\mathrm{T}}+1/2)}{\Gamma(N_{\mathrm{T}})}\right)^2\left(\frac{2^n}{\pi}\sin\frac{\pi}{2^n}\right)^2\gamma, \tag{5.66}$$

where n is the number of bits for feedback of the prerotation phase and the corresponding phase codebook equally divides a unit circle into 2^n segmentations.

Proof. Suppose that Υ is an n-bit phase codebook containing 2^n elements, which divide a unit circle into equal segmentations, then Υ is represented by

$$\Upsilon : \omega_i = \frac{2\pi i}{2^n}, \quad i \in \{0, 1, \ldots, 2^n - 1\}. \tag{5.67}$$

The quantized version of $\bar{\theta}_b$ is chosen as the ω_i with the minimum distance to $-\varphi_b$, which is formulated as

$$\bar{\theta}_b^{\mathrm{q}} = \arg\min_{\omega_i \in \Upsilon}\{|\omega_i - (-\varphi_b)|\}. \tag{5.68}$$

Thus, we recalculate the SINR of the WLP scheme in (5.63) as

$$\begin{aligned}
r_{\mathrm{WLP}}^{\mathrm{q}} &= \frac{\mathbf{H}_{\mathrm{eq}}^{\mathrm{WLP}}\left(\mathbf{H}_{\mathrm{eq}}^{\mathrm{WLP}}\right)^{\mathrm{H}}}{N_0} \\
&= \frac{\sum\limits_{b=1}^{B}\mathbf{H}_b\exp\left(\mathrm{j}\bar{\theta}_b^{\mathrm{q}}\right)\bar{\mathbf{W}}_b\left(\sum\limits_{b=1}^{B}\mathbf{H}_b\exp\left(\mathrm{j}\bar{\theta}_b^{\mathrm{q}}\right)\bar{\mathbf{W}}_b\right)^{\mathrm{H}}}{N_0} \\
&= \sum_{b=1}^{B}\|\mathbf{H}_b\|\exp\left(\mathrm{j}\bar{\theta}_b^{\mathrm{q}}+\mathrm{j}\varphi_b\right)\left(\sum_{b=1}^{B}\|\mathbf{H}_b\|\exp\left(\mathrm{j}\bar{\theta}_b^{\mathrm{q}}+\mathrm{j}\varphi_b\right)\right)^{\mathrm{H}}\gamma \\
&= \sum_{b=1}^{B}\|\mathbf{H}_b\|\exp\left(\mathrm{j}\zeta_b\right)\left(\sum_{b=1}^{B}\|\mathbf{H}_b\|\exp\left(\mathrm{j}\zeta_b\right)\right)^{\mathrm{H}}\gamma,
\end{aligned} \tag{5.69}$$

where $\zeta_b = \bar{\theta}_b^{\mathrm{q}} + \varphi_b$ is the residual error between $\bar{\theta}_b^{\mathrm{q}}$ and $-\varphi_b$. Here, ζ_b conforms to a uniform distribution over $[-\pi/2^n, \pi/2^n)$ because of the assumption on Υ. Therefore, the average SINR of the WLP scheme can be derived as

$$
\begin{aligned}
\gamma_{\mathrm{WLP}}^{\mathrm{q}} &= \mathrm{E}\left\{r_{\mathrm{WLP}}^{\mathrm{q}}\right\} \\
&= \mathrm{E}\left\{\sum_{b=1}^{B} \|\mathbf{H}_b\| \exp\left(\mathrm{j}\zeta_b\right) \left(\sum_{b=1}^{B} \|\mathbf{H}_b\| \exp\left(\mathrm{j}\zeta_b\right)\right)^{\mathrm{H}} \gamma\right\} \\
&= \mathrm{E}\left\{\sum_{b=1}^{B} \|\mathbf{H}_b\|^2 + \sum_{m,n=1,\ m\neq n}^{B} \|\mathbf{H}_m\| \, \|\mathbf{H}_n\| \exp\left(\mathrm{j}\zeta_m - \mathrm{j}\zeta_n\right)\right\} \times \gamma \\
&= \mathrm{E}\left\{\sum_{b=1}^{B} \|\mathbf{H}_b\|^2\right\} \gamma + \mathrm{E}\left\{\sum_{m,n=1,\ m\neq n}^{B} \|\mathbf{H}_m\| \, \|\mathbf{H}_n\| \cos\left(\zeta_m - \zeta_n\right)\right\} \times \gamma \\
&= BN_{\mathrm{T}}\gamma + B(B-1)\mathrm{E}^2\left\{\|\mathbf{H}_b\|\right\} \mathrm{E}\left\{\cos\left(\zeta_m - \zeta_n\right)|_{m\neq n}\right\} \gamma \\
&= BN_{\mathrm{T}}\gamma + B(B-1)\mathrm{E}^2\left\{\|\mathbf{H}_b\|\right\} \times \left(\frac{2^n}{2\pi}\right)^2 \times \int_{-\frac{\pi}{2^n}}^{\frac{\pi}{2^n}} \int_{-\frac{\pi}{2^n}}^{\frac{\pi}{2^n}} \cos\left(\zeta_m - \zeta_n\right) d\zeta_m d\zeta_n \times \gamma \\
&= BN_{\mathrm{T}}\gamma + B\left(B-1\right) \left(\frac{\Gamma\left(N_{\mathrm{T}}+1/2\right)}{\Gamma\left(N_{\mathrm{T}}\right)}\right)^2 \left(\frac{2^n}{\pi} \sin \frac{\pi}{2^n}\right)^2 \gamma.
\end{aligned} \tag{5.70}
$$

The proof is thus concluded with (5.70).

It is interesting to note that from the comparison between (5.60) and (5.66), the phase quantization only affects the term of SINR increase by a factor of $\alpha = \left(\frac{2^n}{\pi} \sin \frac{\pi}{2^n}\right)^2$. When n approaches infinity, α will become one and $\gamma_{\mathrm{WLP}}^{\mathrm{q}}$ will converge to γ_{WLP} of the WLP scheme with ideal feedback of $\bar{\theta}_b$. On the other hand, when n equals zero, α will be zero and $\gamma_{\mathrm{WLP}}^{\mathrm{q}}$ will meet γ_{LP} in (5.58) because the WLP scheme degenerates to the LP scheme, where per-BS precoder only matches each local channel without the BS-specific phase rotation factor.

5.3.2.4 The Average SINR of the SFNP Scheme

Fourth, we investigate the SFNP scheme. According to (5.38), for a single-antenna UE, $\bar{\mathbf{W}}^{\mathrm{S}}$ can be written as

$$
\bar{\mathbf{W}}^{\mathrm{S}} = \sqrt{P} \frac{\left(\sum_{b=1}^{B} \mathbf{H}_b\right)^{\mathrm{H}}}{\left\|\sum_{b=1}^{B} \mathbf{H}_b\right\|} \times \exp\left(\mathrm{j}\varphi^{\mathrm{S}}\right), \tag{5.71}
$$

where φ^{S} is an irrelevant random phase misalignment distributed over $[-\pi, \pi)$. From (5.40), the SINR of the SFNP scheme can be derived as

$$
\begin{aligned}
r_{\mathrm{S}} &= \frac{\mathbf{H}_{\mathrm{eq}}^{\mathrm{S}}\left(\mathbf{H}_{\mathrm{eq}}^{\mathrm{S}}\right)^{\mathrm{H}}}{N_0} \\
&= \frac{\left(\sum\limits_{b=1}^{B} \mathbf{H}_b\right) \mathbf{W}^{\mathrm{S}} \left(\left(\sum\limits_{b=1}^{B} \mathbf{H}_b\right) \mathbf{W}^{\mathrm{S}}\right)^{\mathrm{H}}}{N_0} \\
&= \left\| \left(\sum_{b=1}^{B} \mathbf{H}_b\right) \right\|^2 \gamma.
\end{aligned} \tag{5.72}
$$

The PDF of $\left\|\left(\sum_{b=1}^{B} \mathbf{H}_b\right)\right\|^2$ follows $\chi^2\left(2N_{\mathrm{T}}, B/2\right)$ (Proakis 2001). Thus, the average SINR of the SFNP scheme can be simply calculated as

$$
\begin{aligned}
\gamma_{\mathrm{S}} &= \mathrm{E}\left\{r_{\mathrm{S}}\right\} \\
&= 2N_{\mathrm{T}} \times \frac{B}{2} \times \gamma \\
&= B N_{\mathrm{T}} \gamma.
\end{aligned} \tag{5.73}
$$

From (5.73) and (5.58), we can draw an interesting observation that the LP and SFNP schemes exhibit the same performance in terms of average SINR. That is because the LP and SFNP schemes are essentially similar types of noncoherent precoding methods. To be more specific, the LP scheme first matches the precoders to the local channels then sums the precoded signals, while the SFNP scheme first sums the local channels to form a composite channel then matches the SFN precoder to the said composite channel.

5.3.2.5 The Average SINR of the AS-SFNP Scheme

Finally, as for the proposed AS-SFNP scheme, since the closed-form expression of $\left\{\bar{\mathbf{A}}_b\right\}$ does not exist, we derive a lower bound of its average SINR for a single-antenna UE in the following theorem.

Theorem 5.3. *The average SINR of the AS-SFNP scheme when $N_{\mathrm{R}} = 1$ is lower bounded by*

$$
\gamma_{\text{A-S}} \geq \gamma_{\text{A-S}}^{\mathrm{LB}} = N_{\mathrm{T}} \left(\sum_{i=1}^{B} \sum_{m=1}^{B-i+1} \frac{1}{m} \right) \gamma. \tag{5.74}
$$

Proof. Consider a suboptimal AS scheme where the i-th transmit antenna of the AS-SFN equivalent channel is chosen based on the norm-maximization criterion from the antenna set consisting of all the i-th antennas of the candidate BSs. We denote the BS associated with the selected antenna as b_i. In order to derive an analytical lower bound, we suppose all the other antennas of BS b_i are eliminated from further selection process. Therefore, the selection process for the first $B-1$ antennas is described as

$$a_b(i) = \begin{cases} 1, \text{ if } b = \underset{b=\{1,2,\ldots,B\}/\{b_k|k=1,2,\ldots,i-1\}}{\arg\max} \{\|\mathbf{H}_b(i)\|\} \\ 0, \text{ otherwise.} \end{cases}, i \in \{1,2,\ldots,B-1\}, \tag{5.75}$$

where $\mathbf{H}_b(i)$ is the i-th element of $\mathbf{H}_b$. Without loss of generality, we assume $N_\mathrm{T} \geq B$. Then the last $N_\mathrm{T} - B + 1$ antennas to be selected can only be provided by the remaining BS b_B, that is,

$$a_{b_k}(i) = \begin{cases} 1 & \text{if } k = B \\ 0, & \text{otherwise.} \end{cases}, \quad i \in \{B, B+1, \ldots, N_\mathrm{T}\}. \tag{5.76}$$

Thus, according to (5.43), we have

$$q_{b_i} = \sqrt{N_\mathrm{T}}, (i < B), \tag{5.77}$$

and

$$q_{b_B} = \sqrt{N_\mathrm{T}/(N_\mathrm{T} - B + 1)}. \tag{5.78}$$

Similar to (5.71), when $N_\mathrm{R} = 1, \bar{\mathbf{W}}^{\text{A-S}}$ degenerates to

$$\bar{\mathbf{W}}^{\text{A-S}} = \sqrt{P} \frac{\left(\sum_{b=1}^{B} \mathbf{H}_b \bar{\mathbf{A}}_b^{\text{LB}} q_b\right)^\mathrm{H}}{\left\|\sum_{b=1}^{B} \mathbf{H}_b \bar{\mathbf{A}}_b^{\text{LB}} q_b\right\|} \times \exp\left(\mathrm{j}\varphi^{\text{A-S}}\right), \tag{5.79}$$

where $\bar{\mathbf{A}}_b^{\text{LB}}$ is the antenna selection matrix with its elements defined in (5.75) and (5.76). $\varphi^{\text{A-S}}$ is an irrelevant random phase misalignment distributed over $[-\pi, \pi)$. According to (5.50), the lower bound of the AS-SFNP scheme can be derived as

$$
\begin{aligned}
r_{\text{A-S}}^{\text{LB}} &= \frac{\mathbf{H}_{\text{eq}}^{\text{A-S}}\left(\mathbf{H}_{\text{eq}}^{\text{A-S}}\right)^{\text{H}}}{N_0} \\
&= \frac{\left(\sum_{b=1}^{B}\mathbf{H}_b\bar{\mathbf{A}}_b^{\text{LB}}q_b\right)\bar{\mathbf{W}}^{\text{A-S}}\left(\left(\sum_{b=1}^{B}\mathbf{H}_b\bar{\mathbf{A}}_b^{\text{LB}}q_b\right)\bar{\mathbf{W}}^{\text{A-S}}\right)^{\text{H}}}{N_0} \\
&= \left|\left(\sum_{b=1}^{B}\mathbf{H}_b\bar{\mathbf{A}}_b^{\text{LB}}q_b\right)\right|^2 B\gamma.
\end{aligned}
\tag{5.80}
$$

From (Jakes 1993), the PDF of $\left|\left(\sum_{b=1}^{B}\mathbf{H}_b\bar{\mathbf{A}}_b^{\text{LB}}q_b\right)_i\right|^2$, $(i < B)$ can be written as

$$
p(u) = (B - i + 1)\left(1 - e^{-u}\right)^{B-i}e^{-u},\ u \geq 0,
\tag{5.81}
$$

and hence, its mean value can be derived as

$$
\begin{aligned}
\mathrm{E}\left\{\left|\left(\sum_{b=1}^{B}\mathbf{H}_b\bar{\mathbf{A}}_b^{\text{LB}}q_b\right)_i\right|^2\right\} &= q_{b_i}^2\int_0^{+\infty}p(u)e^{-u}u\,\mathrm{d}u \\
&= N_{\text{T}}\sum_{m=1}^{B-i+1}\frac{1}{m}.
\end{aligned}
\tag{5.82}
$$

Moreover, we have

$$
\begin{aligned}
\sum_{i=B}^{N_{\text{T}}}\mathrm{E}\left\{\left|\left(\sum_{b=1}^{B}\mathbf{H}_b\bar{\mathbf{A}}_b^{\text{LB}}q_b\right)_i\right|^2\right\} &= \sum_{i=B}^{N_{\text{T}}}q_{b_B}^2 \\
&= q_{b_B}^2\left(N_{\text{T}} - B + 1\right) \\
&= N_{\text{T}}.
\end{aligned}
\tag{5.83}
$$

Therefore, combining (5.80), (5.82), and (5.83) yields (5.74), which concludes the proof.

5.4 Simulation and Analysis

In our simulations, we assume $B = 3$, $N_{\text{T}} = 4$, $N_{\text{R}} = 1$, 2 or 4. All channels are assumed to experience uncorrelated Rayleigh fading, and the entries of $\mathbf{H}_b$ are modeled as i.i.d. ZMCSCG random variables with unit covariance. The average

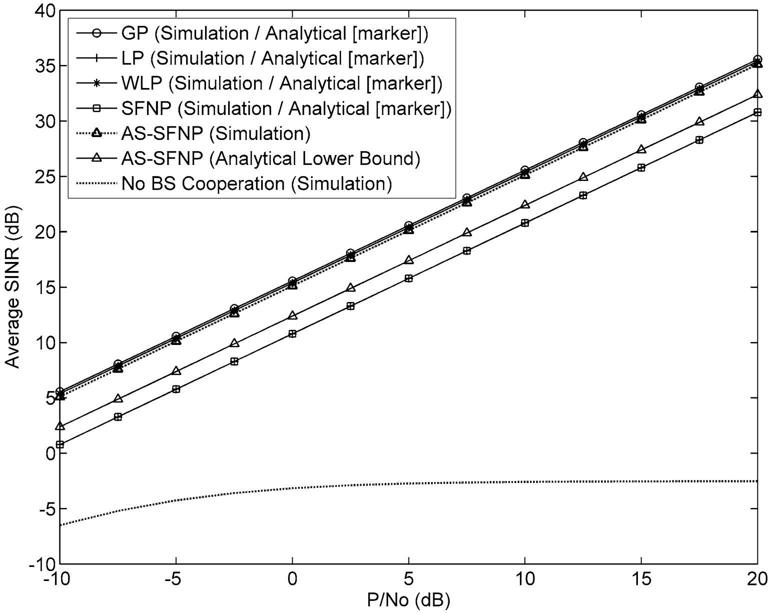

Fig. 5.6 Comparison of the average SINR of various JT precoding schemes for a single-antenna UE (full CSI)

SINR and capacity results are obtained from 10,000 independent random channel realizations.

First, in Fig. 5.6 we show the average SINR results for the GP, LP, WLP SFNP, and AS-SFNP schemes when $N_R = 1$ and full CSI is available at the cooperating BSs. As seen from Fig. 5.6, the simulation results perfectly agree with our analytical results, and the GP scheme achieves the best performance among all the interested schemes. Besides, as predicted by (5.58) and (5.73), the performance curve of the LP scheme coincides with that of the SFNP scheme, with performance gap toward the GP scheme being approximately 5 dB ($\log_{10} B \approx 4.8$ dB), which is caused by noncoherent signal combining so that the antenna array gain is lost. In addition, from (5.64) and (5.55), we can get the performance gap between the GP scheme and the WLP scheme expressed as

$$\log_{10}\left(\frac{\gamma_{\mathrm{GP}}}{\gamma_{\mathrm{WLP}}}\right) = \log_{10}\left(\frac{B^2 N_{\mathrm{T}}\gamma}{B N_{\mathrm{T}}\gamma + B(B-1)\left(\frac{\Gamma(N_{\mathrm{T}}+1/2)}{\Gamma(N_{\mathrm{T}})}\right)^2\gamma}\right)$$
$$= \log_{10}\left(\frac{B N_{\mathrm{T}}}{N_{\mathrm{T}} + (B-1)\left(\frac{\Gamma(N_{\mathrm{T}}+1/2)}{\Gamma(N_{\mathrm{T}})}\right)^2}\right). \tag{5.84}$$

Considering $B = 3$ and $N_{\mathrm{T}} = 4$ in our simulations, the result given by (5.84) is only about 0.179 dB. Thus, if full CSI is available, the WLP and GP schemes will exhibit similar performance in terms of average SINR for single-antenna UEs. Note that the case of limited-bit feedback of phase weights will be discussed in the sequel. Finally, the analytical lower bound of the proposed AS-SFNP scheme takes the place between the SFNP scheme and WLP scheme. However, the curve of the simulated AS-SFNP scheme is very close to that of the WLP scheme. Therefore, the AS-SFNP scheme is shown to be competitive in both performance and feedback overhead. It is worthy of noting that in Fig. 5.6 we also plot the performance of the baseline scheme with no BS cooperation. When γ is high, for example, 10 dB, the average SINR of the baseline scheme is only -3 dB. This is because for a UE without BS joint transmission, it will have one serving BS and two interfering BSs when $B = 3$, and hence, its average SINR can only go as far as $\log_2(1/2) \approx -3$ dB no matter how large γ is. Therefore, the advantage of JT among cooperating BSs has been made very clear in Fig. 5.6 that if JT is operated, then the average SINR will scale linearly with the per-BS SNR increase in dB scale, otherwise the system is severely interference-limited.

Second, in Fig. 5.7 we investigate the average SINR for various precoding schemes when $N_{\mathrm{R}} = 1$, and quantized phase weights, for example, $n \in \{1, 2, 3\}$, are assumed for the WLP scheme. In order to focus on the WLP and AS-SFNP schemes, we drop the performance curves of the LP, SFNP, and baseline schemes in Fig. 5.7. The simulation results in Fig. 5.7 perfectly corroborate our analytical results in (5.70). Compared with Fig. 5.6, it can be observed that the WLP scheme exhibits near-optimal performance when $n = 3$. From (5.70) and (5.55), the performance gap between the GP scheme and the WLP scheme can be calculated as

$$\log_{10}\left(\frac{\gamma_{\mathrm{GP}}}{\gamma_{\mathrm{WLP}}^{\mathrm{q}}}\right) = \log_{10}\left(\frac{B^2 N_{\mathrm{T}}\gamma}{B N_{\mathrm{T}}\gamma + B(B-1)\left(\frac{\Gamma(N_{\mathrm{T}}+1/2)}{\Gamma(N_{\mathrm{T}})}\right)^2\left(\frac{2^n}{\pi}\sin\frac{\pi}{2^n}\right)^2\gamma}\right)$$
$$= \log_{10}\left(\frac{B N_{\mathrm{T}}}{N_{\mathrm{T}} + (B-1)\left(\frac{\Gamma(N_{\mathrm{T}}+1/2)}{\Gamma(N_{\mathrm{T}})}\right)^2\left(\frac{2^n}{\pi}\sin\frac{\pi}{2^n}\right)^2}\right). \tag{5.85}$$

When $B = 3$, $N_{\mathrm{T}} = 4$ and $n = 3$, (5.85) gives approximately 0.403 dB. Considering that the curve of the WLP scheme when $n = 3$ and that of the AS-SFNP scheme almost overlap, we can conclude that the performance of the AS-SFNP scheme is also only about 0.4 dB away from that of the GP scheme in terms of average SINR.

The feedback overhead of the WLP and AS-SFNP schemes in Fig. 5.7 needs to be carefully examined before we can draw the conclusion on which one of the two schemes is more efficient. In the AS-SFNP scheme, the UE needs to indicate

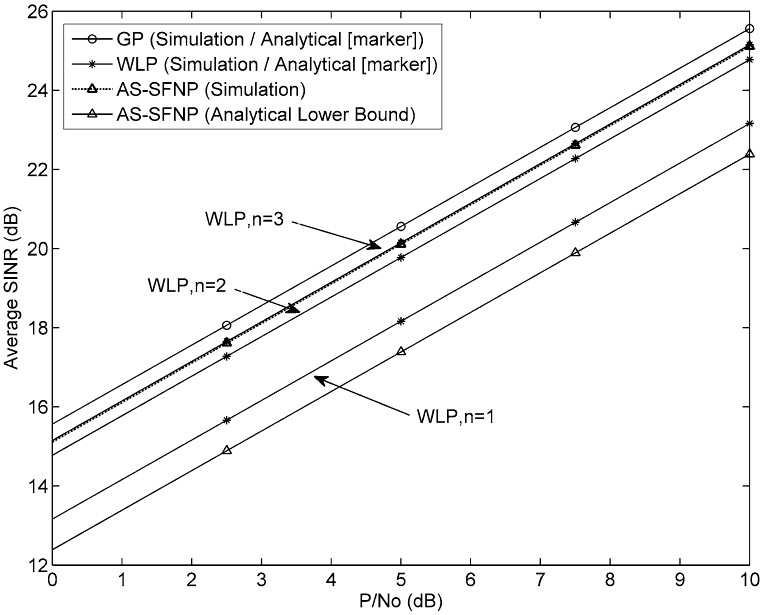

Fig. 5.7 Comparison of the average SINR of various JT precoding schemes for a single-antenna UE (quantized phase in the WLP scheme)

the on-off status of $BN_{\mathrm{T}} = 12$ antennas; thus, a total feedback load of 12 bits is required. As for the WLP scheme when $n = 3$, the number of feedback bits for the phase weights is $(B - 1)n = 6$. The reason why the overhead bits are not $Bn = 9$ is because that the phase weights measure the relative phases between the cooperating BSs, and hence, the default phase weight of the first BS can be set to 1 and doesn't need to be fed back. The feedback overhead comparison has more aspects to cover since for practical systems the precoder(s) should also be reported. Besides the phase weights, the WLP scheme requires the quantized CSI of $B = 3$ local precoders, while the AS-SFNP scheme needs only one SFN precoder. To sum up, the total feedback overhead bits of the WLP and AS-SFNP schemes are, respectively, $((B - 1)n + Bd)$ and $(BN_{\mathrm{T}} + d)$, where d is the number of the quantization bits for each local precoder. Therefore, if d satisfies

$$d > \left(\frac{B}{B-1}\right) N_{\mathrm{T}} - n, \tag{5.86}$$

then the feedback overhead of the WLP scheme will be larger than that of the AS-SFNP scheme. It should be noted that (5.86) holds for the LTE system since $d = 4$ for $N_{\mathrm{T}} = 4$ (3GPP 2010), and we have assumed $B = 3, n = 3$.

Third, in Fig. 5.8 we present the ergodic capacity results for the interested schemes in the multi-antenna UE case when $N_{\mathrm{R}} = 4$ and $L = 4$. For the WLP

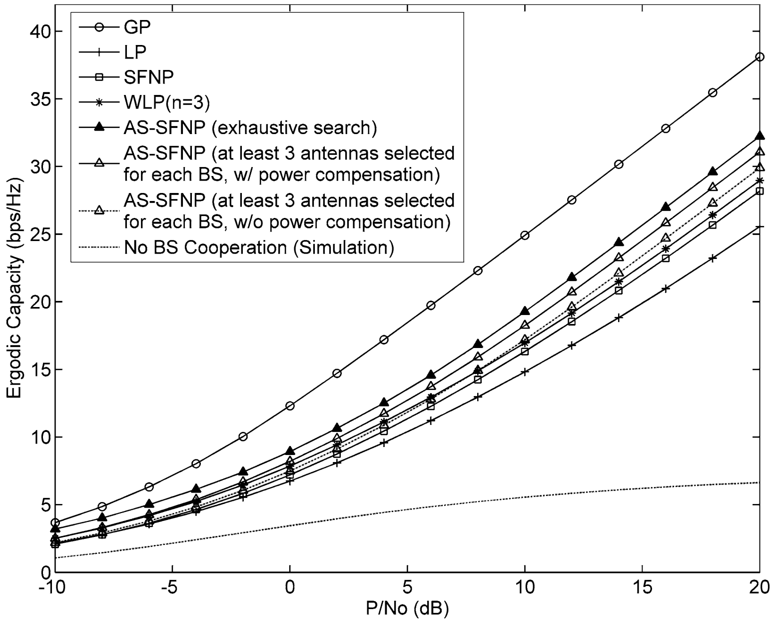

Fig. 5.8 Comparison of the ergodic capacity of various JT precoding schemes for a multi-antenna UE (quantized phase in the WLP scheme and constrained AS in the AS-SFNP scheme)

scheme, n is set to 3. In the baseline scheme, the SINR of each data stream will be limited by about -3 dB as has been explained earlier, and hence, its high-SNR capacity reaches the ceiling of $B \times L \times \log_2(1 + 1/2) \approx 7$ bps/Hz, which can be easily observed from Fig. 5.8. As for the other precoding schemes, in high-SNR regime, the capacity grows linearly with the per-BS SNR in dB. As can be seen from Fig. 5.8, when the SNR is larger than 10 dB, the capacity of the SFNP scheme is approximately 2.5 bps/Hz higher than that of the LP scheme, indicating the importance of the precoding operation for the composite channel. Also in high-SNR regime, the capacity of the WLP scheme is about 3 bps/Hz higher than that of the LP scheme, while the proposed AS-SFNP scheme with full complexity further offers 3 bps/Hz gain over the WLP scheme, which shows considerable advantage of the AS-SFNP scheme in the multi-antenna UE case.

Moreover, in order to decrease the complexity of the AS-SFNP scheme, we add a practical constraint that at least three antennas should be activated from each BS, so the number of possible AS combinations is reduced to $(5)^3 = 125$, which can be represented by 7 bits. Compared with the WLP scheme, the performance of the constrained AS-SFNP scheme still has gains of 2 and 1 bps/Hz for with and without antenna power compensation, respectively, in high-SNR regime. Here, q_b is derived from (5.43) when antenna power compensation is operated; otherwise, $q_b = 1$. In low-SNR regime, the WLP scheme and the AS-constrained AS-SFNP scheme show comparable performance in terms of ergodic capacity. Note that the performance gap between the SFNP and LP schemes also diminishes when the SNR is small, for example, 0 dB. As for the feedback overhead, the number of feedback bits for the AS result (i.e., 7 bits) is similar to that for the phase weights (i.e., 6 bits) in the WLP scheme. Hence, the proposed AS-SFNP scheme can reduce the total overhead by two precoding matrices compared with the WLP scheme.

Fourth, for practical systems, UEs served by JT are usually cell-edge UEs with low SNR due to background interference. Besides, unlike in the previous simulations, precoders should also be quantized to codewords searched from a predefined codebook. Therefore, system-level simulation based on a practical cellular network, for example, the LTE network, should be conducted to compare various JT precoding schemes for a complete performance analysis. The basic principles and methodology of a system-level simulation can be found in Sect. 4.4.1. In our simulation, performance is evaluated in terms of cell-edge spectral efficiency for the SFNP, AS-SFNP, LP, WLP, and GP schemes, as well as the baseline scheme without BS cooperation.

The precoding codebook for the interested schemes is the LTE Release 8 codebook for 4 transmit antennas with 16 codewords (3GPP 2011a). Note that the codebook for the GP scheme is constructed by concatenating multiple LTE Release 8 codebooks. To be more specific, we consider a 3-BS JT in our simulation, with each BS equipped with 4 transmit antennas; thus, we can build a 12-antenna precoding codebook for the GP scheme by concatenating three 4-antenna precoding codebooks. We can expect that the codebook-based GP scheme is of very high computational complexity, since the number of total entries in the 12-antenna global precoding codebook will be as large as $16^3 = 4{,}096$ considering 16 codewords in each 4-antenna precoding codebook, which incurs significant complexity for the UE to find the optimal quantized precoders.

Moreover, in our simulation, we only focused on the cell-edge UEs with potential JT operations. These UEs are chosen as the worst 10-percentile UEs based on path loss measurement, the path loss threshold of which is found empirically from 10,000 UEs generated uniformly in a cell. The cell-edge throughput is obtained from the 50-percent point of the JT throughput, corresponding to the throughput of the 5-percentile cell-edge UE. The detailed simulation parameters are described in Table 5.2, followed by some further explanations:

1. Cellular model and layout: The infrastructure of the considered cellular network is illustrated in Fig. 5.9, where the cells (sectors) are consecutively numbered. And the directional antennas of the sectors are represented by arrows. UEs dropped into each cell site are shown as colored dots with different colors for different sectors.
2. Cells employing JT: Only cells in the interior area of the simulation scenario are allowed to operate JT.
3. JT UE's position: As previously explained and shown in Fig. 5.9, cell-edge UEs are of interest here.
4. Non-JT UE's position: Non-JT UEs are dropped for modeling the realistic intercell interference.

Table 5.2 Parameters of the system-level simulation for various JT precoding schemes

No.	Parameter		Assumption
1	Cellular model and layout		Hexagonal grid, three cell sites, three sectors/cells per cell site (nine cells in total) See Fig. 5.9
2	Cells employing JT		Cells with identification number 1, 5, 9
3	JT UE's position		Cell-edge UEs defined as the worst 10-percentile UEs. See Fig. 5.9
4	Non-JT UE's position		Dropped uniformly in cells
5	Intercell interference modeling		Explicitly modeled for cells with identification number 2, 3, 4, 6, 7, 8
6	Number of JT UEs per cell		15
7	Inter-site distance		500 m
8	BS power class		46 dBm
9	Carrier frequency		2 GHz
10	System bandwidth		8.64 MHz
11	Size of a frequency sub-band		720 KHz
12	Distance-dependent path loss		$L = 128.1 + 37.6\log_{10}(d)$, (in dB), d in km
13	Shadowing standard deviation		8 dB
14	Correlation distance of shadowing		50 m
15	Shadowing correlation	Between cell sites	0.5
16		Between cells	1.0
17	Penetration loss		20 dB
18	Thermal noise density		−174 dBm/Hz
19	Channel model		SCME defined in 3GPP (2011b)
20	Antenna pattern		As in 3GPP (2010) shown below
21	Antenna pattern (horizontal) (for three-sector cell sites with fixed antenna patterns)		$A_H(\varphi) = -\min\left[12\left(\frac{\varphi}{\varphi_{3dB}}\right)^2, A_m\right]$ $\varphi_{3dB} = 70°$, $A_m = 25$ dB
22	Antenna pattern (vertical) (for three-sector cell sites with fixed antenna patterns)		$A_V(\theta) = -\min\left[12\left(\frac{\theta - \theta_{etilt}}{\theta_{3dB}}\right)^2, SLA_v\right]$ $\theta_{3dB} = 10°$, $SLA_v = 20$ dB $\theta_{etilt} = 15°$ Antenna height at the BS is set to 32 m Antenna height at the UE is set to 1.5 m
23	Combining as a 3D antenna pattern		$A(\varphi, \theta) = -\min\{-[A_H(\varphi) + A_V(\theta)], A_m\}$
24	Number of UE antennas		2
25	Number of BS antennas		4
26	Scheduler		Greedy search algorithm based on PF metric (see Sect. 4.3.2)
27	Scheduling granularity in frequency domain		Per frequency sub-band
28	Scheduling granularity in time domain		Per TTI (1 ms)

(continued)

Table 5.2 (continued)

No.	Parameter	Assumption
29	Multilayer transmission	Rank adaptive up to two layers
30	Link adaptation	MCSs based on LTE transport formats according to (3GPP 2011a, b)
31	Retransmission of the error packet	None
32	Traffic model	Full buffer (FB)
33	Quantization bits for phase in the WLP scheme	2 bits (uniform sampling of [0 2π])
34	AS constraint in the AS-SFNP scheme	At least three antennas at each BS should be selected, with power compensation. The corresponding feedback overhead is 7 bits

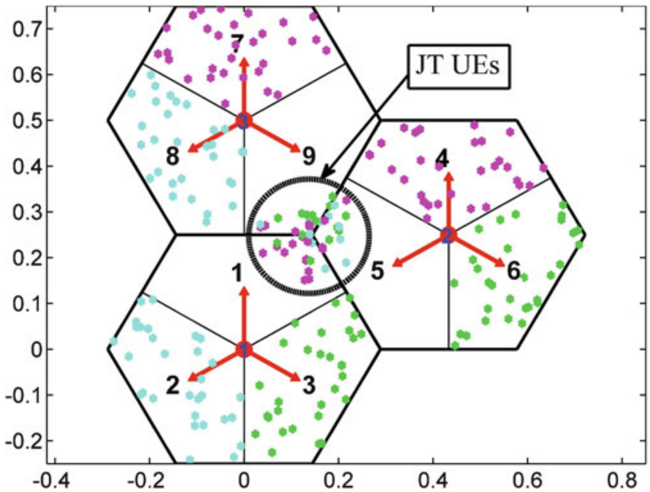

Fig. 5.9 Cellular layout in the system-level simulation for various JT precoding schemes

5. Intercell interference modeling: Except the cells with JT functions, other cells are just constructed for generating interference.
6. Number of JT UEs per cell: The number of JT UEs dropped into cell 1, 5, 9.
7. Inter-site distance: The distance between the center points of adjacent cell sites.
8. BS power class: The maximum transmit power of a BS.
9. Carrier frequency: The carrier frequency of the spectrum for transmission.
10. System bandwidth: The bandwidth of the spectrum for transmission.
11. Size of a frequency sub-band: The frequency granularity for CSI feedback and BS scheduling.
12. Distance-dependent path loss: The formula to model the large-scale channel fading.
13. Shadowing standard deviation: The shadowing value is usually assumed to follow the logarithmic normal distribution (3GPP 2010), the standard deviation of which is denoted as the shadowing standard deviation.

14. Correlation distance of shadowing: The shadowing values have a relatively strong correlation across some distance, which is measured by the correlation distance of shadowing.
15. Shadowing correlation—between cell sites: The correlation coefficient of a UE's shadowing values between cell sites. Due to the distributed deployment of cell sites, this correlation coefficient is relatively low.
16. Shadowing correlation—between cells: The correlation coefficient of a UE's shadowing values between cells. Due to the colocated deployment of cells, this correlation coefficient is relatively high.
17. Penetration loss: Any building which contains a significant thickness of concrete or amount of metal will attenuate the radio wave signal. The corresponding power loss due to penetration through walls and floors is represented by this parameter.
18. Thermal noise density: The power spectrum density of the thermal noise, which relates to the environment temperature.
19. Channel model: The model for fast-fading channels.
20. Antenna pattern: The radiation properties of transmit antennas.
21. Antenna pattern (horizontal): Antenna gain as a function of the horizontal part of the BS-UE angle.
22. Antenna pattern (vertical): Antenna gain as a function of the vertical part of the BS-UE angle.
23. Combining as a 3D antenna pattern: Combination of the horizontal and vertical antenna patterns.
24. Number of UE antennas: The number of receive antennas equipped at UE.
25. Number of BS antennas: The number of transmit antennas equipped at BS.
26. Scheduler: The scheduling algorithms performed by BS have been addressed in Sect. 4.3.2.
27. Scheduling granularity in frequency domain: The granularity of scheduled data transmission in frequency domain.
28. Scheduling granularity in time domain: The granularity of scheduled data transmission in time domain.
29. Multilayer transmission: Simulation of MIMO transmission for the JT UE.
30. Link adaptation: BS chooses an appropriate modulation and coding scheme from a set of candidate schemes (see Sect. 4.3.2.6).
31. Retransmission of the error packet: Treatment of the error packet in JT transmissions.
32. Traffic model: The model that describes how the UE's traffic is generated. The FB model assumes that the buffer for every UE's downlink transmission is fully loaded.
33. Quantization bits for phase in the WLP scheme: The quantization bits of per-BS phase information for the WLP scheme.
34. AS constraint in the AS-SFNP scheme: Constraint on the antenna selection of the AS-SFNP scheme.

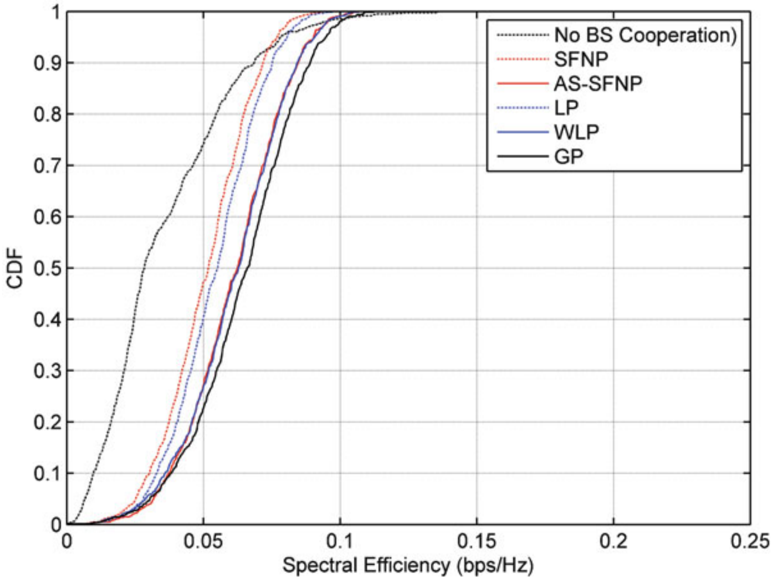

Fig. 5.10 Comparison of the spectral efficiency of various JT precoding schemes for a multi-antenna UE (practical system, full CDF)

Regarding the performance of spectral efficiency, the full CDF results for the interested JT precoding schemes are shown in Fig. 5.10. And the CDF segment containing the cell-edge UE throughput is magnified in Fig. 5.11 for observation purpose.

The detailed numerical results and the involved CSI feedback overhead are compared in Table 5.3.

From the simulation results, we can observe that by using a simple JT precoding scheme, for example, the SFNP or LP scheme, the spectral efficiency performance of cell-edge UEs can be improved by 83–95% compared with the baseline scheme with no BS cooperation. Note that the LP scheme performs relatively better in the practical system because the multiple local precoders pay off in the codebook-based precoding operation. Besides, the WLP and AS-SFNP schemes exhibit a similarly high performance gain around 121% compared with the baseline scheme. However, from Table 5.3 the AS-SFNP scheme requires five less bits of CSI feedback than the WLP scheme, which shows that the AS-SFNP scheme, constructing an effective composite channel with a maximized capacity before precoding, is more efficient than the WLP scheme that combats the interlayer interference using only one phase prerotation for each BS. Furthermore, it is worth noting that although the GP scheme achieves slightly better performance than the AS-SFNP scheme, it will significantly increase the complexity at the UE side.

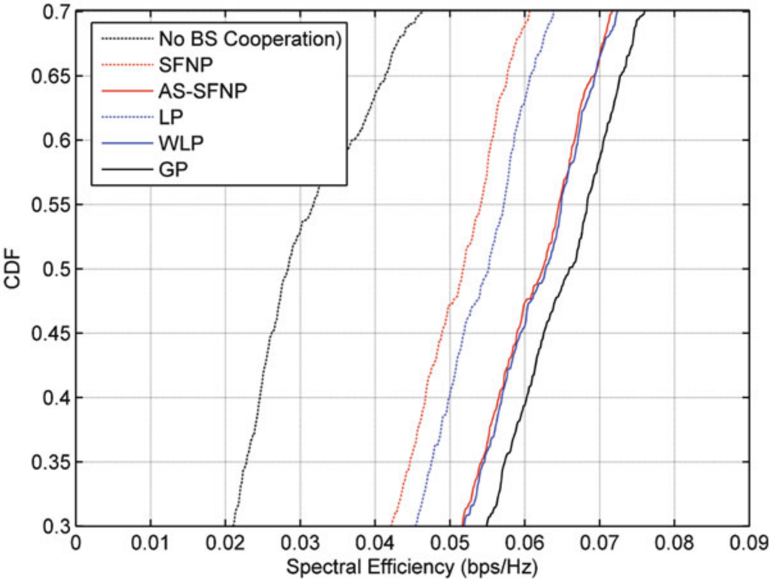

Fig. 5.11 Comparison of the spectral efficiency of various JT precoding schemes for a multi-antenna UE (practical system, CDF segment 0.3 ∼ 0.7)

Table 5.3 Comparison of various linear precoding schemes for multi-BS JT

Scheme	Spectral efficiency of the cell-edge UE (bps/Hz/cell/user)	Gain (%)	Feedback overhead
No BS cooperation	0.0283	–	4 bits for one precoder
SFNP	0.0517	82.7	4 bits for one precoder
AS-SFNP (AS constrained)	0.0624	120.5	4 bits for one SFN precoder + 7 bits for the AS indicator (ASI)
LP	0.0551	94.7	12 bits for three precoders
WLP	0.0628	121.9	12 bits for three precoders + 4 bits for two phase weights
GP	0.0660	133.2	12 bits for three precoders

5.5 Conclusion

In this chapter, we discuss various precoding schemes for JT with ideal backhaul communications among BSs. Based on the discussion, we propose a precoding scheme, which is a combination of antenna selection and single-frequency network precoding. The novelty of the proposed AS-SFNP scheme is that transmit antenna selection is applied to improve the capacity of the composite SFN channel and then the SFNP operation is invoked. Theoretical analysis and simulation results show that in the case of single-antenna UEs, the proposed scheme and the WLP scheme can achieve similarly optimal SINR performance compared with the GP scheme. Furthermore, when considering the case of multi-antenna UEs and more practical scenarios, simulation results show that even if constrained search space is posed on the antenna selection process and the beneficial operation of antenna power compensation is removed, the proposed AS-SFNP scheme still can achieve higher system capacity than those of the LP, WLP, and SFNP schemes. Finally, from a system-level simulation of a practical network, the proposed AS-SFNP scheme is shown to achieve a beneficial balance among the factors of performance, complexity, and feedback overhead, compared with the computationally demanding GP scheme and the feedback-bit consuming WLP scheme.

References

3GPP (2010) TR 36.814: Further advancements for E-UTRA physical layer aspects (V9.0.0). Accessed 2010

3GPP (2011a) TS 36.213 V10.1.0: Physical layer procedures (Release 10). http://www.3gpp.org/ftp/Specs/archive/36_series/36.213/36213-a10.zip. Accessed March 2011

3GPP (2011b) TR 25.996 V10.0.0: Spatial channel model for multiple input multiple output (MIMO) simulations (Release 10). http://www.3gpp.org/ftp/Specs/archive/25_series/25.996/25996-a00.zip. Accessed March 2011

Chae CB, Kim S, Heath RW (2009) Network coordinated beamforming for cell-boundary users: linear and nonlinear approaches. In: IEEE selected topics in signal process, pp 1094–1105

Costa M (1983) Writing on dirty paper. IEEE Trans Inf Theory 29(3):439–441

Dahrouj H, Yu W (2010) Coordinated beamforming for the multicell multi-antenna wireless system. IEEE Trans Wirel Commun 9(5):1748–1759

Ding M, Choudhury S, Khoshnevis A, Nogami T, Shimezawa K (2010) AS-SFN precoding scheme for DL CoMP. In: IEICE Society conference, September, 2010

ETRI (2009) Per-cell precoding methods for downlink joint processing CoMP. In: 3GPP, R1-090882. Accessed 2009

Gesbert D, Hanly S, Huang H, Shamai S, Simeone O, Wei Y (2010) Multi-cell MIMO cooperative networks: a new look at interference. IEEE J Sel Areas Commun 28(9):1380–1408

Golub GH, Loan CFV (1996) Matrix computations. The Johns Hopkins University Press, Baltimore

Grant M, Boyd S, Ye Y (2007) CVX user's guide for cvx version 1.1 (build 565). Accessed November 2007

Huang Y, Palomar DP (2010) Rank-constrained separable semidefinite programming with applications to optimal beamforming. IEEE Trans Signal Process 58(2):664–678

Jakes WC (1993) Microwave mobile communications. IEEE Press, New York, Accessed 1993

Jindal N, Vishwanath S, Goldsmith A (2004) On the duality of Gaussian multiple-access and broadcast channels. IEEE Trans Inf Theory 50(5):768–783

Peel CB, Hochwald B, Swindlehurst AL (2005) A vector perturbation technique for near capacity multi-antenna multi-user communication–Part I: Channel inversion and regularization. IEEE Trans Commun 53(1):195–202

Proakis JG (2001) Digital communication. Mc-Graw Hill Press, New York

Shamai S, Zaidel B (2001) Enhancing the cellular downlink capacity via co-processing at the transmitting end. IEEE Veh Technol Conf 3:1745–1749

Skillermark P, Almgren M, Astely D, Lundevall M, Olsson M (2008) Simplified interference modeling in multi-cell multi-antenna radio network simulations. IEEE Veh Technol Conf (VTC) 2008:1886–1890

TI (2008) Aspects of cooperative MIMO for advanced E-UTRA. In: 3GPP, R1-084444. Accessed 2008

Tse D, Viswanath P (2005) Fundamentals of wireless communication. Cambridge University Press, Cambridge

Venturino L, Prasad N, Wang X (2010) Coordinated linear beamforming in downlink multi-cell wireless networks. IEEE Trans Wirel Commun 9(4):1451–1461

Yu W, Lan T (2007) Transmitter optimization for the multi-antenna downlink with per-antenna power constraints. IEEE Trans Signal Process 55(6):2646–2660

Zhang J, Chen R, Andrews J, Ghosh A, Heath RW (2009) Networked MIMO with clustered linear precoding. IEEE Trans Wirel Commun 8(4):1910–1921

Chapter 6
The Eighth Category: Sequential and Incremental Precoding with Nonideal Backhaul

Abstract For the eighth category of multipoint cooperative communication technology, we discuss the sequential and incremental precoding scheme with nonideal backhaul conditions for the downlink joint transmission (JT) network in this chapter. First, we address the system model of JT and describe the backhaul impairments. Second, we discuss the conventional autonomous global precoding (AGP) scheme, which may suffer from severe performance degradation in the event of partial JT and single-BS transmission (ST) resulted from imperfect backhaul communications. Third, we propose a sequential and incremental precoding (SIP) scheme to overcome the drawbacks of the existing schemes. The objective of our design is to minimize the maximum of the sub-stream mean square errors (MSE), which dominates the average bit error rate (BER) performance of the system. The key problem is first illustrated and solved with a two-BS JT system, and the results are then generalized to multi-BS JT systems. Simulations show that, under the practical backhaul link conditions, our scheme significantly outperforms the AGP scheme in terms of BER performance.

Keywords Joint transmission • Nonideal backhaul • Autonomous global precoding • Sequential and incremental precoding • MSE • BER

6.1 Introduction

In Chap. 5, we have addressed the joint precoding schemes with ideal backhaul communication among multiple transmission points. Now we move forward to treat the precoding design for the joint transmission (JT) with nonideal backhaul conditions, that is, transmission points connected with large latency and limited capacity links. Note that this topic also belongs to the eighth category of multipoint cooperative communication technology discussed in Sect. 2.7.8. In the downlink JT, it requires that the data intended for a user equipment (UE) should be simultaneously transmitted from multiple points in order to improve the received signal quality

M. Ding and H. Luo, *Multi-point Cooperative Communication Systems: Theory and Applications*, Signals and Communication Technology, DOI 10.1007/978-3-642-34949-2_6,

(3GPP 2010). The use of joint processing to reduce the co-channel interference and improve the power gain, channel rank/conditioning, and macro-diversity has been demonstrated in Zhang and Dai (2004). Furthermore, the authors of Somekh et al. (2009) investigated cooperative multipoint system as a means to mitigate co-channel interference and to exploit macro-diversity for the Wyner's model and its variations. Motivated by the recent developments in this area, the JT scheme has been identified in the LTE-A network (Samsung et al. 2010) as one of the key technologies to improve the cell-edge throughput (3GPP 2008a).

As have been discussed in Sect. 2.5, the theoretical capacity of JT with ideal assumptions can be obtained from analysis of a generalized MIMO broadcast channel (BC) (Weingarten et al. 2004) by using the dirty paper coding (DPC) technique (Costa 1983), which is computationally very complex. This has motivated research in linear precoding for JT, such as zero-forcing (ZF) precoders (Huh et al. 2009), which are much more easy-to-implement compared with the DPC technique. Moreover, when a UE is equipped with multiple antennas, the distributed transceiver design (Palomar and Jiang 2006), that is, designing the precoder with UE's receiver structure taken into account, should also be considered for JT. Another relevant issue regarding JT is the imperfect backhaul links (Marsch and Fettweis 2009). In practice, cooperating BSs are connected through imperfect links with finite capacity, unpredictable latency, and limited connectivity. For example, the latency of practical backhaul links such as the copper and wireless interface varies from several milliseconds to tens of milliseconds depending on technology/standard. Besides, when the backhaul communication is based on a generic IP network, the backhaul latency also depends on the number of routers between two cooperative BSs and the network topology, for example, star, ring, tree, and mesh. Furthermore, congestion in the routers causes an extra delay typically of several milliseconds (Orange and Telefónica 2011). It should be noted that limited capacity is another important backhaul issue (Zakhour and Gesbert 2011). Most of the current cellular backhaul networks are designed for handover functions, which are not suited for data exchange in large amount (3GPP 2009). Constraints from lower-capacity/higher-latency backhaul communication in coordinated multipoint (CoMP) operations were studied at the 3GPP LTE-A meetings (MCC Support 2011a, b). Due to the immature status of the study, remote radio head (RRH)-based centralized BS and fiber-based backhaul (Orange et al. 2011) were assumed for the JT as a starting point of the working order for the imperfect backhaul issue (Samsung 2010). Although the current centralized network structure and fiber-based backhaul will not pose serious problems for JT schemes, for future JT operations the impact of imperfect backhaul should be carefully investigated (Ericsson and ST-Ericsson 2011). Up to now, theoretical performance bounds for JT with unreliable backhaul links among the cooperating BSs are still unknown (Gesbert et al. 2010). Finally, it should also be noted that imperfect channel state information (CSI) fed back by the UE is a common assumption in practical frequency division duplex (FDD) systems such as the 3GPP LTE-A network, where the downlink CSI cannot be inferred from the uplink CSI. For imperfect CSI feedback in a practical system (see Sect. 2.6), implicit CSI feedback, that is, feedback of precoder recommendation by UEs

(3GPP 2010), is much more preferred than the explicit CSI feedback, that is, feedback of the channel matrix, due to feedback overhead considerations. In this chapter, we consider the implicit CSI feedback, which has been widely adopted by practical systems such as the 3GPP LTE-A network (3GPP 2010).

6.2 System Model and Existing Technologies

6.2.1 System Model

In this section, we address the system model and briefly discuss the backhaul impairments. We consider a multicell wireless network consisting of B adjacent BSs, where each BS is equipped with N_{T} antennas. The considered B BSs constitute a JT set. A cell-edge UE with N_{R} antennas is served by one serving BS, and the other $B-1$ BSs are helper BSs which adaptively provide service to the UE depending on the backhaul conditions. For JT operations, both the transmission data and CSI must be available at the BSs in the JT set before the transmission starts; otherwise the JT cannot be operated. We assume that UE's data will always arrive at the serving BS from higher-layer entities in a timely and error-free manner, then the serving BS shares the data with the helper BSs by means of imperfect backhaul communications. In practice, the candidates of helper BSs can be decided either by UE based on received reference signal strength of nearby BSs or by the serving BS based on wideband CSI reported by UE. The selection algorithm to decide the helper BSs can be found in Zhou et al. (2009) and Moon and Cho (2011). Here, we assume $B-1$ helper BSs have already been selected based on some existing BS selection algorithms. Moreover, in practical scenarios, values of B are relatively small, usually not larger than 4 (Samsung 2011).

6.2.1.1 The JT Networks with Two BSs

Our basic idea for optimizing the precoders for the B BSs in the JT set is to derive per-BS precoders one by one in a sequential and incremental manner. Hence, the most basic scenario is a JT network with only two BSs. A two-BS JT network ($B=2$) is shown in Fig. 6.1, which serves as an instructive example to formulate the key problem of our concern. An N_{R} -antenna cell-edge UE is associated with a serving $\mathrm{BS}_{1,}$ and the transmission is assisted by a helper BS_2. Note that the results from this model will later be extended to a more general model with multiple BSs in the JT set.

In Fig. 6.1, the baseband channel matrix between the b-th BS and the UE is denoted as $\mathbf{H}_b \in \mathbb{C}^{N_{\mathrm{R}}\times N_{\mathrm{T}}}$. The UE reports the precoder recommendation information either to each individual BS in the JT set or to the serving BS which in turn exchanges this information among helper BSs over backhaul links. Let

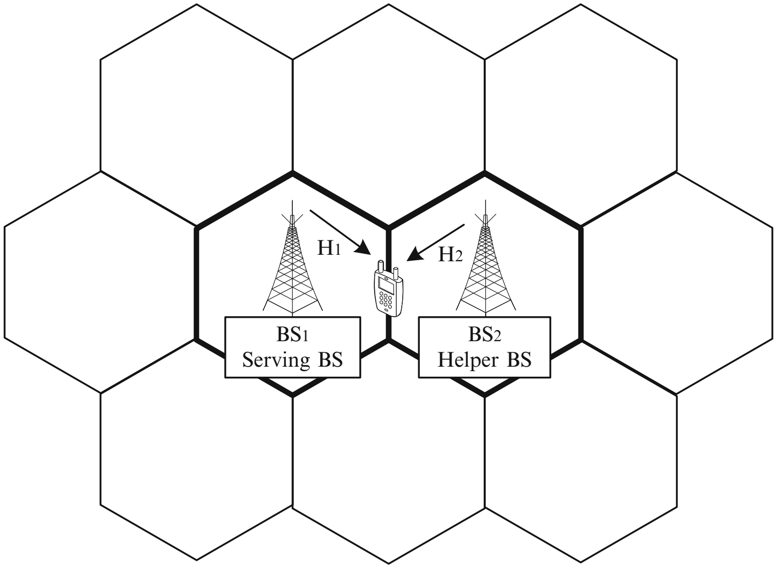

Fig. 6.1 Illustration of a two-BS JT network

$\mathbf{W}_b \in \mathbb{C}^{N_\mathrm{T}\times L}$ be the local precoding matrix of the b-th BS, where L is the number of independent data sub-streams for the UE. Then the signal received at the UE can be described by

$$\mathbf{y} = [\mathbf{H}_1, \mathbf{H}_2]\begin{bmatrix}\mathbf{W}_1\\ \mathbf{W}_2\end{bmatrix}\mathbf{x} + \mathbf{n}, \tag{6.1}$$

where $\mathbf{x} = [x_1, x_2, \ldots, x_\mathrm{L}]^\mathrm{T}$ is the transmission data vector with $\mathrm{E}\left\{\mathbf{x}\mathbf{x}^\mathrm{H}\right\} = \mathbf{R}_\mathrm{n}$ and $\mathbf{n}$ is the noise vector with $\mathrm{E}\left\{\mathbf{n}\mathbf{n}^\mathrm{H}\right\} = \mathbf{R}_\mathrm{n}$. Note that the interference from BSs outside of the interested JT set is incorporated into $\mathbf{n}$. Assume that the interference is white-colored (Skillermark et al. 2008), then $\mathbf{R}_\mathrm{n}$ can be simplified to

$$\mathbf{R}_\mathrm{n} = N_0\mathbf{I}_{N_\mathrm{R}}. \tag{6.2}$$

In addition, $\mathbf{W}_b$ is subjected to a per-BS power constraint shown as

$$\mathrm{tr}\left\{\mathbf{W}_b^\mathrm{H}\mathbf{W}_b\right\} \leq P, \tag{6.3}$$

where P is the maximum transmission power at each BS.

Suppose that a linear receiver $\mathbf{F} \in \mathbb{C}^{L\times N_\mathrm{R}}$ is employed at the UE to detect $\mathbf{x}$. Then the MSE of the i-th ($i \in \{1, 2, \ldots, L\}$) detected sub-stream can be represented by

$$M_i = \mathrm{E}\left\{|\mathbf{F}_{i,:}\mathbf{y} - x_i|^2\right\}. \tag{6.4}$$

In general, the average BER of the system is dominated by the sub-stream with the maximum MSE (Palomar et al. 2002). Therefore, we want to jointly design $\mathbf{W}_1$, $\mathbf{W}_2$, and $\mathbf{F}$ to minimize the maximum of the sub-stream MSEs. This min-max MSE problem is formulated as

$$\begin{aligned} \min_{\mathbf{F},\mathbf{W}_1,\mathbf{W}_2} \quad & \max\{M_i \,|\, i \in \{1, 2, \ldots, L\}\}, \\ \text{s.t.} \quad & \mathrm{tr}\left\{\mathbf{W}_b^{\mathrm{H}}\mathbf{W}_b\right\} \le P, \ \forall b = 1, 2. \end{aligned} \tag{6.5}$$

6.2.1.2 Modeling of Imperfect Backhaul

For full JT operations, the transmission data vector $\mathbf{x}$ and CSI need to be available at the actual transmission points before the transmission starts. Whether both the transmission data and CSI can arrive at a certain helper BS before the time that JT is scheduled to perform is a probabilistic event because of the nonideal backhaul conditions. If a helper BS fails to obtain both the transmission data and CSI in time, then it has to quit the upcoming JT operation. Thereby, whether a helper BS can participate in JT or not is also a probabilistic event.

Here, we are mainly concerned with the impact of BS backhaul latency on system performance. In practice, backhaul links can be generally classified into three categories according to the physical media, that is, optical fiber, copper (ADSL, ATM, VDSL, etc.), and wireless interface. The typical latency of optical fiber is below 1 ms, which can be neglected since the usual delay of channel state information (CSI) exchange and scheduling in cooperative MIMO systems is approximately 10 ms (Orange and Telefónica 2011). However, the latency of copper and wireless interface backhaul links varies from several milliseconds to tens milliseconds depending on technology/standard. Besides, when the backhaul communication is based on a generic IP network, the backhaul latency also depends on the number of routers between two cooperative BSs and the topology of the network, for example, star, ring, tree, and mesh. Furthermore, congestion in the routers causes an extra delay typically of several milliseconds (Orange and Telefónica 2011).

Figure 6.2 illustrates an example of a practical BS backhaul network, which combines the ring and tree topologies. If BS_1 wants to share data with BS_2, it has to set up a backhaul link over several routers. It should be noted that limited capacity is another important backhaul issue (Zakhour and Gesbert 2011). Most of the current cellular backhaul networks are designed for handover functions, which are not suited for data exchange in large amount (3GPP 2010). However, we assume capacity is adequate for backhaul communication throughout this chapter.

According to 3GPP (2008b), the maximum delay for normal backhaul links is around 20 ms and the typical average delay is expected to be within 10 ms. More

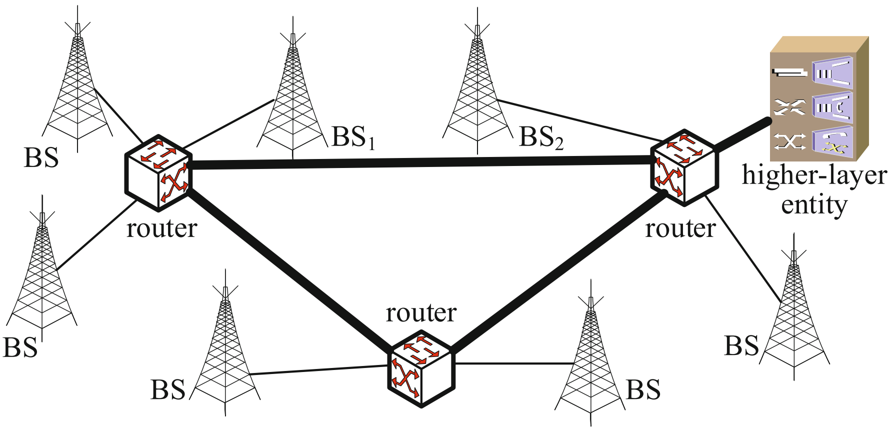

Fig. 6.2 Illustration of a realistic BS backhaul network

Fig. 6.3 Shifted gamma distribution of the backhaul delay

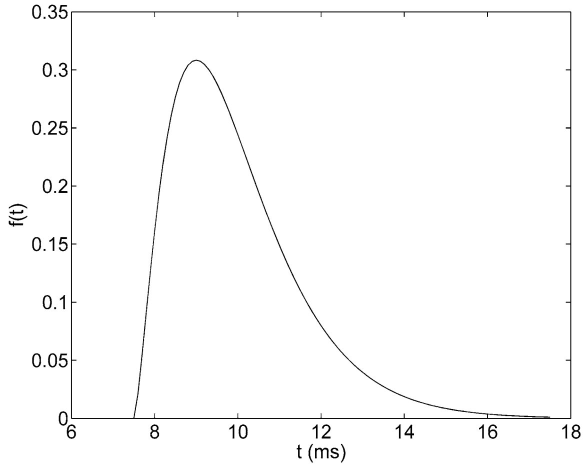

detailed description of the backhaul latency model can be found in IEEE WG 802.20 (2005). The backhaul delay conforms to a shifted gamma distribution (IEEE WG 802.20 2005), and its probability density function (PDF) can be represented by

$$f(t) = \frac{\left(\dfrac{t-t_0}{\alpha}\right)^{\beta-1} \exp\left(-\dfrac{t-t_0}{\alpha}\right)}{\alpha\,\Gamma(\beta)}, \tag{6.6}$$

where α, β and t_0 are the scale, shape and shift parameter, respectively, and $\Gamma(\cdot)$ denotes the gamma function. According to IEEE WG 802.20 (2005), the typical values are $\alpha = 1$, $\beta = 2.5$ and $t_0 = 7.5$ ms. The corresponding PDF curve is plotted in Fig. 6.3 for illustration purpose.

In every transmission slot, the b-th $b \in \{2, 3, \ldots, B\}$ helper BS joins JT with probability p_b, which is determined by the condition of the backhaul link between the serving BS and the b-th helper BS. In the following, p_b will be referred to as participation probability, which can be computed from (6.6). Suppose that the JT operation is scheduled to be performed at a critical time T after the serving cell pushes the UE's data into the backhaul network. Then p_b can be calculated as

$$p_b = \int_0^T f(t)\mathrm{d}t = \frac{\gamma\left(\beta, \frac{T-t_0}{\alpha}\right)}{\Gamma(\beta)}, \tag{6.7}$$

where $\gamma(\cdot,\cdot)$ is the lower incomplete gamma function (Gradshteyn and Ryzhik 2007). In practice, the parameter T will take a reasonably small value to avoid performance degradation caused by outdated CSI. For instance, if $T = 10$ ms, $p_b \approx 0.58$, and if $T = 11$ ms, $p_b \approx 0.78$. Furthermore, if congestion occurs in the routers, $f(t)$ will suffer from additional shift, that is, t_0 will take large values. For instance, let $t_0 = 8.5$ ms, then if $T = 10$ ms, $p_b \approx 0.3$, and if $T = 11$ ms, $p_b \approx 0.58$.

6.2.2 Existing Technologies

In this section, we discuss the advances and drawbacks of the existing schemes, where different aspects such as system performance, required CSI feedback, and limited backhaul connectivity are carefully examined.

6.2.2.1 The Global Precoding Scheme

The optimal precoding strategy for the full JT problem (6.5) is the global precoding (GP), that is, to view the distributed antenna ports from BSs in the JT set as a giant multiple-antenna system and generalize the well-studied point-to-point MIMO transmission strategies to JT across multiple BSs (Gesbert et al. 2010). However, the difficulty lies in how to maintain the distributed per-BS power constraints while extending the point-to-point MIMO schemes to JT MIMO ones. To our best knowledge, the min-max MSE problem is still an open problem for the linear precoding design for JT with distributed per-BS power constraints.

Hence, a sum power constraint is instead assumed for the GP to yield a lower bound for the MSE performance (Gesbert et al. 2010). To formulate GP, rewrite (6.1) as

$$\mathbf{y} = \mathbf{H}\mathbf{W}\mathbf{x} + \mathbf{n}, \tag{6.8}$$

where $\mathbf{H}$ and $\mathbf{W}$ denote the global channel matrix $[\mathbf{H}_1, \mathbf{H}_2]$ and global precoder $[\mathbf{W}_1^{\mathrm{T}}, \mathbf{W}_2^{\mathrm{T}}]^{\mathrm{T}}$, respectively. The min-max MSE problem for GP can be reformulated from (6.5) as

$$\begin{aligned} \min_{\mathbf{F},\mathbf{W}} \quad & \max\{\, M_i \,|\, i \in \{1, 2, \ldots, L\}\} \\ \text{s.t.} \quad & \operatorname{tr}\left\{\mathbf{W}^{\mathrm{H}}\mathbf{W}\right\} \leq 2P. \end{aligned} \tag{6.9}$$

Let $\mathbf{R_H} = \mathbf{H}^{\mathrm{H}}\mathbf{R}_{\mathrm{n}}^{-1}\mathbf{H}$ and its eigenvalue decomposition be

$$\mathbf{R_H} = \mathbf{V}\boldsymbol{\Lambda}\mathbf{V}^{\mathrm{H}}, \tag{6.10}$$

where $\mathbf{V} \in \mathbb{C}^{2N_{\mathrm{T}}\times 2N_{\mathrm{T}}}$ is a unitary matrix and $\boldsymbol{\Lambda} = \operatorname{diag}(\{\lambda_i\})$ is a semi-definite diagonal matrix, with diagonal entries λ_i s being the eigenvalues of $\mathbf{R_H}$. Then, the optimal solution for problem (6.9) is achieved by the joint linear transceiver design (Palomar et al. 2003). The optimal receiver should take the form of the Wiener filter (Tse and Viswanath 2005) shown as

$$\mathbf{F}^{\mathrm{opt}} = \mathbf{H}_{\mathrm{eq}}^{\mathrm{H}}\left(\mathbf{H}_{\mathrm{eq}}\mathbf{H}_{\mathrm{eq}}^{\mathrm{H}} + \mathbf{R}_{\mathrm{n}}\right)^{-1}, \tag{6.11}$$

where $\mathbf{H}_{\mathrm{eq}} = \mathbf{HW}$ denotes the equivalent channel. Note that the Wiener filter has been proved to be the optimum linear receiver in the sense that it minimizes each of the sub-stream MSEs (Palomar et al. 2003). And the optimal transmit precoding matrix $\mathbf{W}^{\mathrm{opt}}$ should be

$$\mathbf{W}^{\mathrm{opt}} = \tilde{\mathbf{W}}\mathbf{Q}^{\mathrm{H}} = \tilde{\mathbf{V}}\boldsymbol{\Sigma}\mathbf{Q}^{\mathrm{H}}, \tag{6.12}$$

where $\tilde{\mathbf{W}} = \tilde{\mathbf{V}}\boldsymbol{\Sigma}$ and the column of $\tilde{\mathbf{V}} \in \mathbb{C}^{2N_{\mathrm{T}}\times L}$ consists of the eigenvectors of $\mathbf{R_H}$ corresponding to the L largest eigenvalues in increasing order. $\boldsymbol{\Sigma} = \operatorname{diag}(\{\sigma_i\})$ is the power loading matrix, where σ_i s are tuned so that the sum MSE with respect to $\tilde{\mathbf{W}}$ is minimized. In Palomar et al. (2003), it is proved that the optimal σ_i s can be obtained by the famous water-filling power allocation (PA) (Tse and Viswanath 2005)

$$\sigma_i = \sqrt{\left(\mu^{-1/2}\lambda_i^{-1/2} - \lambda_i^{-1}\right)^{+}}, \tag{6.13}$$

where $\mu^{-1/2}$ is the water level chosen to satisfy the power constraint in (6.9) with equality.

After minimizing the sum MSE by $\tilde{\mathbf{W}}$, a rotation operation is applied on it. In (6.12), $\mathbf{Q} \in \mathbb{C}^{L\times L}$ is a unitary rotation matrix such that all sub-stream MSEs are equal. Thereby, the minimized sum MSE is equally divided for each sub-stream, leading to a minimized MSE $\hat{M}$ for the maximum of the sub-stream MSEs for the problem (6.9), which can be concisely expressed as (Palomar et al. 2003)

$$\begin{aligned}\hat{M} &= \max\{M_i\} \\ &= \frac{1}{L}\mathrm{tr}\left\{\left(\mathbf{I}_L + \left(\mathbf{W}^{\mathrm{opt}}\right)^{\mathrm{H}}\mathbf{R}_{\mathrm{H}}\mathbf{W}^{\mathrm{opt}}\right)^{-1}\right\}.\end{aligned} \tag{6.14}$$

Though the closed-form expression for $\mathbf{Q}$ does not exist, efficient algorithms to compute $\mathbf{Q}$ can be found in Viswanath and Anantharam (1999). Note that (6.14) is a lower-bound solution for the original problem (6.5) since inter-BS PA implied by (6.12) is usually not the feasible solutions of (6.5). Besides, other practical issues such as limited backhaul and feedback overhead also compromise the performance of GP.

6.2.2.2 The Autonomous Global Precoding Scheme

In practice, full JT, which is assumed by GP, is not always feasible due to backhaul limitations, such as overtime delay leading to incomplete or outdated data at the transmission points. Moreover, it is preferable for practical systems to have distributed schedulers due to considerations of low complexity and low cost, thereby some local scheduling constraints in helper BSs may also force them to temporarily leave the JT set and thus break the full JT operation. Hence, it is desirable to design a flexible JT scheme, in which the serving BS makes the JT scheduling decision and informs the helper BSs, then the helper BSs can adaptively join or quit the upcoming JT operation according to their instantaneous states. If all the helper BSs are temporarily unavailable for JT, the system should be able to fall back to single-BS transmission (ST) smoothly. But this gives rise to a feedback problem. The transmission assumption, based on which the recommended precoder is computed and fed back by the UE, may be inconsistent with the one when the transmission eventually takes place. Consequently, the previously feedback precoder mismatches the transmission channel, causing performance degradation. This problem is not uncommon, especially in 3GPP LTE-A systems (3GPP 2010). A straightforward solution to the above problem is to require the UE to feedback multiple precoder recommendations under different transmission assumptions. For example, in Fig. 6.1 the UE can feedback two precoders, one for JT and another for ST.

However, aside from the issue of necessary inter-BS signaling for switching between JT and ST precoders, additional feedback overhead incurred from multiple precoders will become very large, since the number of transmission assumptions can be as many as 2^{B-1}. To avoid increasing the feedback overhead, another approach would be to instruct the UE to feedback the global precoder $\mathbf{W}^{\mathrm{opt}}$ only. If any helper BSs are not ready for JT, they will mute themselves during the data transmission to keep the interference low, which is called dynamic point muting in the LTE-A system (3GPP 2011). We assume that each helper BS is unaware of the states of other helper BSs, and thus, they should stick to their respective subblock parts of$\mathbf{W}^{\mathrm{opt}}$. Such scheme is hereafter referred to as autonomous global precoding (AGP) and the corresponding precoder $\mathbf{W}^{\mathrm{opt}}$ for the b-th BS can be expressed as

$$\mathbf{W}_b = \begin{cases} \mathbf{0} & \text{(the } b\text{-th BS is absent from JT)} \\ \left[\mathbf{W}^{\text{opt T}}_{(b-1)N_\text{T}+1,:}, \ldots, \mathbf{W}^{\text{opt T}}_{bN_\text{T},:}\right]^\text{T} & \text{(otherwise).} \end{cases} \quad (6.15)$$

In (6.15), $\mathbf{W}_{i,:}$ denotes the i-th row $\mathbf{W}$; thus, $\left[\mathbf{W}^{\text{opt T}}_{(b-1)N_\text{T}+1,:}, \ldots, \mathbf{W}^{\text{opt T}}_{bN_\text{T},:}\right]^\text{T}$ represents the subblock part of $\mathbf{W}^{\text{opt}}$ spanning from the $((b-1)\,N_\text{T}+1)$-th row to the (bN_T)-th row of $\mathbf{W}^{\text{opt}}$.

6.2.2.3 Motivations of Improved Schemes

Since $\mathbf{W}^{\text{opt}}$ is optimized under the assumption of full JT, its subblock part shown in (6.15) may not match individual $\mathbf{H}_b$ very well, which may result in large performance degradation when the system falls back to ST or partial JT. Therefore, we want to propose a precoding scheme that is flexible and achieves satisfactory performance especially for partial JT. In the proposed scheme, we first optimize the precoder at the serving BS and then sequentially optimize the precoders of helper BSs in the JT set according to the descending order of their probabilities of participating in JT. The BS-wise sequential optimization process can improve the system performance when some helper BSs have to temporarily quit the JT operations because of poor instant backhaul conditions. Besides, the precoder of an additional BS is derived in an incremental way, that is, the sequentially optimized precoders of previous BSs are fixed; thus, the additional precoder plays an incremental part in the multi-BS JT operations. Because the BS precoders are generated sequentially and incrementally, our proposed scheme is referred to as the sequential and incremental precoding (SIP) scheme hereafter. Also, an iterative algorithm is designed to jointly optimize the sub-stream precoder and power allocation (PA) for each additional BS in the SIP scheme. To facilitate the optimization, we require that the participation probabilities be determined by the serving BS based on (6.7) and the descending order of the participation probabilities be notified to the UE before it derives the precoders.

There are several benefits offered by our scheme. First, it offers flexibility to the JT since the helper BSs can adaptively decide whether or not to join JT according to their own situation. Such JT scheme enables the network to adaptively switch among single-BS transmission (ST), partial JT, and full JT without inter-BS signaling. Here partial JT refers to the transmission from a subset of BSs within the JT set. Second, the related CSI feedback scheme can easily fit into the current 3GPP LTE-A per-BS feedback framework (3GPP 2010), that is, the feedback operation is performed on a per-BS basis, which facilitates the feedback design. Third, the complexity on the UE side to select a preferred precoder from a codebook is low. Instead of searching for the precoder through a large codebook as done in the conventional GP scheme, the precoder for each BS is obtained from a small per-BS based codebook.

In the following, we first investigate the SIP design for a two-BS JT network. The results are then extended to a multi-BS JT network.

6.3 Sequential and Incremental Precoding Scheme

6.3.1 Precoder Design for the Two-BS JT Network

We address the optimization problem (6.5) for the two-BS JT network introduced in Sect. 6.3.1. We decouple problem (6.5) into two sequential steps. In the first step, we optimize the precoder at the serving BS to ensure the service quality when the system falls back to ST. The problem can be formulated as

$$\begin{aligned} \min_{\mathbf{F},\mathbf{W}_1} \quad & \max\left\{ M_i \,|\, i \in \{1,2,\ldots,L\}\right\}, \\ \text{s.t.} \quad & \operatorname{tr}\left\{\mathbf{W}_1^{\mathrm{H}}\mathbf{W}_1\right\} \le P. \end{aligned} \tag{6.16}$$

Note that the above problem is essentially the same as the problem (6.9) except for the substitution of $\mathbf{W}$ with $\mathbf{W}_1$ and the maximum power. Therefore, the optimal solution for (6.16) can be readily obtained as

$$\mathbf{W}_1^{\mathrm{opt}} = \tilde{\mathbf{V}}_1 \boldsymbol{\Sigma}_1 \mathbf{Q}_1^{\mathrm{H}}, \tag{6.17}$$

where $\tilde{\mathbf{V}}_1$, $\boldsymbol{\Sigma}_1 = \operatorname{diag}(\{\sigma_{1,i}\})$ and $\mathbf{Q}_1$ are derived using the same method as their counterparts in (6.12) without subscripts.

In the second step, we proceed to optimize the performance of the two-BS JT with $\mathbf{W}_1$ fixed as $\mathbf{W}_1 = \mathbf{W}_1^{\mathrm{opt}}$. This problem can be formulated as

$$\begin{aligned} \min_{\mathbf{F},\mathbf{W}_2} \quad & \max\left\{ M_i \,|\, i \in \{1,2,\ldots,L\}\right\}, \\ \text{s.t.} \quad & \operatorname{tr}\left\{\mathbf{W}_2^{\mathrm{H}}\mathbf{W}_2\right\} \le P. \end{aligned} \tag{6.18}$$

Problem (6.18) can be considered as a conditional optimization problem for $\mathbf{W}_2$ with the previously derived $\mathbf{W}_1^{\mathrm{opt}}$ fixed. Direct optimization of problem (6.18) is not an easy task since the aforementioned approach of minimizing the sum MSE followed by unitary rotation for problems (6.9) and (6.16) cannot be applied here. Hence, we resort to an iterative method to minimize the max $\{M_i\}$.

Suppose that we have a precoding matrix $\mathbf{W}_2^{(n)}$ in the n-th iteration. Then the equivalent channel can be written as

$$\mathbf{H}_{\mathrm{eq}}^{(n)} = \mathbf{H}_1 \mathbf{W}_1^{\mathrm{opt}} + \mathbf{H}_2 \mathbf{W}_2^{(n)}. \tag{6.19}$$

Similar to (6.11), at UE side the Wiener filter is also employed in order to minimize the MSE, which is described as

$$\mathbf{F}^{\mathrm{opt},(n)} = \left(\mathbf{H}_{\mathrm{eq}}^{(n)}\right)^{\mathrm{H}} \left(\mathbf{H}_{\mathrm{eq}}^{(n)} \left(\mathbf{H}_{\mathrm{eq}}^{(n)}\right)^{\mathrm{H}} + \mathbf{R}_{\mathrm{n}}\right)^{-1}. \tag{6.20}$$

Then, the MSE of the i-th sub-stream can be written as

$$M_i^{(n)} = \mathrm{E}\left\{\left|\mathbf{F}^{\mathrm{opt},(n)}\left(\mathbf{H}_{\mathrm{eq}}^{(n)}\mathbf{x} + \mathbf{n}\right) - x_i\right|^2\right\}. \tag{6.21}$$

Denote the sub-stream index associated with the maximum sub-stream MSE as

$$j(n) = \arg\max_i \left\{M_i^{(n)}\right\}. \tag{6.22}$$

Next we update $\left(\mathbf{W}_2^{(n+1)}\right)_{:,j(n)}$ subject to a sub-stream power constraint $P_{2,j(n)}^{(n+1)}$ with fixed $\mathbf{F}^{\mathrm{opt},(n)}$ such that $M_{j(n)}^{(n+1)}$ is minimized. Denote $\mathbf{g} = \left(\mathbf{W}_2^{(n+1)}\right)_{:,j(n)}$ for convenience. Then the problem (6.18) can be formulated as

$$\begin{aligned} \min_{\mathbf{g}} \quad & M_{j(n)}^{(n+1)}, \\ \text{s.t.} \quad & \operatorname{tr}\left\{\mathbf{g}^{\mathrm{H}}\mathbf{g}\right\} \le P_{2,j(n)}^{(n+1)}, \end{aligned} \tag{6.23}$$

where $M_{j(n)}^{(n+1)}$ can be represented in detail as

$$\begin{aligned} M_{j(n)}^{(n+1)} =& \mathrm{E}\left\{\left|\mathbf{F}_{j(n),:}^{\mathrm{opt},(n)}\left(\left(\mathbf{H}_1\mathbf{W}_1^{\mathrm{opt}} + \mathbf{H}_2\mathbf{W}_2^{(n+1)}\right)\mathbf{x} + \mathbf{n}\right) - x_{j(n)}\right|^2\right\} \\ =& \sum_{i \ne j(n)} \left|\mathbf{F}_{j(n),:}^{\mathrm{opt},(n)}\left(\mathbf{H}_1\left(\mathbf{W}_1^{\mathrm{opt}}\right)_{:,i} + \mathbf{H}_2\left(\mathbf{W}_2^{(n+1)}\right)_{:,i}\right)\right|^2 \\ & + \left|\mathbf{F}_{j(n),:}^{\mathrm{opt},(n)}\left(\mathbf{H}_1\left(\mathbf{W}_1^{\mathrm{opt}}\right)_{:,j(n)} + \mathbf{H}_2\mathbf{g}\right)\right|^2 \\ & - 2\,\mathrm{Re}\left[\mathbf{F}_{j(n),:}^{\mathrm{opt},(n)}\left(\mathbf{H}_1\left(\mathbf{W}_1^{\mathrm{opt}}\right)_{:,j(n)} + \mathbf{H}_2\mathbf{g}\right)\right] \\ & + \mathbf{F}_{j(n),:}^{\mathrm{opt},(n)}\mathbf{R}_{\mathrm{n}}\left(\mathbf{F}_{j(n),:}^{\mathrm{opt},(n)}\right)^{\mathrm{H}} + N_0. \end{aligned} \tag{6.24}$$

We further fix $(\mathbf{W}_2^{(n+1)})_{:,i}$ for $(i \ne j)$. Omitting the irrelevant terms in (6.24) for simplicity, we get

$$\begin{aligned} \tilde{M}_{j(n)}^{(n+1)} =& \left|\mathbf{F}_{j(n),:}^{\mathrm{opt},(n)}\left(\mathbf{H}_1\left(\mathbf{W}_1^{\mathrm{opt}}\right)_{:,j(n)} + \mathbf{H}_2\mathbf{g}\right)\right|^2 \\ & - 2\,\mathrm{Re}\left[\mathbf{F}_{j(n),:}^{\mathrm{opt},(n)}\left(\mathbf{H}_1\left(\mathbf{W}_1^{\mathrm{opt}}\right)_{:,j(n)} + \mathbf{H}_2\mathbf{g}\right)\right]. \end{aligned} \tag{6.25}$$

Hence, problem (6.23) is equivalent to the following problem

$$\begin{aligned} \min_{\mathbf{g}} \quad & \tilde{M}_{j(n)}^{(n+1)}, \\ \text{s.t.} \quad & \operatorname{tr}\left\{\mathbf{g}^{\mathrm{H}}\mathbf{g}\right\} \leq P_{2,j(n)}^{(n+1)}. \end{aligned} \tag{6.26}$$

It is easy to verify that the problem (6.26) is convex. Thus, we can obtain the optimal $\mathbf{g}$ from the KKT conditions (Boyd and Vandenberghe 2004). The Lagrangian function of (6.26) is given by

$$L(\mathbf{g}, \eta) = \tilde{M}_{j(n)}^{(n+1)} + \eta\left(\operatorname{tr}\left\{\mathbf{g}^{\mathrm{H}}\mathbf{g}\right\} - P_{2,j(n)}^{(n+1)}\right), \tag{6.27}$$

where $\eta \geq 0$ is the Lagrangian multiplier. Taking its derivative with respect to $\mathbf{g}^*$, we have

$$\begin{aligned} \frac{\partial L}{\partial \mathbf{g}^*} = & \mathbf{H}_2^{\mathrm{H}}\left(\mathbf{F}_{j(n),:}^{\mathrm{opt},(n)}\right)^{\mathrm{H}}\mathbf{F}_{j(n),:}^{\mathrm{opt},(n)}\left(\mathbf{H}_1\left(\mathbf{W}_1^{\mathrm{opt}}\right)_{:,j} + \mathbf{H}_2\mathbf{g}\right) \\ & - \mathbf{H}_2^{\mathrm{H}}\left(\mathbf{F}_{j(n),:}^{\mathrm{opt},(n)}\right)^{\mathrm{H}} + \eta\mathbf{g}. \end{aligned} \tag{6.28}$$

The KKT conditions are as follows:

$$\frac{\partial L}{\partial \mathbf{g}^*} = 0, \tag{6.29}$$

$$\eta\left(\operatorname{tr}\left\{\mathbf{g}^{\mathrm{H}}\mathbf{g}\right\} - P_{2,j(n)}^{(n+1)}\right) = 0, \tag{6.30}$$

$$\operatorname{tr}\left\{\mathbf{g}^{\mathrm{H}}\mathbf{g}\right\} \leq P_{2,j(n)}^{(n+1)}. \tag{6.31}$$

From (6.29), (6.30), and (6.31), the closed-form expression for $\mathbf{g}$ can be derived as

$$\begin{aligned} \mathbf{g} = & \left(\mathbf{H}_2^{\mathrm{H}}\left(\mathbf{F}_{j(n),:}^{\mathrm{opt},(n)}\right)^{\mathrm{H}}\mathbf{F}_{j(n),:}^{\mathrm{opt},(n)}\mathbf{H}_2 + \eta\mathbf{I}\right)^{-1} \\ & \times\left(\mathbf{H}_2^{\mathrm{H}}\left(\mathbf{F}_{j(n),:}^{\mathrm{opt},(n)}\right)^{\mathrm{H}} - \mathbf{H}_2^{\mathrm{H}}\left(\mathbf{F}_{j(n),:}^{\mathrm{opt},(n)}\right)^{\mathrm{H}}\mathbf{F}_{j(n),:}^{\mathrm{opt},(n)}\mathbf{H}_1\left(\mathbf{W}_1^{\mathrm{opt}}\right)_{:,j(n)}\right), \end{aligned} \tag{6.32}$$

where η should be chosen such that (6.30) and (6.31) are satisfied.

The remaining problem is the power allocation (PA) strategy for $P_{2,j(n)}^{(n+1)}$. As shown by Palomar et al. (2003), the optimal solution for the min-max MSE problem (6.9) is achieved when the sub-stream MSEs are equal. Motivated by this result, we propose to transfer a small amount of power from the sub-stream with minimum MSE to that with maximum MSE in each iteration. In such way, the maximum MSE $M_{j(n)}^{(n)}$ in the n-th iteration will decrease to $M_{j(n)}^{(n+1)}$ due to the optimized precoding vector $\mathbf{g}$ together with additional power bonus received from the sub-stream with minimum MSE.

Let

$$k(n) = \arg\min_i \left\{ M_i^{(n)} \right\} ; \tag{6.33}$$

we update the PA as follows:

$$\begin{cases} P_{2,j(n)}^{(n+1)} = P_{2,j(n)}^{(n)} + \delta P_{2,k(n)}^{(n)} \\ P_{2,k(n)}^{(n+1)} = P_{2,k(n)}^{(n)} \times (1-\delta) \\ P_{2,i}^{(n+1)} = P_{2,i}^{(n)}, \qquad (\text{for } i \neq j(n), k(n)) , \end{cases} \tag{6.34}$$

where

$$P_{2,l}^{(n)} = \left| \left(\mathbf{W}_2^{(n)} \right)_{:,l} \right|^2, \quad (l = 1, 2, \ldots, L) , \tag{6.35}$$

and δ is the percentage of power transferred from the $k(n)$-th sub-stream to the $j(n)$-th sub-stream. Based on (6.32) and (6.34), $\mathbf{W}_2^{(n+1)}$ can be updated as

$$\begin{cases} \left(\mathbf{W}_2^{(n+1)} \right)_{:,j(n)} = \left\{ \mathbf{g} \,\middle|\, P_{2,j}^{(n+1)} = P_{2,j(n)}^{(n)} + \delta P_{2,k(n)}^{(n)} \right\} \\ \left(\mathbf{W}_2^{(n+1)} \right)_{:,k(n)} = \sqrt{1-\delta} \times \left(\mathbf{W}_2^{(n)} \right)_{:,k(n)} \\ \left(\mathbf{W}_2^{(n+1)} \right)_{:,i} = \left(\mathbf{W}_2^{(n)} \right)_{:,i}, \qquad (\text{for } i \neq j(n), k(n)) . \end{cases} \tag{6.36}$$

Note that the power allocation should be initialized such that $\sum_{l=0}^{L} P_{2,l}^{(1)} = P$ so that in the following iterations, the power constraint of $\mathbf{W}_2^{(n)}$ can always be satisfied. When the iterative algorithm converges, all sub-stream MSEs should be equal. Hence, the termination criterion can be established based on the difference between $M_{j(n)}^{(n)}$ and $M_{k(n)}^{(n)}$. The proposed precoding scheme will be referred to as the sequential and incremental precoding (SIP) scheme hereafter and is summarized in Table 6.1.

Table 6.1 The SIP scheme for two-BS JT

Step 1: Compute $\mathbf{W}_1^{\text{opt}}$ according to (6.17)
Step 2: Obtain $\mathbf{W}_2^{\text{opt}}$ using the following iterative algorithm:
1. Initialization
   Set $\mathbf{W}_2^{(1)} = \sqrt{\frac{P}{L}}\left[\mathbf{I}_L,\ \mathbf{0}_{L\times(N_\text{T}-L)}\right]^\text{T}$ and $n = 1$
2. Iteration
   Compute $\mathbf{H}_{\text{eq}}^{(n)}$ and $\mathbf{F}^{\text{opt},(n)}$ using (6.19) and (6.20), respectively
   Use (6.32) to compute $\mathbf{g}$ and (6.36) to get $\mathbf{W}_2^{(n+1)}$
3. Termination
   The algorithm terminates either when $M_{j(n)}^{(n)}$ and $M_{k(n)}^{(n)}$ converges, that is,
   $\frac{\left|M_{j(n)}^{(n)} - M_{k(n)}^{(n)}\right|}{M_{j(n)}^{(n)}} \leq \xi_\text{th}$ or when $n \geq N_\text{max}$, where ξ_th is a predefined threshold and N_max is the maximum iteration number
   Output $\mathbf{W}_2^{\text{opt}} = \mathbf{W}_2^{(n)}$
   Else, $n = n + 1$, and go to sub-step 2

6.3.2 Extension to the Multi-BS Scenario

In this subsection, we generalize our proposed SIP scheme to a multi-BS scenario, where $B > 2$. Without loss of generality, the $B - 1$ helper BSs are sorted by their participation probabilities in decreasing order as $p_2 \geq p_3 \geq \cdots \geq p_B \geq 0$. Then the corresponding precoders are sequentially and incrementally optimized with $\mathbf{W}_2$ first and $\mathbf{W}_B$ last based on step 2 of the proposed SIP scheme. To be more specific, $\mathbf{W}_b$ ($b \in \{2,3,\ldots,B\}$) is optimized with fixed $\mathbf{W}_i^{\text{opt}}$ ($i \in \{1, 2, \ldots, b-1\}$) previously obtained from the SIP scheme. In addition, the equivalent channel shown in (6.19) now should be computed as

$$\mathbf{H}_{\text{eq}}^{(n)} = \sum_{i=1}^{b-1} \mathbf{H}_i \mathbf{W}_i^{\text{opt}} + \mathbf{H}_b \mathbf{W}_b^{(n)}. \tag{6.37}$$

If helper BS b joins JT, its precoder will be $\mathbf{W}_b^{\text{opt}}$. Otherwise, it mutes its transmission.

To sum up, the proposed SIP scheme can be extended to be employed in a multi-BS JT scenario and is summarized in Table 6.2.

6.3.3 The SIP Scheme with Codebook-based Feedback

If a codebook, denoted as $\boldsymbol{\Omega}$, is employed as the set of precoder candidates, then UE can exhaustively search $\boldsymbol{\Omega}$, find the best precoder, and feedback its index to the BS using just a few bits. In practice, codebook-based feedback is commonly

Table 6.2 The SIP scheme for multi-BS JT

Step 1: Compute $\mathbf{W}_1^{\text{opt}}$ according to (6.17); set b = 2
Step 2: Obtain $\mathbf{W}_b^{\text{opt}}$ using the following iterative algorithm:
1. Initialization
Set $\mathbf{W}_b^{(1)} = \sqrt{\frac{P}{L}}\left[\mathbf{I}_L, \mathbf{0}_{L\times(N_\text{T}-L)}\right]^\text{T}$ and $n = 1$
2. Iteration
Compute $\mathbf{H}_{\text{eq}}^{(n)}$ and $\mathbf{F}^{\text{opt},(n)}$ using (6.37) and (6.20), respectively
Use (6.32) to compute $\mathbf{g}$ and (6.36) to get $\mathbf{W}_b^{(n+1)}$
3. Termination
The algorithm terminates either when $M_{j(n)}^{(n)}$ and $M_{k(n)}^{(n)}$ converges, that is, $\frac{\left\lvert M_{j(n)}^{(n)} - M_{k(n)}^{(n)}\right\rvert}{M_{j(n)}^{(n)}} \leq \xi_\text{th}$ or when $n \geq N_\text{max}$, where ξ_th is a predefined threshold and N_max is the maximum iteration number
Output $\mathbf{W}_b^{\text{opt}} = \mathbf{W}_b^{(n)}$
Else, $n = n + 1$, and go to sub-step 2
Step 3: If $b < B$, then $b = b + 1$, and go to step 2
Else, terminate the algorithm with $\mathbf{W}_b^{\text{opt}}$ $(b \in \{1, 2, \ldots, B\})$ as the per-BS precoders

used in FDD systems such as the LTE-A system (3GPP 2010) due to low overhead costs. Here, we pursue the philosophy of sequential and incremental precoding and propose the SIP scheme with codebook-based feedback.

For $\mathbf{W}_1$, the best precoder in the codebook $\boldsymbol{\Omega}$ can be written as

$$\mathbf{W}_1^{\text{opt,cb}} = \arg\min_{\mathbf{W}_1^{\text{cb}}\in\boldsymbol{\Omega}} \max\left\{M_i \mid i \in \{1, 2, \cdots, L\}\right\}, \tag{6.38}$$

where $M_i = \mathrm{E}\left\{\left\lvert \mathbf{F}_{i,:}^{\text{opt}}\left(\mathbf{H}_1\mathbf{W}_1^{\text{cb}}\mathbf{x} + \mathbf{n}\right) - x_i\right\rvert^2\right\}$.

For $\mathbf{W}_b$, we fix the previously optimized precoders and incrementally find the best precoder for $\mathbf{W}_b$ from

$$\mathbf{W}_b^{\text{opt,cb}} = \arg\min_{\mathbf{W}_b^{\text{cb}}\in\boldsymbol{\Omega}} \max\left\{M_i \mid i \in \{1, 2, \ldots, L\}\right\}, \tag{6.39}$$

where $M_i = \mathrm{E}\left\{\left\lvert \mathbf{F}_{i,:}^{\text{opt}}\left(\mathbf{H}_{\text{eq}}\mathbf{x} + \mathbf{n}\right) - x_i\right\rvert^2\right\}$ and $\mathbf{H}_{\text{eq}} = \sum_{i=1}^{b-1}\mathbf{H}_i\mathbf{W}_i^{\text{opt,cb}} + \mathbf{H}_b\mathbf{W}_b^{\text{cb}}$.

In the AGP scheme, the best precoder from the global codebook $\boldsymbol{\Omega}_{\text{GP}}$ can be represented as

$$\mathbf{W}^{\text{opt,cb}} = \arg\min_{\mathbf{W}^{\text{cb}}\in\boldsymbol{\Omega}_{\text{GP}}} \max\left\{M_i \mid i \in \{1, 2, \ldots, L\}\right\}, \tag{6.40}$$

where $M_i = \mathrm{E}\left\{\left|\mathbf{F}^{\mathrm{opt}}_{i,:}\left(\mathbf{HW}^{\mathrm{cb}}\mathbf{x}+\mathbf{n}\right)-x_i\right|^2\right\}$. Then the $\mathbf{W}^{\mathrm{opt,cb}}_b$ s of the AGP scheme can be readily obtained from (6.15) with $\mathbf{W}^{\mathrm{opt}}$ replaced by $\mathbf{W}^{\mathrm{opt,cb}}$.

Suppose that the cardinality of $\mathbf{\Omega}$ is 2^d, then for each BS d bits are needed to feedback $\mathbf{W}^{\mathrm{opt,cb}}_b$ from 2^d precoder candidates. In order to make a fair comparison between the SIP and AGP schemes, the cardinality of $\mathbf{\Omega}_{\mathrm{GP}}$ should be 2^{Bd}, that is, a total overhead of Bd bits is assumed for the feedback of precoders in both schemes.

6.3.4 Extension to the Multi-UE Scenario

In this subsection, we briefly discuss the further extension of the proposed SIP scheme to the multi-UE scenarios and more sophisticated evaluations using system-level simulations. When multiple UEs are involved, the Wiener filter in (6.20) can be replaced by a block diagonal matrix to reflect the factors that individual UE's receive processing capability is captured by the corresponding block matrix and no receive cooperation is assumed among different UEs. Then the precoders for multiple UEs can be derived using the proposed SIP scheme. However, the closed-form expression for $\mathbf{W}^{\mathrm{opt}}_1$ shown by (6.17) no longer exists. The algorithms for optimizing $\mathbf{W}^{\mathrm{opt}}_1$ with various objective functions can be found in Palomar et al. (2002), which needs further study.

6.4 Simulation and Analysis

In this section, we present simulation results to compare the maximum MSE and average BER performances of the proposed SIP scheme with those of the AGP scheme. We consider a practical setup where a single multi-antenna UE with $N_{\mathrm{R}} = 2$ or 4 is served by a multi-BS JT set with $B = 2$ or 3 and $N_{\mathrm{T}} = 4$. Suppose that the critical time $T = 11$ ms, and t_0 for BS_2 and BS_3 are set to $t_{0,2} = 7.5$ ms and $t_{0,3} = 8.5$ ms, respectively. As explained in Sect. 6.3.1, the corresponding participation probabilities for BS_2 and BS_3 can be calculated using (6.7), and we get $p_2 \approx 0.78$ and $p_3 \approx 0.58$. Note that the water-filling PA for the AGP and SIP schemes may lead to rank adaptation, that is, dropping sub-streams with poor channel gains. For fairness, rank adaptation should be forbidden in our simulations. Therefore, when $N_{\mathrm{R}} = 4$, we fix $L = 4$ to prevent rank adaptation and apply equal sub-stream PA to $\mathbf{W}_1$, that is, set $\sigma_{1,i} = P/L$ in (6.17), whereas the power transfer shown in (6.34) is applied for $\mathbf{W}_b$ s when $b \neq 1$. The water-filling PA is only engaged for $\mathbf{W}_1$ in the case of $N_{\mathrm{R}} = 2$, when rank adaptation rarely happens. At the UE side, we assume that the Wiener filter is always employed.

We define per-BS signal-to-interference-plus-noise ratio (SINR) by $SINR = P/N_0$. All channels are assumed to experience uncorrelated Rayleigh fading, and

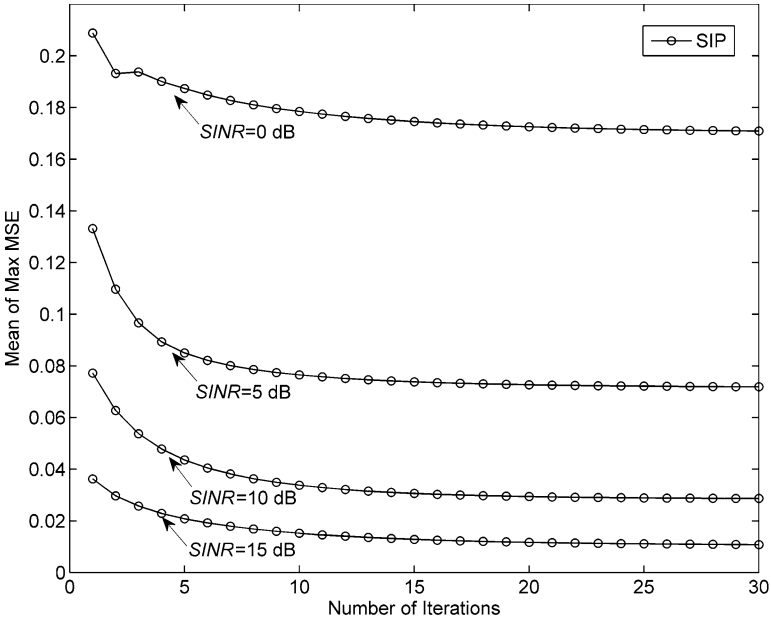

Fig. 6.4 Convergence of the SIP scheme for $B = 2$, $N_{\mathrm{R}} = 2$ (perfect feedback)

the entries of $\mathbf{H}_b$ are i.i.d. zero-mean circularly symmetric complex Gaussian (ZMCSCG) random variables with unit variance. The results are averaged over 10, 000 independent channel realizations. As for the BER results, 1,000,000 symbols obtained from the QPSK constellation are transmitted in each channel realization for each simulated SINR point. In addition, for the proposed SIP scheme, we set the convergence threshold $\xi_{\mathrm{th}} = 0.01$, power transfer percentage $\delta = 1\%$, and the maximum iteration number $N_{\max} = 100$.

6.4.1 Convergence of the SIP Scheme

Before discussing the numerical results of the system performance, we first investigate the convergence behavior of the proposed SIP scheme summarized in algorithm 1. Figures 6.4 and 6.5 show the mean of the maximum of sub-stream MSEs versus number of iterations for $B = 2$ and $N_{\mathrm{R}} = 2$ or 4 with different $SINR$. As seen from these two figures, the MSE always converges. When $N_{\mathrm{R}} = 2$, the MSE converges typically after 20 iterations, and more iterations are needed for the case of $N_{\mathrm{R}} = 4$. Moreover, the convergence of the SIP scheme for multi-BS JT is straightforward since the mathematical form of $\mathbf{H}_{\mathrm{eq}}^{(n)}$ in algorithm 2 is essentially the same as that in algorithm 1. Therefore, here we omit the illustration of algorithm convergence for the case of $B = 3$.

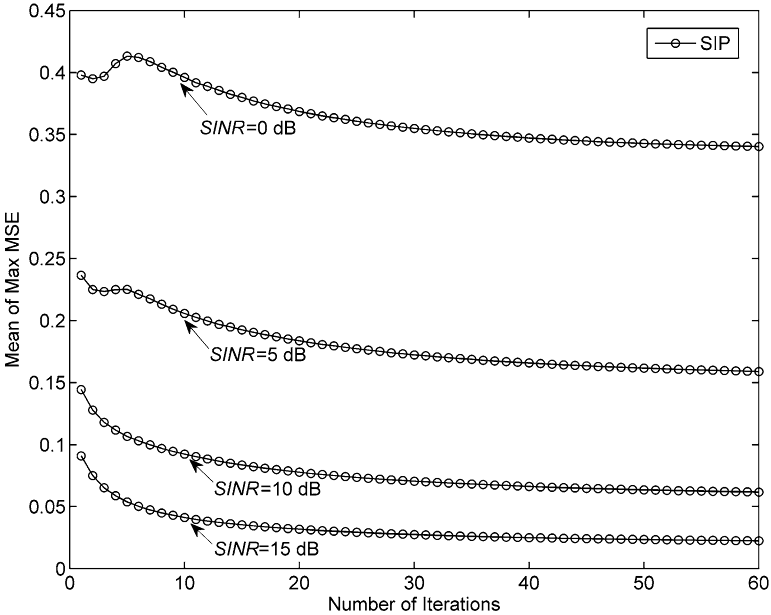

Fig. 6.5 Convergence of the SIP scheme for $B = 2$, $N_R = 4$ (perfect feedback)

6.4.2 *Performance of the Mean of the Maximum of Sub-stream MSE*

Figures 6.6 and 6.7 show the average performance of the maximum of sub-stream MSEs for $B = 2$ and $N_R = 2$ or 4 with different p_2. For the case of $p_2 = 0$, the system degenerates to ST due to broken backhaul, while the case of $p_2 = 1$ corresponds to full JT with perfect backhaul. As explained in Sect. 6.3.2 and observed in Figs. 6.6 and 6.7, the precoder for the AGP scheme is optimized under the assumption of full JT, which incurs large performance degradation when the system falls back to ST or partial JT. When the practical backhaul is considered, that is, $p_2 = 0.78$, the proposed SIP scheme offers significant performance gain, and the gain is more pronounced in high-SINR regimes because the sequentially and incrementally designed precoder matches the actual transmission channel better than the precoder in AGP which is optimized for full JT.

6.4.3 *Performance of Average BER*

Figures 6.8 and 6.9 show the average BER performance for $B = 2$ and $N_R = 2$ or 4 with different p_2. As seen from Figs 6.8 and 6.9, our proposed SIP scheme

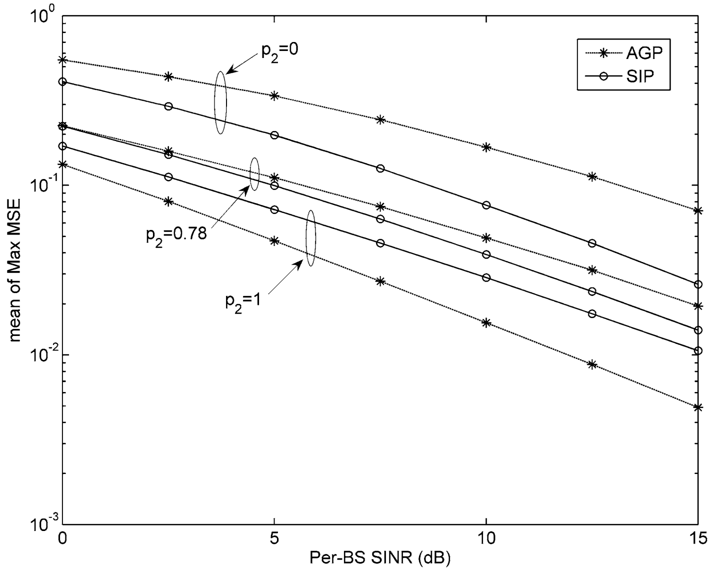

Fig. 6.6 Mean of the maximum of sub-stream MSEs for $B = 2$, $N_{\mathrm{R}} = 2$ (perfect feedback)

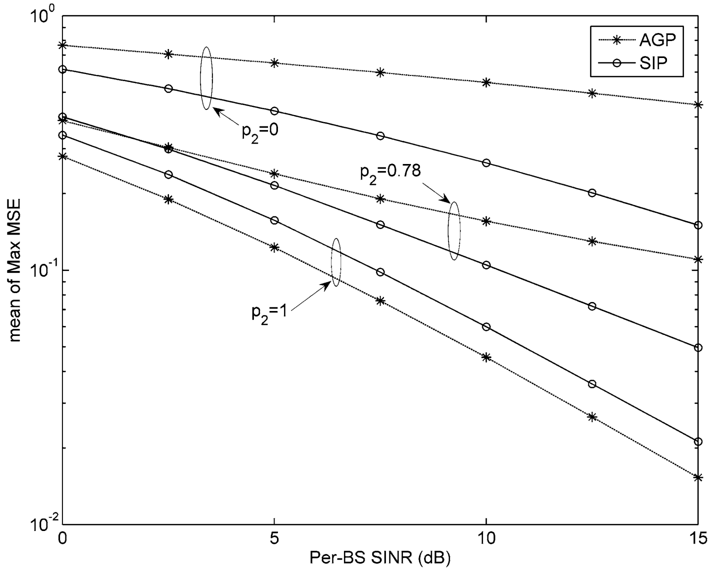

Fig. 6.7 Mean of the maximum of sub-stream MSEs for $B = 2$, $N_{\mathrm{R}} = 4$ (perfect feedback)

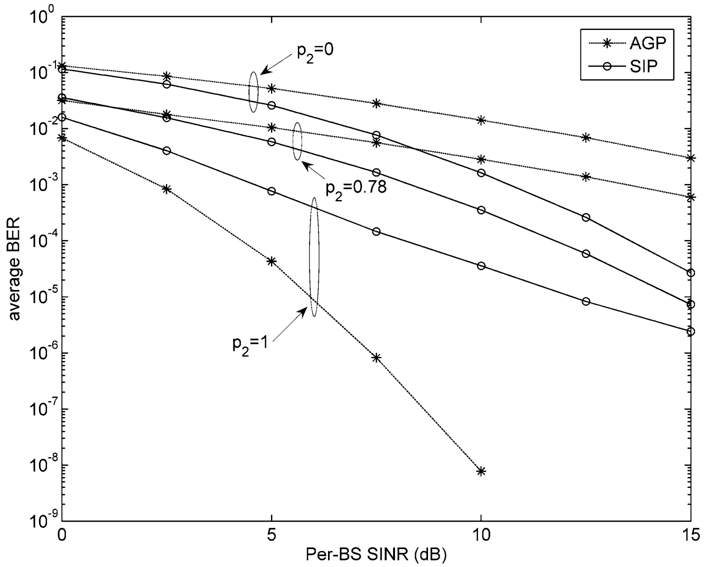

Fig. 6.8 Average BER for $B = 2$, $N_R = 2$ (perfect feedback)

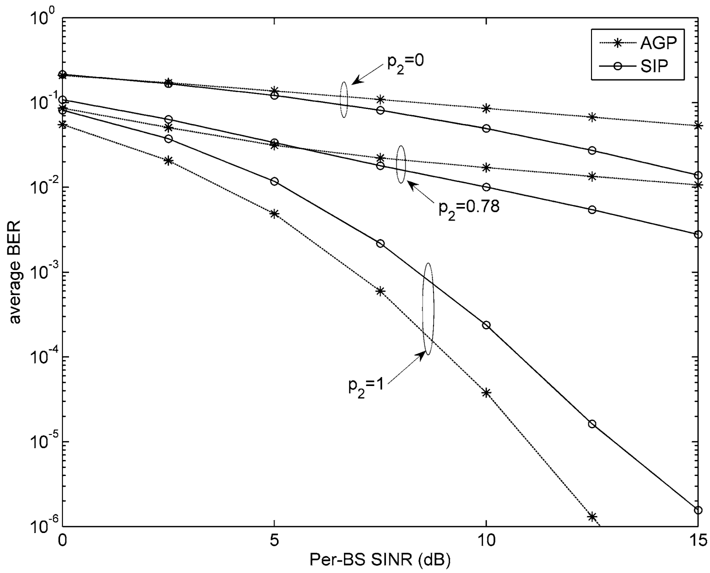

Fig. 6.9 Average BER for $B = 2$, $N_R = 4$ (perfect feedback)

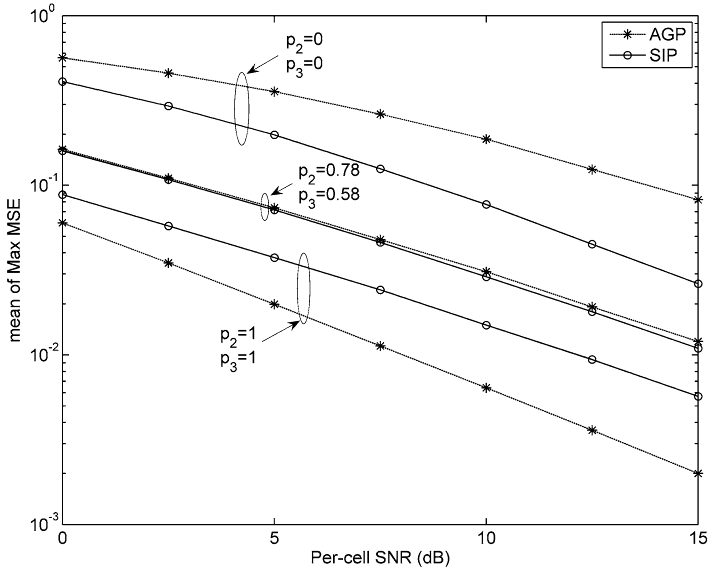

Fig. 6.10 Mean of the maximum of sub-stream MSEs for $B = 3$, $N_{\mathrm{R}} = 2$ (perfect feedback)

also shows superior BER performance when $p_2 = 0.78$, especially in high-SINR regimes. When $SINR = 15$ dB, compared with the AGP scheme, the proposed SIP scheme can reduce the average BER from 0.5×10^{-3} to 1×10^{-5} and from 1×10^{-2} to 3×10^{-3} for the case of $N_{\mathrm{R}} = 2$ and $N_{\mathrm{R}} = 4$, respectively.

6.4.4 Performance of the Extended SIP Scheme

For the extended case of $B = 3$, we show the average performance of the maximum of sub-stream MSEs in Figs 6.10 and 6.11 and the corresponding BER results in Figs. 6.12 and 6.13 for $N_{\mathrm{R}} = 2$ or 4 with different (p_2, p_3). Much like what we have observed previously, when the backhaul suffers from limited connectivity, for example, $(p_2, p_3) = (0.78, 0.58)$, the proposed SIP scheme significantly outperforms the AGP scheme in terms of average BER when SINR is high. It is very interesting to note that the SIP and AGP schemes exhibit close averaged maximum MSE curves when $(p_2, p_3) = (0.78, 0.58)$ in Fig. 6.10, but they have notable BER difference in favor of the SIP scheme in Fig. 6.12. One possible explanation might be that the overall MSE is also important to determine the BER performance and the average MSE of the AGP scheme may not be well controlled as the maximum MSE. To investigate this issue, we conduct simulations to show the average MSE performance in Fig. 6.14 using parameters given in Fig. 6.10. From Fig. 6.14, we observe that the proposed SIP scheme doesn't outperform the AGP

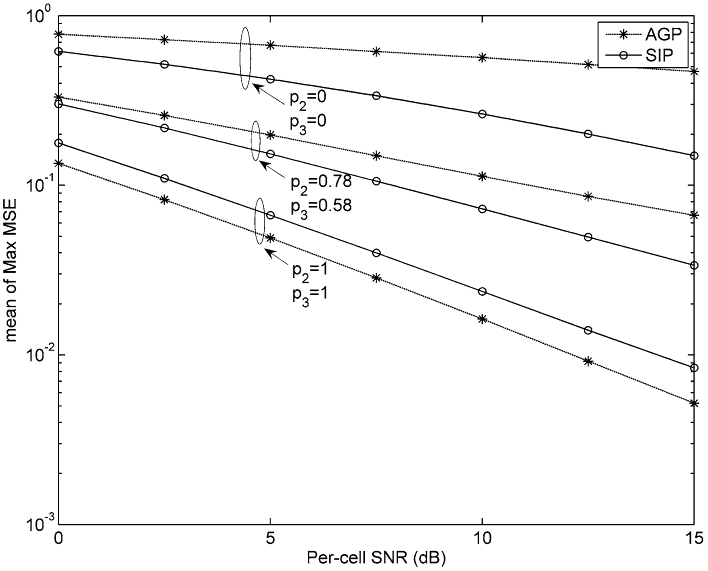

Fig. 6.11 Mean of the maximum of sub-stream MSEs for $B = 3$, $N_R = 4$ (perfect feedback)

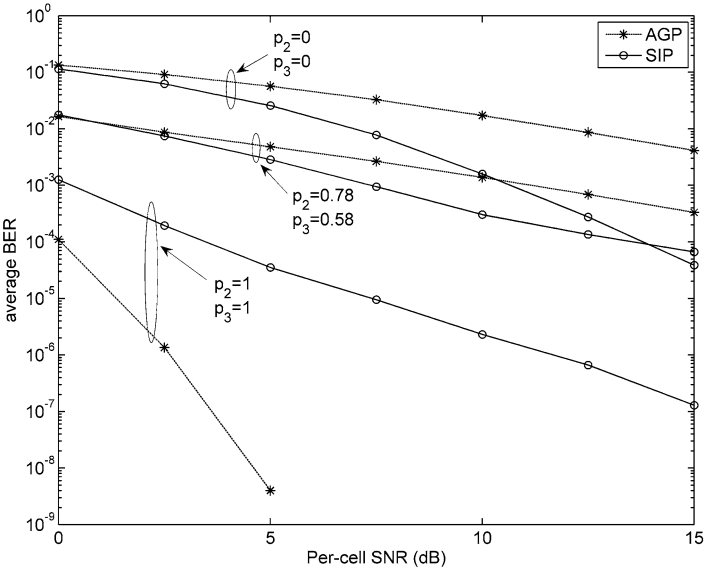

Fig. 6.12 Average BER for $B = 3$, $N_R = 2$ (perfect feedback)

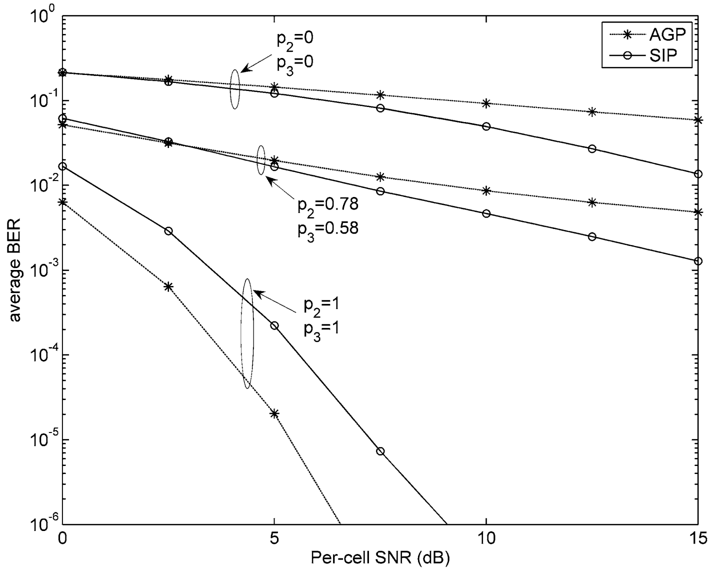

Fig. 6.13 Average BER for $B = 3$, $N_{\mathrm{R}} = 4$ (perfect feedback)

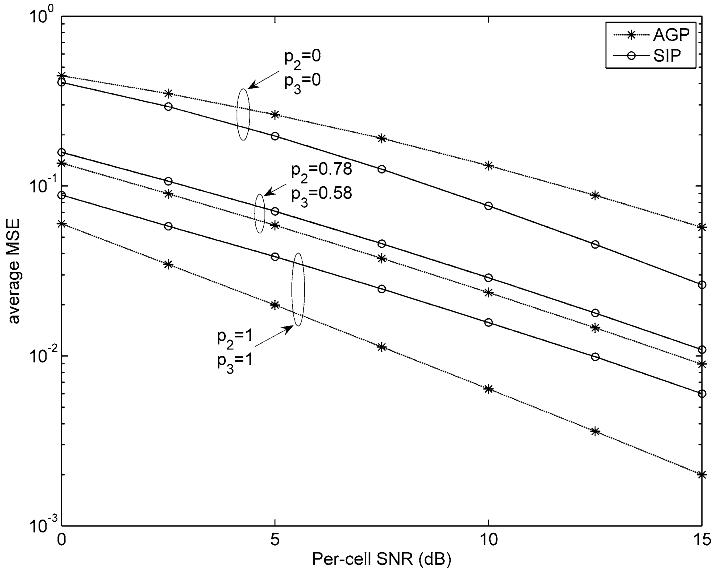

Fig. 6.14 Average MSE for $B = 3$, $N_{\mathrm{R}} = 2$ (perfect feedback)

scheme in terms of average MSE, because the SIP scheme targets the optimization of the maximum sub-stream MSE shown in problem (6.18), not the average MSE. Hence, the comparison of the average MSE performance does not highly relate to that of the BER performance. We suppose that the reason is that although the average maximum MSE performance is similar, the maximum sub-stream MSE of the AGP scheme varies more widely than that of the SIP scheme, as can be observed from Fig. 6.10 where the variant range of the maximum sub-stream MSE is roughly bounded by the "curves of mean of max MSE" for $(p_2, p_3) = (0, 0)$ and $(p_2, p_3) = (1, 1)$, and obviously the variant range of SIP is narrower than that of AGP. The variant range of the maximum sub-stream MSE indicates that the AGP scheme tends to generate larger maximum sub-stream MSE than the SIP scheme does in some poor cases, and the average BER performance is dominated by the large BERs resulted from poor-case maximum sub-stream MSEs, which will lead to a higher BER performance for the AGP scheme.

6.4.5 Performance with Codebook-based Feedback

Since the proposed SIP scheme is developed under the assumption of perfect feedback, it is highly motivated to investigate whether the SIP scheme still works in case of practical finite-rate feedback systems, that is, the indices of the optimal codeword $\mathbf{W}_b^{\text{opt,cb}}$ s rather than $\mathbf{W}_b^{\text{opt}}$ s themselves are fed back. First, we investigate the choice of d in the codebook-based feedback. In Figs. 6.15 and 6.16, average BER performance of the SIP and AGP schemes is shown for $B = 2 p_2 = 0.78$ or $B = 3 (p_2, p_3) = (0.78, 0.58)$, $N_\text{R} = 2$ and $d = 1 \sim 5$. We can observe in both figures that the performance gain suffers from a diminishing return as d increases and $d = 4$ seems to be a good trade-off between performance improvement and feedback overhead. Moreover, $d = 4$ is a common assumption for codebook designs for BSs with four transmit antennas in the LTE-A system (3GPP 2010). Thus, in the following we provide new simulation results plotted in Figs. 6.17, 6.18, 6.19, 6.20, 6.21, 6.22, 6.23, and 6.24 for $d = 4$ to illustrate the performance degradation because of limited-bit feedback in compare with Figs. 6.6, 6.7, 6.8, 6.9, 6.10, 6.11, 6.12, and 6.13. In our simulations, precoder candidates in the codebook are randomly generated as matrix composed of orthogonal normalized vectors (Santipach and Honig 2004) for each channel realization. It can be observed from these figures that although the performance degradation is notable, the gains of the SIP scheme shown in Figs. 6.6, 6.7, 6.8, 6.9, 6.10, 6.11, 6.12, and 6.13 are safely preserved.

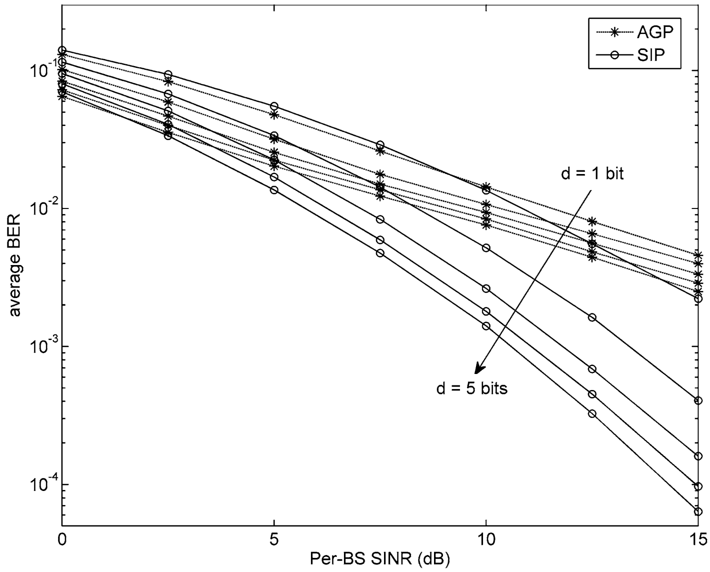

Fig. 6.15 Average BER for $B = 2$, $N_{\mathrm{R}} = 2$, $d = 1 \sim 5$ (codebook-based feedback)

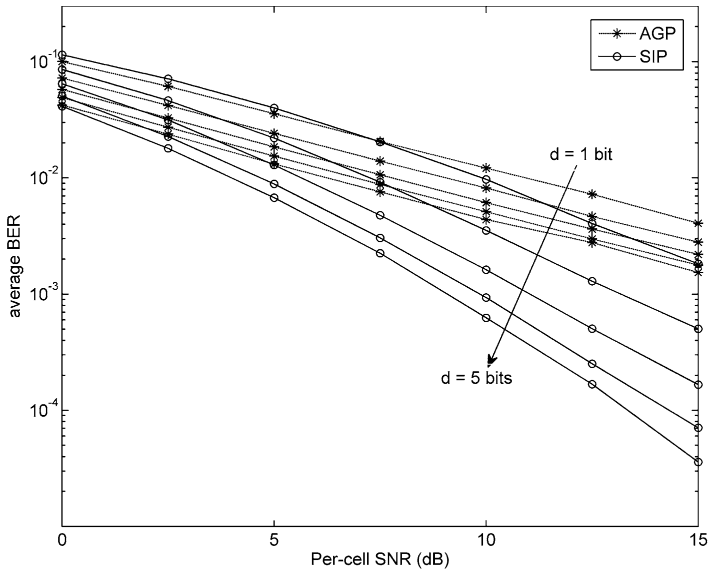

Fig. 6.16 Average BER for $B = 3$, $N_{\mathrm{R}} = 2$, $d = 1 \sim 5$ (codebook-based feedback)

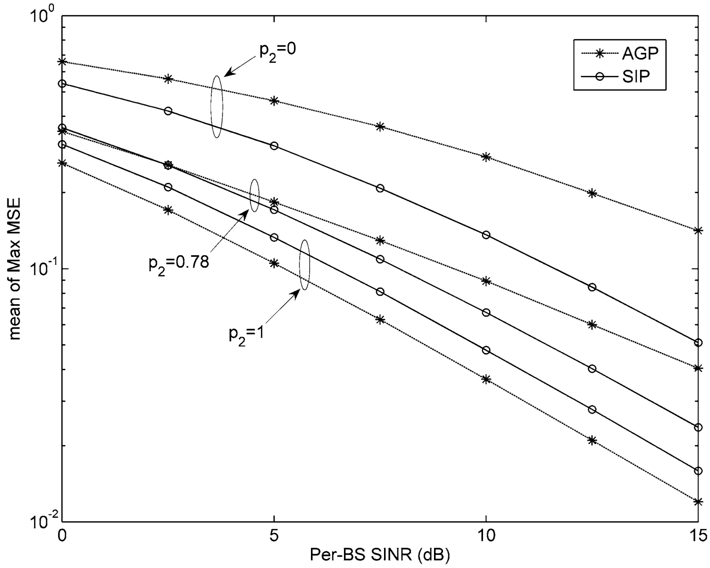

Fig. 6.17 Mean of the maximum of sub-stream MSEs for $B = 2$, $N_R = 2$, $d = 4$ (codebook-based feedback)

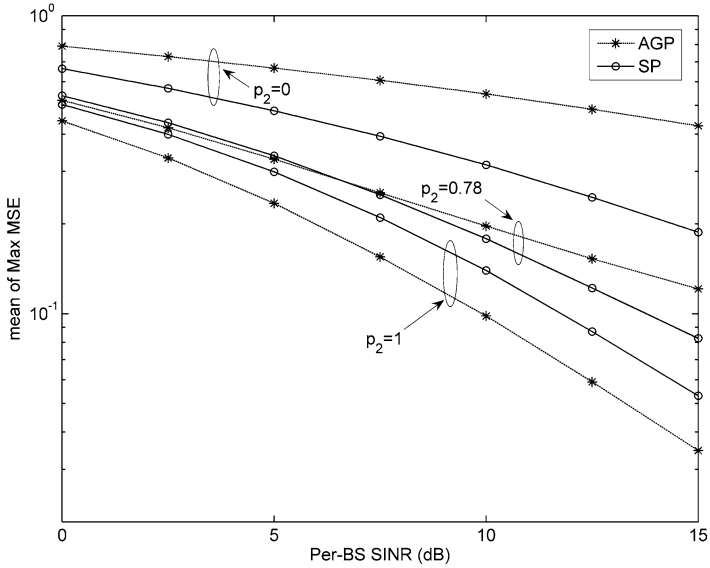

Fig. 6.18 Mean of the maximum of sub-stream MSEs for $B = 2$, $N_R = 4$, $d = 4$ (codebook-based feedback)

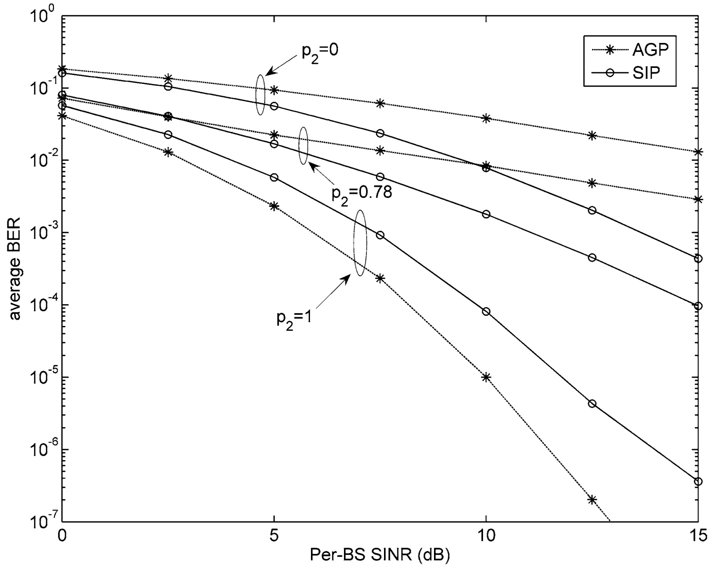

Fig. 6.19 Average BER for $B = 2$, $N_R = 2$, $d = 4$ (codebook-based feedback)

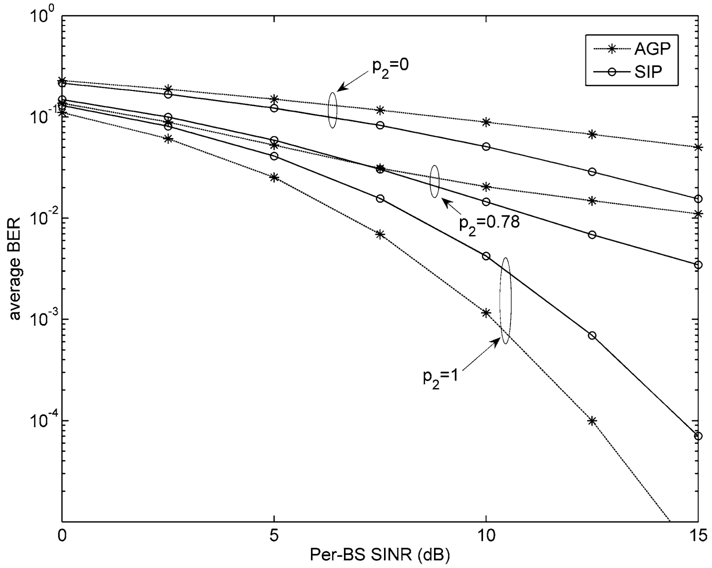

Fig. 6.20 Average BER for $B = 2$, $N_R = 4$, $d = 4$ (codebook-based feedback)

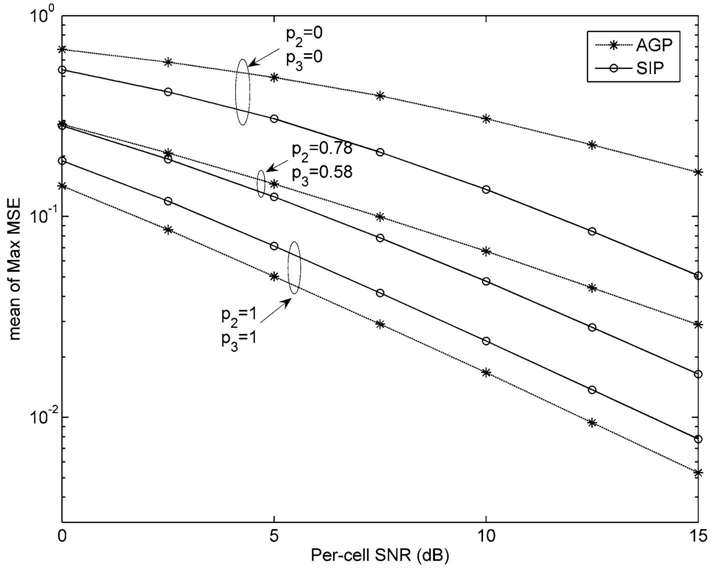

Fig. 6.21 Mean of the maximum of sub-stream MSEs for $B = 3$, $N_R = 2$, $d = 4$ (codebook-based feedback)

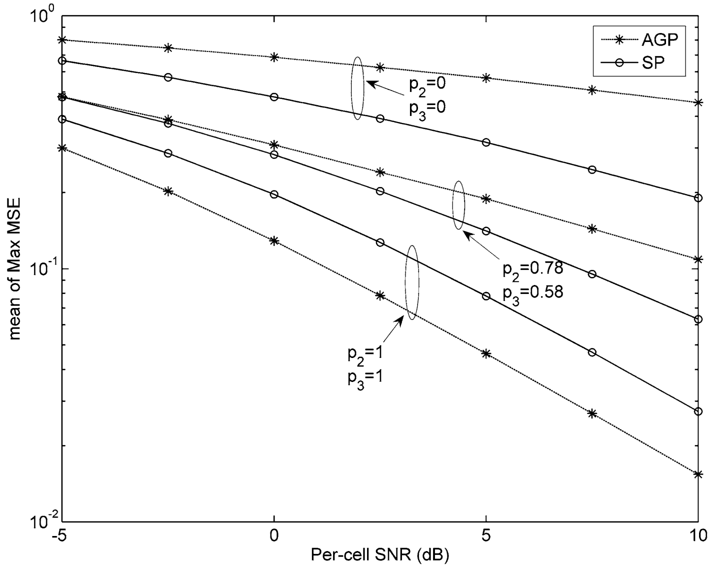

Fig. 6.22 Mean of the maximum of sub-stream MSEs for $B = 3$, $N_R = 4$, $d = 4$ (codebook-based feedback)

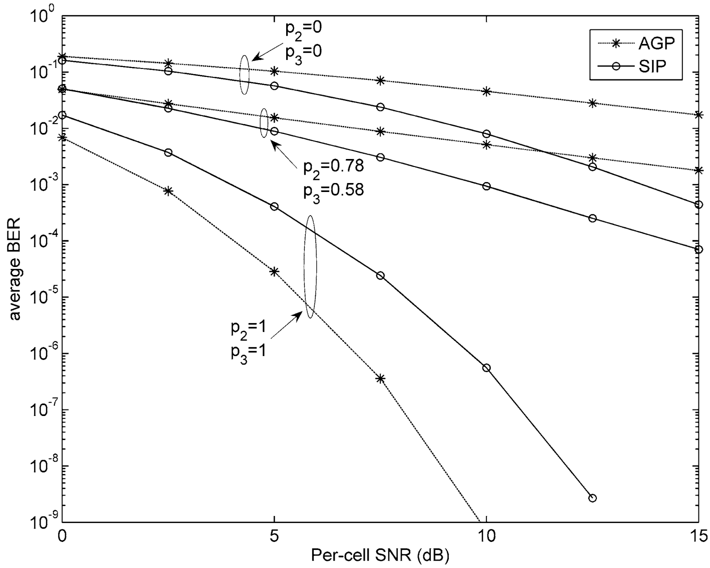

Fig. 6.23 Average BER for $B = 3$, $N_{\mathrm{R}} = 2$, $d = 4$ (codebook-based feedback)

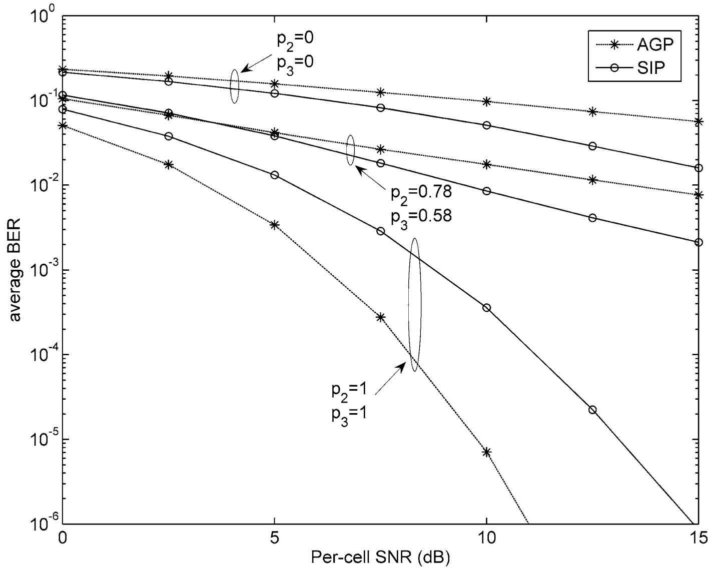

Fig. 6.24 Average BER for $B = 3$, $N_{\mathrm{R}} = 4$, $d = 4$ (codebook-based feedback)

6.5 Conclusion

In the joint precoding for distributed BSs with imperfect backhaul communications, we propose a SIP scheme based on the criterion of minimizing the largest sub-stream MSE. The novelty of the proposed scheme is that the imperfectness of the backhaul communications is modeled as probabilistic events and considered as a relevant factor in the optimization process. We first optimize the precoding matrix for the channel between the serving BS and the UE. Then according to the descending order of the activation probabilities of the helper BSs, we sequentially generate the optimal precoding matrix for each helper BS by an iterative algorithm with the previously optimized precoders fixed. Simulation results show that when the backhaul links are relatively reliable, the proposed scheme can obtain similar maximum sub-stream MSE performance compared with conventional AGP scheme. However, when the backhaul communications suffer from more serious connectivity problems, the proposed scheme exhibits considerable performance gains compared with the AGP scheme. And the robustness of the proposed scheme is more evident in the high-SINR regime or when the equal power allocation over the sub-streams is employed. In addition, through simulations for codebook-based limited-bit feedback systems, the proposed scheme retains the aforementioned advantages. Hence, considering practical backhaul conditions and limited-bit feedback methods, the proposed scheme is very useful for theoretical study and implementation.

References

3GPP (2008a) TR 36.913: requirements for further advancements for E-UTRA (LTE-Advanced) (V8.0.0). Accessed 2008

3GPP (2008b) TS 23.401 (V8.1.0), General Packet Radio Service (GPRS) enhancements for Evolved Universal Terrestrial Radio Access Network (E-UTRAN) access (Release 8), March 2008: p 129

3GPP (2009) Evolved Universal Terrestrial Radio Access Network (E-UTRAN); X2 Application Protocol (X2AP). Accessed Sept 2009

3GPP (2010) TR 36.814: further advancements for E-UTRA physical layer aspects (V9.0.0). Accessed 2010

3GPP (2011) TR 36.819: coordinated multi-point operation for LTE (V2.0.0). Accessed Sept 2011

Boyd S, Vandenberghe L (2004) Convex optimization. Cambridge University Press, Cambridge

Costa M (1983) Writing on dirty paper. IEEE Trans Inform Theor 29(3):439–441

Ericsson, ST-Ericsson (2011) R1-110452: deployment and backhaul constraints for CoMP. In: 3GPP TSG-RAN1#63bis meeting, Dublin, Ireland, Jan 2011

Gesbert D, Hanly S, Huang H, Shamai S, Simeone O, Wei Y (2010) Multi-cell MIMO cooperative networks: a new look at interference. IEEE J Sel Area Commun 28(9):1380–1408

Gradshteyn IS, Ryzhik IM (2007) Tables of integrals, series, and products, 7th edn. Academic Press, New York. Accessed 2007

Huh H, Papadopoulos H, Caire G (2009) MIMO broadcast channel optimization under general linear constraints. In: IEEE International Symposium on Information Theory (ISIT), Los Angeles, CA, USA, pp 2664–2668

IEEE WG 802.20 (2005) 802.20 evaluation criteria (V1.0), Sept. 2005

Marsch P, Fettweis G (2009) On downlink network MIMO under a constrained backhaul and imperfect channel knowledge. In: IEEE Global telecommunication conference (Globecom), Honolulu, HI, USA, Nov 2009, pp 5059–5064

MCC Support (2011a) R1-110611: final report of 3GPP TSG RAN WG1 #63bis v1.0.0. In: 3GPP TSG-RAN1#64 meeting, Taipei, Taiwan, Feb 2011

MCC Support (2011b) R1-111226: final report of 3GPP TSG RAN WG1 #64 v1.0.0. In: 3GPP TSG-RAN1#65 meeting, Barcelona, Spain, May 2011

Moon J, Cho D (2011) Efficient cell-clustering algorithm for inter-cluster interference mitigation in network MIMO systems. IEEE Commun Lett 15(3):326–328

Orange, Telefónica (2011) R1-111174: backhaul modeling for CoMP. In: 3GPP TSG-RAN1#64 meeting, Taipei, Taiwan, Feb 2011

Orange, Deutsche Telekom, NTT DOCOMO, Telecom Italia, Telefónica, Vodafone (2011) R1-110546: views on CoMP evaluation methodology. In: 3GPP TSG-RAN1#63bis meeting, Dublin, Ireland, Jan 2011

Palomar DP, Jiang Y (2006) MIMO transceiver design via majorization theory. Found Trends Commun Inform Theor 3(4):331–551

Palomar DP, Cioffi JM, Lagunas MA (2003) Joint Tx-Rx beamforming design for multicarrier MIMO channels: a unified framework for convex optimization. IEEE Trans Signal Process 51(9):2381–2401

Palomar DP, Lagunas MA, Cioffi JM (2002) On the optimal structure of transmit-receive linear processing for MIMO systems. In: IEEE annual Allerton conference on communication, control, and computing, Monticello, IL, USA

Samsung (2010) RP-101425: revised SID proposal: coordinated multi-point operation for LTE. In: 3GPP TSG RAN#50 meeting, Istanbul, Turkey, Dec 2010

Samsung (2011) R1-114223: discussion on the size of CoMP measurement set. In: 3GPP TSG RAN1#67 meeting, San Francisco, USA, Nov 2011

Samsung, Alcatel-Lucent, Alcatel-Lucent Shanghai Bell, CATR, CATT, CHTTL, CMCC, Deutsche Telekom, Hitachi, HTC, Huawei, ITRI, KDDI, LG Electronics, NEC, NTT DOCOMO, Orange, Panasonic, Pantech, Qualcomm, Research In Motion UK Limited, SK Telecom, ZTE (2010) New study item proposal: coordinated multi-point operation for LTE. In: 3GPP RP-100370. Accessed 2010

Santipach W, Honig M (2004) Asymptotic capacity of beamforming with limited feedback. In: IEEE international symposium on information theory, Los Angeles, CA, USA, p 290

Skillermark P, Almgren M, Astely D, Lundevall M, Olsson M (2008) Simplified interference modeling in multi-cell multi-antenna radio network simulations. IEEE Vehicular Technology Conference (VTC), 2008, pp 1886–1890

Somekh O, Simeone O, Bar-Ness Y, Haimovich A, Shamai S (2009) Cooperative multicell zero-forcing beamforming in cellular downlink channels. IEEE Trans Inform Theor 55(7): 3206–3219

Tse D, Viswanath P (2005) Fundamentals of wireless communication. Cambridge University Press, Cambridge

Viswanath P, Anantharam V (1999) Optimal sequences and sum capacity of synchronous CDMA systems. IEEE Trans Inform Theor 45:1984–1991

Weingarten H, Steinberg Y, Shamai S (2004) The capacity region of the Gaussian MIMO broadcast channel. In: Conference on information sciences and systems, Princeton, NJ, USA, p 174

Zakhour R, Gesbert D (2011) Optimized data sharing in multicell MIMO with finite backhaul capacity. IEEE Trans Signal Process 59(12):6102–6111

Zhang H, Dai H (2004) Cochannel interference mitigation and cooperative processing in downlink multicell multiuser MIMO networks. EURASIP J Wireless Commun Netw 2004(2):222–235

Zhou S, Gong J, Niu Z, Jia Y, Yang P (2009) A decentralized framework for dynamic downlink base station cooperation. In: IEEE Global Telecommunications Conference (GLOBECOM), Dec 2009, Honolulu, HI, USA, pp 1–6

Chapter 7
Coordinated Multipoint System

Abstract In this chapter, the application of multipoint cooperative communication in the 4G networks, that is, the coordinated multipoint (CoMP) system, is addressed from a variety of aspects. First, we review the development of CoMP in the standardization of Long-Term Evolution-Advanced (LTE-A) networks and analyze the reason of its preclusion from the LTE Release 10 specification. Second, we discuss the renewed campaign of CoMP in LTE Release 11, including the downlink transmission and uplink reception schemes of CoMP, as well as the related specification works. Third, we analyze the simulation results from the 3GPP CoMP study item to show the advantages of CoMP system in practical cellular networks.

Keywords CoMP • Implicit CSI feedback • CoMP scenarios • CoMP schemes • Performance evaluation • LTE Release 8/9 • LTE Release 10 • LTE Release 11

7.1 Introduction

The formal discussions of multipoint cooperative communication technology in the 4G networks began in the Third Generation Partner Project (3GPP) technical specification group (TSG) radio access network (RAN) international mobile telecommunications (IMT) advanced workshop meeting (ETSI MCC 2008). Some well-organized elaborations on this new technology within the standardization framework can be found in Alcatel-Lucent (2008a). In the Long-Term Evolution-Advanced (LTE-A) network, cooperative communication scheme is generally named coordinated multipoint (CoMP) transmission or reception, which is employed as a tool to improve the coverage of high data rates, the cell-edge throughput, and also to increase the system throughput (3GPP 2009a).

The basic idea of CoMP is to evolve the conventional single-cell multiuser equipment (UE) system structure to a multicell multi-UE network topology so that the concept of cell-edge UE will blur since a UE close to the cell boundaries can be at the same time on the central point of an area triangulated by several

M. Ding and H. Luo, *Multi-point Cooperative Communication Systems: Theory and Applications*, Signals and Communication Technology, DOI 10.1007/978-3-642-34949-2_7,

operational base stations (BSs). Hence, UEs with low signal qualities will get much better service if nearby BSs can work together in cooperation or coordination. The involved BSs will constitute a CoMP cooperating set. The effectiveness of CoMP was well analyzed in Nortel (2008a) and references therein.

In 3GPP (2009a), two kinds of CoMP schemes have been identified, that is, coordinated scheduling/coordinated beamforming (CS/CB) and joint processing/joint transmission (JP/JT). The difference between CS/CB and JP/JT lies in whether UE's data can be transmitted from a single point (CS/CB) or from multiple points (JP/JT), which implies that JP/JT necessitates data sharing among CoMP points. During the early stage of discussions, beamforming coordination or spatial-domain coordination drew most of the attention in CS/CB (Alcatel-Lucent 2008b; CATT 2008a; Hitachi 2008; Huawei 2008; Philips 2008a; Samsung 2008), while JP/JT included a wider range of topics, such as the overall mechanism and the corresponding reference signal (RS) design (Ericsson 2008; NTT DoCoMo 2008; ETRI 2008a; Nokia 2008; ZTE 2008a, b), control signaling provision (Alcatel-Lucent 2008a; Ericsson 2008; NTT DoCoMo 2008; Philips 2008b), and preprocessing schemes, for example, precoding and transmit diversity (TD) (CATT 2008b; ETRI 2008b; LGE 2008; Mitsubishi 2008; TI 2008; ZTE 2008c). In addition, some papers from a high-level viewpoint tried to provide a unified framework for CoMP, covering both CS/CB and JP/JT. For instance, the author of Samsung (2008) wanted to put all CoMP schemes into a general category of intercell interference coordination technology. Besides, 14 CoMP schemes were investigated and classified in Nortel (2008b). In Motorola (2008), CS/CB was viewed as a constrained optimization problem of JP/JT. Finally, a general utility function was proposed in Qualcomm (2008) to price the performance of various CoMP schemes.

7.2 Standardization Progress

7.2.1 The Failed Campaign of CoMP in LTE Release 10

In the 3GPP TSG RAN working group 1 (WG1) denoted as 3GPP RAN1 for short hereafter, at the #54 and #54bis meetings (MCC Support 2008a, b), most companies actively joined the discussions on CoMP and many details about various CoMP schemes were disclosed, which focused on JP/JT algorithms, UE feedback, RS design, etc. Some proposals on beam coordination/collision avoidance were also treated in the CoMP session of the 3GPP RAN1 #55 meeting (MCC Support 2008c). In the first quarter of year 2009, more than 50 papers of this topic appeared at each 3GPP RAN1 meeting (MCC Support 2009a, b, c), and a way forward on CoMP was agreed that downlink control signaling should be sent from a single point, that is, an anchor cell, and new precoded RS should be introduced for CoMP demodulation. The purpose of introducing a new demodulation RS (DM RS) is to make transmission schemes transparent to UE, since what a UE needs to do is to first detect the precoded DM RS usually in the form of a UE-specific sequence, and then decode its data using the detected RS as a reference for demodulation. Compared with the conventional common RS (CRS) design that UE needs to know the exact transmit operation at BS for correct demodulation (3GPP 2008), the employment of the UE-specific and precoded DM RS leaves more freedom for radio resource management (RRM) control at the network side. Terminology of CoMP-related point sets was debated during the 3GPP RAN1 #57 meeting (MCC Support 2009d) and e-mail discussions on CoMP that took place between the 3GPP RAN1 #57 and #57bis meetings were mainly concentrated on channel state information (CSI) feedback design in support of downlink CoMP (MCC Support 2009e). As a result, a constructive way forward was agreed that CoMP CSI feedback should be in the form of per-cell feedback as a baseline and complementary intercell feedback might be needed (MCC Support 2009f). In the following 3GPP meeting (MCC Support 2009g), the topic of CoMP CSI feedback became a fighting ground with the conventional implicit feedback paradigm (see Sect. 2.6 and Sect. 7.2.2 in the following) defending the offensive from a new design of reporting explicit CSI. In the end, it was observed that extension from the previous LTE design, that is, implicit feedback, to accommodate CoMP operations seemed like a more logical choice. Moreover, spatial domain interference coordination, that is, the seventh category of multipoint cooperative communication technology (see Sect. 2.7.7.2), became a hotly discussed topic for CoMP during the meeting.

The setback of the standardization of CoMP occurred in Nov 2009, when at the 3GPP RAN1 #59 meeting (MCC Support 2009h) CoMP raised wide concerns about its large complexity and heavy feedback overhead, especially for JT, that is, the eighth category of multipoint cooperative communication technology (see Sect. 2.7.8.2). Thus, it was agreed that the standardization priority should be put on single-cell multiple-input multiple-output (MIMO) operations while its extension to CoMP system should be kept in mind. In particular, CSI feedback issues attracted most of the attention during the online discussions for single-cell single-user (SU)/multiuser (MU) MIMO transmissions and possible extensions to CoMP operations. At the 3GPP RAN1 #59bis meeting, several network operators jointly presented their views on CoMP (Vodafone et al. 2010) that for the LTE-A network, that is, LTE Release 10, 3GPP RAN1 should only target for intra-BS CoMP, which is largely an implementation issue. And hence, it was agreed that (MCC Support 2010a):

- No inter-BS backhaul communication protocols should be included in LTE Release 10.
- Design of RS for channel state information (CSI) measurement, that is, CSI RS, should take potential needs of downlink CoMP into account.
- Additional CSI feedback requirements for CoMP in future LTE releases should be consistent with the feedback framework for single-cell SU/MU MIMO defined in LTE Release 10.

At the 3GPP RAN1 #60 meeting held in February 2010 (MCC Support 2010b), the above agreement was reconfirmed with emphasis placed on the design of CSI RS that it should allow for accurate intercell measurements, which would potentially facilitate the fifth to eighth categories of multipoint cooperative communication schemes (see Sects. 2.7.5, 2.7.6, 2.7.7, and 2.7.8) in the future.

Nevertheless, the co-source companies of NTT DOCOMO et al. (2010) recommended to continue the studies on downlink CoMP in the timeframe of a new LTE study item, which would generate a technical report guiding the second wave of CoMP standardization activities when the time is right. Consequently, one month later in March 2010, at the 3GPP #47 plenary meeting held in Vienna, that is, the 3GPP TSG RAN #47 meeting, a new study item description on the CoMP system for future LTE networks (Samsung et al. 2010) was jointly proposed by many companies, and it was agreed that work on this study item should be started in June 2010 (ETSI MCC 2010a). But due to the slow progress in the standardization on the basic features of the LTE-A network, such as enhanced downlink/uplink MIMO operations, frequency carrier aggregation, and interference management in heterogeneous networks, the study on CoMP was considered to have a much lower priority. Therefore, it was concluded that the CoMP-related studies would be further postponed to September 2010 (ETSI MCC 2010b). However, standardization campaigns on the other fronts of the LTE-A network turned out to be much tougher than expected. As a result, at the 3GPP TSG RAN #49 meeting (ETSI MCC 2010c), the endeavor on the design of an advanced CoMP system was again deemed as not urgent and was put off by another 3 months. Some companies were beginning to lose their patience on this topic because the ambious CoMP campaign had been staying inactive for almost a whole year since the 3GPP RAN1 #59 meeting held in Nov 2009 (MCC Support 2009h). So the following 3GPP #50 plenary meeting scheduled in December 2010, seemed to be vital in determining the future of CoMP in LTE networks.

To offer some in-depth background information, the suspension of LTE standardization on CoMP in year 2010 was mainly due to lack of coordination between CoMP and MIMO sessions in the 3GPP RAN1 meetings, leading to immature discussions on CoMP-oriented technologies, for example, explicit CSI feedback, which was incompatible with the MIMO framework at that time. As the LTE-A specifications were scheduled to be finished before the International Telecommunication Union (ITU) officially announcing the 4G standards in the end of 2010, the CoMP operation had to be dropped in the LTE-A network because of its low priority compared with the basic MIMO functionality.

As expected, at the 3GPP TSG RAN #50 meeting, the study on CoMP operation for LTE was finally agreed to restart from December 2010, based on a revised study item description proposal (Samsung 2010a). The scope of this study item included performance evaluation of various CoMP schemes, recommendation of CoMP technologies, and identification of standardization impacts on related specifications. This study item was estimated to be completed in 9 months (ETSI MCC 2011), and four areas were identified as the focal points of study:

1. For the performance evaluation, it should be considered whether further refinements to the simulation assumptions from the agreements reached during the previous study item were needed to align with the potential CoMP deployment scenarios.

2. Concrete numerical results should be provided to evaluate the performance benefits of enhanced CoMP operation and the required specification support for both intra-BS and inter-BS CoMP.
3. Potential enhancements for downlink CoMP operation should be carefully investigated to assist the system design, such as contents of required CSI feedback, uplink RS enhancement for exploiting the channel reciprocity, and control procedures to support CoMP transmission.
4. Potential standardization impact on higher layer protocols for CoMP should be considered, if possible.

7.2.2 CSI Feedback for Single-Cell MIMO in LTE Release 8/9/10

While the CoMP discussion was kept silent in 3GPP RAN1 during the year 2010, the study on downlink MIMO stood up to lead the specification progress in the aspect of enhanced physical layer technologies. The major challenges in downlink MIMO were closely related to the new deployment scenario of eight transmission antennas at BS. Some hotly discussed topics were design of the codebook for precoding, generation of eight-layer DM RSs, and new CSI feedback to support the upgraded single-cell SU/MU MIMO operation. Among them, the feedback framework for the single-cell SU/MU MIMO defined in LTE Release 10 had a profound implication for CoMP since any additional CSI feedback enhancement designed for CoMP should be compatible with the existing framework (MCC Support 2010a). Hence, in the following, we review the CSI feedback design for the single-cell downlink MIMO in LTE-A networks.

7.2.2.1 Implicit CSI Feedback in LTE Release 8/9

First, it is helpful to elaborate on the conventional implicit CSI feedback methods in more details. In general, the implicit CSI feedback refers to the approach of UE reporting transmission recommendations based on codebook searching to BS, which have been briefly introduced in Sect. 2.6. In LTE Release 8/9 systems, that is, the predecessors of the LTE-A network, the implicit CSI feedback serves well considering its reasonable performance gain based on a very limited load of uplink overhead.

The contents of implicit CSI feedback are divided into three categories based on their time-variant properties as follows:

- Rank indicator (RI), which indicates the number of usable layers of a MIMO channel. RI changes very slowly both in time and frequency domains, for example, one RI is typically valid for a bandwidth of 10 MHz during a period of several hundreds of milliseconds (3GPP 2008). A rank-deficient channel often occurs when there is a line-of-sight (LoS) link between BS and UE. It should be noted that rank deficiency can be useful for coverage extension since the low-rank precoding, also known as beamforming, can concentrate the limited transmission power onto one or two beams with high antenna array gain (see Sect. 2.3.3). In a non-LoS (NLoS) channel environment with plenty of scattering objects, full-rank transmission can be considered to reap the multiplexing gain of the MIMO system (see Sect. 2.3.1).

- Precoding matrix indicator (PMI), which indicates the beamforming vector(s) or precoding matrix employed at the transmitter. As explained earlier, the beamforming vector is usually associated with the low-rank transmission, while the precoding matrix supports the high-rank one. Nevertheless, both the beamforming vector and precoding matrix convey the information of proper preprocessing before the transmission (see Sect. 2.3). PMI changes relatively slowly in time domain for UEs with low moving speed, but it may vary between adjacent sub-bands in frequency domain depending on the existence of strong LoS links. In an NLoS case, the channel becomes a frequency-selective one for precoding due to the increased uncertainty of the multi-path phase-combining on a subcarrier from waves bouncing off different scattering objects, which are located randomly in the environment. In contrast, an LoS channel is usually able to accommodate a transmission with a wideband precoder due to the conspicuous channel direction, the beam(s) derived from which is invariable for a wide frequency spectrum. For a UE moving at a typical speed below 10 km/h, one single-cell PMI is valid for a frequency sub-band of about 1 MHz (non-LoS case) or a system wideband of 10 MHz (LoS case), during a period of tens of milliseconds (3GPP 2008).
- Channel quality indicator (CQI), which indicates the adaptive modulation and coding (AMC) scheme having a packet error rate (PER) typically no more than 0.1 (3GPP 2011a). CQI changes fast both in time and frequency domains because a small variation of time or frequency can be interpreted into large phase shifts for the channel frequency response components associated with different time taps considering the relatively high carrier frequency, for example, 2 GHz, and the large phase shifts will lead to constructive or destructive combining of channel frequency response components across the time-frequency resources. For a UE moving at a speed below 10 km/h, one single-cell CQI typically measures the average channel quality for a frequency sub-band of about 1 MHz in a period of 10$\sim$20 ms or for a wideband of 10 MHz in a period of tens of milliseconds (3GPP 2008).

Regarding the container of the above implicit CSI, there are two feedback channels in the LTE system, that is, a physical uplink control channel (PUCCH) and a physical uplink shared channel (PUSCH). The PUCCH is usually configured for transmission of periodic, basic CSI with low payload since PUCCH is essentially a capacity-limited control channel, the main role of which is to assist the downlink data transmission on the physical downlink shared channel (PDSCH). For CSI feedback on the PUCCH, different CSI contents, for example, RI, PMI, and CQI, are transmitted with different periodicity depending on their time-variant properties. To be more specific, CQI is reported with a small periodicity T_0, PMI is updated less frequently, for example, by a periodicity of several T_0, and RI is heavily protected by multi-sequence combinations with its feedback periodicity being tens of times of T_0. On the other hand, the PUSCH is employed for transmission of one-shot, extended CSI with high payload. Due to the large size of a PUSCH transport block (TB), a complete report of all CSI contents can be transmitted within one subframe for the BS to quickly acquire the UE's instantaneous CSI over the entire system bandwidth.

For the PUCCH, there are four feedback types in LTE Release 8/9 networks as follows (3GPP 2009b):

1. Type 1: Location index of one preferred sub-band in a band part (BP), which is a subset of the system bandwidth and information of CQI for the selected sub-band. The respective overhead includes L bits for the sub-band location, 4 bits for the CQI of the first data stream, and 3 bits for the CQI of the possible second data stream which is differentially coded with respect to the CQI of the first data stream.
2. Type 2: Wideband CQI and wideband PMI. The respective overhead includes 4 bits for the wideband CQI of the first data stream, 3 bits for the wideband CQI of the possible second data stream which is differentially coded with respect to the wideband CQI of the first data stream, and 2 or 4 bits for the wideband PMI depending on the transmit antenna configuration at BS. To be more specific, a 2-bit PMI is for a 2-antenna BS, while 4-bit PMI for a 4-antenna BS.
3. Type 3: RI. The overhead for RI is 1 bit for a 2-antenna BS or 2 bits for a 4-antenna BS.
4. Type 4: Wideband CQI of the first data stream. The overhead is constantly 4 bits.

Based on the combination of the above four CSI feedback types, there are four CSI feedback modes defined in LTE Release 8/9 networks (3GPP 2009b), that is, mode 1-0, mode 1-1, mode 2-0, and mode 2-1.

1. The mode 1-0 is a combination of type 3 and type 4. That is, the feedbacks of type 3 and type 4 are operated by different periodicities and/or with different subframe offsets. This mode only provides basic CSI of RI and wideband CQI to BS, thus it mainly targets for wideband TD technologies without precoding (see Sect. 2.3.2).
2. The mode 1-1 is a combination of type 3 and type 2. Similar to the mode 1-0, the feedbacks of type 3 and type 2 are operated by different periodicities and/or with different subframe offsets. This mode includes additional wideband PMI into the feedback compared with the mode 1-0, and hence it is suitable for precoding in frequency nonselective channels, for example, LoS channels.
3. The mode 2-0 is a combination of type 3, type 4, and type 1. This mode contains the wideband and sub-band CQIs for the first data stream as well as the RI if necessary. Compared with the mode 1-0, this mode is also designed for TD technologies, but with frequency-selective sub-band CQIs.
4. The mode 2-1 is a combination of type 3, type 2, and type 1, which is the most sophisticated one among the four modes. In the mode 2-1, the RI if necessary,

the wideband PMI and CQI, as well as one preferred sub-band location in each BP and the associated sub-band CQI, are available to BS. This mode can support multilayer precoding operation with sub-band link adaptation.

The purpose of introducing several CSI feedback modes is to assist the BS to perform various transmission schemes. In LTE Release 8/9 networks (3GPP 2009b), the following eight MIMO transmission modes (TMs) for downlink communication are defined:

1. TM 1: Single-antenna transmission, where only a single layer of data can be transmitted in this degraded MIMO mode. It is designed for BS with one transmission antenna or used as a fallback mode for the system in case of unexpected link failure.
2. TM 2: TD, which has been discussed in Sect. 2.3.2. In a MIMO system, multiple signal replicas transmitted in time/spatial/frequency domain can improve the quality of the received signal but at the cost of sacrificing the multiplexing gain of the MIMO system.
3. TM 3: Open-loop spatial multiplexing, which is an SU multilayer MIMO transmission with predetermined PMI hopping designed for high-speed UE. Note that the term "open loop" means that no precoder information needs to be fed back to BS. However, RI and a reference CQI based on the assumption of TM 2 are still needed so that the reference CQI can serve as a rough measure of the channel quality for the link adaptation operation in TM 3.
4. TM 4: Closed-loop spatial multiplexing, which is an SU multilayer MIMO transmission based on CSI feedback of PMI, as well as RI and CQI.
5. TM 5: MU MIMO, which is a MU version of TM 4. In TM 5, multiple UEs can be simultaneously served on the same downlink time-frequency resource.
6. TM 6: Closed-loop single-layer beamforming, where only a single layer of data is transmitted using MIMO beamforming and the PMI feedback from UE is required.
7. TM 7: Open-loop single-layer beamforming, which is an open-loop version of TM 6. In TM 7, the PMI and RI feedbacks from UE are not required, and a dedicated reference signal, that is, DM RS, is used for data demodulation at UE. Note that a reference CQI based on the assumption of TM 2 should also be reported for link adaptation at BS in TM 7.
8. TM 8: Dual-layer beamforming with DM RSs. In TM 8, UE can be configured with PMI/RI reporting, or otherwise. Note that if no PMI/RI reporting is required, UE still needs to feed back a reference CQI based on the assumption of TM 2 for link adaptation at BS.

For each TM discussed above, two CSI feedback modes are assigned to support its operation. The association between the TM and the supportive CSI feedback modes is summarized as follows:

1. TM 1: Mode 1-0 and mode 2-0
2. TM 2: Mode 1-0 and mode 2-0
3. TM 3: Mode 1-0 and mode 2-0

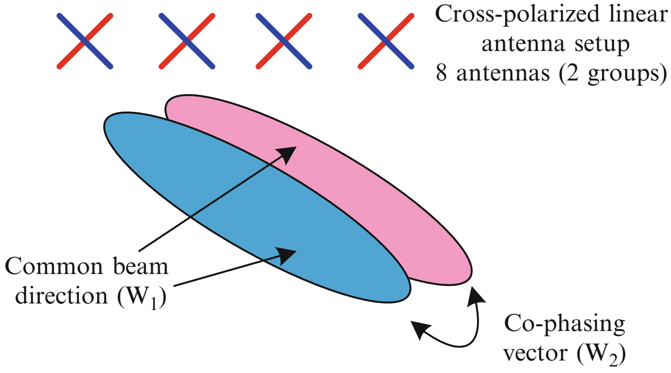

Fig. 7.1 Illustration of the double precoder design

4. TM 4: Mode 1-1 and mode 2-1
5. TM 5: Mode 1-1 and mode 2-1
6. TM 6: Mode 1-1 and mode 2-1
7. TM 7: Mode 1-0 and mode 2-0
8. TM 8 with PMI/RI feedback from UE: Mode 1-1 and mode 2-1; TM 8 without PMI/RI feedback from UE: mode 1-0 and mode 2-0

7.2.2.2 Implicit CSI Feedback in LTE Release 10

The implicit CSI feedback methods in LTE Release 8/9 systems are designed for BS with 1, 2, or 4 transmit antennas. As the MIMO technology continues to evolve in the LTE Release 10 network, CSI feedback for 8-antenna BS should be considered. At the 3GPP RAN1 #60 and #60bis meetings, respectively, held in February and April of year 2010, it was agreed that implicit feedback contents, that is, PMI/RI/CQI, should also be used for LTE Release 10 networks (MCC Support 2010b). And the precoder **W** for a frequency sub-band should be the multiplication of two matrices (MCC Support 2010c) written as

$$\mathbf{W} = \mathbf{W}_1 \mathbf{W}_2, \tag{7.1}$$

where $\mathbf{W}_1$ targets wideband/long-term channel properties and $\mathbf{W}_2$ measures frequency-selective/short-term CSI. Equation (7.1) is usually referred to as the double precoder design, the basic idea of which is to optimize the cross-polarized linear antenna setup as illustrated by Fig. 7.1.

As can be seen from Fig. 7.1, eight transmission antennas are divided into two groups of linear antenna arrays, both with the same polarization direction illustrated in red and blue beams. For both antenna groups, a common beamforming direction is represented by a 4×1 vector. Furthermore, a co-phasing vector is employed to coherently combine the signals transmitted from the two antenna groups. Therefore, $\mathbf{W}_1$ is written in the form of a block diagonal matrix shown as

$$\mathbf{W}_1 = \begin{bmatrix} \mathbf{F} & \\ & \mathbf{F} \end{bmatrix}, \tag{7.2}$$

where $\mathbf{F} \in \mathbb{C}^{4\times L}$ is the multilayer precoding matrix for each antenna group containing L vectors. And $\mathbf{W}_2$ becomes a $2L$ by L co-phasing matrix, which combines the L vector pairs of the two antenna groups using appropriate phase weights. Mathematically, $\mathbf{W}_2$ can be described as

$$\mathbf{W}_2 = \begin{bmatrix} 1 & 0 & \cdots & 0 \\ 0 & 1 & \cdots & 0 \\ \vdots & \vdots & \cdots & \vdots \\ 0 & 0 & \cdots & 1 \\ \exp(\mathrm{j}\varphi_1) & 0 & \cdots & 0 \\ 0 & \exp(\mathrm{j}\varphi_2) & \cdots & 0 \\ \vdots & \vdots & \cdots & \vdots \\ 0 & 0 & \cdots & \exp(\mathrm{j}\varphi_L) \end{bmatrix}. \tag{7.3}$$

Regarding the feedback design of $\mathbf{W}_1$ and $\mathbf{W}_2$, good progress was made at the 3GPP RAN1 #61 meeting (MCC Support 2010d). Following the basic principles established in LTE Release 8/9, the report on PUSCH should be self-contained in the same subframe, and hence one PUSCH CSI report should contain both $\mathbf{W}_1$ and $\mathbf{W}_2$. For feedback on PUCCH, $\mathbf{W}_1$ and $\mathbf{W}_2$ can be signaled in separate subframes (CSI mode 1). Alternatively, $\mathbf{W}_2$ might be divided into a wideband part and a sub-band one and $\mathbf{W}_1$ and wideband $\mathbf{W}_2$ can be transmitted in the same subframe (CSI mode 2). Besides, details of RI and CQI reporting should be further studied. In June 2010, at the 3GPP RAN1 #61bis meeting, three way-forward proposals on CSI mode 1/2 were discussed successively, but none of them got through. A weak consensus was that for CSI mode 2 the total overhead of $\mathbf{W}_1$, $\mathbf{W}_2$, and CQI should be no more than 11 bits. As the clock was ticking toward the end of the evaluation for 4G candidate systems, the specification work of the LTE-A network must move forward and fast. Hence, at the 3GPP RAN1 #62 meeting (MCC Support 2010e), six way-forward files were crafted by various companies trying to settle the open issues of CSI feedback in a swift way. After tough negotiations and necessary compromises, the $\mathbf{F}$ in $\mathbf{W}_1$ was agreed to be composed of discrete Fourier transform (DFT) vectors, and the detailed codebooks of $\mathbf{W}_1$ and $\mathbf{W}_2$ were firmed up (3GPP 2011a). For CSI feedback on PUCCH, it was agreed that only two modes should be considered for CSI mode 1, that is, extensions of LTE Release 8/9 PUCCH mode 1-1 and mode 2-1, and only one mode should be supported for CSI mode 2, that is, extension of LTE Release 8/9 PUCCH mode 1-1. For CSI feedback on PUSCH, most issues were quickly settled and the remaining open question was whether to introduce a new CSI feedback mode containing complete information of sub-band PMI and CQI across the system bandwidth. If such advanced CSI feedback mode were agreed, refinements that reduce the overhead should be considered even for the large-size PUSCH packet. Before the end of year 2010, all the remaining details of CSI feedback for LTE Release 10 networks were confirmed and carefully specified (MCC Support 2010f, g). Note that at the 3GPP RAN1 #63 meeting it was concluded that due to lack of time no new CSI feedback mode would be introduced for PUSCH, and enhanced CQI for MU MIMO would be considered in future LTE releases.

In the LTE Release 10 network, a new transmission mode, that is, TM 9, was introduced. The TM 9 can be viewed as the combination of TM 4 and TM 8 since it defines a closed-loop spatial multiplexing up to 8 layers with dedicated RSs for demodulation. Like TM 8, UE can be configured with or without PMI/RI reporting in TM 9. If no PMI/RI reporting is required, UE still needs to feed back a reference CQI based on the assumption of TM 2 for link adaptation at BS. In order to keep the feedback modes for a UE consistent with those corresponding to TM 4/8 and to support the new TM 9, the PUCCH CSI feedback mode 1-1 and mode 2-1 in the LTE-A system are modified as follows.

Based on transmission methods of $\mathbf{W}_1$ and $\mathbf{W}_2$, that is, CSI mode 1 or 2, mode 1-1 is splitted into two new sub-modes: mode 1-1 sub-mode 1 (CSI mode 1) and mode 1-1 sub-mode 2 (CSI mode 2). Besides, mode 2-1 (CSI mode 1) is also properly revised. In order to support the newly defined feedback modes, several types of feedbacks are introduced in the LTE-A system (3GPP 2011a):

1. Type 1a: Location index of one preferred sub-band in a BP, as well as CQI and indicator of $\mathbf{W}_2$ for the selected sub-band. The overhead for the sub-band location is L bits, and the total overhead for the sub-band CQI(s) and sub-band $\mathbf{W}_2$ is 8 bits (when RI $=$ 1), 9 bits (when $2 \leq \text{RI} \leq 4$), or 7 bits (when $5 \leq \text{RI} \leq 8$), respectively.
2. Type 2a: Indicator of $\mathbf{W}_1$, the overhead of which is 4 bits (when $1 \leq \text{RI} \leq 2$), 2 bits (when $3 \leq \text{RI} \leq 7$), or 0 bit (when RI $=$ 8), respectively. Note that $\mathbf{W}_1$ always targets for wideband precoding according to its definition.
3. Type 2b: Wideband $\mathbf{W}_2$ indicator and wideband CQI, the total overhead of which is 8 bits (when RI $=$ 1), 11 bits (when $2 \leq \text{RI} \leq 3$), 10 bits (when RI $=$ 4), or 7 bits (when $5 \leq \text{RI} \leq 8$), respectively.
4. Type 2c: Wideband CQI, $\mathbf{W}_1$ indicator and wideband $\mathbf{W}_2$ indicator. The total overhead for type 2c is 8 bits (when RI $=$ 1), 11 bits (when $2 \leq \text{RI} \leq 4$), 9 bits (when $5 \leq \text{RI} \leq 7$), or 7 bits (when RI $=$ 8), respectively. It should be noted that, in order to limit the feedback overhead, the $\mathbf{W}_1$ and wideband $\mathbf{W}_2$ take values from certain subsets of their codebooks, which are obtained by downsampling the $\mathbf{W}_1$ and $\mathbf{W}_2$ codebooks.
5. Type 5: RI and $\mathbf{W}_1$ indicator, the total overhead of which is 4 bits in the case of up to 2-layer data multiplexing or 5 bits in the case of up to 4/8-layer data multiplexing. Also, it is to be noted that, in order to limit the feedback overhead, the $\mathbf{W}_1$ takes values from a codebook subset by downsampling.

6. Type 6: RI and precoding type indicator (PTI). The overhead for PTI is fixed to 1 bit, indicating the type of precoding information. The total overhead of type 6 is 2, 3, and 4 bits in the case of up to 2-layer, 4-layer, and 8-layer data multiplexing, respectively.

The mode-to-type relations between the new mode 1-1/2-1 and the above new feedback types are as follows:

1. The mode 1-1 sub-mode 1 is a combination of type 5 and type 2b. That is, the feedbacks of type 5 and type 2b are operated by different periodicities and/or with different subframe offsets.
2. The mode 1-1 sub-mode 2 is a combination of type 3 and type 2/2c. When the MIMO transmission mode is TM 4 or 8, the mode 1-1 sub-mode 2 is composed of type 3 and type 2, that is, the conventional mode 1-1. When the MIMO transmission mode is the new TM 9, the mode 1-1 sub-mode 2 consists of type 3 and type 2c.
3. The new mode 2-1 is specified to support the new TM 9 and is a combination of type 6, type 2b, and type 2a/1a. When the PTI in the type 6 is 0, the new mode 2-1 is composed of wideband CSI only, that is, type 6, type 2a, and type 2b. Otherwise, the new mode 2-1 consists of type 6, type 2b, and type 1a.

7.2.3 The Renewed Campaign of CoMP in LTE Release 11

With the CSI feedback schemes for single-cell MIMO in LTE-A networks being specified to the last detail at the end of year 2010, the time for launching a second campaign of CoMP had finally come (ETSI MCC 2011). Although the double precoder design together with the new CSI feedback mode 1-1/2-1 largely constrained the framework of CoMP study, there were still many open issues that should be solved as discussed in the concluding remarks of Sect. 7.2.1. In the revised study item description proposal (Samsung 2010a), some nontraditional deployment scenarios are addressed such as heterogeneous networks, where the macro-cell coverage is overlaid with those of distributed remote radio heads (RRHs).

The 3GPP RAN1 #63bis meeting marked the beginning of renewed efforts on the CoMP study in LTE Release 11. During the meeting, various companies presented their general views on the CoMP system. A number of homogeneous and heterogeneous CoMP scenarios were proposed and agreed for further study (MCC Support 2011a):

1. Scenario 1: Homogeneous network with intra-site CoMP.
2. Scenario 2: Homogeneous network with high-power RRHs performing inter-site CoMP.
3. Scenario 3: Heterogeneous network with low-power RRHs within the macro-cell coverage, where the transmission/reception points created by the RRHs have separate cell IDs as the macro cell.

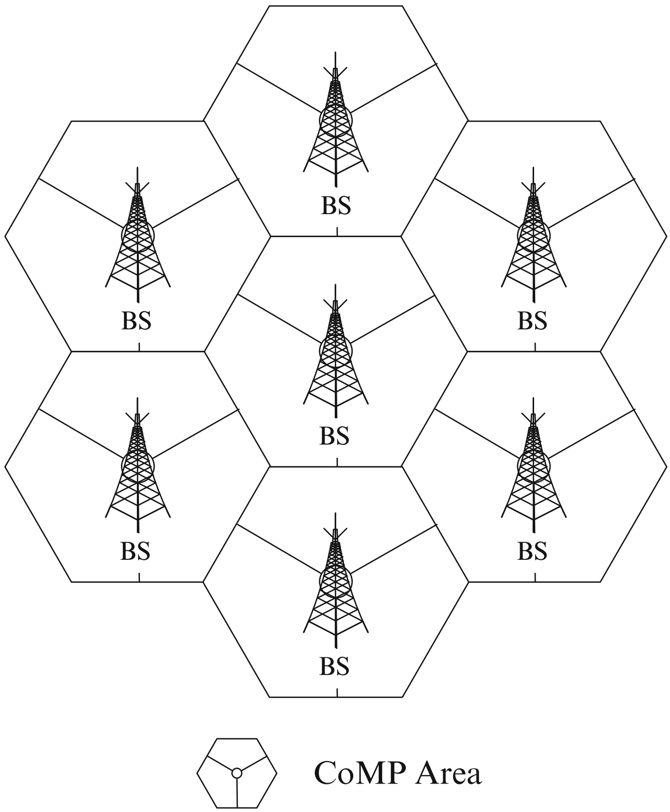

Fig. 7.2 CoMP scenario 1: homogeneous network with intra-site CoMP (7 cell sites plotted)

4. Scenario 4: Heterogeneous network with low-power RRHs within the macro-cell coverage, where the transmission/reception points created by the RRHs have the same cell IDs as the macro cell.

Scenarios 1 and 2 describe the homogeneous networks, that is, all nodes in the network are of the same power class and the coverage areas of two adjacent nodes barely overlay with each other. On the other hand, scenarios 3 and 4 characterize the heterogeneous networks, where low-power nodes coexist with the macro-BSs and hot-spot areas are doubly covered by both the low-power nodes and the macro-BSs.

To explain it in more details, scenario 1 defines a homogeneous network with intra-site CoMP, where a cell site is composed of several cells (sectors) and all radio resources of a cell site are controlled by one macro-BS. Thus, intra-site CoMP operations are mostly left to transparent implementation in BS. The schematic model of CoMP scenario 1 is illustrated in Fig. 7.2.

Scenario 2 represents a more advanced homogeneous network compared with scenario 1. In practice, a fully operational BS with both RF functions and baseband signal processing capabilities is usually of high cost. Therefore, RRH equipment

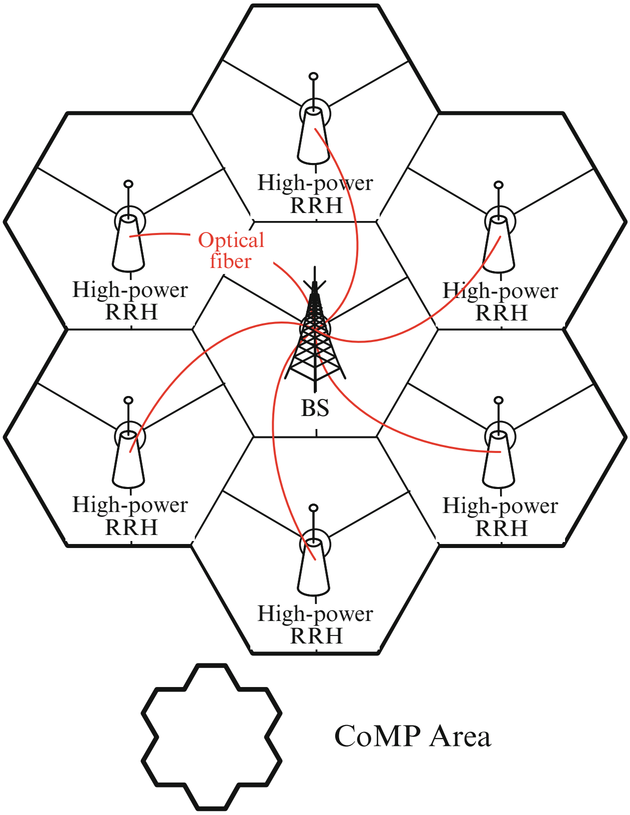

Fig. 7.3 CoMP scenario 2: homogeneous network with CoMP operated among macro-BS and high-power RRHs (7 cell sites plotted)

that only has RF modules and optical fiber connection to the macro-BS is widely used as an efficient means to extend the system coverage. Here, the power level of a RRH node is comparable with that of a BS and this type of RRH is called high-power RRH. As the RRM functions of RRHs are relegated to the master BS, CoMP can be operated among macro-BS and high-power RRHs in a wide area, which is considered in CoMP scenario 2 as illustrated in Fig. 7.3.

CoMP scenarios 3 and 4 relate to a heterogeneous network illustrated in Fig. 7.4, where multiple low-power RRHs are located inside the coverage area of a macro-BS so that the plane of RRH coverage is overlaid with that of the macro-BS coverage. The difference between scenarios 3 and 4 lies in that each RRH has a distinct cell ID in scenario 3, while RRHs share the same cell ID with the associated macro-BS in scenario 4.

As explained in Sect. 6.1, due to the immature study of CoMP with higher latency/lower capacity backhaul communication (Gesbert et al. 2010), optical fiber-based backhaul with zero latency and infinite capacity (Orange et al. 2011) was

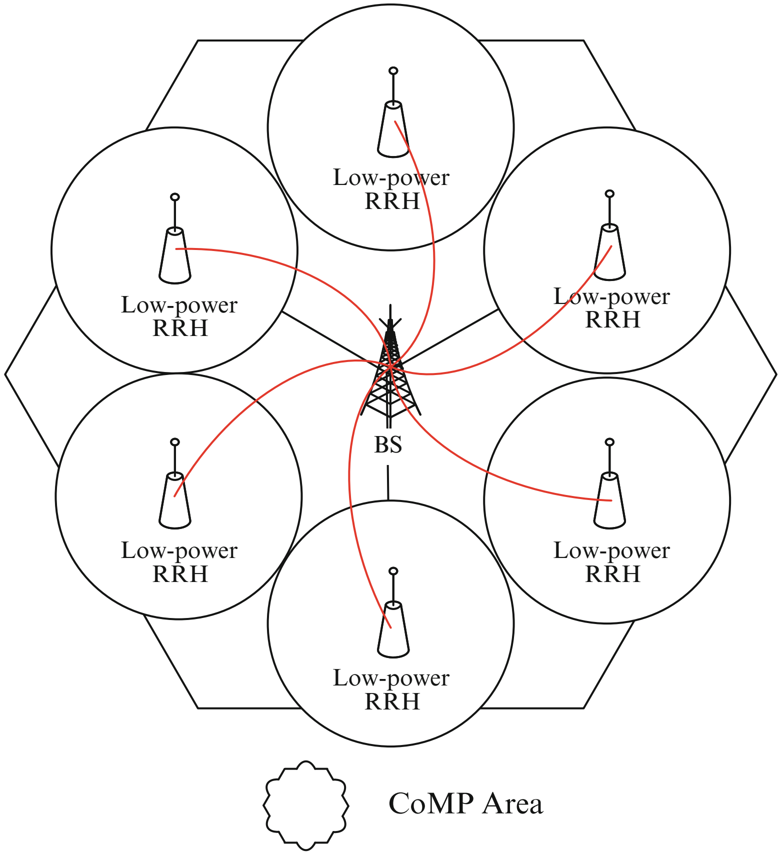

Fig. 7.4 CoMP scenario 3/4: heterogeneous network with low-power RRHs within the macro-cell coverage (1 cell site plotted)

assumed for all the CoMP scenarios in the LTE Release 11 network as a starting point of the working order for the imperfect backhaul issue (Samsung 2010b). In the future, the impact of imperfect backhaul should be carefully investigated for CoMP operations (Ericsson and ST-Ericsson 2011). In particular, for scenarios 2 and 3, RRHs may belong to different BSs, in which case backhaul information exchange may require some additional standardization support (3GPP 2011b).

According to MCC Support (2011a), the CoMP studies were organized into two phases with some priorities set among the defined scenarios. In a first phase, CoMP for scenarios 1 and 2 would be studied to evaluate the potential gains, and this phase was aimed to be concluded in May 2011. In a second phase scheduled to start from Feb 2011, CoMP for heterogeneous deployments, that is, scenarios 3 and 4, would be investigated to show its performance gain in practical systems.

In addition, during the 3GPP RAN1 #63bis meeting and through the following communications on the e-mail reflector, extensive discussions on simulation

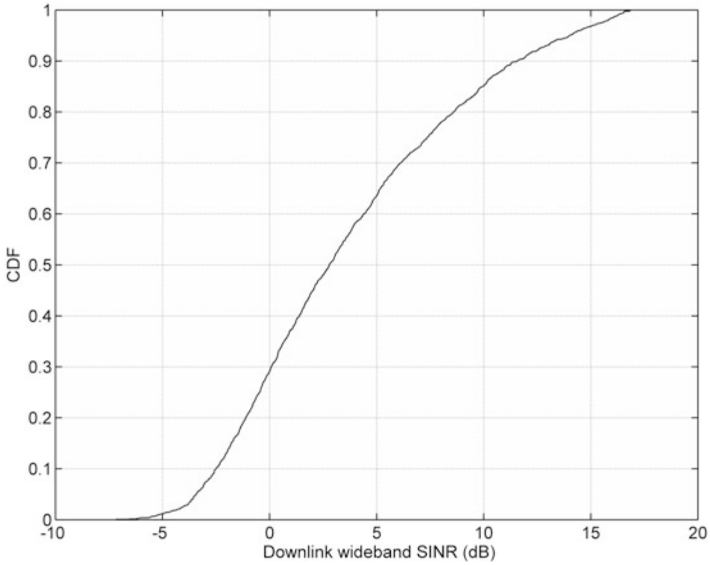

Fig. 7.5 CDF of downlink wideband SINR (3GPP Case 1 with 2D transmission antennas (3GPP 2006))

assumptions were observed. Many companies tried to calibrate their simulators for the convenience of comparing different schemes and evaluating the performance gain. Simulation assumptions included (NTT DOCOMO 2011), for example, performance metrics for full-buffer traffic and non-full-buffer traffics, simulation case (3GPP Case 1 models (3GPP 2006, 2010), or ITU channel model (ITU-R 1997)), node power setting, CoMP transmission schemes, antenna configuration, CSI feedback assumptions, and UE receiver capability.

Based on the agreed simulation assumptions, companies can compare and calibrate their performance curves for some basic configurations so that the cellular infrastructure and system functionalities are modeled correctly. For instance, using a downlink system-level simulator extended from the one addressed in Sect. 5.4, we can obtain the cumulative distribution function (CDF) curves of wideband signal-to-interference-plus-noise ratio (SINR) for 3GPP Case 1 with 2D transmission antennas (3GPP 2006), and 3D transmission antennas (3GPP 2010), as shown in Figs. 7.5 and 7.6, respectively. The results in Figs. 7.5 and 7.6 are in accordance with those calibrated ones provided by a variety of worldwide companies in Ericsson (2009). If large performance deviations from the curves in Figs. 7.5 and 7.6 are observed in some test runs, then the simulator should be double checked and carefully revised until it works properly.

In Feb 2011, at the 3GPP RAN1 #64 meeting, preliminary results for CoMP scenarios 1 and 2 were presented by many companies. However, the disclosed results were drastically diverse among different sources. Thus, it seemed to be necessary to further exchange the updated results in the following meetings (MCC

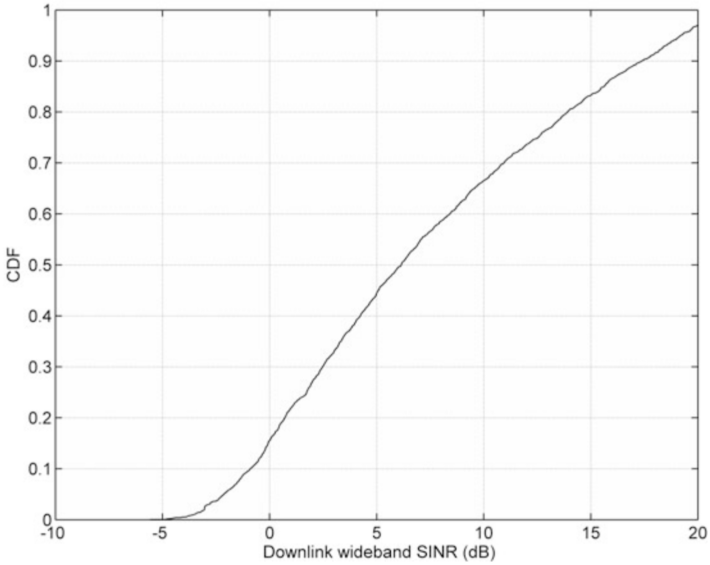

Fig. 7.6 CDF of downlink wideband SINR (3GPP Case 1 with 3D transmission antennas (3GPP 2010))

Support 2011b). Upon the deadline of the first phase of CoMP study, final results for CoMP scenarios 1 and 2 were collected at the 3GPP RAN1 #65 meeting in May 2011 (MCC Support 2011c). An important observation was that the relative CoMP performance gain over the non-CoMP scheme is decreased for high load compared to low load in non-full-buffer traffic model, because idle resources in a low-load system can be activated by CoMP operations to improve the quality of received signals. Besides, the downlink CoMP performance gain seems to be larger in ITU channel models compared with 3GPP Case 1 models. Also at the 3GPP RAN1 #65 meeting, simulation parameter alignment for CoMP study Phase 2 was agreed and the placement of BS, low-power RRH, and UE was regulated as illustrated in Fig. 7.7.

It should be noted that an interesting paper (TI 2011) appeared in a parallel session on the enhanced downlink MIMO, in which it was pointed out that CoMP scenario 4 is actually a single-cell scenario with geographically separated antennas, that is, distributed antenna system (DAS). Thus, the corresponding discussion should be moved from CoMP to the item of enhanced downlink MIMO. Moreover, RRH/antenna selection technologies, that is, the sixth category of multipoint cooperative communication technology (see Sect. 2.7.6.2), were proposed in TI (2011) to improve the spectral efficiency in DAS.

At the 3GPP RAN1 #66 meeting held in Aug 2011, the final evaluation results for CoMP scenarios 3 and 4 were discussed (MCC Support 2011d). It was observed that considerable performance gain can be offered by both downlink and uplink CoMP schemes. In view of the positive evaluation results obtained from the CoMP study item, 3GPP RAN1 concluded that the upcoming work item should specify downlink CoMP operations and investigate the extent to uplink CoMP schemes.

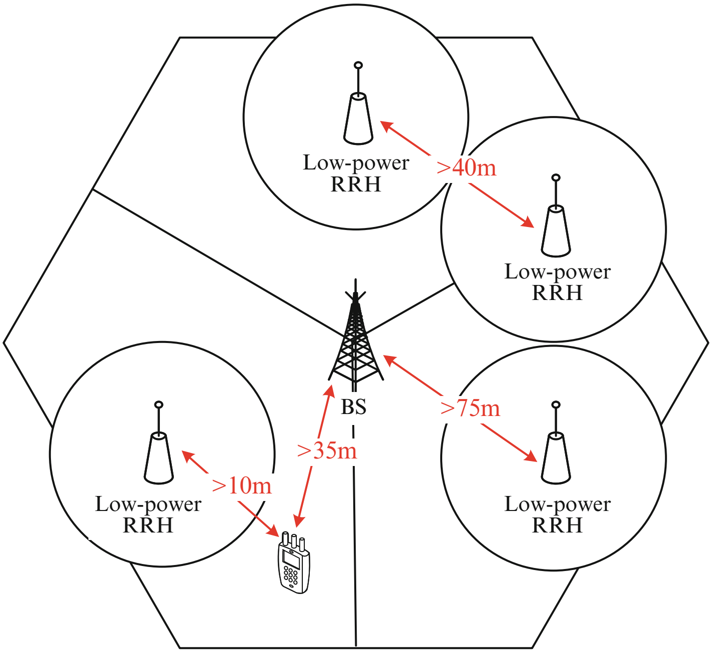

Fig. 7.7 Regulations on the placement of BS, low-power RRH, and UE in CoMP scenario 3/4

7.3 CoMP Schemes in LTE Release 11

During the CoMP study item, a variety of CoMP schemes were identified. All of them have been well covered by our proposed framework of multipoint co-operative communication technologies (see Chap. 2). In this section, we briefly review the downlink and uplink CoMP schemes captured by the LTE Release 11 system (3GPP 2011b). Note that the following CoMP schemes were treated with unequal importance in standardization considering their potential gains and required complexity/overhead. Some recommendations on the work priority of the CoMP schemes can be found in Ericsson et al. (2011) and Huawei et al. (2011).

7.3.1 Downlink CoMP Transmission Schemes

In the downlink CoMP transmission, dynamic coordination among multiple geographically separated transmission points is operated. According to 3GPP (2011b), the term "point" means a set of geographically colocated transmit antennas, which is similar to our definition throughout this book. It should be noted that in CoMP scenario 1, sectors of the same cell site correspond to different points. In the Release

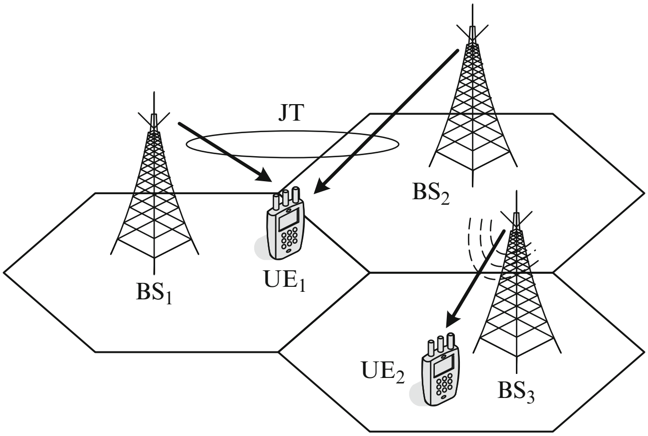

Fig. 7.8 Illustration of a partial JT scheme

11 LTE-A network, two types of downlink CoMP transmission schemes have been identified with high working priority, that is, joint processing (JP) and coordinated scheduling/coordinated beamforming (CS/CB) (3GPP 2011b).

7.3.1.1 Joint Processing

In JP CoMP, both data and CSI are shared among multiple points. If time-frequency synchronized transmission (TFST) is operated, that is, a UE data is simultaneously transmitted from multiple points on a time-frequency resource to improve the received signal quality and/or data throughput, then JP will become joint transmission (JT), which has been discussed in the eighth category of multipoint cooperative communication technology (see Sect. 2.7.8). On the other hand, if non-TFST is allowed, then a UE data will be transmitted from a selected point, possibly with additional muted point(s). This JP scheme degrades to dynamic point selection (DPS) and/or dynamic point blanking (DPB), which has been treated in the sixth category of multipoint cooperative communication technology (see Sect. 2.7.6). It should be noted that DPS and JT schemes can be combined to form a partial JT scheme, in which more than one point, but not all the available points, are selected for JT operation. An illustration of a partial JT scheme is shown in Fig. 7.8, where BS_3 is unselected in the JT for UE_1.

7.3.1.2 Coordinated Scheduling/Coordinated Beamforming

In the second type of downlink CoMP transmission, that is, CS/CB, a UE data is only available at one transmission point but multipoint CSI is exchanged in

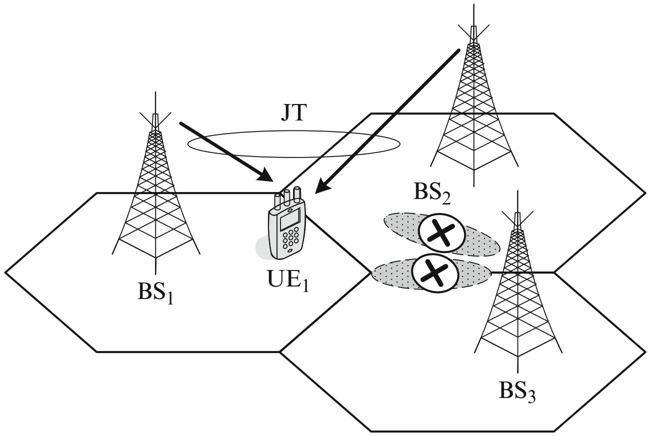

Fig. 7.9 Illustration of a hybrid JP and CS/CB scheme

the network for interpoint coordination of scheduling and/or beamforming. Such scheme belongs to the seventh category of multipoint cooperative communication technology (see Sect. 2.7.7). Note that if point muting is considered, CS/CB schemes will fall into the fifth category of multipoint cooperative communication technology (see Sect. 2.7.5).

In 3GPP (2011b), it also doesn't preclude the possibility of a hybrid JP and CS/CB scheme, which is essentially an interesting combination of the 5th, 6th, 7th, and 8th multipoint cooperative communication technologies. In this general scheme, some points are denoted as JP points and other points serve as CS/CB points. Interpoint CSI is shared among the JP and CS/CB points, but data only arrives at the JP points. Among the JP points, some points will be activated to perform JT, while the CS/CB points will conduct dynamic or semi-static interference coordination. An illustration of a hybrid JP and CS/CB scheme is shown in Fig. 7.9, where BS_1 and BS_2 are performing JT for UE_1 while BS_3 avoids pointing its spatial-domain beams at UE_1 as a CB operation.

7.3.2 Uplink CoMP Reception Schemes

Similar to the downlink CoMP transmission, uplink CoMP reception also features on JP and CS/CB. The uplink JP reception implies joint reception (JR) of the transmitted signal at multiple points to improve the receive SINR, which belongs to the eighth category of multipoint cooperative communication technology (see Sect. 2.7.8). The uplink CS/CB operation involves multicell UE scheduling, power control, low-interference precoder design, etc. The related schemes have been discussed in Sects. 2.7.5 and 2.7.7.

7.4 Specification Works

In standardization activities, identifying the technical schemes is just the first step. Detailed protocols and necessary information provisions should be carefully specified so that the interested schemes can be put to practical use with both the BS and UE knowing how to conduct the operations.

Regarding the downlink CoMP schemes, for scenarios 2–4, inter-BS coordination is obviously needed. Thus, protocols of information exchange over the backhaul links should be designed for BSs. Besides, control signaling should be specified to assist the information acquisition between the BS and UE, such as multicell CSI report from the UE to the BS, enhanced RSs broadcasted from BSs to facilitate the CSI measurement at the UE side, and radio resource control of CoMP schemes configured by the BS. Among the mentioned specification works, the most effort-demanding area is the design of CSI report because it directly impacts the trade-off between system performance and feedback overhead. As have been explained in Sect. 2.6, more CSI generally promises better performance and the problem is that full CSI cannot be obtained at the transmitter side even for the time division duplex (TDD) system. Therefore, to what level and with what contents the CSI shall be provided to the system always arouse hot debates in standardization meetings.

As for the uplink CoMP schemes, the situation is less complicated since the UE is only able to perform simple transmission and most of the signal processing burden is transferred to the BS receiver, which can be left to vendor implementations. Nevertheless, several specification areas include inter-BS data exchange, enhancement of uplink RSs to increase the RS capacity and improve the RS orthogonality, and low-interference-oriented transmission power decrease at UE due to high reliability of multipoint reception or coordination.

7.5 Simulation and Analysis

Large performance gain can be foreseen for the uplink CoMP schemes since any enhanced receiver can achieve performance gains by using advanced signal processing algorithms. Therefore, during the CoMP study item, most simulation efforts were devoted to evaluate the performance of downlink CoMP schemes, where various nonideal assumptions about the BS coordination may offset the theoretical gain promised by the downlink CoMP. In the following, we will review the simulation and analysis results for the downlink CoMP schemes in 3GPP.

In phase I of the performance evaluation for CoMP scenarios 1 and 2, about 20 companies provided their simulation results in Samsung (2011). In spite of the fact that tremendous work had already been devoted to the unification of evaluation methodology and calibration of system-level simulators from various companies, so that comparable results could be obtained from multiple sources to double-check the true gain of CoMP schemes in practical systems, it was a bit discouraging to find that large performance differences still existed in the reported results because the detailed software implementation in each simulator still can be very different among the source companies (see the references in Samsung (2011)). One prominent example of the nontransparent implementation issue is the BS scheduler, which has a significant impact on the distribution of UE throughputs and thus greatly influences the results of cell-edge throughput and the proportional fairness factor of the interested schemes.

The baseline simulation parameters for phase I evaluation can be found in 3GPP (2010, 2011b), and the performance metrics are cell average spectral efficiency in bps/Hz/cell and 5% point cell-edge UE spectral efficiency in bps/Hz/user (3GPP 2011b). From practical considerations, it is assumed that every UE reports CSI based on the assumption of SU MIMO transmission.

For CoMP scenario 1 illustrated in Fig. 7.2, simulations were conducted for frequency division duplex (FDD)/time division duplex (TDD) downlink with closely spaced cross-polarized antenna deployment and full-buffer (FB) traffic for the 3GPP case 1 and ITU channel models. For BS and UE equipped with four and two antennas, respectively, the JT MU-MIMO scheme was shown to achieve an average performance gain about 20–30% in terms of cell-edge UE spectral efficiency as well as some moderate gains in cell average spectral efficiency compared with the single-cell MU-MIMO scheme. On the other hand, the performance gain offered by CS/CB MU MIMO seemed to be rather limited, less than 5% for FDD and around 10% for TDD in terms of cell-edge UE spectral efficiency.

For CoMP scenario 2 illustrated in Fig. 7.3, similar simulation assumptions were adopted as those for CoMP scenario 1. As for the set of cooperating cells, JT in a nine-cell coordination area was considered as the baseline. In addition, uniform linear array (ULA) was considered as an alternative antenna configuration. Similar observations can be drawn for JT and CS/CB when BS and UE are, respectively, equipped with four and two antennas (3GPP 2011b). Besides, a notable finding is that increasing the BS coordination area, that is, conducting CoMP operation among more than nine cells, has a positive effect on CS/CB while it is not helpful for JT because JT MU-MIMO across too many cells will have to sacrifice considerable performance gain in exchange for complexity reduction in practical systems.

In phase II of the performance evaluation for CoMP scenarios 3 and 4, the system-level simulation parameters for the heterogeneous networks are specified in 3GPP (2011b) and a total of 25 companies presented their simulation results. In addition to the traffic model used in CoMP study item phase I, a non-full-buffer model was considered in phase II for simulations of dynamic traffic in hot spots. For FDD systems and FB traffic models, both CS/CB and JP schemes can achieve 25–30% gain in cell-edge UE spectral efficiency compared with a baseline scheme without interference management. Note that the performance gains become even larger for non-full-traffic models because idle resources in a low- or medium-loaded system can be utilized by the network to operate non-time-frequency-synchronized transmission or reception (TFSTR) CoMP schemes, that is, the third, fourth, fifth, and sixth categories of multipoint cooperative communication technologies (see Sect. 2.7).

To sum up, from the performance evaluation results in the 3GPP CoMP study item, it can be concluded that both the downlink and uplink CoMP schemes can offer performance benefits in all defined scenarios. But it is also found that performance of CoMP schemes with spatial information exchange is sensitive to the delay between two transmission points (3GPP 2011b). Therefore, aspects related to the delay issue, such as limited-bit CSI feedback and/or nonideal backhaul conditions, should be further investigated.

7.6 Conclusion

After several years of study in academic communities, the seventh and eighth categories of multipoint cooperative communication technologies were considered to be applied in practical cellular networks, for example, in the LTE Release 10 system. The applications are generally called CoMP transmission or reception. Although the CoMP function is failed to be adopted by the LTE Release 10 specifications due to some incompatible CSI feedback designs with the single-cell MIMO framework, it has eventually come back for the LTE Release 11 standardization. Several interested CoMP schemes have been identified as JT/JR or CS/CB. The corresponding specification works are related to aspects such as backhaul communication protocols, control signaling provision, and multipoint CSI feedback design. The performance evaluation results of various CoMP schemes show that considerable gains can be expected from CoMP, but the multipoint delay issue should be further investigated for practical applications.

References

3GPP (2006) TR 25.814 V7.1.0: physical layer aspects for evolved Universal Terrestrial Radio Access (UTRA) (Release 7). http://www.3gpp.org/ftp/Specs/archive/25_series/25.814/25814-710.zip. Accessed Oct 2006

3GPP (2008) TS 25.213 V8.0.0: physical layer procedures (Release 8). http://www.3gpp.org/ftp/Specs/archive/25_series/25.213/25213-800.zip. Accessed Mar 2008

3GPP (2009a) TR 36.814 V1.0.0: further advancements for E-UTRA: physical layer aspects. http://www.3gpp.org/ftp/Specs/archive/36_series/36.814/36814-100.zip. Accessed Feb 2009

3GPP (2009b) TS 25.213 V9.0.0: physical layer procedures (Release 9). http://www.3gpp.org/ftp/Specs/archive/25_series/25.213/25213-900.zip. Accessed Sept 2009

3GPP (2010) TR 36.814: further advancements for E-UTRA, physical layer aspects. http://www.3gpp.org/ftp/Specs/archive/36_series/36.814/36814-900.zip. Accessed Mar 2010

3GPP (2011a) TS 36.213 V10.1.0: physical layer procedures (Release 10). http://www.3gpp.org/ftp/Specs/archive/36_series/36.213/36213-a10.zip. Accessed Mar 2011

3GPP (2011b) TR 36.819 V11.1.0: coordinated multi-point operation for LTE physical layer aspects (Release 11). http://www.3gpp.org/ftp/Specs/archive/36_series/36.819/36819-b10.zip. Accessed Dec 2011

Alcatel-Lucent (2008a) R1-082812: collaborative MIMO for LTE-A downlink. In: 3GPP TSG RAN WG1 meeting #54, Jeju, Korea, 18–22 Aug 2008. http://www.3gpp.org/ftp/tsg_ran/WG1_RL1/TSGR1_54/Docs/R1-082812.zip
Alcatel-Lucent (2008b) R1-084141: UE PMI feedback signalling for user pairing/coordination. In: 3GPP TSG RAN WG1 #55, Prague, Czech Republic, 10–14 Nov 2008. http://www.3gpp.org/ftp/tsg_ran/WG1_RL1/TSGR1_55/docs/R1-084141.zip
CATT (2008a) R1-084290: proposal of multiple sites coordination for LTE-A TDD. In: 3GPP TSG RAN WG1 meeting #55, Prague, Czech Republic, 10–14 Nov 2008. http://www.3gpp.org/ftp/tsg_ran/WG1_RL1/TSGR1_55/docs/R1-084290.zip
CATT (2008b) R1-083630: a technique to enhance the cell edge performance. In: 3GPP TSG RAN WG1 #54bis, Prague, Czech Republic, September 29–October 3 2008. http://www.3gpp.org/ftp/tsg_ran/WG1_RL1/TSGR1_54b/Docs/R1-083630.zip
Ericsson (2008) R1-084377: downlink coordinated transmission–impact on specification. In: 3GPP TSG-RAN WG1 #55, Prague, Czech Republic, 10–14 Nov 2008. http://www.3gpp.org/ftp/tsg_ran/WG1_RL1/TSGR1_55/docs/R1-084377.zip
Ericsson (2009) R1-092019: summary from email discussion on calibration step1+2. In: 3GPP TSG RAN1 meeting #57, San Francisco, 4–8 May 2009. http://www.3gpp.org/ftp/tsg_ran/wg1_rl1/TSGR1_57/Docs/R1-092019.zip
Ericsson, ST-Ericsson (2011) R1-110452: deployment and backhaul constraints for CoMP. In: 3GPP TSG-RAN1#63bis meeting, Dublin, Ireland, 17–21 Jan 2011. http://www.3gpp.org/ftp/tsg_ran/WG1_RL1/TSGR1_63b/Docs/R1-110452.zip
Ericsson et al (2011) R1-112852: proposal for DL CoMP standardization impact. In: 3GPP TSG-RAN WG1 meeting #66, Athens, Greece, 22–26 Aug 2011. http://www.3gpp.org/ftp/tsg_ran/wg1_rl1/TSGR1_66/Docs/R1-112852.zip
ETRI (2008a) R1-082896: coordinated multi-cell transmission for LTE-advanced downlink. In: 3GPP TSG-RAN WG1 #54, Jeju, South Korea, 18–22 August 2008. http://www.3gpp.org/ftp/tsg_ran/WG1_RL1/TSGR1_54/Docs/R1-082896.zip
ETRI (2008b) R1-084144: per-cell precoding methods for downlink joint processing CoMP. In: 3GPP TSG RAN WG1#55, Prague, Czech Republic, 10–14 Nov 2008. http://www.3gpp.org/ftp/tsg_ran/WG1_RL1/TSGR1_55/docs/R1-084144.zip
ETSI MCC (2010a) Report of 3GPP TSG RAN meeting #47. In: 3GPP TSG RAN #47, Vienna, Austria, 16–19 Mar 2010. http://www.3gpp.org/ftp/tsg_ran/TSG_RAN/TSGR_47/Report/RP-100648.zip
ETSI MCC (2010b) Report of 3GPP TSG RAN meeting #48. In: 3GPP TSG RAN meeting #48, Seoul, Korea, 1–4 June 2010. http://www.3gpp.org/ftp/tsg_ran/TSG_RAN/TSGR_48/Report/RP-100969.zip
ETSI MCC (2010c) Report of 3GPP TSG RAN meeting #49. In: 3GPP TSG RAN meeting #49, San Antonio, 14–17 Sept 2010. http://www.3gpp.org/ftp/tsg_ran/TSG_RAN/TSGR_49/Report/RP-101373.zip
ETSI MCC (2011) Report of 3GPP TSG RAN meeting #50. In: 3GPP TSG RAN meeting #50, Istanbul, Turkey, 7–12 Dec 2010. http://www.3gpp.org/ftp/tsg_ran/TSG_RAN/TSGR_50/Report/RP-110361.zip
ETSI Mobile Competence Centre (MCC) (2008) REV-080060: report of the 3GPP TSG RAN IMT advanced workshop. In: 3GPP TSG RAN IMT advanced workshop, Shenzhen, China, 7–8 Apr 2008. http://www.3gpp.org/ftp/workshop/2008-04-07_RAN_IMT_Advanced/Docs/REV-080060.zip
Gesbert D, Hanly S, Huang H, Shamai S, Simeone O, Wei Y (2010) Multi-cell MIMO cooperative networks: a new look at interference. IEEE J Sel Areas Commun 28(9):1380–1408
Hitachi (2008) R1-083689: proposal of inter cell interference coordination scheme. In: 3GPP TSG RAN WG1 #54bis, Prague, Czech Republic, September 29–October 3, 2008. http://www.3gpp.org/ftp/tsg_ran/WG1_RL1/TSGR1_54b/Docs/R1-083689.zip
Huawei (2008) R1-084352: DL coordinated beam switching for interference management in LTE-advanced. In: 3GPP TSG RAN WG1#55, Prague, Czech Republic, 10–14 Nov 2008. http://www.3gpp.org/ftp/tsg_ran/WG1_RL1/TSGR1_55/docs/R1-084352.zip

Huawei et al (2011) R1-112829; way forward on CoMP performance gains. In: 3GPP TSG-RAN WG1 meeting #66, Athens, Greece, 22–26 Aug 2011. http://www.3gpp.org/ftp/tsg_ran/wg1_rl1/TSGR1_66/Docs/R1-112829.zip
ITU-R (1997) Recommendation ITU-R M.1225: guidelines for evaluation of radio transmission technologies for IMT-2000. http://www.itu.int/dms_pubrec/itu-r/rec/m/R-REC-M.1225-0-199702-I!!PDF-E.pdf. Accessed 1997
LGE (2008) R1-084202: multi-layered rate control for CoMP in LTE-advanced. In: 3GPP TSG RAN WG1#55, Prague, Czech Republic, 10–14 Nov 2008. http://www.3gpp.org/ftp/tsg_ran/WG1_RL1/TSGR1_55/docs/R1-084202.zip
MCC Support (2008a) Final report of 3GPP TSG RAN WG1 #54 v1.0.0. In: 3GPP TSG RAN WG1 #54, Jeju Island, South Korea, 18–22 Aug 2008. http://www.3gpp.org/ftp/tsg_ran/WG1_RL1/TSGR1_54/Report/Final_ReportWG1#54_v100.zip
MCC Support (2008b) Draft report of 3GPP TSG RAN WG1 #54b v0.2.0. In: 3GPP TSG RAN WG1 #54b, Czech Republic, September 29–October 3, 2008. http://www.3gpp.org/ftp/tsg_ran/WG1_RL1/TSGR1_54b/Report/Draft_ReportWG1#54b_v020.zip
MCC Support (2008c) Final report of 3GPP TSG RAN WG1 #55 v1.0.0. In: 3GPP TSG RAN WG1 #55, Czech Republic, 10–14 Nov 2008. http://www.3gpp.org/ftp/tsg_ran/WG1_RL1/TSGR1_55/Report/Final_ReportWG1#55_v100.zip
MCC Support (2009a) Final report of 3GPP TSG RAN WG1 #55bis v3.0.0. In: 3GPP TSG RAN WG1 #55bis, Ljubljana, Slovenia, 12–16 Jan 2009. http://www.3gpp.org/ftp/tsg_ran/WG1_RL1/TSGR1_55b/Report/Final_ReportWG1#55bis_v300.zip
MCC Support (2009b) Final report of 3GPP TSG RAN WG1 #56 v1.0.0. In: 3GPP TSG RAN WG1 #56, Athens, Greece, 9–13 Feb 2009. http://www.3gpp.org/ftp/tsg_ran/WG1_RL1/TSGR1_56/Report/Final_ReportWG1#56_v100.zip
MCC Support (2009c) Final report of 3GPP TSG RAN WG1 #56bis v2.0.0. In: 3GPP TSG RAN WG1 #56bis, Seoul, South Korea, 23–27 Mar 2009. http://www.3gpp.org/ftp/tsg_ran/WG1_RL1/TSGR1_56b/Report/Final_ReportWG1#56b_v200.zip
MCC Support (2009d) Final report of 3GPP TSG RAN WG1 #57 v1.0.0. In: 3GPP TSG RAN WG1 #57, San Francisco, 4–8 May 2009. http://www.3gpp.org/ftp/tsg_ran/WG1_RL1/TSGR1_57/Report/Final_ReportWG1#57_v100.zip
MCC Support (2009e) Final report of 3GPP TSG RAN WG1 #57bis v1.0.0. In: 3GPP TSG RAN WG1 #57bis, Los Angeles, June 29–July 3 2009. http://www.3gpp.org/ftp/tsg_ran/WG1_RL1/TSGR1_57b/Report/Final_ReportWG1#57b_v100.zip
MCC Support (2009f) Final report of 3GPP TSG RAN WG1 #58 v1.0.0. In: 3GPP TSG RAN WG1 #58, Shenzhen, China, 24–28 Aug 2009. http://www.3gpp.org/ftp/tsg_ran/WG1_RL1/TSGR1_58/Report/Final_ReportWG1#58_v100.zip
MCC Support (2009g) Final report of 3GPP TSG RAN WG1 #58bis v1.0.0. In: 3GPP TSG RAN WG1 #58bis, Miyazaki, Japan, 12–16 Oct 2009. http://www.3gpp.org/ftp/tsg_ran/WG1_RL1/TSGR1_58b/Report/Final_ReportWG1#58b_v100.zip
MCC Support (2009h) Final report of 3GPP TSG RAN WG1 #59 v1.0.0. In: 3GPP TSG RAN WG1 #59, Jeju, South Korea, 9–13 Nov 2009. http://www.3gpp.org/ftp/tsg_ran/WG1_RL1/TSGR1_59/Report/Final_ReportWG1#59_v100.zip
MCC Support (2010a) Draft report of 3GPP TSG RAN WG1 #59bis v0.1.0. In: 3GPP TSG RAN WG1 #59bis, Valencia, Spain, 18–22 Jan 2010. http://www.3gpp.org/ftp/tsg_ran/WG1_RL1/TSGR1_59b/Report/Draft_ReportWG1#59b_v020.zip
MCC Support (2010b) Final report of 3GPP TSG RAN WG1 #60 v1.0.0. In: 3GPP TSG RAN WG1 #60, California, 22–26 Feb 2010. http://www.3gpp.org/ftp/tsg_ran/WG1_RL1/TSGR1_60/Report/R1-101711.zip
MCC Support (2010c) Final report of 3GPP TSG RAN WG1 #60bis v1.0.0. In: 3GPP TSG RAN WG1 #60bis, Beijing, China, 12–16 Apr 2010. http://www.3gpp.org/ftp/tsg_ran/WG1_RL1/TSGR1_60b/Report/R1-102601.zip
MCC Support (2010d) Final report of 3GPP TSG RAN WG1 #61 v3.0.0. In: 3GPP TSG RAN WG1 #61, Montreal, Canada, 10–14 May 2010. http://www.3gpp.org/ftp/tsg_ran/WG1_RL1/TSGR1_61/Report/Final_ReportWG1#61_v300.zip

MCC Support (2010e) Draft report of 3GPP TSG RAN WG1 #62 v0.1.0. In: 3GPP TSG RAN WG1 #62, Madrid, Spain, 23–27 Aug 2010. http://www.3gpp.org/ftp/tsg_ran/WG1_RL1/TSGR1_62/Report/Draft_ReportWG1#62_v010.zip

MCC Support (2010f) Draft report of 3GPP TSG RAN WG1 #62bis v0.1.0. In: 3GPP TSG RAN WG1 #62bis, Xian, China, 11–15 Oct 2010. http://www.3gpp.org/ftp/tsg_ran/WG1_RL1/TSGR1_62b/Report/Draft_ReportWG1#62b_v010.zip

MCC Support (2010g) Final report of 3GPP TSG RAN WG1 #63 v1.0.0. In: 3GPP TSG RAN WG1 #63, Florida, 15–19 Nov 2010. http://www.3gpp.org/ftp/tsg_ran/WG1_RL1/TSGR1_63/Report/Final_ReportWG1#63_v100.zip

MCC Support (2011a) Final report of 3GPP TSG RAN WG1 #63bis v1.0.0. In: 3GPP TSG RAN WG1 #63bis, Dublin, Ireland, 17–21 Jan 2011. http://www.3gpp.org/ftp/tsg_ran/WG1_RL1/TSGR1_63b/Report/Final_ReportWG1#63b_v100.zip

MCC Support (2011b) Final report of 3GPP TSG RAN WG1 #64 v1.3.0. In: 3GPP TSG RAN WG1 #64, Taipei, Taiwan, 21–25 Feb 2011. http://www.3gpp.org/ftp/tsg_ran/WG1_RL1/TSGR1_64/Report/Final_ReportWG1#64_v130.zip

MCC Support (2011c) Draft report of 3GPP TSG RAN WG1 #65 v1.0.0. In: 3GPP TSG RAN WG1 #65, Barcelona, Spain, 9–13 May 2011. http://www.3gpp.org/ftp/tsg_ran/WG1_RL1/TSGR1_65/Report/Final_ReportWG1#65_v100.zip

MCC Support (2011d) Final report of 3GPP TSG RAN WG1 #66 v1.0.0. In: 3GPP TSG RAN WG1 #66, Athens, Greece, 22–26 Aug 2011. http://www.3gpp.org/ftp/tsg_ran/WG1_RL1/TSGR1_66/Report/Final_ReportWG1#66_v100.zip

Mitsubishi (2008) R1-084482: low-complexity precoding for LTE-A collaborative MIMO: a signal leakage approach. In: 3GPP TSG RAN WG1#55, Prague, Czech Republic, 10–14 Nov 2008. http://www.3gpp.org/ftp/tsg_ran/WG1_RL1/TSGR1_55/docs/R1-084482.zip

Motorola (2008) R1-084407: coordinated multi-point transmission – exploring possible system operations and UE support. In: 3GPP TSG RAN WG1#55, Prague, Czech Republic, 10–14 Nov 2008. http://www.3gpp.org/ftp/tsg_ran/WG1_RL1/TSGR1_55/docs/R1-084407.zip

Nokia (2008) R1-084322: scalable CoMP solutions for LTE advanced. In: 3GPP TSG RAN WG1#55, Prague, Czech Republic, 10–14 Nov 2008. http://www.3gpp.org/ftp/tsg_ran/WG1_RL1/TSGR1_55/docs/R1-084322.zip

Nortel (2008a) R1-084464: cell clustering for CoMP transmission/reception. In: 3GPP TSG-RAN WG1 #55, Prague, Czech Republic, 10–14 Nov 2008. http://www.3gpp.org/ftp/tsg_ran/WG1_RL1/TSGR1_55/docs/R1-084464.zip

Nortel (2008b) R1-084465: discussion and link level simulation results on LTE-A downlink multi-site MIMO cooperation. In: 3GPP TSG RAN WG1#55, Prague, Czech Republic, 10–14 Nov 2008. http://www.3gpp.org/ftp/tsg_ran/WG1_RL1/TSGR1_55/docs/R1-084465.zip

NTT DoCoMo (2008) R1-084252: views on coordinated multipoint transmission/reception in LTE-advanced. In: 3GPP TSG RAN WG1#55, Prague, Czech Republic, 10–14 Nov 2008. http://www.3gpp.org/ftp/tsg_ran/WG1_RL1/TSGR1_55/docs/R1-084252.zip

NTT DOCOMO (2011) R1-110598: CoMP simulation assumptions. In: 3GPP TSG RAN1 #63bis, Dublin, Ireland, 17–21 Jan 2011. http://www.3gpp.org/ftp/tsg_ran/WG1_RL1/TSGR1_63b/Docs/R1-110598.zip

NTT DOCOMO et al (2010) R1-101599: way forward for CoMP in release 10. In: 3GPP TSG RAN WG1 #60, California, 22–26 Feb 2010. http://www.3gpp.org/ftp/tsg_ran/wg1_rl1/TSGR1_60/Docs/R1-101599.zip

Orange et al (2011) R1-110546: views on CoMP evaluation methodology. In: 3GPP TSG-RAN1#63bis meeting, Dublin, Ireland, 17–21 Jan 2011. http://www.3gpp.org/ftp/tsg_ran/WG1_RL1/TSGR1_63b/Docs/R1-110546.zip

Philips (2008a) R1-084100: multi-cell co-operative beamforming: operation and performance. In: 3GPP TSG RAN WG1#55, Prague, Czech Republic, 10–14 Nov 2008. http://www.3gpp.org/ftp/tsg_ran/WG1_RL1/TSGR1_55/docs/R1-084100.zip

Philips (2008b) R1-084099: interference management for LTE-advanced. In: 3GPP TSG RAN WG1#55, Prague, Czech Republic, 10–14 Nov 2008. http://www.3gpp.org/ftp/tsg_ran/WG1_RL1/TSGR1_55/docs/R1-084099.zip

Qualcomm (2008) R1-084400: coordinated multi-point downlink transmission in LTE-advanced. In: 3GPP TSG RAN WG1#55, Prague, Czech Republic, 10–14 Nov 2008. http://www.3gpp.org/ftp/tsg_ran/WG1_RL1/TSGR1_55/docs/R1-084400.zip

Samsung (2008) R1-084173: inter-cell interference mitigation through limited coordination. In: 3GPP TSG RAN WG1#55, Prague, Czech Republic, 10–14 Nov 2008. http://www.3gpp.org/ftp/tsg_ran/WG1_RL1/TSGR1_55/docs/R1-084173.zip

Samsung (2010a) RP-101425: revised SID proposal: coordinated multi-point operation for LTE. In: 3GPP TSG RAN#50, Istanbul, Turkey, 7–10 Dec 2010. http://www.3gpp.org/ftp/tsg_ran/TSG_RAN/TSGR_50/Docs/RP-101425.zip

Samsung (2010b) RP-101425: revised SID proposal: coordinated multi-point operation for LTE. In: 3GPP TSG RAN#50 meeting, Istanbul, Turkey, 7–10 Dec 2010. http://www.3gpp.org/ftp/tsg_ran/TSG_RAN/TSGR_50/Docs/RP-101425.zip

Samsung (2011) R1-111944: RAN1 phase 1 CoMP results. In: 3GPP TSG RAN WG1 Meeting #65, Barcelona, Spain, 9–13 May 2011. http://www.3gpp.org/ftp/tsg_ran/WG1_RL1/TSGR1_65/Docs/R1-111944.zip

Samsung et al (2010) RP-100370: new study item proposal: coordinated multi-point operation for LTE. In: TSG RAN meeting #47, Vienna, Austria, 16–19 Mar 2010. http://www.3gpp.org/ftp/tsg_ran/tsg_ran/TSGR_47/Docs/RP-100370.zip

Texas Instruments (2011) R1-111342: Rel.11 DL MIMO enhancements for single-cell with RRHs. In: 3GPP TSG RAN WG1 65, Barcelona, Spain, 9–13 May 2011. http://www.3gpp.org/ftp/tsg_ran/WG1_RL1/TSGR1_65/Docs/R1-111342.zip

TI (2008) R1-084444: aspects of cooperative MIMO for advanced E-UTRA. In: 3GPP TSG RAN WG1#55, Prague, Czech Republic, 10–14 Nov 2008. http://www.3gpp.org/ftp/tsg_ran/WG1_RL1/TSGR1_55/docs/R1-084444.zip

Vodafone et al (2010) R1-100764: proposal for intra-eNB/inter-site eNB CoMP. In: 3GPP TSG RAN WG1 meeting #59bis, Valencia, Spain, 18–22 Jan 2010. http://www.3gpp.org/ftp/tsg_ran/WG1_RL1/TSGR1_59b/Docs/R1-100764.zip

ZTE (2008a) R1-082847: on consideration for CoMP in LTE-A. In: 3GPP TSG-RAN WG1 #54, Jeju, South Korea, 18–22 Aug 2008. http://www.3gpp.org/ftp/tsg_ran/WG1_RL1/TSGR1_54/Docs/R1-082847.zip

ZTE (2008b) R1-083611: consideration on COMP antenna port mapping in LTE-A. In: 3GPP TSG RAN WG1 #54bis, Prague, Czech Republic, September 29–October 3 2008. http://www.3gpp.org/ftp/tsg_ran/WG1_RL1/TSGR1_54b/Docs/R1-083611.zip

ZTE (2008c) R1-084115: downlink CoMP transmitting scheme based on beamforming. In: 3GPP TSG RAN WG1#55, Prague, Czech Republic, 10–14 Nov 2008. http://www.3gpp.org/ftp/tsg_ran/WG1_RL1/TSGR1_55/docs/R1-084115.zip

Chapter 8
Common Feedback Framework for Downlink CoMP

Abstract In this chapter, we address the common feedback framework (CFF) for downlink coordinated multipoint (CoMP) transmissions in Long-Term Evolution (LTE) Release 11 networks. First, we introduce the work item of CoMP in LTE Release 11 and the ambitious goal of standardizing a CFF to support all interested CoMP schemes. Second, we discuss four candidates of CFF options, with the emphases on feedbacks of co-phase information (CFF option 2) and aggregated CQI (CFF option 3). From system-level simulation results, it can be observed that both CFF options 2 and 3 are able to offer considerable cell-edge throughput gains compared with the non-CoMP scheme. Third, we review the relevant standardization activities and explain why it is another CFF option that will eventually be adopted in LTE Release 11. Finally, some concluding remarks are provided to forecast the further development of CoMP CFF in the future.

Keywords CoMP • CSI feedback • Common feedback framework • Co-phase • Aggregated CQI • System-level simulation • LTE Release 11 • LTE Release 12

8.1 Introduction

As have been discussed in Chap. 7, downlink coordinated multipoint (CoMP) transmission and uplink CoMP reception are considered for LTE Release 11 in order to improve the coverage of high data rates and to increase the cell-edge throughput as well as the overall throughput. At the Third Generation Partner Project (3GPP) technical specification group (TSG) radio access network (RAN) #50 meeting, a 9-month study item on CoMP operation was agreed for LTE Release 11 networks (Samsung 2010). The performance gains and standardization impacts of CoMP were the primary targets of this study item, which had been successfully closed in September 2011. The decisive conclusion of this study item was that both downlink and uplink CoMP operations can offer considerable gains in homogeneous and

M. Ding and H. Luo, *Multi-point Cooperative Communication Systems: Theory and Applications*, Signals and Communication Technology, DOI 10.1007/978-3-642-34949-2_8,

heterogeneous scenarios. As a result, a CoMP work item description proposal was treated and adopted during the 3GPP TSG RAN #53 meeting (3GPP 2011a).

As a start point of the CoMP work item, a general working assumption was agreed at the 3GPP TSG RAN working group 1 (WG1) (shorten as 3GPP RAN1 hereafter) #66bis meeting (MCC Support 2011a), which aimed to standardize a common feedback/signaling framework suitable for CoMP scenarios 1∼4 (see Sect. 7.2.3) that can support all the interested downlink CoMP transmissions, that is, DPS/DPB, JT, and CS/CB (see Sect. 7.3). Most research scientists and engineers in this field were quite enthusiastic about the common feedback framework (CFF) because it might eventually offer a total solution for CoMP so that all fragmented designs, for example, CSI feedback for DPS in CoMP scenario 3 or that for JT in CoMP scenario 4, could be unified into one design. To begin with, the playground of the CFF was set to be rather large. According to MCC Support (2011a), the CFF should be composed from one or more of the following, including at least one of the first three sub-bullets:

- Aggregated feedback across multiple channel state information (CSI)-reference signal (RS) resources
- Per-CSI-RS-resource feedback with inter-CSI-RS-resource feedback
- Per-CSI-RS-resource feedback
- Per-cell Release 8 common reference signal (CRS)-based feedback

It should be noted that CSI-RS is the RS for CSI measurement in LTE Release 10/11, while CRS is the predecessor of CSI-RS for legacy UEs in LTE Release 8/9. Main features of CSI-RS include low density in time-frequency domain and UE-specific configuration. So CSI-RS is suitable for the support of BS with a large number of antennas and that of flexible association between logical antenna ports and UEs. It should also be noted that the definition of "CSI-RS resource" is even more general than that of "point" in CoMP. According to 3GPP (2011b), the term "point" means a set of geographically colocated transmit antennas, while a CSI-RS resource corresponds to a number of logical antenna ports that may be mapped from a set of non-colocated antennas 3GPP (2011c).

Following the working assumption, various CFF schemes were proposed by many companies and extensively discussed in the 3GPP RAN1#67 meeting at the end of year 2011. A preliminary way-forward proposal (Alcatel-Lucent et al. 2011) was crafted trying to narrow down the CFF candidates as follows:

- CoMP CSI feedback in LTE Release 11 should support reporting inter-CSI-RS-resource feedback on top of per-CSI-RS-resource feedback.

  1. Inter-CSI-RS-resource feedback includes at least co-phase information.
  2. Inter-CSI-RS-resource feedback reporting is configurable.
  3. When configured, N bits are used to report the inter-CSI-RS-resource feedback between two per-CSI-RS-resource feedback (further study whether $N = 2$, 3, or 4).

The mentioned co-phase information refers to the per-BS phase prerotation factor addressed in the weighted local precoding (WLP) scheme (see Sect. 5.2.2.3). Although this way-forward proposal was not agreed due to immature study on CoMP CFF, the interested companies were encouraged to continue the discussions, particularly investigating how many bits should be required for the CSI feedback (MCC Support 2011b).

8.2 Candidates of Common Feedback Framework

8.2.1 CFF Option Matrix

Before following the discussions led by Alcatel-Lucent et al. (2011), it is beneficial to perform a full analysis of CoMP CFF options in order to get a large picture about the design principles in this area. According to MCC Support (2011a, b), it is quite safe to conclude that per-CSI-RS-resource feedback provides the most basic CSI elements for CoMP operations; thus, it should be the baseline for the CFF design. On top of that, we may add inter-CSI-RS-resource feedback and/or aggregated feedback to create more advanced CFF schemes. Hence, all the papers on CFF at the 3GPP RAN1#67 meeting can be classified into four categories summarized in a 2×2 matrix shown in Table 8.1. The two dimensions of this CFF option matrix, respectively, indicate whether inter-CSI-RS-resource feedback is required and whether aggregated feedback should be operated.

Table 8.1 CoMP CFF options (till the 3GPP RAN1#67 meeting)

	With aggregated feedback	*Without* aggregated feedback
With inter-CSI-RS-resource feedback	Option 1 Supporters: Huawei and HiSilicon (2011a, b), New Postcom (2011a, b), ZTE (2011a, b), Panasonic (2011), InterDigital and LLC (2011a, b), Marvell (2011), Motorola (2011), RIM (2011), and Hitachi and LLC (2011)	Option 2 Supporters: Huawei and HiSilicon (2011a, b), Intel (2011a, b), Sony (2011), Sharp (2011), Alcatel-Lucent (2011), Qualcomm (2011), CATT (2011), and LG (2011a)
Without inter-CSI-RS-resource feedback	Option 3 Supporters: Huawei and HiSilicon (2011a, b), Intel (2011a, b), Texas Instruments (2011), Motorola (2011), Fujitsu (2011), Ericsson and ST-Ericsson (2011), RIM (2011), Hitachi and LLC (2011), and LG (2011a, b)	Option 4 Supporters: Texas Instruments (2011), Motorola (2011), Samsung (2011), Nokia Siemens and Nokia (2011a), and Hitachi (2011)

In CFF option 1, inter-CSI-RS-resource co-phase information feedback was recommended by ZTE (2011a), Panasonic (2011), and Motorola (2011). The authors of Huawei and HiSilicon (2011a, b) took a further step to propose that not only co-phase information but magnitude information should be included in the contents of inter-CSI-RS-resource feedback. Similar opinions can be found in Marvell (2011) that the overhead of 2 bits for co-phase reporting and optional 2 bits for magnitude reporting seemed to be quite efficient. Moreover, ZTE (2011b) addressed how aggregated statistical interference information can help to implicitly derive the CQIs for various CoMP transmissions, while Panasonic (2011) and InterDigital and LLC (2011b) favored aggregated CQI feedback in order to facilitate JT operations. Furthermore, the rank restriction issue of aggregated CQI was considered in Motorola (2011). The authors of Huawei and HiSilicon (2011a, b) also agreed with Panasonic (2011) and InterDigital and LLC (2011b) that additional aggregated CQI feedback might be useful for DPS/CB operations. Proposals in New Postcom (2011a) and New Postcom (2011b) required that the overhead of inter-CSI-RS-resource feedback should be less than 2 bits and legacy design principles should be adopted to design the codebook of channel direction component for aggregated PMI feedback. However, the idea of aggregated PMI was generally not so popular, though it was briefly addressed in other papers (Huawei and HiSilicon 2011a; RIM 2011; Hitachi and LLC 2011), where configurations of aggregated CSI reporting were discussed.

In CFF option 2, co-phase information was supported by many companies as the major content of inter-CSI-RS-resource feedback, with common rank restriction (Intel 2011b; CATT 2011; LG 2011a), or without any rank restriction (Intel 2011a; Sony 2011; Sharp 2011; Alcatel-Lucent Shanghai 2011; Qualcomm 2011). A reasonable overhead of co-phase information was probably 2$\sim$3 bits per CSI-RS resource according to LG (2011a) and Alcatel-Lucent (2011). Besides, other contents such as magnitude information were addressed in Huawei and HiSilicon (2011a, b) and Alcatel-Lucent (2011). However, aggregated feedback wasn't well received by the companies supporting CFF option 2. For instance, the authors of Huawei and HiSilicon (2011b) argued that aggregated CQI could be derived from per-CSI-RS-resource CQIs.

In CFF option 3, emphasis was laid on the comparison of the effectiveness of aggregated PMI and that of aggregated CQI, both without reporting of inter-CSI-RS-resource information (Huawei and HiSilicon 2011a, b; Intel 2011a, b; Texas Instruments 2011; Fujitsu 2011; Ericsson and ST-Ericsson 2011; LG 2011a, b). Among them, the authors of Texas Instruments (2011), Fujitsu (2011), Ericsson and ST-Ericsson (2011), LG (2011a, b) expressed their preference toward the feedback of aggregated CQI over that of aggregated PMI. At first glance, reporting aggregated CQI alone can only support noncoherent JT, which may seem inadequate for coherent JT operations. However, we may think noncoherent JT as a form of opportunistic coherent JT, that is, sometimes dummy co-phase information happens to be optimal to perform a coherent JT. And the opportunity of such event can be well captured by the report of a high aggregated CQI, which will later be exploited by the BS scheduler. The above reason explains why Texas Instruments

(2011), Ericsson and ST-Ericsson (2011), LG (2011a, b) asserted that considerable gains could be expected from noncoherent JT. However, whether the BS scheduler can indeed enjoy the opportunities of coherent JT using CFF, option 3 depends on many factors, such as the availability of accurate aggregated CQI, the system bandwidth, the number of CoMP UEs, and the extent of frequency selectivity in the composite JT channel. The author of Fujitsu (2011), on the other hand, resorted to another approach that co-phase information could be implicitly reported when UE jointly selecting multiple per-CSI-RS-resource PMIs, that is, the global precoding (GP) scheme (see Sect. 5.2.2.1). Thus, the feedback of aggregated CQI alone was sufficient.

In CFF option 4, the authors of Texas Instruments (2011) and Nokia Siemens and Nokia (2011a) were major opponents to any kind of new CSI reporting on top of the per-CSI-RS-resource feedback. Concerns in Texas Instruments (2011) and Nokia Siemens and Nokia (2011a) were mainly focused on marginal performance gains, inter-CSI-RS-resource synchronization problems, and substantial specification efforts. Furthermore, CFF option 4 also included other interesting CFF designs besides those in CFF option 1∼3, such as the independent precoding CoMP scheme (Motorola 2011), the dynamic selection of CSI-RS-resource feedback at the UE side (Samsung 2011), and the new feedback contents of eigenvector and eigenvalue information per CSI-RS resource (Hitachi 2011).

Finally, a more high-level CoMP CFF can be found in Huawei and HiSilicon (2011a), wherein network-centric semi-static configuration of CoMP CFF among CFF options 1, 2, and 3 was proposed.

8.2.2 Discussions on CFF Options

In CFF option 2, each UE needs to feed back not only a PMI for each CSI-RS resource in the CoMP cooperating set but also the co-phase information and possibly amplitude difference among multiple CSI-RS resources. The serving transmission point (TP) then sends the per-CSI-RS-resource PMI(s) and co-phase information to non-serving TP(s) in the CoMP cooperating set to generate distributed precoding matrices for JT operations. Suppose that the number of non-serving TPs is B, then the optimal relative phase θ_i of the i-th ($i \in \{1, 2, \ldots, B\}$) non-serving TP can be found by exhaustive search described as

$$\left\{\theta_1^{\text{opt}}, \ldots, \theta_i^{\text{opt}}, \ldots, \theta_B^{\text{opt}}\right\} = \underset{\theta_i \in \boldsymbol{\Omega},\, i \in \{1,2,\ldots,B\}}{\arg\max} \left\{ \text{gen\_CQI} \left(\mathbf{H}_0 \mathbf{F}_0 + \sum_{i=1}^{B} \mathbf{H}_i \mathbf{F}_i \mathrm{e}^{\mathrm{j}\theta_i} \right) \right\}, \tag{8.1}$$

where $\boldsymbol{\Omega}$ is the codebook for θ_i. Here, we consider a simple co-phase codebook that equally divides a unit circle into 2^n segmentations and n is the number of quantization bits for co-phase information. Then $\boldsymbol{\Omega}$ can be represented as

$$\Upsilon : \omega_i = \frac{2\pi i}{2^n}, \quad i \in \{0, 1, \ldots, 2^n - 1\}. \tag{8.2}$$

Besides, in (8.1), $\mathbf{H}_0$ is the matrix between the serving TP and the UE, $\mathbf{F}_0$ is the precoding matrix at the serving TP, $\mathbf{H}_i$ is the channel matrix between the i-th non-serving TP and the UE, and $\mathbf{F}_i$ is the precoding matrix at the i-th non-serving TP. Function gen_CQI $(\cdot)$ generates the CQI of the effective channel according to a 4-bit CQI table defined in 3GPP (2011e). Note that in academic research, (8.1) usually takes a more general form shown in Sect. 5.2.2.3, where the CQI in (8.1) is replaced by a capacity metric defined in the information theory. Considering coherent JT, the estimated aggregated CQI derived at the serving TP can be roughly written as

$$Agg\_CQI^{\text{Est}}_{\text{Co-JT}} = \sum_{i=0}^{B} CQI_i + 2 \times \sum_{i=0}^{B-1} \sum_{k=i+1}^{B} \sqrt{CQI_i CQI_k} \times \mathrm{E}\left\{\cos\left(\varphi_{i,k}\right)\right\}, \tag{8.3}$$

where CQI_i is the per-CSI-RS-resource CQI for the i-th TP with interference out of the CoMP cooperating set (NTT 2012b), $\mathrm{E}\{\cdot\}$ is the expectation operator, and $\varphi_{i,k}$ is the residual phase error between the i-th and the k-th TP. $\mathrm{E}\{\cos(\varphi_{i,k})\}$ can be obtained from numerical simulation or can be directly derived according to Wu et al. (2011) as

$$\mathrm{E}\left\{\cos\left(\varphi_{i,k}\right)\right\} = \frac{2^{2n}}{2\pi^2}\left(1 - \cos\left(\frac{2\pi}{2^n}\right)\right). \tag{8.4}$$

If the co-phase information is used to facilitate the CQI computation in noncoherent JT, then an alternative formula for the estimated aggregated CQI can be found in (NTT 2011) shown as

$$Agg\_CQI^{\text{Est}}_{\text{NonCo-JT}} = \sum_{i=0}^{B} CQI_i + 2 \times \sum_{i=0}^{B-1} \sum_{k=i+1}^{B} \sqrt{CQI_i CQI_k} \times \cos\left(\theta_i^{\text{opt}} + \theta_k^{\text{opt}}\right). \tag{8.5}$$

It should be noted that although (8.3) and (8.5) exhibit similar mathematical forms, the transmission schemes represented by these two equations are totally different. The expectation of $Agg\_CQI^{\text{Est}}_{\text{Co-JT}}$ can be as high as $\sum_{i=0}^{B} CQI_i + 2 \times \sum_{i=0}^{B-1} \sum_{k=i+1}^{B} \sqrt{CQI_i CQI_k}$ if n approaches infinite, which achieves the full array gain of coherent JT. On the other hand, the expectation of $Agg\_CQI^{\text{Est}}_{\text{NonCo-JT}}$ is only $\sum_{i=0}^{B} CQI_i$ considering $\mathrm{E}\left\{\cos\left(\theta_i^{\text{opt}} + \theta_k^{\text{opt}}\right)\right\} = 0$, which suffers from considerable SINR loss caused by noncoherent signal combining. In order to make full use of the reported co-phase information, we suppose that we should evaluate the performance of co-phase feedback (CFF option 2) based on (8.3), not based on (8.5) proposed in (NTT 2011). It should be noted that the form of the CQI result in (8.3) is similar to that of the theoretical SINR result in (5.64).

Furthermore, in CFF option 1, the aggregated CQI resulted from $\left\{\theta_i^{\text{opt}}\right\}$ is fed back to the serving TP, and it is given by

$$Agg\_CQI_{\text{Co-JT}}^{\text{FB}} = \text{gen\_CQI}\left(\mathbf{H}_0\mathbf{F}_0 + \sum_{i=1}^{B}\mathbf{H}_i\mathbf{F}_i \mathrm{e}^{\mathrm{j}\theta_i^{\text{opt}}}\right). \tag{8.6}$$

In CFF option 3, co-phase is not required and can be assumed to be zero. And hence, the reported aggregated CQI of the noncoherent JT scheme can be readily obtained from (8.6) with $\theta_i^{\text{opt}} = 0$, yielding

$$Agg\_CQI_{\text{NonCo-JT}}^{\text{FB}} = \text{gen\_CQI}\left(\sum_{i=0}^{B}\mathbf{H}_i\mathbf{F}_i\right). \tag{8.7}$$

To complete the analysis of CFF options, we briefly discuss CFF option 4, in which neither co-phase nor aggregated CQI is reported from the UE. A straightforward way for the serving TP to estimate the aggregated CQI for JT is to blindly assume $\cos\left(\theta_i^{\text{opt}} + \theta_k^{\text{opt}}\right) = 0$ in (8.5), which leads to

$$Agg\_CQI_{\text{NonCo-JT}}^{\text{Blind-Est}} = \sum_{i=0}^{B} CQI_i. \tag{8.8}$$

Other practical issues should also be considered for CFF options 1 and 2, such as outdated co-phase information and inter-CSI-RS-resource frequency errors. The outdated co-phase information is caused by the delay from the measurement of co-phase to the actual JT transmission using co-phase, which can be divided into three parts, that is, transmission time intervals (TTIs) from measurement to feedback, those from feedback to scheduling, and those from scheduling to transmission. Let the three parts of co-phase delay be sequentially denoted as "delay1," "delay2," and "delay3," which are illustrated in Fig. 8.1. Usually, "delay1" and "delay3" are constant values, the sum of which can be represented by a parameter L_{13}^{JT}, while "delay2" is upper bounded by the co-phase feedback periodicity T_{coph}. When evaluating the performance of JT, the impact of L_{13}^{JT} and T_{coph} should be carefully investigated.

Another potential issue of inter-CSI-RS-resource co-phase feedback is that the performance of coherent JT degrades in the presence of frequency error due to the unreliable co-phase information (Nokia Siemens and Nokia 2011b). In fact this issue is not as severe as it may seem. According to NEC et al. (2011), a frequency offset of 30 Hz was assumed between different frequency carriers, and hence, similar value can be assumed for CoMP cases. Obviously, a frequency offset of 30 Hz will not

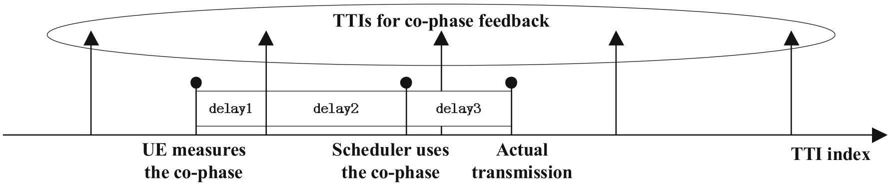

Fig. 8.1 Illustration of co-phase delays

pose a serious problem for the validity of co-phase information from the simulation results provided in Nokia Siemens and Nokia (2011b).

8.2.3 Co-phase Versus Aggregated CQI

At the 3GPP RAN1 #68 meeting, a follow-up way-forward proposal (Huawei et al. 2012a) was presented that CoMP CSI feedback should support reporting inter-CSI-RS-resource co-phase information in addition to per-CSI-RS-resource PMI. Besides, the inter-CSI-RS-resource co-phase feedback is configurable, that is, the system should allow for switch between CFF options 2 and 4. If configured, the corresponding co-phase bits are at least 2 for rank-one CoMP transmission. Regarding this way-forward proposal, many concerns were raised about the performance gain of inter-CSI-RS-resource co-phase compared with aggregated CQI and the respective overhead costs (3GPP 2012). Thereby, the fight between the inter-CSI-RS-resource co-phase (CFF option 2) and the aggregated CQI (CFF option 3) became the focus of discussions during the CoMP session. Since both CFF options were supported by numerous companies, no agreement was reached at the 3GPP RAN1#68 meeting (MCC Support 2012a). But it was reconfirmed that CSI feedback for CoMP should at least include per-CSI-RS-resource feedback, that is, at least CFF option 4 should be supported (MCC Support 2012a). To continue our analysis of the CoMP CFF options, Table 8.1 is updated to Table 8.2 based on new inputs provided by various sources at the 3GPP RAN1#68 meeting.

In CFF option 1, the authors of Huawei and HiSilicon (2012a, c) proposed that if the co-phase feedback were adopted, then aggregated CSI such as some sort of interference information should also be needed. Otherwise, aggregated PMI should be introduced. In ZTE (2012b), it was shown that for low-rank JT inter-CSI-RS-resource co-phasing was beneficial, while for high-rank JT aggregated PMI might be useful. Moreover, aggregated CQI should be further studied. The rank restriction issue for JT was discussed in LG (2012b, c) and Motorola (2012a). The former two papers derived the JT rank as the minimum of all per-CSI-RS-resource ranks and indicated that aggregated CQI should be useful especially for high-rank SU JT. On the other hand, the author of Motorola (2012a) argued that JT rank should be the maximum of all per-CSI-RS-resource ranks due to reduced channel correlation

Table 8.2 CoMP CFF options (till the 3GPP RAN1#68 meeting)

	With aggregated feedback	*Without* aggregated feedback
With inter-CSI-RS-resource feedback	Option 1 Supporters: Huawei and HiSilicon (2012a, c), ZTE (2012b), LG (2012b, c), and Motorola (2012a)	Option 2 Supporters: Huawei and HiSilicon (2012a, b), CHTTL (2012), Hitachi (2012a), Sharp (2012), ZTE (2012a), Alcatel-Lucent (2012), Qualcomm (2012a), ITRI (2012), CATT (2012a, b), and LG (2012a)
Without inter-CSI-RS-resource feedback	Option 3 Supporters: Intel (2012a, b), Renesas (2012b, c, d), Motorola (2012b), MediaTek (2012a, b, c), Fujitsu (2012), Ericsson and ST-Ericsson (2012a, b), and Nokia Siemens and Nokia (2012b)	Option 4 Supporters: Samsung (2012a), Hitachi (2012b), Renesas (2012a), NTT (2012a, b), Texas Instruments (2012), and Nokia Siemens and Nokia (2012a)

among the distributed JT points. Besides, it was addressed in ZTE (2012b) and Motorola (2012a) that co-phase should be useful for rank-one JT, while it was discussed in LG (2012c) and Motorola (2012a) that aggregated CQI could help to improve the performance of rank-two JT.

In CFF option 2, the authors of Huawei and HiSilicon (2012a, b) proposed that the number of co-phase bits should be four and co-phase reporting could be turned off by network configuration. However, most companies wanted to keep the co-phase overhead as low as 2 bits (CHTTL 2012; Sharp 2012; ZTE 2012a; Alcatel-Lucent 2012; CATT 2012a, b; LG 2012a), though this overhead issue might be revisited for high-rank JT later (Sharp 2012; ZTE 2012a). Other contents such as timing offset information and magnitude information were addressed in Qualcomm (2012a) and ITRI (2012), respectively. Besides, the authors of CHTTL (2012) and Hitachi (2012a), respectively, encouraged further study of aggregated CQI and aggregated PMI; thus, they were open with CFF option 1.

In CFF option 3, a large portion of efforts was dedicated to show that noncoherent JT with aggregated CQI feedback can achieve good performance close to that of CFF option 1 (Renesas 2012b, c; Motorola 2012b; MediaTek 2012a, b, c; Ericsson and ST-Ericsson 2012a); thus, the feedback of aggregated CQI alone is sufficient to support JT. Further justification of aggregated CQI can be found in Renesas (2012d) and Ericsson and ST-Ericsson (2012b) that implicit derivation of JT CQI based on per-CSI-RS-resource CQIs seemed to be not very accurate. In addition, it was addressed in Intel (2012a, b) and Motorola (2012b) that aggregated CQI should be adopted for high-rank JT especially for cross-polarized antenna setups, and interference measurement for JT should also be carefully considered. Some potential supporters of CFF option 3 include the authors of Qualcomm (2012b) and Nokia Siemens and Nokia (2012b) because they expressed some interests in aggregated CQI at the meeting.

In CFF option 4, most papers are resubmissions. The authors of Texas Instruments (2012) and Nokia Siemens and Nokia (2012a), reinforced by those of Renesas (2012a), and NTT (2012a, b), objected to adopt any new kind of CSI reporting on top of the per-CSI-RS-resource feedback. Furthermore, two interesting CFF designs were re-proposed, that is, dynamic selection of CSI-RS-resource feedback at the UE side (Samsung 2012a) and new feedback contents of eigenvector and eigenvalue information per CSI-RS resource (Hitachi 2012b).

A noteworthy observation from Table 8.2 is that the forces in CFF option 3 have been growing substantially stronger thanks to new comers such as the authors of Renesas (2012b, c), and MediaTek (2012a, b, c). Although the companies in CFF option 2 still outnumber those in CFF option 3, rugged resistance from the side of CFF option 3 can be expected in the following 3GPP RAN1 meetings.

8.3 Performance Evaluation

8.3.1 Simulation Description

At the 3GPP RAN1#68 meeting, many companies that have presented negative views on co-phase feedback (NTT 2012b; MediaTek 2012c; Renesas 2012a; Motorola 2012a; Ericsson and ST-Ericsson 2012a) argued that the performance gain offered by CFF option 1 over CFF option 3 cannot justify the additional feedback of co-phase. However, it seemed that the true value of co-phase information should be revealed based on the comparison between CFF options 2 and 3, not between CFF options 1 and 3, because we are concerned with the co-phase information alone, not the additional co-phase information on top of the aggregated CQI feedback.

In order to investigate the performance of various CFF options, we conduct system-level simulations (see Sect. 4.4.1) to compare the throughput performance for six schemes as follows:

1. Baseline scheme: SU single-cell processing (SCP) scheme. Overhead in addition to per-CSI-RS-resource feedback is 0 bit per frequency sub-band.
2. Scheme (a): Noncoherent SU JT of CFF option 4, in which the estimated aggregated CQI is derived from per-CSI-RS-resource CQIs as shown in (8.8). Overhead in addition to per-CSI-RS-resource feedback is 0 bits per frequency sub-band.
3. Scheme (b): Noncoherent SU JT of CFF option 3, in which the reported aggregated CQI is computed according to (8.7) with the periodicity of aggregated CQI feedback being $T_{\mathrm{aggCQI}} = 10$ ms. Overhead in addition to per-CSI-RS-resource feedback is 4 bits per frequency sub-band.
4. Scheme (c): Noncoherent SU JT of CFF option 2 (lower bound), in which the estimated aggregated CQI is obtained from (8.5) with the periodicity of co-phase feedback being $T_{\mathrm{coph}} = 10$ ms. Overhead in addition to per-CSI-RS-resource

feedback is 2 bits (2-CSI-RS-resource JT) or 4 bits (3-CSI-RS-resource JT) of co-phase information per frequency sub-band.

5. Scheme (d): Coherent SU JT of CFF option 2, in which the estimated aggregated CQI is derived from (8.3) with the periodicity of co-phase feedback being $T_{\mathrm{coph}} = 10$ ms. Overhead in addition to per-CSI-RS-resource feedback is 2 bits (2-CSI-RS-resource JT) or 4 bits (3-CSI-RS-resource JT) of co-phase information per frequency sub-band.
6. Scheme (e): Coherent SU JT of CFF option 1, in which the reported aggregated CQI is calculated using (8.6) with the periodicities of co-phase and aggregated CQI feedbacks being $T_{\mathrm{coph}} = T_{\mathrm{aggCQI}} = 10$ ms. Overhead in addition to per-CSI-RS-resource feedback is 2 bits (2-CSI-RS-resource JT) or 4 bits (3-CSI-RS-resource JT) of co-phase information and 4 bits of aggregated CQI per frequency sub-band.

The detailed simulation parameters as well as the CoMP scenario are described in Table 8.3.

Also we provide some further explanations for the above parameters as follows:

1. CoMP scenario: Currently, there are four CoMP scenarios defined in LTE Release 11 (see Sect. 7.2.3), that is, homogeneous networks (CoMP scenarios 1 and 2) and heterogeneous networks (CoMP scenario 3 and 4). In our simulations, we adopt CoMP scenario 2, which features on intercell site CoMP with fiber connections among transmission points.
2. Cellular model and layout: The infrastructure of the considered cellular network is illustrated in Fig. 8.2, where the cells (sectors) are consecutively numbered. And the directional antennas of the sectors are represented by red arrows. UEs dropped into each cell site are shown as colored hexagrams with different colors for different sectors. It should be noted that the outmost tires of cells, that is, cells with number 58–111, are the virtual cells generated by the wraparound technique (Sallabi et al. 2005). The introduced virtual cells can improve the validity of the performance results collected from the cells around the rim of the simulated area by duplicating specific interior cells and placing them outside the simulation area for generating realistic interference. Also note that UEs shown by hollow hexagrams in the virtual cells are virtual UEs born from the wraparound cell mapping procedure.
3. Number of UEs per cell: The number of UEs dropped into each cell should be set to a reasonable value. UEs that can be simultaneously served by a BS are usually limited by the system bandwidth and capacity of the control channel.
4. Inter-site distance: The distance between the center points of adjacent cell sites.
5. Minimum distance between UE and cell site: UEs should be positioned at a distance from BSs to avoid entering of the blind spots incurred from the BS antenna down-tilt.
6. UE's speed: For CoMP transmissions, only low-speed UEs are of interest due to more accurate tracking of the CSI variations.
7. BS power class: The maximum transmit power of a BS.

Table 8.3 Parameters of the system-level simulation for SCP and JT

No.	Parameter		Assumption
1	CoMP scenario		Scenario 2 (see Sect. 7.2.3)
2	Cellular model and layout		Hexagonal grid, 19 cell sites, 3 sectors/cells per cell site (57 cells in total), wraparound layout (Sallabi et al. 2005)
3	Number of UEs per cell		10
4	Inter-site distance		500 m
5	Minimum distance between UE and cell site		35 m (see Fig. 7-7)
6	UE's speed		3 km/h (maximum Doppler frequency = 5.56 Hz)
7	BS power class		43 dBm
8	Carrier frequency		2 GHz
9	System bandwidth		5 MHz
10	Number of subcarriers		300
11	Number of subcarriers per resource block (RB)		12
12	Number of RBs for data transmission		24
13	Size of a frequency sub-band		4 RBs
14	Distance-dependent path loss		$L = 128.1 + 37.6\log_{10}(d)$, (in dB), d in km
15	Shadowing standard deviation		8 dB
16	Correlation distance of shadowing		10 m
17	Shadowing correlation	Between cell sites	0.5
18		Between cells	1.0
19	Penetration loss		20 dB
20	Thermal noise density		−174 dBm/Hz
21	Channel model		SCME defined in 3GPP (2011d)
22	Antenna pattern		As in 3GPP (2010) shown below

23	Antenna pattern (horizontal)	$A_H(\varphi) = -\min\left[12\left(\frac{\varphi}{\varphi_{3dB}}\right)^2, A_m\right]$
	(For 3-sector cell sites with fixed antenna patterns)	$\varphi_{3dB} = 70^\circ, A_m = 25$ dB
24	Antenna pattern (vertical)	$A_V(\theta) = -\min\left[12\left(\frac{\theta-\theta_{etilt}}{\theta_{3dB}}\right)^2, SLA_v\right]$
	(For 3-sector cell sites with fixed antenna patterns)	$\theta_{3dB} = 10^\circ$, $SLA_v = 20$ dB $\theta_{etilt} = 15^\circ$ Antenna height at the BS is set to 32 m Antenna height at the UE is set to 1.5 m
25	Combining as a 3D antenna pattern	$A(\varphi,\theta) = -\min\{-[A_H(\varphi) + A_V(\theta)], A_m\}$
26	Number of UE antennas	2, co-polarized
27	Number of BS antennas	4, co-polarized
28	Maximum number of CSI-RS resources for JT operation	3
29	CSI-RS-resource selection threshold for path loss comparison	6 dB
30	Maximum rank of SCP	2
31	Maximum rank of JT	1
32	Scheduler	Greedy search algorithm based on PF metric (see Sect. 4.3.2) Dynamic switch between SCP and JT
33	Scheduling granularity in frequency domain	Per sub-band
34	Scheduling granularity in time domain	Per TTI (1 ms)
35	Link adaptation	MCSs based on LTE transport formats according to (3GPP 2011e)
36	Expected PER of the first transmission	0.1
37	Scheduling of the retransmission	Dynamic
38	Maximum number of retransmissions	4

(continued)

Table 8.3 (continued)

No.	Parameter	Assumption
39	Traffic model	Full buffer (FB)
40	Downlink overhead	30% of total time-frequency resources
41	Receiver type	MMSE (option 1 of LG et al. (2011))
42	Periodicity of per-CSI-RS-resource feedback for SCP UEs	10 ms
43	Per-CSI-RS-resource feedback periodicity for JT UEs	10 ms
44	L_{13}^{SCP} for SCP UEs	5 ms
45	L_{13}^{JT} for JT UEs	10 ms
46	Periodicity of co-phase feedback for JT UEs T_{coph}	10, 20, 30 ms
47	Periodicity of aggregated CQI feedback for JT UEs T_{aggCQI}	10, 20, 30 ms
48	Codebook for PMI feedback	LTE Release 8 codebook
49	Number of co-phase bits	0 or 2 bits (uniform sampling of $[0\ 2\pi]$)

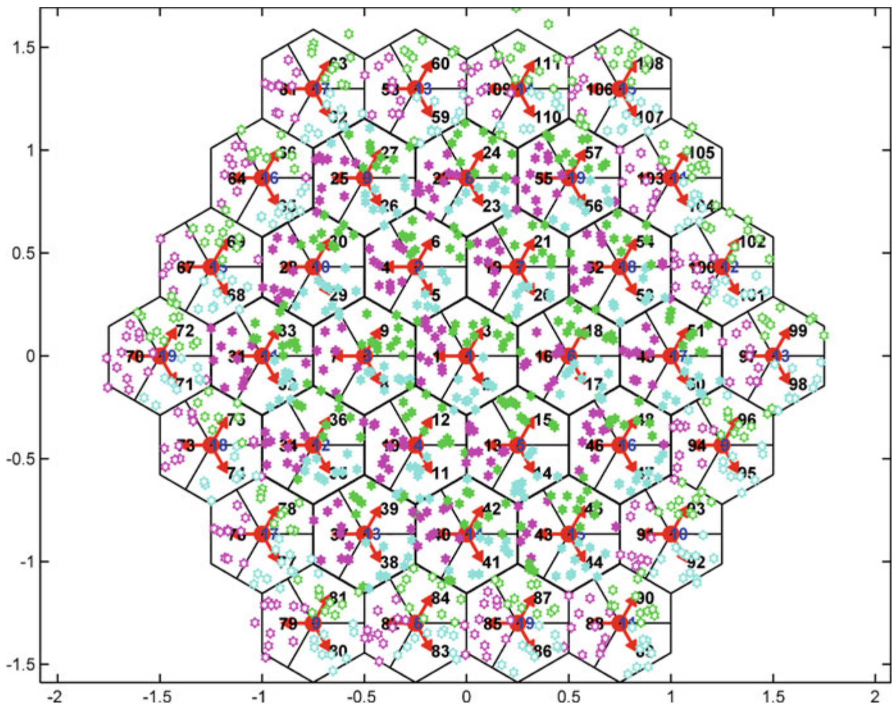

Fig. 8.2 Illustration of the layout of the simulated cellular network (57 cells)

8. Carrier frequency: The carrier frequency of the spectrum for transmission.
9. System bandwidth: The bandwidth of the spectrum for transmission.
10. Number of subcarriers: The number of available subcarriers in the OFDM system without guard bands.
11. Number of subcarriers per RB: The number of subcarriers contained in one unit of resource block.
12. Number of RBs for data transmission: The number of available RBs for data transmission in the OFDM system without the guard bands, downlink broadcasting, and synchronization channels.
13. Size of a frequency sub-band: The frequency granularity for CSI feedback and BS scheduling.
14. Distance-dependent path loss: The formula to model the large-scale channel fading.
15. Shadowing standard deviation: The shadowing value is usually assumed to follow the logarithmic normal distribution (3GPP 2010), the standard deviation of which is denoted as the shadowing standard deviation.
16. Correlation distance of shadowing: The shadowing values have a relatively strong correlation across some distance, which is measured by the correlation distance of shadowing.

17. Shadowing correlation—between cell sites: The correlation coefficient of a UE's shadowing value between cell sites. Due to the distributed deployment of cell sites, this correlation coefficient is relatively low.
18. Shadowing correlation—between cells: The correlation coefficient of a UE's shadowing value between cells. Due to the colocated deployment of cells, this correlation coefficient is relatively high.
19. Penetration loss: Any building which contains a significant thickness of concrete or amount of metal will attenuate the radio wave signal. The corresponding power loss due to penetration through walls and floors is represented by this parameter.
20. Thermal noise density: The power spectrum density of the thermal noise, which relates to the environment temperature.
21. Channel model: The model for fast-fading channels.
22. Antenna pattern: The radiation properties of transmit antennas.
23. Antenna pattern (horizontal): Antenna gain as a function of the horizontal part of the BS-UE angle.
24. Antenna pattern (vertical): Antenna gain as a function of the vertical part of the BS-UE angle.
25. Combining as a 3D antenna pattern: Combination of the horizontal and vertical antenna patterns.
26. Number of UE antennas: The number of receive antennas equipped at UE.
27. Number of BS antennas: The number of transmit antennas equipped at BS.
28. Maximum number of CSI-RS resources for JT operation: This parameter limits the CSI-RS resources in JT, which helps to reduce the system complexity.
29. CSI-RS-resource selection threshold for path loss comparison: Only CSI-RS resources with their path loss differences below a threshold will be considered for JT.
30. Maximum rank of SCP: Maximum layers of MIMO transmission in SCP.
31. Maximum rank of JT: Maximum layers of MIMO transmission in JT.
32. Scheduler: The scheduling algorithms performed by BS have been addressed in Sect. 4.3.2.
33. Scheduling granularity in frequency domain: The granularity of scheduled data transmission in frequency domain.
34. Scheduling granularity in time domain: The granularity of scheduled data transmission in time domain.
35. Link adaptation: BS chooses an appropriate modulation and coding scheme from a set of candidate schemes (see Sect. 4.3.2.6).
36. Expected PER of the first transmission: The PER target for the first transmission with link adaptation.
37. Scheduling of the retransmission: The scheduling algorithm for retransmissions should be performed by BS when the first transmission fails.
38. Maximum number of retransmissions: When several attempts of retransmission still cannot recover a data packet, it is necessary to discard the transmission process to prevent further wasting of communication resources in case the corrupted packet is beyond repair (3GPP 2010).

39. Traffic model: The model that describes how the UE's traffic is generated. The FB model assumes that the buffer for every UE's downlink transmission is fully loaded.
40. Downlink overhead: Not all of the subcarriers and OFDM symbols in a RB can be used for data transmission, so the downlink resources for, for example, control signaling, CSI-RS and DM-RS, should be excluded from throughput calculation.
41. Receiver type: The receiver structure and capability at the UE side.
42. Periodicity of per-CSI-RS-resource feedback for SCP UEs: The CSI report periodicity of per-CSI-RS-resource feedback for SCP UEs.
43. Per-CSI-RS-resource feedback periodicity for JT UEs: The CSI report periodicity of per-CSI-RS-resource feedback for JT UEs.
44. L_{13}^{SCP} for SCP UEs: As previously explained in Sect. 8.2.2, a constant CSI delay is composed of TTIs from CSI measurement to CSI feedback and those from scheduling to transmission. This parameter gives the constant CSI delay for SCP UEs.
45. L_{13}^{JT} for JT UEs: Similar to the constant CSI delay L_{13}^{SCP} for SCP UEs, this parameter indicates the constant CSI delay for JT UEs.
46. Periodicity of co-phase feedback for JT UEs: The co-phase report periodicity for JT UEs.
47. Periodicity of aggregated CQI feedback for JT UEs: The aggregated CQI report periodicity for JT UEs.
48. Codebook for PMI feedback: For both SCP and JT UEs, the codebook for PMI in per-CSI-RS-resource feedback is defined here.
49. Number of co-phase bits: The quantization bits of co-phase information for JT UEs.

8.3.2 Performance Comparison

Regarding the throughput performance, the full CDF results for the interested schemes are shown in Fig. 8.3. And the CDF segment containing the cell-edge UE throughput is magnified in Fig. 8.4 for observation purpose.

The comparison of detailed numerical results for various CFF schemes is summarized in Table 8.4.

From the simulation results shown in Table 8.4, we can see that the average spectral efficiencies of the interested schemes show little difference. However, we can clearly observe that compared with the baseline SCP, CFF option 4 shows modest improvement (11.64%) on the cell-edge throughput, while CFF options 1, 2, and 3 achieve around or more than 25% cell-edge throughput gain. Among them, CFF option 1 seems not very efficient due to its high overhead and limited performance gain compared with CFF options 2 and 3. In addition, CFF option 2 shows comparable performance with CFF option 3 with a lower overhead of CSI feedback. Besides, the suboptimal scheme of CFF option 2, that is, scheme (c),

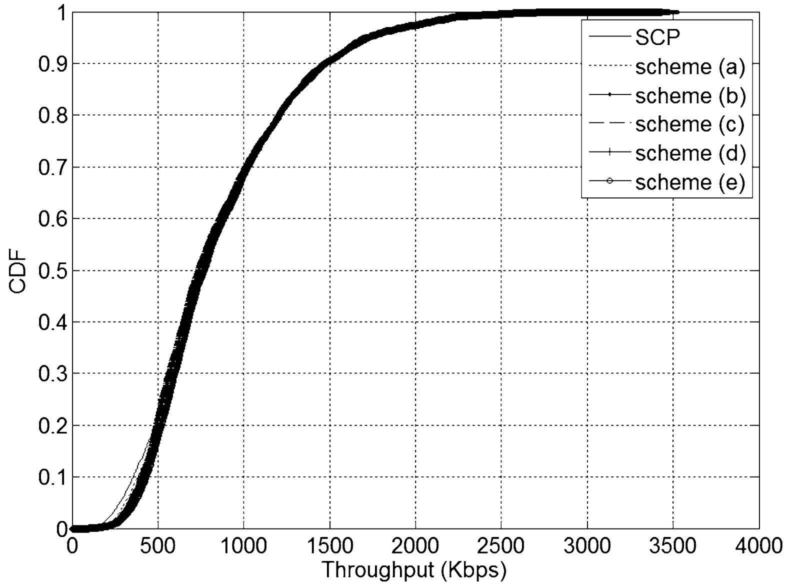

Fig. 8.3 Comparison of various CFF schemes (full CDF)

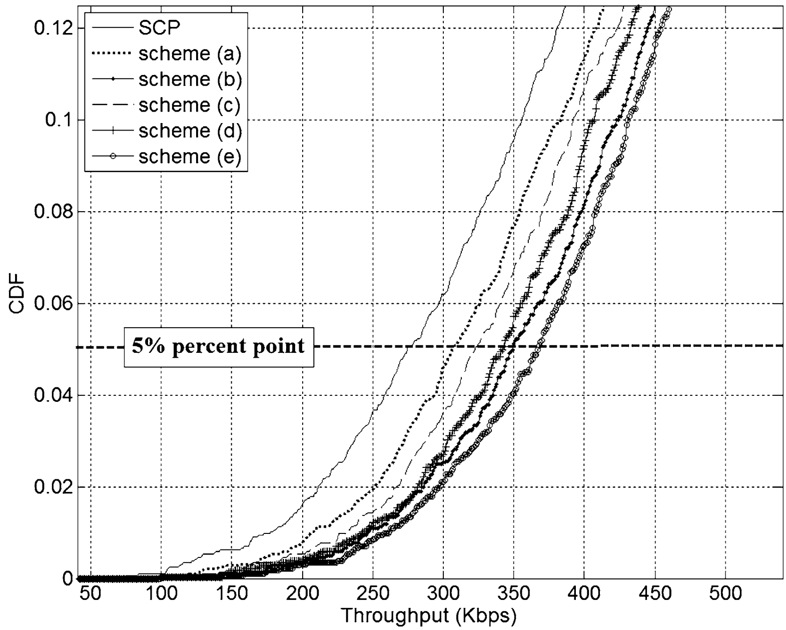

Fig. 8.4 Comparison of various CFF schemes (CDF segment: 0∼0.12)

Table 8.4 Numerical results of various CFF schemes

Scheme description	Average spectral efficiency (bps/Hz)	5-percentile UE spectral efficiency (bps/Hz)	Average spectral efficiency gain by using JT (%)	5-percentile UE spectral efficiency gain by using JT (%)
Baseline scheme (SCP)	1.7391	0.0550	–	–
Scheme (a) [option 4]	1.7213	0.0614	−1.03	11.64
Scheme (b) [option 3] [$T_{aggCQI} = 10$ ms]	1.7597	0.0700	1.18	27.27
Scheme (c) [option 2, LB] [$T_{coph} = 10$ ms]	1.7151	0.0646	−1.38	17.45
Scheme (d) [option 2] [$T_{coph} = 10$ ms]	1.7238	0.0686	−0.88	24.73
Scheme (e) [option 1] [$T_{coph} = T_{aggCQI} = 10$ ms]	1.7634	0.0736	1.39	33.82

exhibits less improvement in terms of the cell-edge throughput in comparison to the common practice of CFF option 2, that is, scheme (d). Nevertheless, the availability of scheme (c) is still useful since it provides the flexibility for BS to decide how to use the co-phase information, that is, employing coherent JT (scheme (d)) or noncoherent JT (scheme (c)). Therefore, with co-phase fed back from the UE, coherent or noncoherent JT transmission can be made transparent to the UE, whereas noncoherent JT based on the aggregated CQI (scheme (b)) does not have this merit. To sum up, it is shown that both CFF options 2 and 3 are competitive, which achieve different trade-offs between performance gain and feedback overhead.

Another pertinent concern is about the performance degradation due to outdated co-phase or aggregated CQI information. To investigate the delay issue of the JT CSI reporting, especially for CFF options 2 and 3, we present simulation results to compare the throughput performance for another 9 schemes listed as follows:

1. Baseline scheme: SU SCP scheme.
2. Scheme (b-0): Noncoherent SU JT of CFF option 3, in which the reported aggregated CQI is based on (8.7) with $T_{aggCQI} = 10$ ms
3. Scheme (b-1): Noncoherent SU JT of CFF option 3, in which the reported aggregated CQI is based on (8.7) with $T_{aggCQI} = 20$ ms
4. Scheme (b-2): Noncoherent SU JT of CFF option 3, in which the reported aggregated CQI is based on (8.7) with $T_{aggCQI} = 30$ ms
5. Scheme (b-3): Noncoherent SU JT of CFF option 3, in which the reported aggregated CQI is based on (8.7) with $T_{aggCQI} = 40$ ms
6. Scheme (d-0): Coherent SU JT of CFF option 2, in which the estimated aggregated CQI is derived from (8.3) with the periodicity of co-phase feedback being $T_{coph} = 10$ ms

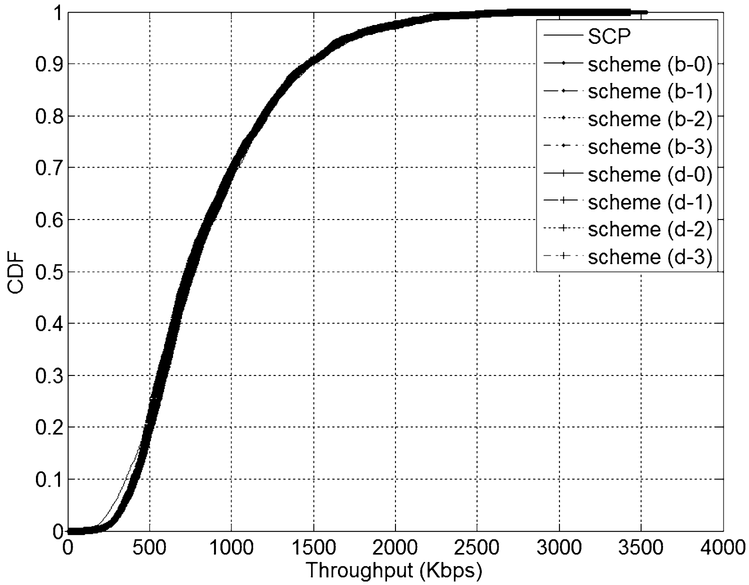

Fig. 8.5 Comparison of CFF schemes with different T_{coph} and T_{aggCQI} (full CDF)

7. Scheme (d-1): Coherent SU JT of CFF option 2, in which the estimated aggregated CQI is derived from (8.3) with the periodicity of co-phase feedback being $T_{\text{coph}} = 20$ ms
8. Scheme (d-2): Coherent SU JT of CFF option 2, in which the estimated aggregated CQI is derived from (8.3) with the periodicity of co-phase feedback being $T_{\text{coph}} = 30$ ms
9. Scheme (d-3): Coherent SU JT of CFF option 2, in which the estimated aggregated CQI is derived from (8.3) with the periodicity of co-phase feedback being $T_{\text{coph}} = 40$ ms

As described in Sect. 8.3.1, for schemes (b-0), (b-1), (b-2), and (b-3), the overhead in addition to per-CSI-RS-resource feedback is 4 bits per frequency sub-band. And for schemes (d-0), (d-1), (d-2), and (d-3), the overhead in addition to per-CSI-RS-resource feedback is 2 bits (2-CSI-RS-resource JT) or 4 bits (3-CSI-RS-resource JT) of co-phase information per frequency sub-band.

The detailed simulation parameters and CoMP scenario are described in Table 8.3, and the full CDF results of throughput are shown in Fig. 8.5. Moreover, the CDF segment containing the cell-edge UE throughput is magnified in Fig. 8.6 for observation purpose.

The comparison of numerical results of CFF schemes with different T_{coph} and T_{aggCQI} is summarized in Table 8.5.

From the results shown in Table 8.5, we can find that the performance gap between CFF options 2 and 3 remains small when the feedback periodicity of co-

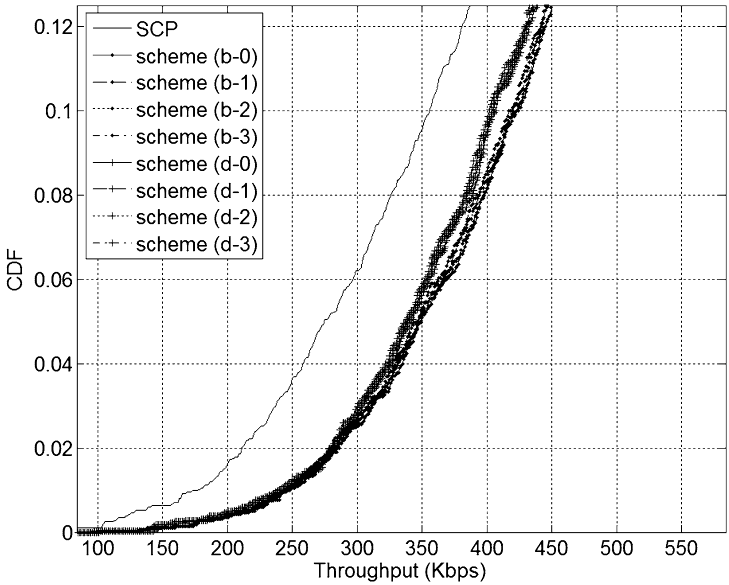

Fig. 8.6 Comparison of CFF schemes with different T_{coph} and T_{aggCQI} (CDF segment: 0∼0.12)

phase or aggregated CQI becomes large. More importantly, it can be concluded from the numerical results that large periodicity of co-phase or aggregated CQI reporting, for example, 30 or 40 ms, has a marginal impact on the performance of JT due to slow channel variation of low-speed UEs. Therefore, the overhead of co-phase or aggregated CQI feedback can be kept very low in practice.

In conclusion, from the simulation results provided in this section, we observe that around 25% cell-edge throughput gain at the cost of very small loss on the average throughput can be achieved by CFF options 2 and 3. Moreover, an additional 6∼8% cell-edge throughput gain can be offered by CFF option 1 with a larger overhead. Another valuable finding is that large periodicity of co-phase or aggregated CQI reporting has a very small impact on the performance of JT when UE moves at a relatively low speed, for example, 3 km/h.

8.4 The Final Winner of CFF

From the performance evaluation results shown in Sect. 8.3, it can be concluded that CFF option 2 or 3 is the logical choice to guide the design for CSI feedback in CoMP operations, especially in JT. Thereby, at the 3GPP RAN1 #68bis meeting in Mar 2012, CFF option 2 was treated with a high priority to see whether it was agreeable to introduce co-phase information in LTE Release 11 networks (MCC Support 2012b).

Table 8.5 Numerical results of CFF schemes with different T_{coph} and T_{aggCQI}

Scheme description	Average spectral efficiency (bps/Hz)	5-percentile UE spectral efficiency (bps/Hz)	Average spectral efficiency gain by using JT (%)	5-percentile UE spectral efficiency gain by using JT (%)
Baseline scheme (SCP)	1.7391	0.0550	–	–
Scheme (b-0) [option 3] [$T_{aggCQI} = 10$ ms]	1.7597	0.0700	1.18	27.27
Scheme (b-1) [option 3] [$T_{aggCQI} = 20$ ms]	1.7536	0.0698	0.83	26.91
Scheme (b-2) [option 3] [$T_{aggCQI} = 30$ ms]	1.7465	0.0694	0.42	26.18
Scheme (b-3) [option 3] [$T_{aggCQI} = 40$ ms]	1.7422	0.0694	0.18	26.18
Scheme (d-0) [option 2] [$T_{coph} = 10$ ms]	1.7238	0.0686	−0.88	24.73
Scheme (d-1) [option 2] [$T_{coph} = 20$ ms]	1.7174	0.0678	−1.25	23.27
Scheme (d-2) [option 2] [$T_{coph} = 30$ ms]	1.7103	0.0676	−1.66	22.91
Scheme (d-3) [option 2] [$T_{coph} = 40$ ms]	1.7060	0.0678	−1.91	23.27

During the meeting, a way-forward proposal (Intel et al. 2012) was first presented by a number of companies that inter-CSI-RS-resource co-phase information feedback for 2-CSI-RS-resource JT CoMP could be transparently supported by UE feeding back a 2-antenna PMI, that is, no explicit inter-CSI-RS-resource co-phase feedback should be specified for LTE Release 11. This proposal was questioned by some companies that there were no benefits in this scheme considering the increased complexity and overhead when the number of CSI-RS resources in CoMP operations being more than two. With no satisfactory answers, this proposal was rejected.

Next, another try to move CFF option 2 forward was made by (Huawei et al. 2012b), which stated that inter-CSI-RS-resource co-phase indicator with 2 bits for rank-one JT should be supported and aggregated CSI report should be precluded from the specification. This proposal was objected by companies supporting CFF options 1, 3, and 4, and hence, it was also turned down during the meeting. With no other way-forward proposals available, it was concluded that inter-CSI-RS-resource co-phase indicator feedback would not be supported in LTE Release 11. Although it was agreed to further consider CFF option 3 at the following 3GPP RAN1 meeting, it seemed that CFF option 3 would inevitably share the same fate with CFF option 2 because the views on CFF options shown in Table 8.2 were so fragmented that it was nearly impossible to reach any consensus in the LTE Release 11 time framework.

Besides the intense debate in CoMP CFF, other issues related to CoMP were also treated at the 3GPP RAN1 #68bis meeting. Some interesting discussions were devoted to a new RS resource for interference measurement, that is, interference measurement resource (IMR), which was introduced in LTE Release 11 to assist the assessment of interference at the UE side. As a constructive result in this topic, it was agreed that at least one IMR should be configured for an LTE Release 11 UE (MCC Support 2012b). In another aspect, the maximum size of CSI-RS resources in CoMP drew a lot of attention since it might have a significant impact on the design of CSI feedback formats. The prevailing opinion was to support an up to 3-CSI-RS-resource CoMP, while several companies wanted to simplify the system design by only allowing for a 2-CSI-RS-resource CoMP at the cost of some performance degradation (MCC Support 2012b).

At the 3GPP RAN1 #69 meeting in May 2012 (MCC Support 2012c), a quick decision regarding CFF option 3 was made that no aggregated CQI should be introduced in LTE Release 11 since the positive and negative opinions on this design were equally strong. With CFF options 2 and 3 and their combination, that is, CFF option 1 being discarded, the previously agreed CFF option 4 (MCC Support 2012a) seemed to be the only option for LTE Release 11 networks. Therefore, discussions on per-CSI-RS-resource CSI feedback became the main topic during this meeting. And it was agreed that multiple CSI feedbacks could be configured for one UE and each CSI feedback should be associated with a channel part evaluated from CSI-RS and an interference part measured from IMR. Thus, SCP and various CoMP schemes can be transparently supported by appropriate configurations of UE's CSI-RS(s) and IMR(s) by BS. Although this CFF design cannot fully facilitate dynamic CoMP transmissions since each CSI feedback configuration corresponds to a single preferred transmission assumption, it requires minimal specification efforts because a BS can choose which CoMP transmission(s) should be conducted for a UE so that only some specific CSI feedback reports should be activated and there is no need to consider an all-round CSI feedback scheme to support all CoMP transmissions, including those which might have already been eliminated by the BS scheduler. Regarding the feedback channels of CoMP CSI, periodic PUCCH and control signaling triggered PUSCH were approved with no dispute. Besides the progress in CoMP CFF, during the 3GPP RAN1 #69 meeting, it was also generally agreed that the maximum size of CSI-RS resources in CoMP should be three.

In the very recent 3GPP RAN1 meeting held in Qingdao, China, Aug 2012, a new terminology, "CSI process," is used to define a CSI feedback associated with one channel part and one interference part (MCC Support 2012d). From an implementation point of view, a BS can configure one CSI process to collect the CSI from a UE for one CoMP transmission assumption. If a BS has identified more than one candidate CoMP transmission for a UE, then it should configure multiple

CSI processes. Note that for multiple CSI processes, RI and frequency sub-band constraints should be further considered for the support of JT because constructive signal combining must take place on the same data transmission layer and frequency sub-band (Ericsson et al. 2012). Moreover, it was agreed that all the LTE Release 10 CSI reporting types and modes should be reused for CoMP operations in LTE Release 11 so that the remaining details of CSI feedback formats will be quite similar to those addressed in Sect. 7.2.2.

It is estimated that all the specifications with regard to CoMP in LTE Release 11 will be completed in December 2012, just a couple of months from now. Therefore, it is safe to conclude that CFF option 4 will become the final winner as the CoMP CFF design in LTE Release 11. It may seem somewhat unexpected to find that CFF option 4 prevails in the end because its performance gain shown in Table 8.4 is the least one among the existing CFF options. In the future, if the fragmented views on CFF options 1, 2, and 3 summarized in Table 8.2 can somehow converge, then the CFF issue may be reopened and an enhanced CFF option 4 will be sought for. It should be noted that a new work item description on enhanced CoMP for LTE Release 12 was proposed and well received at the most recent 3GPP #57 plenary meeting (Samsung 2012b). This new work item proposed that from the year 2013 3GPP RAN1 should identify and specify necessary enhancements on CSI-RS-based feedback mechanisms and support of JT, including intracell site and intercell site. Hence, preparations for the third campaign of CoMP in future LTE releases are already on the move, and some exciting activities in this area can be expected with great anticipation.

8.5 Conclusion

In review of the renewed campaign of CoMP in LTE Release 11 started from December 2010, the study item of which confirmed the advantages of multipoint cooperative communication technologies in practical cellular systems, and the work item of which set the primary battle ground on the CFF design. As an ambitious goal, the CoMP CFF targeted for proposing a total solution for CoMP so that all transmission-specific designs could be unified into one scheme. However, all of the existing CFF options were supported by numerous companies, and hence, the views were divided and fragmented. Although system-level simulations showed that both the co-phase information (CFF option 2) and the aggregated CQI (CFF option 3) were able to provide considerable cell-edge throughput gains compared with the SCP baseline, these two CFF options were eventually rejected by 3GPP RAN1 due to lack of consensus on which option should be adopted. As a result, CFF option 4, that is, per-CSI-RS-resource CSI feedback, was agreed to guide the designs of CSI reporting for CoMP in LTE Release 11. The major benefit of CFF option 4 is that it requires minimal specification efforts to include CoMP into the LTE network as a new and competitive feature. However, the potential problem about CFF option 4 is that it may not be able to support JT very well since any information of inter-CSI-

RS-resource or aggregated CSI is not available in this framework. Therefore, a third campaign of CoMP for LTE Release 12 and onward will be launched in the future, with one of the aims to enhance the feedback mechanisms for better support of JT, including intracell site and intercell site.

References

3GPP (2010) TR 36.814: further advancements for E-UTRA, physical layer aspects. http://www.gpp.org/ftp/Specs/archive/36_series/36.814/36814-900.zip. Accessed 30 Mar 2010

3GPP (2011a) RP-111365: coordinated multi-point operation for LTE. In: 3GPP TSG RAN#53 meeting, Fukuoka, Japan, 13–16 Sept 2011. http://www.3gpp.org/ftp/tsg_ran/TSG_RAN/TSGR_53/Docs/RP-111365.zip

3GPP (2011b) TR 36.819 V11.1.0: coordinated multi-point operation for LTE physical layer aspects (Release 11). http://www.3gpp.org/ftp/Specs/archive/36_series/36.819/36819-b10.zip. Accessed 22 Dec 2011

3GPP (2011c) TS 36.211 V10.1.0: physical channels and modulation (Release 10). http://www.3gpp.org/ftp/Specs/archive/36_series/36.211/36211-a10.zip. Accessed 30 Mar 2011

3GPP (2011d) TR 25.996 V10.0.0: spatial channel model for Multiple Input Multiple Output (MIMO) simulations (Release 10). http://www.3gpp.org/ftp/Specs/archive/25_series/25.996/25996-a00.zip. Accessed 30 Mar 2011

3GPP (2011e) TS 36.213 V10.1.0: physical layer procedures (Release 10). http://www.3gpp.org/ftp/Specs/archive/36_series/36.213/36213-a10.zip. Accessed 30 Mar 2011

3GPP (2012) Chairman notes. In: 3GPP TSG RAN WG1 meeting #68, Dresden, Germany, 6–10 Feb 2012

Alcatel-Lucent Shanghai Bell (2011) R1-114048: CoMP feedback based on multiple CSI-RS Resources. In: 3GPP TSG RAN WG1 meeting #67, San Francisco, USA, 14–18 Nov 2011. http://www.3gpp.org/ftp/tsg_ran/WG1_RL1/TSGR1_67/Docs/R1-114048.zip

Alcatel-Lucent Shanghai Bell (2012) R1-120492: analysis of inter-CSI-RS-resource phase feedback. In: 3GPP TSG RAN WG1 Meeting #68, Dresden, Germany, 6–10 Feb 2012. http://www.3gpp.org/ftp/tsg_ran/wg1_rl1/TSGR1_68/Docs/R1-120492.zip

Alcatel-Lucent, Alcatel-Lucent Shanghai Bell, CATT, CMCC, ETRI, HiSilicon, Hitachi, Huawei, Intel, LG Electronics, New Postcom, Orange, Sharp, ZTE (2011) R1-114420: way forward on reporting inter-CSI-RS-resource feedback. In: 3GPP TSG RAN WG1 meeting #67, San Francisco, USA, 14–18 Nov 2011. http://www.3gpp.org/ftp/tsg_ran/WG1_RL1/TSGR1_67/Docs/R1-114420.zip

CATT (2011) R1-113728: CSI feedback to support CoMP transmission. In: 3GPP TSG RAN WG1 meeting #67, San Francisco, USA, 14–18 Nov 2011. http://www.3gpp.org/ftp/tsg_ran/WG1_RL1/TSGR1_67/Docs/R1-113728.zip

CATT (2012a) R1-120094: discussion on inter-CSI-RS-resource feedback. In: 3GPP TSG RAN WG1 meeting #68, Dresden, Germany, 6–10 Feb 2012. http://www.3gpp.org/ftp/tsg_ran/wg1_rl1/TSGR1_68/Docs/R1-120094.zip

CATT (2012b) R1-120098: feedback mechanism for CoMP. In: 3GPP TSG RAN WG1 meeting #68, Dresden, Germany, 6–10 Feb 2012. http://www.3gpp.org/ftp/tsg_ran/wg1_rl1/TSGR1_68/Docs/R1-120098.zip

CHTTL (2012) R1-120120: discussion on inter-CSI-RS-resource feedback for DL CoMP. In: 3GPP TSG RAN WG1 meeting #68, Dresden, Germany, 6–10 Feb 2012. http://www.3gpp.org/ftp/tsg_ran/wg1_rl1/TSGR1_68/Docs/R1-120120.zip

Ericsson, ST-Ericsson (2011) R1-114258: CSI feedback for DL CoMP. In: 3GPP TSG RAN WG1 meeting #67, San Francisco, USA, 14–18 Nov 2011. http://www.3gpp.org/ftp/tsg_ran/WG1_RL1/TSGR1_67/Docs/R1-114258.zip

Ericsson, ST-Ericsson (2012a) R1-120783: performance of incoherent and coherent JT CoMP. In: 3GPP TSG RAN WG1 meeting #68, Dresden, Germany, 6–10 Feb 2012. http://www.3gpp.org/ftp/tsg_ran/wg1_rl1/TSGR1_68/Docs/R1-120783.zip

Ericsson, ST-Ericsson (2012b) R1-120784: CSI feedback operation for CoMP. In: 3GPP TSG RAN WG1 meeting #68, Dresden, Germany, 6–10 Feb 2012. http://www.3gpp.org/ftp/tsg_ran/wg1_rl1/TSGR1_68/Docs/R1-120784.zip

Ericsson, Alcatel Lucent, Alcatel-Lucent Shanghai Bell, CATT, ST-Ericsson, Huawei, Hi Silicon, LG Electronics, New Postcom, Samsung (2012) R1-123976: way forward on rank and sub-band constraints between CSI Processes. In: 3GPP TSG RAN WG1 #70, Qingdao, China, 13–17 Aug 2012. http://www.3gpp.org/ftp/tsg_ran/wg1_rl1/TSGR1_70/Docs/R1-123976.zip

Fujitsu (2011) R1-114180: consideration on CSI feedback to support DL CoMP. In: 3GPP TSG RAN WG1 meeting #67, San Francisco, USA, 14–18 Nov 2011. http://www.3gpp.org/ftp/tsg_ran/WG1_RL1/TSGR1_67/Docs/R1-114180.zip

Fujitsu (2012) R1-120745: consideration on CSI feedback framework to support DL CoMP. In: 3GPP TSG RAN WG1 meeting #68, Dresden, Germany, 6–10 Feb 2012. http://www.3gpp.org/ftp/tsg_ran/wg1_rl1/TSGR1_68/Docs/R1-120745.zip

Hitachi Ltd (2011) R1-114338: CQI definition for CoMP. In: 3GPP TSG RAN WG1 meeting #67, San Francisco, USA, 14–18 Nov 2011. http://www.3gpp.org/ftp/tsg_ran/WG1_RL1/TSGR1_67/Docs/R1-114338.zip

Hitachi Ltd. (2012a) R1-120242: consideration on CSI feedback for JT CoMP. In: 3GPP TSG RAN WG1 meeting #68, Dresden, Germany, 6–10 Feb 2012. http://www.3gpp.org/ftp/tsg_ran/wg1_rl1/TSGR1_68/Docs/R1-120242.zip

Hitachi Ltd. (2012b) R1-120243: CQI definition for CoMP. In: 3GPP TSG RAN WG1 meeting #68, Dresden, Germany, 6–10 Feb 2012. http://www.3gpp.org/ftp/tsg_ran/wg1_rl1/TSGR1_68/Docs/R1-120243.zip

Hitachi Ltd, LLC (2011) R1-113968: consideration on aggregated CSI feedback. In: 3GPP TSG RAN WG1 meeting #67, San Francisco, USA, 14–18 Nov 2011. http://www.3gpp.org/ftp/tsg_ran/WG1_RL1/TSGR1_67/Docs/R1-113968.zip

Huawei, HiSilicon (2011a) R1-113638: framework for aggregated and per CSI-RS-resource feedback for CoMP. In: 3GPP TSG RAN WG1 meeting #67, San Francisco, USA, 14–18 Nov 2011. http://www.3gpp.org/ftp/tsg_ran/WG1_RL1/TSGR1_67/Docs/R1-113638.zip

Huawei, HiSilicon (2011b) R1-113639: CQI feedback for CoMP. In: 3GPP TSG RAN WG1 meeting #67, San Francisco, USA, 14–18 Nov 2011. http://www.3gpp.org/ftp/tsg_ran/WG1_RL1/TSGR1_67/Docs/R1-113639.zip

Huawei, HiSilicon (2012a) R1-120027: overview of CSI and CQI feedback for CoMP. In: 3GPP TSG RAN WG1 meeting #68, Dresden, Germany, 6–10 Feb 2012. http://www.3gpp.org/ftp/tsg_ran/wg1_rl1/TSGR1_68/Docs/R1-120027.zip

Huawei, HiSilicon (2012b) R1-120028: inter-CSI-RS-resource feedback for CoMP. In: 3GPP TSG RAN WG1 meeting #68, Dresden, Germany, 6–10 Feb 2012. http://www.3gpp.org/ftp/tsg_ran/wg1_rl1/TSGR1_68/Docs/R1-120028.zip

Huawei, HiSilicon (2012c) R1-120124: aggregated CSI feedback for CoMP. In: 3GPP TSG RAN WG1 meeting #68, Dresden, Germany, 6–10 Feb 2012. http://www.3gpp.org/ftp/tsg_ran/wg1_rl1/TSGR1_68/Docs/R1-120124.zip

Huawei, CATT, China Telecom, CHTTL, CMCC, ETRI, HiSilicon, Hitachi, Intel, KDDI, LG Electronics, New Postcom, Sharp, ZTE (2012a) R1-120901: way forward on CSI feedback for CoMP. In: 3GPP TSG RAN WG1 meeting #68, Dresden, Germany, 6–10 Feb 2012. http://www.3gpp.org/ftp/tsg_ran/wg1_rl1/TSGR1_68/Docs/R1-120901.zip

Huawei, Alcatel-Lucent, Alcatel-Lucent Shanghai Bell, CATT, CMCC, ETRI, HiSilicon, KDDI, Sharp (2012b) R1-121890: WF on CoMP CSI feedback. In: 3GPP TSG RAN WG1 #68bis, Jeju, South Korea, 26–30 Mar 2012. http://www.3gpp.org/ftp/tsg_ran/WG1_RL1/TSGR1_68b/Docs/R1-121890.zip

Intel Corporation (2011a) R1-113661: views on CSI feedback for DL CoMP systems. In: 3GPP TSG RAN WG1 meeting #67, San Francisco, USA, 14–18 Nov 2011. http://www.3gpp.org/ftp/tsg_ran/WG1_RL1/TSGR1_67/Docs/R1-113661.zip

Intel Corporation (2011b) R1-113663: unified CSI feedback framework for CoMP scheme. In: 3GPP TSG RAN WG1 meeting #67, San Francisco, USA, 14–18 Nov 2011. http://www.3gpp.org/ftp/tsg_ran/WG1_RL1/TSGR1_67/Docs/R1-113663.zip

Intel (2012a) R1-120198: discussion on aggregated CQI feedback for JT CoMP. In: 3GPP TSG RAN WG1 meeting #68, Dresden, Germany, 6–10 Feb 2012. http://www.3gpp.org/ftp/tsg_ran/wg1_rl1/TSGR1_68/Docs/R1-120198.zip

Intel (2012b) R1-120203: performance analysis of per CSI-RS resource feedback for JT CoMP. In: 3GPP TSG RAN WG1 meeting #68, Dresden, Germany, 6–10 Feb 2012. http://www.3gpp.org/ftp/tsg_ran/wg1_rl1/TSGR1_68/Docs/R1-120203.zip

Intel, Nokia, NSN, ZTE, III (2012) R1-121887: WF on support of inter-point phase feedback for JT CoMP. In: 3GPP TSG RAN WG1 #68bis, Jeju, South Korea, 26–30 Mar 2012. http://www.3gpp.org/ftp/tsg_ran/WG1_RL1/TSGR1_68b/Docs/R1-121887.zip

InterDigital Communications, LLC (2011a) R1-113926: CSI feedback to support downlink CoMP. In: 3GPP TSG RAN WG1 meeting #67, San Francisco, USA, 14–18 Nov 2011. http://www.3gpp.org/ftp/tsg_ran/WG1_RL1/TSGR1_67/Docs/R1-113926.zip

InterDigital Communications, LLC (2011b) R1-113927: CSI feedback for joint transmission. In: 3GPP TSG RAN WG1 meeting #67, San Francisco, USA, 14–18 Nov 2011. http://www.3gpp.org/ftp/tsg_ran/WG1_RL1/TSGR1_67/Docs/R1-113927.zip

ITRI (2012) R1-12077: inter-CSI-RS-resource feedback for downlink CoMP. In: 3GPP TSG RAN WG1 meeting #68, Dresden, Germany, 6–10 Feb 2012. http://www.3gpp.org/ftp/tsg_ran/wg1_rl1/TSGR1_68/Docs/R1-120778.zip

LG Electronics (2011a) R1-113981: evaluation results on CoMP with aggregated CQI or relative phase information. In: 3GPP TSG RAN WG1 meeting #67, San Francisco, USA, 14–18 Nov 2011. http://www.3gpp.org/ftp/tsg_ran/WG1_RL1/TSGR1_67/Docs/R1-113981.zip

LG Electronics (2011b) R1-113982: consideration on CSI feedback for CoMP and feedback container. In: 3GPP TSG RAN WG1 meeting #67, San Francisco, USA, 14–18 Nov 2011. http://www.3gpp.org/ftp/tsg_ran/WG1_RL1/TSGR1_67/Docs/R1-113982.zip

LG Electronics, Motorola Mobility, Intel, Marvell, Samsung, ETRI, Orange, Renesas, Huawei (2011) R1-110586: proposal for UE receiver assumption in CoMP simulations. In: TSG-RAN WG1 #63bis, Dublin, Ireland, 17–21 Jan 2011. http://www.3gpp.org/ftp/tsg_ran/WG1_RL1/TSGR1_63b/Docs/R1-110586.zip

LG (2012a) R1-120432: discussions on inter CSI-RS-resource feedback. In: 3GPP TSG RAN WG1 meeting #68, Dresden, Germany, 6–10 Feb 2012. http://www.3gpp.org/ftp/tsg_ran/wg1_rl1/TSGR1_68/Docs/R1-120432.zip

LG (2012b) R1-120433: consideration on aggregated feedback. In: 3GPP TSG RAN WG1 meeting #68, Dresden, Germany, 6–10 Feb 2012. http://www.3gpp.org/ftp/tsg_ran/wg1_rl1/TSGR1_68/Docs/R1-120433.zip

LG (2012c) R1-120435: consideration on CoMP CQI definition. In: 3GPP TSG RAN WG1 meeting #68, Dresden, Germany, 6–10 Feb 2012. http://www.3gpp.org/ftp/tsg_ran/wg1_rl1/TSGR1_68/Docs/R1-120435.zip

Marvell (2011) R1-114162: joint processing with aggregated feedback. In: 3GPP TSG RAN WG1 meeting #67, San Francisco, USA, 14–18 Nov 2011. http://www.3gpp.org/ftp/tsg_ran/WG1_RL1/TSGR1_67/Docs/R1-114162.zip

MCC Support (2011a) Final report of 3GPP TSG RAN WG1 #66bis v1.1.0. In: 3GPP TSG RAN WG1 #66bis, Zhuhai, P. R. China, 10–14 Oct 2011. http://www.3gpp.org/ftp/tsg_ran/WG1_RL1/TSGR1_66b/Report/Final_ReportWG1#66b_v110.zip

MCC Support (2011b) Final report of 3GPP TSG RAN WG1 #67 v1.0.0. In: 3GPP TSG RAN WG1 #67, San Francisco, USA, 14–18 Nov 2011. http://www.3gpp.org/ftp/tsg_ran/WG1_RL1/TSGR1_67/Report/Final_ReportWG1#67_v100.zip

MCC Support (2012a) Final report of 3GPP TSG RAN WG1 #68 v1.0.0. In: 3GPP TSG RAN WG1 #68, Dresden, Germany, 6–10 Feb 2012. http://www.3gpp.org/ftp/tsg_ran/WG1_RL1/TSGR1_68/Report/Final_ReportWG1#68_v100.zip

MCC Support (2012b) Final report of 3GPP TSG RAN WG1 #68bis v1.0.0. In: 3GPP TSG RAN WG1 #68bis, Jeju, South Korea, 26–30 Mar 2012. http://www.3gpp.org/ftp/tsg_ran/WG1_RL1/TSGR1_68b/Report/Final_ReportWG1#68b_v100.zip

MCC Support (2012c) Final report of 3GPP TSG RAN WG1 #69 v1.0.0. In: 3GPP TSG RAN WG1 #69, Prague, Czech Republic, 21–25 May 2012. http://www.3gpp.org/ftp/tsg_ran/WG1_RL1/TSGR1_69/Report/Final_ReportWG1#69_v100.zip

MCC Support (2012d) Draft Report of 3GPP TSG RAN WG1 #70 v0.1.0. In: 3GPP TSG RAN WG1 #70, Qingdao, China, 13–17 Aug 2012. http://www.3gpp.org/ftp/tsg_ran/WG1_RL1/TSGR1_70/Report/Draft_ReportWG1#70_v010.zip

MediaTek Inc. (2012a) R1-120623: on the need of aggregated CQI and inter-CSI-RS-resource feedback for CoMP. In: 3GPP TSG RAN WG1 meeting #68, Dresden, Germany, 6–10 Feb 2012. http://www.3gpp.org/ftp/tsg_ran/wg1_rl1/TSGR1_68/Docs/R1-120623.zip

MediaTek Inc. (2012b) R1-120624: aggregated CSI feedback and configuration. In: 3GPP TSG RAN WG1 meeting #68, Dresden, Germany, 6–10 Feb 2012. http://www.3gpp.org/ftp/tsg_ran/wg1_rl1/TSGR1_68/Docs/R1-120624.zip

MediaTek Inc. (2012c) R1-120625: CQI for multi-CSI-RS-resource feedback for Rel-11. In: 3GPP TSG RAN WG1 meeting #68, Dresden, Germany, 6–10 Feb 2012. http://www.3gpp.org/ftp/tsg_ran/wg1_rl1/TSGR1_68/Docs/R1-120625.zip

Motorola Mobility (2011) R1-114025: feedback designs for downlink CoMP. In: 3GPP TSG RAN WG1 meeting #67, San Francisco, USA, 14–18 Nov 2011. http://www.3gpp.org/ftp/tsg_ran/WG1_RL1/TSGR1_67/Docs/R1-114025.zip

Motorola Mobility (2012a) R1-120520: inter-CSI-RS resource feedback for CoMP. In: 3GPP TSG RAN WG1 meeting #68, Dresden, Germany, 6–10 Feb 2012. http://www.3gpp.org/ftp/tsg_ran/wg1_rl1/TSGR1_68/Docs/R1-120520.zip

Motorola Mobility (2012b) R1-120521: CQI definition for CoMP. In: 3GPP TSG RAN WG1 meeting #68, Dresden, Germany, 6–10 Feb 2012. http://www.3gpp.org/ftp/tsg_ran/wg1_rl1/TSGR1_68/Docs/R1-120521.zip

NEC, Motorola Mobility, Renesas Mobile Europe Ltd, ZTE, Huawei, HiSilicon, LGE, Intel, Ericsson, ST-Ericsson, Samsung, Fujitsu, CATT (2011) R4-115498: way forward on CA demodulation requirements. In: 3GPP TSG-RAN WG4 meeting #60bis, Zhuhai, China, 10–14 Oct 2011. http://www.3gpp.org/ftp/tsg_ran/WG4_Radio/TSGR4_60bis/docs/R4-115498.zip

New Postcom (2011a) R1-113696: PMI feedback for DL CoMP. In: 3GPP TSG RAN WG1 meeting #67, San Francisco, USA, 14–18 Nov 2011. http://www.3gpp.org/ftp/tsg_ran/WG1_RL1/TSGR1_67/Docs/R1-113696.zip

New Postcom (2011b) R1-113697: CQI feedback for DL CoMP. In: 3GPP TSG RAN WG1 meeting #67, San Francisco, USA, 14–18 Nov 2011. http://www.3gpp.org/ftp/tsg_ran/WG1_RL1/TSGR1_67/Docs/R1-113697.zip

Nokia Siemens Networks, Nokia (2011a) R1-114316: feedback framework integrating CRS and CSI-RS based feedback. In: 3GPP TSG RAN WG1 meeting #67, San Francisco, USA, 14–18 Nov 2011. http://www.3gpp.org/ftp/tsg_ran/WG1_RL1/TSGR1_67/Docs/R1-114316.zip

Nokia Siemens Networks, Nokia (2011b) R1-114317: CSI feedback using multiple CSI-RS resources. In: 3GPP TSG RAN WG1 meeting #67, San Francisco, USA, 14–18 Nov 2011. http://www.3gpp.org/ftp/tsg_ran/WG1_RL1/TSGR1_67/Docs/R1-114317.zip

Nokia Siemens Networks, Nokia (2012a) R1-120718: need for inter CSI-RS resources feedback. In: 3GPP TSG RAN WG1 meeting #68, Dresden, Germany, 6–10 Feb 2012. http://www.3gpp.org/ftp/tsg_ran/wg1_rl1/TSGR1_68/Docs/R1-120718.zip

Nokia Siemens Networks, Nokia (2012b) R1-120719: aggregated feedback for CoMP. In: 3GPP TSG RAN WG1 meeting #68, Dresden, Germany, 6–10 Feb 2012. http://www.3gpp.org/ftp/tsg_ran/wg1_rl1/TSGR1_68/Docs/R1-120719.zip

NTT DOCOMO (2011) R1-113292: CSI feedback scheme for JT CoMP. In: 3GPP TSG RAN WG1 meeting #66bis, Zhuhai, China, 10–14 Oct 2011. http://www.3gpp.org/ftp/tsg_ran/WG1_RL1/TSGR1_66b/Docs/R1-113292.zip

NTT DOCOMO (2012a) R1-120403: views on TM9 and CA based approaches for Rel-11 CoMP. In: 3GPP TSG RAN WG1 meeting #68, Dresden, Germany, 6–10 Feb 2012. http://www.3gpp.org/ftp/tsg_ran/wg1_rl1/TSGR1_68/Docs/R1-120403.zip
NTT DOCOMO (2012b) R1-120404: CSI feedback scheme for Rel-11 CoMP. In: 3GPP TSG RAN WG1 meeting #68, Dresden, Germany, 6–10 Feb 2012. http://www.3gpp.org/ftp/tsg_ran/wg1_rl1/TSGR1_68/Docs/R1-120404.zip
Panasonic (2011) R1-113807: CSI feedback in support of DL CoMP. In: 3GPP TSG RAN WG1 meeting #67, San Francisco, USA, 14–18 Nov 2011. http://www.3gpp.org/ftp/tsg_ran/WG1_RL1/TSGR1_67/Docs/R1-113807.zip
Qualcomm Incorporated (2011) R1-114110: feedback schemes in support of downlink CoMP. In: 3GPP TSG RAN WG1 meeting #67, San Francisco, USA, 14–18 Nov 2011. http://www.3gpp.org/ftp/tsg_ran/WG1_RL1/TSGR1_67/Docs/R1-114100.zip
Qualcomm Incorporated (2012a) R1-120544: on the need for inter-CSI-RS-resource feedback. In: 3GPP TSG RAN WG1 meeting #68, Dresden, Germany, 6–10 Feb 2012. http://www.3gpp.org/ftp/tsg_ran/wg1_rl1/TSGR1_68/Docs/R1-120544.zip
Qualcomm Incorporated (2012b) R1-120545: on the need for supporting aggregated feedback for CoMP. In: 3GPP TSG RAN WG1 meeting #68, Dresden, Germany, 6–10 Feb 2012. http://www.3gpp.org/ftp/tsg_ran/wg1_rl1/TSGR1_68/Docs/R1-120545.zip
Renesas Mobile Europe Ltd. (2012a) R1-120373: need for inter-CSI-RS-resource feedback. In: 3GPP TSG RAN WG1 meeting #68, Dresden, Germany, 6–10 Feb 2012. http://www.3gpp.org/ftp/tsg_ran/wg1_rl1/TSGR1_68/Docs/R1-120373.zip
Renesas Mobile Europe Ltd. (2012b) R1-120374: on aggregated CoMP feedback. In: 3GPP TSG RAN WG1 meeting #68, Dresden, Germany, 6–10 Feb 2012. http://www.3gpp.org/ftp/tsg_ran/wg1_rl1/TSGR1_68/Docs/R1-120374.zip
Renesas Mobile Europe Ltd. (2012c) R1-120375: DL CoMP rank reporting. In: 3GPP TSG RAN WG1 meeting #68, Dresden, Germany, 6–10 Feb 2012. http://www.3gpp.org/ftp/tsg_ran/wg1_rl1/TSGR1_68/Docs/R1-120375.zip
Renesas Mobile Europe Ltd. (2012d) R1-120376: CQI feedback options for CoMP. In: 3GPP TSG RAN WG1 meeting #68, Dresden, Germany, 6–10 Feb 2012. http://www.3gpp.org/ftp/tsg_ran/wg1_rl1/TSGR1_68/Docs/R1-120376.zip
Research In Motion, UK Limited (2011) R1-113960: on support of aggregated feedback for CoMP transmission. In: 3GPP TSG RAN WG1 meeting #67, San Francisco, USA, 14–18 Nov 2011. http://www.3gpp.org/ftp/tsg_ran/WG1_RL1/TSGR1_67/Docs/R1-113960.zip
Sallabi F, Lakas A, Shuaib K, Boulmalf M (2005) WCDMA downlink simulator with efficient wrap-around technique. In: IEEE second IFIP international conference on wireless and optical communications networks, Dept. of Electron. & Electr. Eng., Strathclyde Univ., Glasgow, UK, pp 472–476
Samsung (2010) RP-101425: revised SID proposal: coordinated multi-point operation for LTE. In: 3GPP TSG RAN#50, Istanbul, Turkey, 7–10 Dec 2010. http://www.3gpp.org/ftp/tsg_ran/TSG_RAN/TSGR_50/Docs/RP-101425.zip
Samsung (2011) R1-114224: CSI feedback mechanism for multiple transmission points. In: 3GPP TSG RAN WG1 meeting #67, San Francisco, USA, 14–18 Nov 2011. http://www.3gpp.org/ftp/tsg_ran/WG1_RL1/TSGR1_67/Docs/R1-114224.zip
Samsung (2012a) R1-120169: CSI feedback mechanism for CoMP. In: 3GPP TSG RAN WG1 meeting #68, Dresden, Germany, 6–10 Feb 2012. http://www.3gpp.org/ftp/tsg_ran/wg1_rl1/TSGR1_68/Docs/R1-120169.zip
Samsung (2012b) RP-121453: new WID proposal: enhanced CoMP for LTE. In: TSG RAN#57, Chicago, USA, 4–7 Sept 2012. http://www.3gpp.org/ftp/tsg_ran/TSG_RAN../TSGR_57/Docs/RP-121453.zip
Sharp (2011) R1-113821: CSI feedback content: the need for per CSI-RS-resource feedback. In: 3GPP TSG RAN WG1 meeting #67, San Francisco, USA, 14–18 Nov 2011. http://www.3gpp.org/ftp/tsg_ran/WG1_RL1/TSGR1_67/Docs/R1-113821.zip

Sharp (2012) R1-120275: performance evaluation of JT CoMP with inter-CSI-RS feedback. In: 3GPP TSG RAN WG1 meeting #68, Dresden, Germany, 6–10 Feb 2012. http://www.3gpp.org/ftp/tsg_ran/wg1_rl1/TSGR1_68/Docs/R1-120275.zip
Sony Corporation (2011) R1-113684: discussion on CSI feedback schemes for DL CoMP. In: 3GPP TSG RAN WG1 meeting #67, San Francisco, USA, 14–18 Nov 2011. http://www.3gpp.org/ftp/tsg_ran/WG1_RL1/TSGR1_67/Docs/R1-113684.zip
Texas Instruments (2011) R1-113784: CSI feedback to support downlink CoMP. In: 3GPP TSG RAN WG1 meeting #67, San Francisco, USA, 14–18 Nov 2011. http://www.3gpp.org/ftp/tsg_ran/WG1_RL1/TSGR1_67/Docs/R1-113784.zip
Texas Instruments (2012) R1-120463: CSI feedback to support downlink CoMP. In: 3GPP TSG RAN WG1 meeting #68, Dresden, Germany, 6–10 Feb 2012. http://www.3gpp.org/ftp/tsg_ran/wg1_rl1/TSGR1_68/Docs/R1-120463.zip
Wu Y, Luo H, Ding M et al (2011) Efficient limited feedback for MIMO-relay Systems. IEEE Commun Lett 15(2):181–183
ZTE (2011a) R1-113763: discussion on CSI feedback for CoMP based on carrier aggregation feedback structure. In: 3GPP TSG RAN WG1 meeting #67, San Francisco, USA, 14–18 Nov 2011. http://www.3gpp.org/ftp/tsg_ran/WG1_RL1/TSGR1_67/Docs/R1-113763.zip
ZTE (2011b) R1-113766: CQI computation for CoMP. In: 3GPP TSG RAN WG1 meeting #67, San Francisco, USA, 14–18 Nov 2011. http://www.3gpp.org/ftp/tsg_ran/WG1_RL1/TSGR1_67/Docs/R1-113766.zip
ZTE (2012a) R1-120298: evaluation of inter-CSI-RS-resource feedback for CoMP. In: 3GPP TSG RAN WG1 meeting #68, Dresden, Germany, 6–10 Feb 2012. http://www.3gpp.org/ftp/tsg_ran/wg1_rl1/TSGR1_68/Docs/R1-120298.zip
ZTE (2012b) R1-120299: evaluation of aggregated feedback for CoMP. In: 3GPP TSG RAN WG1 meeting #68, Dresden, Germany, 6–10 Feb 2012. http://www.3gpp.org/ftp/tsg_ran/wg1_rl1/TSGR1_68/Docs/R1-120299.zip

Chapter 9
Conclusion

Abstract In this chapter, we summarize the key points of this book and look forward to the future of multipoint cooperative communication technologies. It is pointed out that multipoint cooperative communication with new features will continue to be one of the key technologies in the future 5G cellular networks.

Keywords Conclusion • Multipoint cooperative communication • 5G

9.1 Key Points of This Book

Two distinct features characterize the modern wireless mobile communication systems. The first feature is broadband high-speed transmission, for example, the downlink bandwidth of the fourth generation (4G) wireless communication network is as large as 100 MHz, which can accommodate a peak data rate of 1 Gbps (Sesia et al. 2009). The second feature is mobile Internet. According to Fujitsu (2012), at present more than 70% of Internet access comes from mobile handsets, which indicates a paradigm shifting from old-fashioned PC Internet to a new era of mobile Internet, which gives birth to a great number of new applications such as cloud services, social networks, mobile video streaming, and real-time navigation.

However, the mentioned two features pose serious challenges for design of communication systems, such as intercell interference management, reliable connection and efficient handover during movement, self-optimization networks, and distributed/centralized signal processing. To respond to these challenges, many technologies have been proposed, and among them multipoint cooperative communication is regarded as a very effective tool to enhance the performance of existing networks (Kramer et al. 2006). In particular, it has been shown that cooperative communication is capable of improving the cell-edge throughput as well as the overall throughput (Marsch and Fettweis 2011). Therefore, investigations of multipoint cooperative communication technologies are of high value both in academic studies and in practical applications.

M. Ding and H. Luo, *Multi-point Cooperative Communication Systems: Theory and Applications*, Signals and Communication Technology, DOI 10.1007/978-3-642-34949-2_9,

In Chap. 2 of this book, recent theoretical research activities in cooperative communications as well as backgrounds of multiple-input multiple-output (MIMO) systems are comprehensively addressed and systematically analyzed. Based on whether data sharing is conducted, whether channel state information (CSI) sharing is allowed, and whether time-frequency synchronized transmission or reception (TFSTR) is operated, all the existing multipoint cooperative communication schemes are classified into eight categories. In the proposed framework of eight technology categories, the first four categories don't require sharing of CSI so that they treat the intercell interference as unpredictable and useless signals, leading to passive and simple multipoint cooperative communication schemes. On the other hand, the latter four categories take advantage of the multipoint CSI and perform more active signal processing functionalities in an interference-cognitive way. Theoretical studies in this book focus on the latter four technology categories, including interference coordination technologies, antenna selection (AS) techniques, and linear precoding in multipoint joint transmission (JT).

For the sixth category of multipoint cooperative communication technology, we investigate the relay/antenna selection schemes for the amplify-and-forward (AF) MIMO relay network in Chap. 3. In this chapter, we propose three greedy antenna selection algorithms, which are doubly zero-forcing (ZF) greedy capacity maximization (DZF-GCM), greedy capacity maximization (GCM), and greedy mean square error (MSE) minimization (GMM) algorithms. The effectiveness of the proposed schemes is verified by simulation results followed by comprehensive discussions on the performance comparison of various algorithms to provide more insights on this topic. Under the assumption of ZF processing at both transmitter and receiver, simulation results show the proposed DZF-GCM algorithm can achieve higher system capacity than the existing schemes, and the gain is more pronounced in the low signal-to-noise ratio (SNR) regime at the relay nodes. Under the assumption of general processing at both transmitter and receiver, simulation results show that the system capacity obtained from the existing schemes increases with the relay number by the rate of $O(\log\log K)$, while the proposed GCM algorithm can make the system capacity scale like $O(\log K)$ with the relay number, achieving the upper bound of system capacity in the sense of asymptotic capacity. Under the assumption of general processing at both transmitter and receiver, the proposed GMM algorithm can achieve higher diversity gain and lower bit error rate (BER) than the existing algorithms, even without the power bonus given by activating more independently powered relay nodes. The novelty of the proposed schemes is that the closed-form expressions of the capacity increase and MSE decrease resulted from adding one more antenna pair to the AF MIMO relay network are carefully derived, followed by designs of low-complexity greedy relay/antenna selection algorithms.

For the seventh category of multipoint cooperative communication technology, we address the interference coordination schemes for the uplink frequency division multiple access (FDMA) cellular network in Chap. 4. In this chapter, we propose an advanced interference coordination scheme that consists of six steps with the key design lying in the enhanced user equipment (UE) categorization and resource-access control policies from an altruistic perspective, which aims to reduce the interference to adjacent cells. To verify the effectiveness of the proposed scheme, we resort to the approach of system-level simulation based on a cellular network, the methodology and implementation of which are addressed in great details. Simulation results show that compared with the existing schemes, the proposed scheme can increase the efficiency of the trade-off between the cell-edge throughput and the overall throughput by more than 50%. Therefore, the proposed scheme exhibits high performance in interference coordination and can be implemented with small load of inter-BS signaling, which is very beneficial for the uplink FDMA cellular network. The novelty of the proposed scheme is that the BS assigns different levels of authorization for UEs to access the frequency resource based on the UEs' resistance of interference and tendency of producing interference. If a UE tends to produce a large amount of interference to adjacent cells, the BS will restrict the frequency resource for the UE to use, thus reducing the interference level in the network from an altruistic perspective, and hence, the cell-edge throughput can be increased. On the other hand, if a UE is not likely to cause much interference to adjacent cells, the BS will grant the UE to have access to the edge UE resource of the cell if it is available; thus, the overall throughput can be improved.

For the eighth category of multipoint cooperative communication technology, we discuss joint precoding schemes for the downlink cellular network with ideal backhaul conditions and those with nonideal backhaul conditions in Chaps. 5 and 6, respectively. In Chap. 5, we introduce some of the well-known precoding schemes for JT, that is, the global precoding (GP), local precoding (LP), weighted local precoding (WLP), and single-frequency network precoding (SFNP) schemes. Based on the discussion, we propose a precoding scheme that is a combination of antenna selection (AS) and SFNP, that is, the AS-SFNP scheme. Theoretical analysis and simulation results show that in the case of single-antenna users, the proposed scheme and the weighted local precoding scheme can achieve similar optimal SINR performance compared with the global precoding scheme. Furthermore, when considering the case of multi-antenna users and more practical scenarios, simulation results show that even if restricted search space is exerted on the antenna selection process and the beneficial operation of antenna power compensation is removed, the proposed scheme still can achieve higher system capacity than those of the local precoding, weighted local precoding, and single-frequency network precoding schemes. Thus, the proposed scheme effectively closes the performance gap with the optimal global precoding scheme. In addition, the proposed scheme, compared to the weighted local precoding scheme, requires a lower load of feedback overhead and is easy to implement. Finally, from a system-level simulation of a practical network, the proposed AS-SFNP scheme is shown to achieve a beneficial balance among the factors of performance, complexity, and feedback overhead, compared with the computationally demanding GP scheme and the feedback-bit consuming WLP scheme. The novelty of the proposed AS-SFNP scheme is that transmit antenna selection is applied to improve the capacity of the composite SFN channel, and then, the SFNP operation is invoked.

In Chap. 6, we propose a sequential and incremental precoding (SIP) scheme based on the criterion of minimizing the largest sub-stream MSE. Simulation results show that when the backhaul links are relatively reliable, the proposed scheme can obtain similar maximum sub-stream MSE performance compared with the existing schemes. However, when the backhaul communications suffer from more serious connectivity problems, the proposed scheme exhibits considerable performance gains compared with the existing schemes. And the robustness of the proposed scheme is more evident in the high signal-to-interference-plus-noise ratio (SINR) regime or when the equal power allocation over the sub-streams is engaged. In addition, through simulations for limited-bit feedback systems, the proposed scheme retains the aforementioned advantages. Hence, considering the practical backhaul conditions and the limited-bit feedback methods, the proposed scheme is very useful for implementation. The novelty of the proposed scheme is that the imperfectness of the backhaul communications is modeled as probabilistic events and considered as a relevant factor in the optimization process. We first optimize the precoding matrix for the channel between the serving base station and the user. Then, according to the descending order of the activation probabilities of the helper base stations, we sequentially generate the optimal precoding matrix for each helper base station by an iterative algorithm with the previously optimized precoders fixed.

After completing the discussions on the selected areas of theoretical studies on multipoint cooperative communication technologies, we turn our attention to the practical applications of cooperative communications.

In Chaps. 7 and 8, we address the coordinated multipoint system (CoMP) system which will be adopted by the enhanced 4G networks, that is, the Long-Term Evolution (LTE) Release 11 system. In CoMP transmission or reception, schemes in the seventh and eighth categories of multipoint cooperative communication technologies have been considered, for example, JT/joint reception (JR) and coordinated scheduling (CS)/coordinated beamforming (CB). Although the CoMP system was failed to be adopted by LTE Release 10 specifications due to some incompatible CSI feedback designs with the single-cell MIMO framework, it has eventually come back for the LTE Release 11 standardization. The corresponding specification works are related to aspects such as backhaul communication protocols, control signaling provision, and multipoint CSI feedback design. Also we analyze the simulation results from the 3GPP CoMP study item to show the advantages of CoMP system in practical cellular networks. However, it is concluded from the CoMP study item that the multipoint delay issue should be further investigated for practical applications. One of the closely related topics is the CSI feedback in multipoint scenarios. Hence, in Chap. 8, we address the common feedback framework (CFF) for downlink CoMP transmissions in LTE Release 11 networks. As an ambitious goal, the CoMP CFF targeted for proposing a total solution for CoMP so that all transmission-specific designs could be unified into one scheme. However, all of the existing CFF options were supported by numerous companies, and hence, the views were divided and fragmented. Although system-level simulations showed that both the co-phase information (CFF option 2) and the aggregated channel quality indicator (CQI) (CFF option 3) were able to provide considerable cell-edge throughput gains compared the non-CoMP scheme, these two CFF options were eventually rejected by 3GPP due to lack of consensus on which option should be adopted. As a result, CFF option

4, basically a per-point feedback scheme, was agreed to guide the designs of CSI reporting for CoMP in LTE Release 11. The major benefit of CFF option 4 is that it requires minimal specification efforts to include CoMP into the LTE network as a new and competitive feature. However, the potential problem about CFF option 4 is that it may not be able to support JT very well since any information of inter-CSI-RS-resource or aggregated CSI is not available in this framework. Therefore, a third campaign of CoMP for LTE Release 12 and onward will be launched in the future, with one of the aims to enhance the feedback mechanisms for better support of JT, including intracell site and intercell site.

9.2 Toward the Future

In the next decade, wireless communication systems will face three major challenges, which are data traffic explosion, rise of the mobile Internet, and a gigantic number of upcoming machine-to-machine (M2M) devices (see Sect. 1.2.1). These challenges pose a lot of new requirements for the existing 4G networks. Therefore, the development of modern wireless communication system has entered the enhanced 4G era and began to gradually move toward the 5G front. Higher data rate and better quality of service will continue to be the focal points of research activities both in academic and industrial fields.

During the 3GPP workshop meeting held in June 2012 (Sect. 1.2.3), some preliminary proposals on the key technologies of the 5G mobile telecommunication system were treated with great interests. Compared with the enhanced 4G system, some new trends of the 5G network include ultrahigh rate of wireless transmission, cloud radio access network (RAN), smart communication service provision, and Internet of things (IoT). Several advanced technologies for 5G networks were also briefly discussed.

- Massive MIMO technology (Samsung 2012; ZTE 2012): Considering the communication on high-frequency spectrums in the future, the number of small-size antennas stalled on a transmission point can be very large, for example, 64 or 128, to achieve a very high multiplexing gain in the system.
- Enhanced M2M communication (Fujitsu 2012; LG 2012): Current M2M communication focuses on low-rate and small packet transmissions. However, in the future, enhanced M2M communication should be considered for surveillance, healthcare, and environment monitoring applications.
- D2D communication (Ericsson and ST-Ericsson 2012; Nokia 2012): This new technology allows direction communication between UEs so that a large amount of traffic can be offloaded from the core network.

The discussed technologies for the 5G system also have profound implications for the multipoint cooperative communication. It can be foreseen that multi-UE based cooperative communications and multi-point transmissions involving massive-antenna BSs and a large number of UEs/machines will see some interesting activities in the future 5G networks.

9.3 Conclusion

This book addresses the theory and applications of multipoint cooperative communication systems. In the first part, a thorough technical survey is presented and four selected areas of theoretical studies are treated, while in the second part the CoMP transmission and reception in the enhanced 4G networks are discussed from a variety of aspects. Finally, we briefly share our views on the 5G system and point out two directions for future studies on the multipoint cooperative communication technology.

References

Ericsson, ST-Ericsson (2012) RWS-120003: views on Rel-12. In: 3GPP Workshop on Release 12 Onward, Ljubljana, Slovenia, 11–12 June 2012. http://www.3gpp.org/ftp/workshop/2012-06-11_12_RAN_REL12/Docs/RWS-120003.zip

Fujitsu Limited (2012) RWS-120016: requirements and technical considerations for RAN Rel.12 & Onwards. In: 3GPP workshop on Release 12 Onward, Ljubljana, Slovenia, 11–12 June 2012. http://www.3gpp.org/ftp/workshop/2012-06-11_12_RAN_REL12/Docs/RWS-120016.zip

Kramer G, Mari'c I, Yates RD (2006) Foundations and trends in networking. Cooperative Commun 1(3):271–425

LG Electronics (2012) RWS-120050: LG's view on evolution of LTE in Release 12 and beyond. In: 3GPP workshop on Release 12 Onward, Ljubljana, Slovenia, 11–12 June 2012. http://www.3gpp.org/ftp/workshop/2012-06-11_12_RAN_REL12/Docs/RWS-120050.zip

Marsch P, Fettweis GP (2011) Coordinated multi-point in mobile communications. Cambridge University Press, New York

Nokia Corporation (2012) RWS-120004: LTE evolving towards Local Area in Release 12 and beyond. In: 3GPP workshop on Release 12 Onward, Ljubljana, Slovenia, 11–12 June 2012. http://www.3gpp.org/ftp/workshop/2012-06-11_12_RAN_REL12/Docs/RWS-120004.zip

Samsung Electronics (2012) RWS-120046: technologies for Rel-12 and onwards. In: 3GPP workshop on Release 12 Onward, Ljubljana, Slovenia, 11–12 June 2012. http://www.3gpp.org/ftp/workshop/2012-06-11_12_RAN_REL12/Docs/RWS-120046.zip

Sesia S, Toufik I, Baker M (2009) LTE: the UMTS long term evolution. Wiley, Chichester

ZTE (2012) RWS-120034: views on 3GPP Rel-12 and beyond. In: 3GPP workshop on Release 12 Onward, Ljubljana, Slovenia, 11–12 June 2012. http://www.3gpp.org/ftp/workshop/2012-06-11_12_RAN_REL12/Docs/RWS-120034.zip